AD NUMBER

AD001778

NEW LIMITATION CHANGE

TO

Approved for public release, distribution unlimited

FROM

Distribution: No foreign.

AUTHORITY

ONR ltr., 26 Oct 1977

AD- 1778

UNCLASSIFIED

ADDITIONS AND CORRECTIONS

TO THE REPORT

AN INVESTIGATION OF THE LOAD-DEFORMATION CHARACTERISTICS OF REINFORCED CONCRETE BEAMS UP TO THE POINT OF FAILURE

The following additions and corrections are to be made to the report An Investigation of the Load-Deformation Characteristics of Reinforced Concrete Beams Up to the Point of Failure, by J. R. Gaston, C. P. Siess and N. M. Newmark, which was issued to the Office of Naval Research under Contract N6ori-071(34), Task Order 34, Project NR-064-372 in December 1952:

BEAM DESIGNATION

The significance of the letter and numeral symbols used to designate the various beam specimens was not given in the original report.

The letters and numerals serve to identify the various beams in the following manner:

For beams reinforced in tension only:

The letter T indicates that the beam was reinforced in tension only in the region of pure flexure.

The numeral following the letter T is the value of the reinforcing index $q = \frac{pf_y}{f'_c}$ in tenths, rounded to the nearest tenth.

The letter L, M, or H appearing next designates the concrete strength; that is low, medium, or high, where low is from 2000 psi to 3000 psi, medium is from 3000 psi to 4000 psi and high is from 4000 psi to 5000 psi.

The lower case letter a, b, or c following the concrete strength designation identifies the individual beams when two or more similar specimens were tested.

For beams reinforced in compression as well as tension:

The letter C indicates that the beam was reinforced in compression as well as tension in the region of pure flexure.

The numeral following the letter C is the value of $q = \frac{pf_y}{f'_c}$ in tenths, as before.

The letter w, x, y, or z appearing next indicates the spacing of the ties in the region of pure flexure. The letter w refers to compression reinforcement without ties; x indicates that the tie spacing was equal to that specified by ACI 318-51; y indicates that the tie spacing was one-half that specified by ACI 318-51; and z indicates that the tie spacing was one-fourth that specified by ACI 318-51.

The letters n or m indicate the type of tie used, as shown in Fig. 4 of the report.

The lower case letter a or b, where it appears, indicates that two similar specimens were tested.

Examples:

Beam T1La is reinforced in tension only, has a value of the reinforcing index q equal to 0.1, a concrete strength between 2000 and 3000 psi, and is one of two or more similar beams.

Beam C3yna is reinforced in compression as well as tension, has a value of q equal to 0.3, has a tie spacing in the region of pure flexure one-half that specified by ACI 318-51, has type n ties, and is one of two or more similar beams.

ADDITION TO TABLE NO. 2

SUMMARY OF RESULTS

FOR BEAMS REINFORCED IN TENSION AND COMPRESSION

Beam	k^n +
C2w	0.897
C2xw	0.878
C3w	0.857
C3xw	0.857
C3yna	0.866
C3ynb	0.850
C4xna	0.884
C4xnb	0.856
C4xn	0.857
C5yn	0.833
C6xn	0.833
C7.	0.833

k"d ... tance between the centroid... of ... tens'on and compression reinforcement; where d = distance from the top of the beam to the centroid of the ... reinforcement.

CORRECTION TO TABLE 9a

COMPARISON OF EXPERIMENT AND THEORETICAL VALUES

OF YIELD-POINT MOMENT

Beams with Tension and
Compression Reinforcement

Beam	M_y - kip-ft		
	Exp	Theo	Exp / Theo
C2w	32.4	31.1	1.04
C2xm	38.0	35.4	1.07
C3w	62.4	60.4	1.03
C3xm	66.3	61.5	1.09
C3yna	41.0	40.1	1.02
C3xnb	62.4	62.0	1.01
C4xna	40.1	41.4	0.97
C4xnb	42.8	42.2	1.01
C4zn	59.3	60.7	0.98
C5yn	87.8	89.5	0.98
C6xm	84.9	85.2	1.00
C7w	84.0	84.7	0.99
	Average Ratio		1.02
	Range		0.98-1.09

OTHER CORRECTIONS AND ADDITIONS

A value of the modulus of elasticity of the reinforcing steel, E, of 30 x 10^6 psi was used throughout the report.

Page 32:

Equation (31) should read:

$$f_c = \frac{pf_y}{\frac{1}{2}k' + \frac{np'(k' + k''-1)}{k'}}$$

Equation (32) should read:

$$f'_s = \left[\frac{k'' + k'-1}{k'}\right] nf_c$$

Page 38:

Third line below Eq. (47)

"For $q' > q'_{cr}$, . . ."

Fifth line below Eq. (47)

" . . ., that is, $f_s < f_y$ "

Second line below Eq. (48)

" . . . and $f_s > f_y$ "

TABLE 1, "SUMMARY OF RESULTS FOR BEAMS REINFORCED IN TENSION ONLY"

The entry under the column entitled "Stirrups" should read "None" for beam T1M8 instead of "Clamp-on".

TABLE 2, "SUMMARY OF RESULTS FOR BEAMS REINFORCED IN TENSION AND COMPRESSION

The heading for column 9 should read " p'- %", instead of " p -%".

TABLE 4, PROPERTIES OF REINFORCING STEEL

The heading for column 9 should read "Elongation in 8 in., %" instead of "Elongation in 6 in., %".

Fig. 1/ BEAM AND TESTING APPARATUS

The following note should be added, "The 8"-dimension of all bearing plates is parallel to the axis of the beam".

CONTENTS

TABLES

FIGURES

I. SUMMARY AND CONCLUSIONS

The objective of these tests and studies was to establish the relationships between load and deformation for reinforced concrete members subjected to static flexural loading. The approach to this problem has been mainly experimental, guided by theoretical considerations.

The tests were made on 33 reinforced concrete beams, 6 in. by 12 in. in cross section, having a span length of 9 ft., and loaded at the third points. Twenty-one of these beams were provided with tension reinforcement, while 12 were provided with both tension and compression reinforcement. The main variables in these tests were the concrete strength, the percentages of tension or compression reinforcement, and the method of tying the compression reinforcement.

The tests have been described, and the test results have been presented in both tabular and graphical form. Comparisons of the test results of various beams have been made to show the effects of the variables introduced.

An analysis has been developed that predicts the load-deflection diagrams for the beams tested. This analysis consists of expressing the conditions at the critical points of the load-deformation curves.

In the equations expressing the conditions at the yield point, a transformed section and a linear stress-strain relationship for the concrete are assumed. Although these assumptions are rather crude for beams near balanced design, the equations give satisfactory results.

The equations expressing the conditions at the maximum load-carrying capacity involve the values of k_2/k_1k_3, k_1k_3 and ϵ_{cu}, where k_1 and

k_2 are coefficients defining the magnitude and position of the internal compressive force in the concrete, k_3 is the ratio of maximum compressive strength of concrete in a beam to the corresponding compressive strength of standard test cylinders, and ϵ_u is the ultimate strain in the concrete. These values were determined empirically. In this investigation, the value of k_2/k_1k_3 has been found to be approximately 0.5, $k_1k_3 = 0.625 + \frac{600}{f'_c - 1500}$, and $\epsilon_u = 0.003$.

Comparisons between the theoretical and experimental results have been made. These are presented in both tabular and graphical form.

The following conclusions can be drawn from the test results:

(1) Concrete strength has little effect on the energy absorbing capacity of beams failing initially in tension but does have an effect on the energy absorbing capacity of beams failing initially in compression.

(2) The ductility of a beam is dependent upon the reinforcing index as can be seen from the test results. The midspan deflection of beams with a cross section of 6 x 12 in., an effective depth of approximately 10 in., and a span of 9 ft. varied from less than 1 in. to more than 6 in. when carrying the maximum load. This is a variation in deflection of from 0.9 to 5.5 percent of the span length.

(3) The compression reinforcement adds to the ductility of a beam. The addition of compression reinforcement strengthens the compression zone and thus raises the neutral axis. This enables a larger angle change to take place before the

concrete crushes and thereby increases the deflection which the beam can undergo and still carry near maximum loads.

(4) In order for the compression reinforcement to be the most effective, it must be well tied.

II INTRODUCTION

1. Object

The ultimate aim of this investigation is the development of methods for predicting the load-deflection or moment-rotation characteristics of reinforced concrete members subjected to dynamic loading. However, in order to plan an intelligent investigation of these characteristics, the load deflection or moment-rotation characteristics of reinforced concrete members subjected to static loading must be known. A review of the available data shows that very little is known about the deformations required to develop the maximum load-carrying capacity of reinforced concrete members. Therefore, the object of this phase of the investigation is to establish the relationships between load and deformation for reinforced concrete members subjected to static loading.

The reason for determining the load-deformation characteristics of reinforced concrete members is to ascertain the energy-absorbing capacity of the members. Since the greatest part of the energy absorbed by a member is absorbed after the member has yielded, the load-deformation characteristics of a member subjected to stresses in the plastic range are of particular interest.

In an actual structure there are many kinds of stresses and stress combinations which contribute to the energy absorbing capacity of the entire structure. However, since very little is known about even the energy absorbing capacity of a reinforced concrete member subjected to the simplest kind of stress, it was deemed necessary to establish by experiment the complete load-deformation relations for the simple case of pure

flexure before complicated stress combinations were considered.

2. Scope

Although a great many variables must be considered in a complete study of the flexural load-deformation characteristics of reinforced concrete members, it was not considered practicable to introduce all of them in this phase of the investigation. However, studies of previous investigations, and analyses made in connection with this study, indicated that the most important variables are the concrete strength and the steel percentage and properties; therefore, these were chosen as the principal quantities to be studied.

The results of both analytical and experimental investigations are presented in this report. The analysis was developed to predict the load-deflection curves for simple beams in flexure. The results of the analysis were tested by comparison with test results. It was found that the method is capable of predicting with a fair degree of accuracy the following properties of the load-deflection curves obtained from the tests:

(1) The load at first yielding of reinforcement

(2) The deflection of the beam or the rotation in the constant moment section at a load corresponding to (1)

(3) The maximum load carried by the beam

(4) The deflection or rotation corresponding to the maximum load.

With these four quantities the load-deflection diagram for beams with tension reinforcement only or with both tension and compression reinforcement may be constructed, and the energy-absorbing capacity computed.

The results of static load tests of 33 reinforced concrete beams in flexure are reported herein and compared with the predictions of the analysis. Twenty-one of these beams were provided with tension reinforcement only, while 12 were provided with compression as well as tension reinforcement. Adequate provisions against shear failure were made in practically all beams. The principal variables were the strength of the concrete, the amount of tension or compression reinforcement and the manner of tying the compression reinforcement.

3. Acknowledgments

The tests and studies reported herein were made as a part of an investigation of the relation between load and deformation for reinforced concrete joints and members conducted by the Structural Research Laboratory in the Engineering Experiment Station of the University of Illinois, in cooperation with the Office of Naval Research, under contract N6 onr-07134, Task Order 34, Project Designation No. N.R.-064-372. This investigation was initiated 1 February 1951.

The program of the investigation was guided by Dr. N. M. Newmark, Research Professor of Structural Engineering. The program was under the immediate direction of Dr. C. P. Siess, Research Associate Professor of Civil Engineering.

Appreciation is expressed to Mr. G. D. T. Wright for his work in the early stages of the investigation and to Lt. A. F. Dill, Civil Engineer Corps, U. S. Navy, for his able assistance in connection with the development of the analysis. The manuscript of this report was critically studied by Mr. J. H. Appleton, Research Associate, and his helpful comments are gratefully acknowledged.

4. Notation

The following notation is used in this report:

A_s = area of tension reinforcement

A'_s = area of compression reinforcement

a = depth of stress block in concrete at maximum load-carrying capacity

b = width of a rectangular beam

C_1 = compressive force in concrete

C_2 = compressive force in the compression reinforcement

d = distance from centroid of tension reinforcement to compression edge of beam

E_c = modulus of elasticity of concrete; assumed approximately equal to $1{,}800{,}000 + 460\ f'_c$

E_s = modulus of elasticity of reinforcing steel in the elastic region

E_o = slope of stress-strain curve for reinforcing steel in work-hardening region (See Fig. 1)

f'_c = compressive strength of concrete as determined from tests of 6 x 12-in. cylinders

f_o = defined in Fig. 1

f_s = stress in tension reinforcement

f'_s = stress in compression reinforcement

f_y = yield point of tension reinforcement

f'_y = yield point of compression reinforcement

I_y = moment of inertia of beam cross-section transformed to concrete

k = ratio indicating relative depth to neutral axis of transformed section of beams reinforced in tension only. (straight-line theory)

k' = ratio indicating relative depth to neutral axis of transformed section of beams reinforced in tension and compression (straight-line theory)

k'' = a factor which when multiplied by d yields the distance between tension and compression reinforcement

k_1, k_2 = coefficients defining the magnitude and position of the internal compressive force in concrete (See Fig. 2)

k_3 = ratio of maximum compressive strength of concrete in beam to compressive strength of standard test cylinders, f'_c

L = length of beam span

M_y = bending moment at yield point

M_{max} = maximum bending moment at maximum load-carrying capacity

$n = E_s/E_c$ = modular ratio

$p = A_s/bd$

$p' = A'_s/bd$

$$q = \frac{pf_y}{f'_c}$$

$$q' = \frac{p'f_y - p'f'_y}{f'_c}$$

T = force in tension reinforcement

Δ_y = midspan deflection at yield point

Δ_{ult} = midspan deflection at maximum load-carrying capacity

ε_s = strain in steel*

ε_y = strain in steel at yield point*

ε_o = strain in steel at beginning of work-hardening*

ε_u = ultimate strain in concrete*

Φ_y = curvature of beam at yield point, in region of constant moment

Φ_{ult} = curvature of beam at maximum load-carrying capacity, in region of constant moment

---

* In all cases the absolute values of strain are used in the analysis

III. DESCRIPTION OF TEST SPECIMENS, MATERIALS AND FABRICATION

5. Description of Test Specimens

The choice of the size of the test specimens was influenced by two factors. First, it was desired that the beams be sufficiently large so the smallest steel percentage could be attained by using two commercial-size deformed bars as longitudinal reinforcement. And second, the beams should be sufficiently small so future tests under dynamic loading could possibly be made with the same size specimen. With these considerations in mind, a beam cross section of 6 in. by 12 in. and a beam span length of 9 ft. were chosen. The overall length of the test beams was 10 ft.

The beams were loaded at the third points in order to subject a considerable portion of the specimen to pure flexure and still keep within reasonable load and shear requirements. Load was applied through bearing blocks which were 8 in. square and 3 in. thick.

In the series of tests employing tension reinforcement only, the reinforcing index $q = pf_y/f'_c$ was varied in such a manner as to cover the range from beams having less reinforcement than specified by usual design codes to beams having sufficient reinforcement to obtain initial concrete compression failures. This is shown in the plot of q vs. f'_c in Fig. 3.

In order to vary the parameter q in the series of beams reinforced in tension only, the concrete strength, f'_c, was varied from 2000 to 6000 psi, and the percentage of tension reinforcement p, was varied from 0.34 to 7.22 percent as shown in Table 1. In order to vary the tensile and compressive resistance of the beams reinforced in tension and compression, the following factors were varied as shown in Table 2: concrete strength,

f'_c, from 2000 to 5000 psi; the percentage of tension reinforcement, p, from 1.38 to 5.61 percent; the percentage of compression reinforcement, p', from 0.625 to 2.80 percent; the ratio of the area of compression reinforcement, p', to the area of the tension reinforcement, p, from 0.454 to 0.733; the ties in the region of pure flexure, from no ties to ties at one-quarter of the spacing required by the A.C.I. Code (318-51); and the manner of tying the compression reinforcement as shown in Fig. 4.

Since the shear requirements of A.C.I. 318-51 were satisfied, no shear reinforcement was provided in the first eight beams. However, the first two beams tested failed in diagonal tension, and shear reinforcement was therefore provided in the subsequent tests. Outside "clamp-on" stirrups, as shown in Fig. 5, were used on the beams already fabricated without web reinforcement, and conventional vertical stirrups were provided in the remaining beams. These stirrups were designed to carry all of the predicted maximum shearing force at a computed unit stress in the stirrups of 30,000 psi.

6. Materials

(a) Cement Type I Portland Cement was used in all test beams. The cement was purchased in paper bags in two lots from a local dealer and stored under proper conditions.

(b) Fine and Coarse Aggregates The fine aggregate was Wabash River torpedo sand having an average fineness modulus of 3.1. The coarse aggregate was Wabash River gravel of 1-in. maximum size. The gravel had a rather high percentage of fines. The aggregate sieve analyses are given in Table 3. The specific gravities were 2.65 and 2.70 for sand and gravel, respectively. The absorption of both fine and coarse aggregate was about

one percent by weight of the surface dry aggregate.

The origin of these aggregates is a glacial outwash, mainly of the Wisconsin glaciation. The major consituents of the gravel were limestone and dolomite, and there were minor quantities of quartz, granite, gneiss, etc. The sand consisted mainly of quartz with the coarser fractions similar to the gravel.

The aggregates were purchased in three lots from a local dealer and stored under proper conditions.

(c) Reinforcing Steel Seven sizes of deformed bars were used as longitudinal reinforcement; No. 3 through No. 9. All of the deformed bars used met the minimum requirements for deformations of deformed steel bars for concrete reinforcement, ASTM Designation A 305-50T. A photograph of samples of these bars is given in Fig. 6. One beam was reinforced with plain bars. All bars were of intermediate grade steel meeting the requirements of ASTM Designation A 15-39.

The steel reinforcement was purchased in 22-ft. lengths from a commercial dealer. All bars were from the same lot except the bars in the first two beams fabricated which were from the laboratory stock. Properties of each bar used, determined from tension tests, are listed in Table 4, and a typical stress-strain curve for each size of bar is given in Figs. 7, 8, 9, and 10. The tests were made in a 120,000-lb. capacity Baldwin Southwark Tate-Emery hydraulic testing machine, and strains were measured with an 8-in. extensometer and recorded with an automatic recording device. The extensometer employs a "microformer" coil in measuring strain. As used, the extensometer had a range of 4-percent strain and an error of less than one percent of the reading.

7. Fabrication and Curing

(a) Preparation of Steel Reinforcement The first step in the manufacture of the specimens was to cut the longitudinal bars to length. The bars, as supplied, were of such dimensions that two lengths of longitudinal reinforcement and one tension test coupon could be obtained from each bar. The gage lines for the mechanical strain gages were then marked and the gage holes punched and drilled. A small piece of electrician's tape was placed over each gage hole to protect it during the casting of the concrete. Corks were wired to the bars at each gage-hole location in order to form core holes in the sides of the beam to provide access to the bars. The core holes may have slightly influenced the formation of tension cracks, but such cracks would have occured in any event before the steel stresses became large.

The stirrups and ties were fabricated in the laboratory, and the reinforcement was assembled into a unit before it was placed in the forms as shown in Fig. 6. The longitudinal steel was placed inside the stirrups or ties and securely wired to them as shown in Figs. 11 and 12. Spacer bars and chairs were used to insure accurate spacing of these bars. All bars had approximately one inch of concrete covering at any surface.

In six of the twelve beams with compression reinforcing, SR-4 electric resistance strain gages were mounted on this reinforcement. To facilitate mounting of these gages, the lugs were ground off over half the perimeter of the bar for a length of about 1.5 in. It has been found in other investigations that the yield point and ultimate strength of the bar is little affected by the local removal of the lugs.*

---

* Hognestad, E., "A Study of Combined Bending and Axial Load in Reinforced Concrete Members", University of Illinois Engineering Experiment Station Bulletin No. 399, Nov. 1951, P. 16.

(b) Casting of Concrete. All concrete was mixed in a non-tilting drum type mixer of 6-cu. ft. capacity and placed with the aid of a high frequency laboratory-type internal vibrator. Two batches were used in each beam. In spite of the use of a butter mix to condition the mixer prior to the first batch, the strength of the two separate batches having the same nominal proportions varied to some extent. In order that the concrete in the constant moment section of the beam be from the same batch, the first batch of each mix was placed in the outer quarters of the beam and the second batch in the central half. The properties of the mixes are given in Table 5 and the test-day and 7-day strengths are plotted against the cement-water ratio in Fig. 13.

Although the mix was designed to have a slump of 2 to 3 in., the actual slumps varied from 0.5 to 7 in. as shown in Table 5. The consistency was difficult to control because the moisture content of the aggregate varied and the mixing of only two batches afforded little chance for adjustment.

The beams were cast in steel forms. The forms were removed the day after the beams were cast, and the beams were stored under moist conditions for an additional six days. They were then stored in the air of the laboratory until tested. Six 6 by 12-in. control cylinders were cast from each batch of concrete and were vibrated and cured in the same manner as the beams. Three of these cylinders were tested at seven days to give some indication of the compressive strength; the remaining three cylinders were tested on the day the beam itself was tested.

IV DESCRIPTION OF APPARATUS AND TEST PROCEDURE

8. Description of Test Apparatus

(a) Loading Apparatus The beams were tested on a 9-ft. span with loads applied at each one-third point. The beams were tested in a 300,000-lb. capacity Riehle screw-type testing machine and were offset in the machine to provide access to the entire length of the beam for mechanical strain gage readings, as shown in Figs. 14 and 15. The jack on the west end of the loading rig was used to keep the loading beam approximately level during testing. The testing machine was used to apply deformation, and a 125,000-lb. elastic-ring dynamometer was used to measure the applied load. The weight of the distributing beam, 600 lb., was taken into account in all calculations since the dynamometer did not measure this load.

b. Instrumentation Tensile strains in the steel were measured on six-inch gage lengths with a mechanical type strain gage. A Berry type mechanical strain gage was used until the strains exceeded its range, after which a direct-reading type strain gage was employed. The Berry gage had a multiplication ratio of 5.32, and was equipped with a 0.001-in. dial micrometer. The precision of readings with this gage was on the order of 0.00003 strain. The direct-reading gage was equipped with a 0.001-in. dial micrometer and was read to the nearest 0.001-in.

As shown in Fig. 16, the six-inch mechanical gage lines on each bar of the tension reinforcement were continuous throughout the entire span on the first 16 beams tested. However, after a study of the test data obtained from these beams, it was decided to eliminate the gage lines in the outer thirds of the span on the remaining 17 beams.

The compressive strain on the top surface of the concrete was measured with SR-4 electric resistance strain gages. These gages were located as shown in Fig. 16. The three central SR-4 gages (Nos. 2,3,4) were of type A-9, with six-inch gage lengths and were located so as to be directly above the three central gage lines on the tension reinforcement in order that the angle-change at midspan could be measured. The outer two gages (Nos. 1 and 5) were of type A-11, with one-inch gage lengths, and were used as check gages at the outer extremities of the constant moment section.

The strains in the compression steel at midspan of six of the twelve beams reinforced in compression were measured by means of SR-4 electric resistance strain gages, type A-11, with one-inch gage lengths. These gages were mounted on the bars and carefully waterproofed with Petrolastic asphaltic compound or Cycleweld C-14 cement so that they would function properly after being embedded in the fresh concrete.

The deflections of the beams with respect to the bed of the testing machine were measured to the nearest one-hundredth of an inch by means of a steel scale and cross-section paper targets on the sides of the beams. These deflections were measured at seven locations along each side of the first 11 beams tested, and at nine locations on each side of the remaining 22 beams as shown in Fig. 17. In order to determine the midspan deflection curves more accurately for the last eight beams tested a 0.001-in. dial indicator deflectometer was used.

The appearance of the failure of the first beam suggested that the diagonal tension failure could have been initiated by a bond failure; therefore 0.0001-in. dial indicators were mounted on the second beam in order to detect any end-slip of the tension reinforcement. The failure of

the second beam was similar to the first beam and, since no end-slip was observed, these measurements were not made on the remaining beams.

9. Description of Test Procedure

The beams were tested at ages from 28 to 70 days as shown in Table 5.

The increments of loading were based upon the critical factors during each stage of the testing procedure. Up to the yield load, the increments were based upon the dynamometer readings which measured the applied load. The load which caused yielding could be estimated closely from calculations based on an ultimate theory or from the results of previous tests. After yielding, the increments of loading were based upon the concrete strain until the concrete in the compression zone crushed. After the concrete crushed, the increments were based upon the measured deflections until the beam collapsed or until the test was stopped because of the instability of the loading apparatus. From four to six approximately equal increments of load were applied between zero load and the yield load, and depending upon the ductility of the beam a total of 9 to 25 increments were applied between zero load and collapse.

The following measurements were recorded after the application of each increment of deformation: the maximum load attained during the application of the deformation, the deflections along the beam, the strains in the concrete, the strains in the reinforcement, and the load the beam was carrying after all measurements had been taken. In addition to these measurements, the crack pattern was marked after each increment and a running log of any significant change in the behavior of the test was kept.

A continuous photographic record was made of the beams during test-

ing. These photographs were taken at every significant change in the crack pattern or in the general appearance of the beam. These records were made on 35 mm. film from which positive film strips were printed. By projecting these photographs on a screen the appearance of the beams during testing and the development of cracks could be studied.

The applications of each increment of load and the taking of all the measurements required about 20 minutes. The entire testing of one beam required from five to eight hours.

On the day the beam was tested, six concrete control cylinders were tested, three from each batch of concrete in the beam.

V. DERIVATION OF EXPRESSIONS FOR CRITICAL MOMENTS AND DEFORMATIONS

10. Assumptions

The following are the assumptions made in the calculations for theoretical load-deflection relations:

(1) Linear strain distribution. Linear distribution of strains throughout the depth of the beam is assumed at all stages.

(2) Stress-strain relationship for steel. The stress-strain relationship for the steel is assumed to be known. In the theory, the actual stress-strain curve of the steel is approximated by an idealised curve consisting of three straight lines as shown in Fig. 1.

(3) No tension resisted by concrete. Tension stresses in the concrete are neglected. Although some tension stresses must always exist, their effect on the moment-carrying capacity and deformations of interest in this report can be neglected with little error.

(4) Crushing of concrete at a limiting strain. The theory is based upon the assumption that the maximum flexural capacity is reached when the concrete crushes. The crushing of the concrete is assumed to occur when the concrete strain reaches some limiting value that is assumed to be a function of the compressive strength of the concrete.

(5) Buckling of compression steel. The compression steel is assumed to buckle as soon as the concrete crushes.

(6) Bond between concrete and steel. The bond condition between the reinforcement and the concrete influences the condition of compatibility of strains. Perfect bond is assumed to exist between the concrete and steel. This assumption is not strictly correct since local bond failures occur in the vicinity of cracks.

A. BEAMS REINFORCED IN TENSION ONLY

11. At Yield Point

The load and deformation at the yield point can be satisfactorily determined by use of the conventional "straight-line" theory which assumes a linear stress-strain relationship for the concrete and thus leads to a linear stress distribution in the concrete. In reality, the stress distribution in the concrete will be linear only if the maximum fiber stress at the top of the beam is well below the compressive strength of the concrete. This will be true only for under-reinforced beams; that is, beams having percentages of reinforcement or values of q below those necessary to produce simultaneous failure by crushing of the concrete and yielding of the steel. If a more precise calculation is desired, a concrete stress block similar to that shown in Fig. 2 may be employed.

If linear stress-strain distribution in the concrete is assumed, as shown in the sketch on the following page, the yield-point moment and deformations for beams reinforced in tension only and failing by yielding of the reinforcement can be computed as follows:

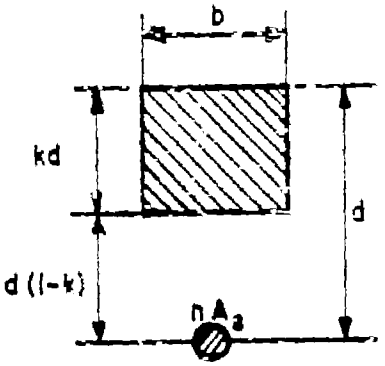

Transformed Area

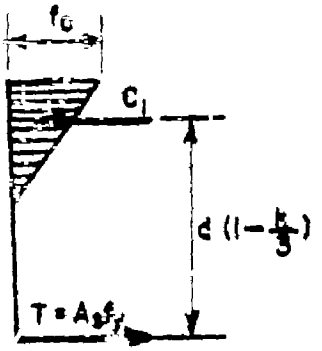

Stress Distribution

If we define

$$n = \frac{E_s}{E_c} \tag{1}$$

and

$$p = \frac{A_s}{bd} \tag{2}$$

then, as in the conventional "straight-line" theory, the depth to the neutral axis is kd where

$$k = \sqrt{2pn + (pn)^2} - pn \tag{3}$$

The moment acting on the beam when the reinforcement is stressed to the yield point, f_y, is then:

$$M_y = Td\left(1 - \frac{k}{3}\right) = A_s f_y d\left(1 - \frac{k}{3}\right) \tag{4}$$

The moment of inertia of the section, transformed to concrete, is:

$$I_y = \frac{bd^3}{3} k^3 + nA_s d^2 (1 - k)^2 \qquad (5)$$

And the curvature of the beam due to moment is:

$$\Phi_y = \frac{M_y}{E_c I_y} \qquad (6)$$

Since the $M - \Phi$ curve is approximately a straight line up to yielding of the reinforcement, the distribution of curvature along the beam is the same as that for moment. Therefore the yield point deflection at midspan of a beam with third-point loading is:

$$\Delta_y = \frac{23}{216} \frac{M_y}{E_c I_y} L^2 \qquad (7)$$

where L is the span of the beam.

12. At Maximum Load-Carrying Capacity

The load and deformations at maximum load-carrying capacity can be determined by the use of an ultimate theory, derived in the following paragraphs. In this theory it is necessary to assume a stress block in the concrete which is represented by three parameters k_1, k_2, and k_3 as shown

in Fig. 2 and in the sketch below.

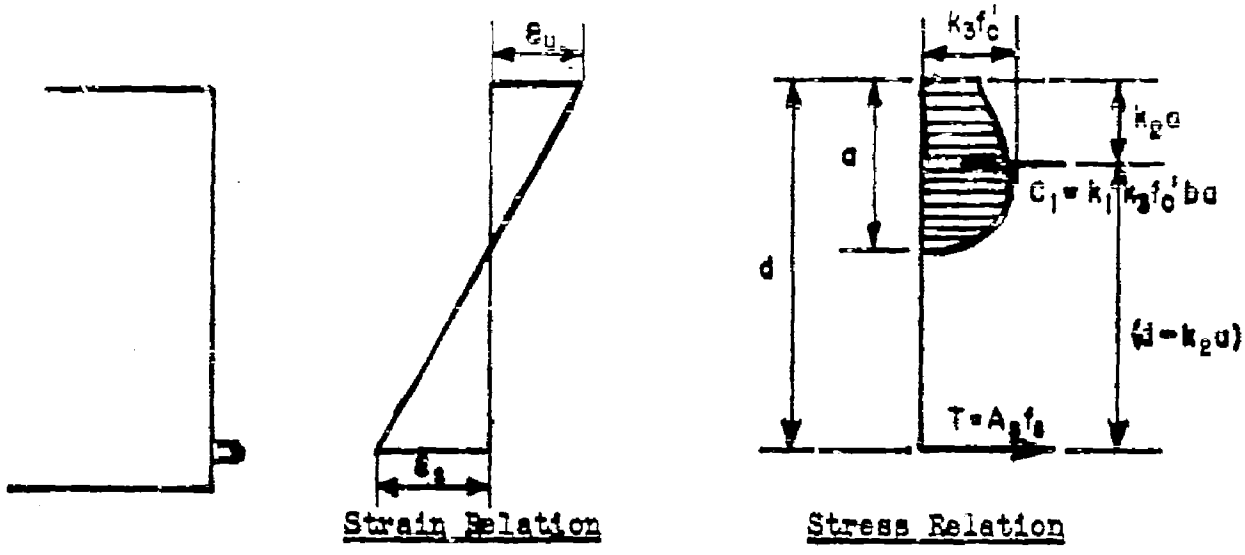

(a) Maximum Moment The maximum flexural load-carrying capacity of a concrete beam can be computed as follows:

From statics, referring to the preceding sketch:

$$k_1k_3f'_cba = A_sf_s = pbdf_s \tag{8}$$

$$a = \frac{pdf_s}{k_1k_3f'_c} \tag{8a}$$

$$M_{max} = T(d - k_2a) = pbdf_s\ (d - k_2a) \tag{9}$$

By substituting Eq. (8a) in Eq. (9), M_{max} is obtained as follows:

$$M_{max} = pf_sbd^2\left(1 - \frac{k_2}{k_1k_3}\frac{pf_s}{f'_c}\right) \tag{9a}$$

The maximum moment given by Eq. (9a) can be determined if f_s and the quantity $\frac{k_2}{k_1 k_3}$ are known. The value of $\frac{k_2}{k_1 k_3}$ varies somewhat with f'_c, but from this and other investigations, a value of 0.5 has been found to provide the best agreement with the results of experiment. The steel stress f_s may be at the yield point, above, or below it, depending on the properties of the beam. Expressions for f_s are derived subsequently.

(b) Maximum Moment Deformations The deformations corresponding to the maximum moment can be computed if the ultimate strain, ε_u, in the top of the beam and the corresponding steel strain, ε_s, are known. Ultimate concrete strains measured in the tests of these beams are shown in Fig. 18. For the calculations included in this report, it has been assumed that ε_u is independent of f'_c and equal to 0.004.

If the strain in the tension reinforcement, ε_s, and the ultimate concrete strain, ε_u, in the top of the beam are known, the curvature of the beam at the location of maximum moment can be expressed as:

$$\Phi_{ult} = \frac{\varepsilon_s + \varepsilon_u}{d} \tag{10}$$

The strain in the tension reinforcement may be computed as follows:

From the strain relations:

$$\frac{a}{d} = \frac{\varepsilon_u}{\varepsilon_s + \varepsilon_u} \tag{11}$$

while from the stress relations:

$$\frac{a}{d} = \frac{pf_s}{k_1 k_3 f'_c} \tag{12}$$

From Eqs. (11) and (12):

$$\varepsilon_s = \varepsilon_u \left(\frac{k_1 k_3 f'_c}{pf_s} - 1\right) \tag{13}$$

Values of k_1k_3 determined from the test results are plotted as a function of the concrete strength in Fig. 19. For the calculations in this report the following empirical equation has been used.

$$k_1 k_3 = 0.625 + \frac{600}{f'_c - 1500} \tag{14}$$

The relation of this empirical expression to the results of the tests is discussed further in Section 18a.

If k_1k_3 and f_s are known, the steel strain, ε_s, can be determined, thus enabling the curvature of the beam at the location of maximum moment to be computed. Expressions for f_s are derived in the following section.

(c) Determination of Stress in Tension Reinforcement at Maximum Moment The stress in the tension reinforcement, f_s, at maximum moment can be computed if the ultimate concrete strain, ε_u, in the top of the beam, the values of k_1k_3, and the stress-strain relationship for the steel are known. The ultimate concrete strain, ε_u, is taken as 0.004; k_1k_3 is computed from Eq. (14); and the stress-strain relationship for the steel is determined

by coupon test or from an idealized stress-strain curve as shown in Fig. 1.

Solving Eqs. (11) and (12) for f_s:

$$f_s = \frac{k_1 k_3 f'_c \varepsilon_u}{p(\varepsilon_u + \varepsilon_s)} \tag{15}$$

If the stress in the tension reinforcement is below the yield point:

$$\varepsilon_s = \frac{f_s}{E_s} \qquad \text{(from Fig. 1)} \tag{16}$$

And solving Eqs. (15) and (16) for f_s, gives

$$f_s = \sqrt{\frac{E_s \varepsilon_u k_1 k_3 f'_c}{p} + \frac{1}{4}(\varepsilon_u E_s)^2} - \frac{\varepsilon_u E_s}{2} \tag{17}$$

If the stress in the tension reinforcement is above the yield point:

$$f_s = f_o + \varepsilon_s E_o \qquad \text{(from Fig. 1)} \tag{18}$$

and

$$\varepsilon_s = \frac{f_s - f_o}{E_c} \tag{18a}$$

And solving Eqs. (15) and (18a) for f_s, gives

$$f_s = \sqrt{\frac{E_o k_1 k_3 f'_c \varepsilon_u}{p} + \frac{1}{4}(E_o \varepsilon_u - f_o)^2} - \frac{1}{2}(E_o \varepsilon_u - f_o) \qquad (19)$$

The remaining case is for the stress in the tension reinforcement at the yield point, for which

$$f_s = f_y \qquad \text{(from Fig. 1)} \qquad (20)$$

In order to determine whether the stress in the tension reinforcement is above, at, or below the yield point, the critical values of $q = \frac{pf_y}{f'_c}$ corresponding to $\varepsilon_s = \varepsilon_y$ and $\varepsilon_s = \varepsilon_o$ must be known. These may be computed as follows:

Solving Eqs. (11) and (12) for $\frac{pf_s}{f'_c}$:

$$\frac{pf_s}{f'_c} = \frac{k_1 k_3}{1 + \frac{\varepsilon_s}{\varepsilon_u}} \qquad (21)$$

At both $\varepsilon_s = \varepsilon_y$ and $\varepsilon_s = \varepsilon_o$, $f_s = f_y$ and thus

$$\frac{pf_y}{f'_c} \simeq q = \frac{k_1 k_3}{1 + \frac{\varepsilon_s}{\varepsilon_u}} \qquad (22)$$

The upper critical value of q is designated as q_{cr}. It marks the boundary between initial failure of the beam by crushing of the concrete and by yielding of the reinforcement. For $q > q_{cr}$, failure occurs initially by crushing of the concrete while the reinforcement is still stressed below the yield point; that is, $f_s < f_y$. The strain in the reinforcement, ε_s, at the limiting condition for yield failures is equal to ε_y. Substituting this value in Eq. (22), q_{cr} is obtained as follows:

$$q_{cr} = \frac{k_1 k_3}{1 + \frac{\varepsilon_y}{\varepsilon_u}} \tag{23}$$

The lower critical value of q, differentiating between $f_s = f_y$ and $f_s > f_y$ at failure, is designated as q_o. The strain in the reinforcement for this limiting condition is $\varepsilon_s = \varepsilon_o$. Substituting this value in Eq. (22), q_o is obtained as follows:

$$q_o = \frac{k_1 k_3}{1 + \frac{\varepsilon_o}{\varepsilon_u}} \tag{24}$$

(d) Determination of Midspan Deflection at Maximum Moment

The deflection of a beam can be computed if the relation between moment and curvature is known. The moment to which a beam was subjected is known from the measured load and the dimensions of the beam. The relation between the moment and curvature can be determined from measured strains at a given load. However, the maximum moment-carrying capacity of a reinforced concrete beam can be computed from Eq. (9a) and the curvature of

the beam due to pure flexure from Eq. (10).

The moment and curvature at the yield point can be computed from Eqs. (4) and (6), and the moment and curvature at the maximum load-carrying capacity can be computed as stated above. From these values, the diagram of moment vs. curvature can be represented approximately by straight lines as follows:

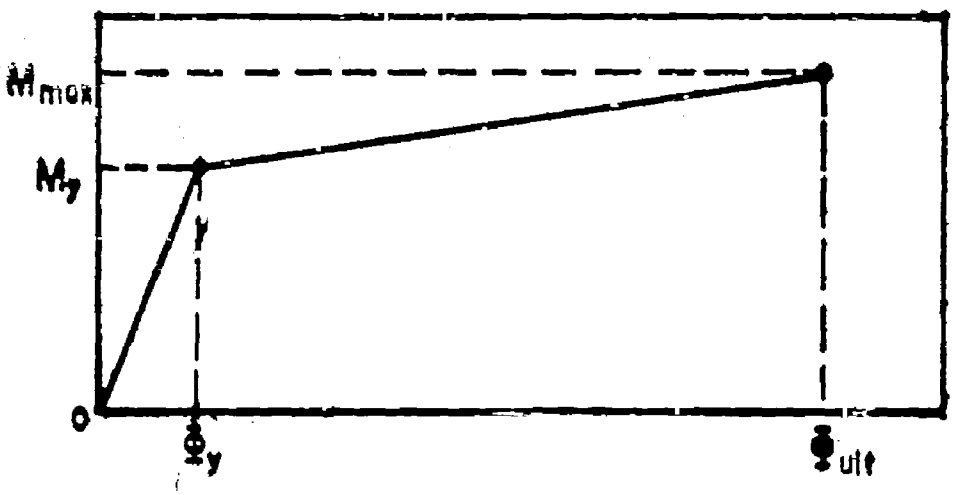

The general nature of this curve agrees very well with the results obtained from measured strains in the constant moment region of the test beams.

At the maximum load-carrying capacity of a beam, the maximum moment can be computed by Eq. (9a), and the distribution of moment along the beam can be determined from statics. The $M - \Phi$ relationship determined for the section of pure moment is assumed to apply throughout the entire length of the beam if the cracking due to shear is negligible. If this assumption is made, the following distribution of curvature at the maximum load-carrying capacity of a beam loaded at the third points is

obtained:

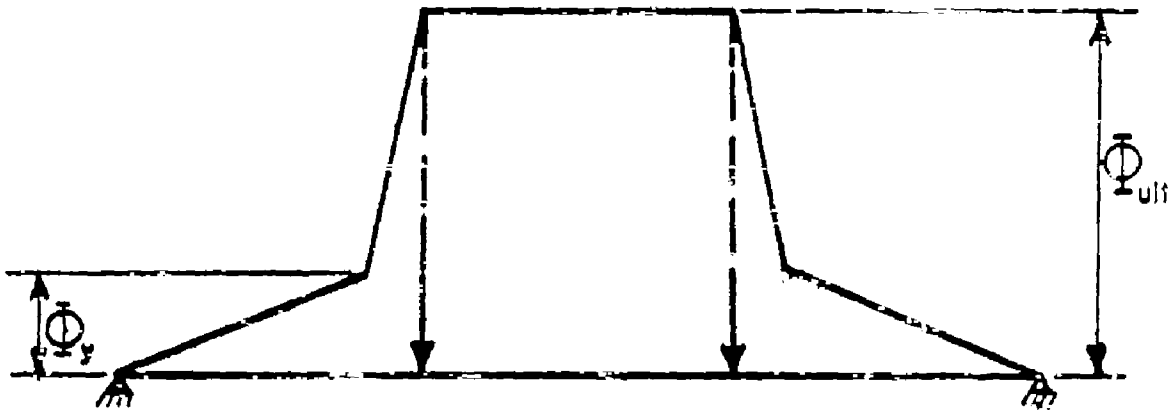

However the deflection of the beam is little affected by the shape or magnitude of the curvature diagram in the outer third of the beam. Consequently, a simplified distribution of curvature has been assumed as follows:

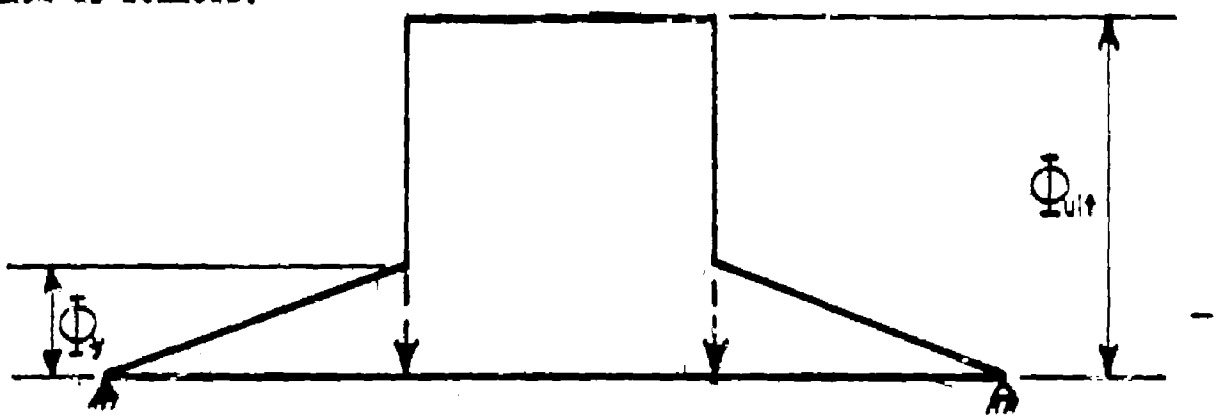

For the above distribution of curvature along a beam loaded at the third points, the midspan deflection at maximum load-carrying capacity can be expressed as follows:

$$\Delta_{ult} = \frac{L^2}{216} \Phi_{ult} \left[15 + 8 \frac{\Phi_y}{\Phi_{ult}} \right] \qquad (25)$$

The above computations for Δ_{ult} are valid only if the cracking

due to shear is negligible. This is true for the beams which were reinforced for shear with the clamp-on stirrups because the stirrups prestressed the beam vertically in the outer-thirds of the beam. With the cracking due to shear thus inhibited, the beams acted as if they were subjected to pure moment which was constant in the central third of the beam span and varied linearly from maximum to zero in the outer thirds.

However, the beams which were reinforced for shear with conventional type stirrups showed extensive shear cracking in the outer thirds of the beam span. This is due to the fact that the concrete must crack before the stirrups can become effective. In most cases the cracking in the outer thirds due to combined shear and moment was as extensive as the cracking in the central third of the beams. Therefore, for calculation of the deflections of the beams reinforced in shear with conventional stirrups, the effective cross section which theoretically existed in the central third of the beam was assumed to act throughout the entire length of the beam. If this assumption is made the distribution of curvature corresponds to the distribution of moment at maximum load-carrying capacity as shown below.

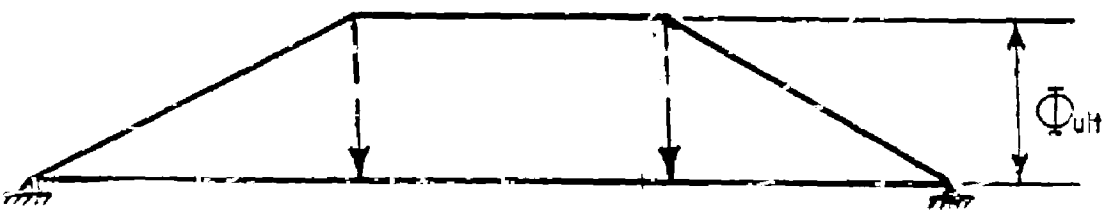

For the above distribution of curvature along a beam loaded at the third points, the midspan deflection at maximum load-carrying capacity can be expressed as follows:

$$\Delta_{ult} = \frac{23}{216} L^2 \Phi_{ult} \qquad (26)$$

B. BEAMS REINFORCED IN TENSION AND COMPRESSION

13. At Yield Point

As in the case of beams reinforced in tension only, the load and deformation at the yield point of beams reinforced in both tension and compression can be determined satisfactorily by use of the conventional "straight-line" theory. However, if a more precise calculation is desired, a concrete stress block similar to that shown in Fig. 2 may be employed.

If a linear stress-strain distribution in the concrete is assumed, as shown in the sketch below, the yield-point moment and deformations for beams reinforced in tension and compression and failing by yielding of the reinforcement can be computed as follows:

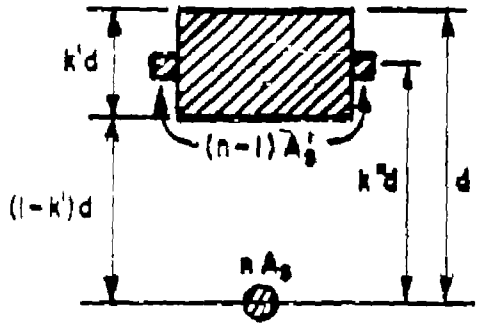

Transformed Area

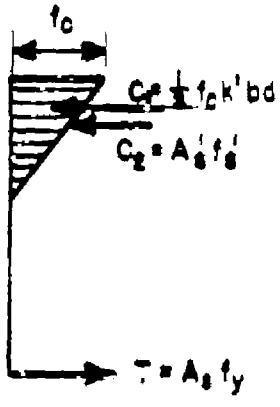

Stress Distribution

From the properties of the transformed section:

$$k' = \sqrt{2\left[np + (1 - k'')\,(n - 1)p'\right] + \left[(n - 1)p' + np\right]^2} - \left[(n - 1)p' + np\right] \tag{27}$$

where

$$n = E_s/E_c \tag{28}$$

and

$$p = \frac{A_s}{bd} \tag{29}$$

and

$$p' = \frac{A'_s}{bd} \tag{30}$$

From statics, $$f'_s = \frac{pf_y}{\frac{1}{2}k' + \frac{p'(k' + k'' - 1)}{k'}} \tag{31}$$

and, from geometry,

$$f'_s = \left[\frac{k'' + k' - 1}{k'}\right] f_c \tag{32}$$

The moment acting on the beam when the tension reinforcement is stressed to the yield point, f_y, is:

$$M_y = \tfrac{1}{2} f_c k' d^2 b \left[1 - \frac{k'}{3}\right] + k'' d A'_s f'_s \tag{33}$$

The moment of inertia of the section, transformed to concrete is:

$$I_y = \frac{b(k'd)^3}{3} + pnbd^3 (1 - k')^2 + p'(n - 1)bd^3 \left[k' + k'' - 1\right]^2 \tag{34}$$

and the curvature of the beam due to moment is:

$$\Phi_y = \frac{M_y}{E_c I_y} \tag{35}$$

Since the $M - \Phi$ curve is approximately a straight line up to yielding of the tension reinforcement and the diagonal tension cracks are negligible, the distribution of curvature along the beam is the same as that for moment. Therefore, the yield point deflection at midspan of a beam with third-point loading is:

$$\Delta_y = \frac{23}{216} \frac{M_y}{E_c I_y} L^2 \tag{36}$$

where L is the span of the beam.

14. At Maximum Load-Carrying Capacity

The load and deformation at maximum load-carrying capacity can be determined by the use of an ultimate theory, derived in the following paragraphs. In this theory, which is a modification of the theory used for beams reinforced in tension only, it is necessary to assume a stress block in the concrete which is represented by three parameters, k_1, k_2, k_3, as shown in Fig. 2, and the stress in the compression steel to be at the yield point. The theory, presented in the following paragraphs, assumes that the compression steel has yielded at the maximum load and that it buckled when the concrete crushed.

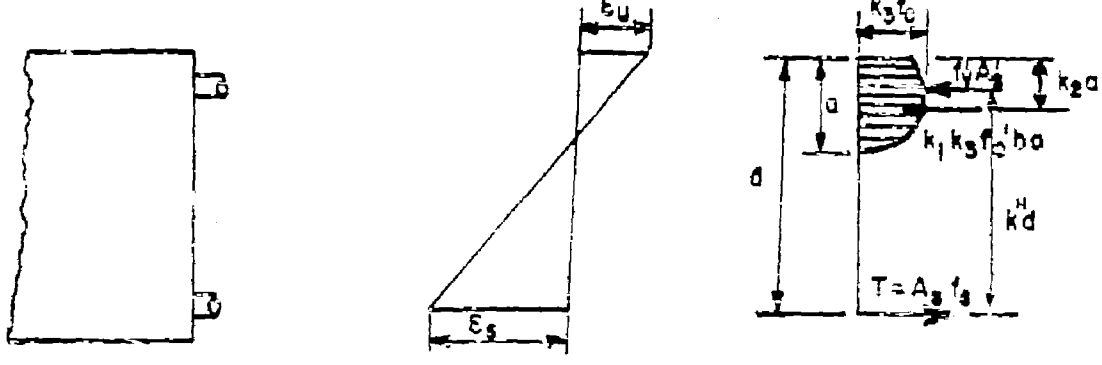

Strain Relation Stress Relation

(a) Maximum Moment The maximum flexural load-carrying capacity can be computed as follows:

From statics:

$$k_1 k_3 f'_c ba + f'_y p'bd = pbdf_s \tag{37}$$

$$a = \frac{pf_s - p'df'_y}{k_1 k_3 f'_c} \tag{37a}$$

and

$$M_{max} = k_1 k_3 f'_c ba(d - k_2 a) + f'_y p'bd^2 k' \tag{38}$$

By substituting the value of a from Eq. (37a) into Eq. (38), M_{max} is obtained as follows:

$$M_{max} = bd^2\left[pf_s - p'f'_y\right]\left[1 - \frac{k_2}{k_1 k_3}\frac{(pf_s - p'f'_y)}{f'_c}\right] + f'_y p'bd^2 k' \tag{38a}$$

The maximum flexural capacity of a beam can be determined by Eq. (38a) if f_s and the quantity $\frac{k_2}{k_1 k_3}$ are known. As in the computations of the maximum flexural capacity of beam reinforced in tension only, $\frac{k_2}{k_1 k_3}$ is assumed to be 0.5. The value of f_s may be at the yield point, above, or below it, depending on the properties of the beam. Expressions for f_s are derived subsequently.

(b) Maximum Moment Deformations The deformations corresponding to the maximum moment can be computed employing the same principals used in the computation of the deformations of the beams reinforced in tension only.

For these computations ε_u is assumed to be independent of f'_c and equal to 0.004.

From the strain relations:

$$\Phi_{ult} = \frac{\varepsilon_s + \varepsilon_u}{d} \tag{39}$$

The strain in the tension reinforcement may be computed as follows:

$$\frac{k}{d} = \frac{\varepsilon_u}{\varepsilon_s + \varepsilon_u} \tag{40}$$

while from the stress relations:

$$\frac{k}{d} = \frac{pf_s - p'f'_y}{k_1 k_3 f'_c} \tag{41}$$

From Eqs. (40) and (41):

$$\varepsilon_s = \varepsilon_u \left[\frac{k_1 k_3 f'_c}{pf_s - p'f'_y} - 1 \right] \tag{42}$$

The values of $k_1 k_3$ are obtained from equation (14).

If $k_1 k_3$ and the expression for f_s are known, the steel strain, ε_s, can be determined, and the curvature of the beam at the location of maximum moment can be computed. The expressions for f_s are derived in the following section.

(c) Determination of the Stress in Tension Reinforcement at Maximum Moment. With the assumption that the beam reaches its maximum flexural capacity when the concrete crushes, the stress at maximum moment can be computed if the ultimate concrete strain, ε_u, in the top of the beam, the values of k_1k_3, and the stress-strain relationship for the steel are known. The ultimate concrete strain, ε_u, is assumed to be 0.004; k_1k_3 is computed from Eq. (14); and the stress-strain relationship for the steel is determined by coupon test or from an idealized stress-strain curve as shown in Fig. 1.

Solving Eqs. (40) and (41) for f_s:

$$f_s = \frac{1}{p}\left[\frac{k_1k_3f'_c\varepsilon_u}{\varepsilon_s + \varepsilon_u} + p'f'_y\right] \tag{43}$$

If the stress in the tension reinforcement is below the yield point:

$$\varepsilon_s = \frac{f_s}{E_s} \tag{16}$$

then solving Eq. (43) and Eq. (16) for f_s:

$$f_s = \sqrt{\frac{\varepsilon_u E_s}{p}\left[k_1k_3f'_c + p'f'_y\right] + \frac{1}{4}\left[\varepsilon_u E_s - \frac{p'f'_y}{p}\right]^2} - \frac{1}{2}\left[\varepsilon_u E_s - \frac{p'f'_y}{p}\right] \tag{44}$$

If the stress in the tension reinforcement is above the yield point:

$$f_s = f_o + \epsilon_s E_o \tag{18}$$

and

$$\epsilon_s = \frac{f_s - f_o}{E_o} \tag{18a}$$

then solving Eq. (43) and Eq. (18a) for f_s:

$$f_s = \sqrt{\frac{E_o k_1 k_3 f'_c \epsilon_u}{p} + E_o \epsilon_u p' f'_y - p' f'_y f_o} + \tfrac{1}{2}\left[E_o \epsilon_u - f_o - \frac{p' f'_y}{p}\right]^2$$

$$- \tfrac{1}{2}\left[E_o \epsilon_u - f_o - \frac{p' f'_y}{p}\right] \tag{45}$$

The remaining case is for the stress in the tension reinforcement at the yield point, for which:

$$f_s = f_y \tag{20}$$

In order to determine whether the stress in the tension reinforcement is above, at, or below the yield point, the critical values of $q' = \frac{pf_y - p'f'_y}{f'_c}$ corresponding to $\epsilon_s = \epsilon_y$ and $\epsilon_s = \epsilon_o$ must be known. These may be computed as follows:

Solving Eqs. (40) and (41) for $\frac{pf_s - p'f'_y}{f'_c}$

$$\frac{pf_s - p'f'_y}{f'_c} = \frac{k_1 k_2 \varepsilon_u}{\varepsilon_u + \varepsilon_s} \tag{46}$$

At both $\varepsilon_s = \varepsilon_y$ and $\varepsilon_s = \varepsilon_o$, $f_s = f_y$, and thus:

$$\frac{pf_y - p'f'_y}{f'_c} = q' = \frac{k_1 k_2 \varepsilon_u}{\varepsilon_u + \varepsilon_s} \tag{47}$$

The upper critical value of q' is designated as q'_{cr}. It establishes the boundary between initial failure of the beam by crushing of the concrete and by yielding of the reinforcement. For $q' \; q'_{cr}$, failure occurs initially by crushing of the concrete while the reinforcement is still stressed below the yield point; that is, $f_s \; f_y$. The strain in the tension reinforcement, ε_s, at the limiting condition for yield failures is equal to ε_y. Substituting this value in Eq. (47) q'_{cr} is obtained as follows:

$$q'_{cr} = \frac{k_1 k_2}{1 + \frac{\varepsilon_y}{\varepsilon_u}} \tag{48}$$

The lower critical value of q', marking the boundary between $f_s = f_y$ and $f_s \; f_y$ at failure, is designated as q'_o. The strain in the tension reinforcement for this limiting case is $\varepsilon_s = \varepsilon_o$. Substituting this value in Eq. (47) q'_o is obtained as follows:

$$q'_o = \frac{k_1 k_2}{1 + \frac{\varepsilon_o}{\varepsilon_u}} \tag{49}$$

(d) Determination of Midspan Deflection at Maximum Moment. The midspan deflection of a beam can be computed if the relation between moment and curvature is known. All the beams reinforced in compression had conventional stirrups as shear reinforcement. Therefore, the cracking due to shear was extensive for the same reasons stated in the case of beams reinforced in tension only and reinforced for shear by conventional stirrups. Since the beams were extensively cracked in the outer thirds of the beam span at the maximum load, the distribution of curvature along the beams is assumed to correspond to the distribution of moment at the maximum load-carrying capacity of the beam as shown below:

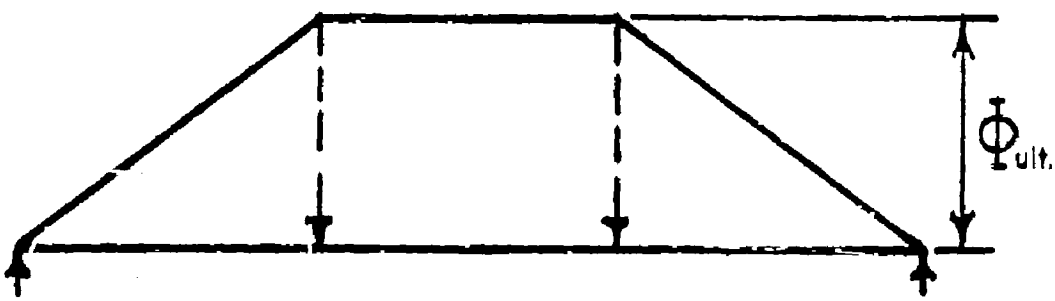

For the above distribution of curvature along a beam loaded at the third points, the midspan deflection at maximum load-carrying capacity can be computed as follows:

$$\Delta_{ult} = \frac{23}{216} L^2 \Phi_{ult} \qquad (50)$$

15. Summary of Equations

The following equations, which were derived in the preceding sections, can be used to compute the critical quantities for the determination of the load-deflection curves or the moment-rotation curves for

reinforced concrete beams

Beams reinforced in tension only:

$$M_y = A_s f_y d\left(1 - \frac{k}{3}\right) \tag{4}$$

$$\Phi_y = \frac{M_y}{E_c I_y} \tag{6}$$

$$\Delta_y = \frac{23}{216} \frac{M_y}{E_c I_y} L^2 \tag{7}$$

$$M_{max} = \rho f_s b d^2 \left[1 - \frac{k_2}{k_1 k_3} \frac{\rho f_s}{f'_c}\right] \tag{9a}$$

$$\Phi_{ult} = \frac{\epsilon_s + \epsilon_u}{d} \tag{10}$$

for beams in which the shear cracking was inhibited:

$$\Delta_{ult} = \frac{L^2}{216} \Phi_{ult}\left[15 + 8 \frac{\Phi_y}{\Phi_{ult}}\right] \tag{25}$$

for beams in which the shear cracking was not inhibited:

$$\Delta_{ult} = \frac{23}{216} \Phi_{ult} L^2 \tag{26}$$

Beams reinforced in tension and compression:

$$M_y = \tfrac{1}{2} f_c k' d^2 b\left[1 - \frac{k'}{3}\right] + k'' d A'_s f'_s \tag{33}$$

$$\Phi_y = \frac{M_y}{E_c I_y} \tag{35}$$

$$\Delta_y = \frac{22}{216} \frac{M_y}{E_c I_y} L^2 \tag{36}$$

$$M_{max} = bd^2\left[pf_s - p'f'_y\right]\left[1 - \frac{k_2}{k_1 k_3}\frac{pf_s - p'f'_y}{f'_c}\right] + f'_y pbd^2 k'' \tag{38a}$$

$$\Phi_{ult} = \frac{\epsilon_s + \epsilon_u}{d} \tag{39}$$

$$\Delta_{ult} = \frac{23}{216} L^2 \Phi_{ult} \tag{50}$$

(All beams exhibited extensive shear cracking)

The quantities which are essential in the determination of the above quantities can be obtained from the following:

Beams reinforced in tension only:

$$q = \frac{pf_y}{f'_c} \tag{22}$$

$$q_{cr} = \frac{k_1 k_3}{1 + \frac{\epsilon_y}{\epsilon_u}} \tag{23}$$

$$q_o = \frac{k_1 k_3}{1 + \frac{\epsilon_o}{\epsilon_u}} \tag{24}$$

If $q > q_{cr}$

$$f_s = \sqrt{\frac{E_s \varepsilon_u k_1 k_3 f'_c}{p} + \tfrac{1}{4}(\varepsilon_u E_s)^2} - \frac{\varepsilon_u E_s}{2} \qquad (17)$$

If $q_{cr} > q > q_o$

$$f_s = f_y \qquad (20)$$

If $q < q_o$

$$f_s = \sqrt{\frac{E_o k_1 k_3 f'_o \varepsilon_u}{p} + \tfrac{1}{4}(E_o \varepsilon_u - f_o)^2} - \tfrac{1}{2}(E_o \varepsilon_u - f_o) \qquad (19)$$

Beams reinforced in tension and compression:

$$q' = \frac{pf_y - p'f'_y}{f'_c} \qquad (47)$$

$$q'_{cr} = \frac{k_1 k_3}{1 + \frac{\varepsilon_y}{\varepsilon_u}} \qquad (48)$$

$$q'_o = \frac{k_1 k_3}{1 + \frac{\varepsilon_o}{\varepsilon_u}} \qquad (49)$$

If $q' > q'_{cr}$

$$f_s = \sqrt{\frac{\varepsilon_u E_s}{p}\left[k_1 k_3 f'_c + p' f'_y\right] + \frac{1}{4}\left[\varepsilon_u E_s - \frac{p' f'_y}{p}\right]^2} - \frac{1}{2}\left(\varepsilon_u E_s - \frac{p' f'_y}{p}\right) \tag{44}$$

If $q'_{cr} > q' > q'_o$

$$f_s = f_y \tag{20}$$

If $q' < q'_o$

$$f_s = \sqrt{\frac{E_o k_1 k_3 f'_c \varepsilon_u + E_o \varepsilon_u p' f'_y - p f'_y f_o}{p} + \frac{1}{4}\left[E_o \varepsilon_y - f_o - \frac{p' f'_y}{p}\right]^2} - \frac{1}{2}\left[E_o \varepsilon_y - f_o - \frac{p' f'_y}{p}\right] \tag{45}$$

The values of $k_1 k_3$, $\frac{k_2}{k_1 k_3}$, and ε_u were obtained empirically as follows:

$$\varepsilon_u = 0.004 \qquad \text{(Fig. 18)}$$

$$\frac{k_2}{k_1 k_3} = 0.5$$

$$k_1 k_3 = 0.625 + \frac{60}{f'_c - 1500} \qquad \text{(Fig. 19)} \tag{14}$$

VI TEST RESULTS

16. Measured and Derived Quantities

The following measurements were recorded after the application of each increment of load or deformation: the maximum load attained during the application of the increment, the deflection along the beam, the strains in the concrete and in the reinforcement; and the load the beam was carrying after all measurements had been taken. In addition to these measurements, the crack pattern was marked after each increment, a running log of any significant change in the behavior of the test was kept, and a continuous photographic record was made of the beams during testing.

Auxiliary tests were made to determine the concrete strength and the stress-strain characteristics of the reinforcement. The concrete strength was determined from three concrete cylinders cast from each batch of concrete, and the stress-strain characteristics of the steel were determined from a tension coupon taken from each bar used in the fabrication of the beams. These tests are described in Section 3.

The following quantities were derived from the measured quantities: maximum moment attained during an increment of load or deformation, and the ratio of that moment to the maximum moment carried by the beam; angle change in the region of pure flexure, from the measured concrete and steel strains; stress in the reinforcement, from measured strains and the stress-strain characteristics obtained from coupon tests; and the deflection of the central portion of the beam due to pure flexure, obtained by subtracting the third-point deflection from the midspan deflection.

The measured and derived quantities are presented graphically in the figures of the appendix. The figures in the appendix contain the

following plots for each beam tested: applied load vs. tension steel strain at midspan; applied load vs. concrete strain on top of beam at midspan; applied load vs. midspan deflection; applied load vs. load-point deflection; deflection along the beam at various stages during testing; ratio of applied moment to maximum moment attained during test vs. angle change at midspan; ratio of applied moment to maximum moment attained during test vs. deflection of midspan with respect to load-point; ratio of applied load to maximum load attained in test vs. midspan deflection; and ratio applied load to maximum load attained in test vs. load-point deflection.

17. Mode of Failure

(a) Initial Tension Failure. The beams which failed initially in tension exhibited large deflections between the yield load and the load causing collapse, as shown by the load-deflection curves in the appendix. The relative magnitudes of these deflections are dependent upon the parameter q for beams reinforced in tension only, as can be seen in Fig. 20.

The following stages were observed during the loading to collapse of beams reinforced in tension only: The concrete cracked in tension under a relatively small load; as the load was increased the tension reinforcement yielded; then the beam underwent a relatively large deflection with little further increase in load. When the concrete in the compression zone reached its limiting strain, the maximum load-carrying capacity of the beam was reached and compression failure occurred.

In a beam reinforced in tension only, the distance down from the top of the beam over which crushing occurred was dependent upon the relative magnitude of the tensile force and the concrete strength. This

ratio is best represented by the quantity $q = \frac{pf_y}{f'_c}$. When the depth of initial compression failure is small compared to the depth of the beam, there is ample concrete remaining after initial failure to carry the compressive force that existed at maximum load. However, the lever arm between the tensile and compressive forces is reduced. Consequently the load-carrying capacity is lowered and it continues to decrease as the compression failure progresses down through the depth of the beam. On the other hand, if the depth of initial compression failure is large, the remaining concrete in the compression zone may be able to carry only a small portion of the compressive force that existed at maximum load. Consequently, the load-carrying capacity drops to a very small fraction of that at maximum load as soon as the concrete crushes. The above discussion shows that q is a major factor in the determination of the rate of drop in the load-carrying capacity once the maximum load-carrying capacity is reached. This is also shown in Fig. 20 where the rate of drop in the load-carrying capacity, in percent of the maximum load attained, is seen to vary with the reinforcing index q.

Until the tension steel yields, beams which are reinforced in both tension and compression exhibit much the same behavior as the beams reinforced in tension only. The behavior after crushing of the concrete depends largely upon the amount of compression reinforcement and the effectiveness of the ties. If the compression reinforcement is not tied or is poorly tied it will buckle as soon as the concrete crushes. However, if the ties are effective, they will inhibit the buckling of the compression steel after the concrete has crushed. Effective ties also force

the compression reinforcing bars to buckle locally between the ties which enables the beam to exhibit a much more ductile failure than if the compression reinforcement buckles over a long length as in the case of ineffective ties.

Figure 21 shows the influence of effective and ineffective ties on the load deflection curves. The beams chosen for comparison had comparable concrete strengths and identical reinforcement except for the method of tying the compression reinforcement.

As discussed in Chapter IV, the magnitude of the strain in the tension reinforcement at the maximum load-carrying capacity is dependent upon the parameter q for the beams reinforced in tension only and q' for the beams reinforced in tension and compression. If the strain in the tension reinforcement at the maximum load-carrying capacity of a beam is beyond the yield range there will be a larger percent of increase in the load-carrying capacity between the yield and maximum loads than if the strains in the tension reinforcement at failure are within the yield range.

Beams which are reinforced in tension and compression deflect much more before there is a substantial loss of load-carrying capacity than a comparable beam reinforced in tension only. This is due mainly to the much larger strains in the tension reinforcement obtainable in beams reinforced in both tension and compression. Figure 22 illustrates the relative magnitudes of the strains that were attained in the tension reinforcement of comparable beams - one with and one without compression reinforcement. These beams had comparable concrete strengths and identical percentages of tension reinforcement.

(b) Initial Compression Failure. This discussion is concerned with beams reinforced in tension only because in these tests compression

failures were observed only in beams without compression reinforcement.

In order for a beam to fail initially in compression abnormally high percentages of tension reinforcement are required. An over-reinforced beam is one in which the concrete in the compression zone fails before the tension steel reaches its yield point. This mode of failure, exemplified by beam T11L, shows little if any ductility. As the beam is deflected, the concrete in the tension zone cracks, then with a relatively small additional deflection the concrete in the compression zone crushes. Since a rather large tensile force is required to cause a beam to fail in this manner, the depth of concrete involved in the initial compression failure is large compared to the depth of the beam; therefore, the load carrying capacity after a compression failure is only a small percentage of the maximum load-carrying capacity. The load deflection curve of beam T11L, Fig. 8 of the appendix, shows this abrupt drop-off in the load-carrying capacity after the maximum load is attained in an over-reinforced beam.

As shown in Fig. 23, the load-carrying capacity of a beam failing initially in compression is dependent upon the concrete strength. On the other hand, the maximum load-carrying capacity of a beam failing in tension is little effected by the concrete strength.

(c) <u>Balanced Failure</u> A balanced failure is one in which the tension reinforcement yields at the same instant that the concrete crushes. The load-deflection characteristics of beams which fail in this manner are very similar to those of beams with compression failure. It is believed that the failures of beams T4H and T5H are representative of this type failure.

(d) Premature Shear Failure As stated previously, no shear reinforcement was provided in beams T1Mb, T2Ma, T2Mb and T2Mc because the shear requirements of A.C.I. 318-51 for beams without shear reinforcement were satisfied. Beams T2Ma and T2Mb were reinforced in tension with straight deformed bars, beam T2Mc with hooked deformed bars, and beam T1Mb with hooked plain bars.

Beams T2Ma, T2Mb, and T2Mc failed in shear whereas T1Mb failed in flexure with a secondary failure in bond in the middle third of the beam span. Hooking the bars in T2Mb did not prevent the shear failure. Table 6 gives data and comparisons for the beams failing in shear and Fig. 24 shows some views of these beams after failure.

In that the object of this phase of the investigation was to determine the load-deformation characteristics of beams failing in flexure no further studies were made of the phenomena of shear failures.

18. Effect of Variables

(a) Concrete Strength The effect of the concrete strength on the maximum load-carrying capacity is negligible for beams failing initially in tension. This is illustrated by a comparison of the maximum moments resisted by beams T1Lb and T1Ma. Beam T1Lb with f'_c = 2520 and p = 0.62 resisted 20.17 ft.-kips, and beam T1Ma with f'_c = 4600 and p = 0.62 resisted 19.51 ft.-kips. However, the concrete strength has a much greater effect on the maximum load-carrying capacity of beams which fail initially in compression. The load-deflection curves of beams T5H and T1IL in Fig. 23 illustrate this.

The concrete strength had little if any consistent effect upon the deflection at the maximum load-carrying capacity because the ultimate

concrete strain is relatively independent of the concrete strength. This is shown in Fig. 18 in which the ultimate concrete strain is plotted against the concrete strength. Although there is some scatter, there is no trend with concrete strength and a value of 0.004 is a reasonably good average for the ultimate concrete strain.

As shown in Fig. 19, the factor k_1k_3 which is related to shape of the stress block is dependent upon the concrete strength. The exact relationship is unknown but the empirical curve given in Fig. 19 yields values of k_1k_3 which are in fair agreement with the values found in this and in another investigation in this laboratory. By using the values of k_1k_3 determined by this equation, ultimate deflections can be computed which agree with the test results. However, the curve is not accurately defined in the region of low concrete strengths. The empirical curve is not intended to be used for concrete strengths below 2000 psi, and further investigation is needed to establish the relation between k_1k_3 and concrete strength in this region.

(b) Percentage of Tension Reinforcement. In these tests, the magnitude of the tensile resistance of the beams was varied chiefly by employing different percentages of reinforcement; however, minor variations were produced by the differences in the yield strengths of the reinforcing bars. Since the maximum load-carrying capacity of beams which fail initially in tension is dependent on the tensile resistance of the steel, it varied primarily with the percentage of tensile reinforcement. This can be seen in Fig. 25, in which the plots of load vs. deflection of beams with approximately equal concrete strengths and varying percentages of tension reinforcement are presented.

On the other hand, the tensile resistance of the steel is not a critical factor in the determination of the maximum load-carrying capacity of beams which fail initially in compression.

(c) Reinforcing Index. For beams reinforced in tension only the reinforcing index is $q = \frac{pf_y}{f'_c}$, and for beams reinforced in tension and compression it is $q' = \frac{pf_y - p'f'_y}{f'_c}$. In beams with tension reinforcement only, the parameter q was found to be the controlling factor in determining the shape of the load-deflection curve after the yield load was attained. Specimens with low values of q exhibited a ductile failure; that is, they were able to undergo large deformations at relatively constant high loads before the maximum load was attained and the drop-off in the load-carrying capacity was very gradual beyond the maximum. On the other hand, those with high values of q exhibited a brittle failure, that is, they were able to undergo little deflection before the maximum load was attained and the drop-off in load-carrying capacity was abrupt beyond the maximum. The specimens with intermediate values of q had load deformation characteristics between the two extremes described above. The load-deformation characteristics of beams with various values of q are shown in Fig. 20 in which the load-ratio is plotted against midspan deflection for beams with different values of q. It can be seen from this figure that q not only has a definite effect on the deflection at the maximum load-carrying capacity, but also on the overall shape of the load deflection curve.

In the beams provided with compression reinforcement, the effect of q' on the shape of the load-deflection curve is partially masked by the added ductility produced by the effectiveness of the compression reinforcement ties. However, the load-ratio vs. deflection plots of beams G2xm,

C3xx and C6xx in Fig. 26 suggest that, for beams having the compression steel tied in the same manner, the shape of the load-deflection curve beyond yielding is dependent to some degree on the parameter q'. However, a more comprehensive study is needed before this can be definitely stated.

(d) Compression Reinforcement. As a general rule, the addition of a nominal amount of compression reinforcement makes it almost impossible to design a rectangular beam that will fail initially in compression because of the excessive amount of tension reinforcement that would be required. However, no tests have been made in this investigation to validate this statement.

The addition of compression reinforcement did not appreciably increase the maximum load-carrying capacity of a beam which would have failed initially in tension without the compression steel, provided the tension reinforcement was not strained into the work hardening region in either case. This is shown by comparisons of the maximum load-carrying capacities of beams T1B, C2w and C2xx, which were 40.7 kip-ft., 41.7 kip-ft., 44.8 kip-ft., respectively. The tension reinforcement of C2w and C2xx was strained into work hardening but not to a marked degree. However, if a beam would have failed initially in compression without compression reinforcement, the addition of enough compression reinforcement to prevent initial compression failure would force the beam to fail initially in tension and thereby raise the maximum load-carrying capacity.

As shown in Fig. 27, the addition of effectively tied compression reinforcement enabled beam C2xx to carry a load near the maximum with larger deflections than the comparable beam T1A reinforced in tension only. The addition of compression reinforcement strengthens the compression zone and thus raises the neutral axis. This enables a larger angle change to take

place before the concrete crushes, and thereby increases the deflection through which the beam can carry near maximum loads.

(e) Method of Tying Compression Reinforcement In order for the compression reinforcement to add the greatest amount of ductility to a beam it must be effectively tied; that is, the ties must be strong enough to force the bars of the compression reinforcement to buckle locally instead of over a long length. Figure 28 shows photographs of effective and ineffective ties after beam failure. The ties of beam C2xm shown in Fig. 28a were effective and forced the compression steel to buckle locally, whereas the ties of C3xm shown in Fig. 28b were not effective.

Actually, the ties do not come into play until after the concrete has crushed; consequently, the ties affect the shape of the load-deflection curve only after the maximum load-carrying capacity has been reached. This can be seen in Fig. 21 in which the load-ratio vs. the midspan deflection is plotted for comparable beams.

The two methods of tying the compression reinforcement are illustrated in Fig. 4. In this series of tests, method g of fabricating the ties was superior to method g. Since ties fabricated by method g were anchored in the tension zone, the ends of the tie bars could not pull apart when the compression failure of the concrete occurred. Those ties fabricated by method g were anchored in the compression zone and could readily pull apart when the compression failure of the concrete occurred.

(f) Type of Shear Reinforcement The conventional vertical stirrups that were employed in most of the beams of this investigation were not effective until the concrete cracked and consequently could do little to prevent cracking of the concrete. Therefore, even if a beam was heavily

reinforced in shear with conventional stirrups, there would still be cracks in a region of high shear. However, when the clamp-on type stirrups, illustrated in Fig. 5, were used, the beam was prestressed in a vertical direction, and the cracking due to shear was inhibited or in some cases even eliminated. The crack patterns for beams with conventional stirrups and with clamp-on stirrups are shown in the photographs of Fig. 29.

Since the conventional stirrups allowed the beam to crack extensively in the region subjected to shear, the effective stiffness of the beam in this region was reduced. This enabled the beam to deflect more than if the cracks had not formed, as in the case of a beam with clamp-on stirrups.

VII COMPARISON OF EXPERIMENTAL AND ANALYTICAL RESULTS

The results of the theoretical analysis and the experimental investigation are compared in figures and tables. Although the ultimate aim is to develop moment-rotation relationships, most of the comparisons are of measured deflections rather than measured rotations since the deflections could be determined more accurately.

Comparisons of the analytical and test results have been made for the following quantities: tension reinforcement stress at the maximum moment, yield-point moments, maximum moments, midspan deflection at the yield-point, and midspan deflection at the maximum moment. The results are given in Tables 8, 9a, 9b, 10a, and 10b.

The theoretical values of the stress in the tension reinforcement at the maximum moment, from Eqs. (17), (19), or (20) for beams with tension reinforcement only and from Eqs. (44), (45), or (20) for beams with tension and compression reinforcement, compare favorably with the experimental results. As shown in Table 8, the ratio of the experimental to the theoretical values for beams reinforced in tension only has an average of 0.99 with a range of 0.90 to 1.06 and for beams with tension and compression reinforcement an average of 1.06 with a range of 0.98 to 1.18. The assumptions involved in the computations of the stress in the tension reinforcement at the maximum moment are as follows: the maximum moment to be reached when the concrete crushes, an ultimate concrete strain of 0.004, the empirical values of k_1k_3 to be valid, an idealized stress-strain curve for the steel as shown in Fig. 1, and the compression steel to be yielded at the maximum moment.

The theoretical values of the yield-point moments, from Eq. (4) for beams with tension reinforcement only and from Eq. (33) for beams with tension and compression reinforcement, are in reasonably close agreement with the test results. As shown in Table 9a, the ratio of the experimental to the theoretical values for beams reinforced in tension only has an average of 0.97 with a range of 0.82 to 1.05 and for beams reinforced in tension and compression an average of 1.01 with a range of 0.97 to 1.08. The major assumption in these calculations is the straight line distribution of the stress in the concrete. As can be seen in Table 9a, the beams with high values of q have higher experimental values of M_y than the theory gives because the stress distribution in the concrete at the yield point is no longer approximately linear in beams which approach a balanced failure.

The theoretical values of the maximum-moment capacity, from Eq. (9a) for beams reinforced in tension only and from Eq. (38a) for beams reinforced in both tension and compression, are in good agreement with the experimental values. As shown in Table 9b, the ratio of the experimental to the theoretical values for beams reinforced in tension only has an average of 0.99 with a range of 0.85 to 1.08 and for beams reinforced in tension and compression an average of 1.03 with a range of 0.96 to 1.08. All of the assumptions made in the calculation of the tension reinforcement stress plus $k_2/k_1k_3 = 0.5$ are made in these calculations.

The theoretical values of the midspan deflection at the yield point, from Eq. (7) for beams with tension reinforcement only and from Eq. (36) for beams with tension and compression reinforcement, are consistently lower than the test results. The value of the experimental yield-point deflection is taken as the value at which the deflection starts to increase

rapidly with little or no increase in load. As shown in Table 10a, the ratio of the experimental to the theoretical values for beams reinforced in tension only has an average of 1.22 with a range of 1.04 to 1.56 and for beams reinforced in tension and compression an average of 1.29 with a range of 1.15 to 1.53. The consistently low theoretical values probably can be attributed to the values of E_c and the assumption of linear stress distribution in the concrete used in the computations. It also must be realized that the yield point deflection is difficult to ascertain by experiment since the deflection increases rapidly without further increase in load once the yield point is reached. Therefore, the measured value would always be larger than the actual value unless a continuous record were made with an automatic device.

The theoretical values of the midspan deflection corresponding to the maximum-moment capacity, from Eqs. (25) or (26) for beams with tension reinforcement only and from Eq. (36) for beams with tension and compression reinforcement, are in fair agreement with the test results. As shown in Table 10b, the ratio of the experimental to theoretical values for beams reinforced in tension only has an average of 0.93 with a range of 0.76 to 1.28 and for beams reinforced in tension and compression an average of 1.15 with a range of 0.78 to 1.77. The low theoretical value of the deflection of beam T1La can probably be attributed to the uncertainties of the concrete characteristics in a beam with a very small percentage of reinforcement; that is, it is difficult to determine the properties of the concrete when only a very small area is involved in resisting the tension force. The low value of the ratio of experimental to theoretical values of the deflection for beam T1Mb is most likely due to a premature bond failure near the maximum load since this beam was reinforced with plain bars. The

high values of the ratio of experimental to theoretical deflections of the beams reinforced in tension and compression are probably due to the effectiveness of the compression reinforcement ties whereas the low value of the ratio for beam 07w can probably be attributed to ineffectiveness of the compression reinforcement because the large bars used as compression reinforcement were not tied in any manner.

The theoretical and experimental values of the yield-point and maximum loads and the corresponding deflections have also been compared by plotting the theoretical values on the experimental load-deflection curve, for each beam. The theoretical and experimental values are in good agreement as can be seen in the plots presented in Figs. 1 through 33 of the appendix.

The theoretical and experimental values of the maximum moment capacity of the beams provided with tension reinforcement only are compared in Figs. 30 and 31. In Fig. 30 the values of $M_{max}(obs)/bd^2f'_c$ vs. q have been plotted, and in Fig. 31 the values of $M_{max}/bd^2f'_c$ vs. pf_s/f'_c have been plotted. In the computation of q the values of the yield point stress of the tension steel have been used, whereas in the computation of pf_s/f'_c the values of the tension steel stress computed from Eqs. (17), (19) or (20) have been used. It can be seen from Fig. 30 that a fairly accurate result can be obtained by using the yield point stress in the computation of the maximum-moment capacity of beams failing in tension even if the stress in the tension reinforcement is in the work hardening region. However, a much more accurate result can be obtained in the computation of the maximum moment capacity of beams failing in tension if the computed tension steel stress is used. The latter method is also applicable to beams failing in compression whereas the former is not.

The load-deflection curves may be approximated by connecting with straight lines the points corresponding to zero load and deflection, to the yield load and deflection, and to the maximum moment and deflection. Comparisons of the measured and theoretical load-deflection curves are presented in Figs. 1 through 33 of the appendix.

Table 10 gives a comparison of the values of the measured and computed "usable energy". The "usable energy" is the area under the load-midspan deflection curve up to the deflection given in Table 10b where the load starts dropping rapidly. The agreement between the measured and theoretical values is as good as could be expected since the inaccuracies of the computations of the critical moments and deflections are inherent in the computed values of the "usable energy". Also the theoretical load-deflection curve is composed of straight lines whereas the actual curve is irregular. As shown in Table 11 the average ratio of the experimental to theoretical values is 0.88 with a range of 0.63 to 1.27 for beams reinforced in tension only and an average of 1.15 with a range of 0.40 to 1.84 for beams reinforced in tension and compression.

TABLE NO. 1

SUMMARY OF RESULTS

FOR BEAMS REINFORCED IN TENSION ONLY

Beam	f'_c psi	Reinforcement Amount and Size	d in.	f_y psi	p %	Stirrups	M_{max} (obs) kip-ft.	Mode of Failure
T1La	2150	2-3	10.79	54300	0.34	Clamp-on	13.81	Tension
T1Lb	2520	2-4	10.72	46000	0.62	¼ @ 6"	20.17	Tension
T2La	2120	2-5	10.65	40400	0.97	¼ @ 4"	24.24	Tension
T2Lb	2440	2-5	10.65	55400	0.97	Clamp-on	29.84	Tension
T4La	2380	2-7	10.51	44100	1.90	Clamp-on	39.30	Tension
T4Lb	2810	2-8	10.44	43300	2.52	3/8 @ 4"	47.80	Tension
T5L	2500	2-9	10.37	40200	3.22	3/8 @ 4"	53.87	Tension
T11L	2900	4-9	9.23	45300	7.22	3/8 @ 2"	67.56	Comp.
T1Ma	4600	2-4	10.72	46200	0.62	Clamp-on	19.51	Tension
T1Mb	4750	2-6**	10.58	42900	1.38	None	32.83	Tension
T2Ma	4320	2-6	10.58	47700	1.38	None	27.69	Shear
T2Mb	4020	2-6*	10.58	48300	1.38	None	29.31	Shear
T2Mc	4460	2-7	10.51	46800	1.90	None	37.52	Shear
T3Ma	4800	2-9	10.37	41000	3.22	Clamp-on	61.86	Tension
T3Mb	4110	2-9	10.37	41700	3.22	Clamp-on	62.89	Tension
T1Ha	5880	2-6	10.58	44200	1.38	3/8 @ 3½"	35.10	Tension
T1Hb	5180	2-6	10.58	52200	1.38	Clamp-on	40.66	Tension
T2H	5400	2-8	10.44	45600	2.52	3/8 @ 3½"	53.88	Tension
T3H	5920	4-7	9.52	43200	4.20	3/8 @ 2"	67.72	Tension
T4H	5260	4-8	9.38	42000	5.61	Clamp-on	77.97	Tension
T5H	5900	4-9	9.23	40600	7.22	3/8 @ 2"	86.30	Tension

* Deformed bars hooked

** Plain bars hooked

TABLE NO. 2

SUMMARY OF RESULTS

FOR BEAMS EXPOSED TO TORSION AND COMPRESSION

Beam	f'_c	Reinforcement Amount and Size		d	f'_y	f'_y	p	p	Ties* Spacing	Type**	Stirrups	M_{max} (obs)	Mode of Failure
	psi	Tens	Comp.	in.	psi	psi	%	%	in.			kip. ft.	
C2w	3940	2-6	2-4	10.58	45400	44500	1.38	0.62	None	-	3/8 @ 6"	41.7	Torsion
C2xm	4070	2-6	2-4	10.58	53300	47000	1.38	0.62	8	m	3/8 @ 6"	44.8	"
C3w	4310	2-9	2-7	10.37	41800	46700	3.22	1.93	None	-	3/8 @ 3"	70.1	"
C3xm	3890	2-9	2-7	10.37	41800	42500	3.22	1.93	12	m	3/8 @ 3"	70.2	"
C3yna	3330	2-7	2-5	10.51	45200	56100	1.90	0.98	5	n	3/8 @ 5"	34.8	"
C3ynb	4860	2-9	2-7	10.37	42100	47400	3.22	1.93	6	n	3/8 @ 3"	74.2	"
C4xna	2450	2-7	2-5	10.51	45500	41400	1.90	0.98	10	n	3/8 @ 5"	44.0	"
C4xnb	2430	2-7	2-6	10.51	46400	44100	1.90	1.39	12	n	3/8 @ 3"	49.0	"
C4zn	3570	2-9	2-7	10.37	41300	46400	3.22	1.93	3	n	3/8 @ 3"	72.0	"
C5yn	4430	4-8	2-8	9.38	44000	43400	5.61	2.80	6	n	3/8 @ 2½"	90.8	"
C6xm	3680	4-8	2-8	9.38	41800	40200	5.61	2.80	12	m	3/8 @ 2½"	86.6	"
C7w	3480	4-8	2-8	9.38	41600	43600	5.61	2.80	None	-	3/8 @ 2½"	85.2	"

* All ties ¼" diameter

** See Fig. 4

TABLE NO. 3

SIEVE ANALYSES OF AGGREGATES

SAND

Lot	Percent Passing Sieve No.						Fineness Modulus
	4	6	16	30	50	100	
1	94.3	82.6	64.9	32.1	7.1	1.7	3.17
2	93.2	82.8	66.0	37.0	11.6	1.2	3.08
3	98.0	80.6	64.5	34.9	10.4	2.1	3.10

GRAVEL

Lot	Percent Passing Sieve No.					
	1½	3/4	3/8	4	8	16
1	100	76.7	37.4	12.5	9.1	7.6
2	100	56.8	14.1	4.9	4.4	4.1
3	100	76.9	36.1	6.7	2.5	1.6

TABLE NO. 4

PROPERTIES OF REINFORCING STEEL

Bar Size	Bar No.	Yield Point Stress* f_y-psi	Yield Point Strain ϵ_y-%	Strain at Work Hardening ϵ_s-%	f_o** psi	E_o** psi	Ultimate Strength* f_{ult}-psi	Elongation in 6 in. %	Bar Location Beam-Layer+
3	31	54300	0.167	1.98	38000	855000	82800	20.8	T1La-B
4	41	46200	0.153	1.75	30000	920000	74400	-	T1Ma-B
	42	46000	0.153	1.82	30000	875000	74300	22.2	T1Lb-B
	43	44500	0.154	1.34	33000	875000	72300	22.6	C2a-C
	44	47000	0.154	1.54	33000	875000	76900	20.3	C2xm-C
Average		45900	0.154	1.61	31500	886000	74500	21.7	
5	51	55400	0.171	1.48	41000	998000	87300	21.0	T2Lb-B
	52	40400	0.153	1.75	23000	1060000	65800	27.2	T2La-B
	53	41350	0.146	1.62	29000	770000	68500	-	C4xma-C
	54	56100	0.185	1.36	43000	890000	86800	20.3	C3yma-C
Average		48300	0.164	1.56	34000	930000	77100	22.8	
6	61	47700	0.153	1.71	38000	564000	75200	23.0	T2Ma-B
	62	52200	0.173	1.90	39000	690000	77300	24.2	T1Eb-B
	63	44200	0.153	1.82	32000	682000	69600	25.9	T1Ha-B
	64	45400	0.154	1.54	35000	696000	73800	22.8	C2a-B
	65	53300	0.180	1.42	40000	925000	83800	21.3	C2xm-B
	66	47300	0.154	1.65	35000	770000	74200	27.0	T2Mb-NB
	67	49300	0.154	1.57	38000	767000	78200	26.0	T2Mb-SB
	68	44100	0.146	1.98	34000	575000	69400	-	C4xmb-C
Average		47900	0.158	1.70	36000	709000	75200	24.4	
7	71	45000	0.153	0.97	33000	1240000	82500	21.6	T2Fc-B
	72	48600	0.163	0.80	38000	1350000	90700	16.7	T2Mc-B
	73	44100	0.140	1.37	30000	1095000	75900	23.2	T4Ia-B

TABLE NO. 4 (con't)

PROPERTIES OF REINFORCING STEEL

Bar Size No.	Yield Point Stress* f_y-psi	Strain ϵ_y- %	Strain at Work Hardening ϵ_o- %	f_o** psi	E_o** psi	Ultimate Strength* f_{ult}-psi	Elongation in 6 in. %	Bar Location Beam-Layer*
74	42500	0.153	1.36	32000	868000	72500	24.8	T3H-T
75	43300	0.153	1.31	30000	993000	75200	22.5	T3H-B
76	46700	0.154	1.69	31000	868000	75600	24.4	C3w-C
77	42500	0.154	1.35	32000	805000	73200	-	C3xm-C
78	45500	0.135	1.72	31000	853000	74200	26.4	C4xma-B
79	45200	0.139	1.81	33000	730000	73600	26.8	C3yma-B
710	46400	0.127	1.81	37000	640000	74500	26.2	C4xmb-B
711	47400	0.125	1.88	34000	773000	74600	24.0	C3ymb-B
712	46400	0.146	1.66	34000	767000	73400	25.0	C4xm-B
Average	45300	0.145	1.48	33000	915000	76300	23.8	
8 81	43800	0.146	1.67	32000	735000	71500	29.2	T4H-T
82	40200	0.144	1.41	29000	833000	68400	25.4	T4H-B
83	43300	0.145	1.86	28000	800000	71300	25.5	T4Lb-B
84	45900	0.153	1.44	40000	500000	72000	26.3	T2H-B
85	43600	0.135	1.73	29000	858000	63400	28.1	C7w-C
86	40300	0.138	1.92	25000	890000	68300	25.9	C7w-T
87	42800	0.140	1.07	33000	833000	72300	-	C7w-B
88	40250	0.154	1.34	30000	768000	68800	25.0	C6xm-C
89	42800	0.145	1.23	37000	400000	71400	-	C6xm-T
810	40750	0.145	1.50	29000	832000	68250	26.3	C6xm-B
811	43400	0.146	1.32	30000	758000	71200	26.6	C5yn-C
812	43600	0.143	1.66	30000	727000	71400	26.8	C5yn-T
813	44900	0.139	1.73	33000	773000	73000	-	C5yn-B
Average	42670	0.144	1.57	31000	746000	70100	26.5	

TABLE NO. 4 (con't)

PROPERTIES OF REINFORCING STEEL

Bar Size	Bar No.	Yield Point Stress* f_y-psi	Yield Point Strain ϵ_y- %	Strain at Work Hardening ϵ_o- %	f_o** psi	E_o** psi	Ultimate Strength* f_{ult}-psi	Elongation in 6 in. %	Bar Location Beam-Layer+
9	91	41000	0.152	1.71	29000	767000	68400	29.4	T3Mb-B
	92	41700	0.152	2.02	28000	708000	66600	27.5	T3Ma-B
	93	40150	0.133	1.60	27000	822000	68200	30.0	T5L-B
	94	41250	0.134	1.81	27000	786000	68900	27.8	T5M-T
	95	40050	0.154	1.62	28000	788000	65650	29.0	T5M-B
	96	48400	0.154	1.10	36000	1130000	84450	-	T11L-T
	97	42250	0.154	1.73	28000	810000	69500	25.6	T11L-B
	98	41750	0.154	1.92	27000	773000	68450	25.8	C3w-B
	99	41850	0.154	1.73	27000	815000	69420	-	C3xm-B
	910	42100	0.116	1.85	30000	657000	68900	-	C3ynb-B
	911	41300	0.135	2.01	29000	683000	66350	30.4	C4zn-B
Average		42000	0.145	1.74	29000	816000	69500	28.2	
6P	61P++	43300	0.135	2.31	27000	710000	66600	34.0	T1Mb- NB
	62P	42500	0.135	2.23	27000	710000	63600	32.3	T1Mb- SB
Average		42900	0.135	2.27	27000	710000	65100	33.2	

* Based on nominal area

** See Fig. 1

\+ Layer of steel

C - Compression

T - Top layer of tension reinforcement

B - Bottom layer of tension reinforcement

NB - North side of bottom layer of tension reinforcement

SB - South side of bottom layer of tension reinforcement

++ Plain bars

Note: Some bars broke outside gage line; therefore, no elongation recording was made.

TABLE NO. 5

PROPERTIES OF CONCRETE MIXTURES

Beam	Concrete Strength psi		Cement* / Water		Aggregate* / Cement	Aggregate* / Sand	Slump - in.		Age Days
	Batch		Batch				Batch		
	1	2	1	2			1	2	
T1La	1860	2150	0.98	1.00	10.80	2.14	6	2	67
T1Lb	3550	2540	0.88	0.90	10.70	2.10	5½	6	57
T2La	2690	2130	1.13	1.07	10.10	2.15	2	2	59
T2Lb	4740	2440	1.03	0.97	10.30	2.35	9	7	44
T4La	2910	2380	0.99	0.99	11.00	2.26	3	2	63
T4Lb	3420	2810	1.02	1.02	10.80	2.28	1½	1	61
T5L	3720	2500	0.86	0.86	10.80	2.25	2	2½	60
T11L	3500	2900	1.26	1.24	7.86	2.57	2	1	57
T1Ma	3840	4600	1.46	1.42	8.47	2.71	1½	3	28
T1Mb	4850	4720	1.57	1.57	6.71	2.51	3	2	29
T2Ma	4280	4360	1.28	1.37	7.44	2.55	4	1½	36
T2Mb	3860	4015	1.45	1.54	7.40	2.50	6	5	34
T2Mc	4560	4380	1.79	1.79	6.75	2.55	½	1	36
T3Ma	4550	4110	1.47	1.44	8.47	2.68	1½	2	70
T3Mb	4850	4940	1.45	1.42	7.94	2.55	1	1	43
T1Ha	5880	5880	1.89	1.89	5.91	2.60	3	2½	52
T1Hb	4540	5180	1.65	1.61	8.00	2.53	1	1½	43
T2H	5590	5400	1.95	1.95	6.01	2.52	3	2	40
T3H	5790	5920	2.15	2.00	6.05	2.51	2½	2	36
T4H	5100	5260	1.62	1.60	8.00	2.52	3	1½	42
T5H	5940	5900	1.81	1.89	6.02	2.51	2	2½	35
C2w	4100	3940	1.32	1.32	8.60	2.64	2½	3	52
C2xm	3820	4070	1.40	1.46	8.58	2.66	2	2	48
C3w	4650	4310	1.37	1.40	8.60	2.64	2½	3	54
C3xm	3360	3890	1.37	1.37	8.50	2.66	1½	2	48
C3yxa	3530	3330	1.26	1.26	8.74	2.52	3	1½	28
C3ynb	4490	4860	1.52	1.52	8.65	2.64	1	1	47
C4xna	2510	2450	0.94	0.94	10.60	2.22	6	6	34
C4xnb	2000	2430	0.92	0.96	10.60	2.23	6½	6	44
C4yn	3340	3570	1.47	1.37	8.60	2.63	½	4	43
C5yn	4150	4480	1.42	1.42	8.60	2.65	2	3	40
C6xm	3400	3680	1.32	1.34	8.62	2.65	6	3	34
C7w	3570	3480	1.29	1.29	8.54	2.66	2	3	50

* All ratios based on weight

TABLE NO. 6

TEST RESULTS OF BEAMS FAILING

IN SHEAR

Beam Data

	T2M3a	T2M3b	T2M3c
Average concrete strength;			
6 x 12 in. cylinders-psi	4320	4020	4470
Reinforcing steel;			
Percent - p	1.38	1.38	1.90
Yield Point; f_y-psi	47700	48300	46800
Depth to steel; d-in.	10.58	10.58	10.51
Reinforcing Index; $q = \frac{pf_y}{f'_c}$	0.152	0.166	0.199
End Anchorage	None	Hooks	None

Test Results

Ultimate load capacity; P_{ult}(obs)-lb.	17400	18450	23900
Nominal shear stress at P_{ult}(obs) v-psi*	193	204	223
As fraction of f'_c	0.036	0.041	0.046

---

* $v = \frac{V}{bjd}$ where: V = total shear

$j = 1 - \frac{k}{3}$

TABLE NO. 7s

CRITICAL AND ACTUAL VALUES OF THE REINFORCING INDEX FOR BEAMS WITH TENSION REINFORCEMENT ONLY

Beam	q	q_{or}	q_o	Mode of Failure
T1La	0.09	1.09	0.26	Tension
T1Lb	0.11	0.83	0.22	Tension
T2La	0.18	1.15	0.30	Tension
T2Lb	0.22	0.88	0.27	Tension
T4La	0.33	0.97	0.30	Tension
T4Lb	0.39	0.79	0.19	Tension
T5L	0.52	0.92	0.25	Tension
T11L*	1.13	0.67	0.24	Comp.
T1Ma	0.06	0.59	0.15	Tension
T1Mb**	0.12	0.61	0.12	Tension
T2Ma	0.15	0.61	0.16	Shear
T2Mb	0.17	0.62	0.17	Shear
T2Mc	0.20	0.59	0.26	Shear
T3Ma	0.27	0.58	0.13	Tension
T3Mb	0.33	0.62	0.16	Tension
T1Ha	0.10	0.55	0.14	Tension
T1Hb	0.14	0.55	0.14	Tension
T2H	0.21	0.56	0.17	Tension
T3H*	0.30	0.49	0.20	Tension
T4H*	0.46	0.51	0.19	Tension
T5H*	0.50	0.50	0.17	Tension

* Two layers of tension reinforcement

** Plain bars for reinforcement

TABLE NO. 7b

CRITICAL AND ACTUAL VALUES OF THE REINFORCING INDEX FOR BEAMS WITH TENSION AND COMPRESSION REINFORCEMENT

Beam	q'	q'_{cr}	ω'	Mode of Failure
C2w	0.09	0.63	0.18	Tension
C2xm	0.08	0.58	0.18	Tension
C3w	0.10	0.62	0.14	Tension
C3xm	0.14	0.63	0.16	Tension
C3yna	0.09	0.71	0.17	Tension
C3ynb	0.09	0.61	0.14	Tension
C4xma	0.19	0.93	0.24	Tension
C4xmb	0.11	0.97	0.23	Tension
C4xn	0.12	0.68	0.15	Tension
C5yn*	0.28	0.55	0.28	Tension
C6xm*	0.33	0.53	0.21	Tension
C7w*	0.32	0.48	0.17	Tension

* Two layers of tension reinforcement

TABLE NO. 6

COMPARISON OF EXPERIMENTAL AND THEORETICAL VALUES OF STRESS IN THE TENSION REINFORCEMENT AT MAXIMUM MOMENT

Beams with Tension Reinforcement Only

Beam	f_s @ M_{max} - ksi		
	Exp	Theo	Exp / Theo
T1La	71.8	77.7	0.93
T1Lb	58.0	56.9	1.02
T2La	48.4	48.9	0.99
T2Lb	58.7	58.6	1.00
T4La	44.2	44.1	1.00
T4Lb	43.0	43.3	0.99
T5L	40.5	40.2	1.01
T11L	33.2	33.2	1.00
T1Ma	56.0	62.3	0.90
T1Mb	42.7	42.9	1.00
T3Ma	41.0	41.0	1.00
T3Mb	42.0	41.7	1.01
T1Ha	47.7	47.8	1.00
T1Hb	55.7	51.9	1.06
T2H	45.6	45.6	1.00
T3H	43.6	43.2	1.00
T4H	41.5	42.0	0.99
T5H	40.6	40.6	1.00
	Average Ratio		0.99
	Range		0.90 - 1.06

Beams with Tension and Compression Reinforcement

Beam	f_s @ M_{max} - ksi		
	Exp	Theo	Exp / Theo
C2w	51.8	53.2	0.98
C2xm	68.2	60.7	1.12
C3w	45.1	44.7	1.01
C3xm	43.5	43.4	1.00
C3yna	58.3	51.6	1.13
C3ynb	54.5	45.8	1.18
C4xma	50.8	48.2	1.05
C4xmb	57.3	53.8	1.06
C4xn	50.3	43.3	1.17
C5xm	43.8	44.0	1.00
C6xm	40.8	41.8	0.98
C7w	41.2	41.6	0.99
	Average Ratio		1.06
	Range		0.98 - 1.18

TABLE 9a

COMPARISON OF EXPERIMENTAL AND THEORETICAL VALUES

OF YIELD-POINT MOMENT

Beams with Tension Reinforcement Only

Beam	M_y - kip-ft		
	Exp	Theo	Exp / Theo
T1La	10.2	9.9	1.03
T1Lb	15.4	14.8	1.04
T2La	20.6	19.6	1.05
T2Lb	26.1	26.8	0.97
T4La	37.5	39.2	0.96
T4Lb	47.0	49.7	0.95
T5L	48.4	56.8	0.85
T11L*	-	-	-
T1Ma	15.5	15.1	1.03
T1Mb	30.2	29.2	1.03
T3Ma	60.5	59.2	1.02
T3Mb	58.1	59.9	0.97
T1Ha	29.8	30.3	0.98
T1Hb	34.2	35.7	0.96
T2H	51.3	43.4	0.96
T3H	65.1	66.1	0.96
T4H**	-	83.7	-
T5H	81.7	99.5	0.82
	Average Ratio		0.97
	Range	0.82 - 1.05	

Beams with Tension and Compression Reinforcement

Beam	M_y - kip-ft		
	Exp	Theo	Exp / Theo
C2w	32.4	30.9	1.05
C2nn	38.0	36.3	1.05
C3w	62.4	61.3	1.02
C3nn	66.3	61.5	1.08
C3yna	41.0	40.9	1.00
C3nnb	62.4	62.1	1.00
C4nna	40.1	41.3	0.97
C4nnb	42.8	42.3	1.01
C4nn	59.3	60.7	0.98
C5yn	87.8	89.7	0.98
C6nn	84.9	84.9	1.00
C7w	84.0	84.3	1.00
	Average Ratio		1.01
	Range	0.97 - 1.08	

* Compression failure

** Experimental value not recorded

TABLE 9b

COMPARISON OF EXPERIMENTAL AND THEORETICAL VALUES OF THE MAXIMUM MOMENT CAPACITY

Beams with Tension Reinforcement Only

Beam	M_{max} - kip-ft Exp	Theo	Exp / Theo
T1La	13.1	14.4	0.91
T1Lb	19.4	18.8	1.03
T2La	23.5	23.8	0.99
T2Lb	29.1	28.4	1.02
T4La	37.8	38.2	0.99
T4Lb	47.0	47.9	0.98
T5L	53.1	51.8	1.03
T1ILb	66.8	61.7	1.08
T1Ma	18.7	21.2	0.88
T1Mb	32.0	31.0	1.03
T3Ma	62.1	61.5	1.01
T3Mb	61.1	60.7	1.01
T1Ha	34.3	34.8	0.99
T1Hb	39.9	37.2	1.07
T2H	53.1	55.9	0.95
T3H	67.0	69.7	0.96
T4H	77.2	80.4	0.96
T5H	85.5	100.2	0.85
	Average Ratio		0.99
	Range		0.85 - 1.08

Beams with Tension and Compression Reinforcement

Beam	M_{max} - kip-ft Exp	Theo	Exp / Theo
C2w	40.9	38.1	1.07
C2xm	44.1	43.1	1.02
C3w	69.3	68.6	1.01
C3xm	69.5	66.5	1.05
C3yna	49.8	46.3	1.08
C3ynb	73.4	69.4	1.06
C4xma	43.2	45.0	0.96
C4xmb	48.2	50.1	0.96
C4xm	71.3	66.1	1.08
C5yn	90.1	91.0	0.99
C6xm	85.8	86.1	1.00
C7w	84.5	86.0	0.98
	Average Ratio		1.03
	Range		0.96 - 1.08

TABLE 10a

COMPARISON OF EXPERIMENTAL AND THEORETICAL VALUES

OF MIDSPAN DEFLECTION AT YIELD POINT

Beams with Tension Reinforcement Only

Beam	Δ_y - in. Exp	Theo	Exp / Theo
T1La	0.30	0.27	1.11
T1Lb	0.30	0.25	1.20
T2La	0.27	0.25	1.08
T2Lb	0.36	0.34	1.06
T4La	0.38	0.32	1.19
T4Lb	0.46	0.34	1.35
T5L	0.49	0.35	1.40
T11L*	-	-	-
T1Ma	0.25	0.24	1.04
T1Mb	0.34	0.26	1.31
T3Ma	0.50	0.32	1.56
T3Mb	0.38	0.34	1.12
T1Ha	0.37	0.27	1.37
T1Hb	0.37	0.32	1.15
T2H	0.37	0.33	1.12
T3H	0.48	0.39	1.23
T4H*	-	0.44	-
T5H	0.55	0.47	1.17
	Average Ratio		1.22
	Range 1.04 - 1.56		

Beams with Tension and Compression Reinforcement

Beam	Δ_y - in. Exp	Theo	Exp / Theo
C2w	0.36	0.27	1.31
C2xn	0.45	0.32	1.39
C3w	0.46	0.30	1.53
C3xn	0.40	0.31	1.31
C3yna	0.38	0.30	1.27
C3ynb	0.42	0.30	1.39
C4xna	0.37	0.31	1.19
C4xnb	0.38	0.31	1.22
C4sn	0.40	0.30	1.31
C5yn	0.50	0.41	1.22
C6xn	0.50	0.40	1.25
C7w	0.46	0.40	1.15
	Average Ratio		1.29
	Range 1.15 - 1.53		

* Compression Failure

** Deflection at yield-point not obtained

TABLE 10b

COMPARISON OF EXPERIMENTAL AND THEORETICAL VALUES OF MIDSPAN DEFLECTION AT MAXIMUM LOAD CARRYING CAPACITY

Beams with Tension Reinforcement Only

Beam	Δ_{ult} - in. Exp	Theo	Exp/Theo
T1La	4.95	3.87	1.28
T1Lb	3.97	4.01	0.99
T2La	3.07	3.33	0.93
T2Lb	1.83	1.77	1.03
T4La	1.10	1.26	0.87
T4Lb	1.01	1.33	0.76
T5L	1.05	1.13	0.93
T11L*	-	0.58	-
T1Ma	3.30	3.04	1.09
T1Mb	1.92	3.06	0.63
T3Ma	0.97	1.19	0.82
T3Mb	0.93	1.08	0.86
T1Ha	2.64	3.19	0.83
T1Hb	1.87	1.85	1.01
T2H	1.48	1.74	0.85
T3H	1.34	1.29	1.04
T4H	1.87	1.85	1.01
T5H*	-	0.82	-
	Average Ratio		0.93
	Range	0.63 - 1.28	

Beams with Tension and Compression Reinforcement

Beam	Δ_{ult} - in. Exp	Theo	Exp/Theo
C2w	3.23	3.53	0.92
C2xa	4.22	3.10	1.36
C3w	3.46	3.22	1.07
C3xa	4.10	2.81	1.46
C3yna	4.62	3.49	1.32
C3ynb	6.09	3.76	1.62
C4xna	2.98	2.86	1.04
C4xnb	4.29	3.58	1.20
C4xa	5.60	3.16	1.77
C5yn	1.00	1.99	0.50
C6xa	1.21	1.71	0.71
C7w	1.75	2.25	0.78
	Average Ratio		1.15
	Range	0.78 - 1.77	

* Ultimate deflection not observed

TABLE NO. 11

COMPARISON OF EXPERIMENTAL AND THEORETICAL VALUES

OF "USABLE ENERGY"

Beams with Tension Reinforcement Only

Beam	"Usable Energy" kip-in. Exp	Theo	Exp/Theo
T1La	38.5	30.2	1.27
T1Lb	45.7	43.4	1.05
T2La	43.7	46.3	0.95
T2Lb	30.5	29.4	1.04
T4La	22.6	28.4	0.80
T4Lb	24.0	37.8	0.64
T5L	28.0	34.9	0.80
T11L*	-	11.9	-
T1Ma	38.2	35.0	1.09
T1Mb	37.0	58.8	0.63
T3Ma	28.6	41.4	0.69
T3Mb	29.5	36.5	0.81
T1Ha	53.0	66.0	0.81
T1Hb	43.2	41.0	1.05
T2H	44.5	57.2	0.78
T3H	49.1	50.2	0.98
T4H	20.0	29.9	0.67
T5H*	-	38.8	-
	Average Ratio		0.88
	Range		0.63 - 1.27

Beams with Tension and Compression Reinforcement

Beam	"Usable Energy" kip-in Exp	Theo	Exp/Theo
C2w	73.8	77.8	0.95
C2xa	111.3	77.4	1.44
C3w	142.9	132.6	1.08
C3xa	178.4	113.2	1.57
C3ya	135.6	96.9	1.40
C3yb	263.3	158.0	1.66
C4xa	76.8	77.6	0.99
C4xb	122.5	105.0	1.17
C4x	235.0	127.0	1.84
C5y	43.5	107.0	0.40
C6x	53.2	86.0	0.62
C7w	81.8	116.0	0.71
	Average Ratio		1.15
	Range		0.40 - 1.84

* Deflection not obtained at M_{max}

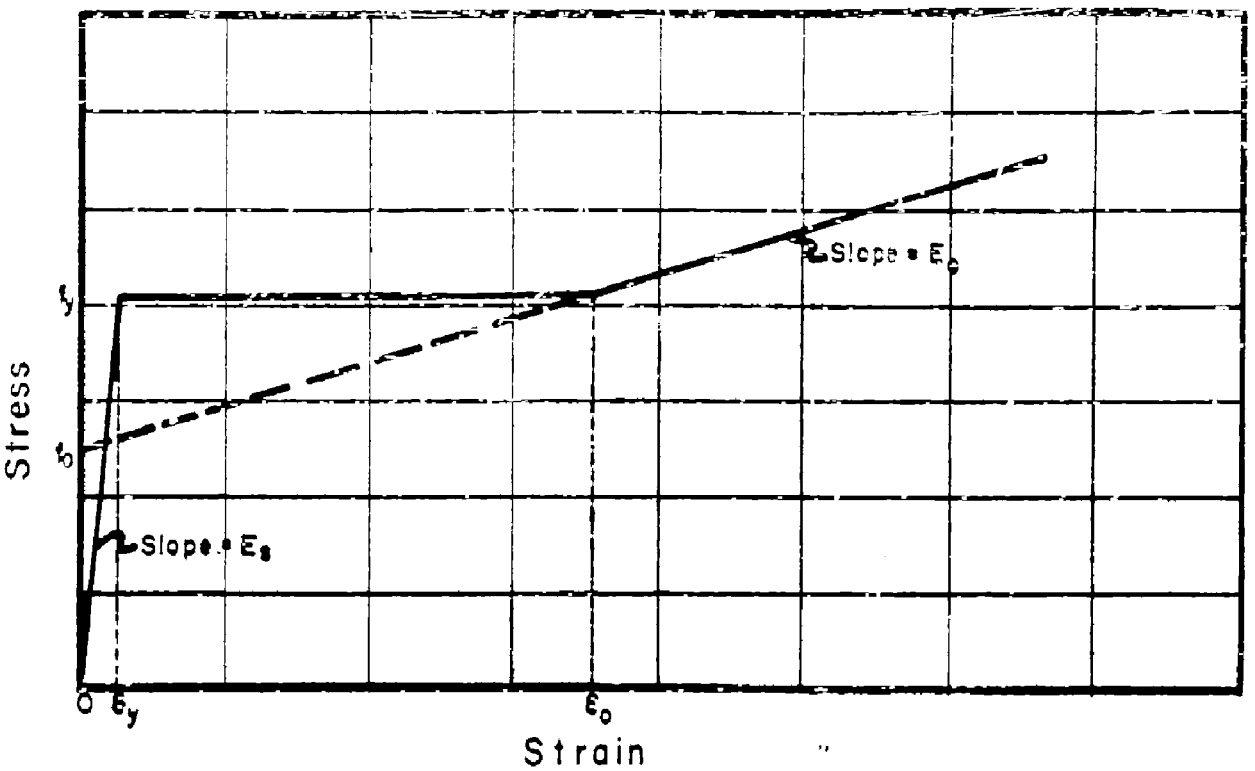

FIG. 1 IDEALIZED STRESS-STRAIN DIAGRAM FOR REINFORCING STEEL

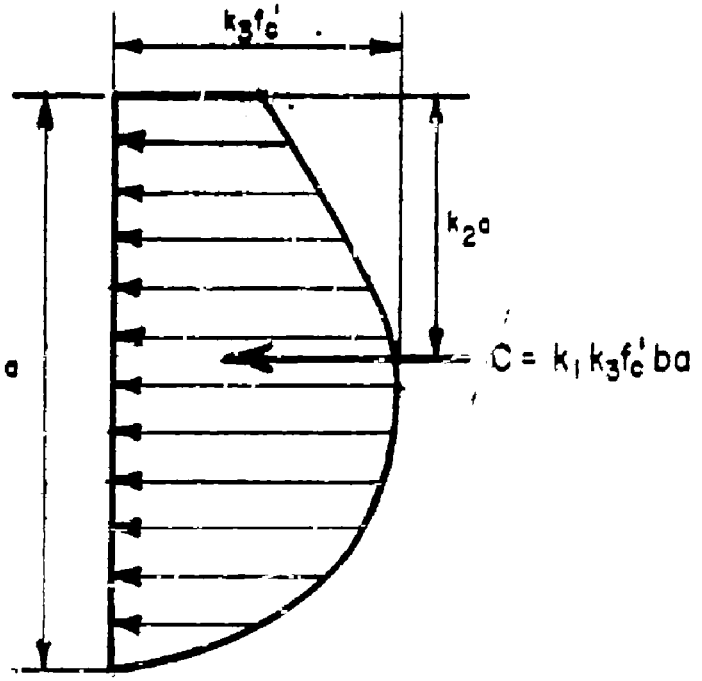

FIG. 2 ASSUMED STRESS BLOCK IN CONCRETE AT ULTIMATE

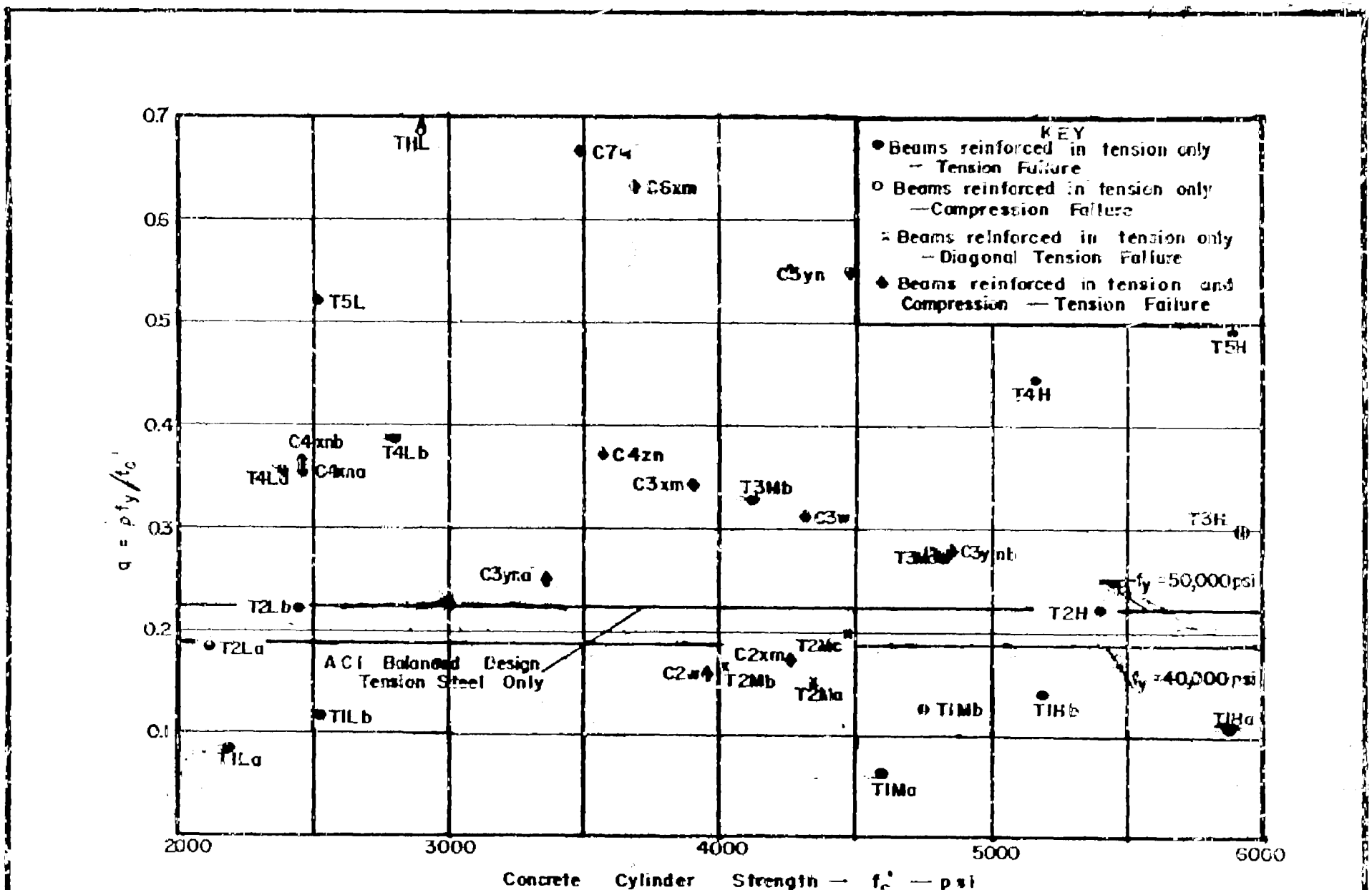

FIG. 3 OUTLINE OF TESTING PROGRAM

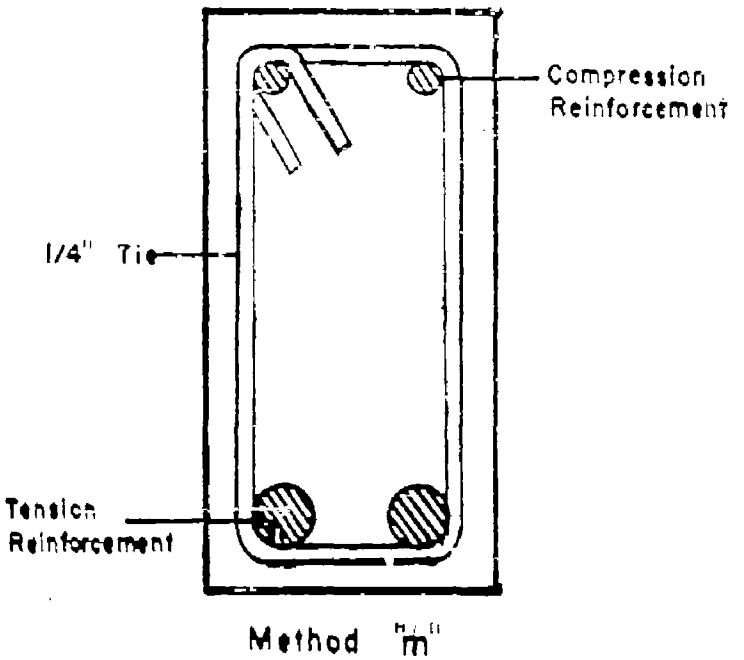

Method "m"

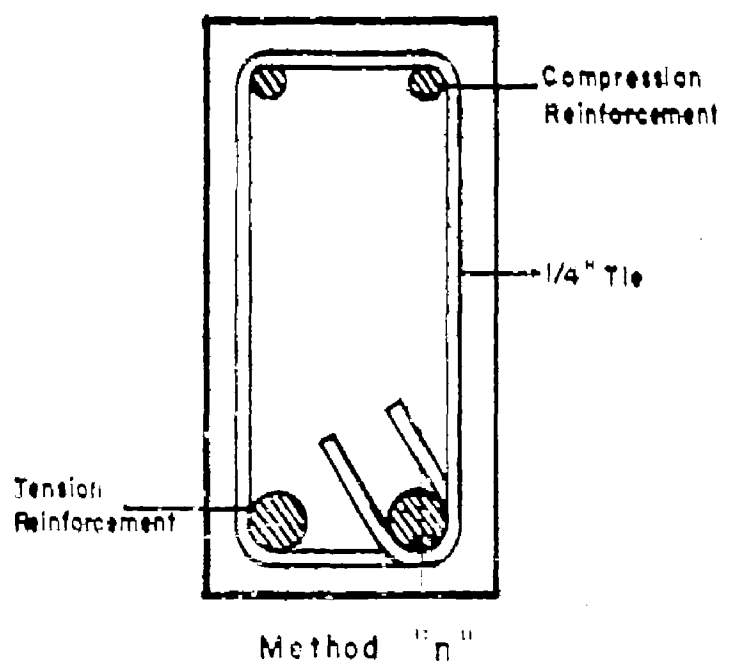

Method "n"

FIG. 4 METHODS OF TYING COMPRESSION REINFORCEMENT

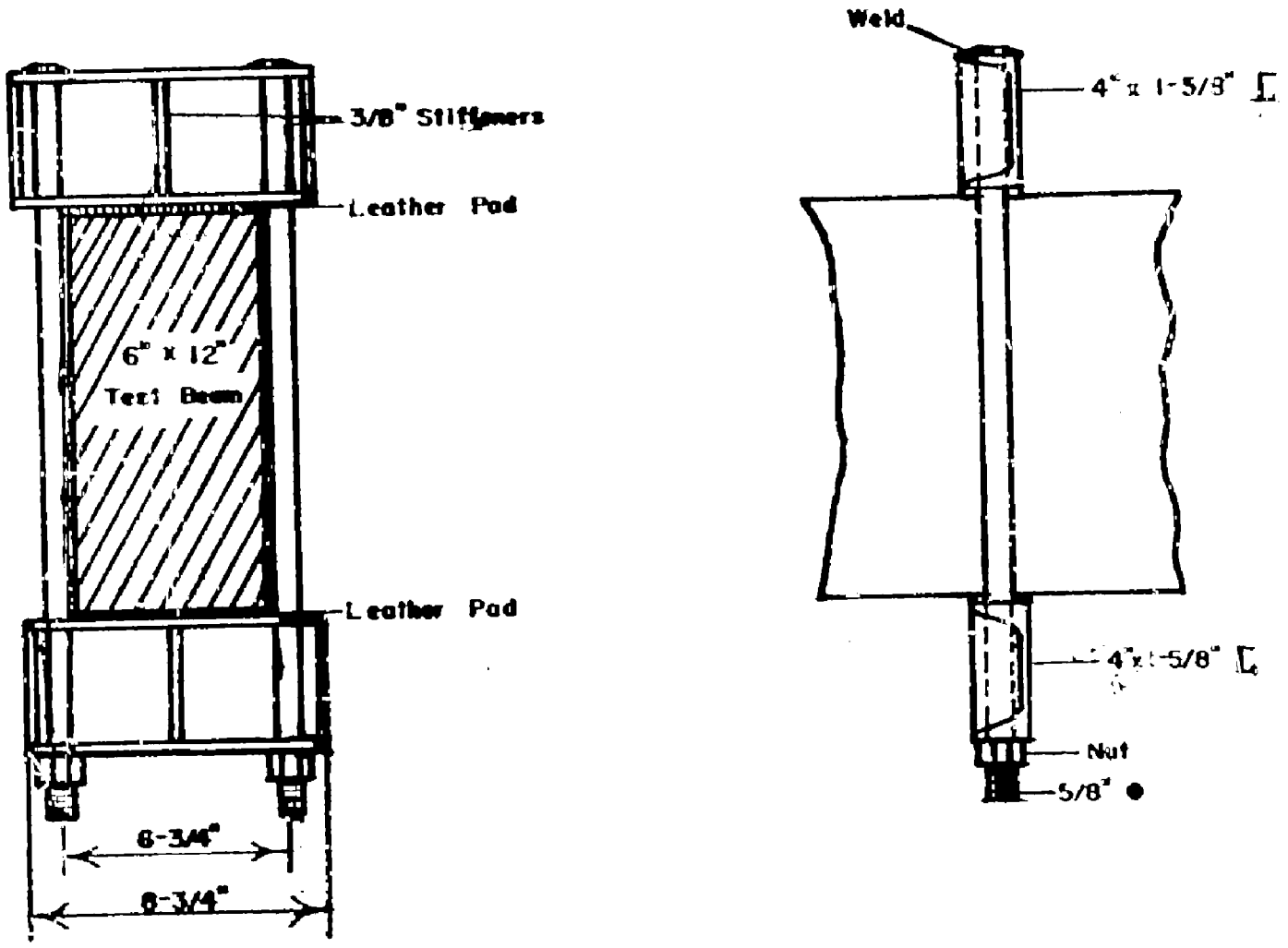

FIG. 5 OUTSIDE CLAMP-ON STIRRUP

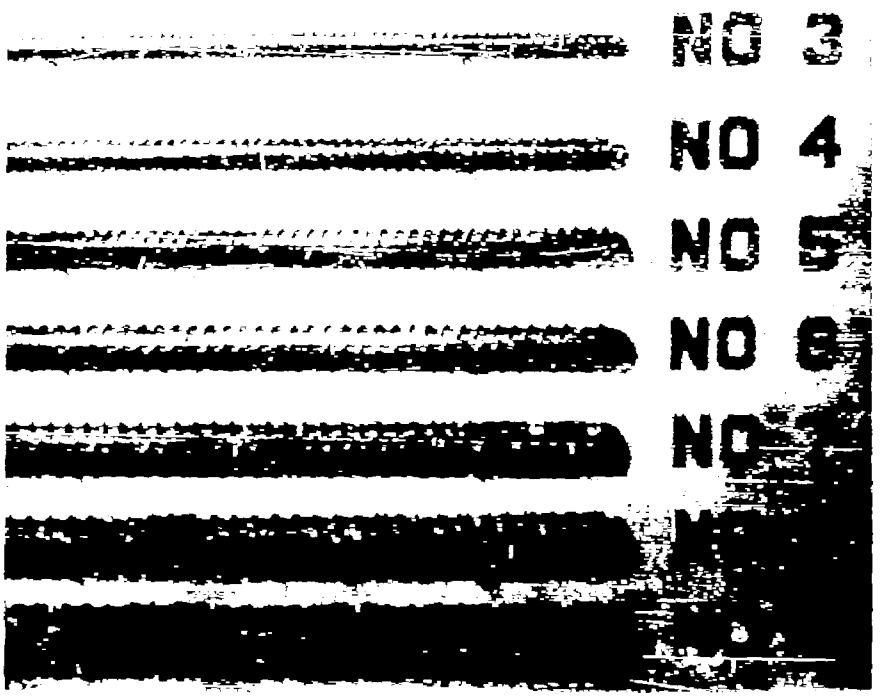

Reinforcing Bars Used in Beams

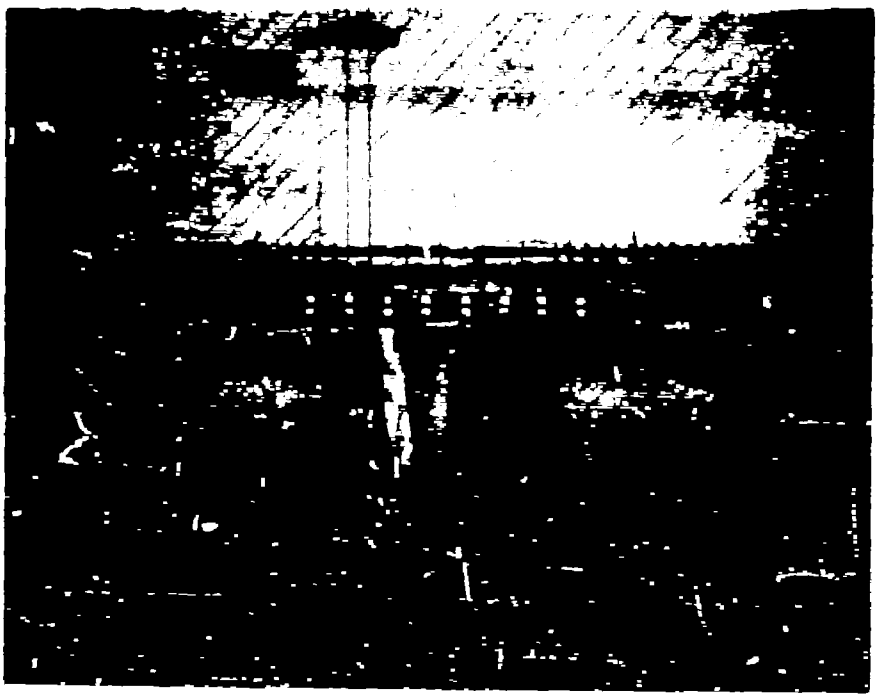

Typical Steel Reinforcing Cage

FIG. 6 REINFORCING STEEL

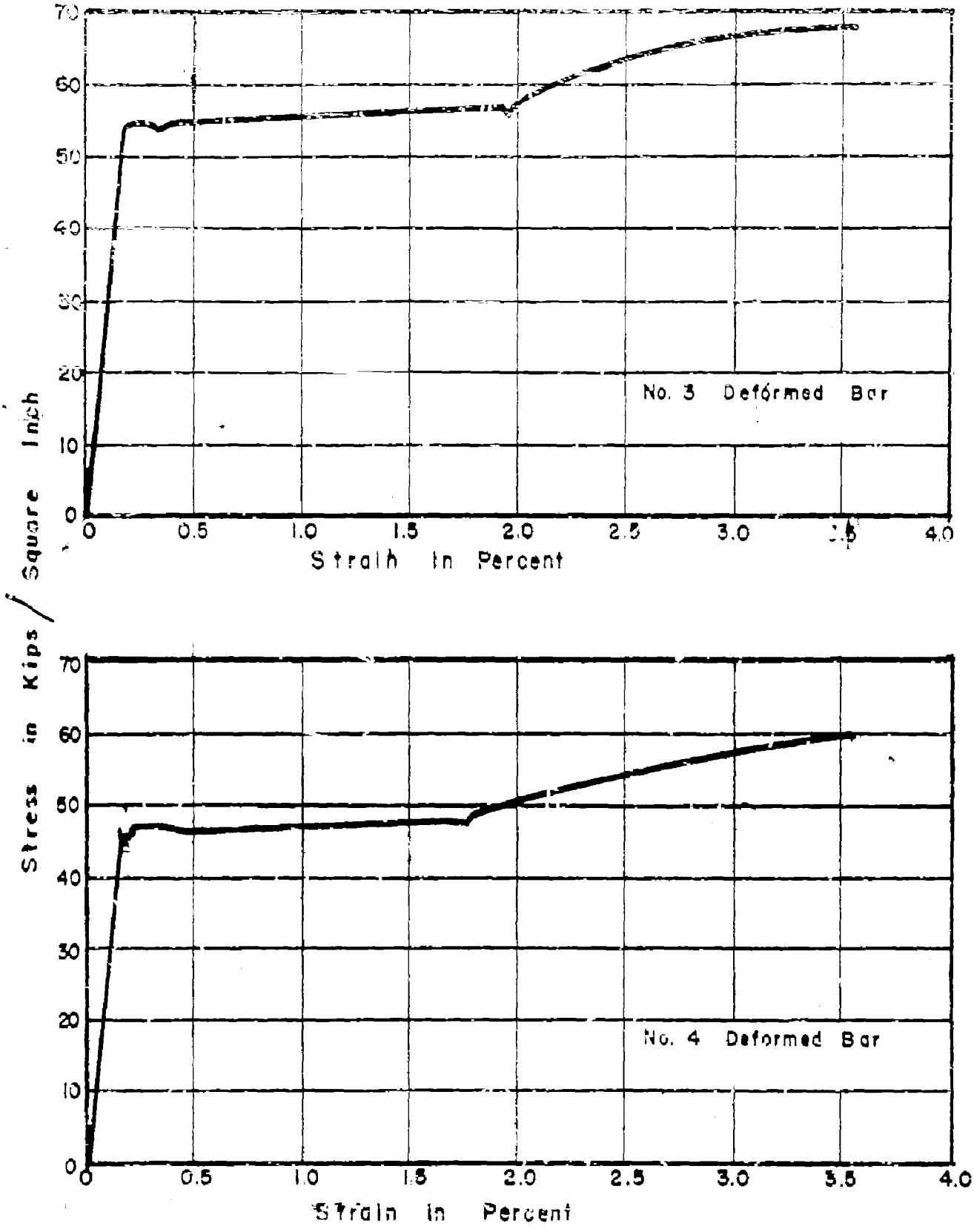

FIG. 7 TYPICAL STRESS-STRAIN CURVES FOR REINFORCING BARS

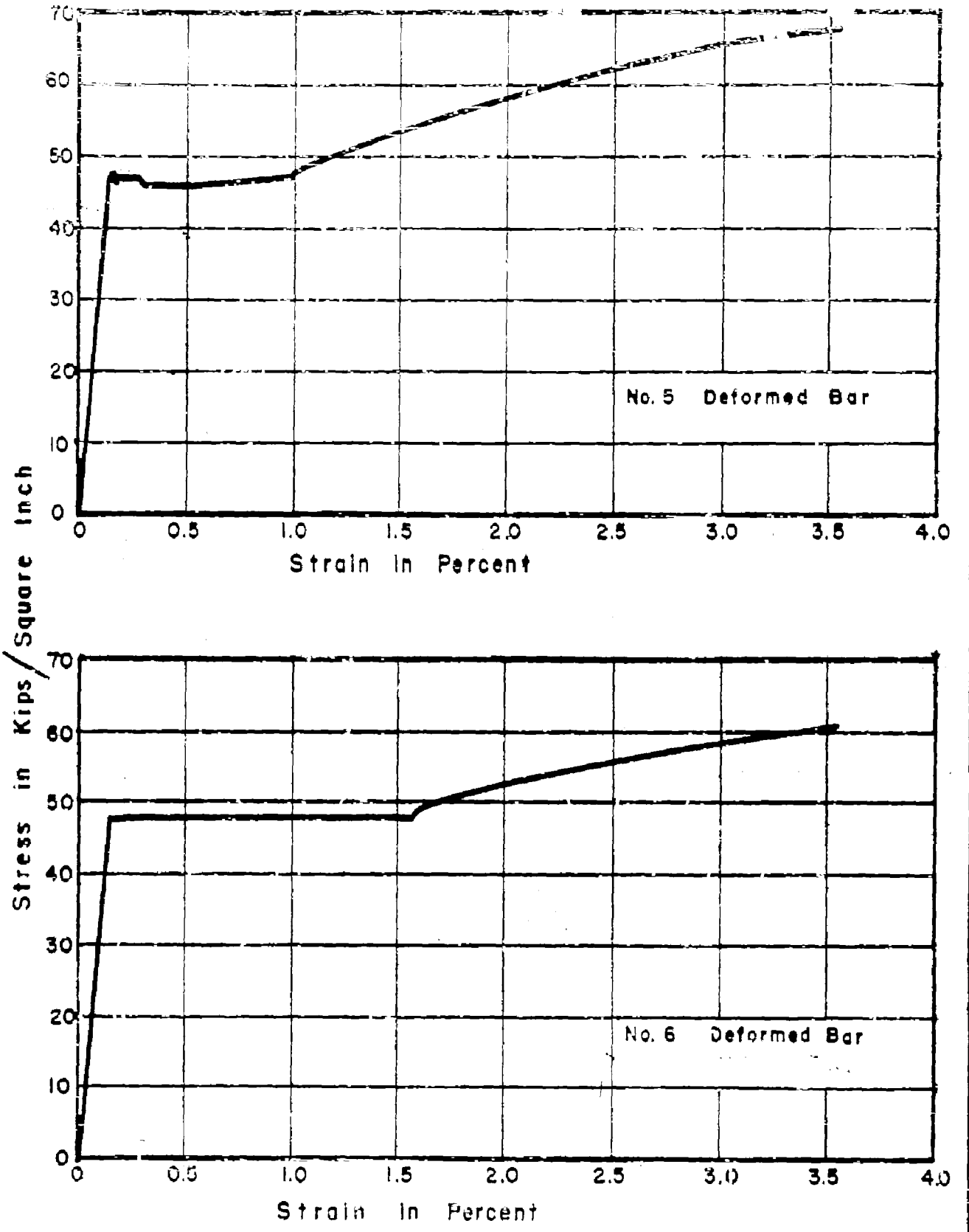

FIG. 8 TYPICAL STRESS – STRAIN CURVES FOR REINFORCING BARS

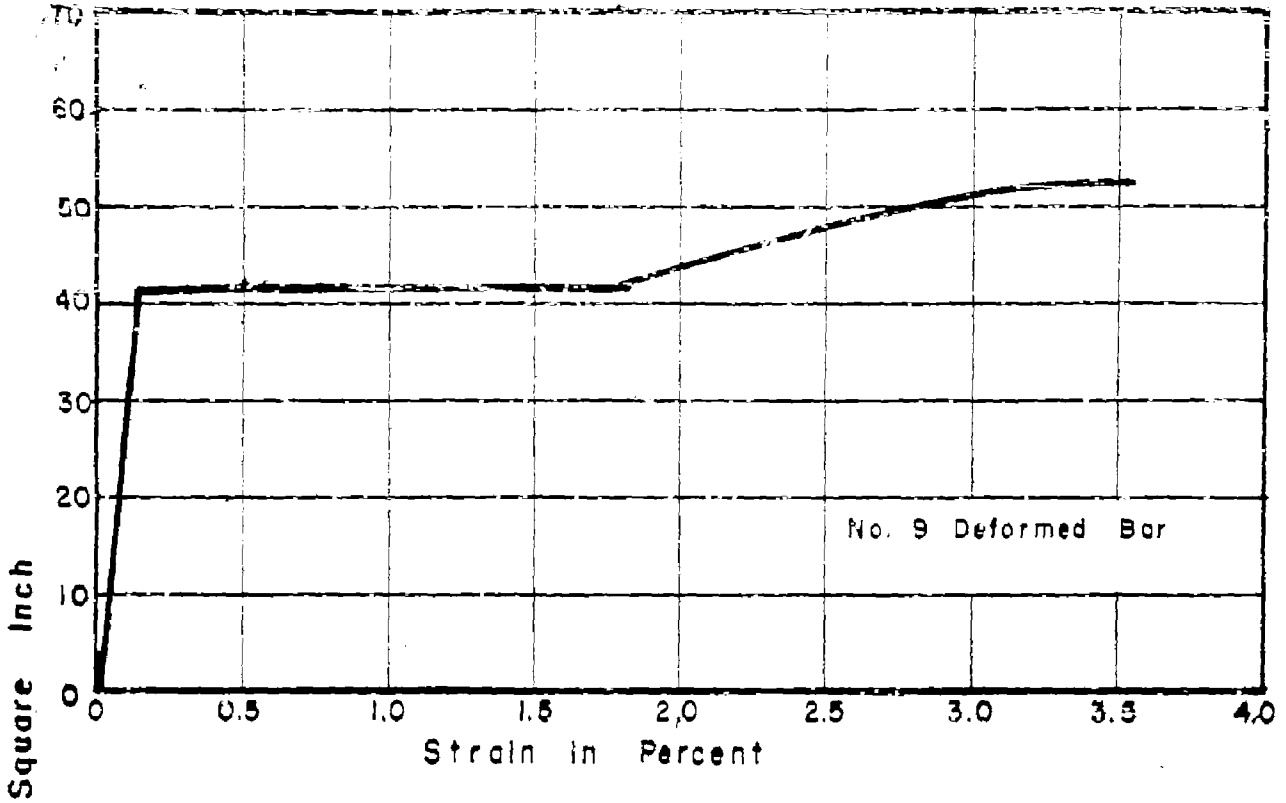

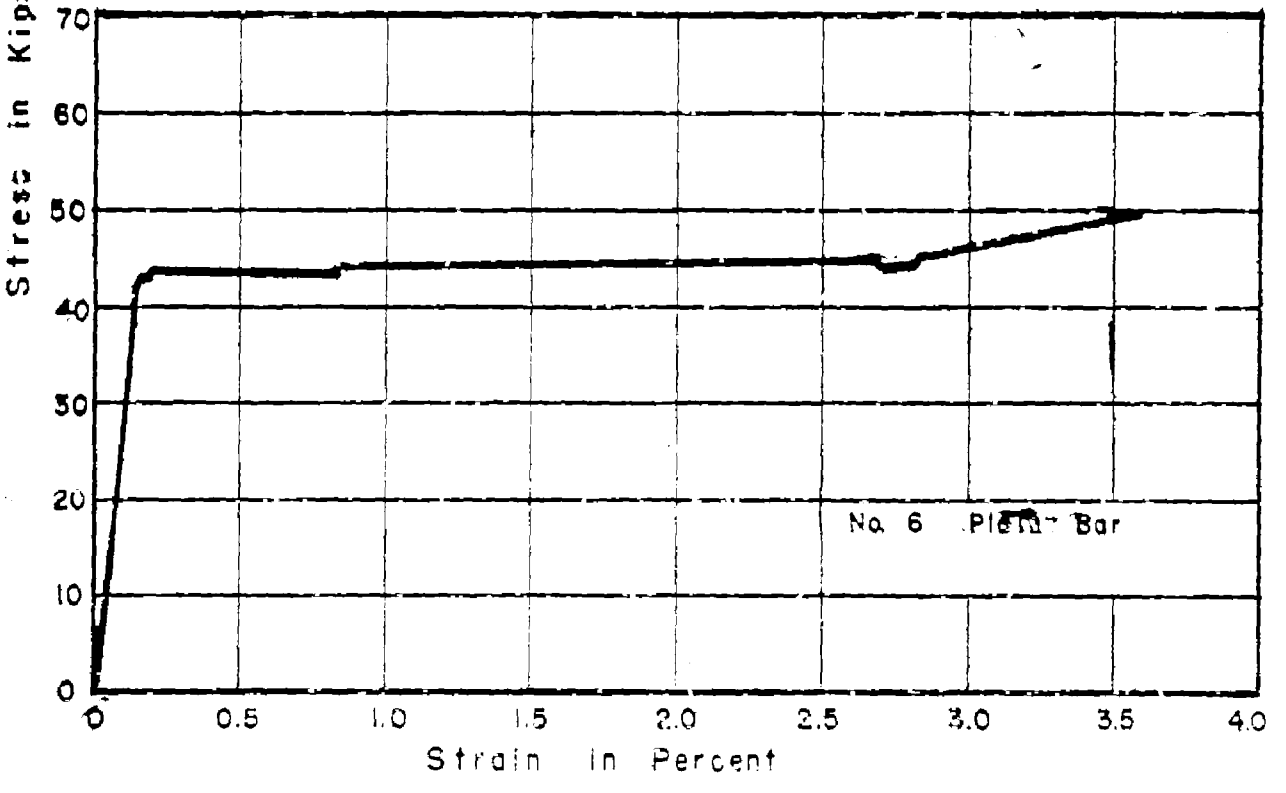

FIG. 10 TYPICAL STRESS — STRAIN CURVES FOR REINFORCING BARS

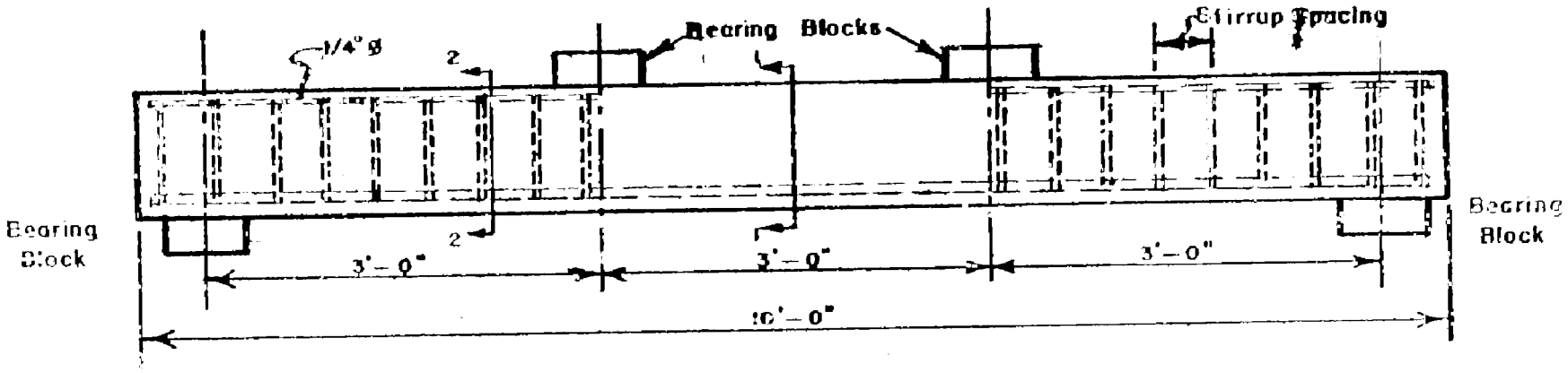

NOTE

Concrete cover of approximately one inch

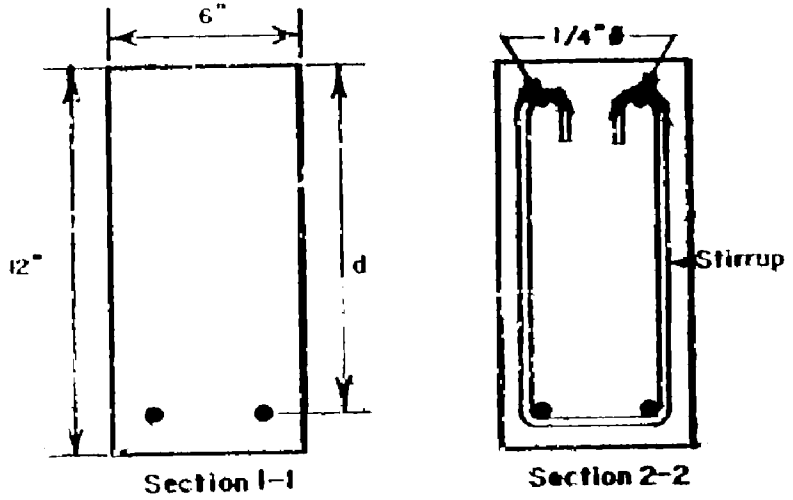

BEAMS WITH ONE LAYER
OF TENSION REINFORCEMENT

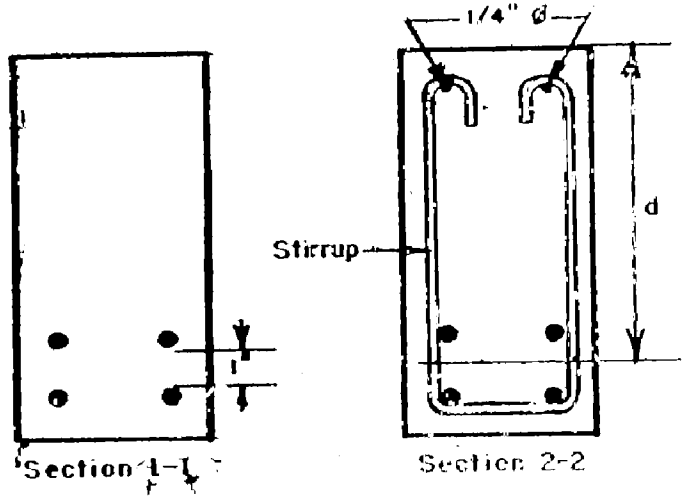

BEAMS WITH TWO LAYERS
OF TENSION REINFORCEMENT

FIG. 1: ARRANGEMENT OF REINFORCEMENT FOR BEAMS REINFORCED IN TENSION ONLY

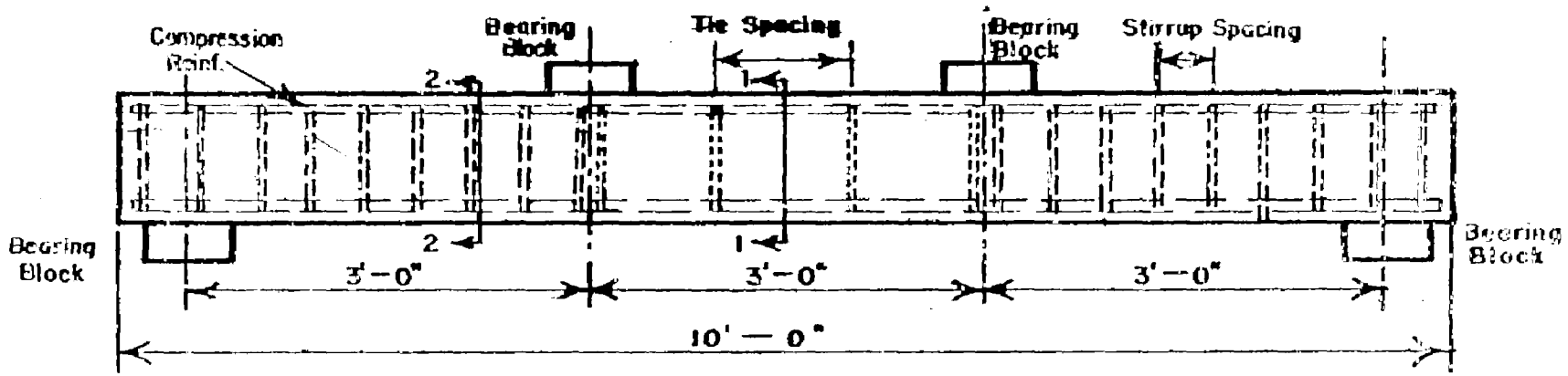

NOTE:
Concrete cover of approximately one inch.

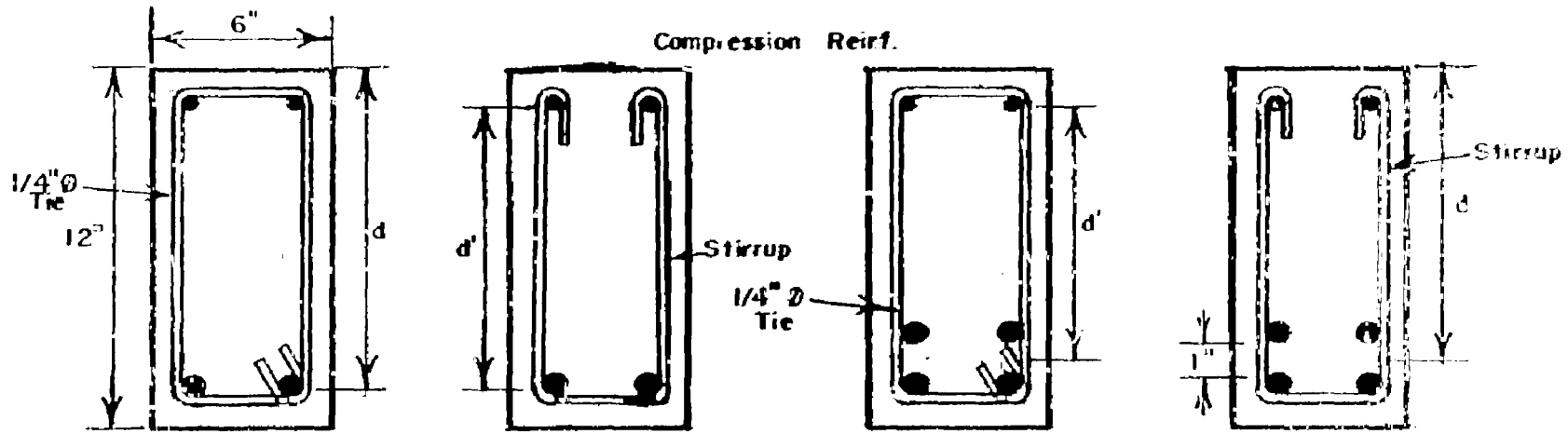

BEAMS WITH ONE LAYER OF TENSION REINFORCEMENT

BEAMS WITH TWO LAYERS OF TENSION REINFORCEMENT

FIG. 12 ARRANGEMENT OF REINFORCEMENT FOR BEAMS REINFORCED IN TENSION AND COMPRESSION

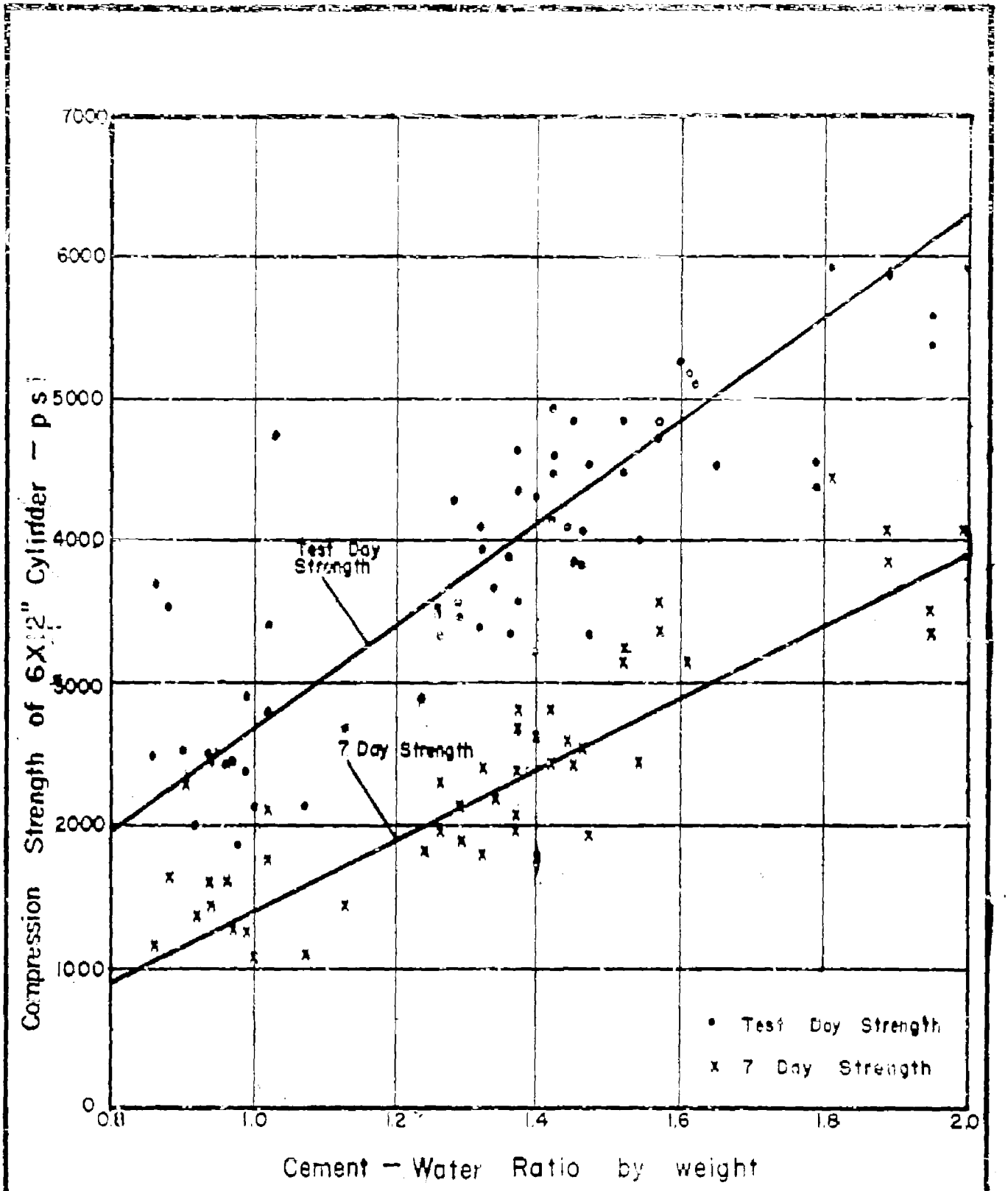

FIG.13 CONCRETE STRENGTH VS CEMENT-WATER RATIO

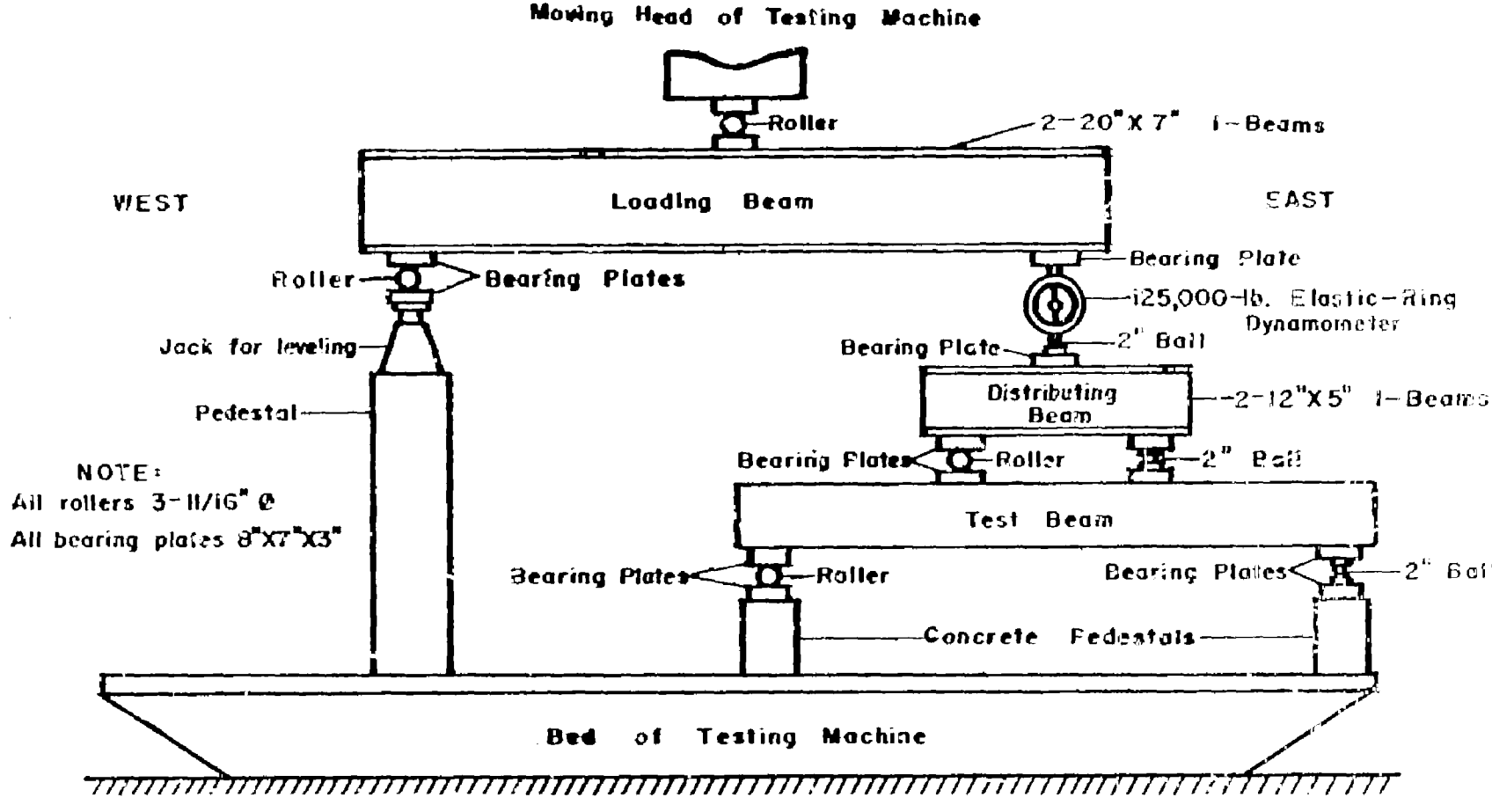

FIG. 14 BEAM AND TESTING APPARATUS

West End

South Side

FIG. 15 VIEWS OF BEAM TESTING APPARATUS

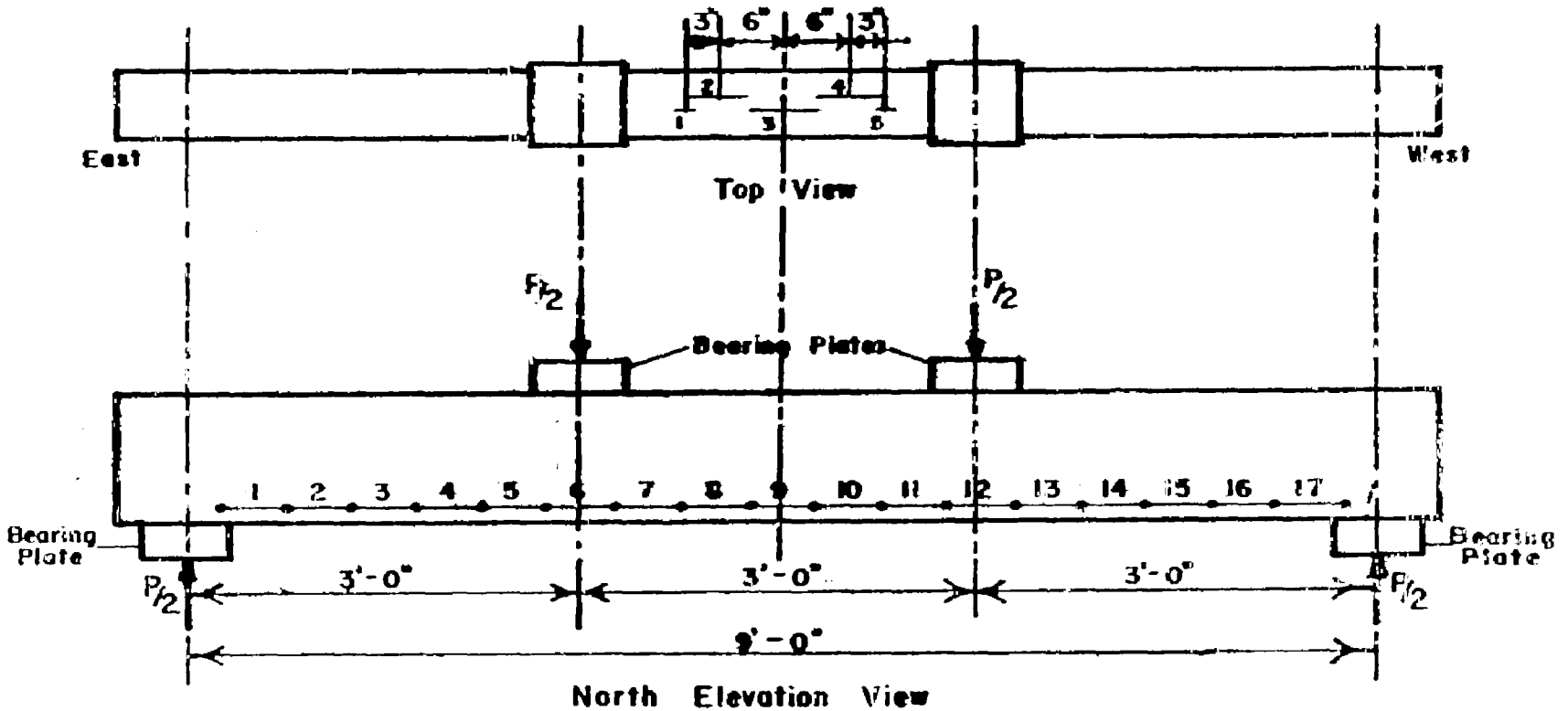

2 — SR-4 Electric Resistance Strain Gage { 1,5 - Type A-11 / 2,3,4 - Type A-9

2 — 6" Mechanical Strain Gage Lines (Berry and Direct)

FIG. 16 STRAIN MEASUREMENT LOCATIONS

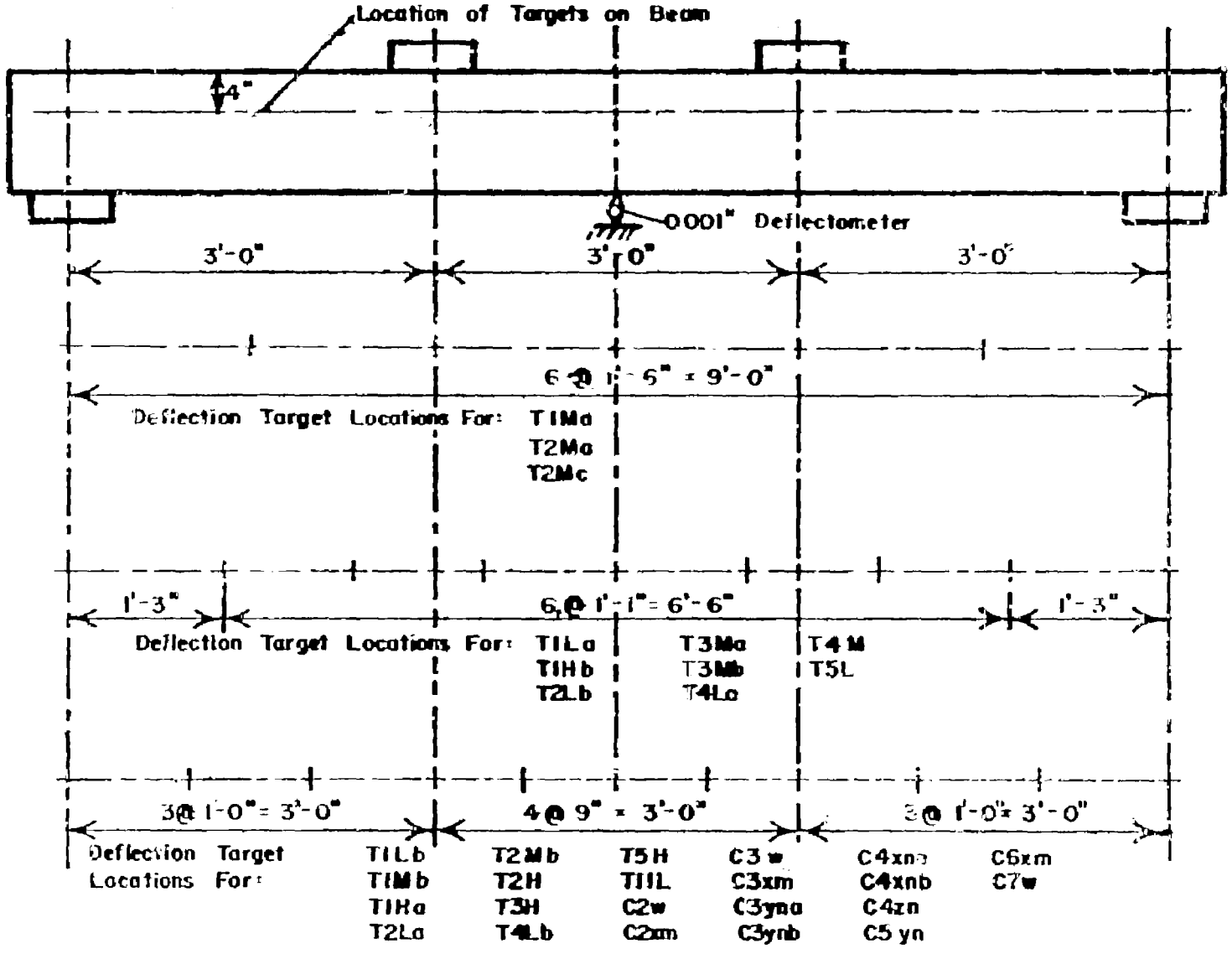

FIG. 17 DEFLECTION MEASUREMENT LOCATIONS

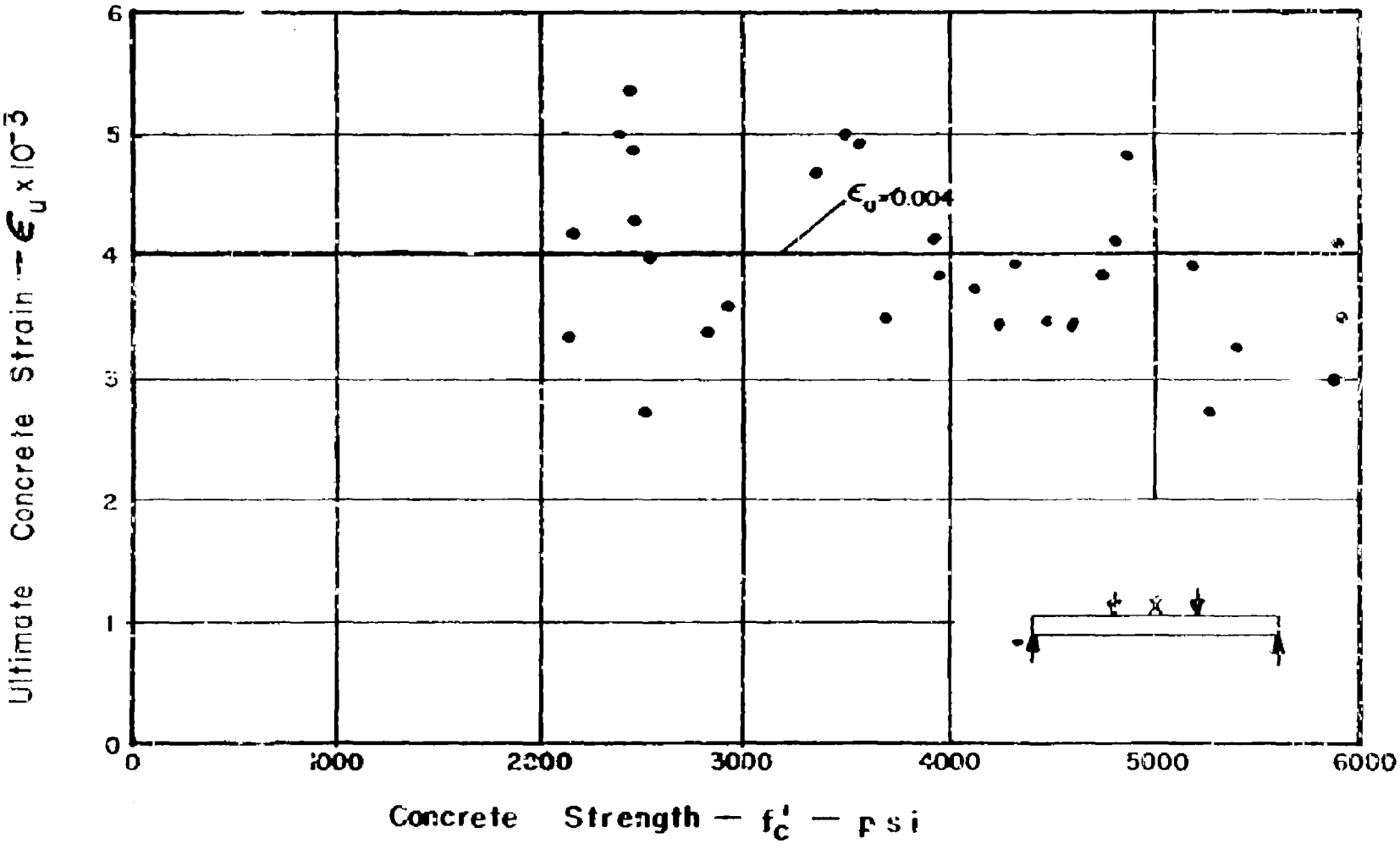

FIG.18 ULTIMATE CONCRETE STRAIN vs CONCRETE STRENGTH

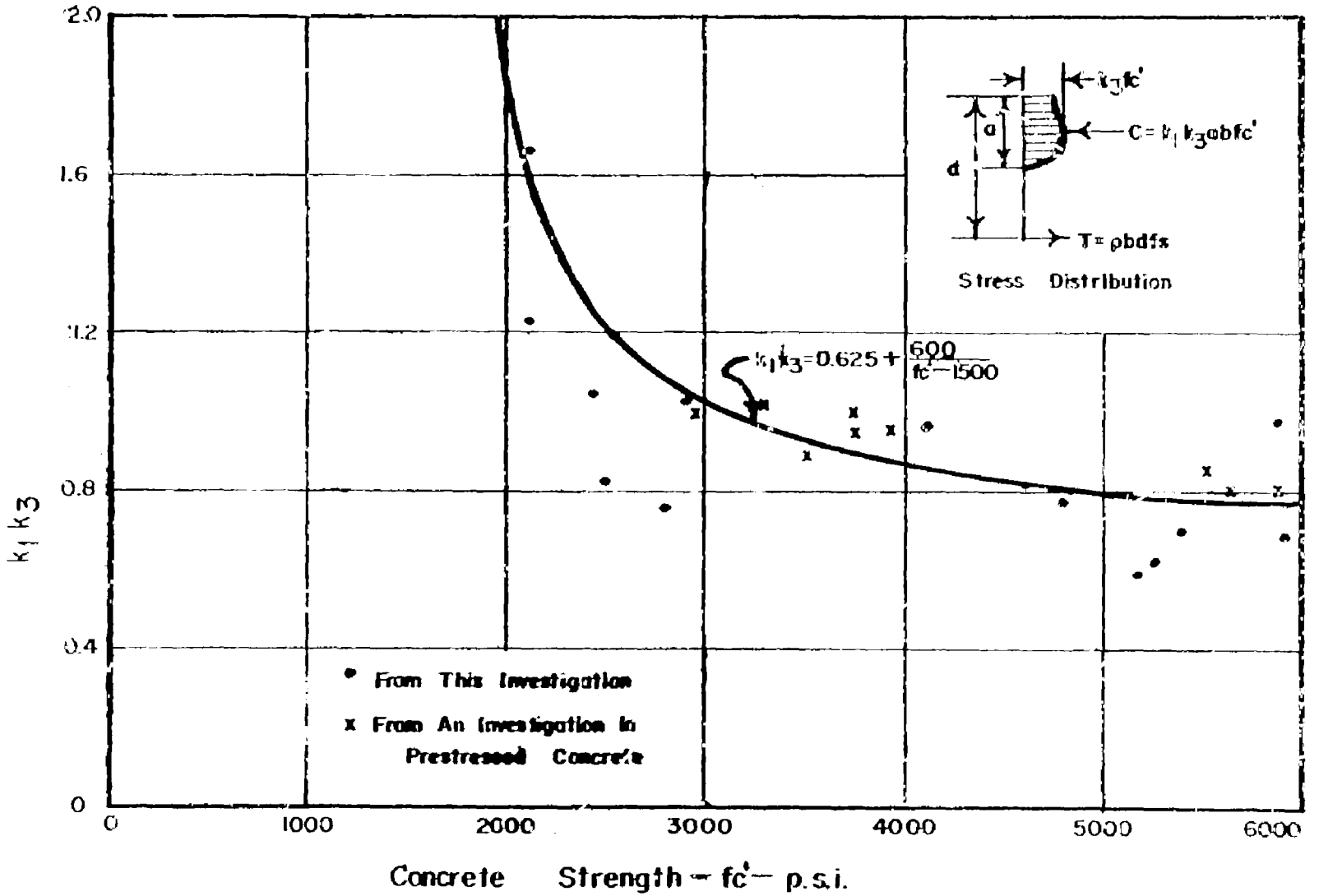

FIG.19 $K_1 K_3$ VS CONCRETE STRENGTH

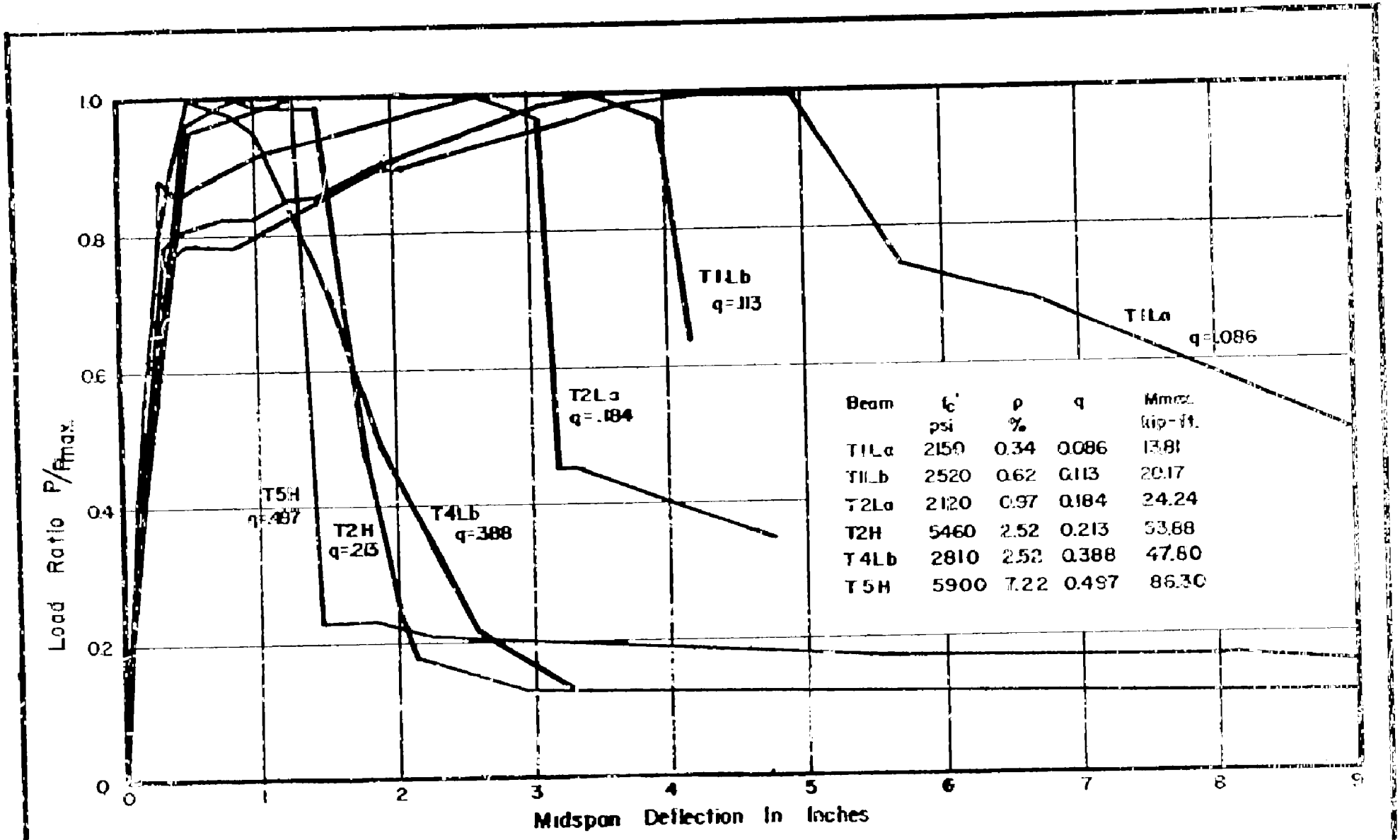

FIG. 20 EFFECT OF q ON THE DROP-OFF IN LOAD-CARRYING CAPACITY

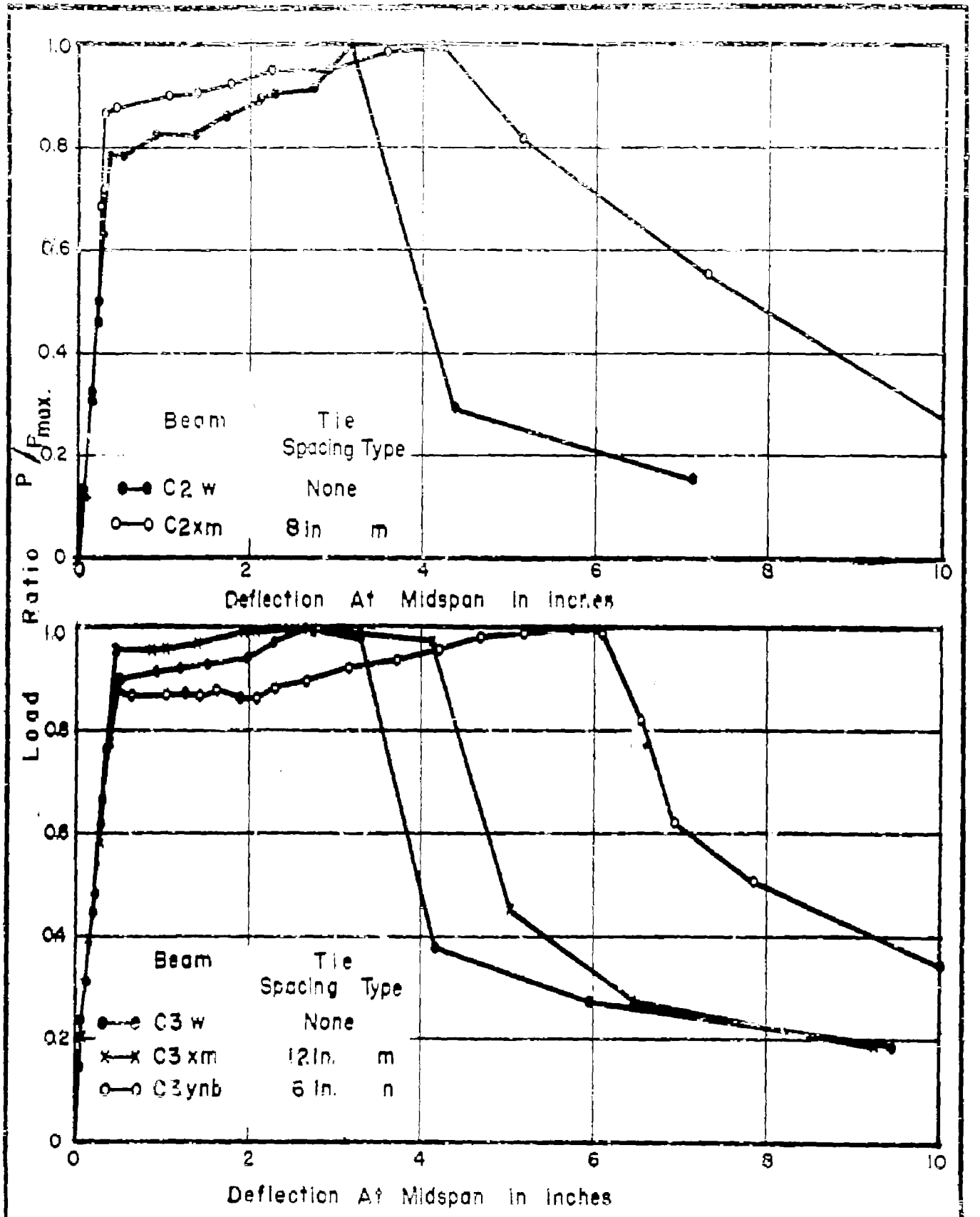

FIG. 21 EFFECT OF METHODS OF TYING COMPRESSION REINFORCEMENT ON LOAD-CARRYING CAPACITY

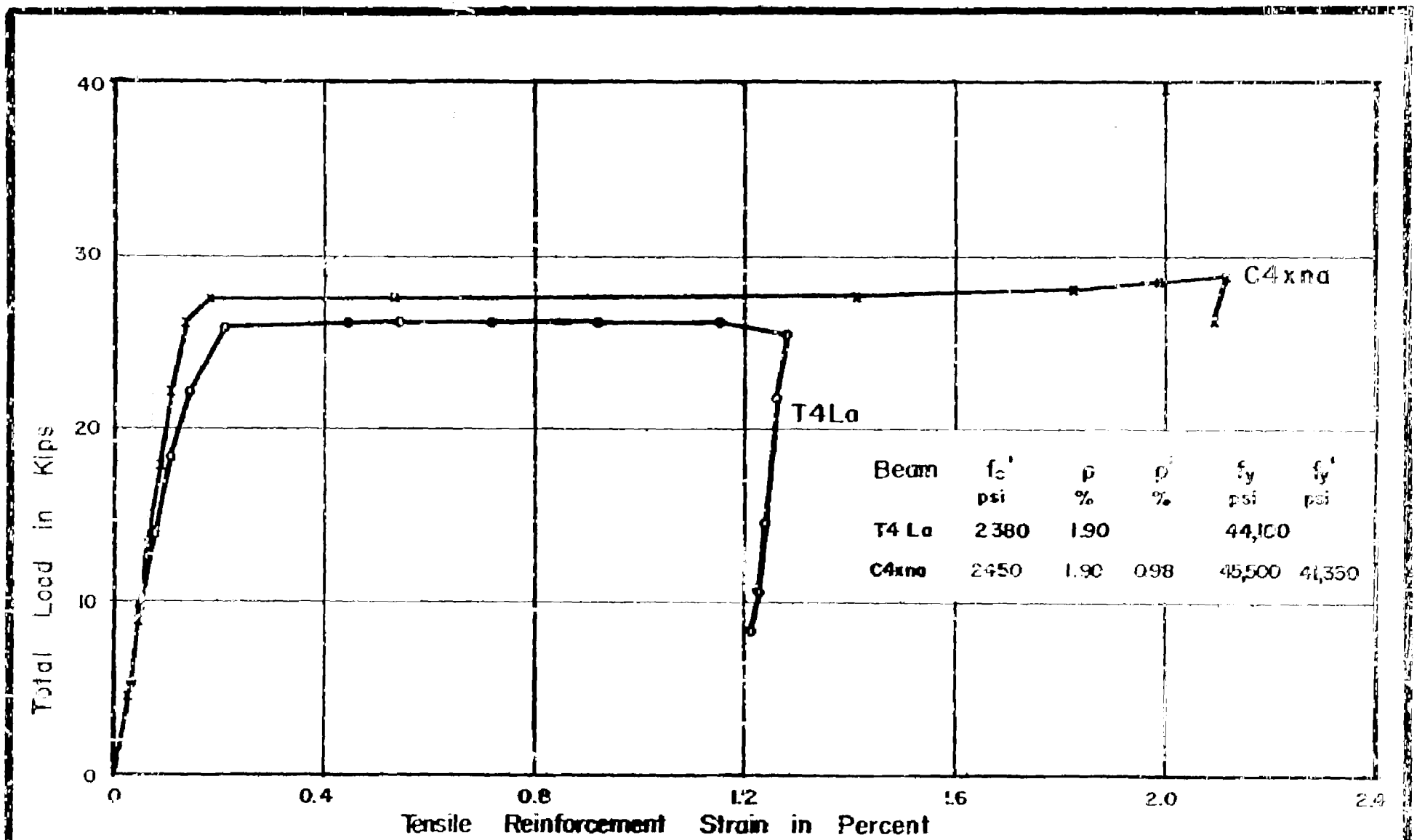

FIG.22 COMPARISON OF TENSION REINFORCEMENT STRAINS OF BEAMS WITH AND WITHOUT COMPRESSION REINFORCEMENT

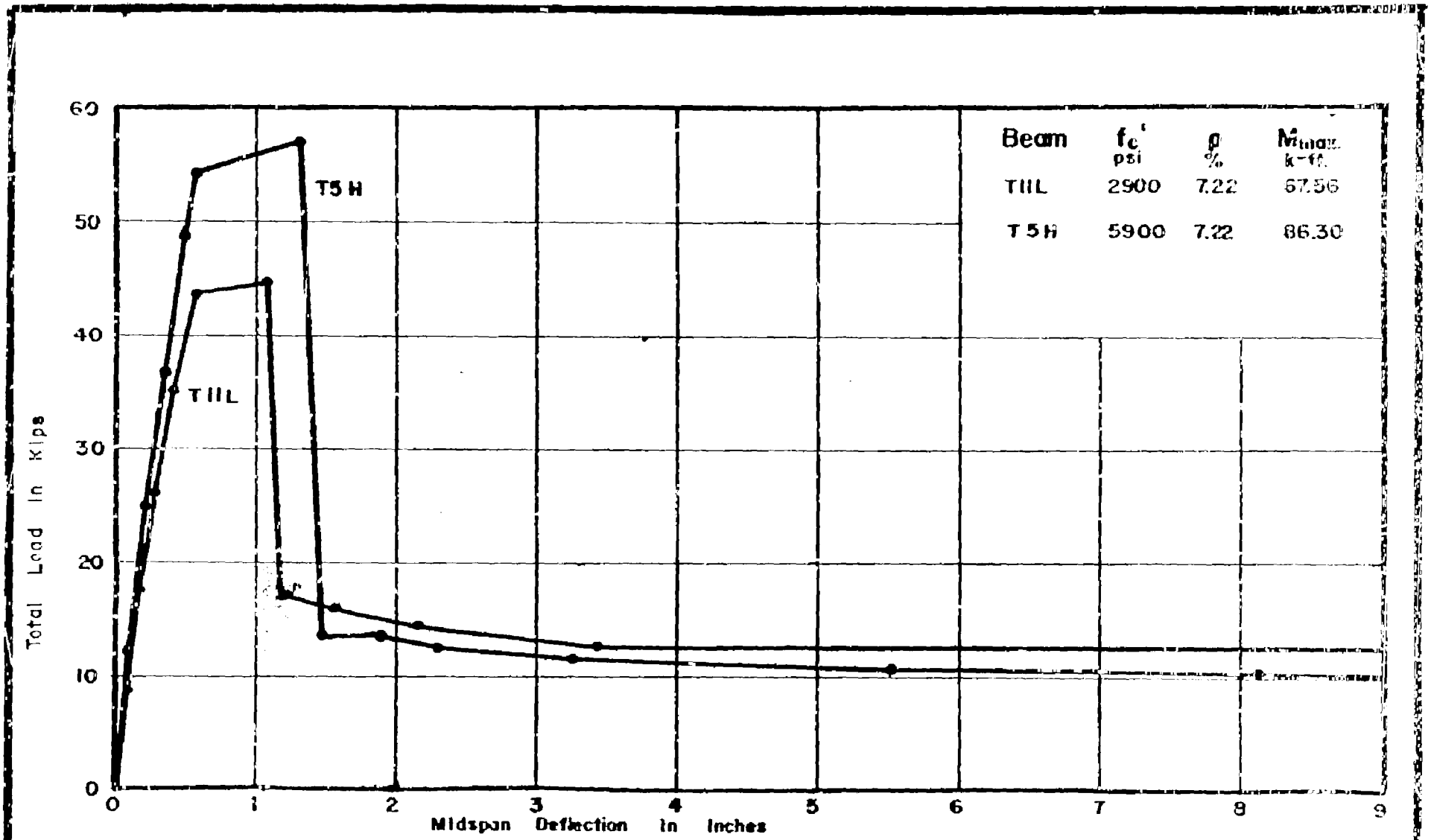

FIG. 23 EFFECT OF CONCRETE STRENGTH ON LOAD DEFLECTION-COMPRESSION FAILURES

North Side of Beam

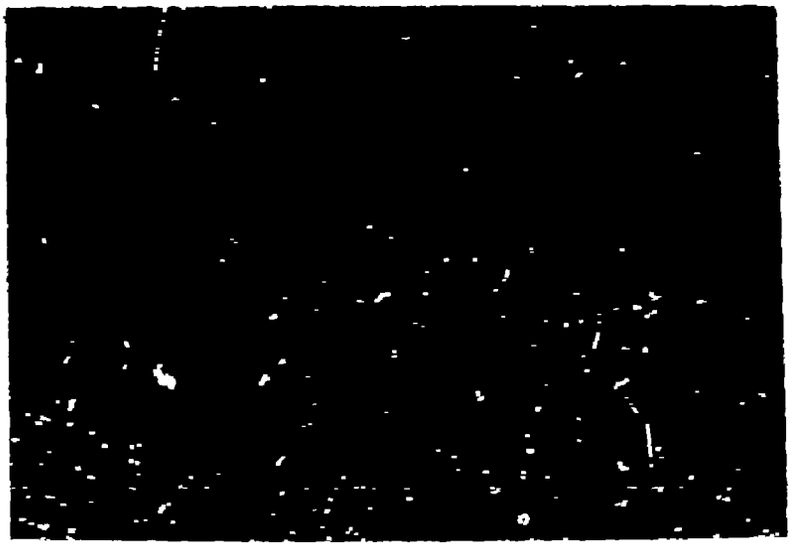

South Side of Beam

FIG. 24 VIEWS OF BEAM T2Mb
AFTER SHEAR FAILURE

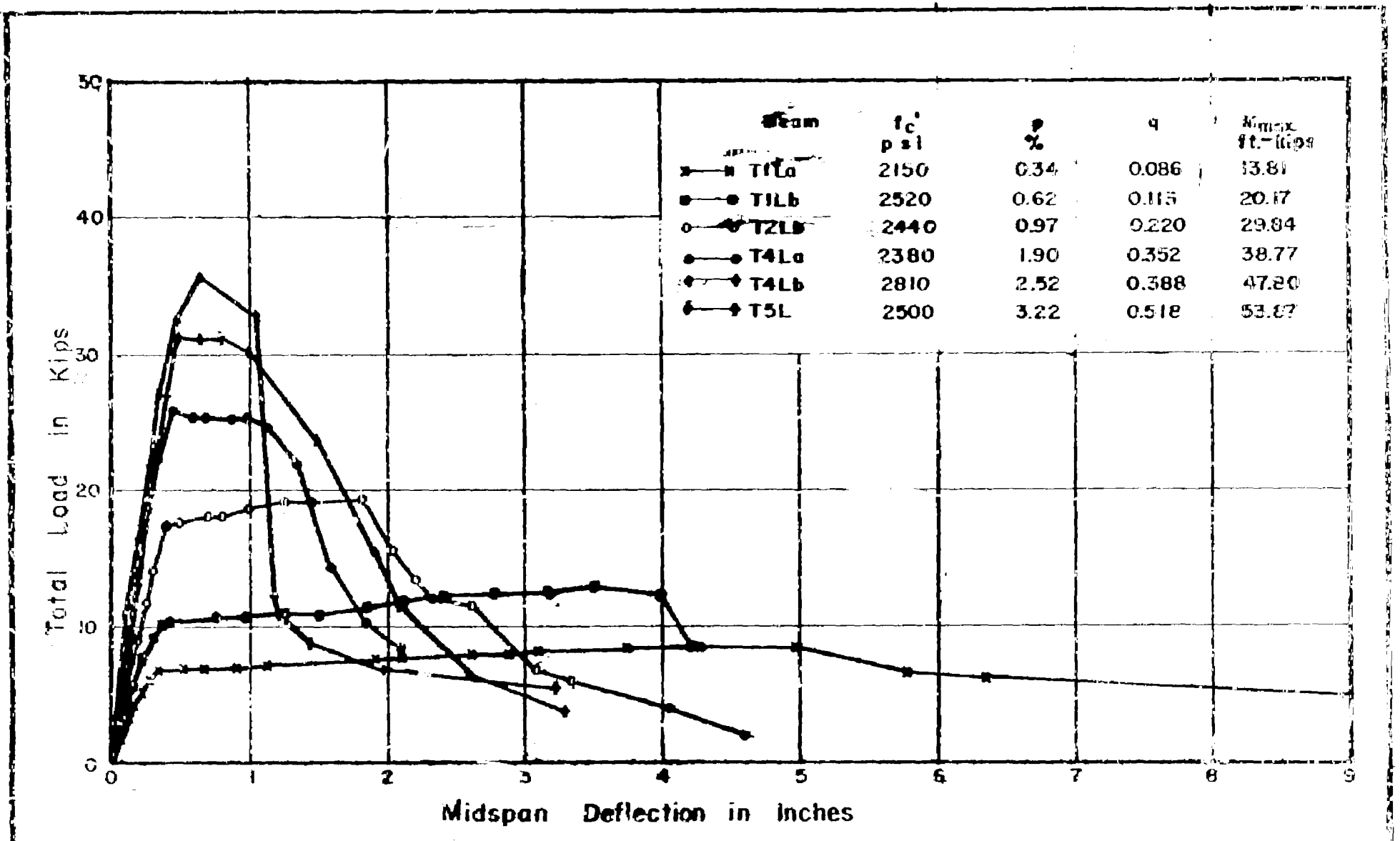

FIG25 EFFECT OF TENSION REINFORCEMENT ON MAXIMUM LOAD CARRYING CAPACITY—TENSILE REINFORCEMENT ONLY

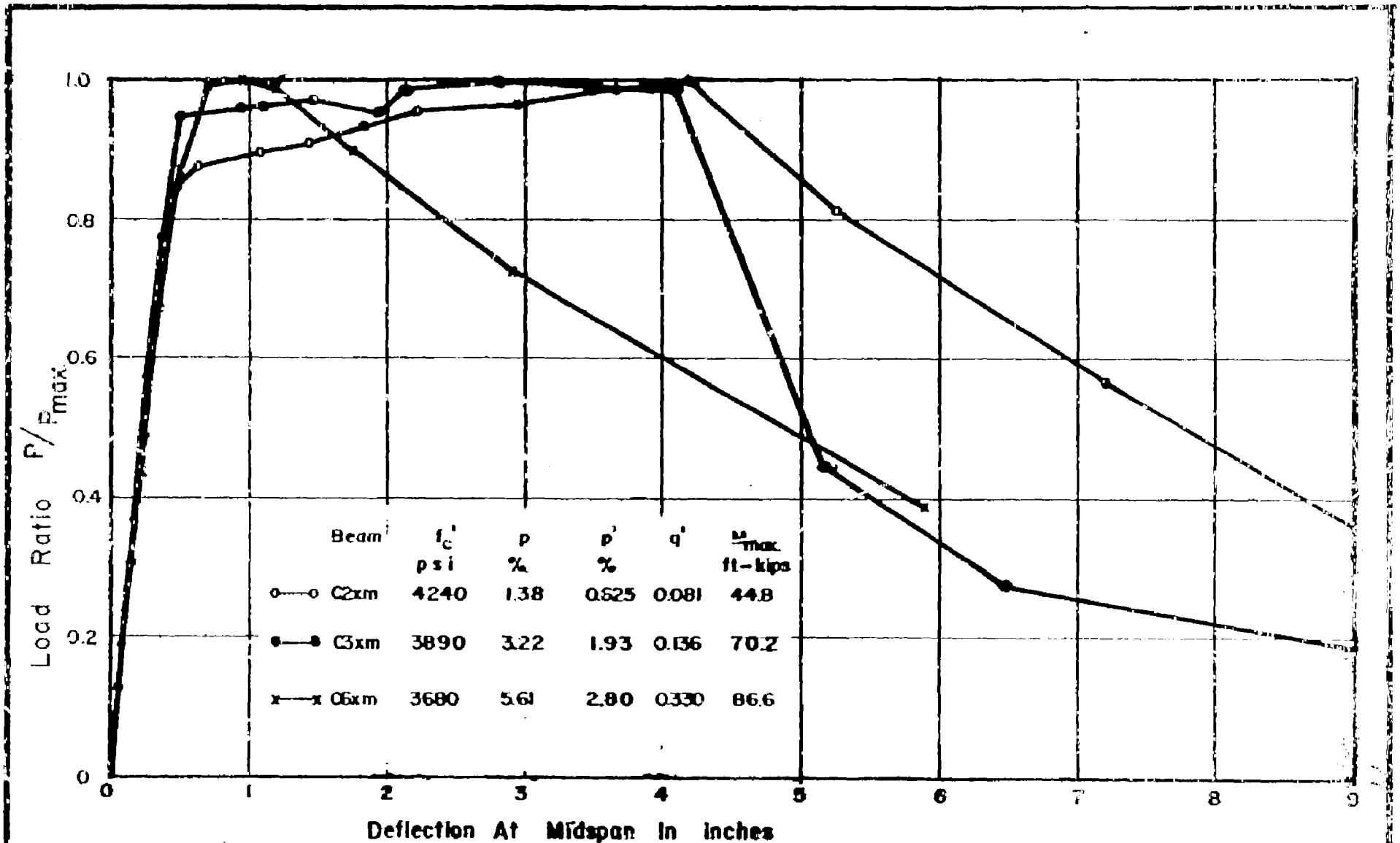

FIG. 26 EFFECT OF q' ON SHAPE OF LOAD — DEFLECTION CURVES

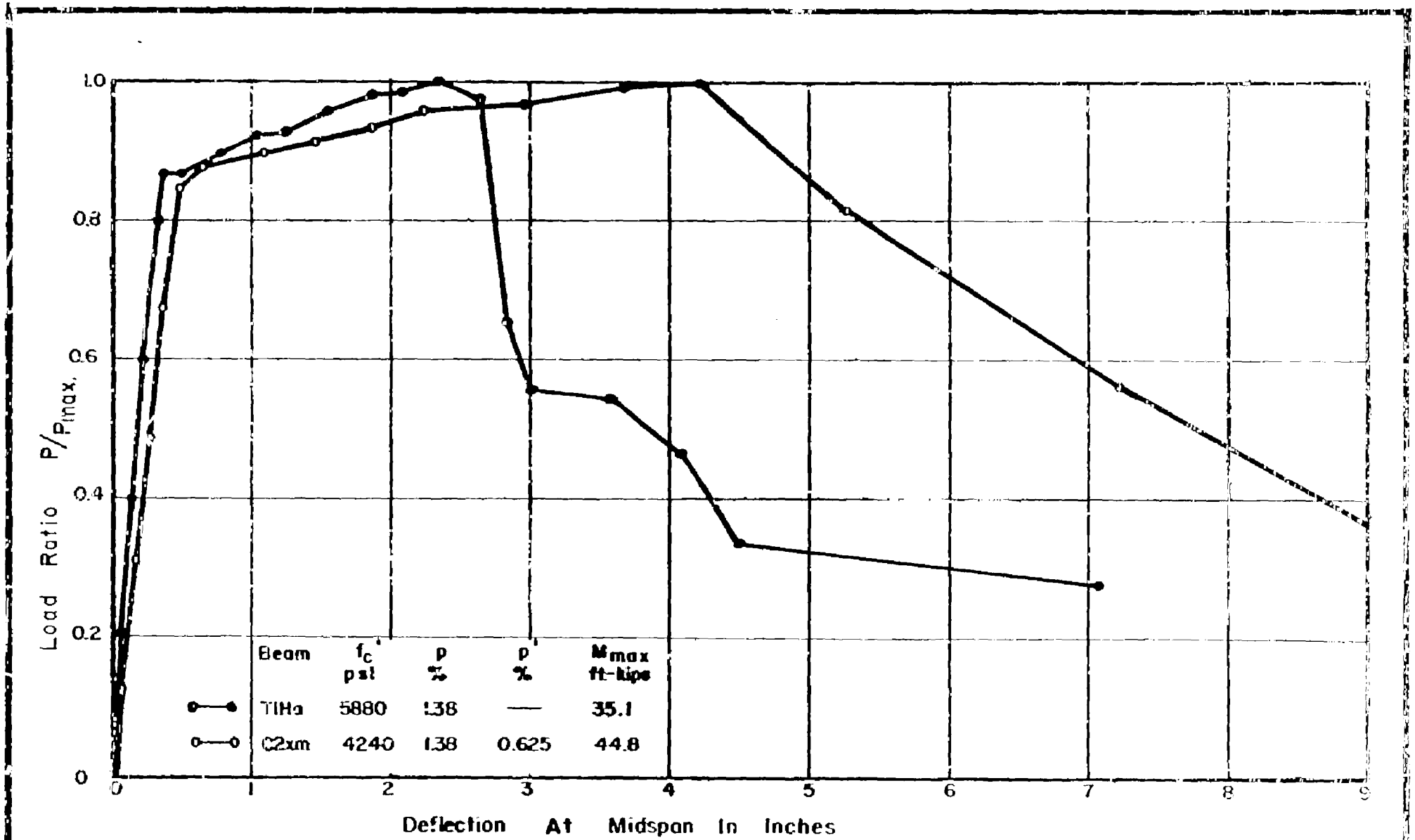

FIG. 27 LOAD-RATIO VS. DEFLECTION FOR BEAMS WITH AND WITHOUT COMPRESSION REINFORCEMENT

Beam C2xm With Effective Ties

Beam C3xm With Ineffective Ties

FIG. 28 VIEWS OF EFFECTIVE AND INEFFECTIVE TIES AFTER BEAM FAILURE

Beam T3Ma With Clamp-on Stirrups

Beam T5L With Conventional Stirrups

FIG. 29 EFFECT OF TYPE OF STIRRUPS ON CRACK DISTRIBUTION

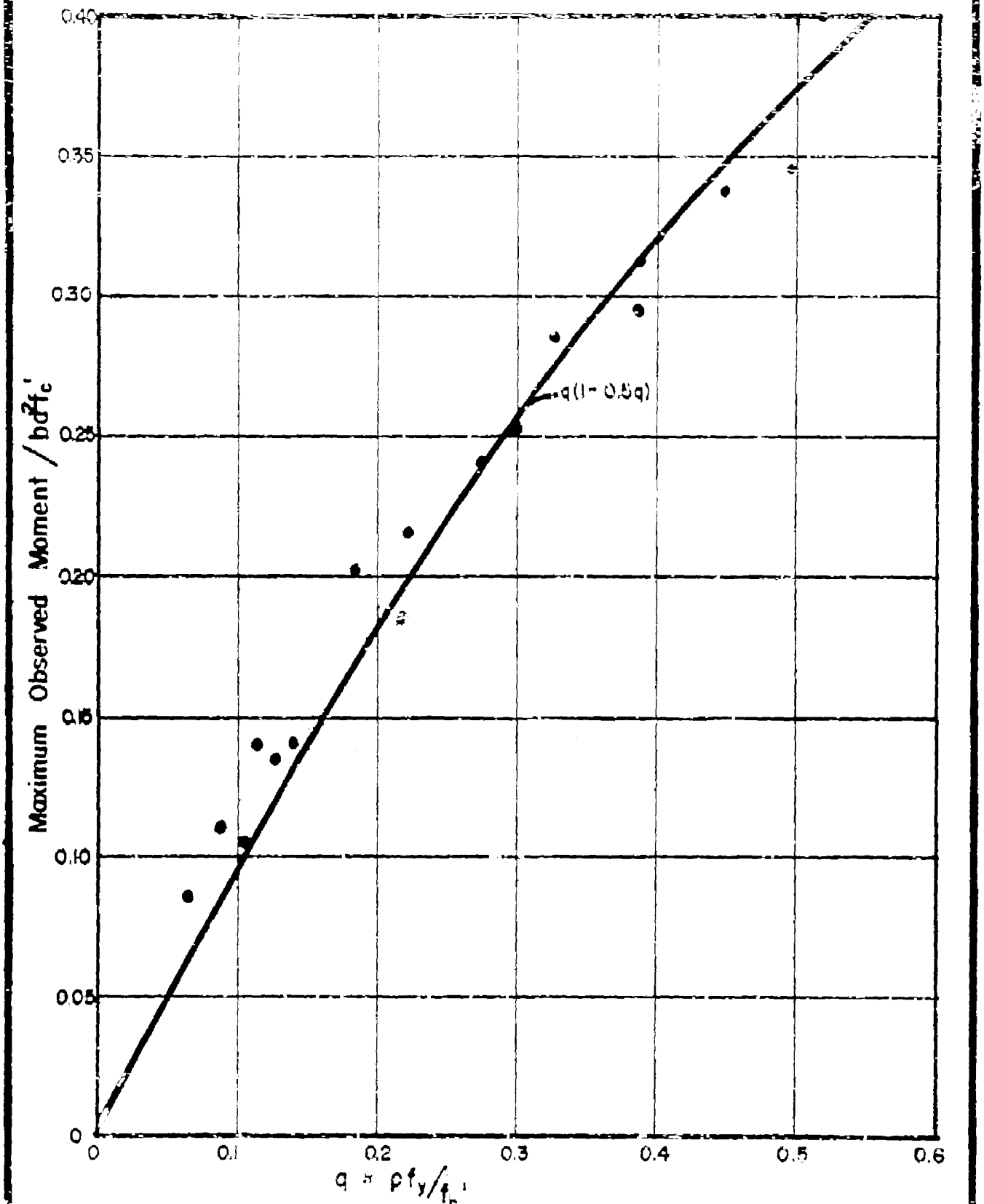

FIG.30 COMPARISON OF THEORETICAL RESISTING MOMENTS WITH EXPERIMENTAL DATA --USING f_y

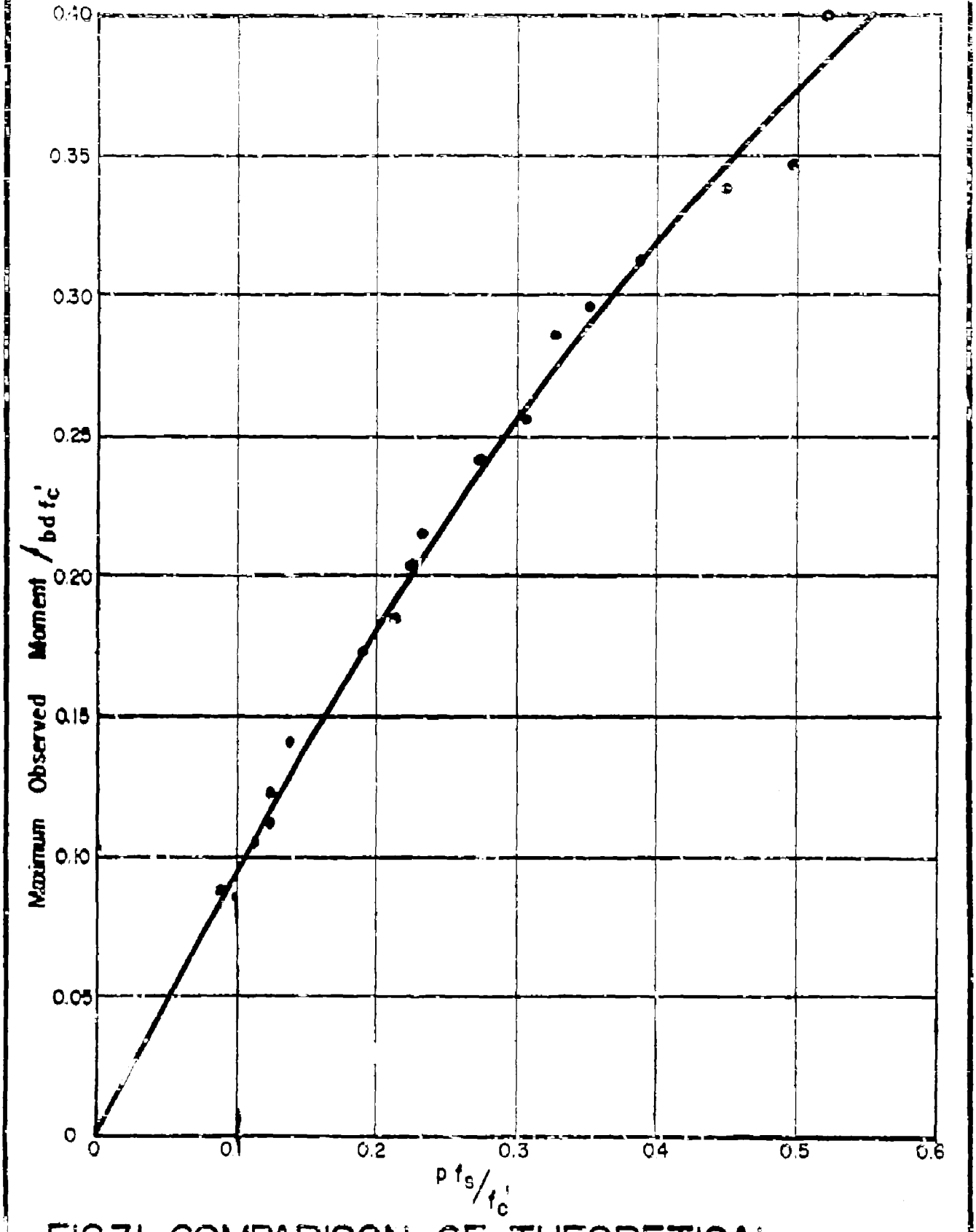

FIG.31 COMPARISON OF THEORETICAL RESISTING MOMENTS WITH EXPERIMENTAL DATA - USING COMPUTED f_s

APPENDIX

GRAPHICAL PRESENTATION OF EXPERIMENTAL DATA

The appendix contains the following plots for each beam tested:

App. Fig. 1 - 33

(a) Load vs. midspan deflection

(b) Load vs. load-point deflection

App. Fig. 34 - 66

(a) Deflections along beam at various load increments

App. Fig. 67 - 99

(a) Load vs. tension steel strain at midspan

(b) Load vs. concrete strain on top of beam at midspan

App. Fig. 100 - 132

(a) Ratio of applied load to maximum load attained in test vs. midspan deflection

(b) Ratio of applied load to maximum load attained in test vs. load-point deflection

App. Fig. 133 - 165

(a) Ratio of applied moment to maximum moment attained in test vs. angle change at midspan of beam

(b) Ratio of applied moment to maximum moment attained in test vs. deflection at midspan with respect to the load points.

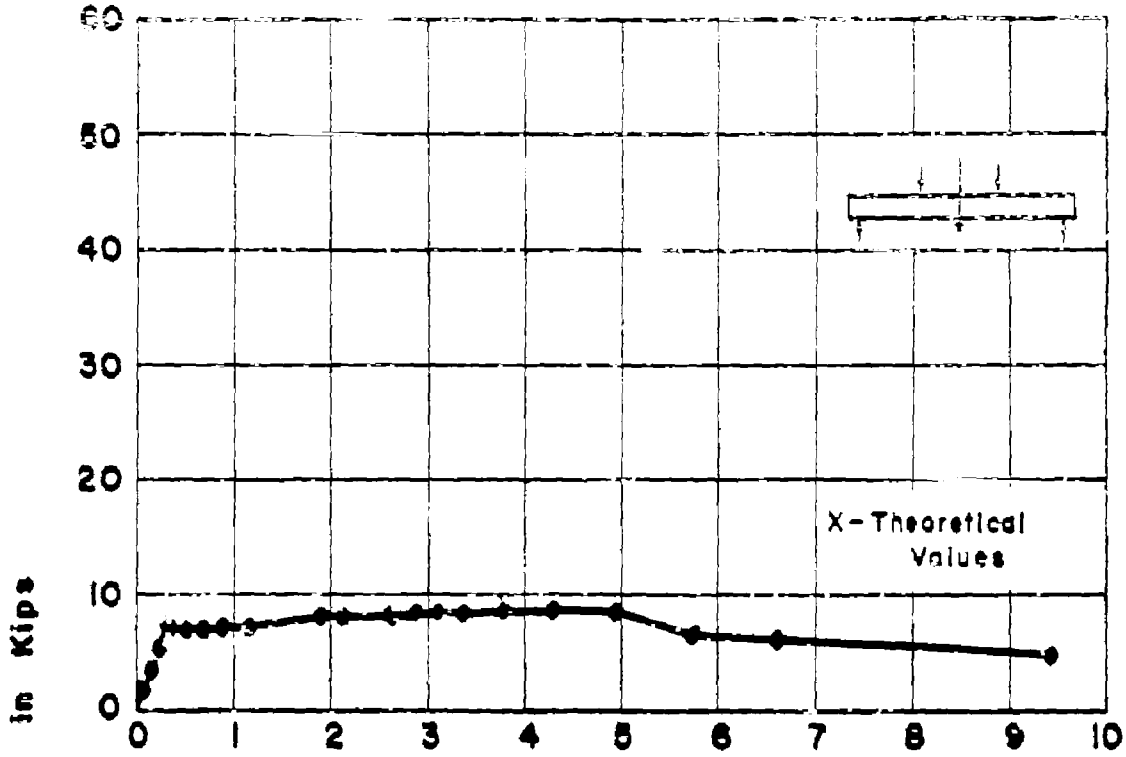

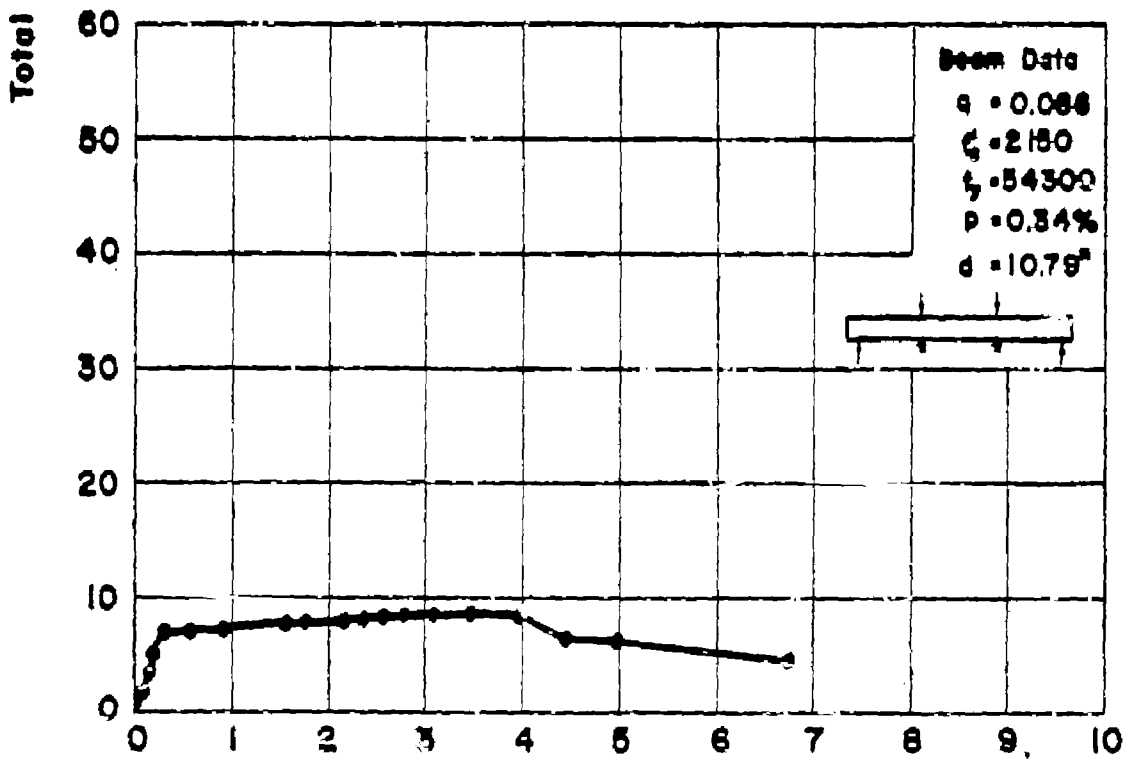

APP. FIG. I LOAD-DEFLECTION CURVES FOR BEAM NO. T1L-a

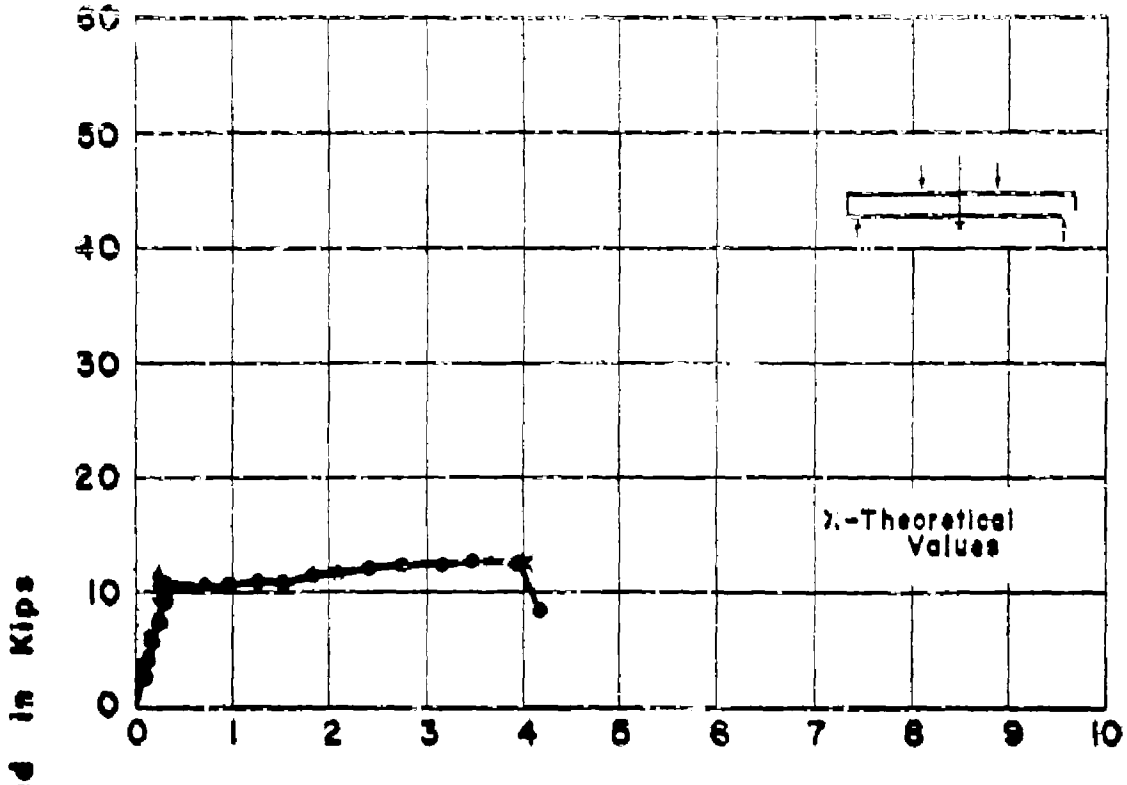

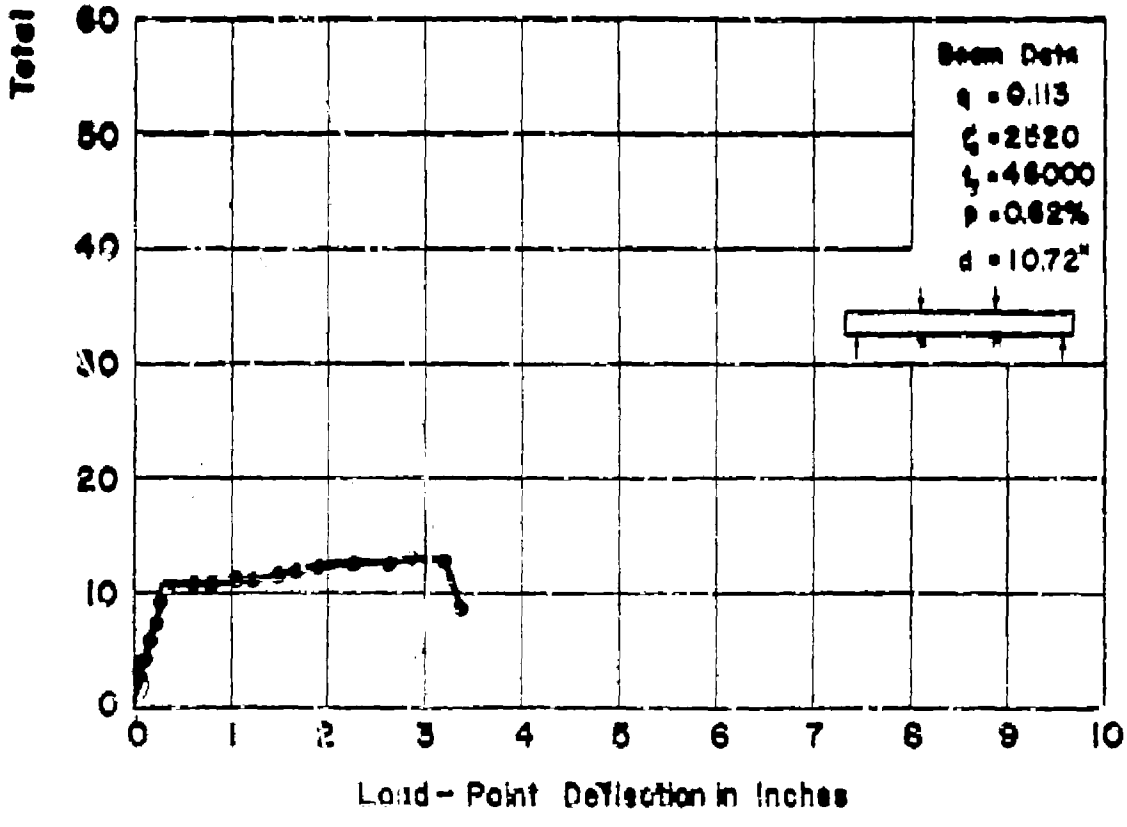

APP. FIG. 2 LOAD-DEFLECTION CURVES FOR BEAM NO. T1L5

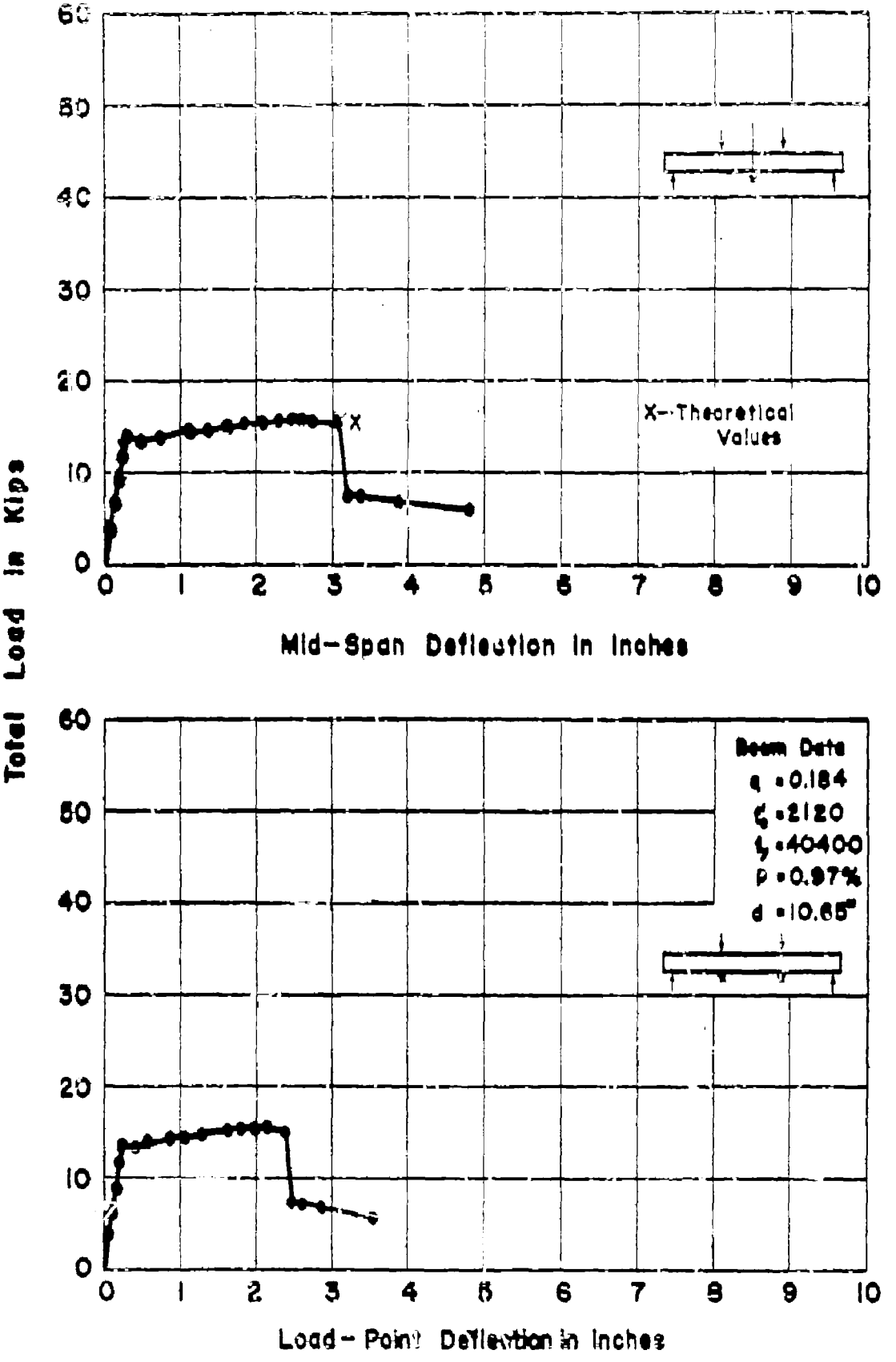

APP. FIG. 3 LOAD-DEFLECTION CURVES FOR BEAM NO. T2La

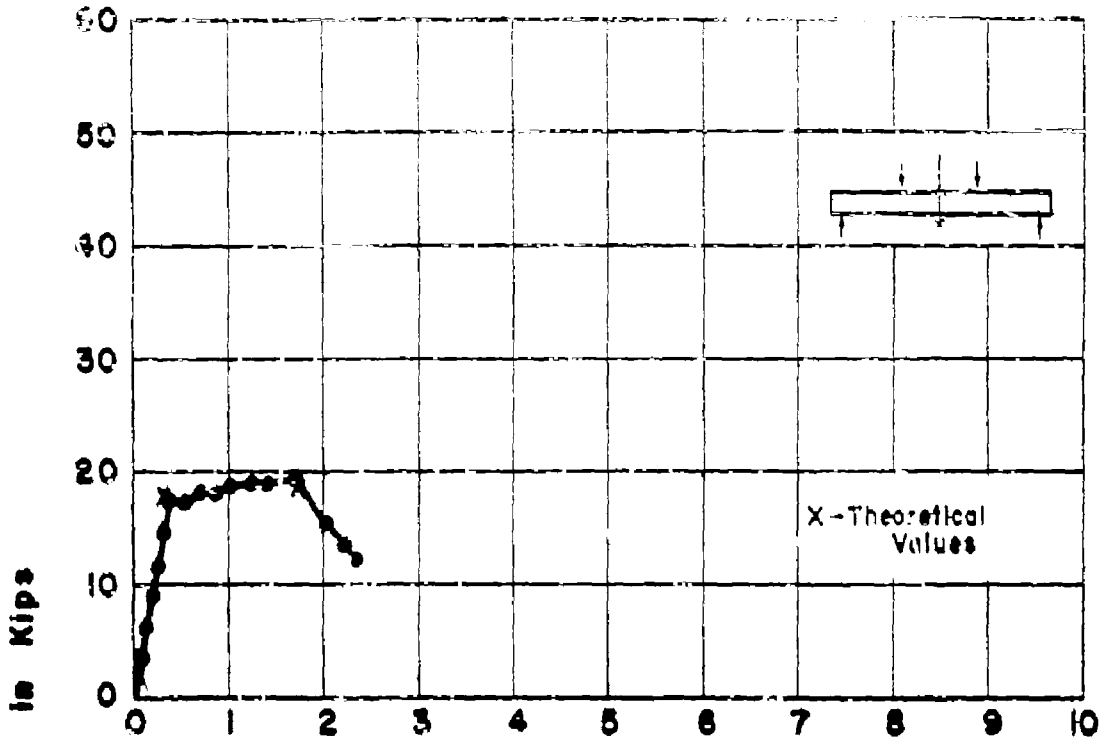

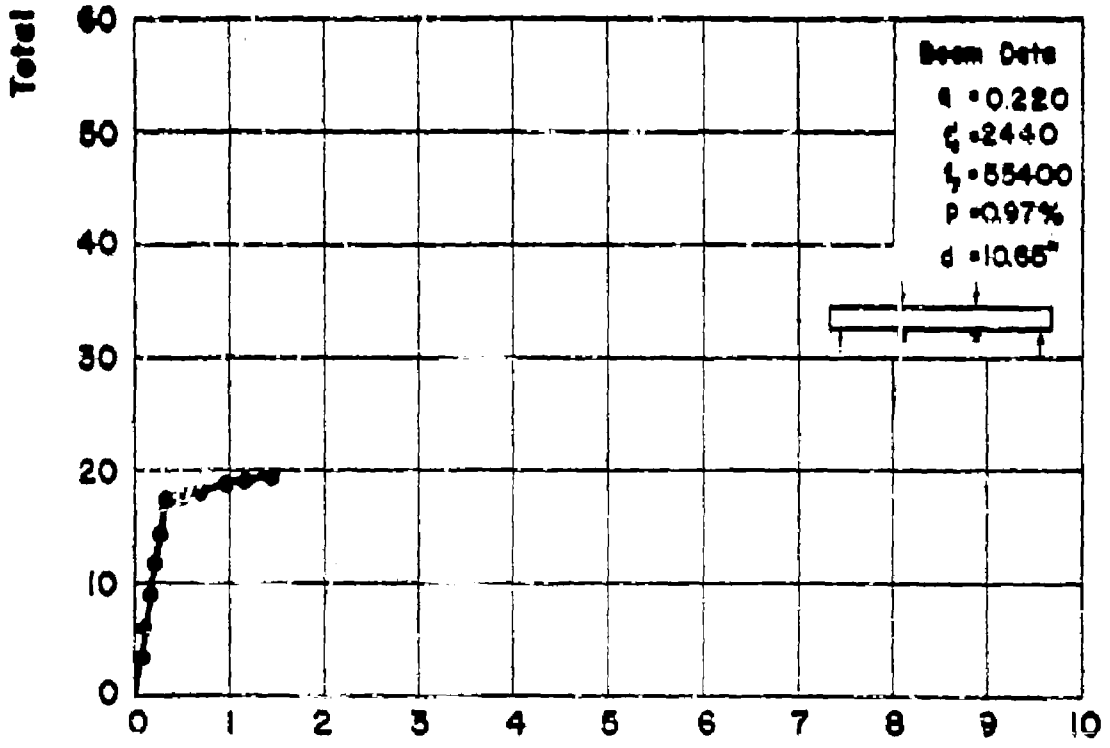

APP. FIG. 4 LOAD-DEFLECTION CURVES FOR BEAM NO. T2Lb

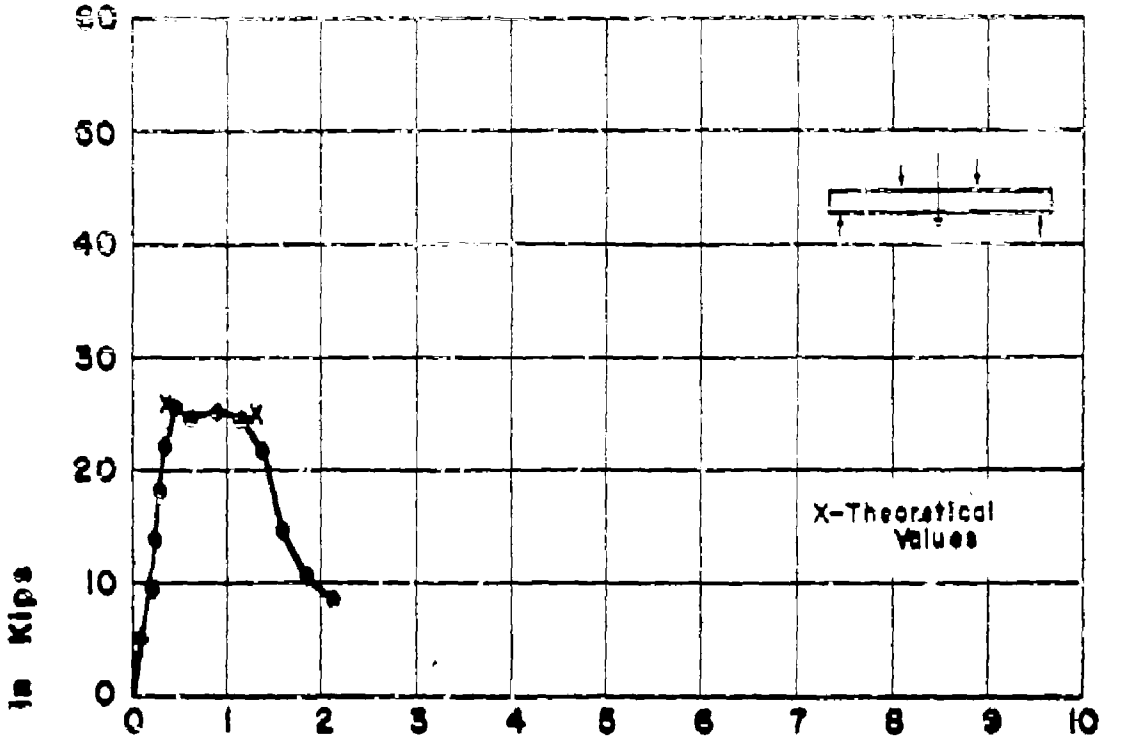

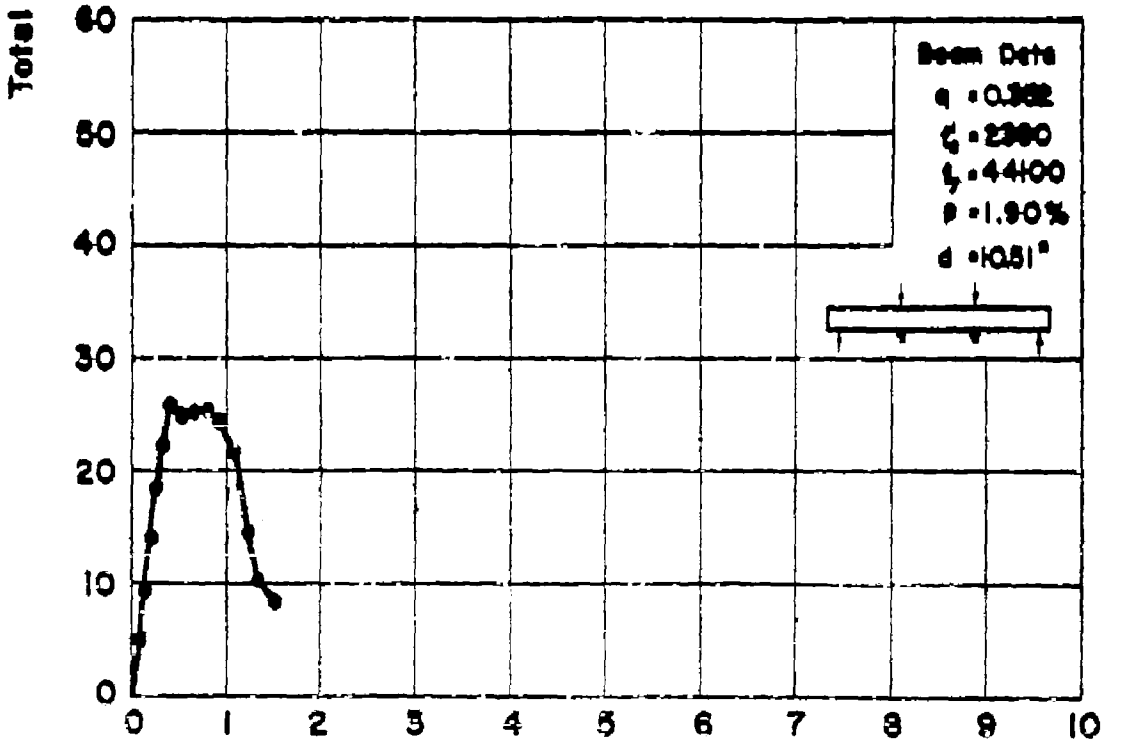

APP. FIG. 5 LOAD-DEFLECTION CURVES FOR BEAM NO. T4Lc

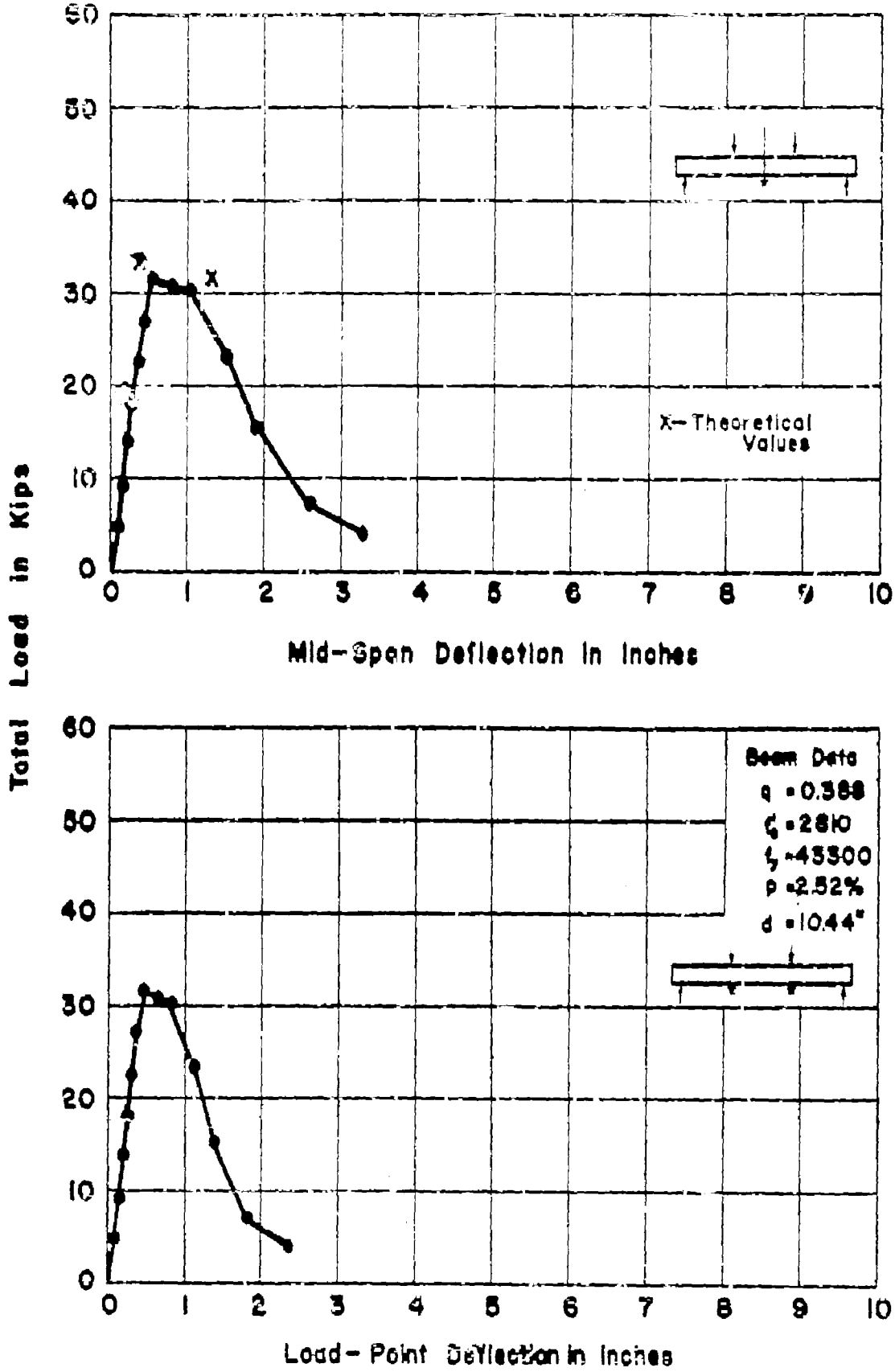

APP. FIG. 6 LOAD-DEFLECTION CURVES FOR BEAM NO. T4Lb

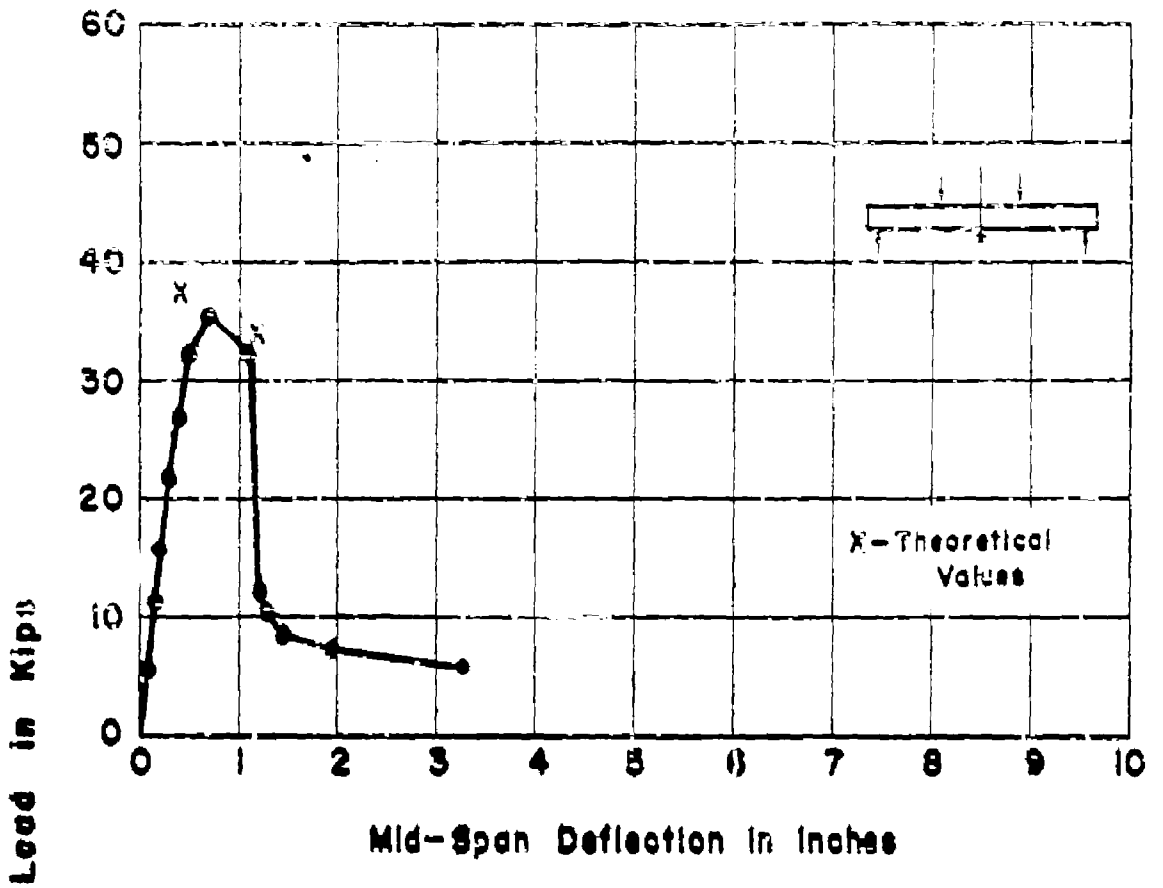

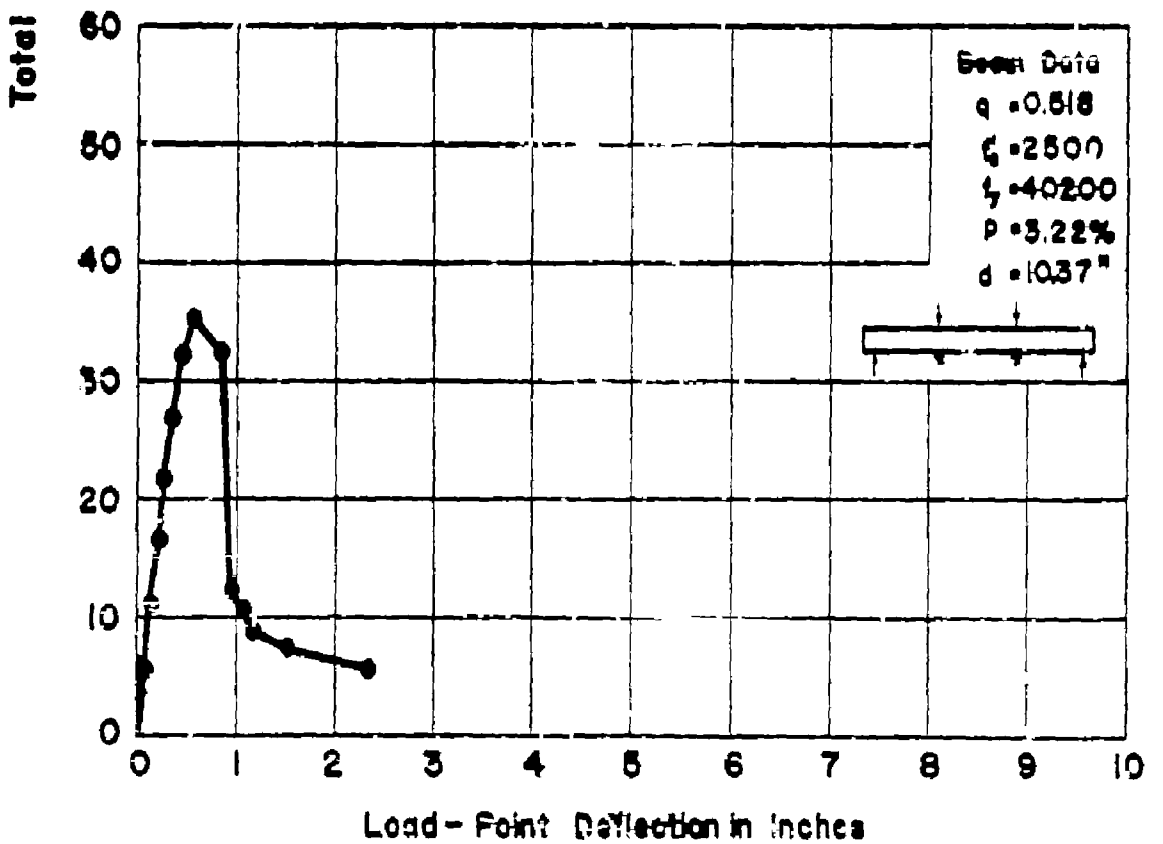

APP. FIG. 7 LOAD-DEFLECTION CURVES FOR BEAM NO. T5L

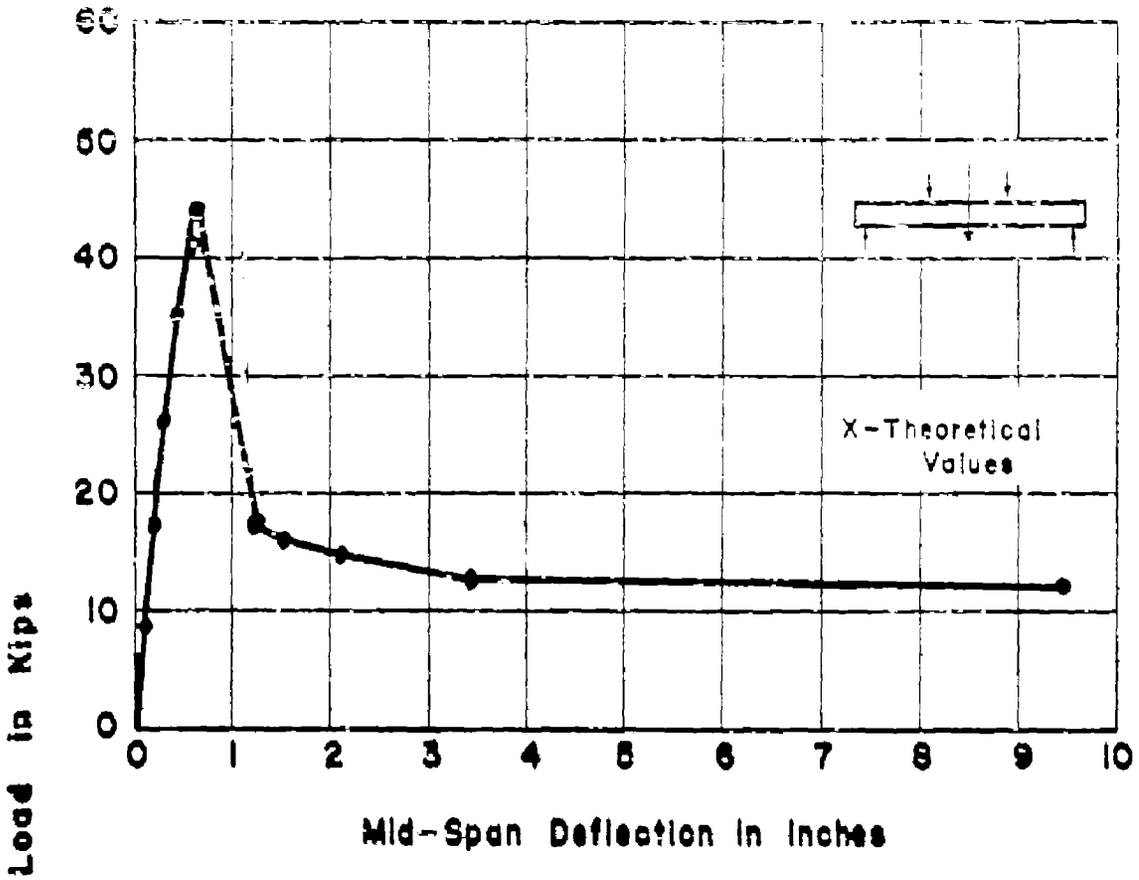

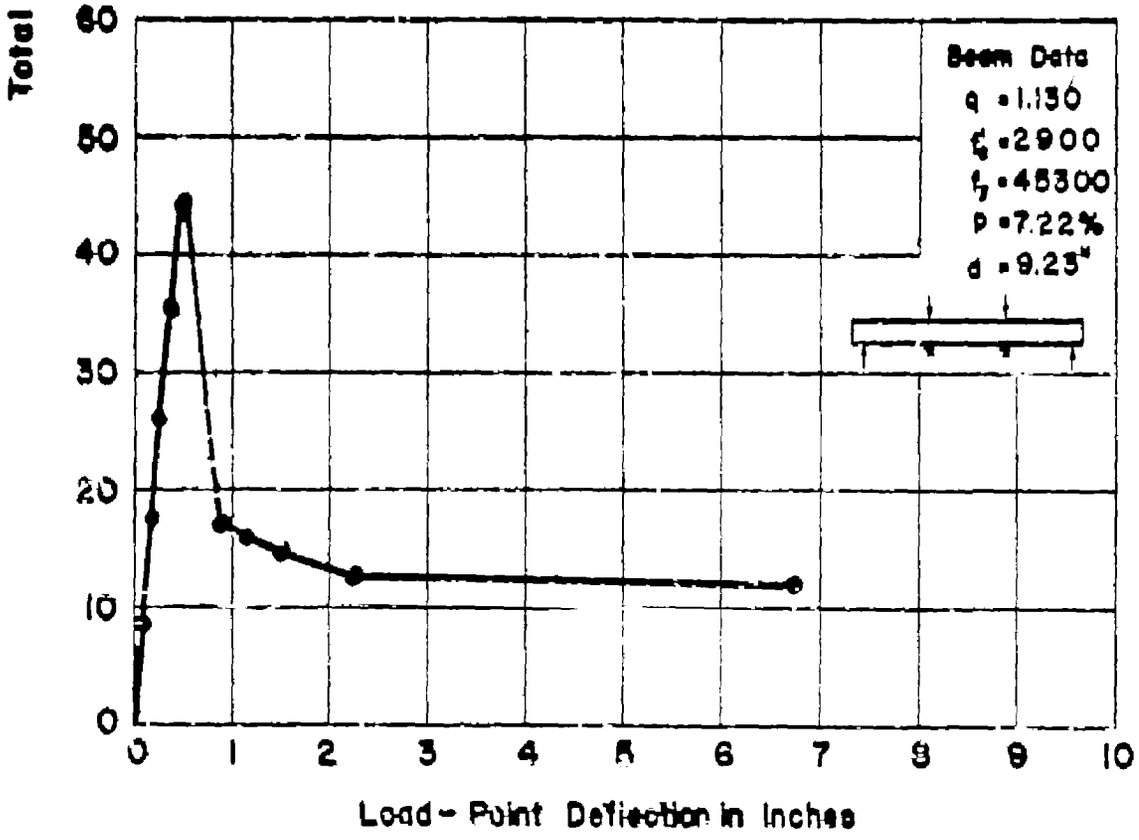

APP. FIG. 8 LOAD-DEFLECTION CURVES FOR BEAM NO. T11L

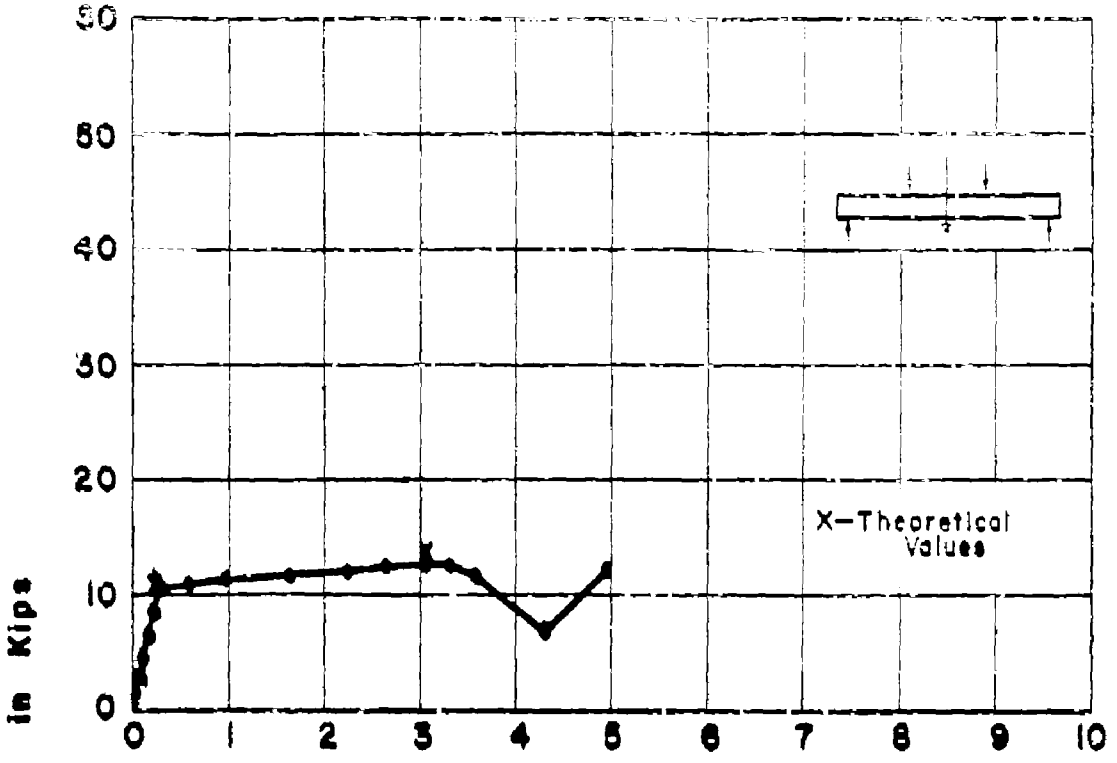

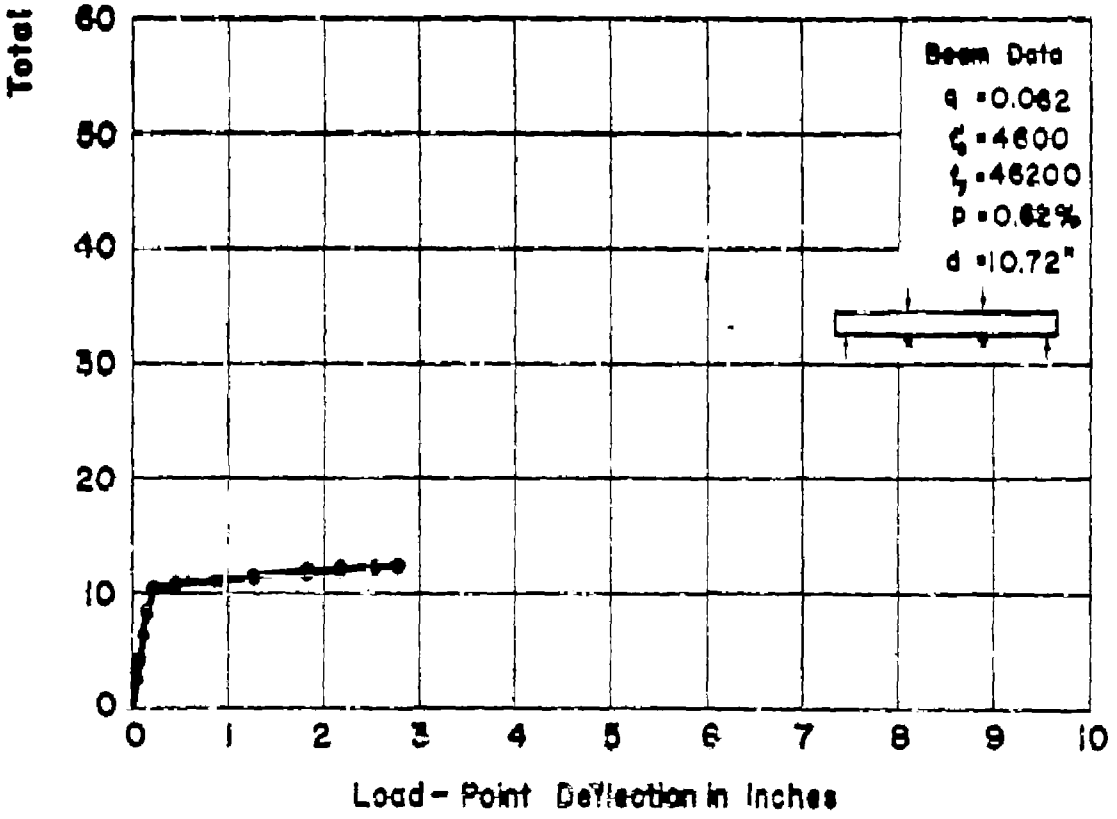

APP. FIG. 9 LOAD-DEFLECTION CURVES FOR BEAM NO. T1Ma

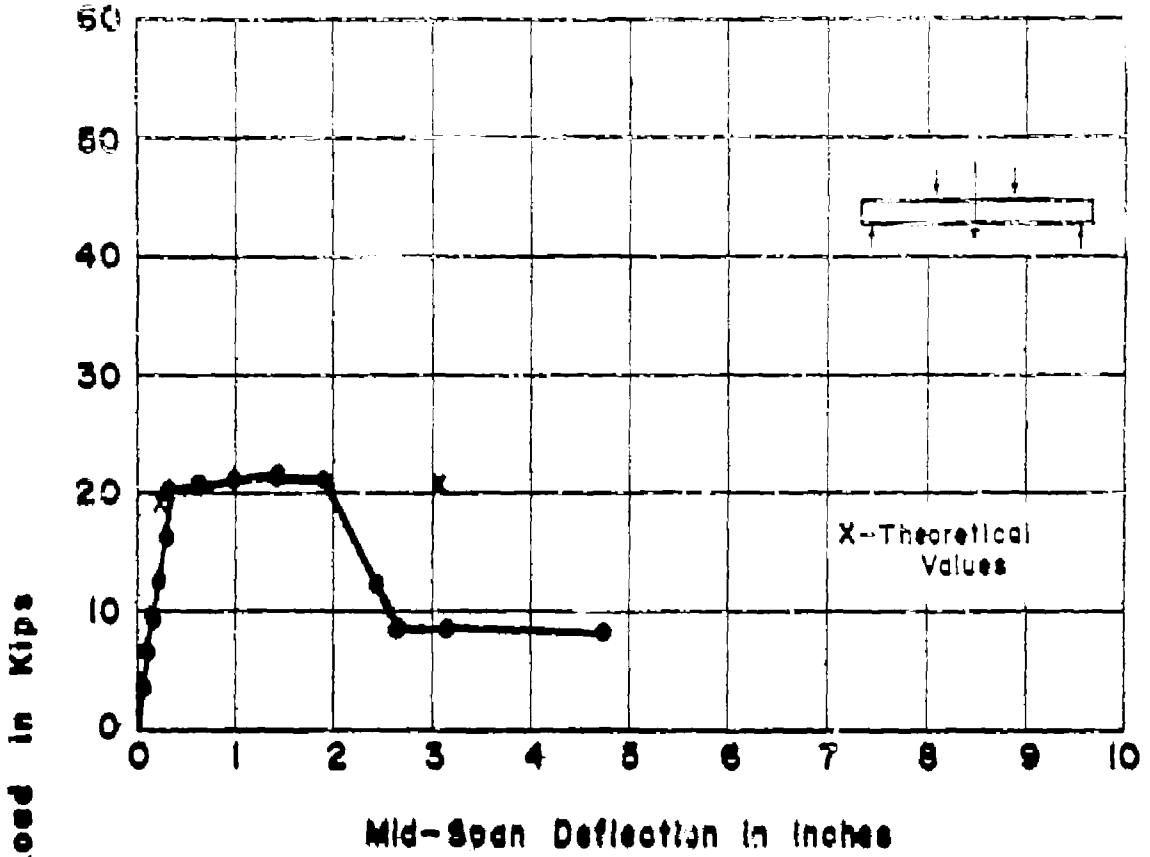

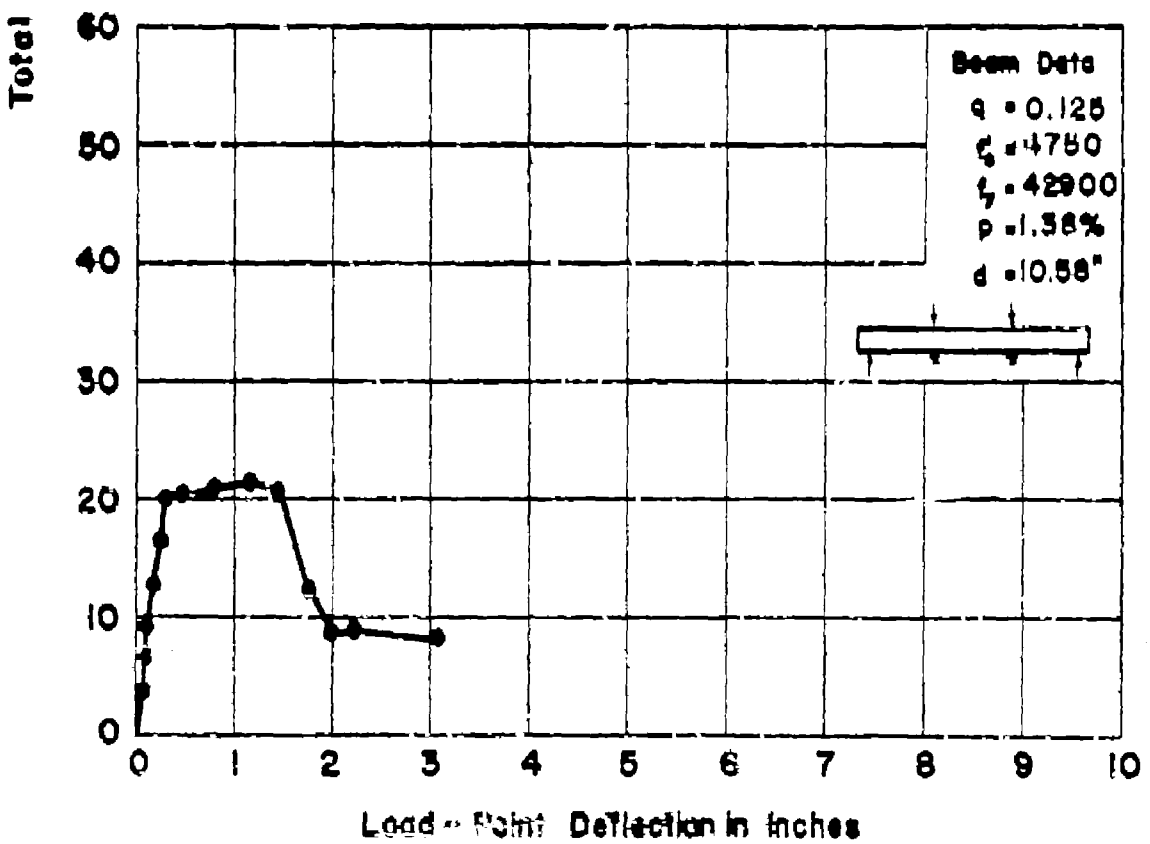

APP. FIG. 10 LOAD-DEFLECTION CURVES FOR BEAM NO. T1M6

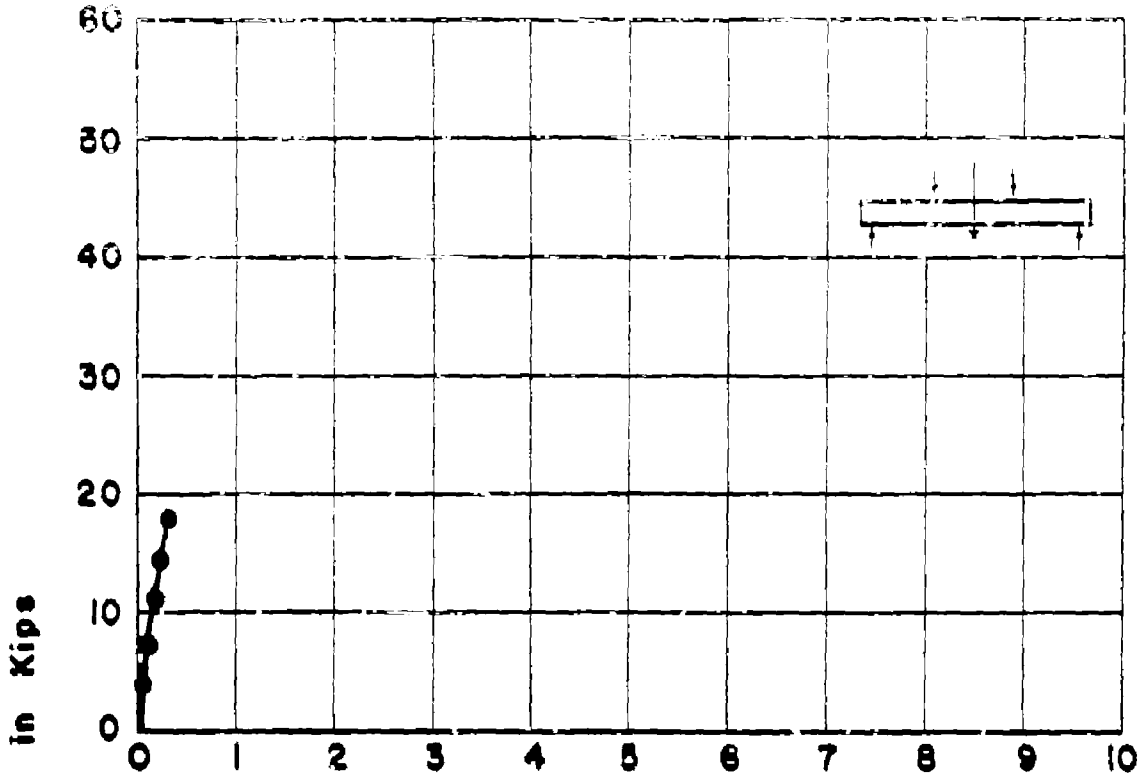

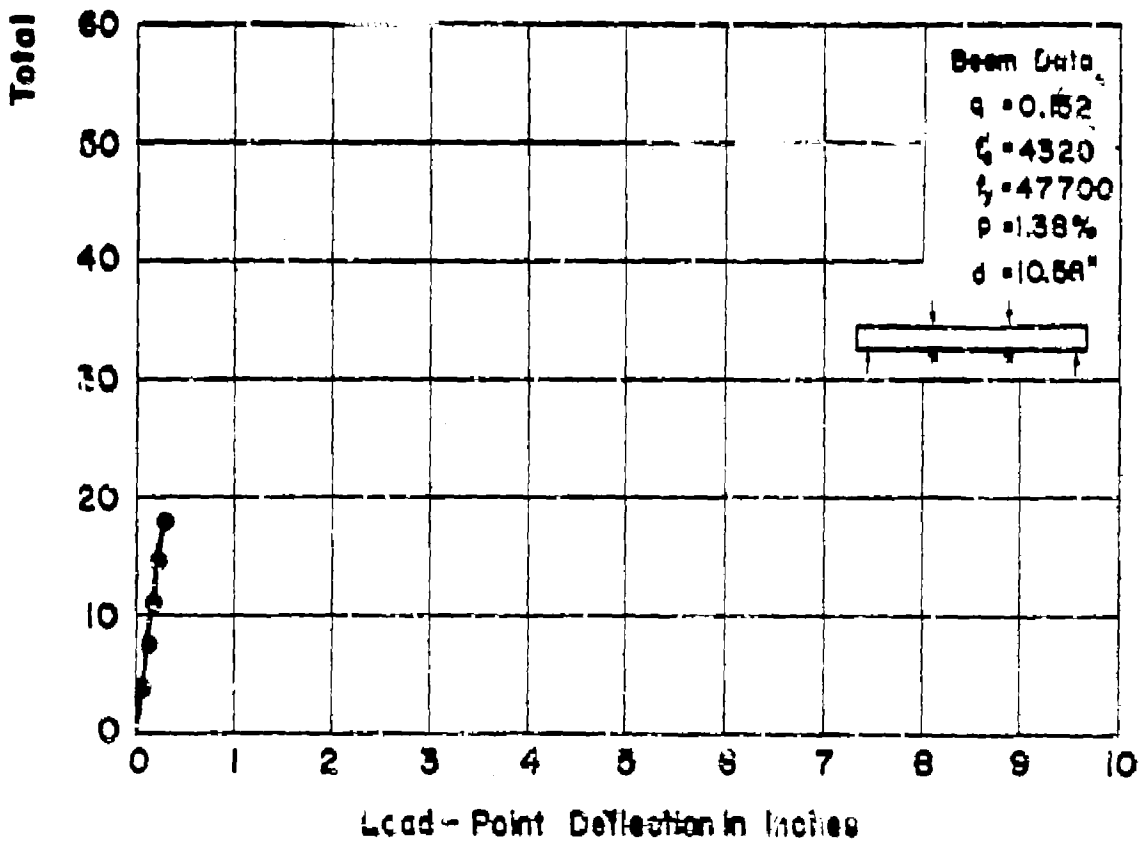

APP. FIG. 11 LOAD-DEFLECTION CURVES FOR BEAM NO. T2M6

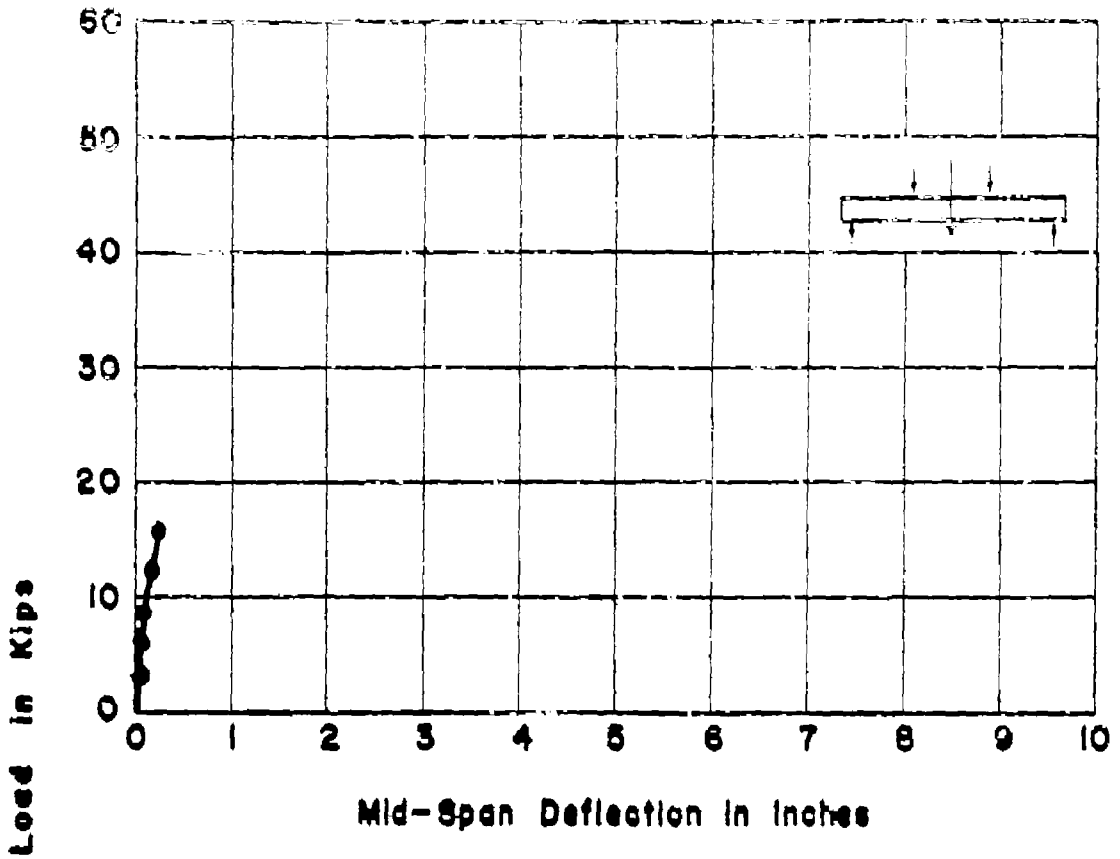

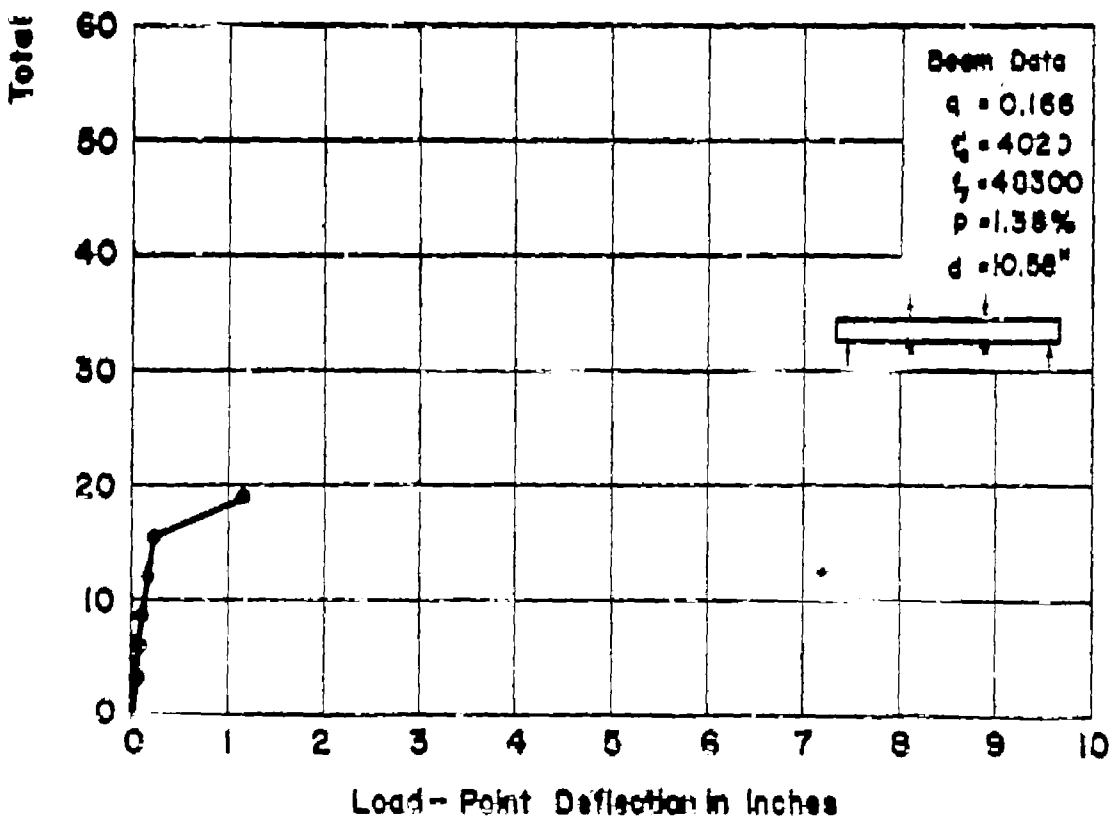

APP. FIG. 12 LOAD-DEFLECTION CURVES FOR BEAM NO. T2Mb

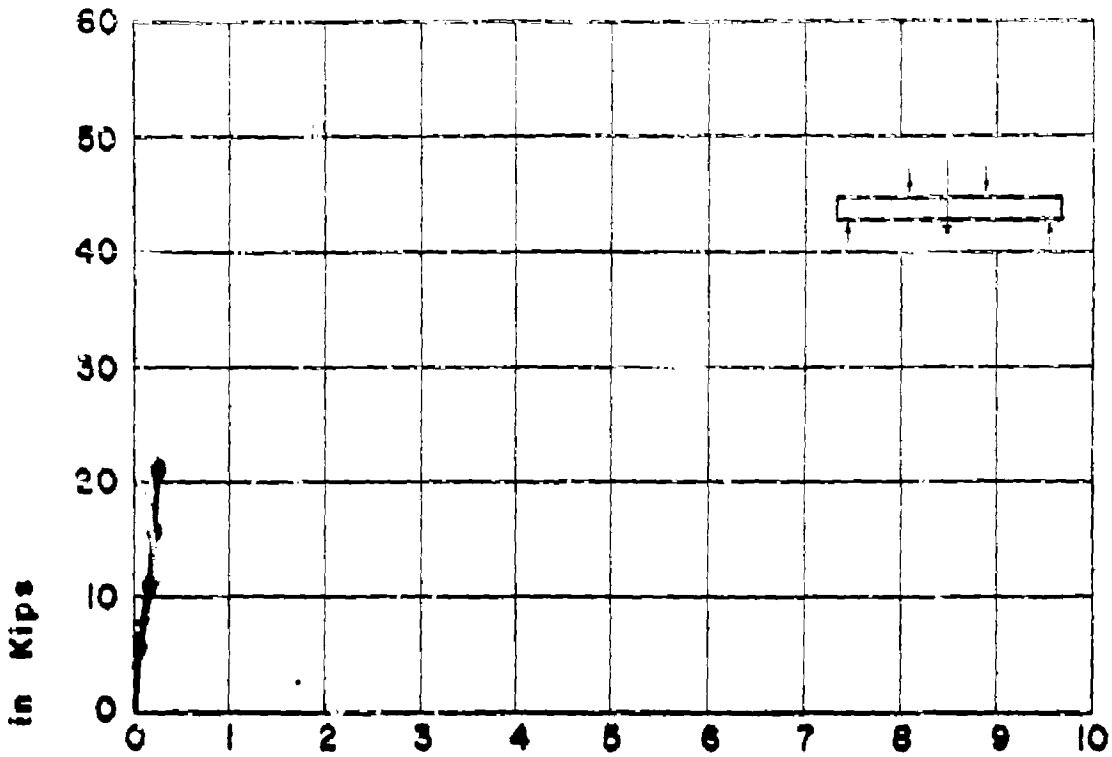

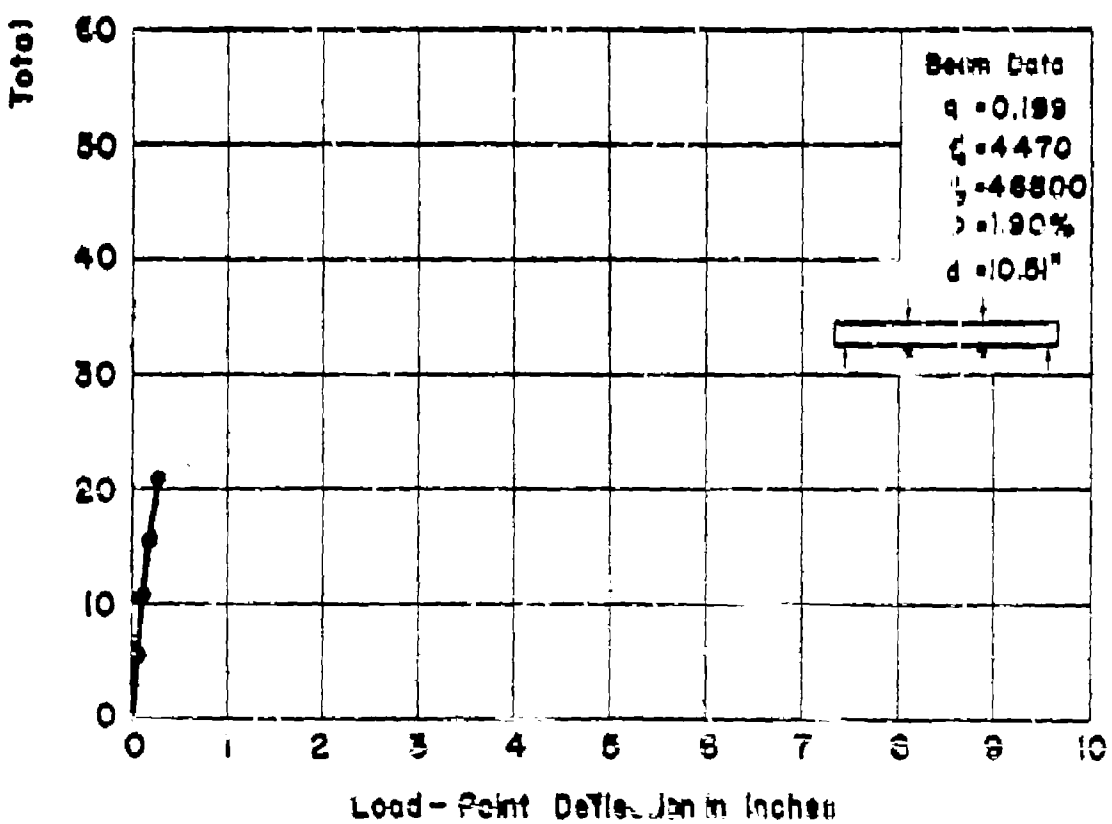

APP. FIG. 13 LOAD-DEFLECTION CURVES FOR BEAM NO. T2Mc

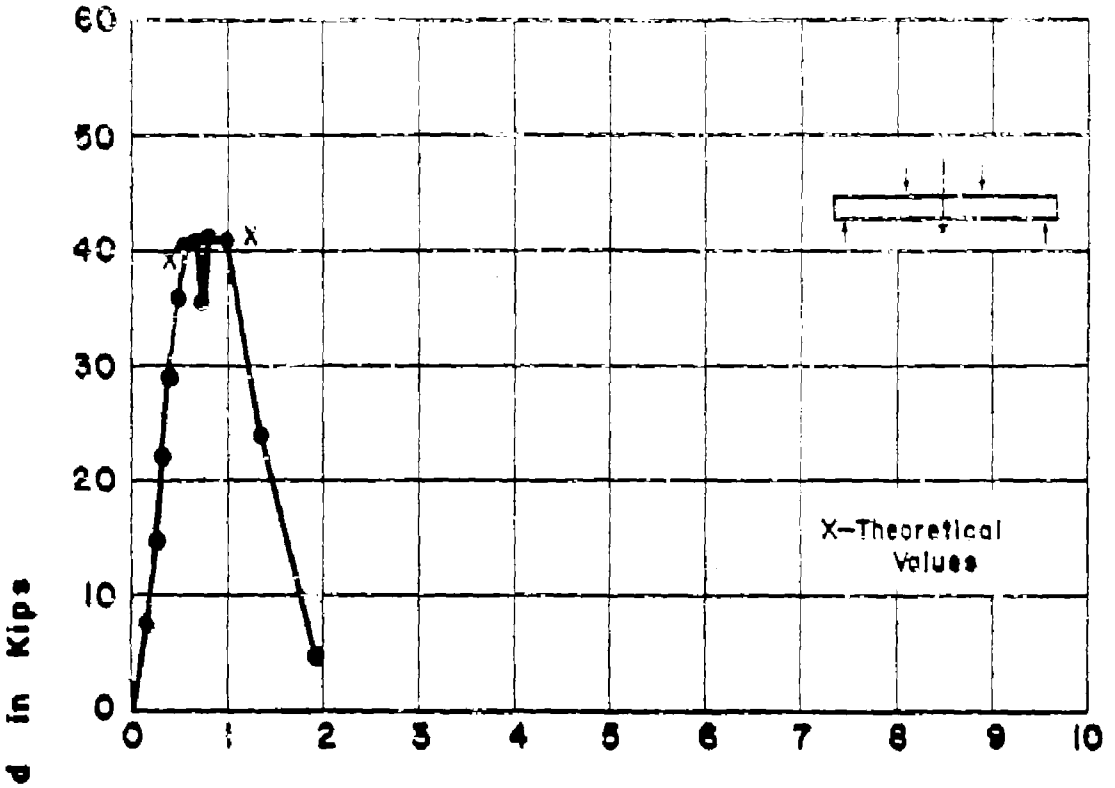

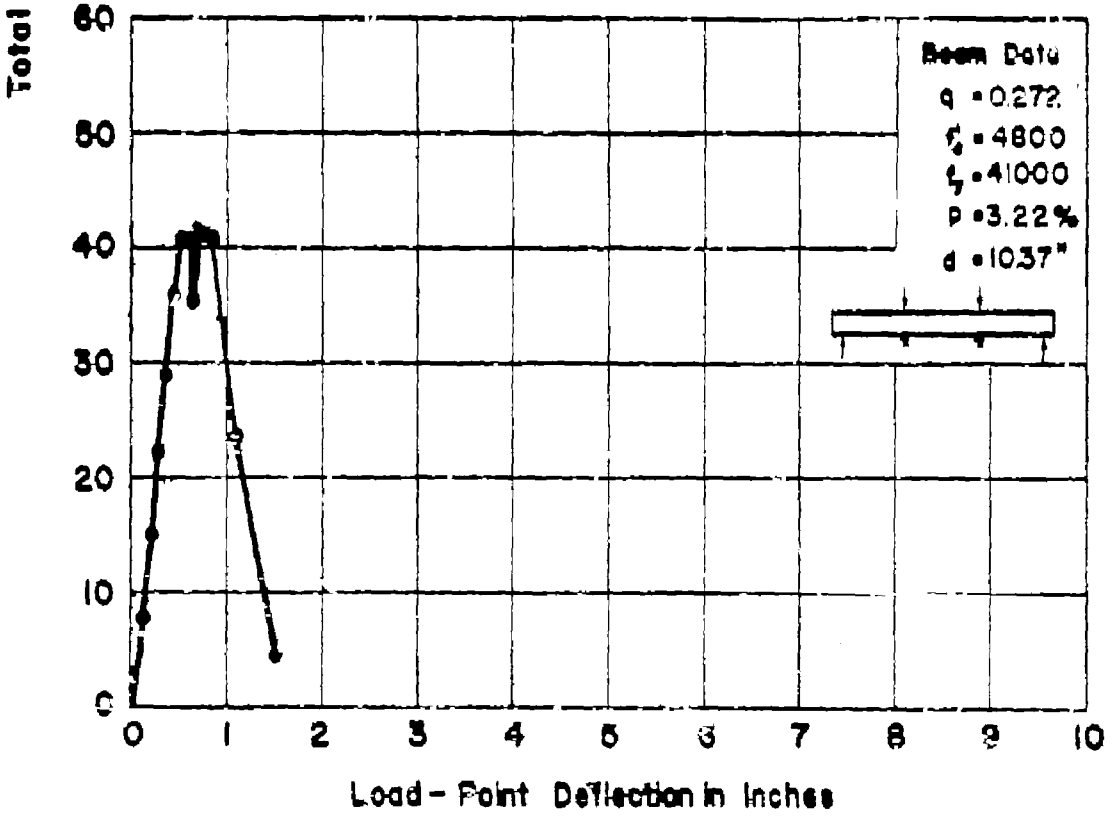

APP. FIG. 14 LOAD-DEFLECTION CURVES FOR BEAM NO. T3Ma

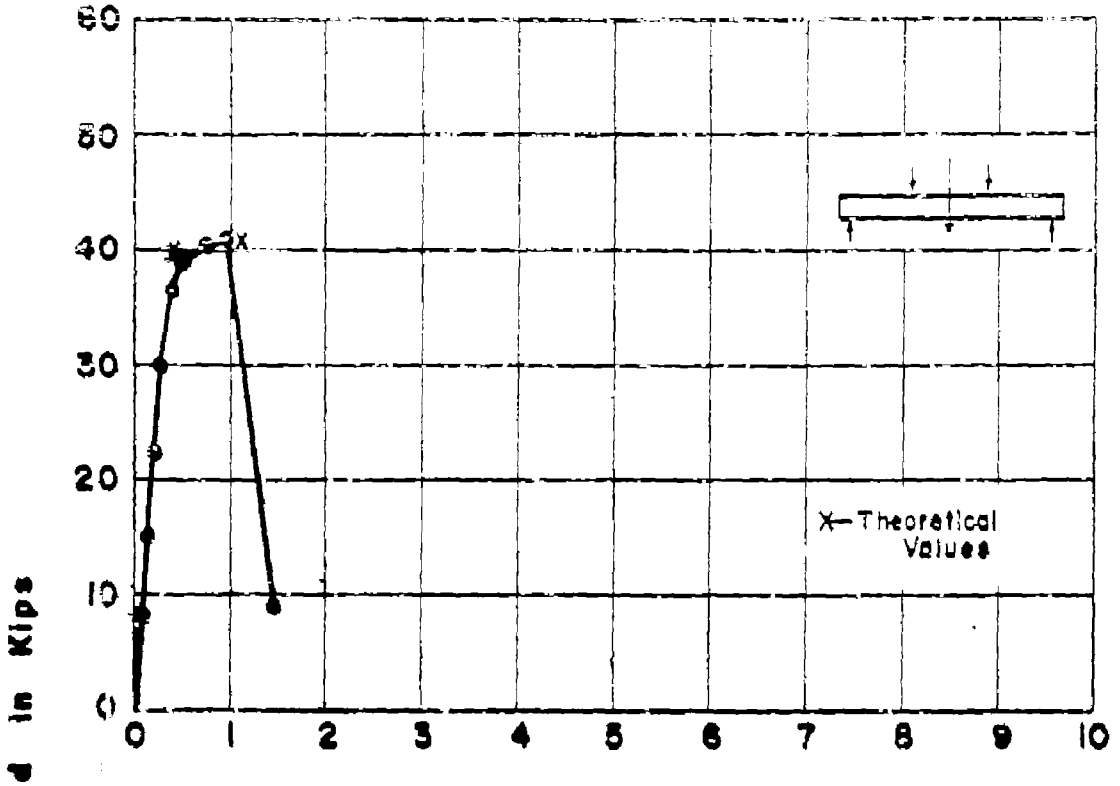

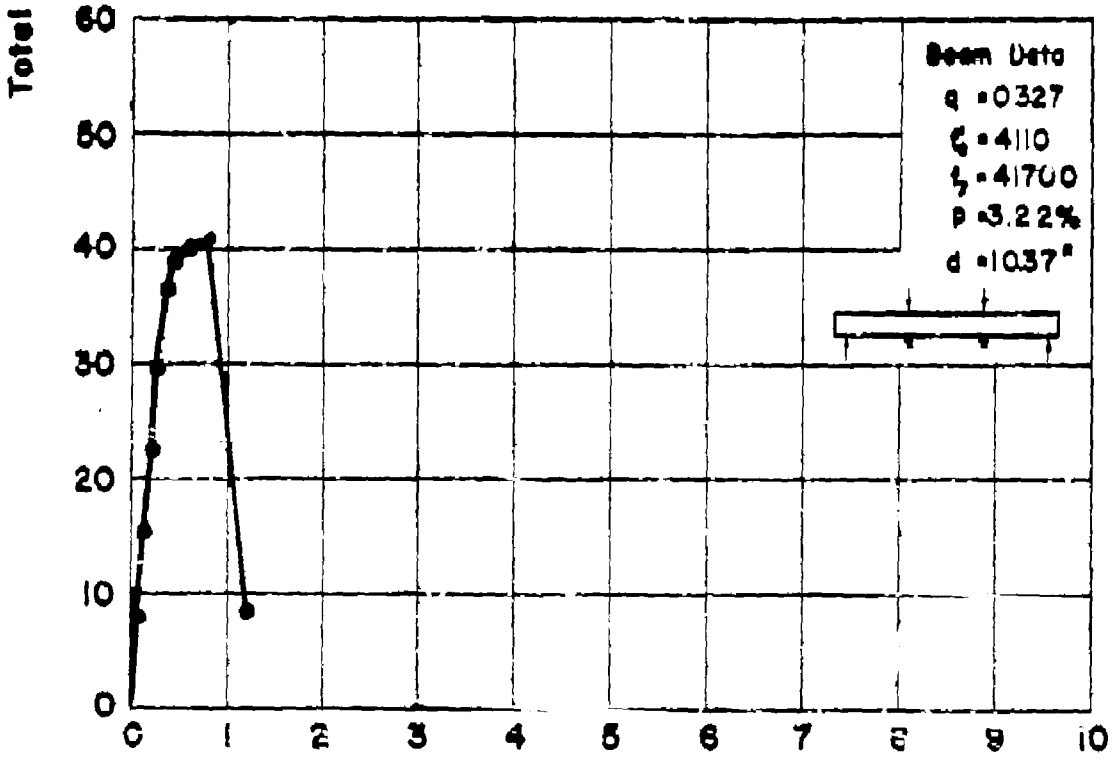

APP. FIG. 15 LOAD-DEFLECTION CURVES FOR BEAM NO. T3Mb

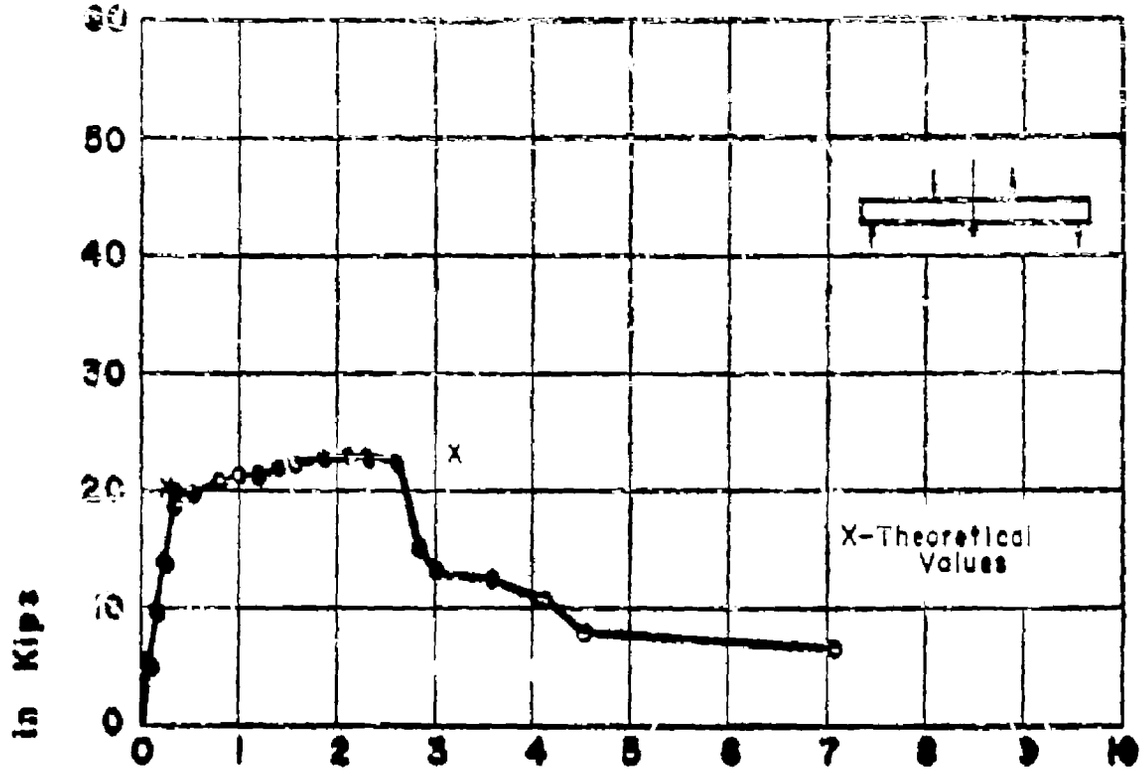

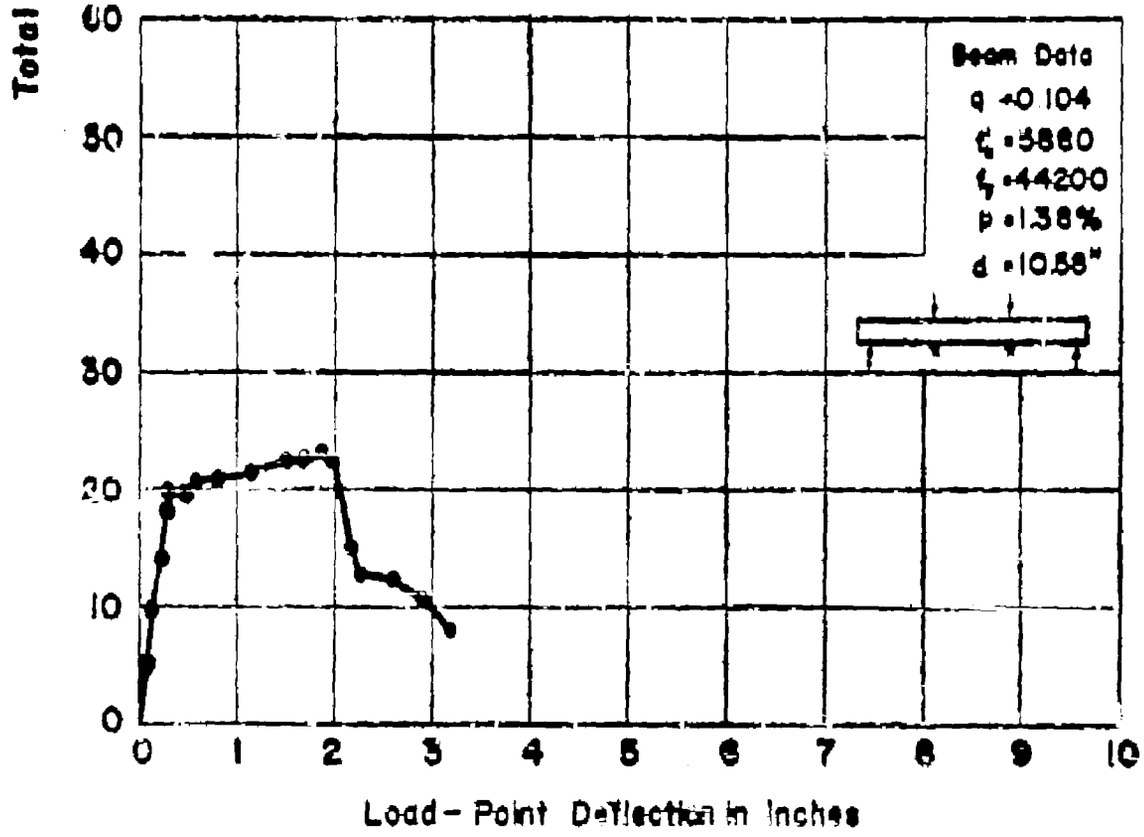

APP. FIG. 15 LOAD-DEFLECTION CURVES FOR BEAM NO. T1H2

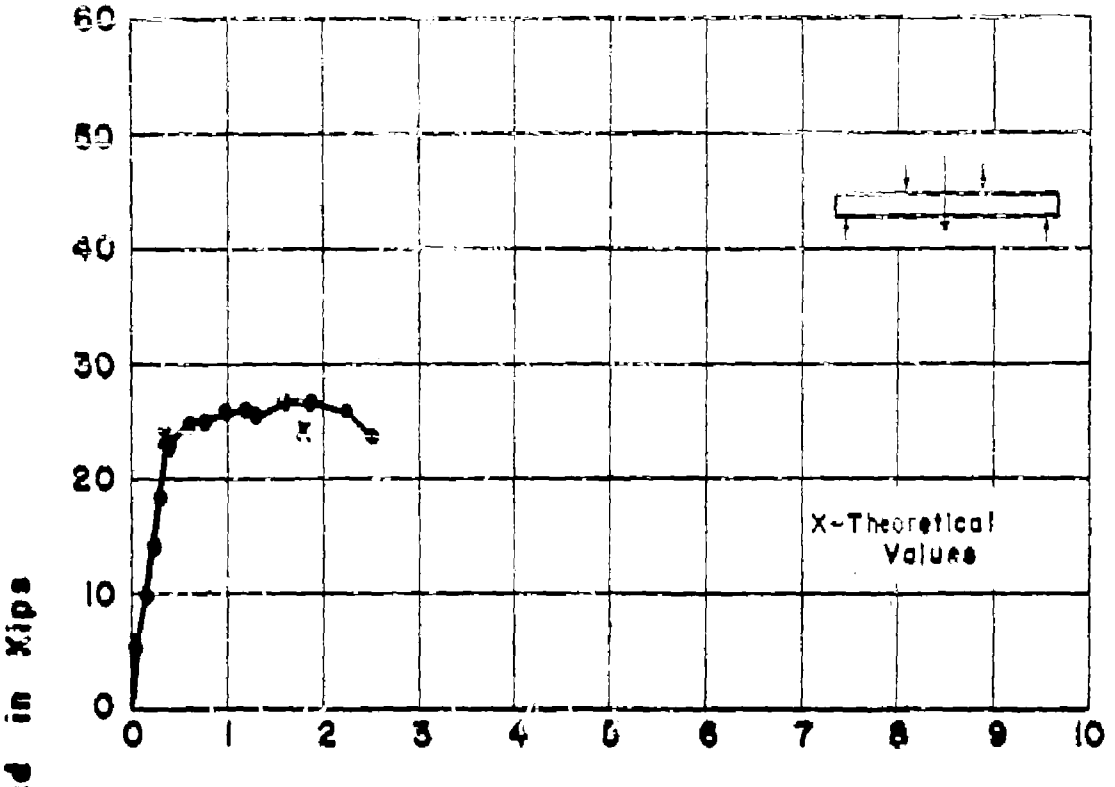

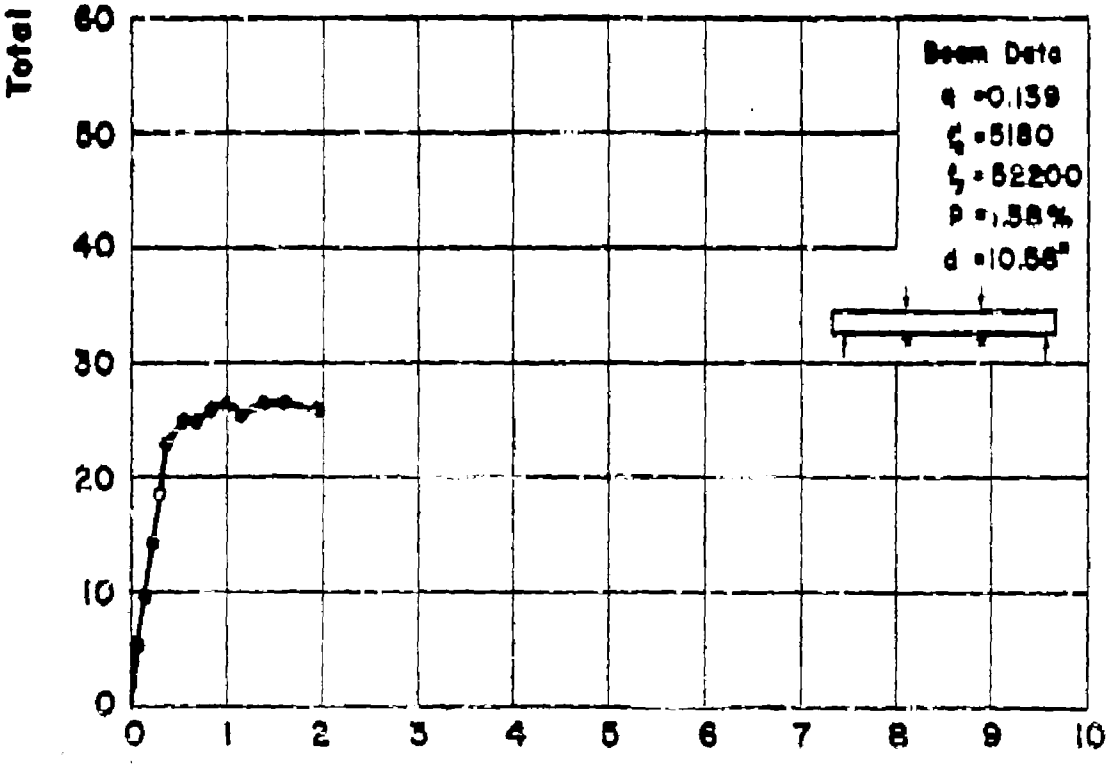

APP. FIG. 17 LOAD-DEFLECTION CURVES FOR BEAM NO. T1Hb

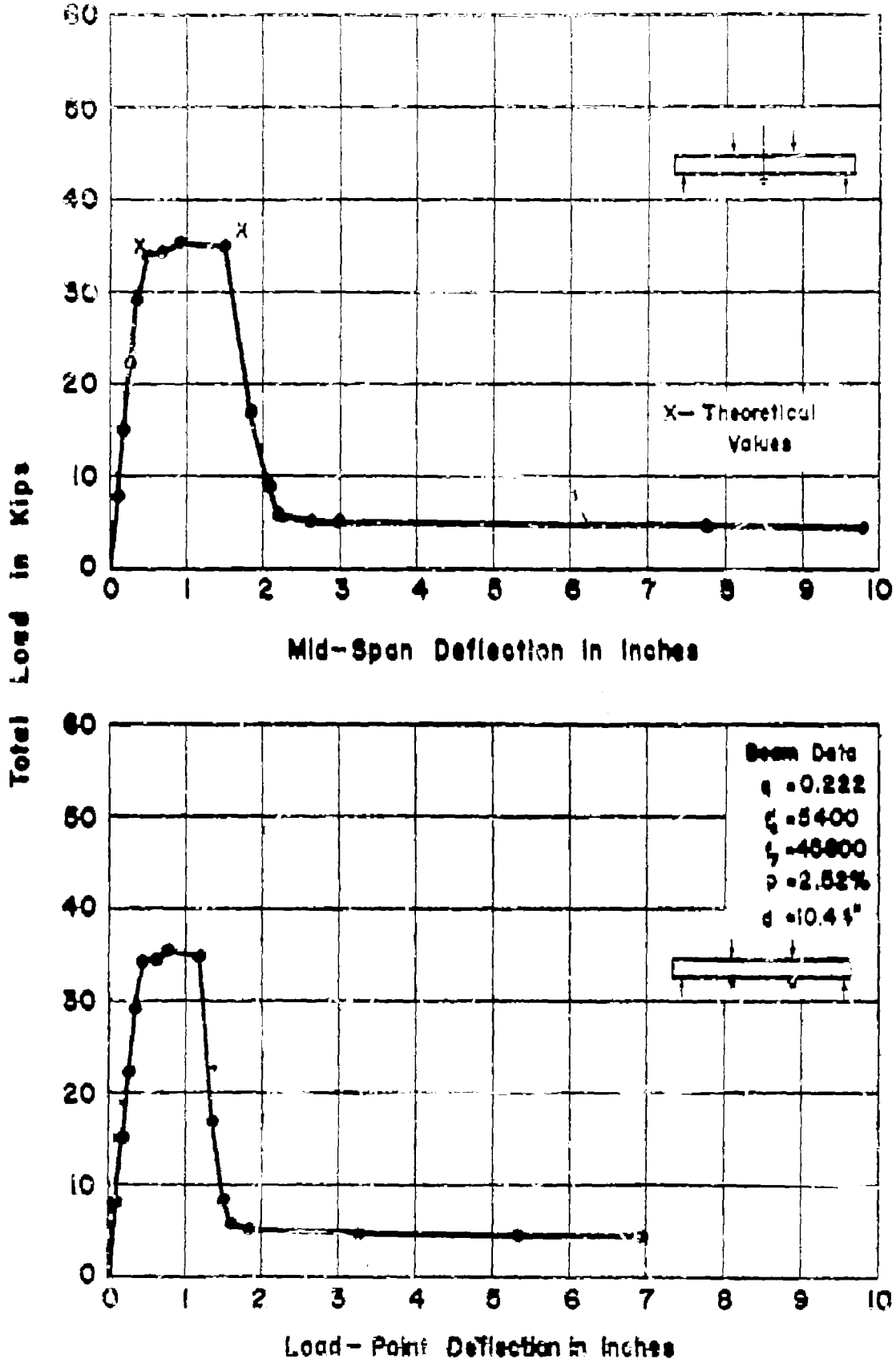

APP. FIG. 18 LOAD-DEFLECTION CURVES FOR BEAM NO. T2H

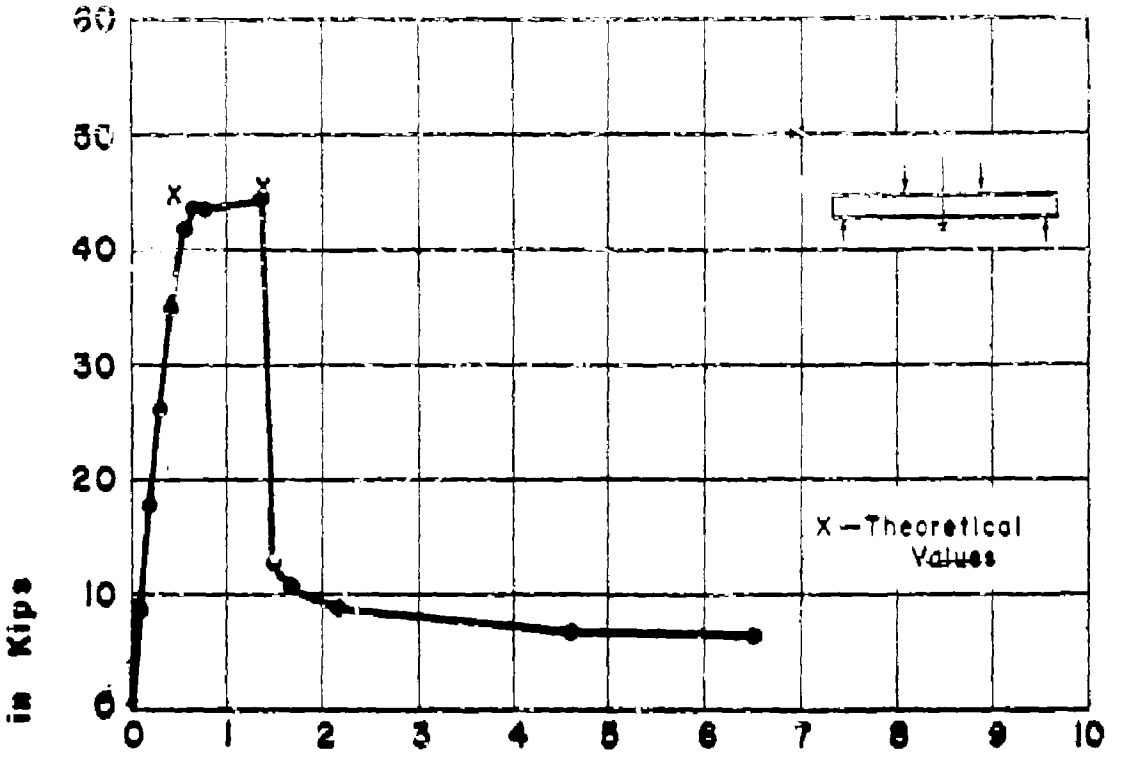

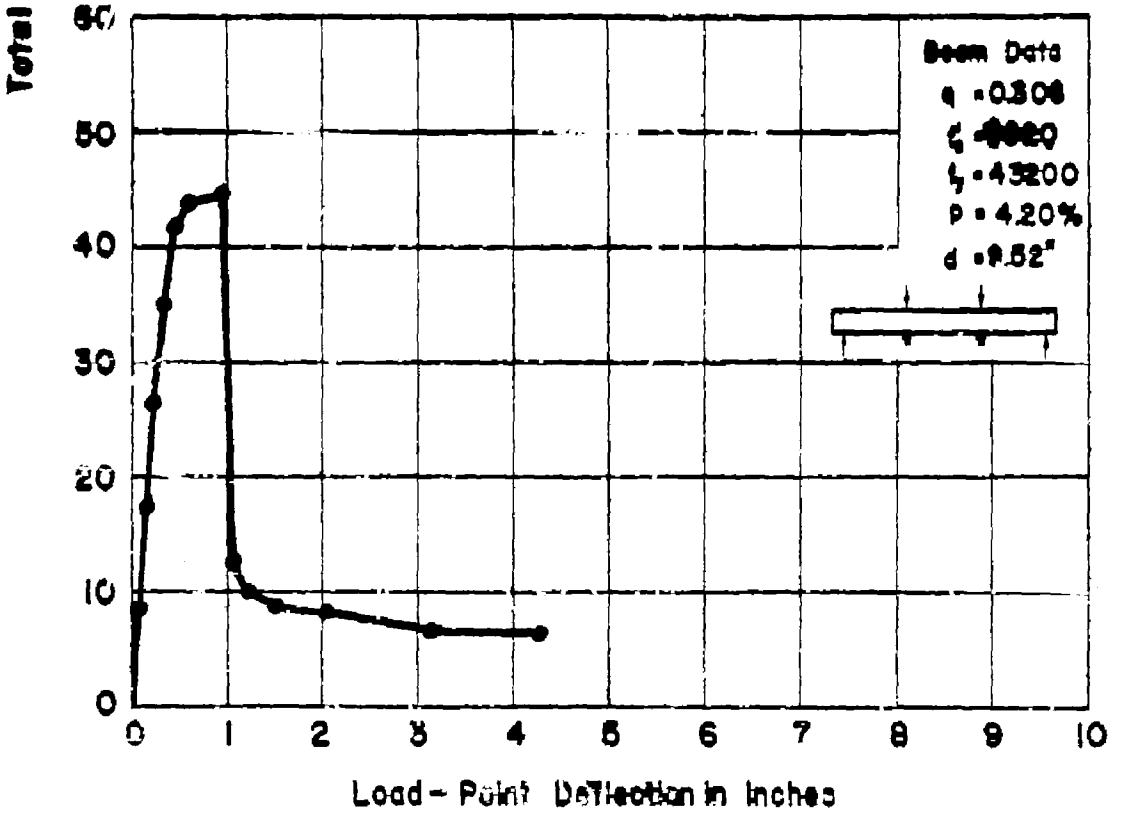

APP FIG. 19 LOAD-DEFLECTION CURVES FOR BEAM NO.T3H

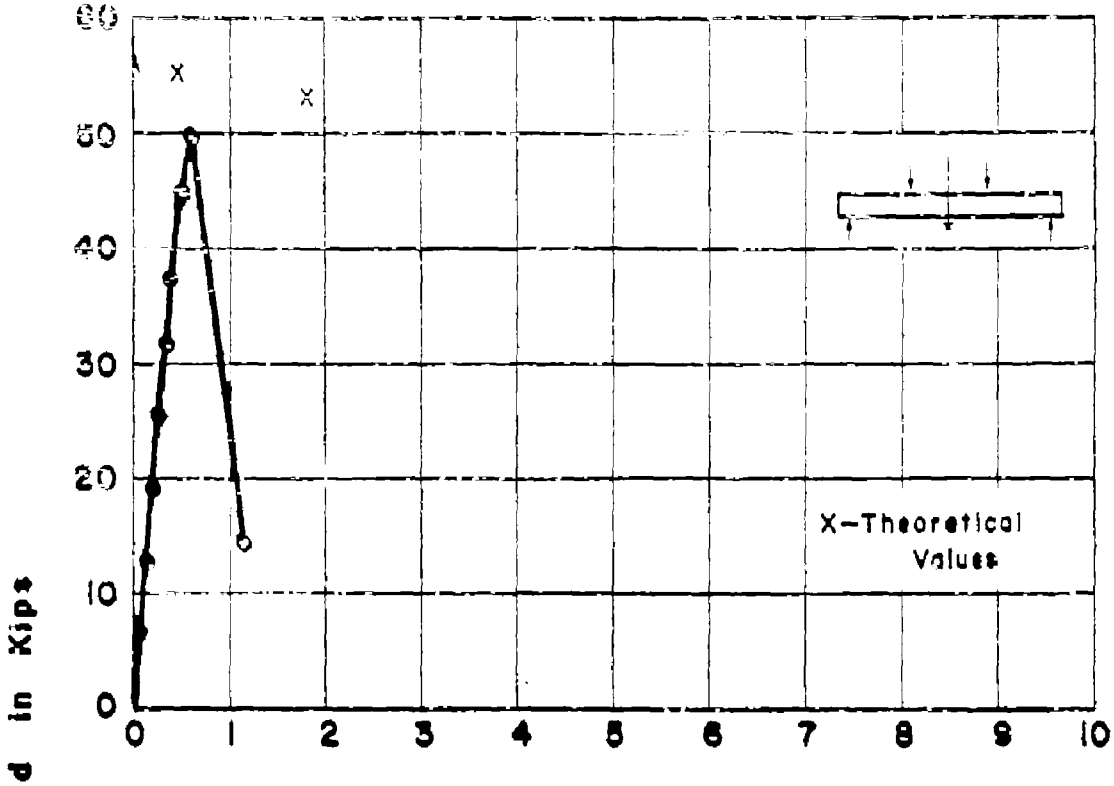

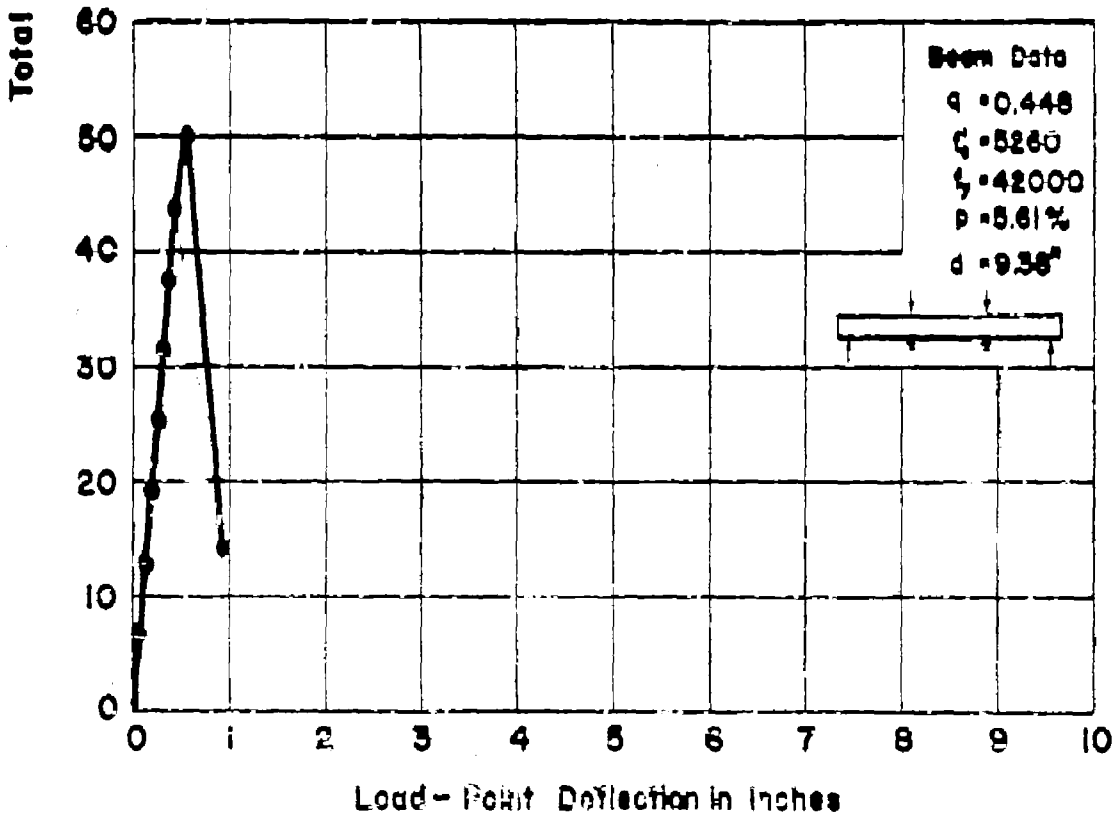

APP. FIG. 20 LOAD-DEFLECTION CURVES FOR BEAM NO. T4H

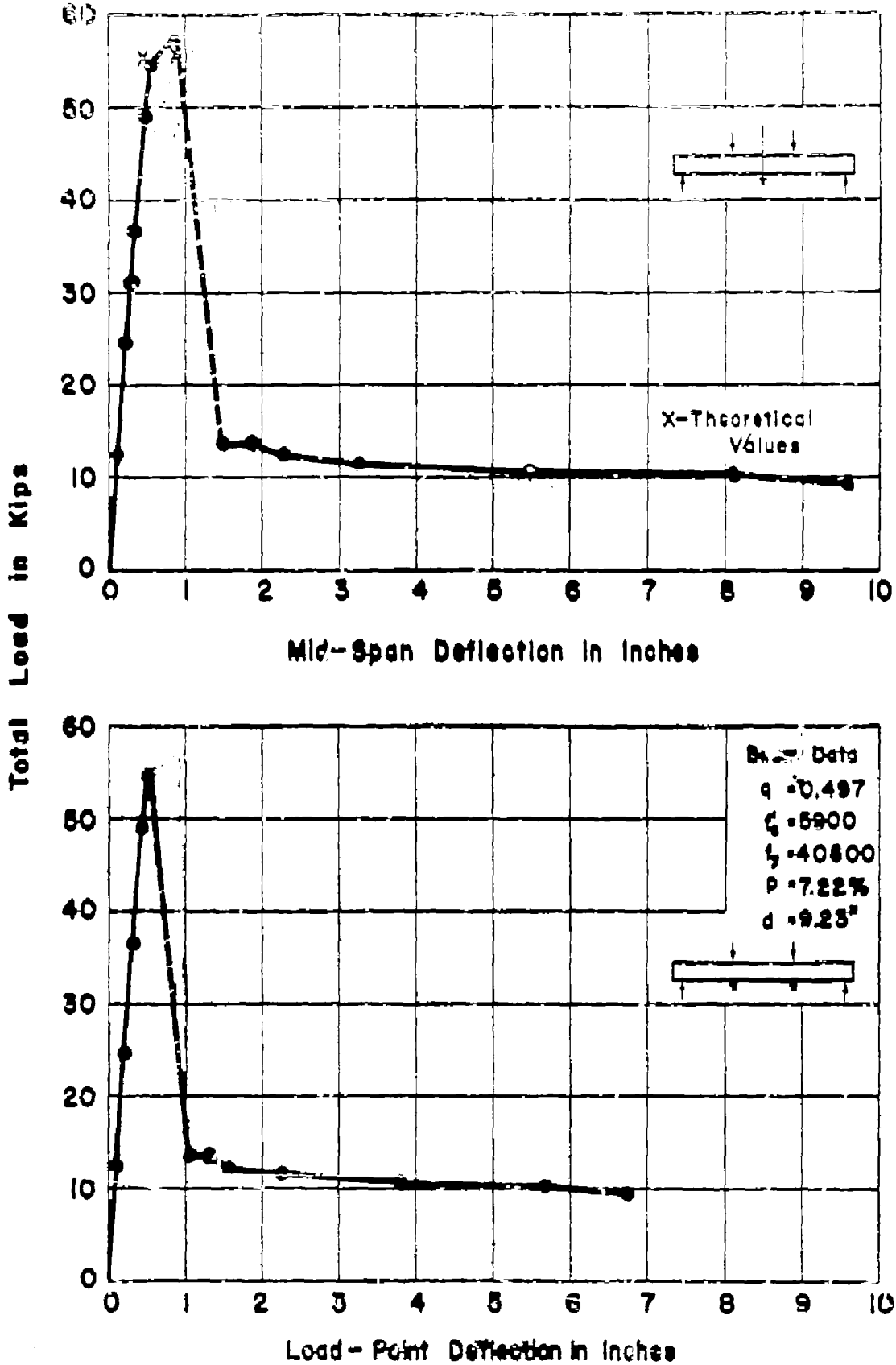

APP. FIG. 21 LOAD-DEFLECTION CURVES FOR BEAM NO. T5H

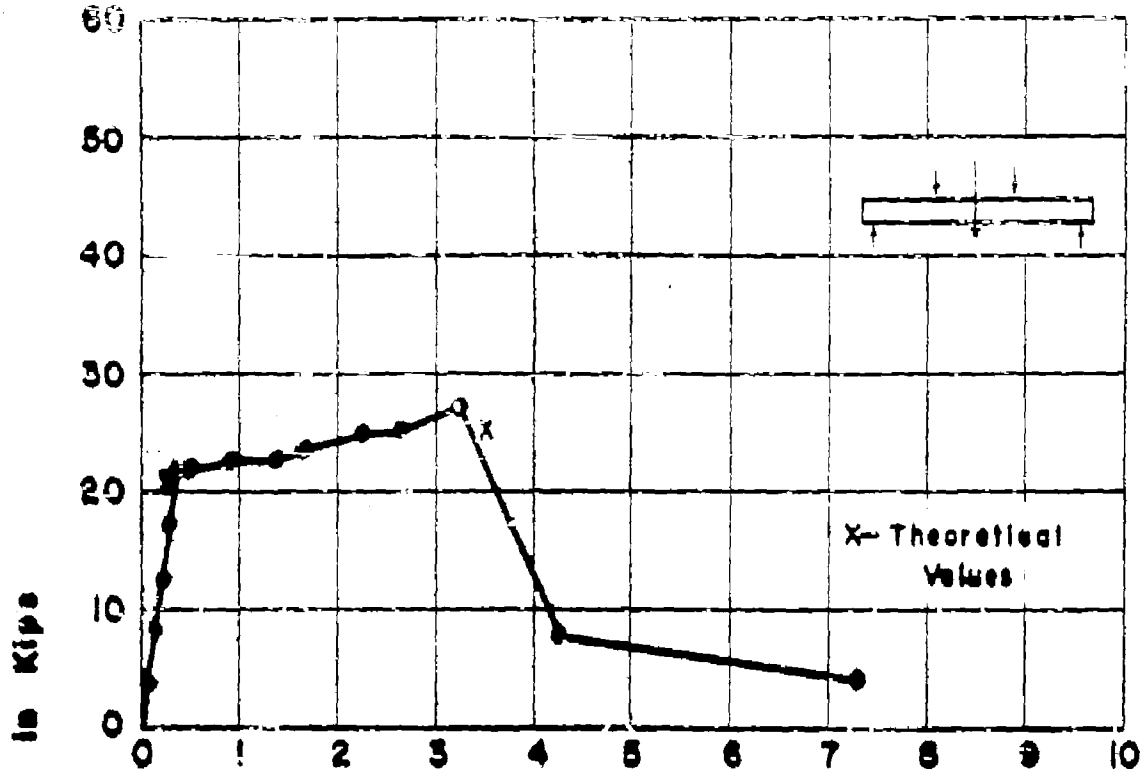

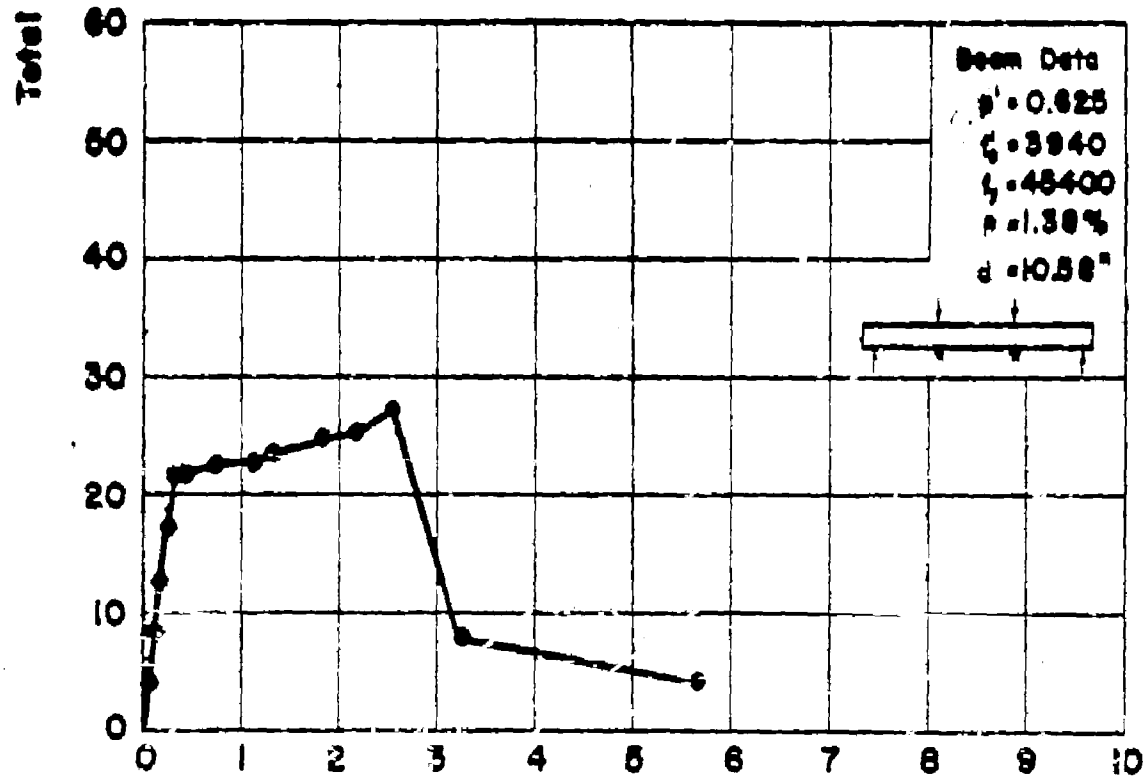

APP. FIG. 22 LOAD-DEFLECTION CURVES FOR BEAM NO. C2w

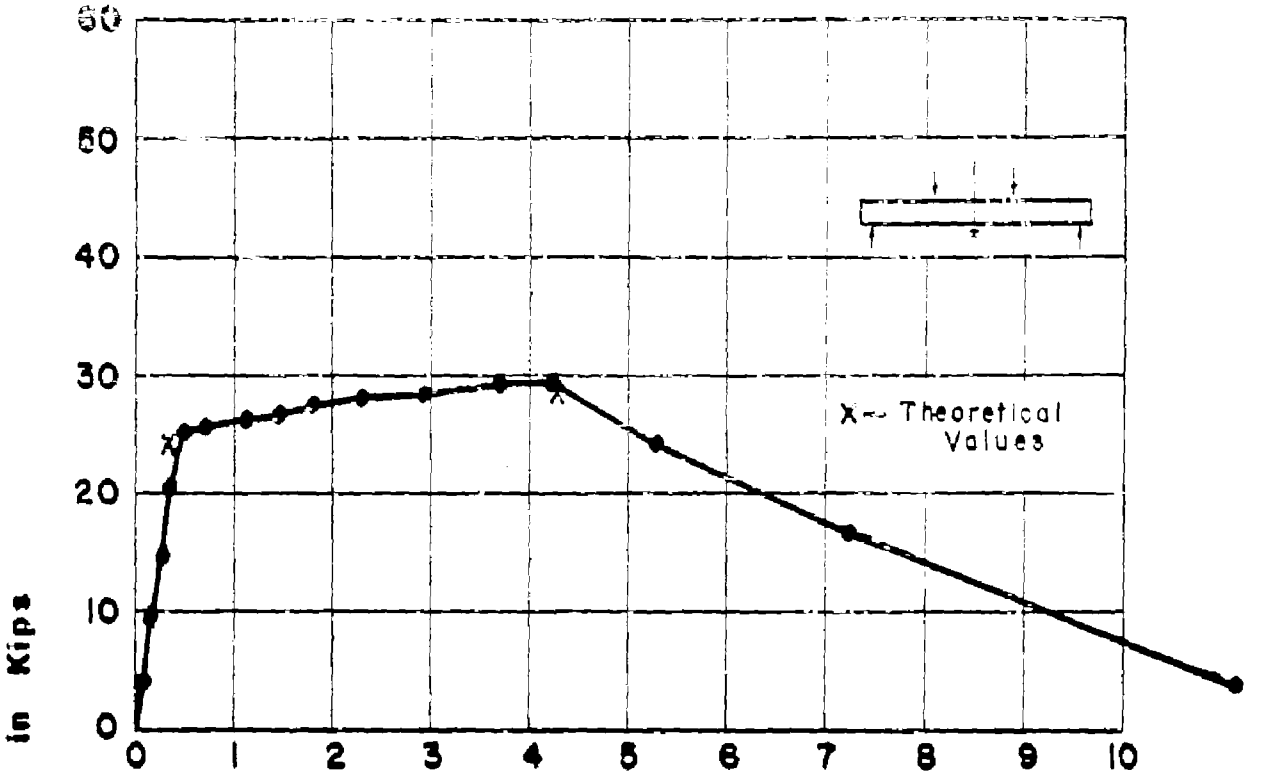

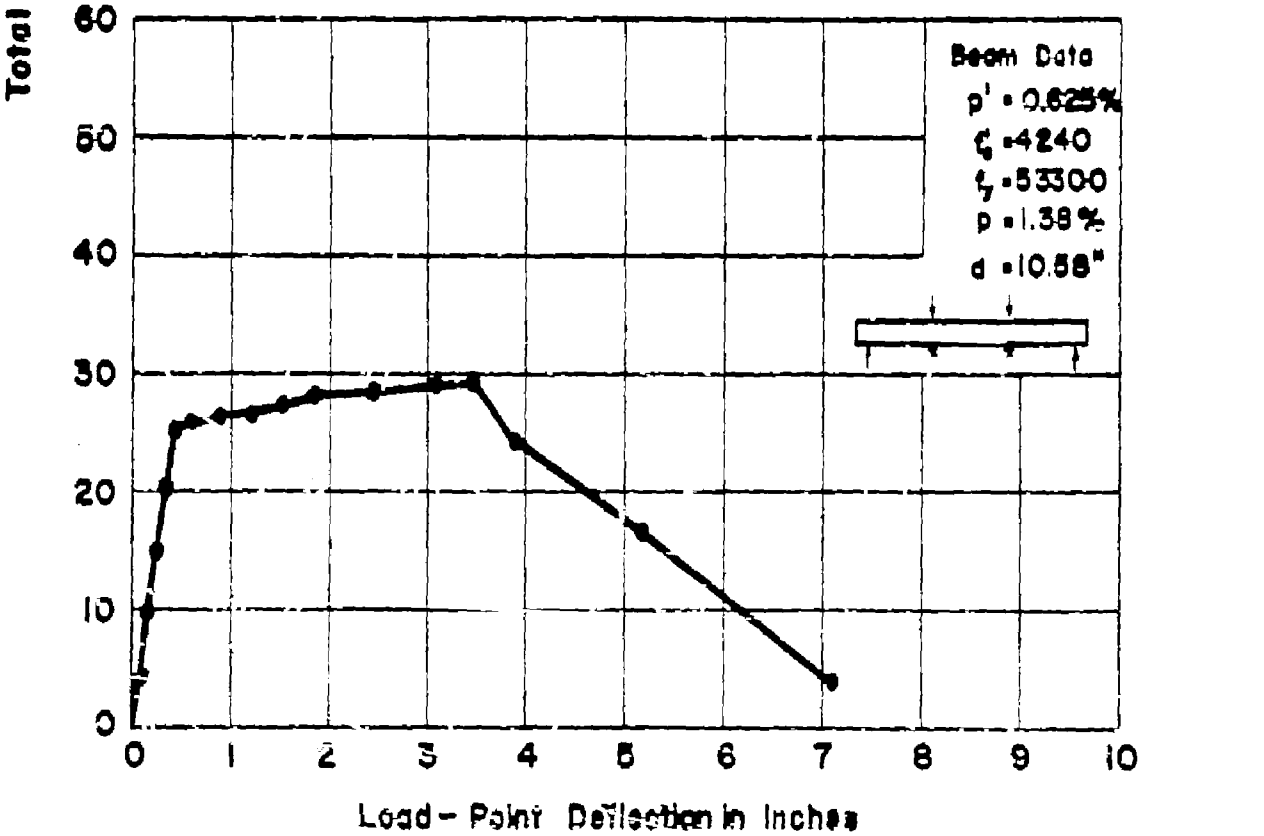

APP. FIG. 23 LOAD-DEFLECTION CURVES FOR BEAM NO. C2xm

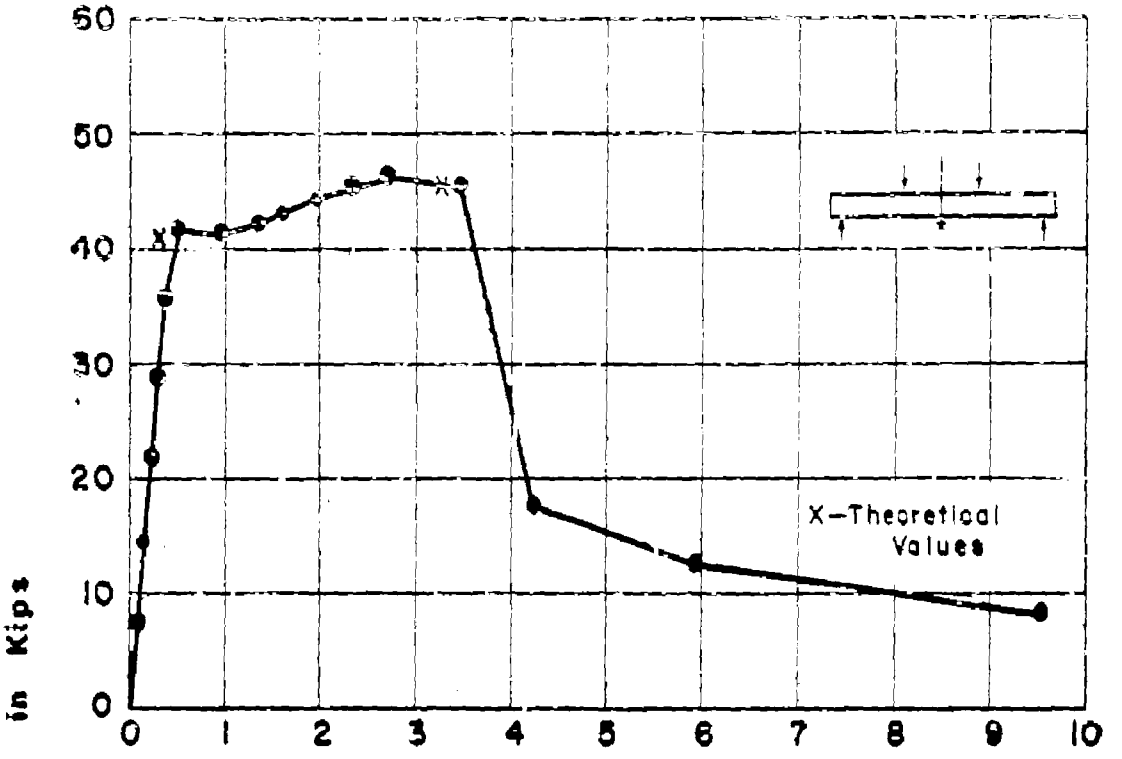

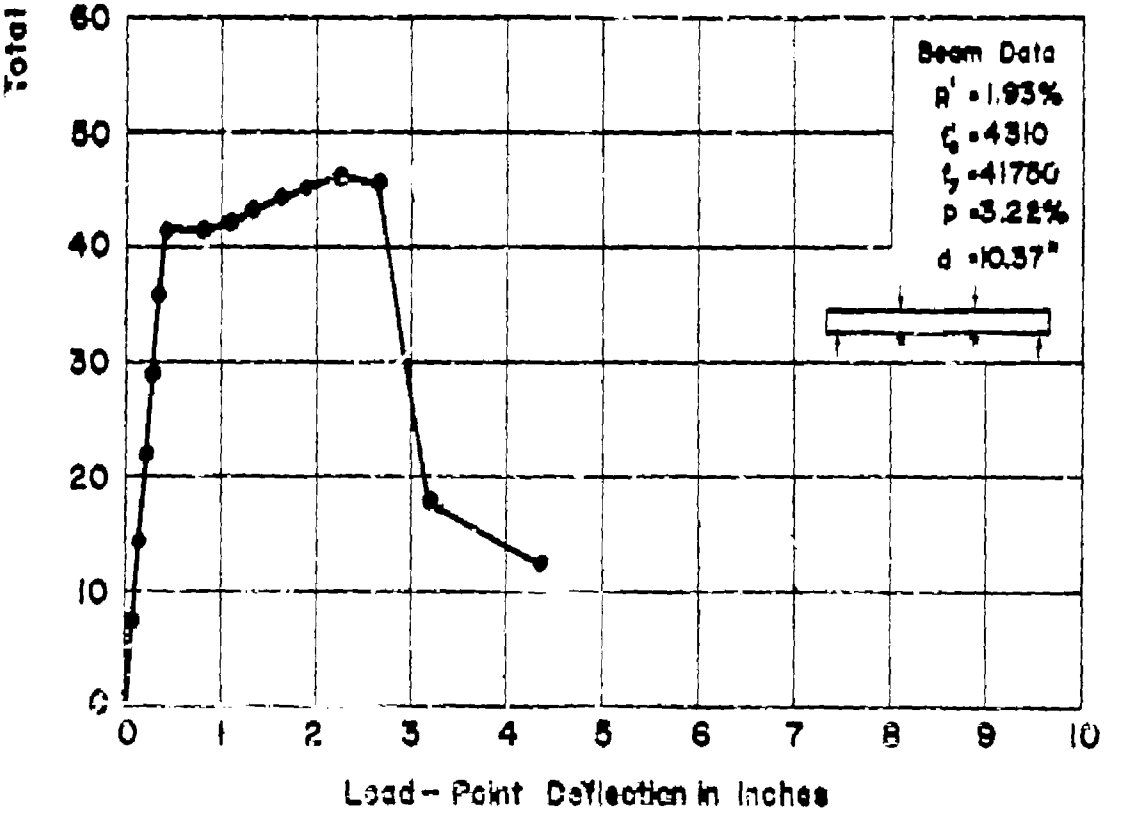

APP. FIG. 24 LOAD-DEFLECTION CURVES FOR BEAM NO. C3w

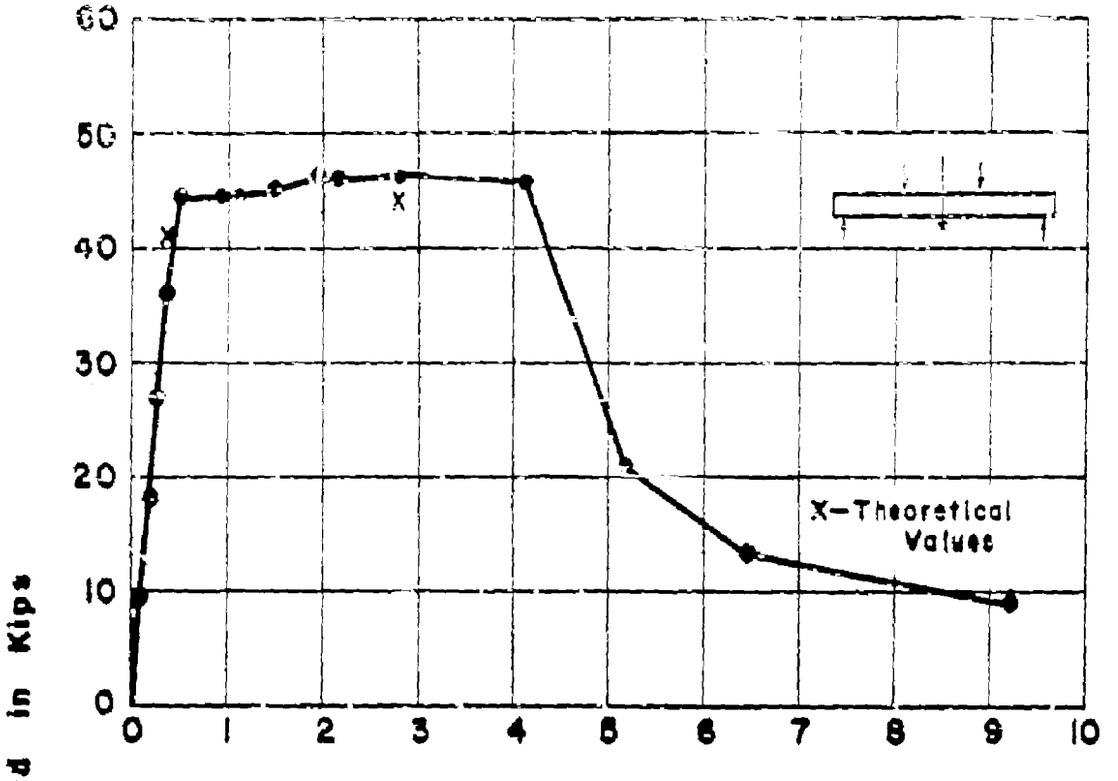

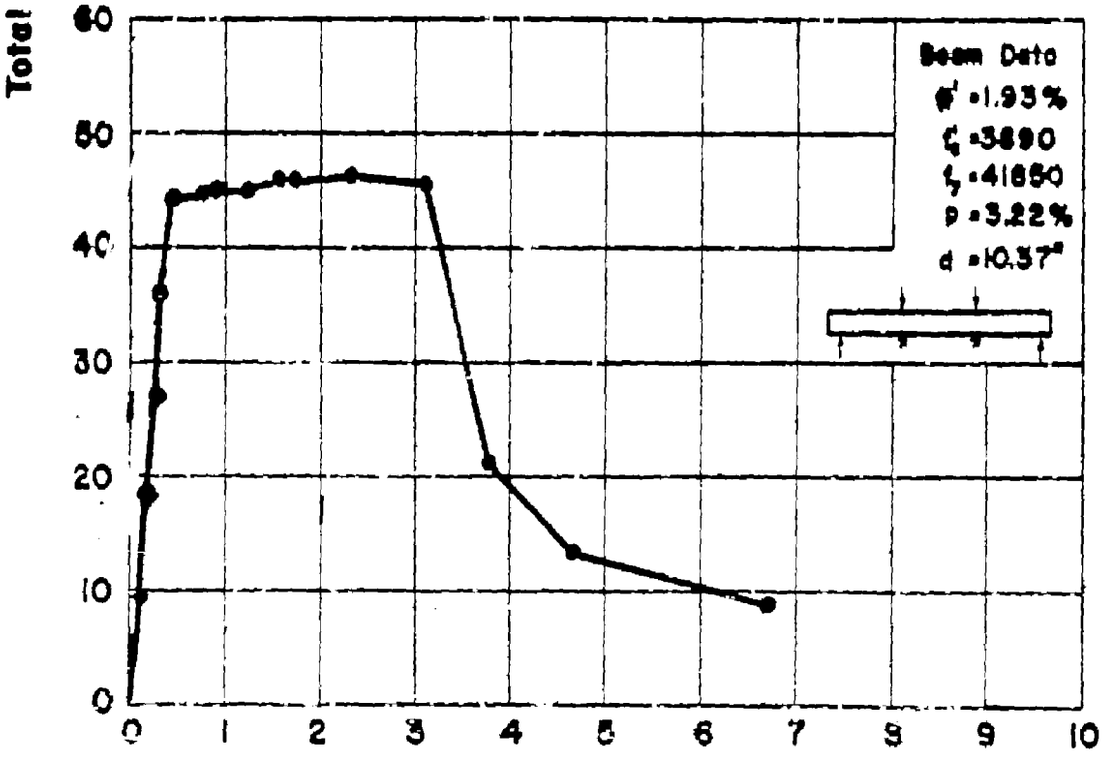

APP. FIG. 25 LOAD-DEFLECTION CURVES FOR BEAM NO. C3xm

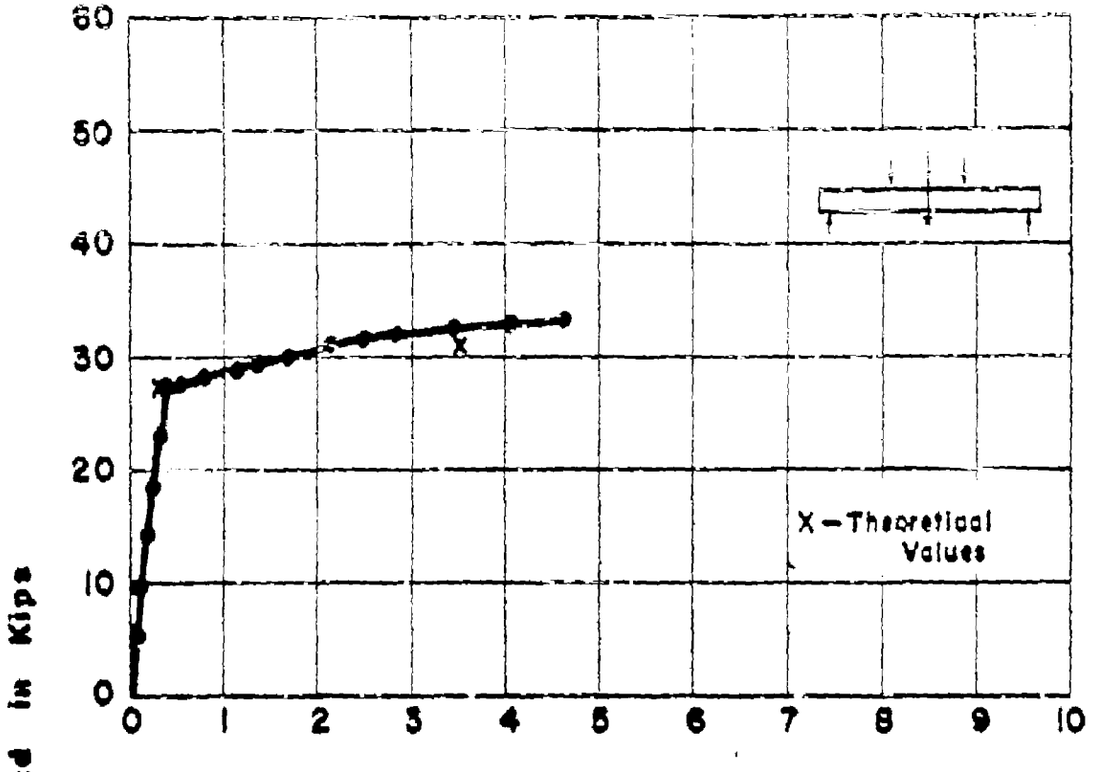

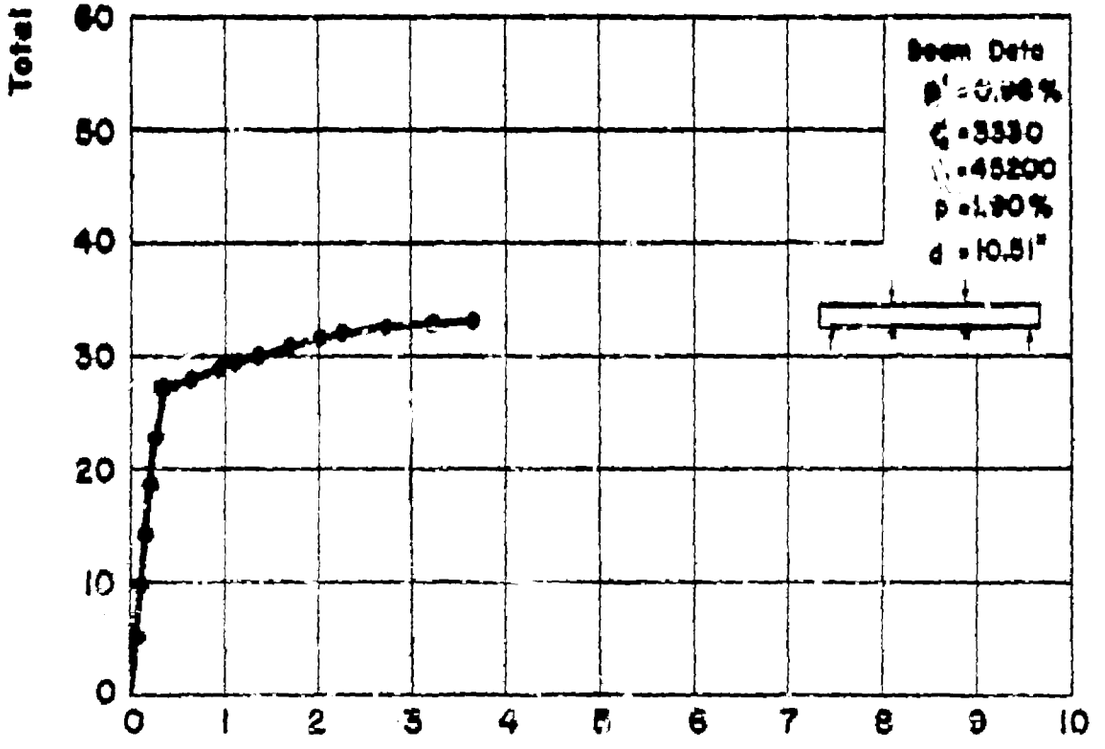

APP. FIG. 26 LOAD-DEFLECTION CURVES FOR BEAM NO. C3yna

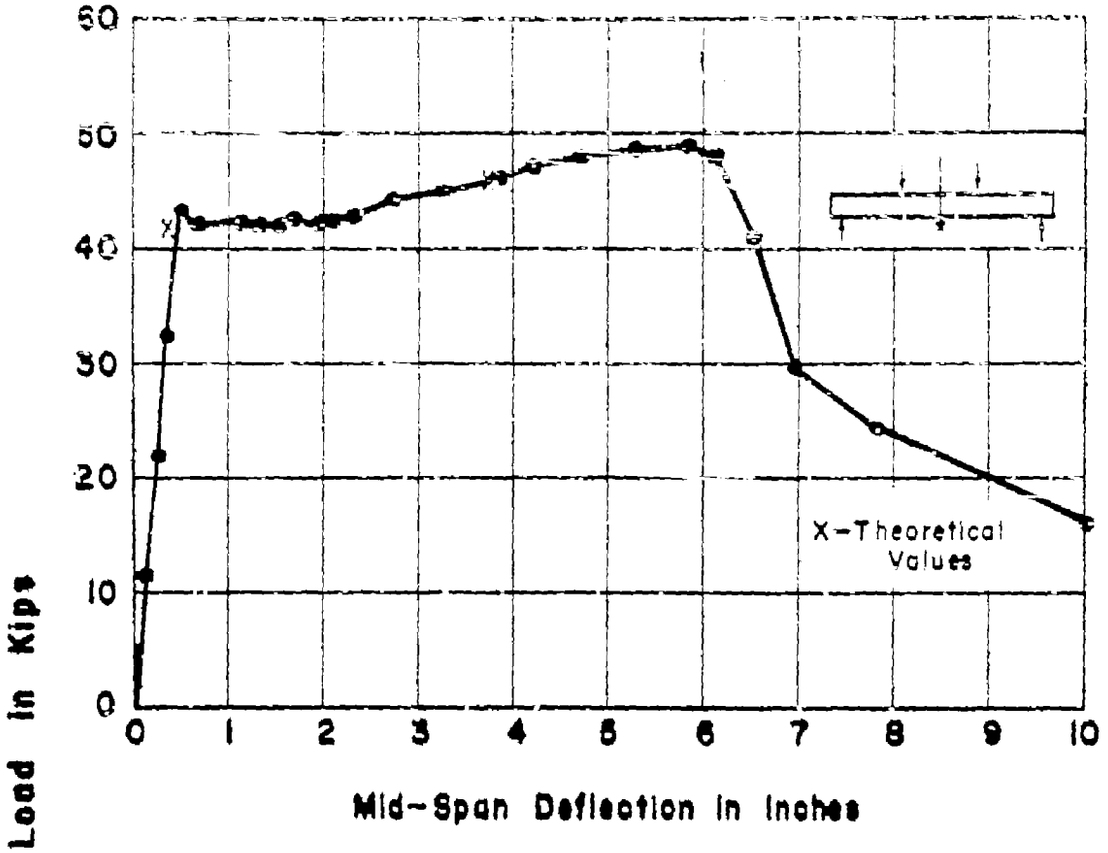

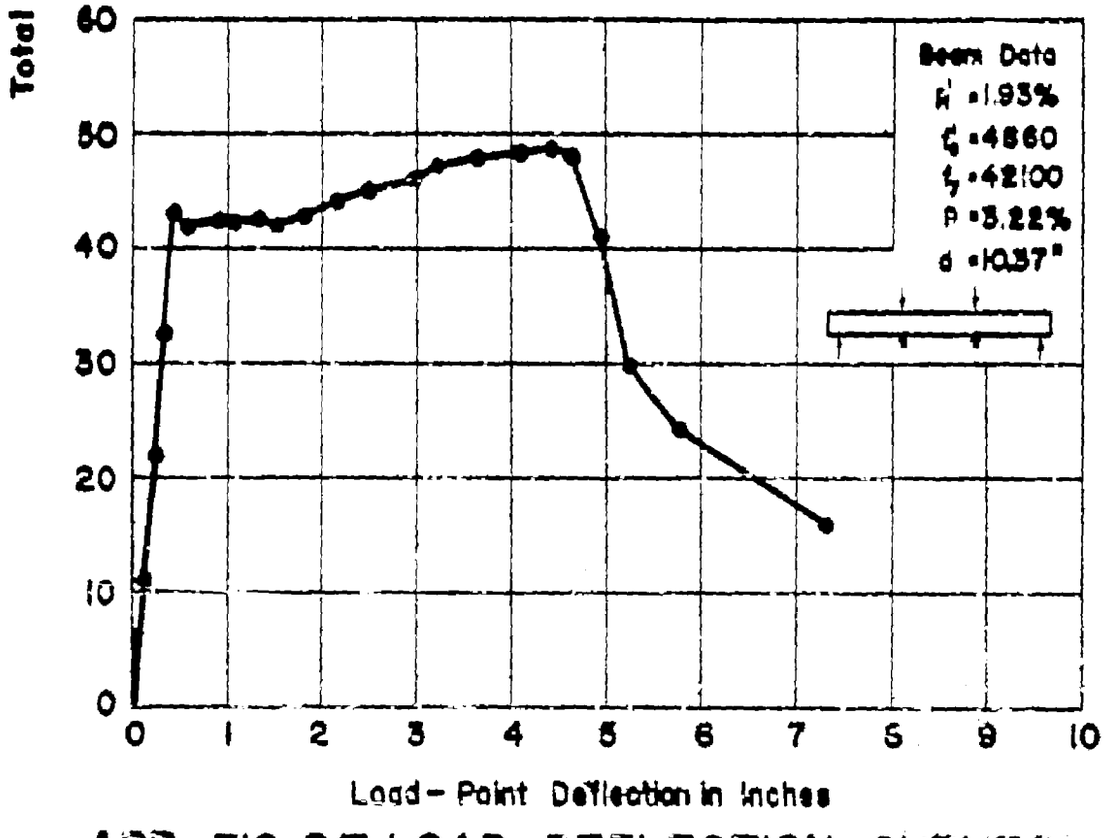

APP. FIG. 27 LOAD-DEFLECTION CURVES FOR BEAM NO. C3ynb

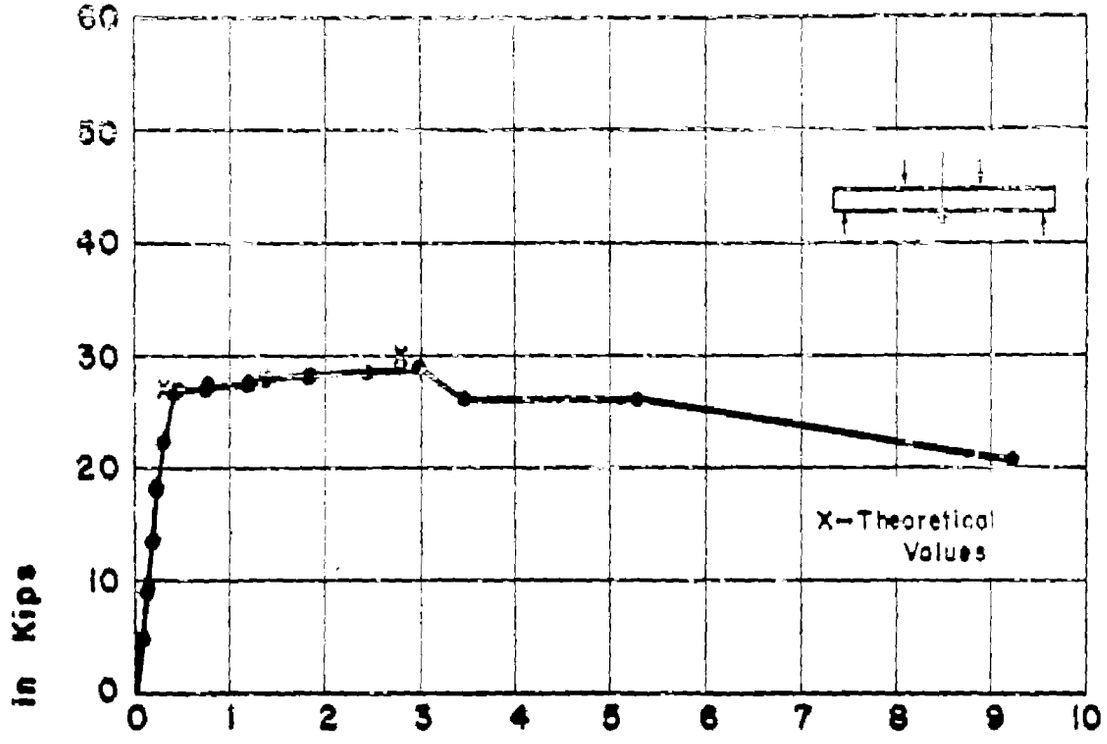

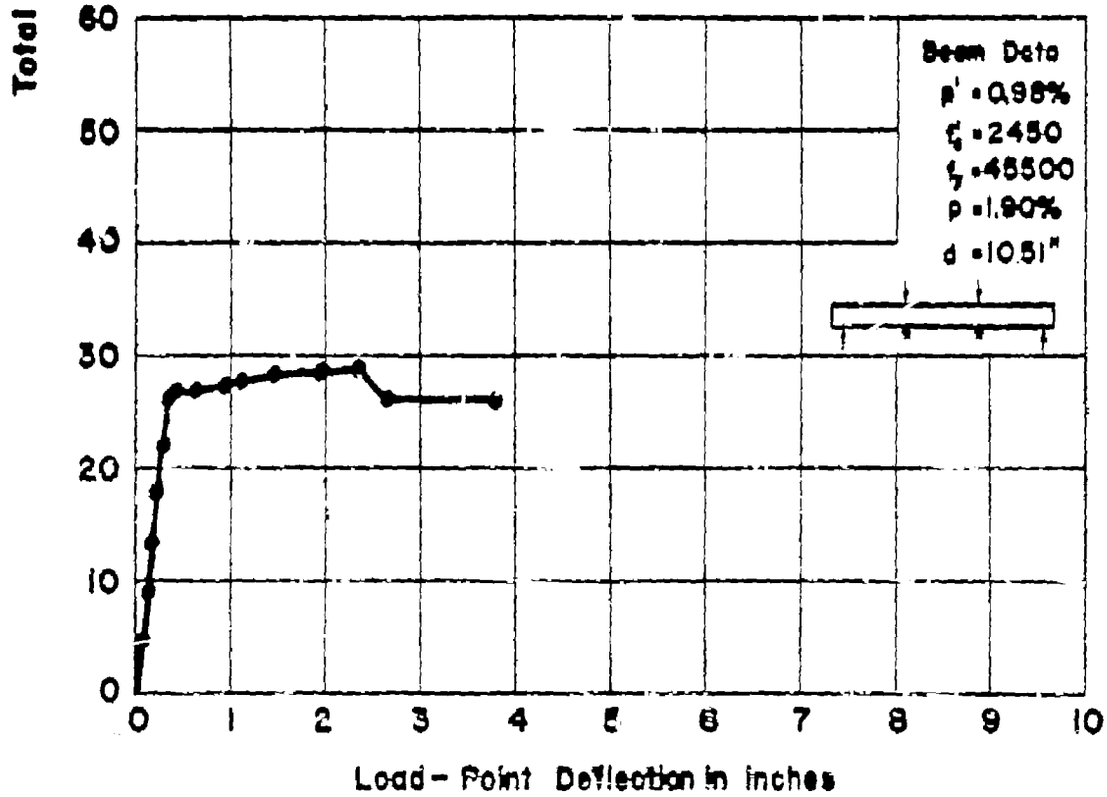

APP. FIG. 23 LOAD-DEFLECTION CURVES FOR BEAM NO. C4xna

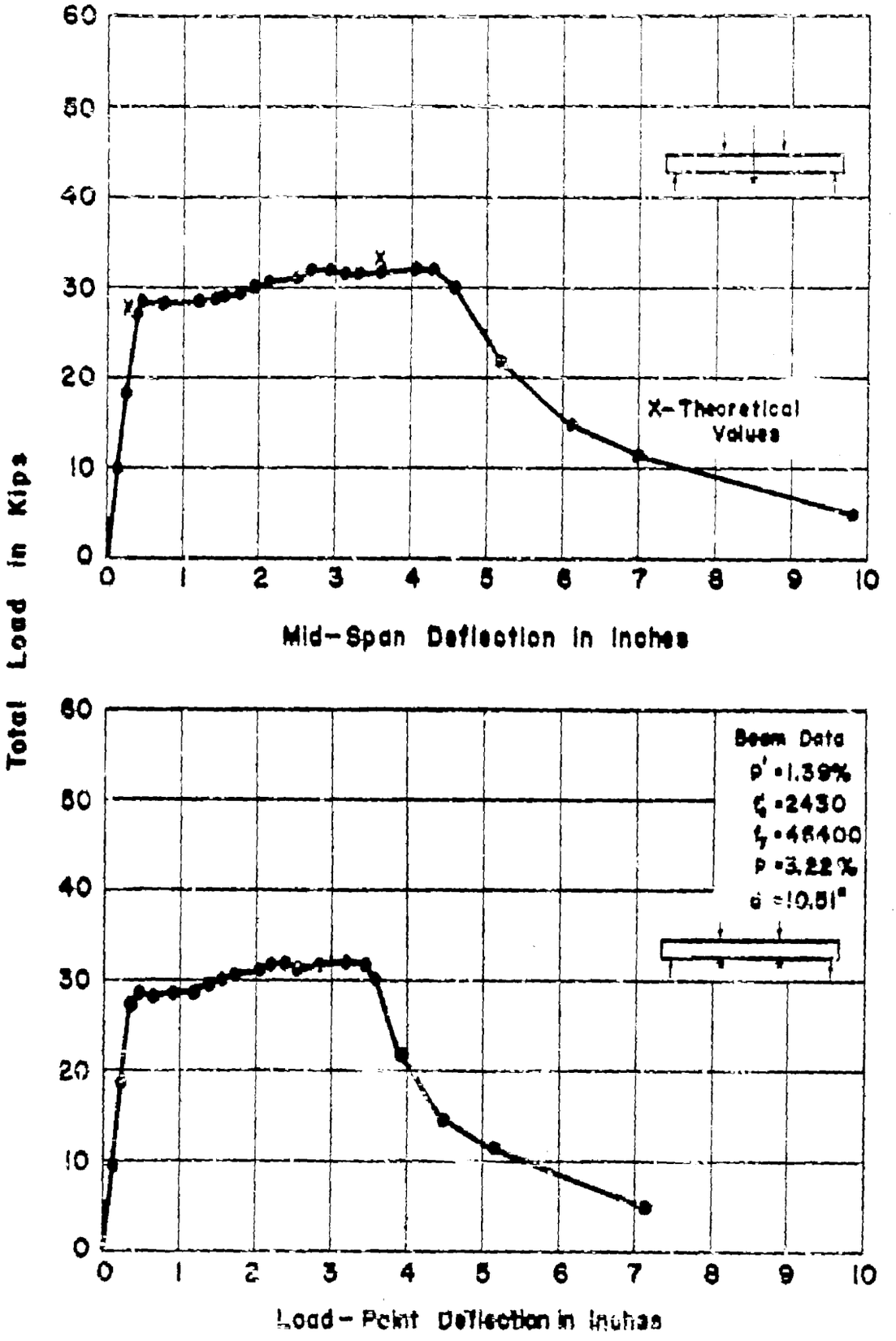

APP. FIG. 29 LOAD-DEFLECTION CURVES FOR BEAM NO. C4xnb

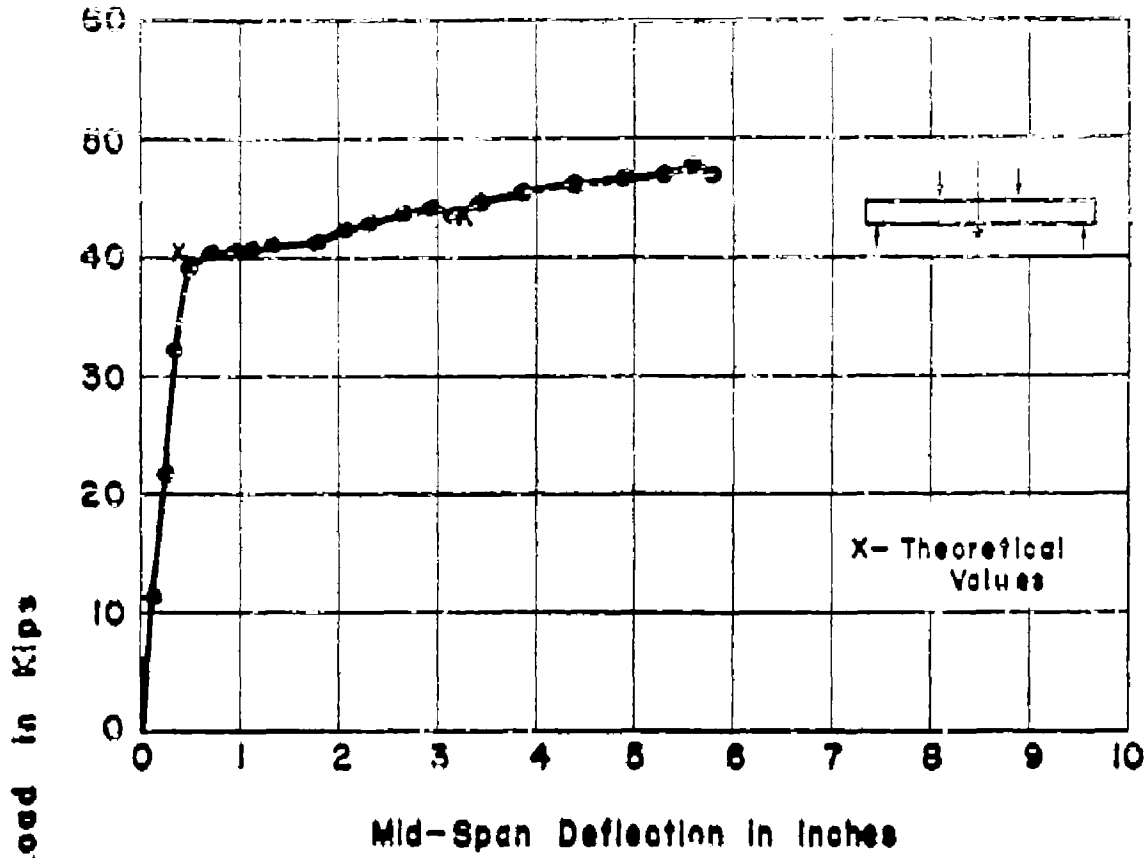

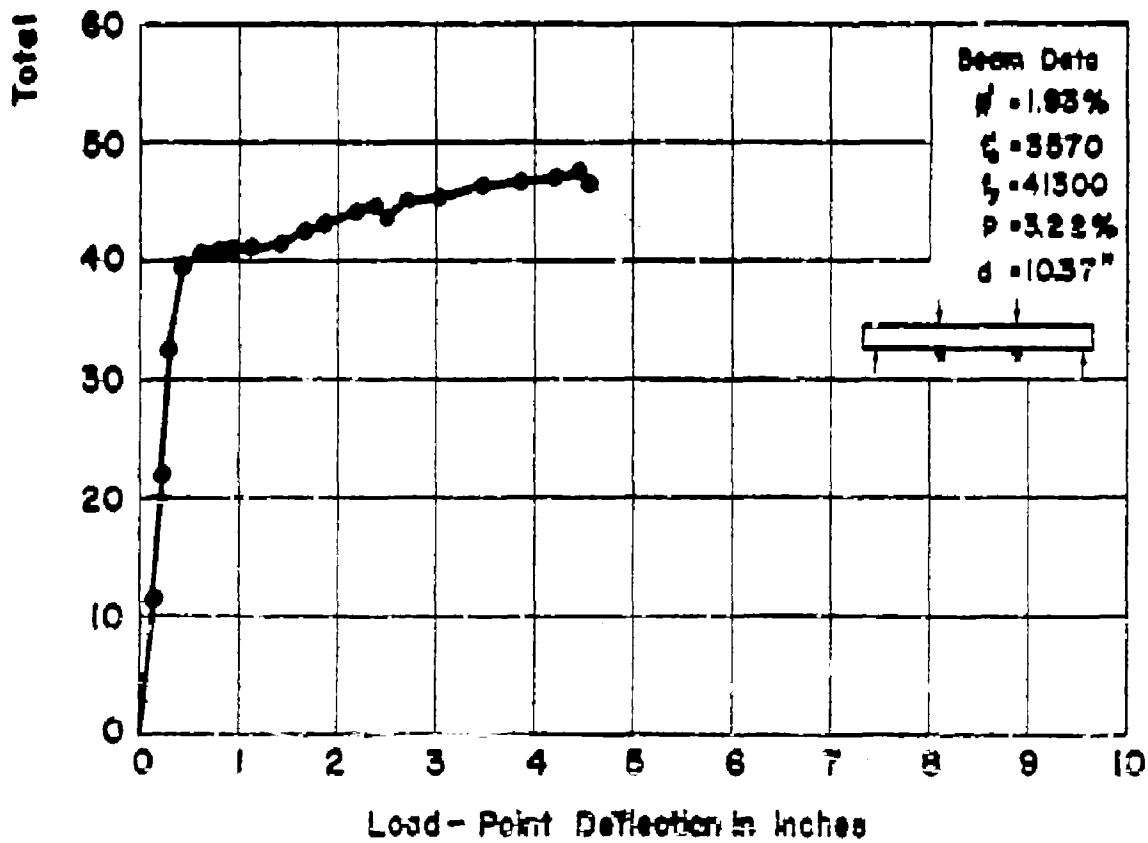

APP. FIG. 30 LOAD-DEFLECTION CURVES FOR BEAM NO. C4zn

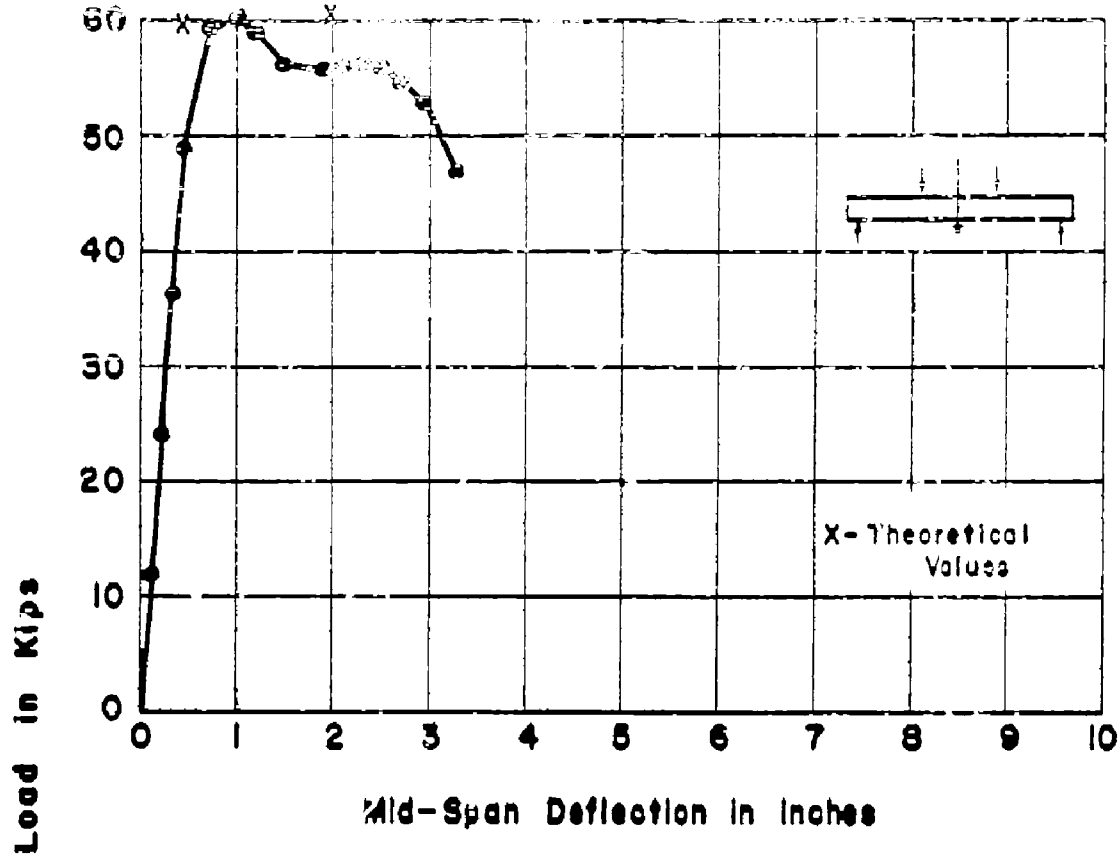

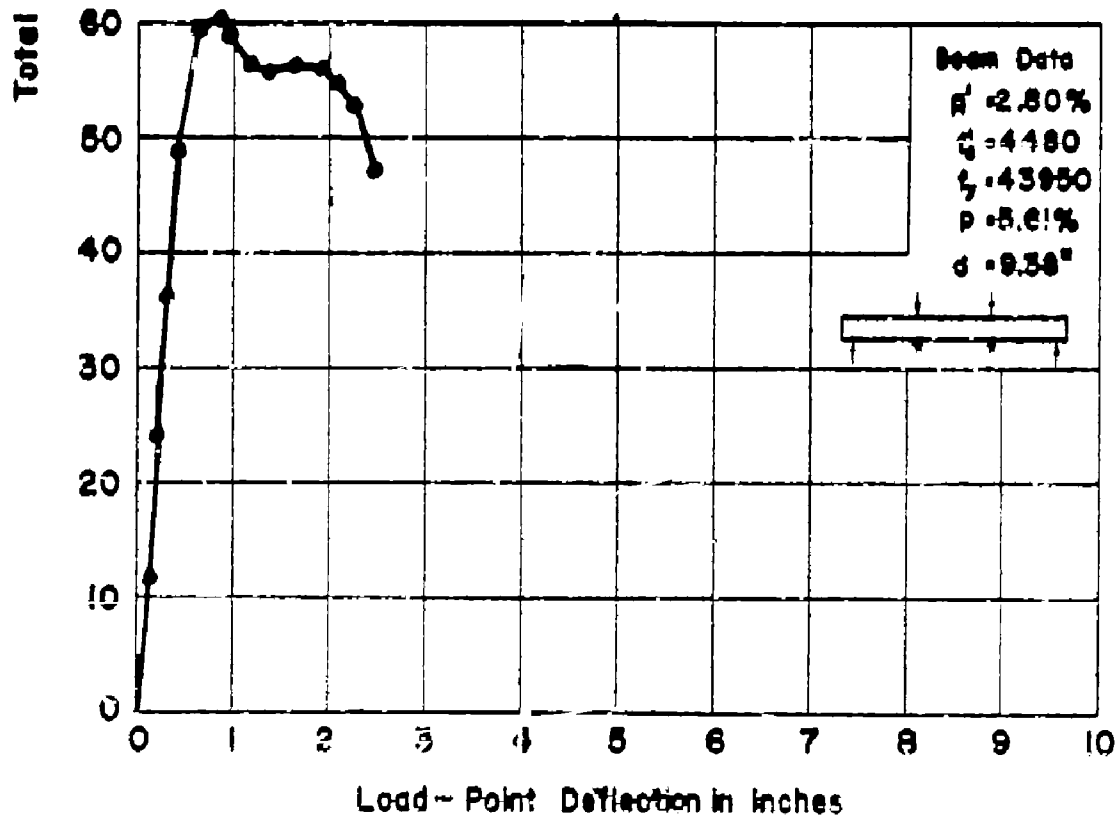

APP. FIG. 31 LOAD-DEFLECTION CURVES FOR BEAM NO. C5yn

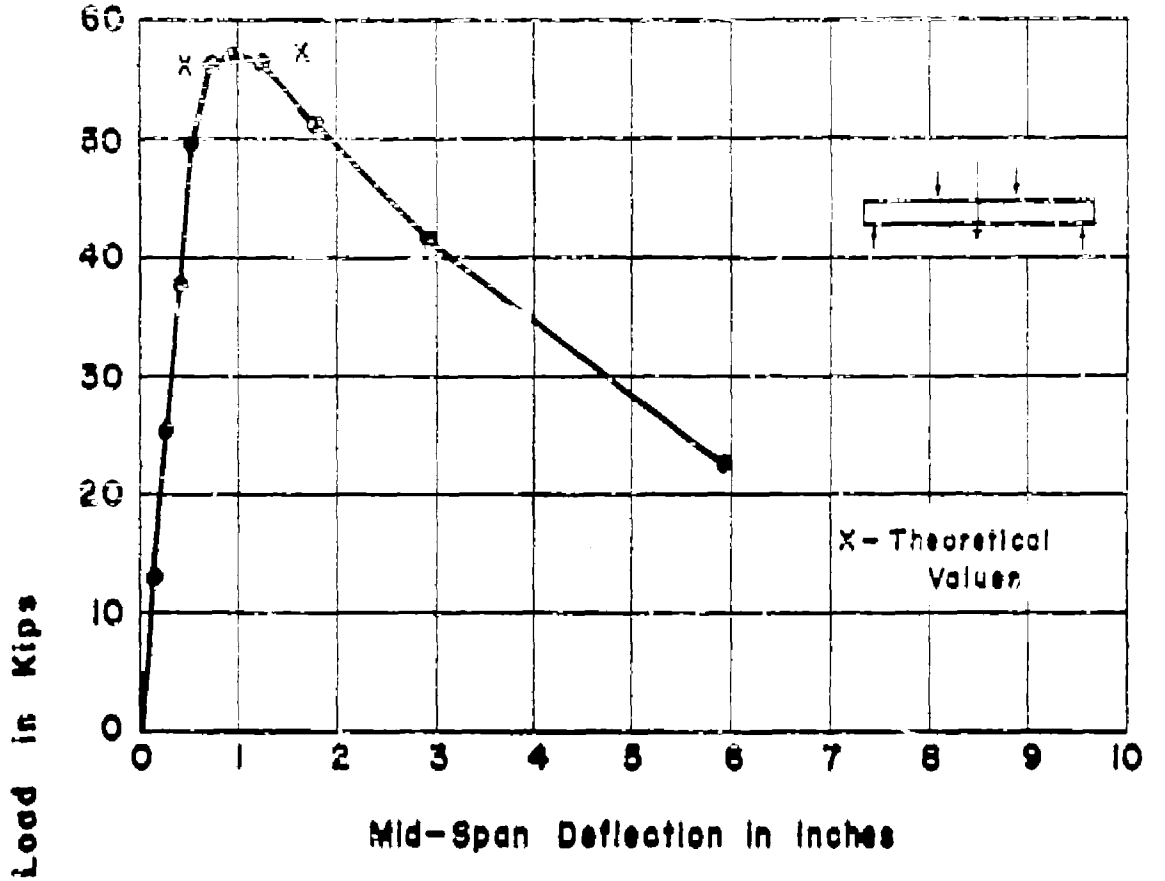

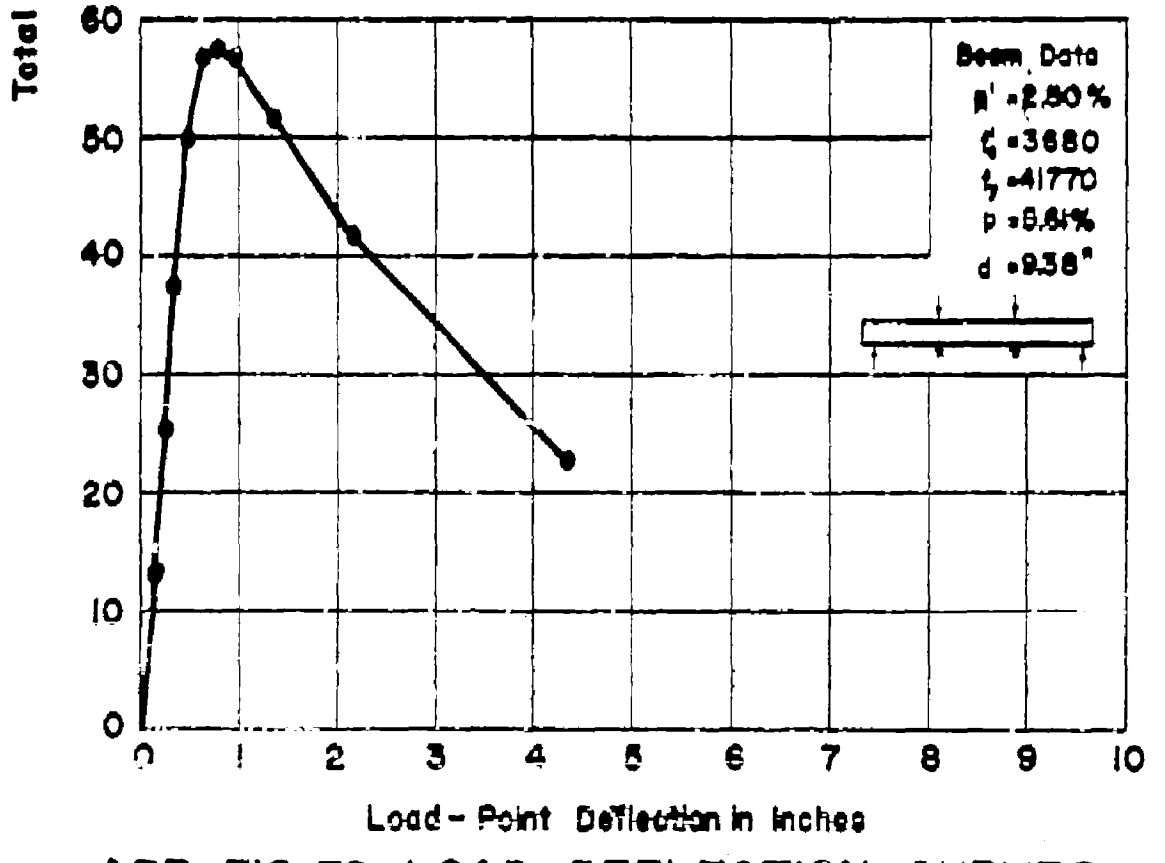

APP. FIG. 32 LOAD-DEFLECTION CURVES FOR BEAM NO. CGxm

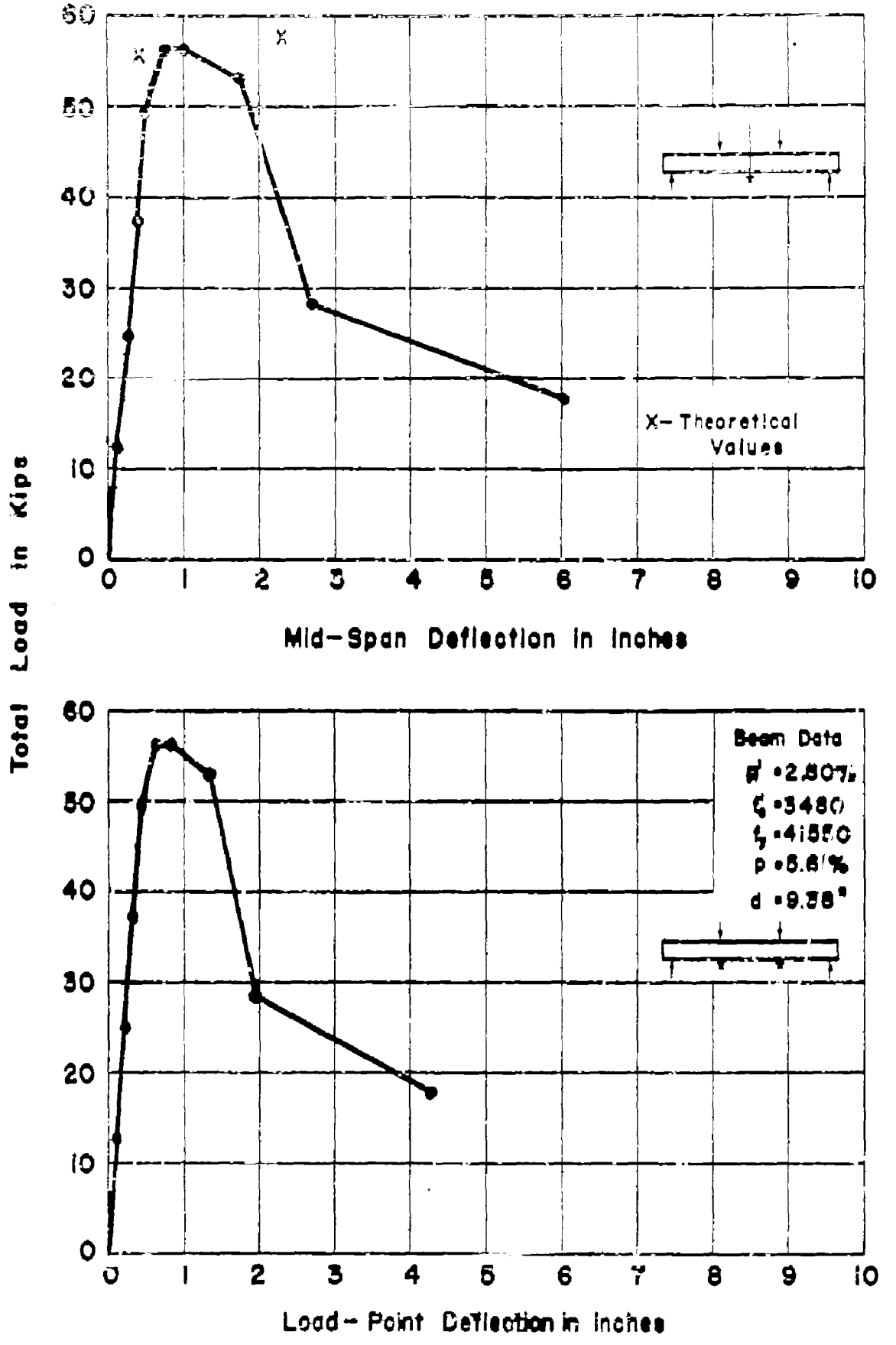

APP. FIG. 33 LOAD-DEFLECTION CURVES FOR BEAM NO. C7w

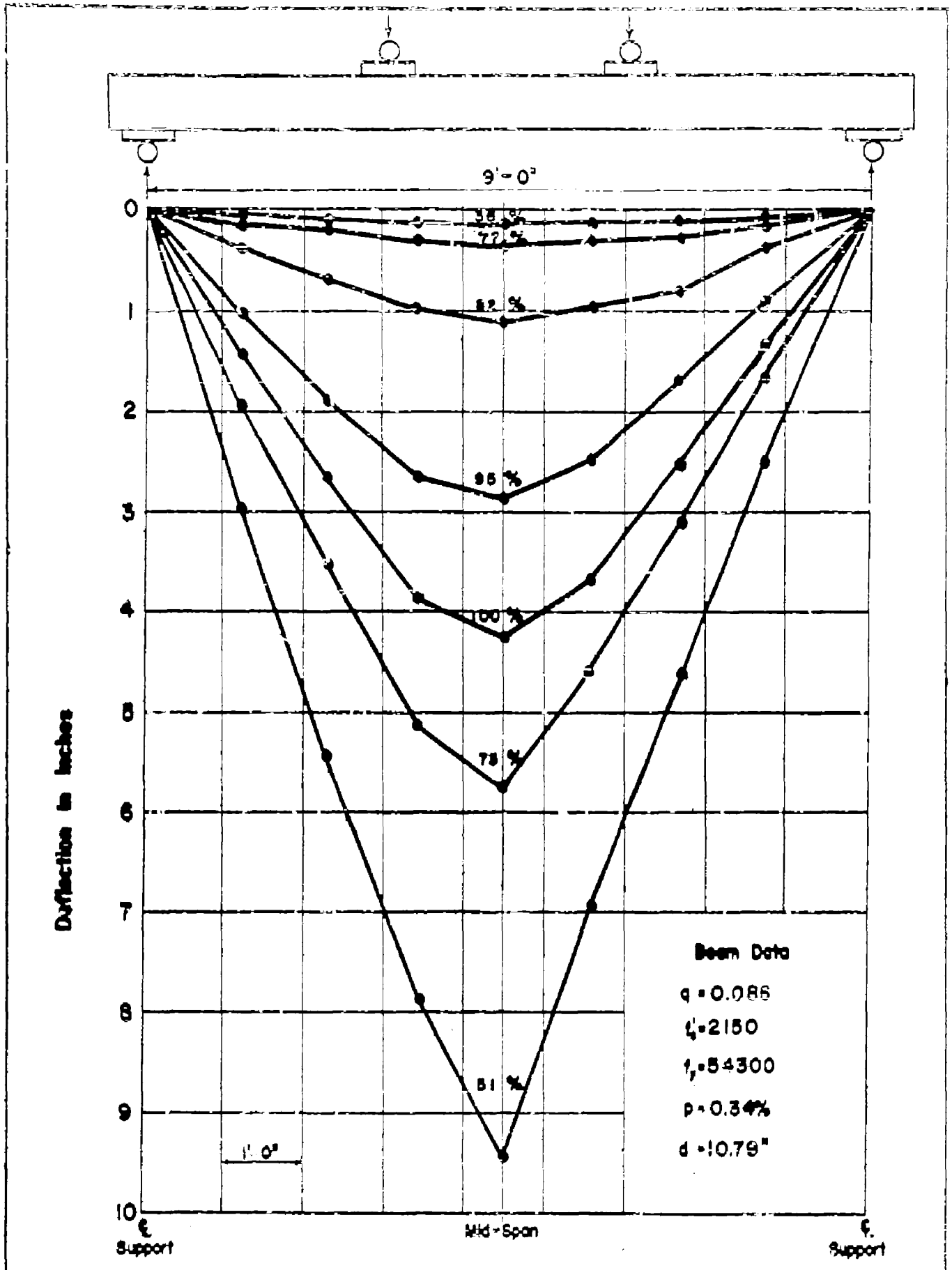

APP. FIG. 34 DEFLECTIONS ALONG BEAM NO. T1L3

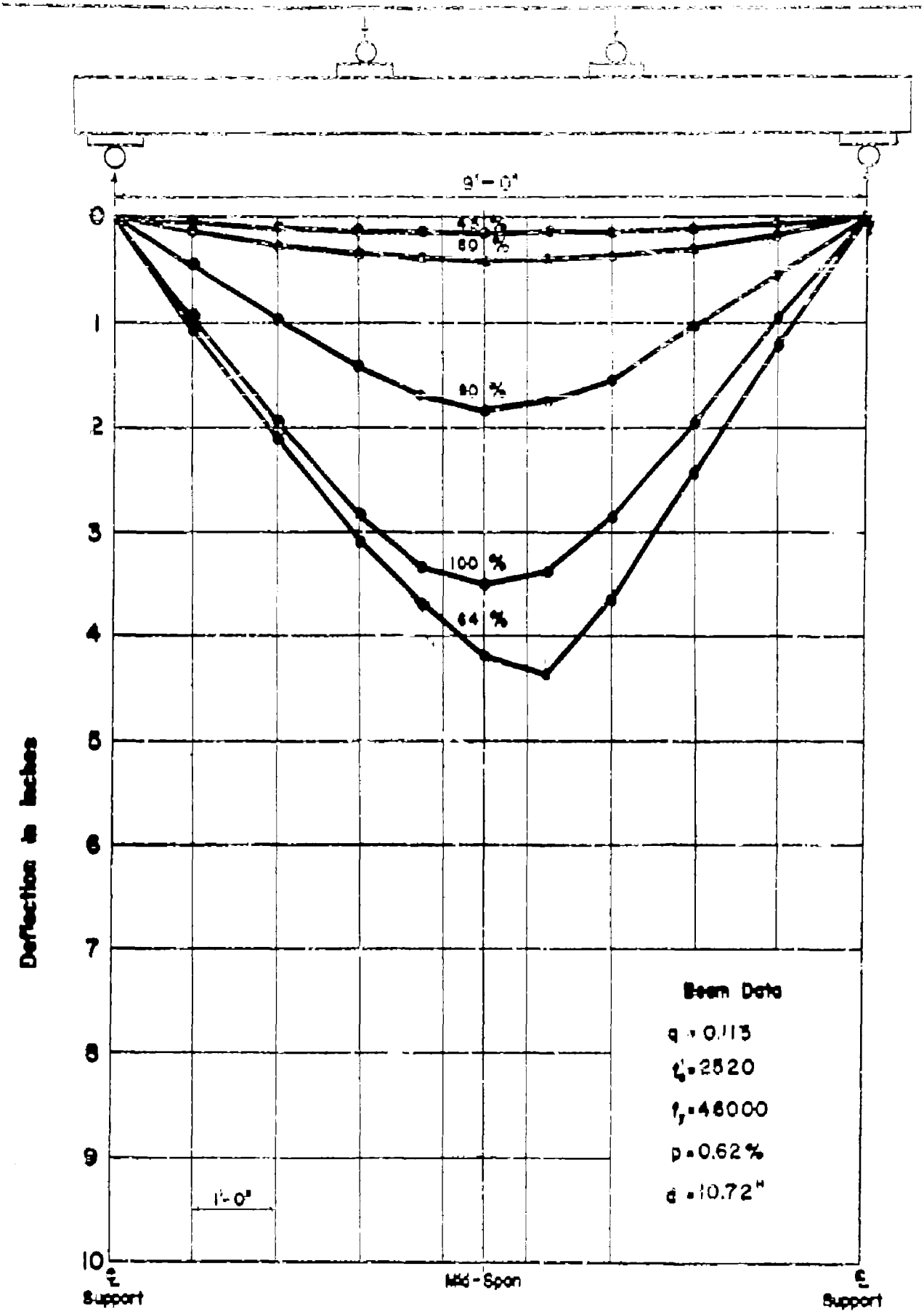

APP FIG. 35 DEFLECTIONS ALONG BEAM NO. T1Lb

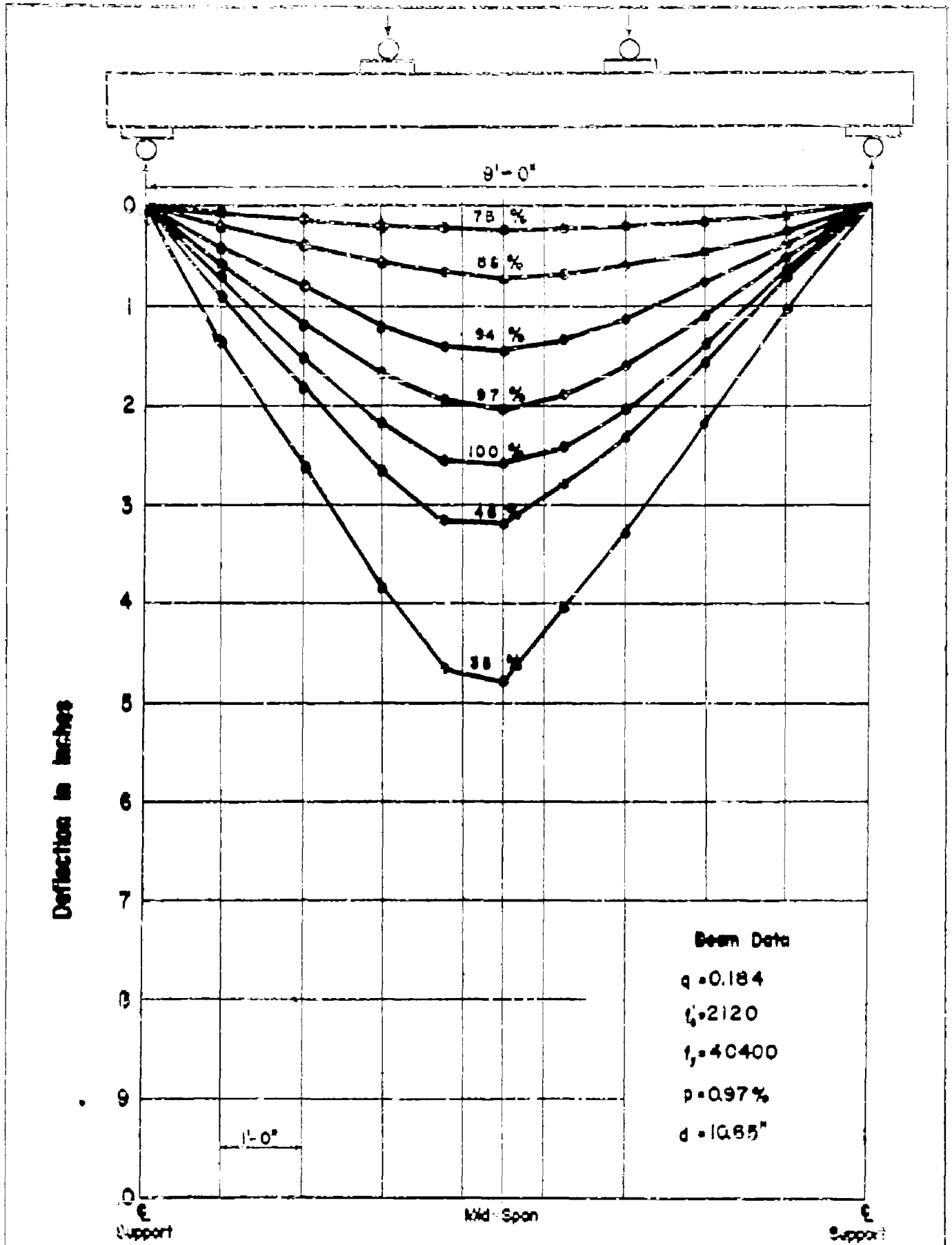

APP FIG. 36 DEFLECTIONS ALONG BEAM NO. T2L0

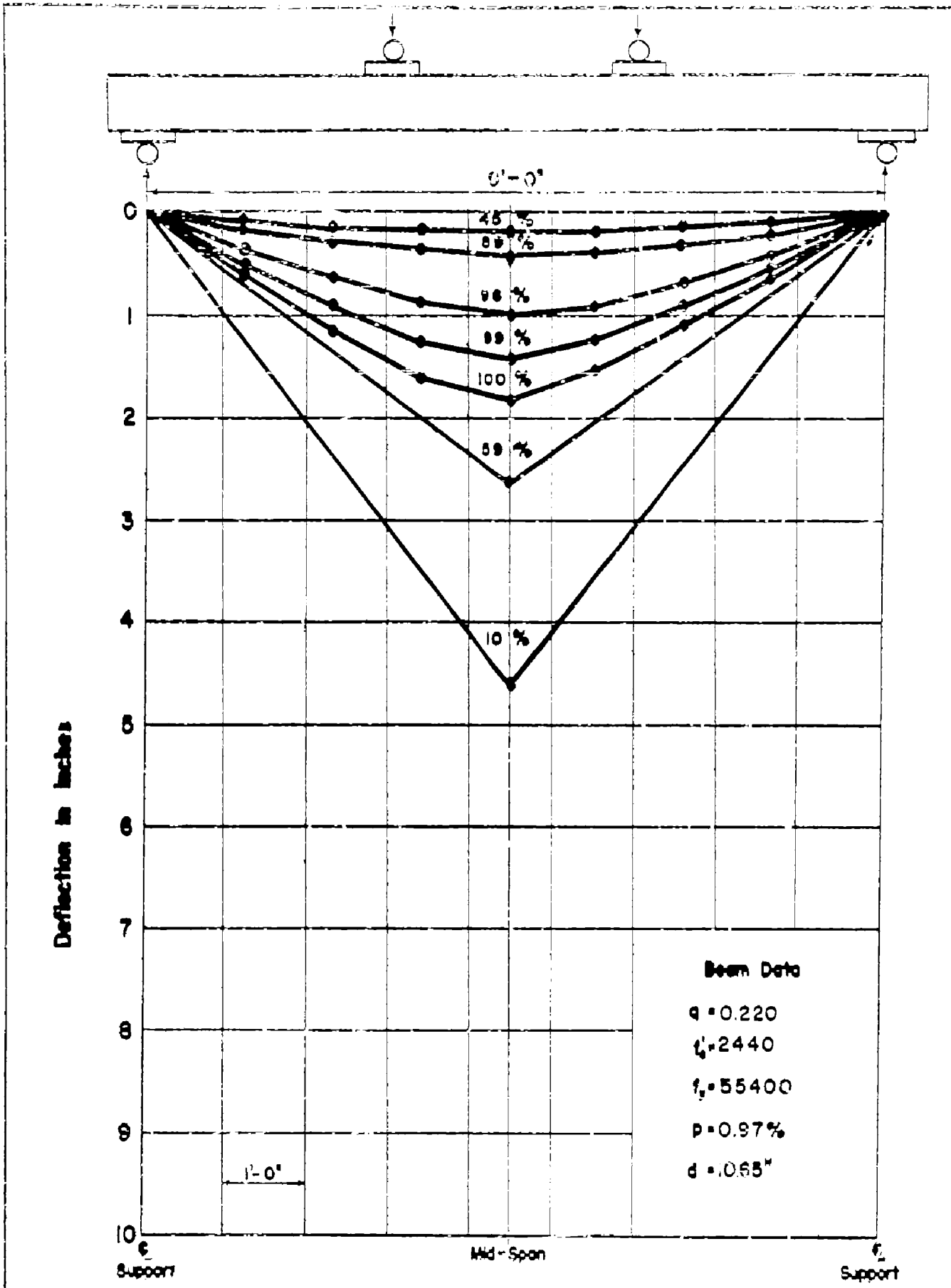

APP. FIG. 37 DEFLECTIONS ALONG BEAM NO. T2L6

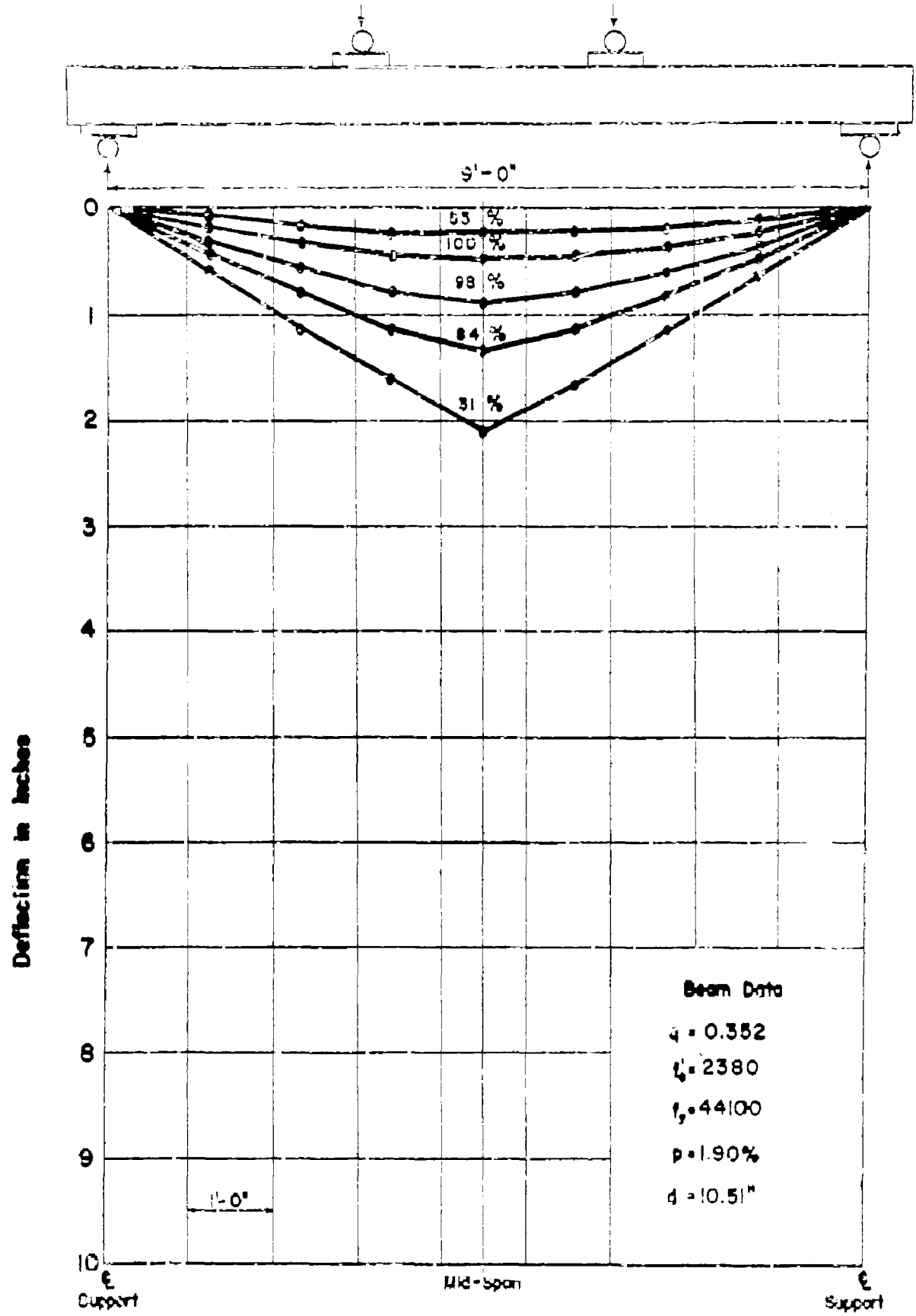

APPFIG. 38 DEFLECTIONS ALONG BEAM NO. T4La

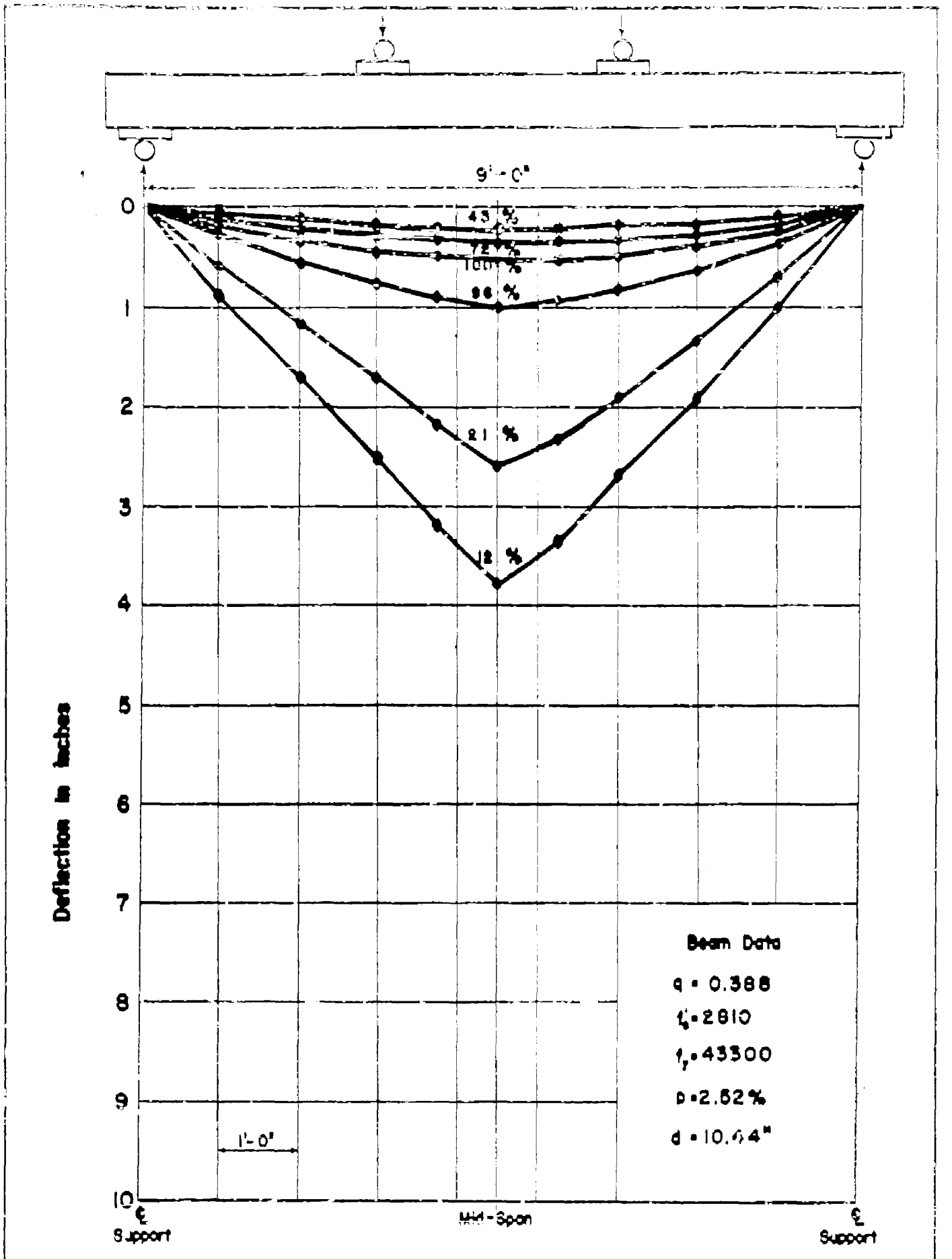

APPFIG. 39 DEFLECTIONS ALONG BEAM NO. T4L1

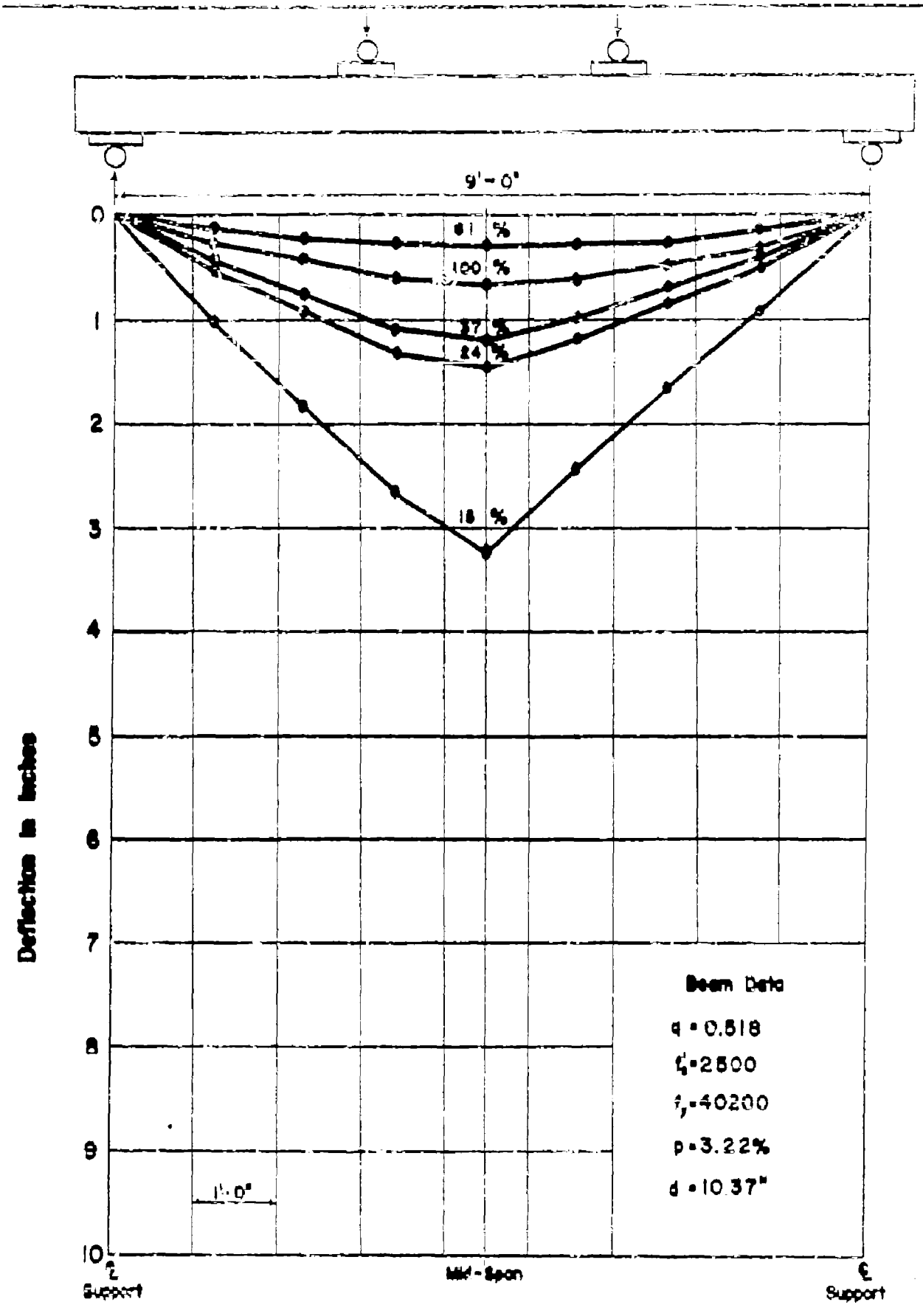

APP. FIG. 40 DEFLECTIONS ALONG BEAM NO. T5L

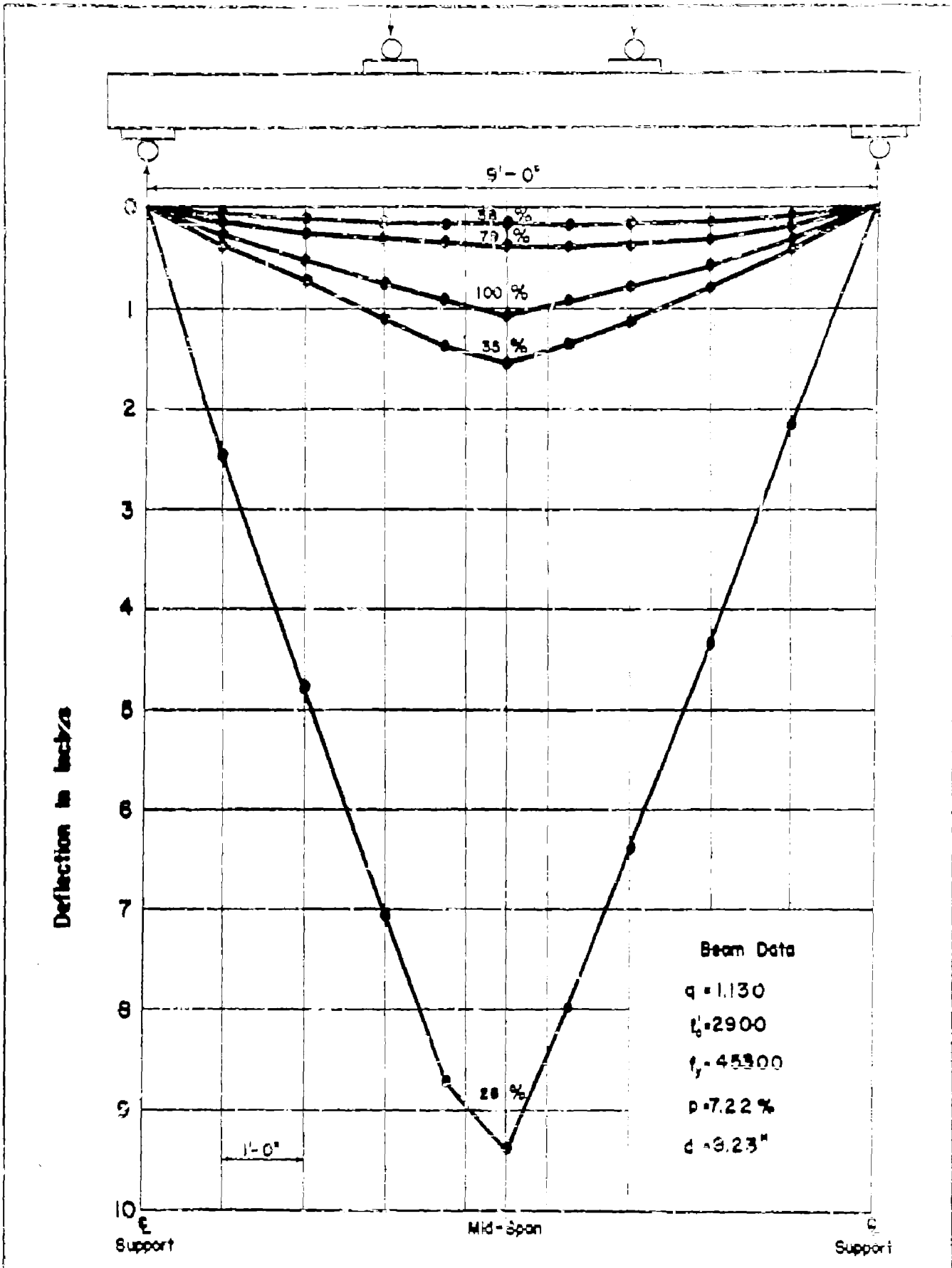

APPFIG. 41 DEFLECTIONS ALONG BEAM NO. T II L

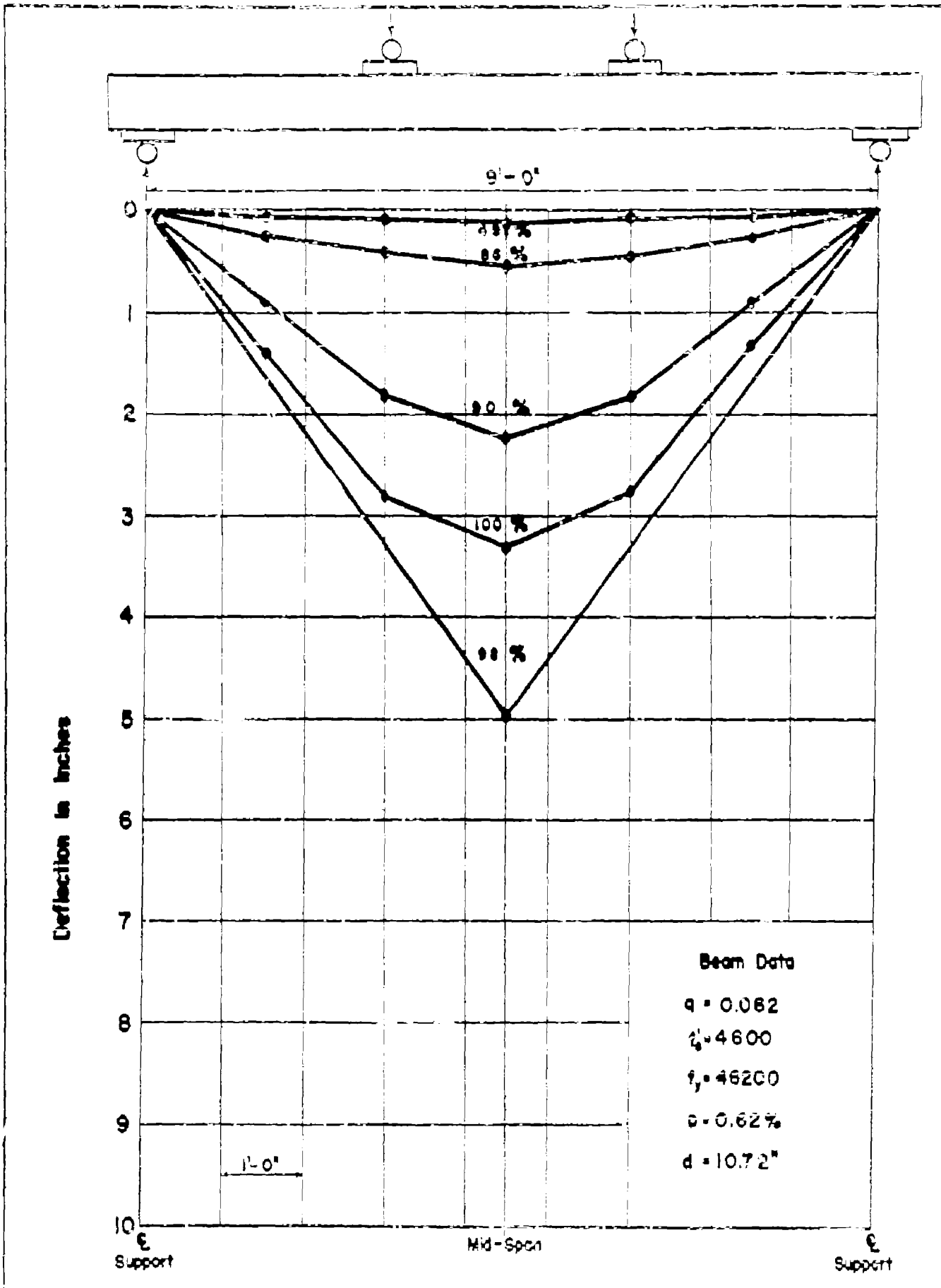

APP. FIG. 42 DEFLECTIONS ALONG BEAM NO. T1Ma

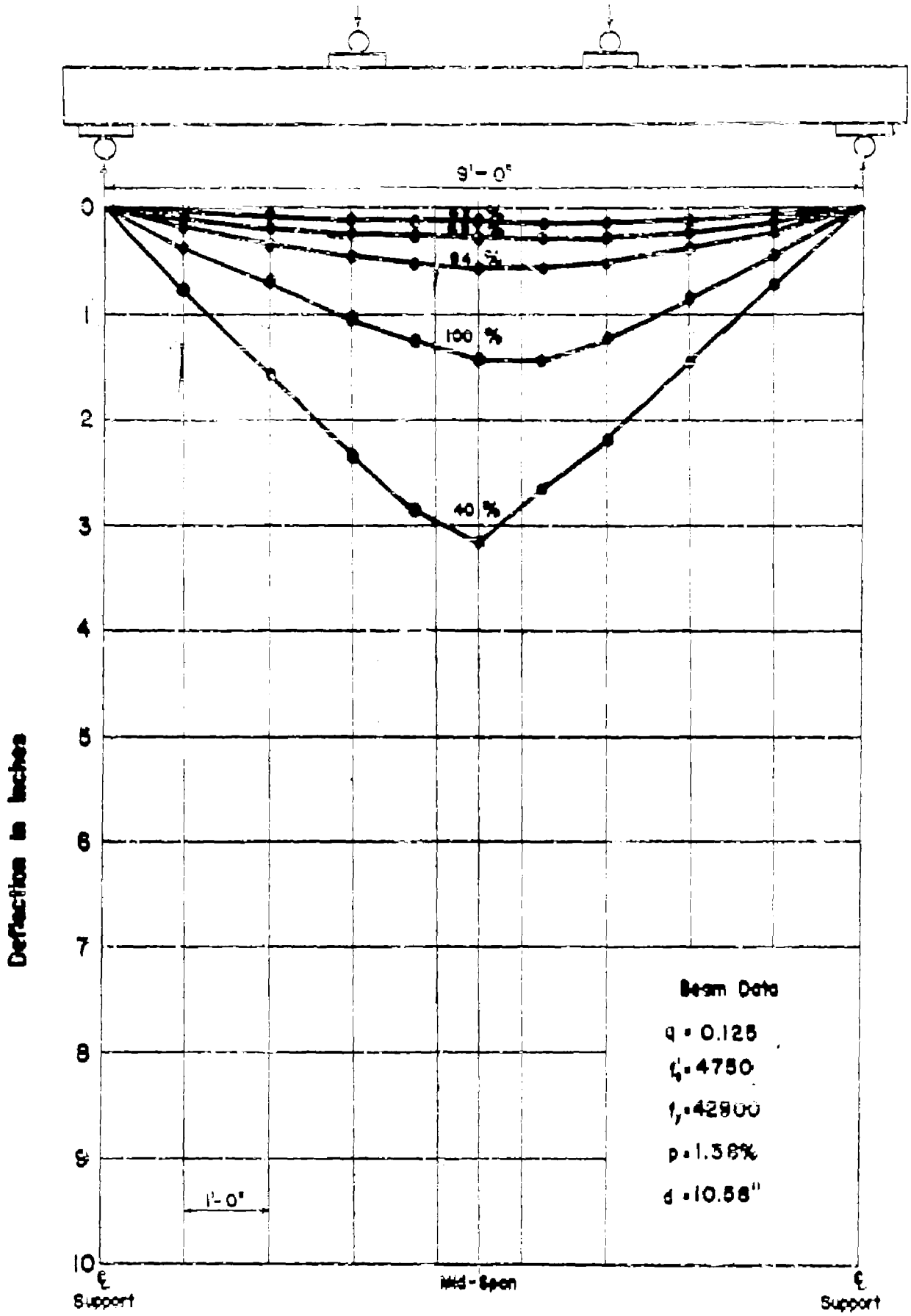

APP. FIG. 43 DEFLECTIONS ALONG BEAM NO. TIMb

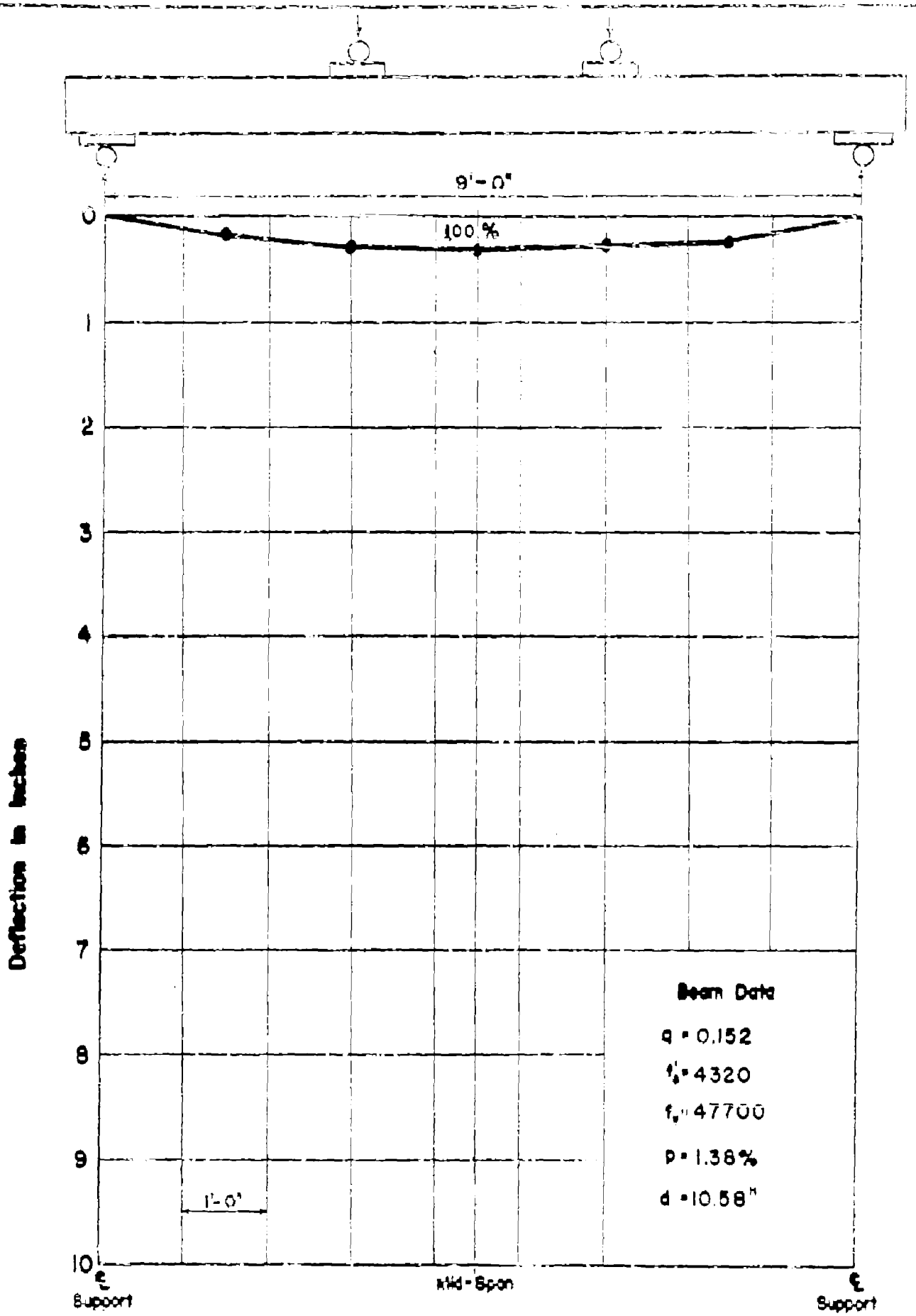

APP. FIG. 44 DEFLECTIONS ALONG BEAM NO. T2Ma

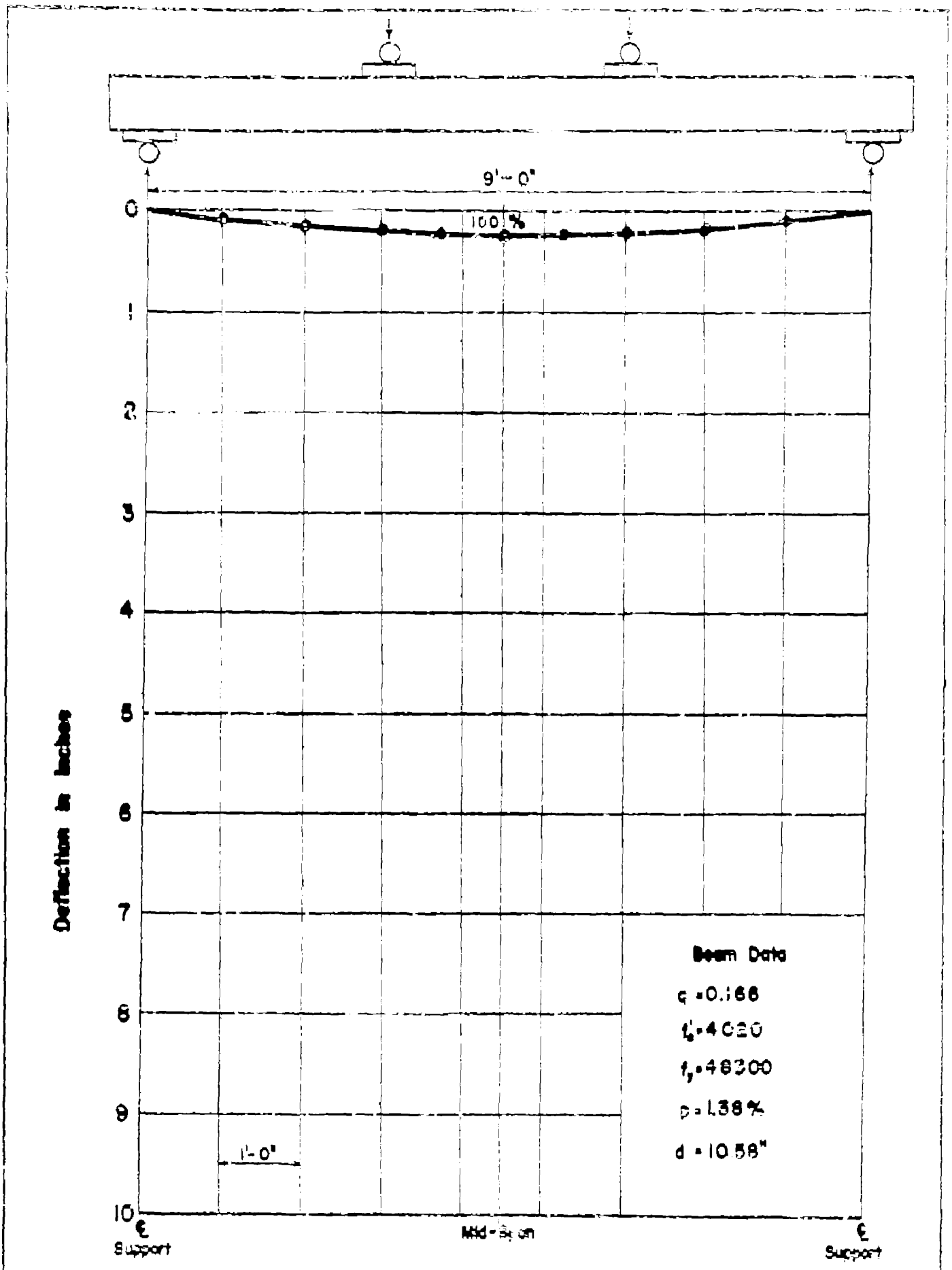

APP. FIG. 45 DEFLECTIONS ALONG BEAM NO. T2Mb

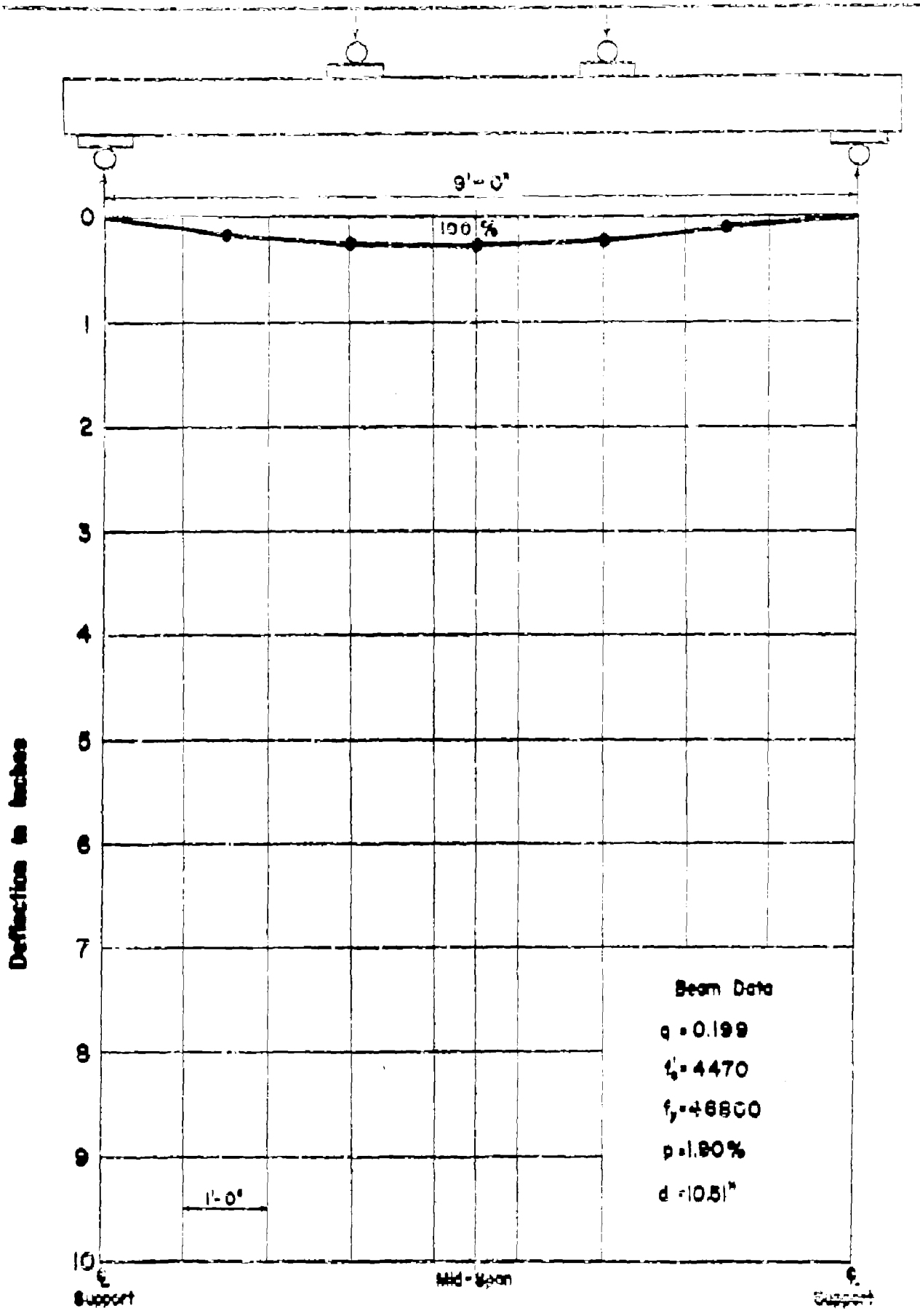

APPFIG. 46 DEFLECTIONS ALONG BEAM NO.T2Mc

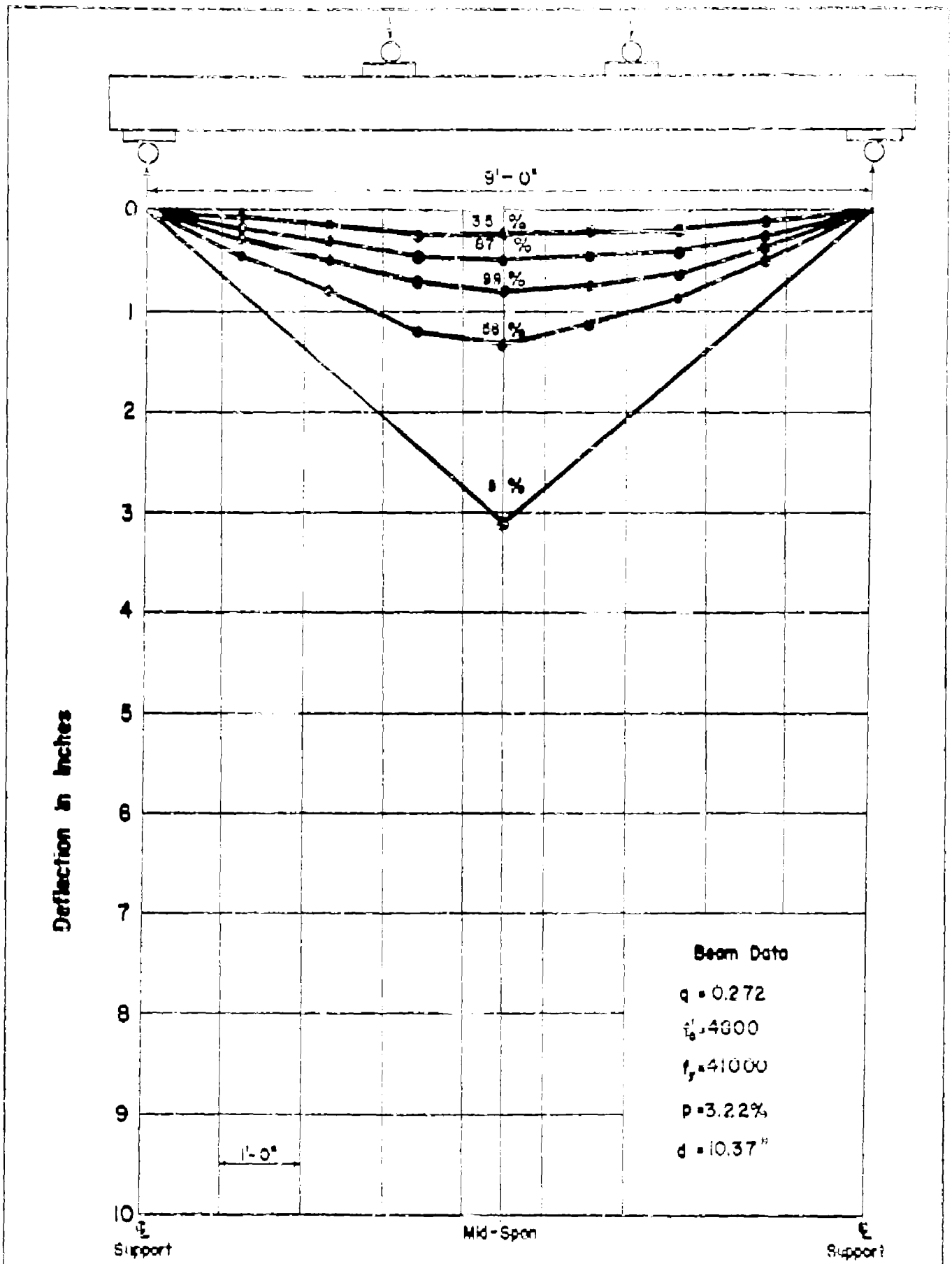

APP. FIG. 47 DEFLECTIONS ALONG BEAM NO. T3Ma

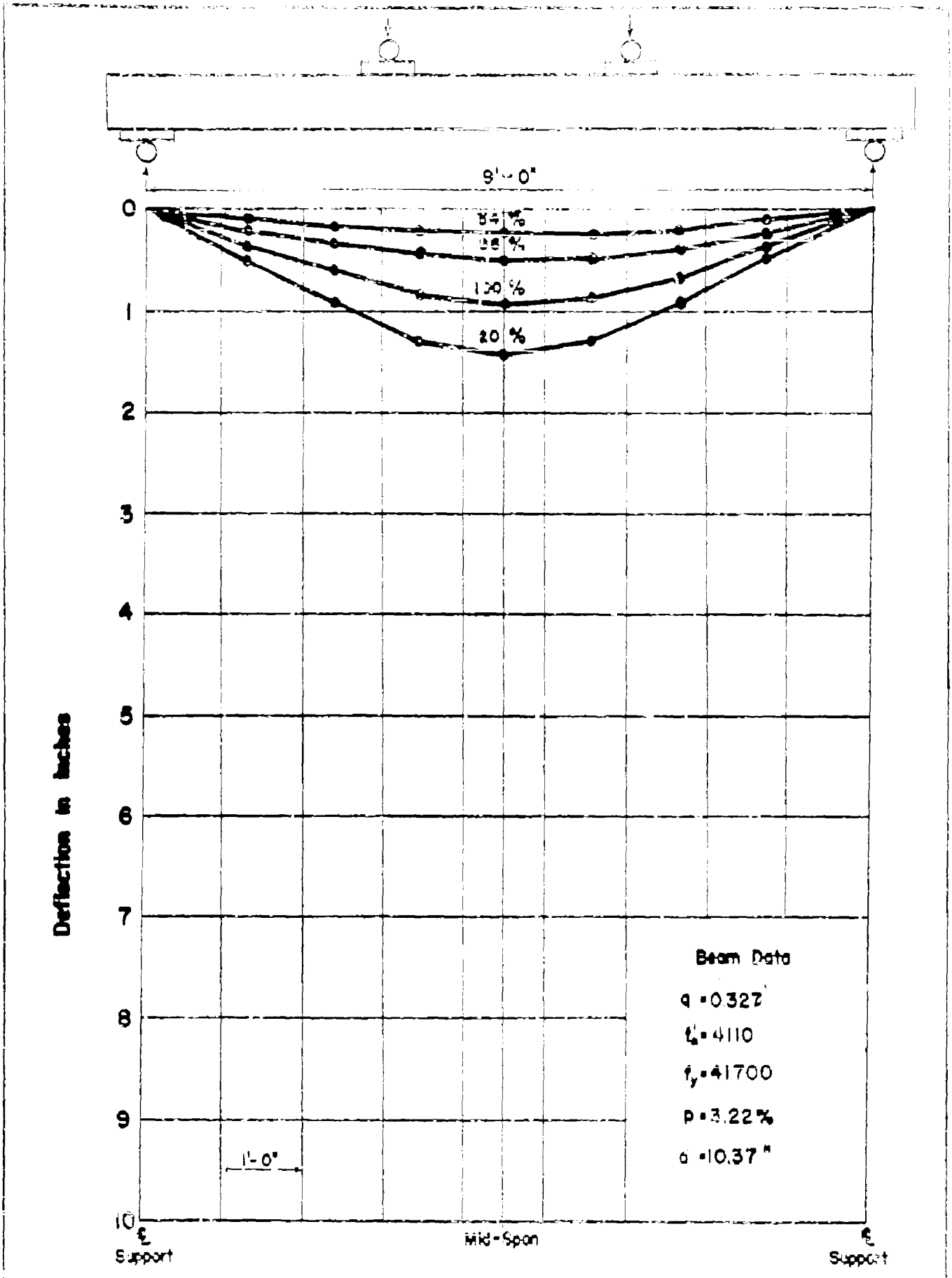

APP.FIG. 48 DEFLECTIONS ALONG BEAM NO. T3Mb

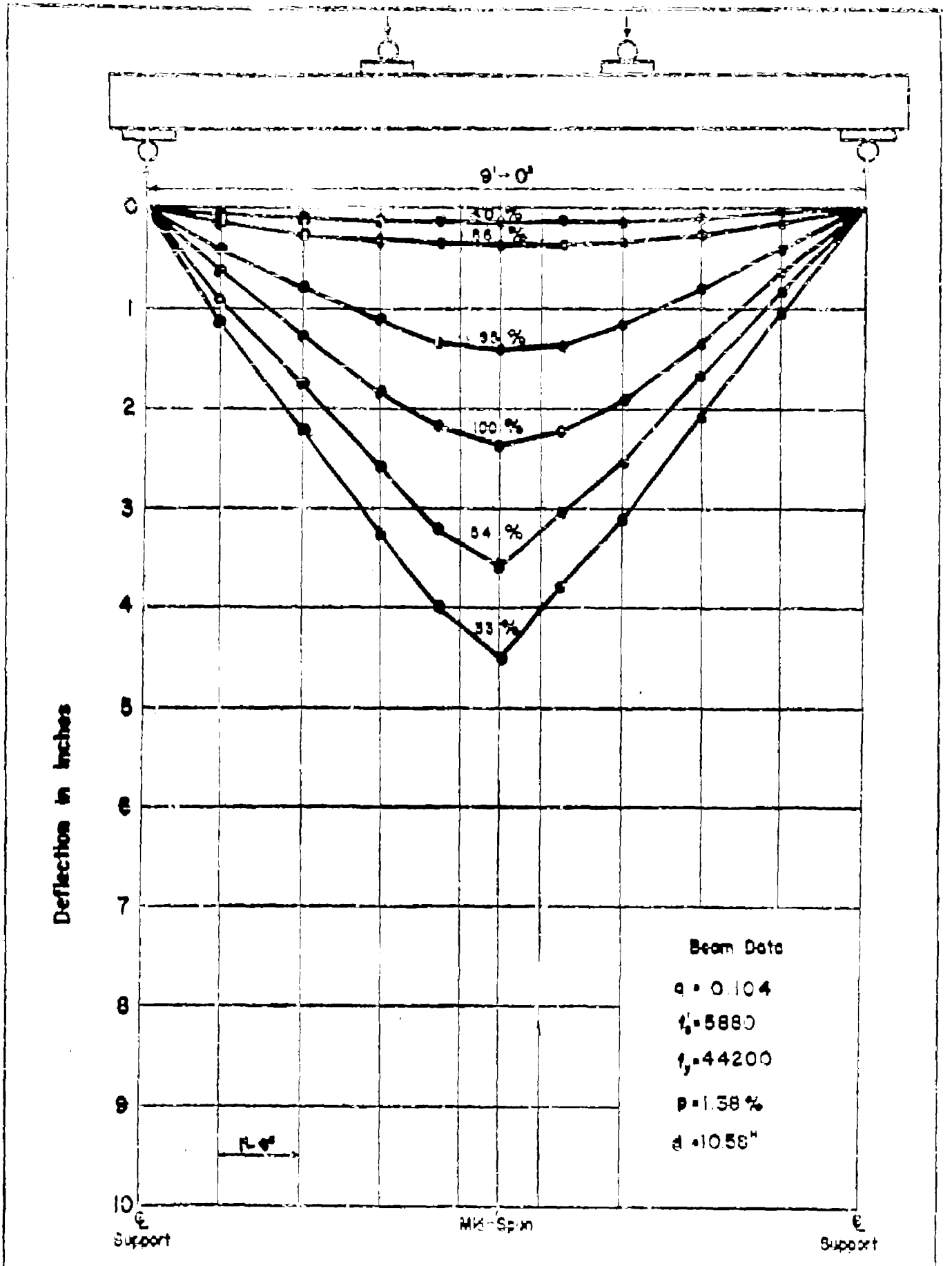

APP FIG. 49 DEFLECTIONS ALONG BEAM NO. IIHa

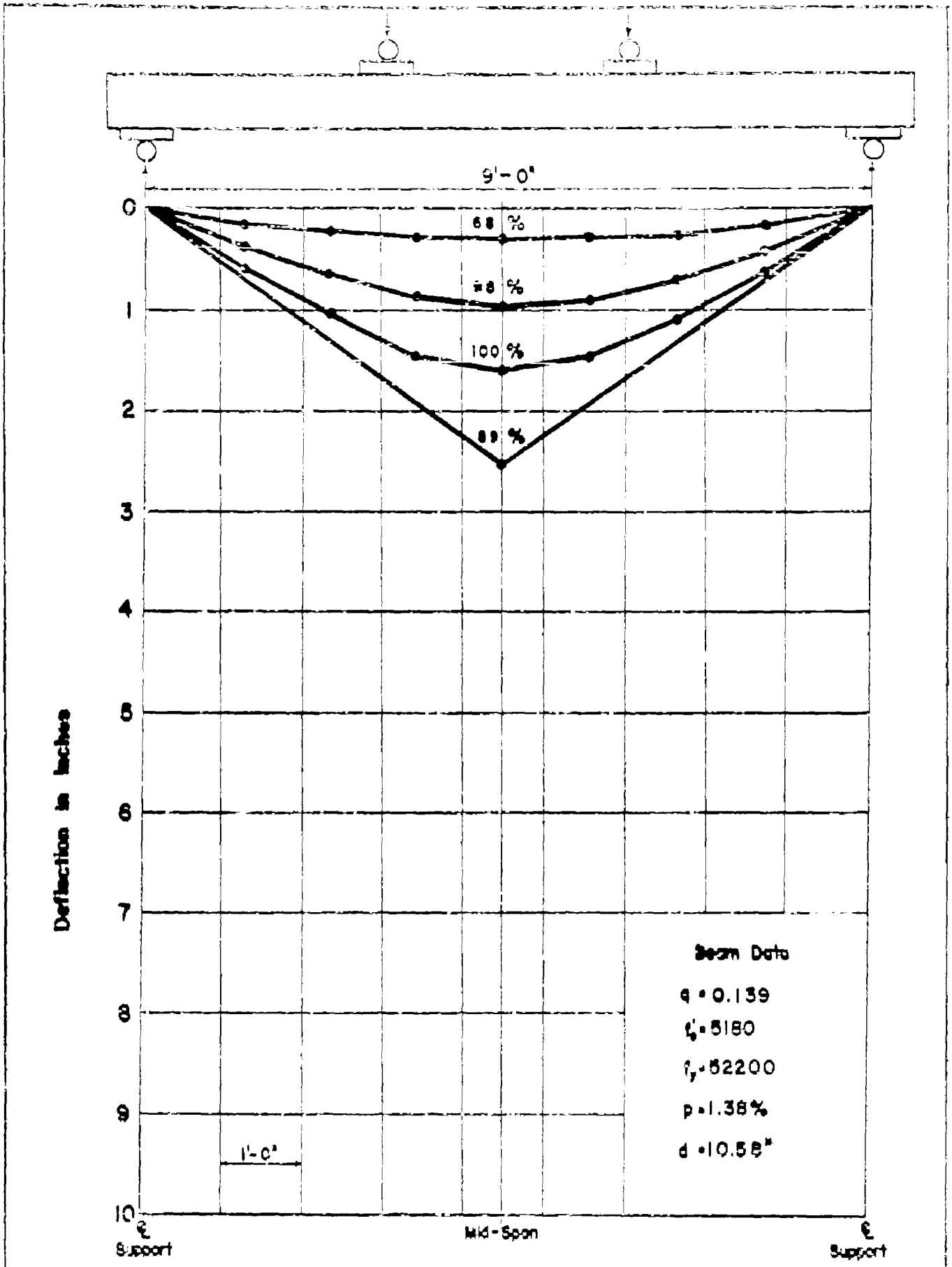

APP FIG. 50 DEFLECTIONS ALONG BEAM NO. TIHb

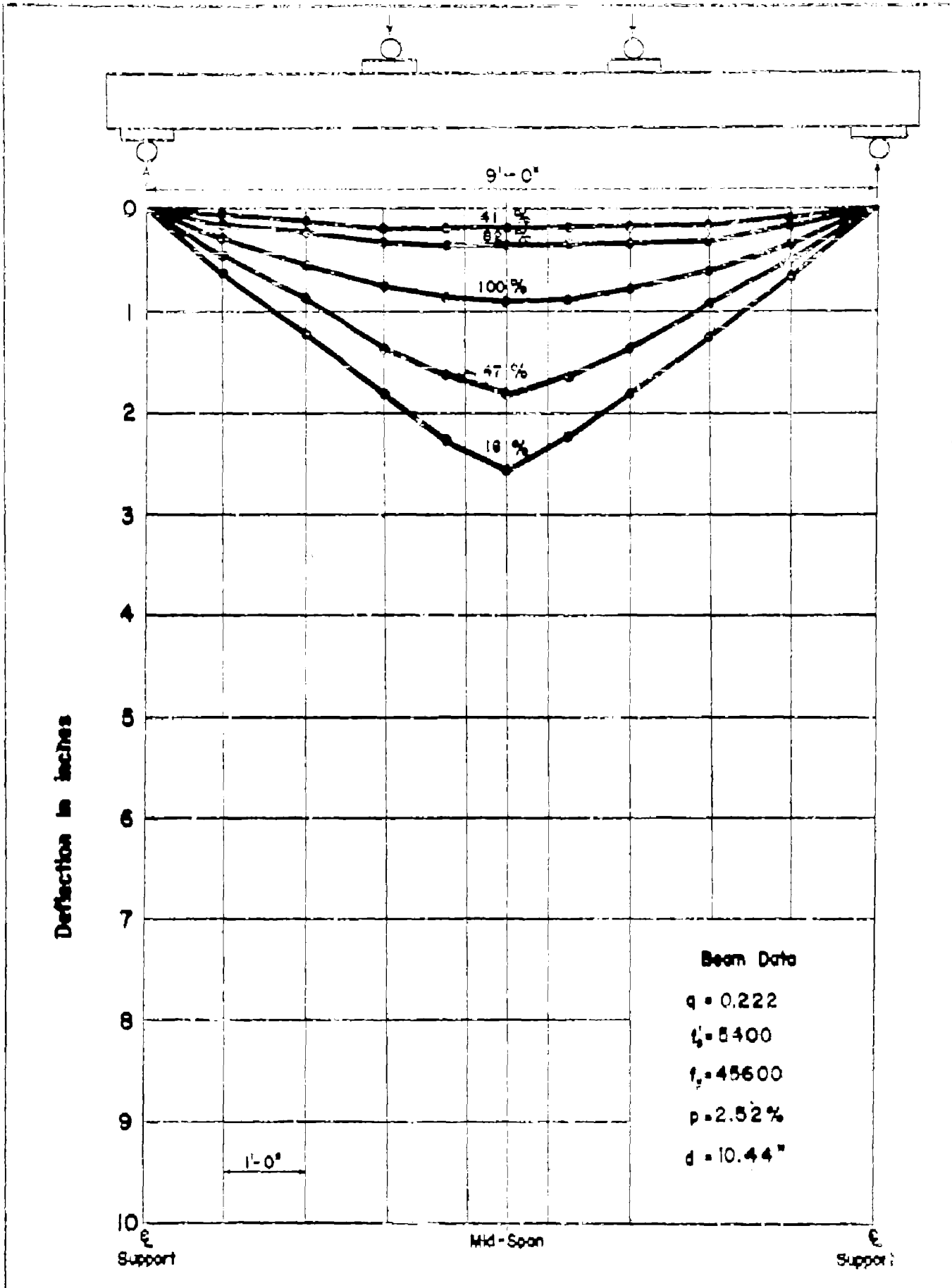

APP. FIG. 51 DEFLECTIONS ALONG BEAM NO. T2H

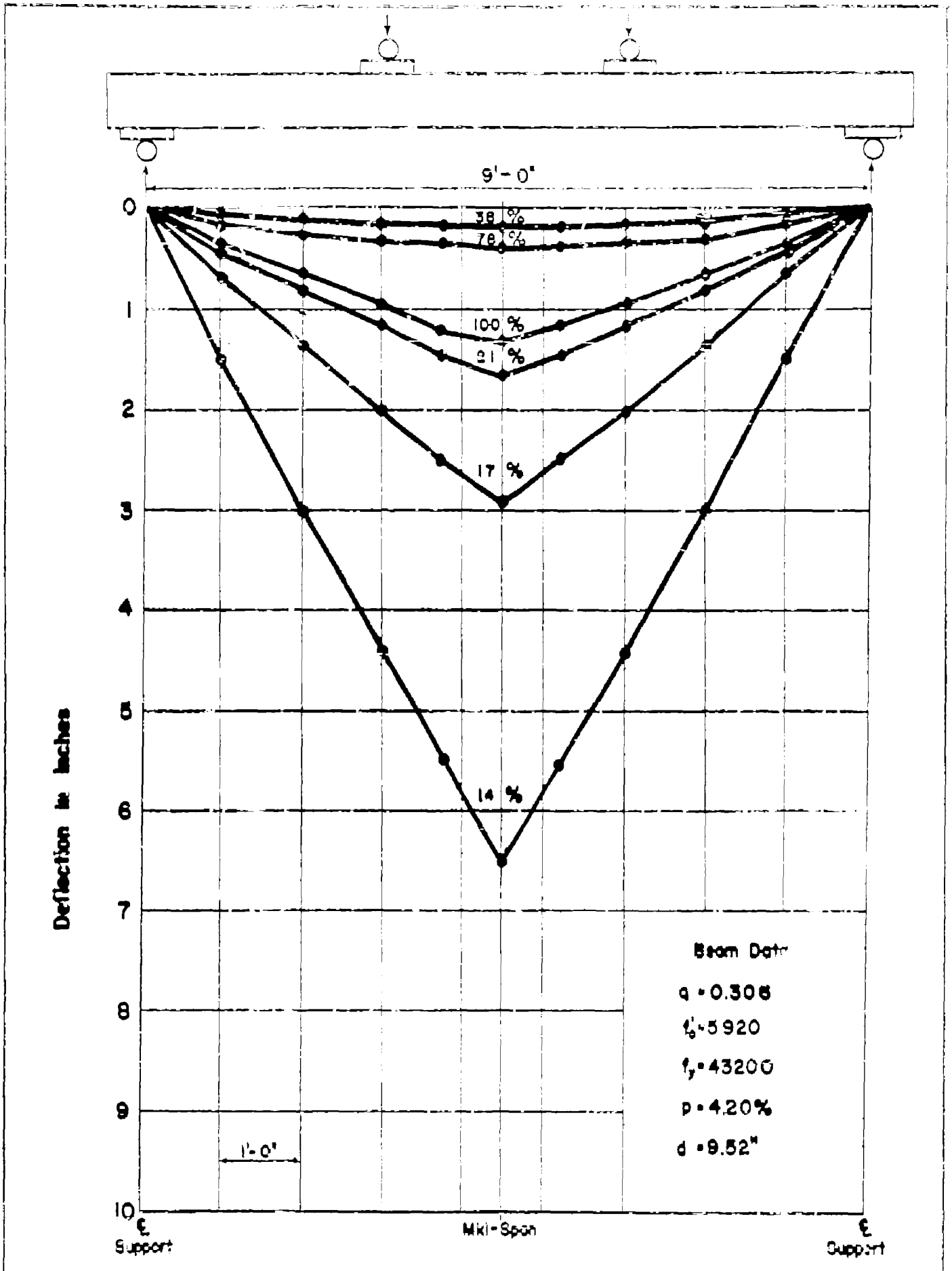

APP.FIG. 52 DEFLECTIONS ALONG BEAM NO. T3H

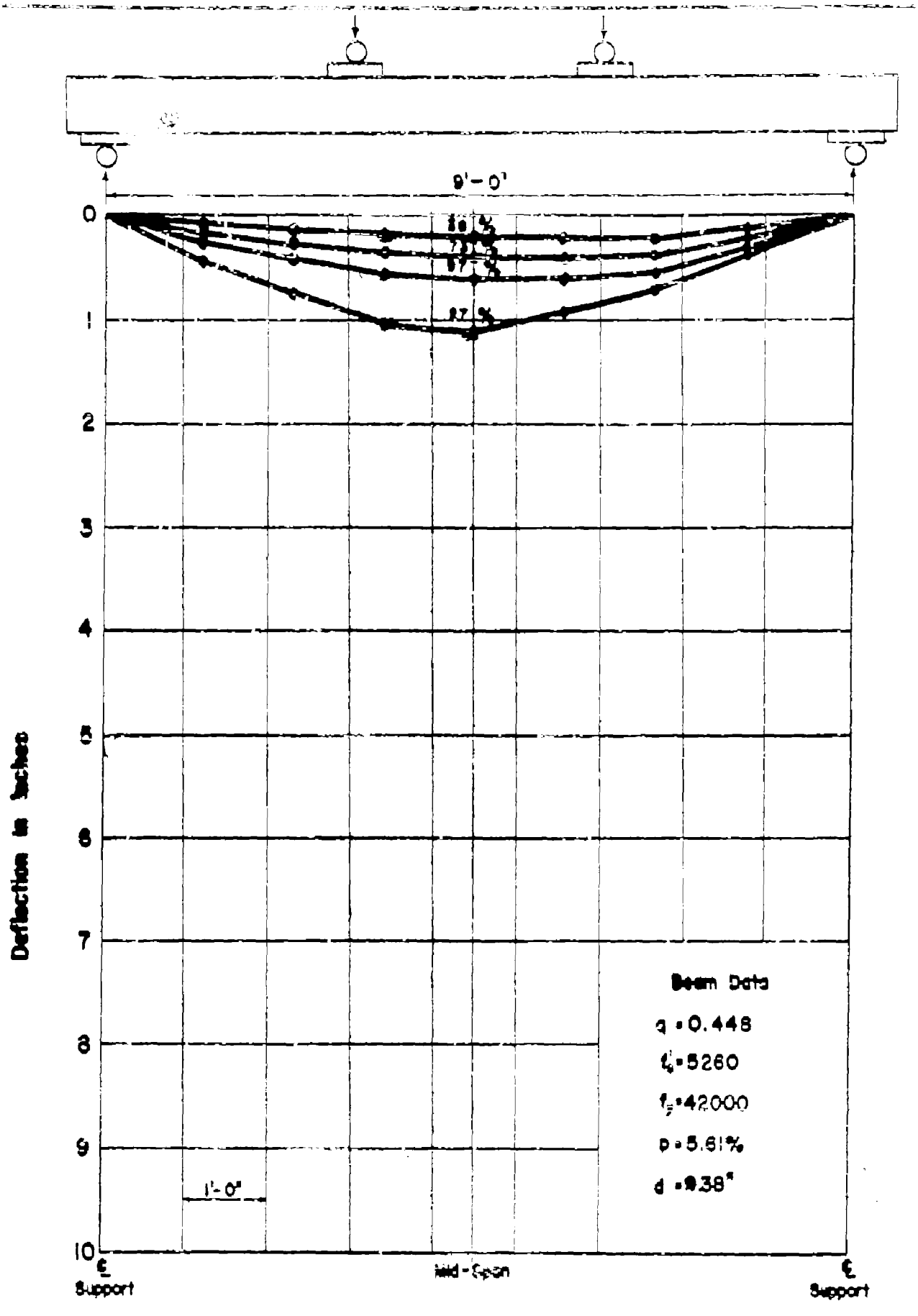

APPFIG. 53 DEFLECTIONS ALONG BEAM NO. T4H

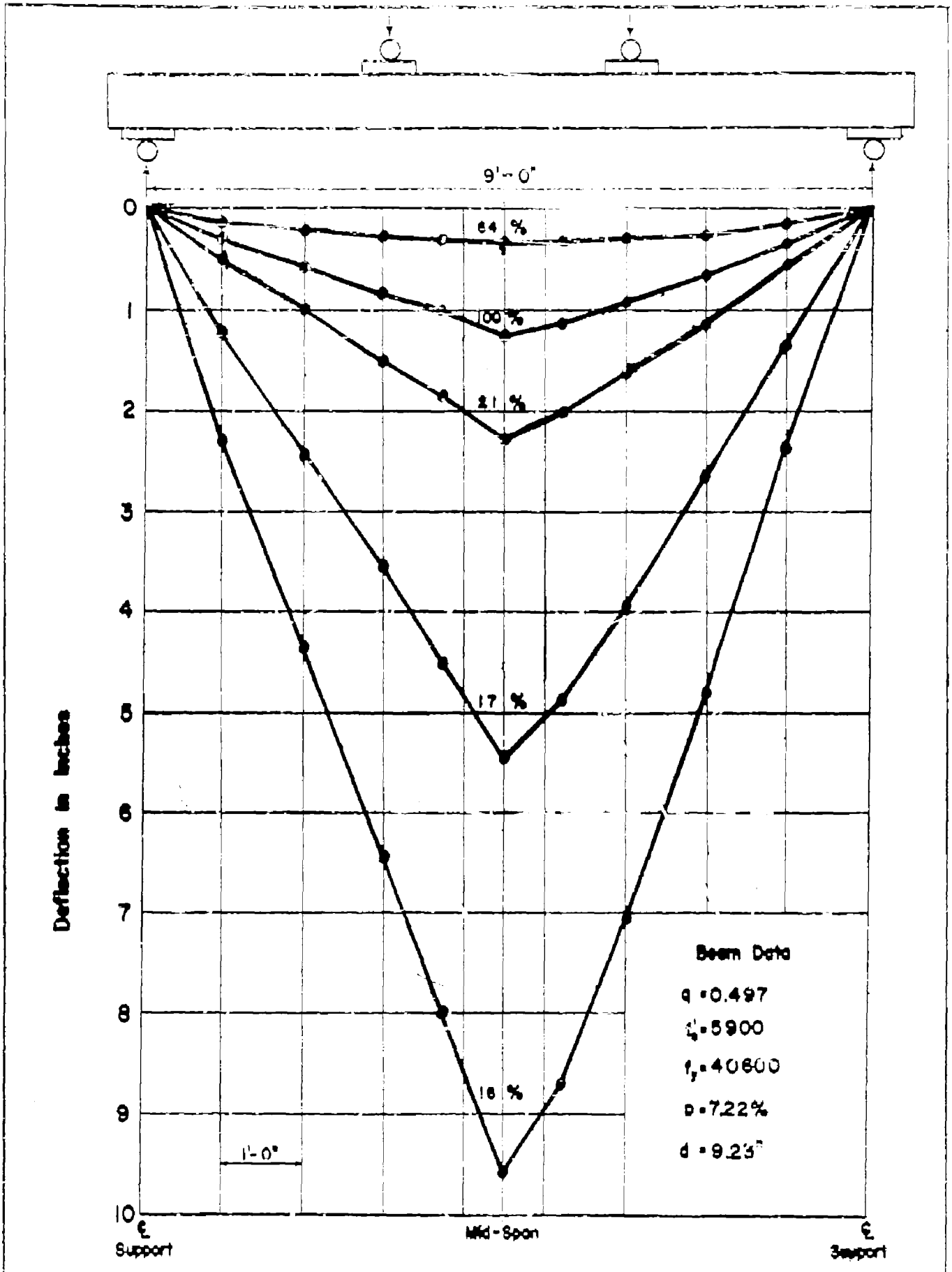

APP. FIG. 54 DEFLECTIONS ALONG BEAM NO. T5H

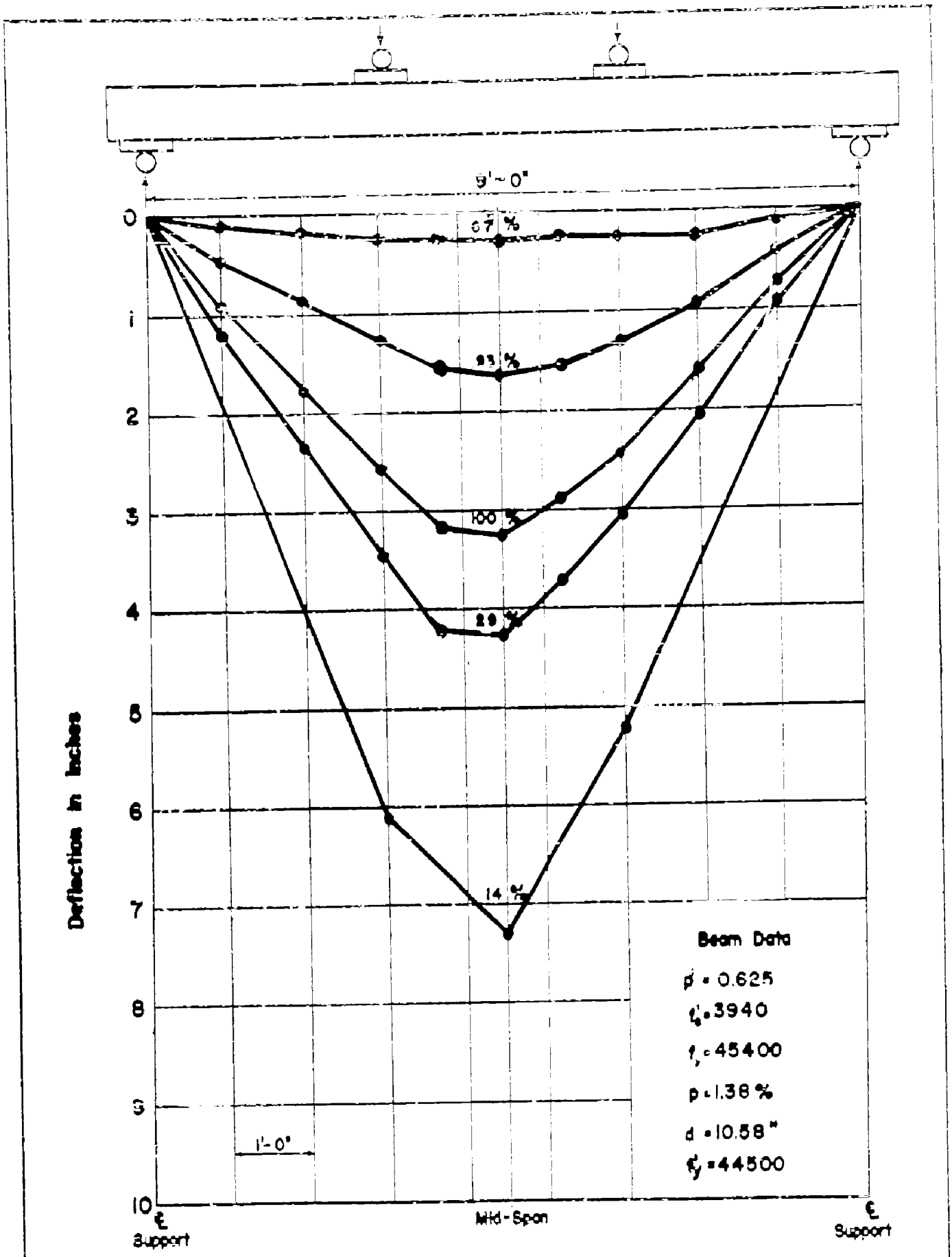

APP. FIG. 55 DEFLECTIONS ALONG BEAM NO. C2W

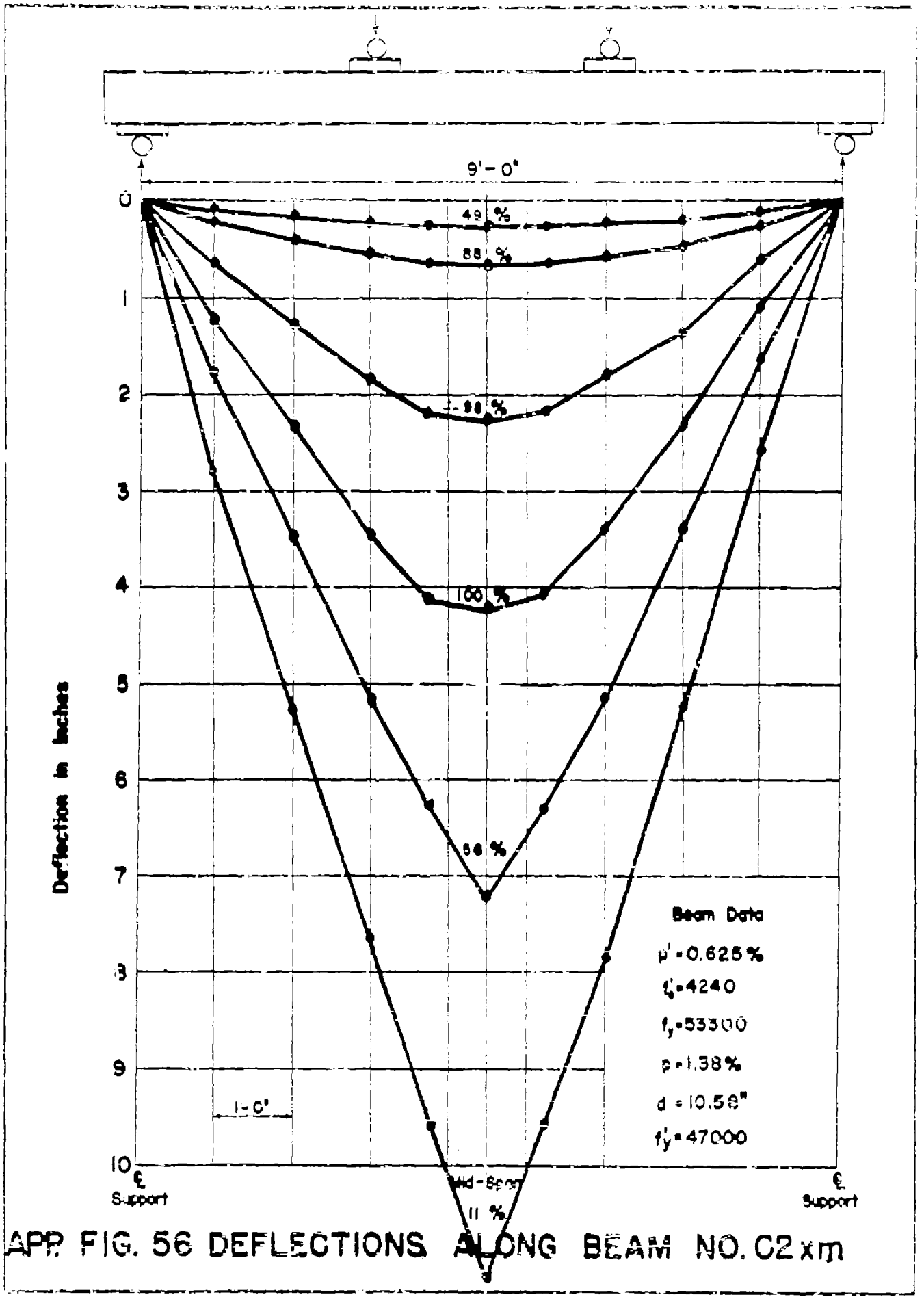

APP. FIG. 56 DEFLECTIONS ALONG BEAM NO. C2xm

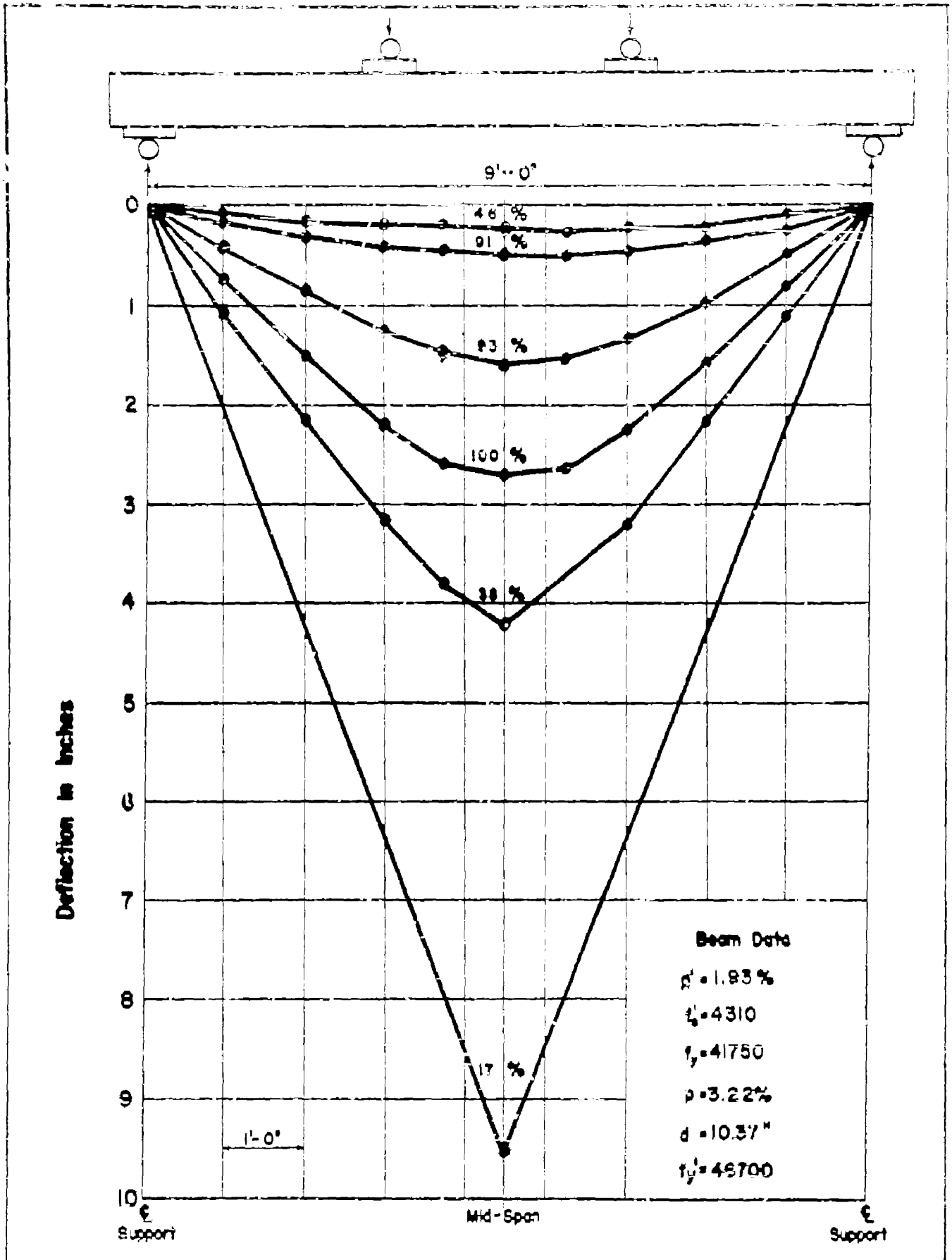

APP. FIG. 57 DEFLECTIONS ALONG BEAM NO. C3W

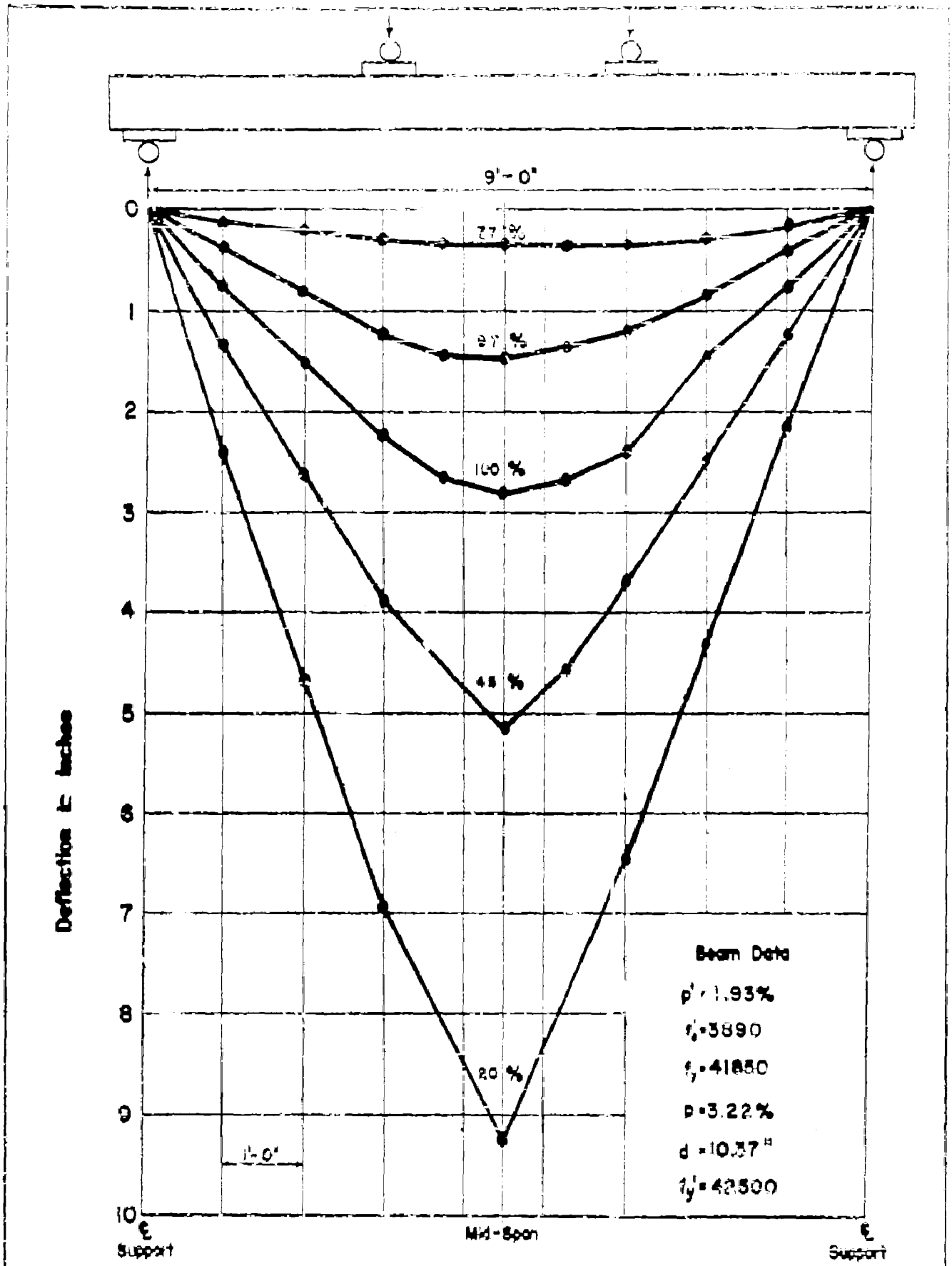

APPFIG. 58 DEFLECTIONS ALONG BEAM NO. C3xm

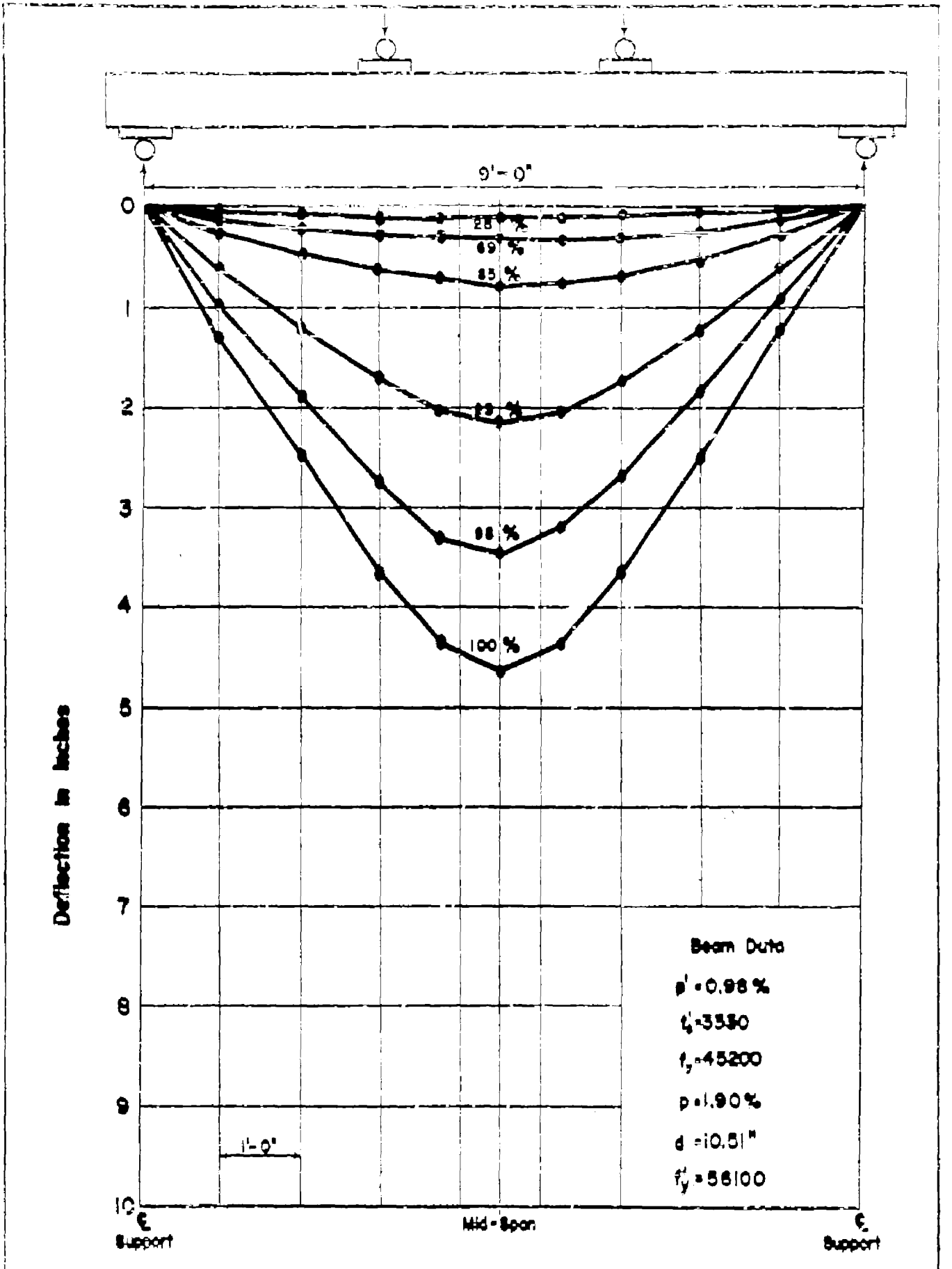

APP. FIG. 59 DEFLECTIONS ALONG BEAM NO. C3yna

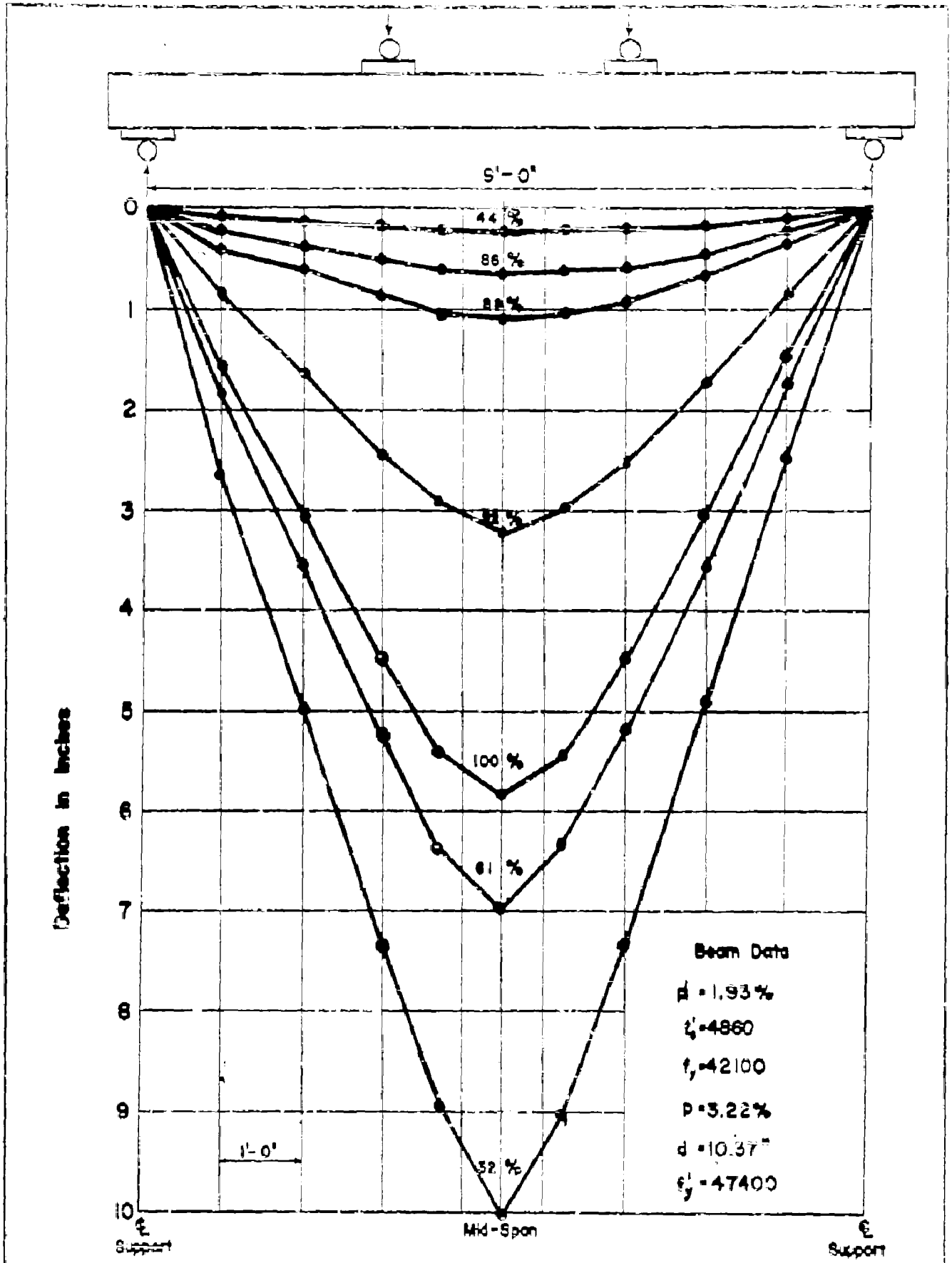

APP. FIG. 60 DEFLECTIONS ALONG BEAM NO. C3ynb

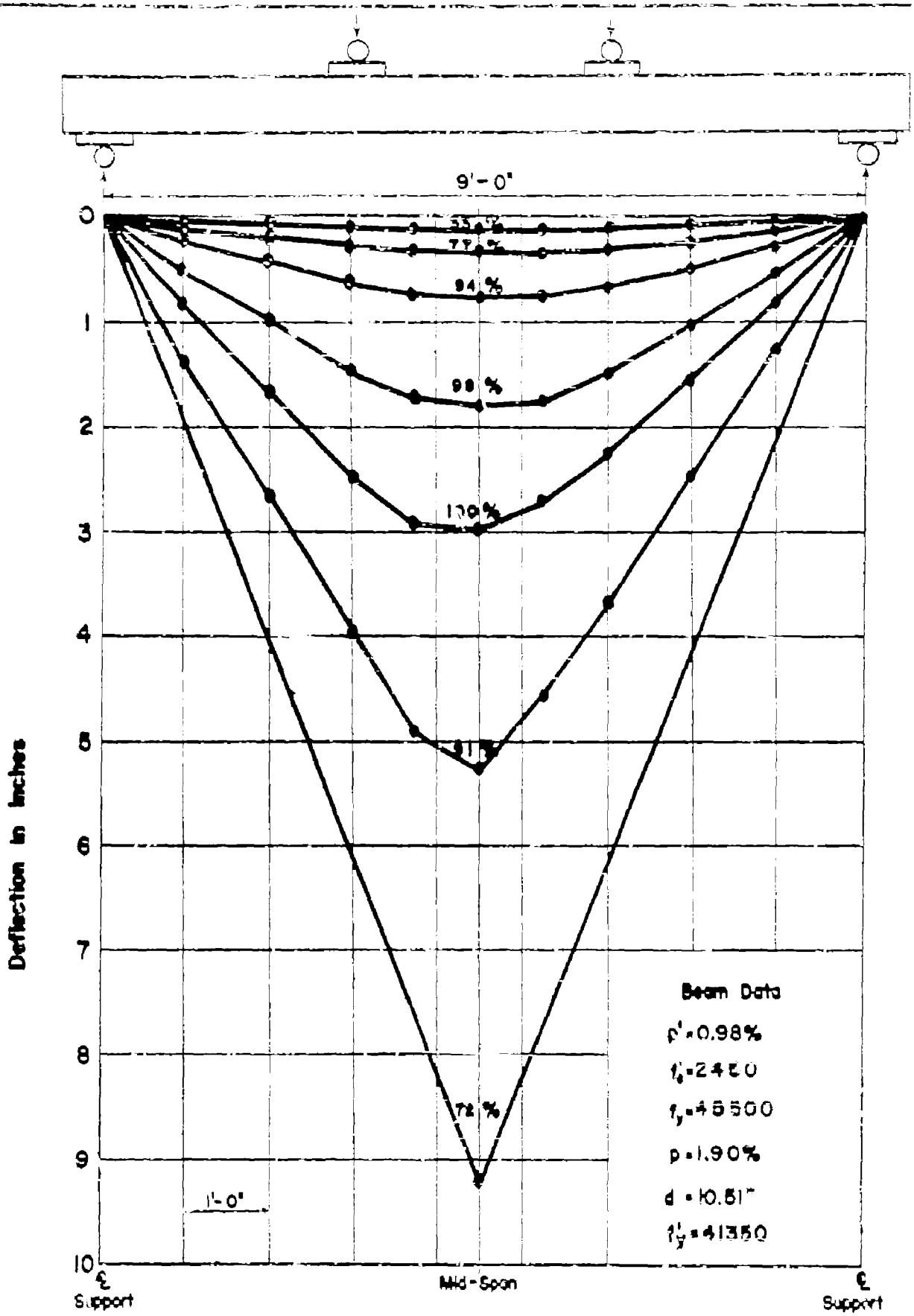

APPFIG. 61 DEFLECTIONS ALONG BEAM NO.C4 xna

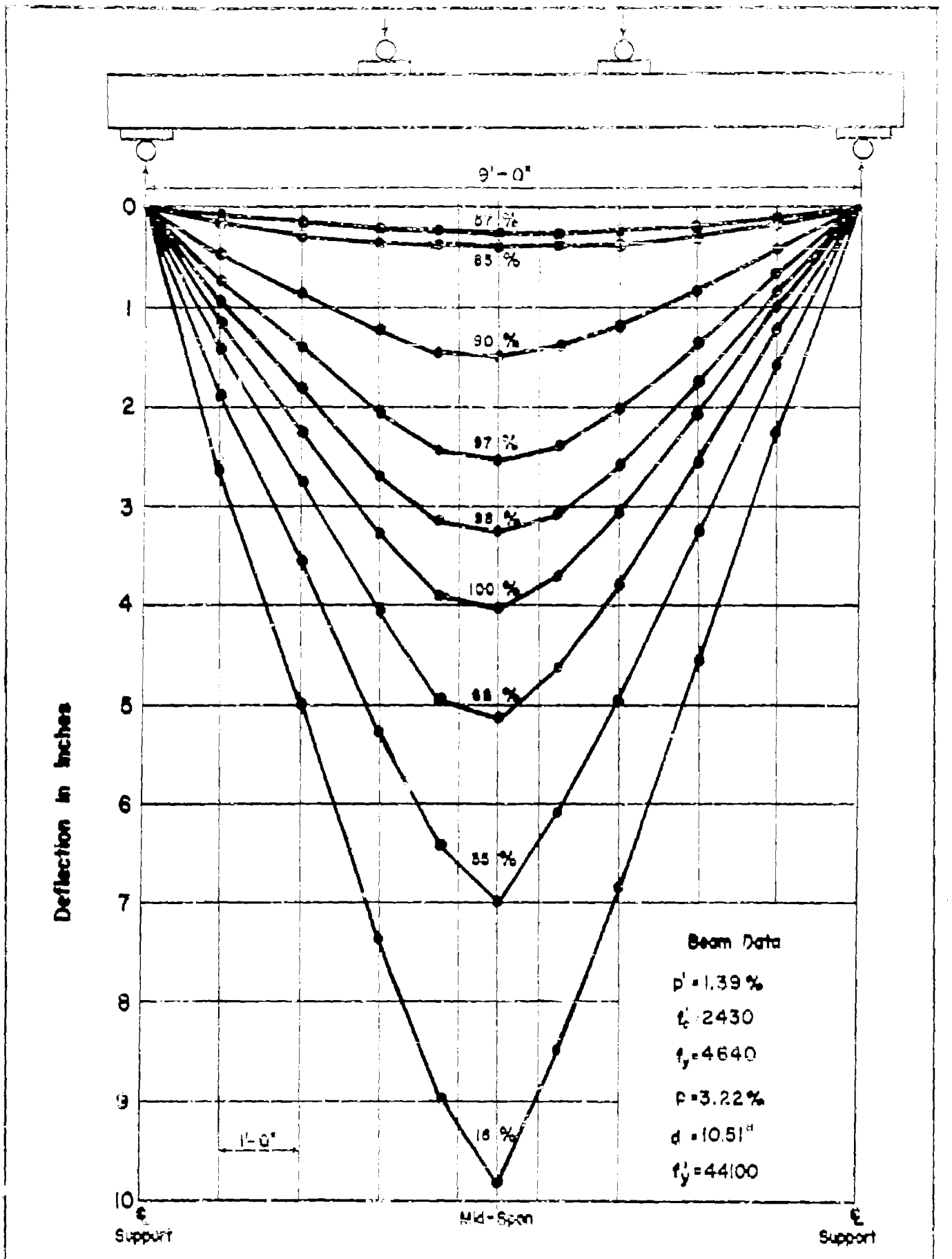

APP. FIG. 62 DEFLECTIONS ALONG BEAM NO. C4xnb

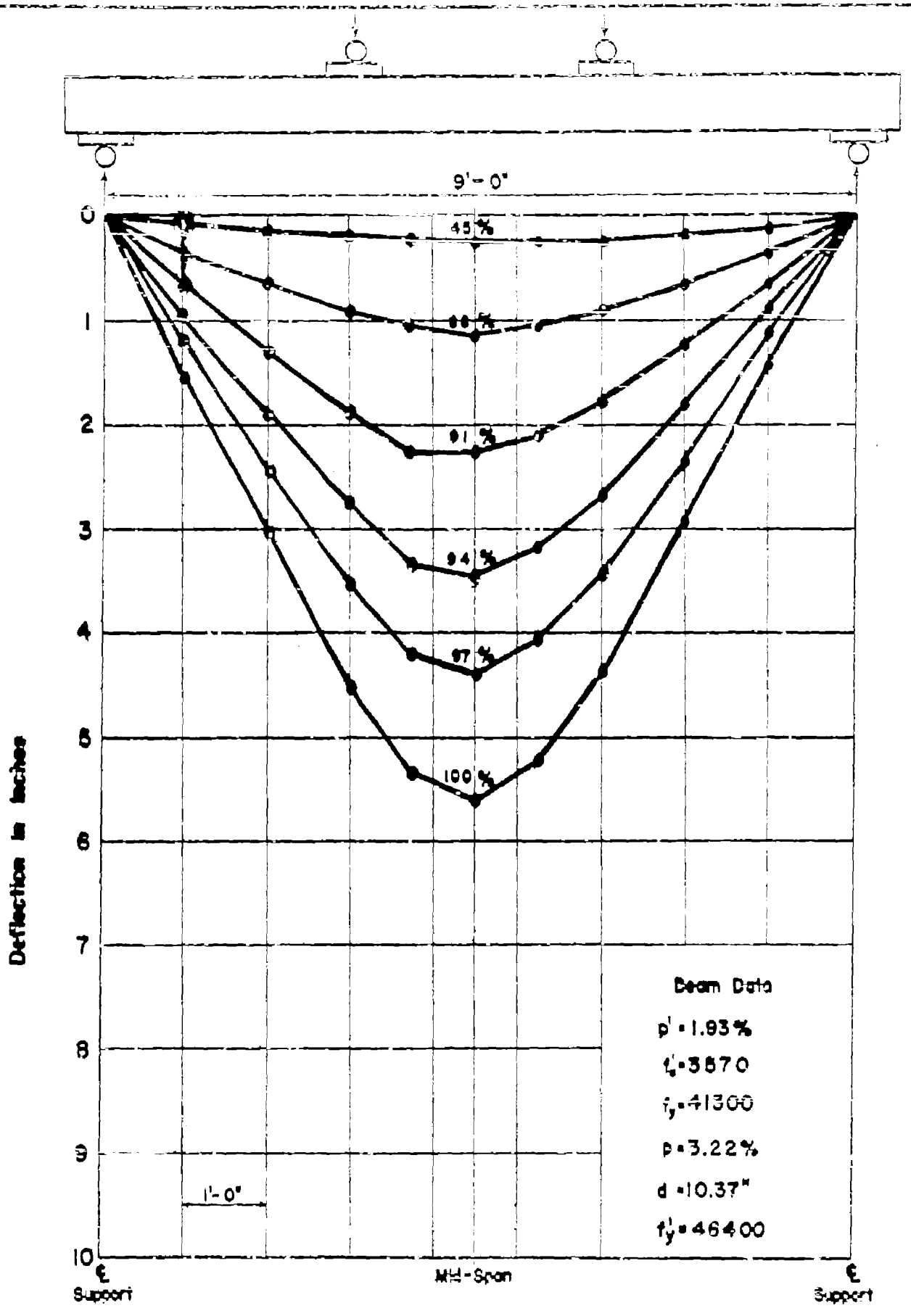

APP. FIG. 63 DEFLECTIONS ALONG BEAM NO. C4zn

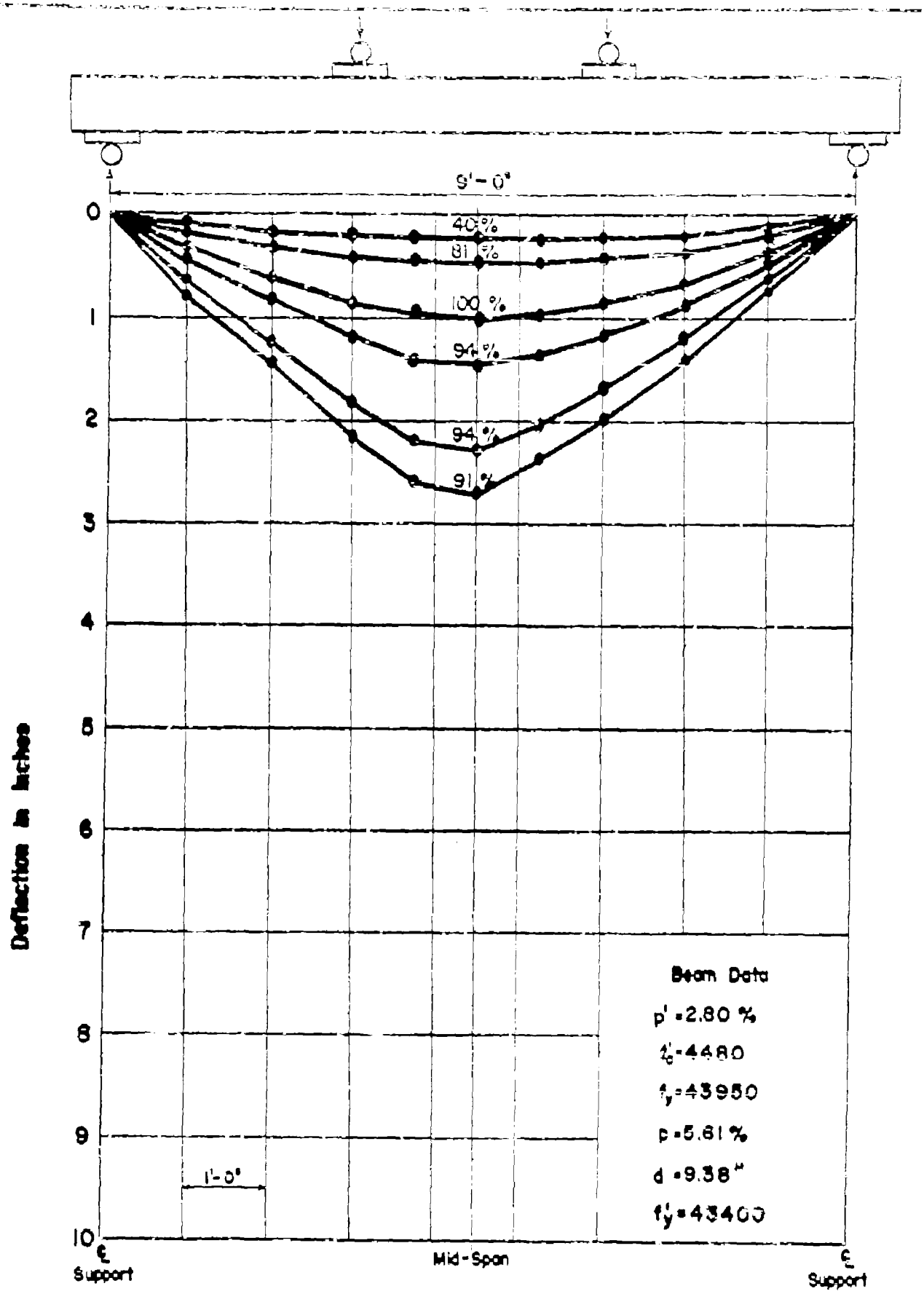

APPFIG. 64 DEFLECTIONS ALONG BEAM NO. C5yn

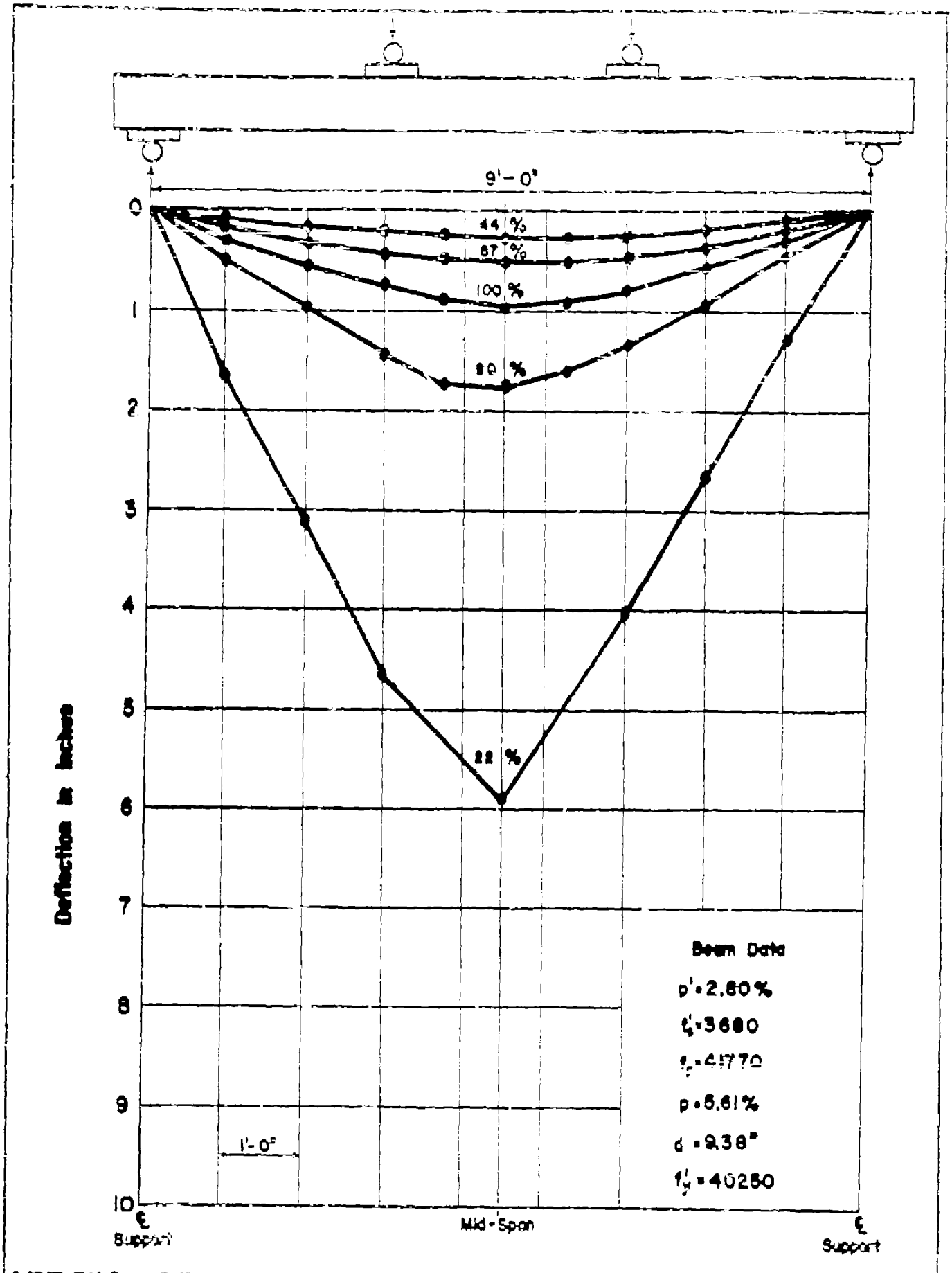

APP. FIG. 65 DEFLECTIONS ALONG BEAM NO. C6xm

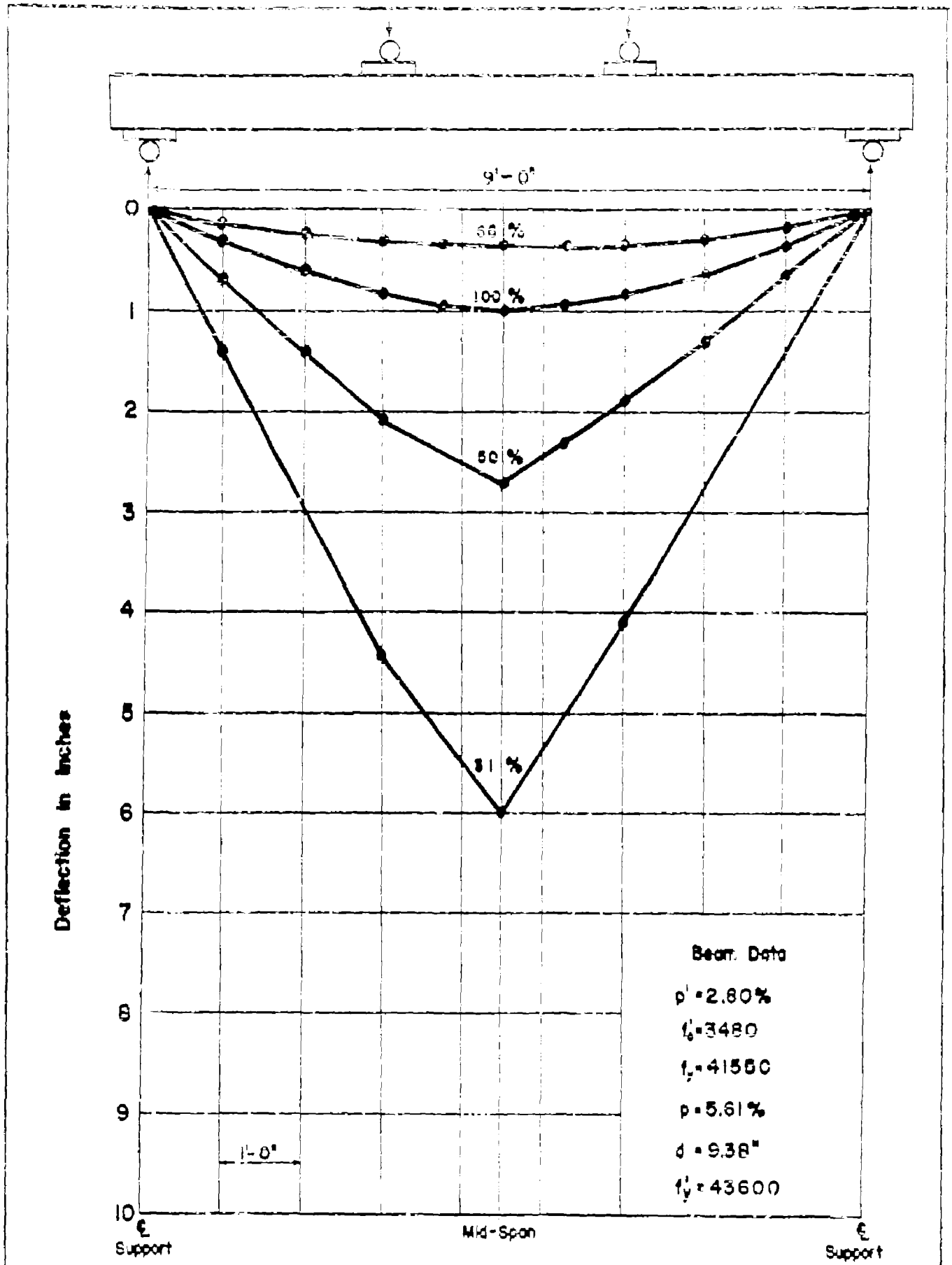

APP. FIG. 66 DEFLECTIONS ALONG BEAM NO. C7w

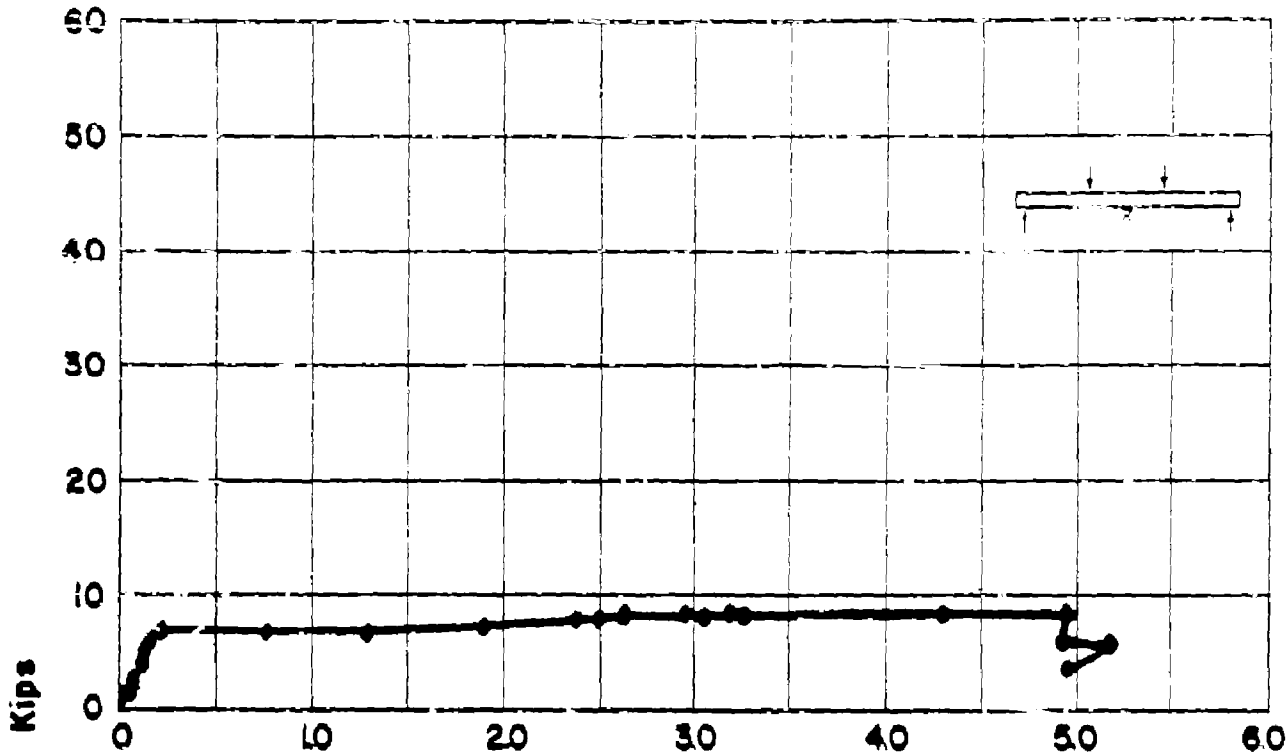

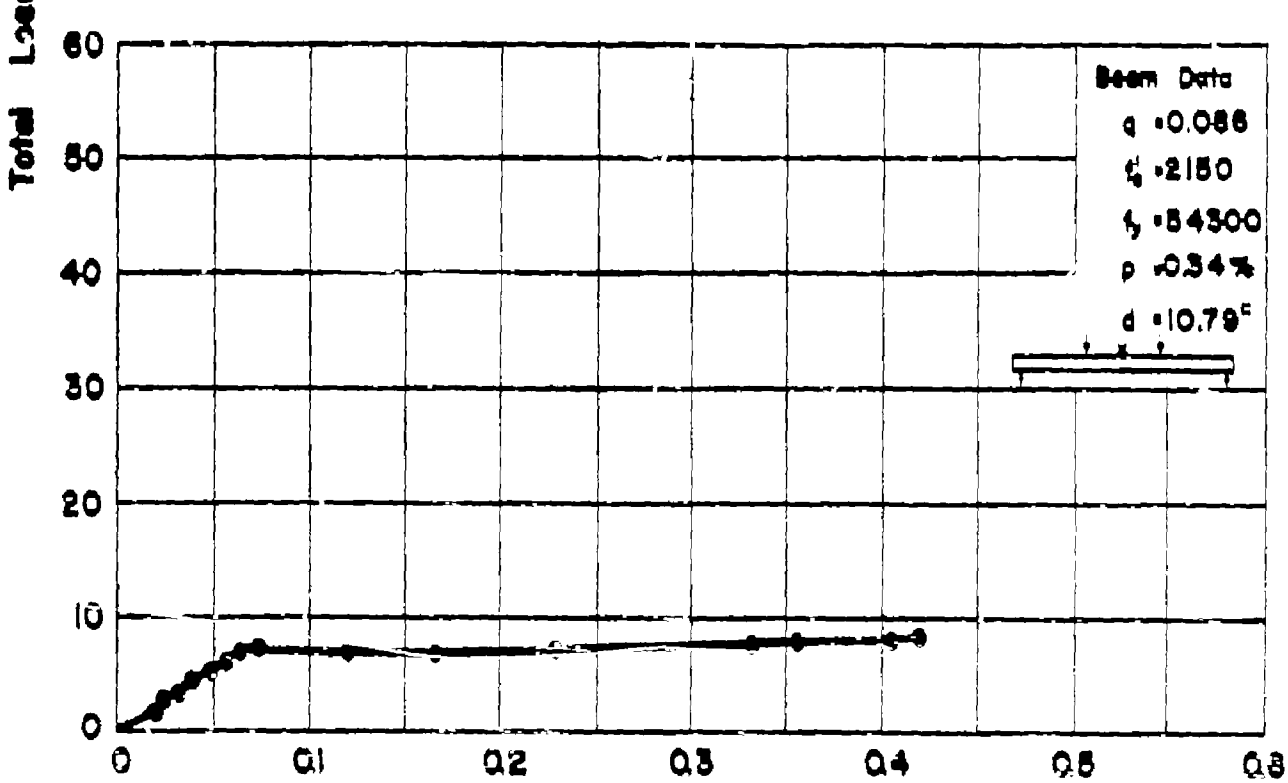

APP. FIG. 67 LOAD-STRAIN CURVES FOR BEAM NO. TILa

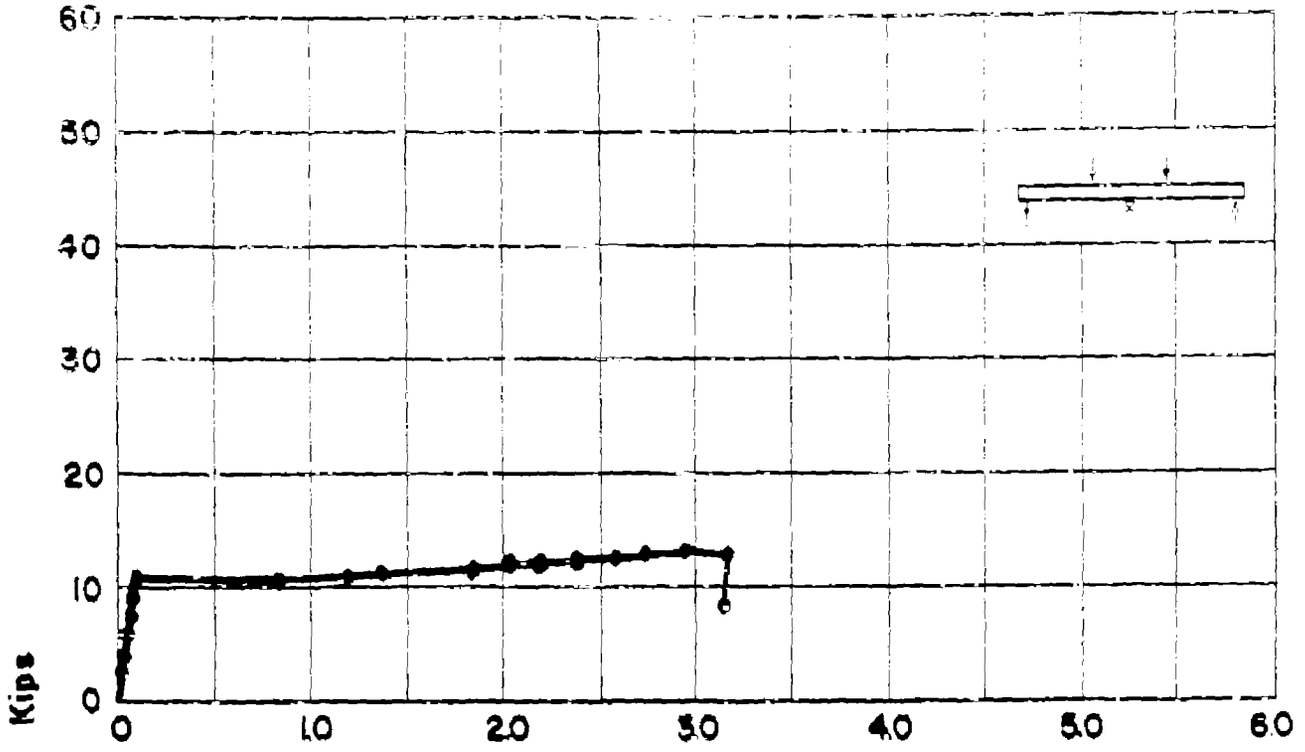

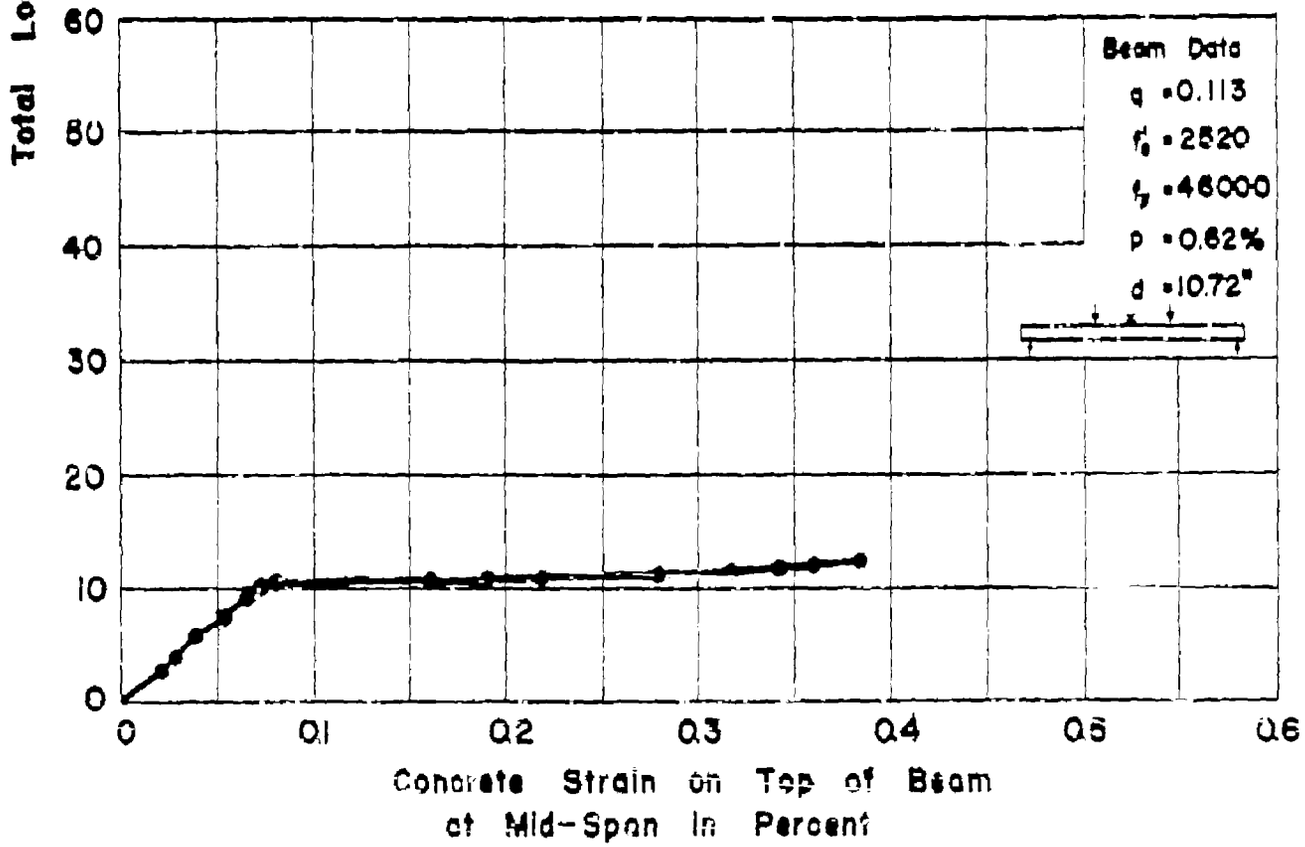

APP. FIG. 68 LOAD-STRAIN CURVES FOR BEAM NO. TILb

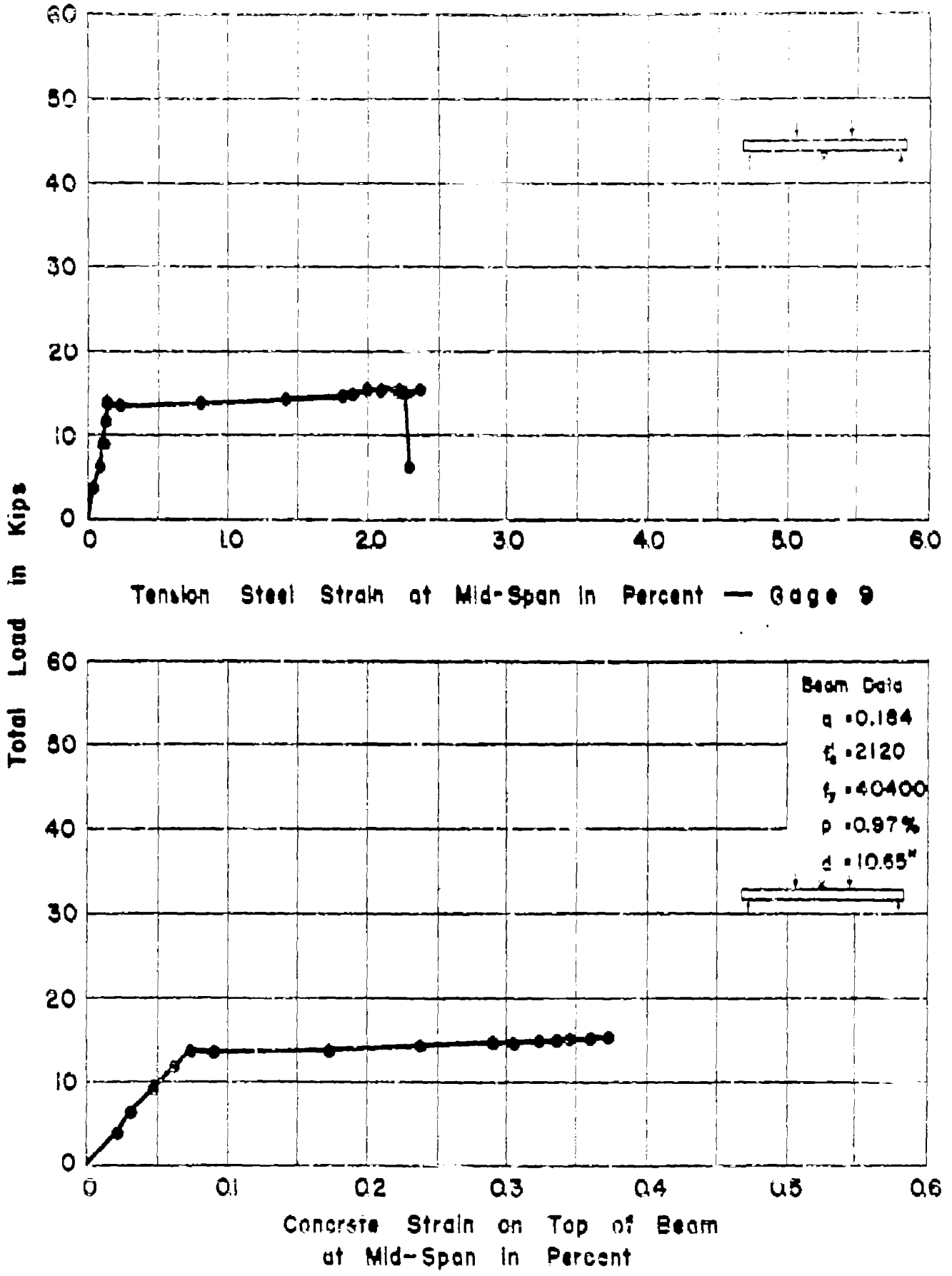

APP. FIG. 69 LOAD-STRAIN CURVES FOR BEAM NO.T2La

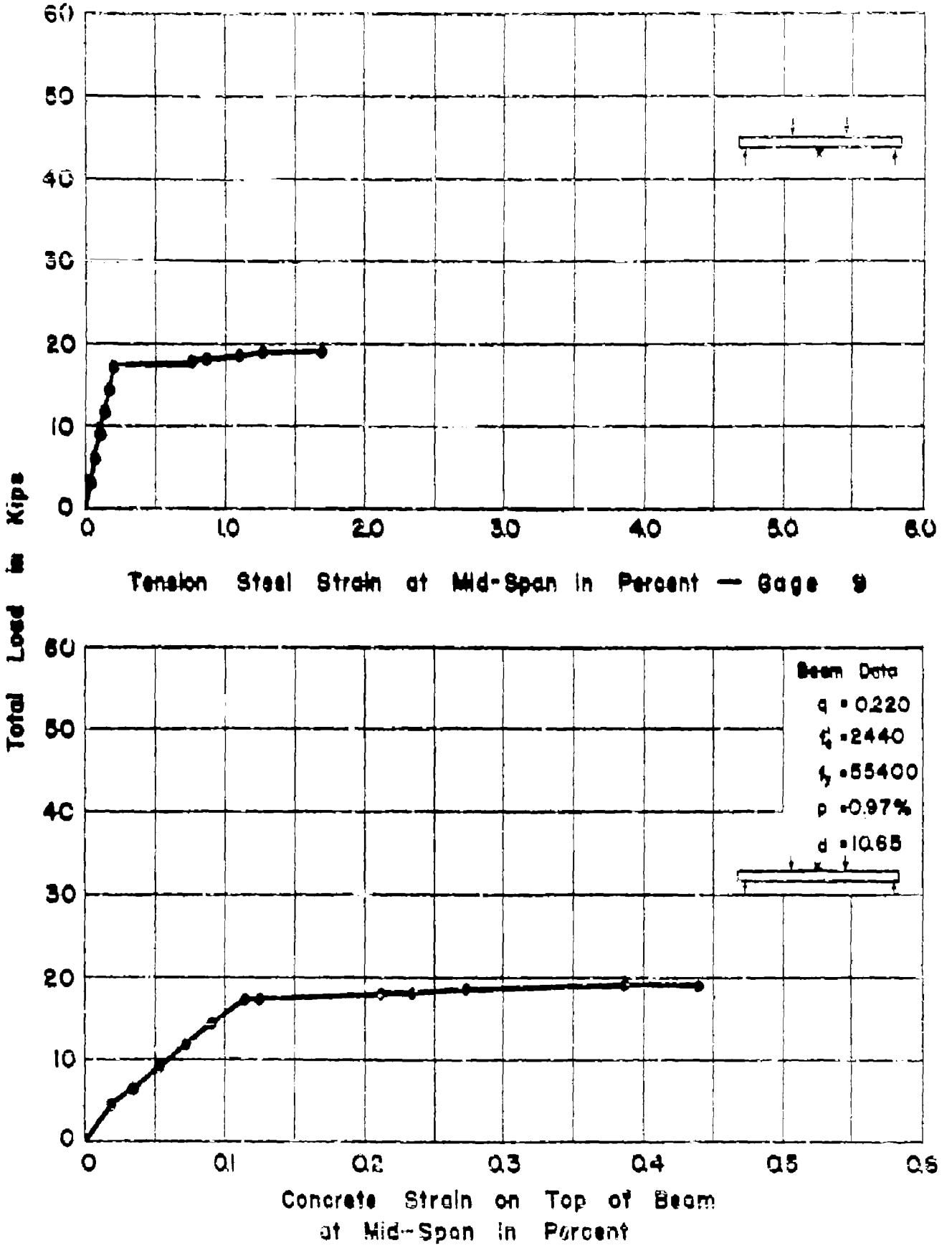

APP. FIG. 70 LOAD-STRAIN CURVES FOR BEAM NO. T2Lb

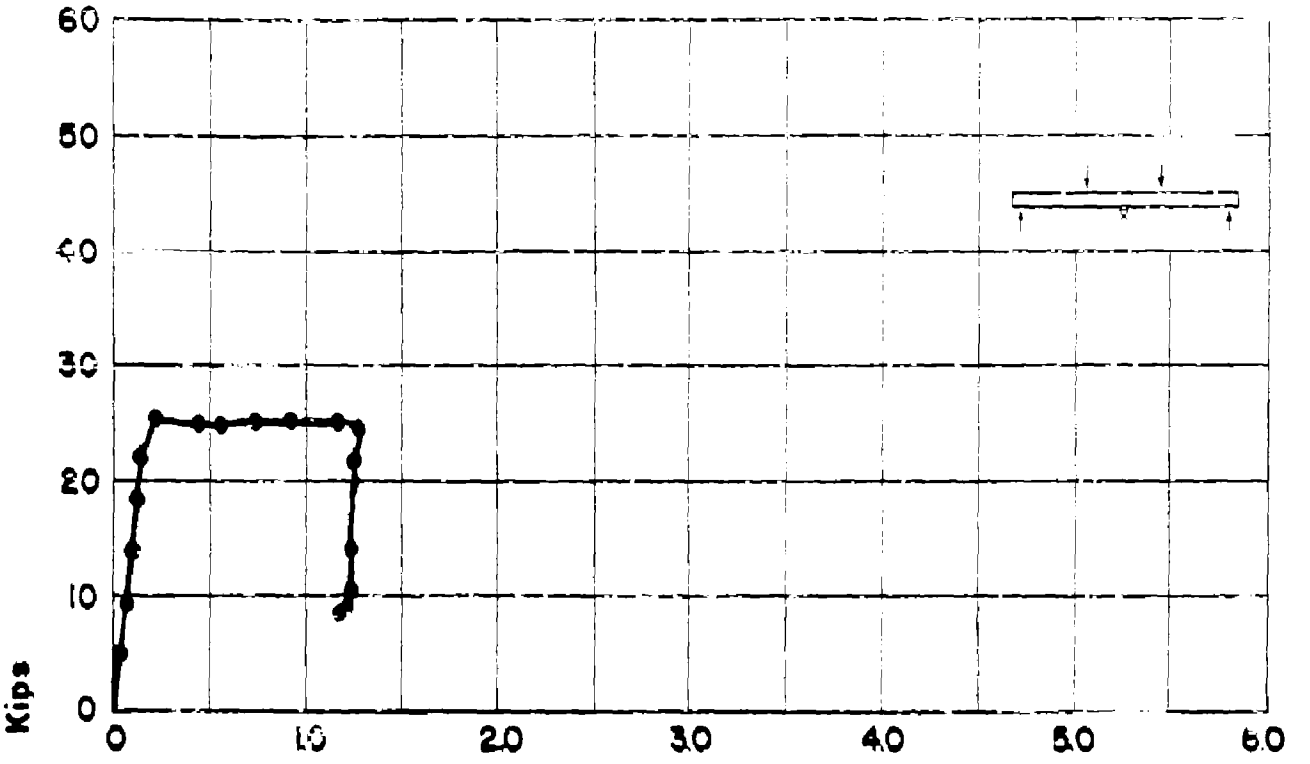

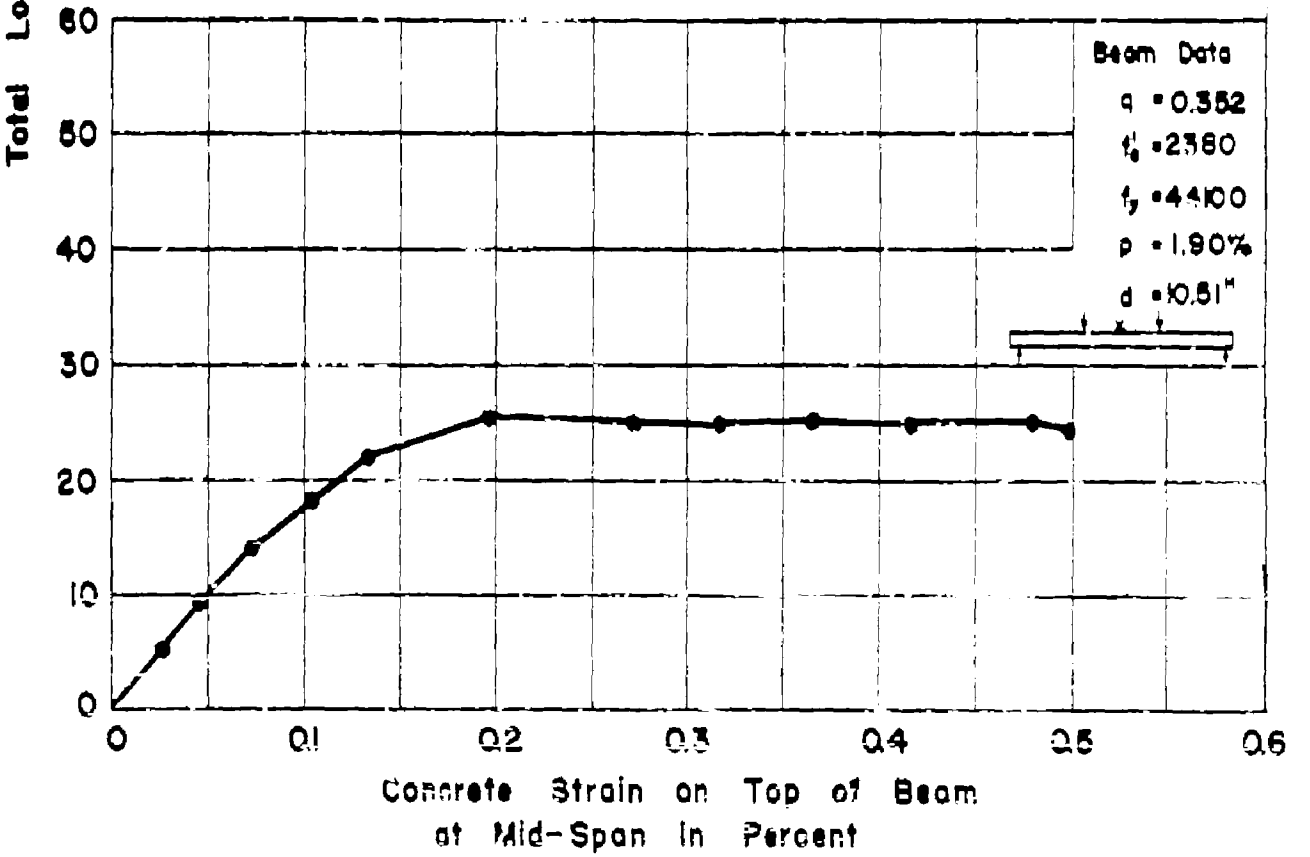

APP FIG 71 LOAD-STRAIN CURVES FOR BEAM NO.T4La

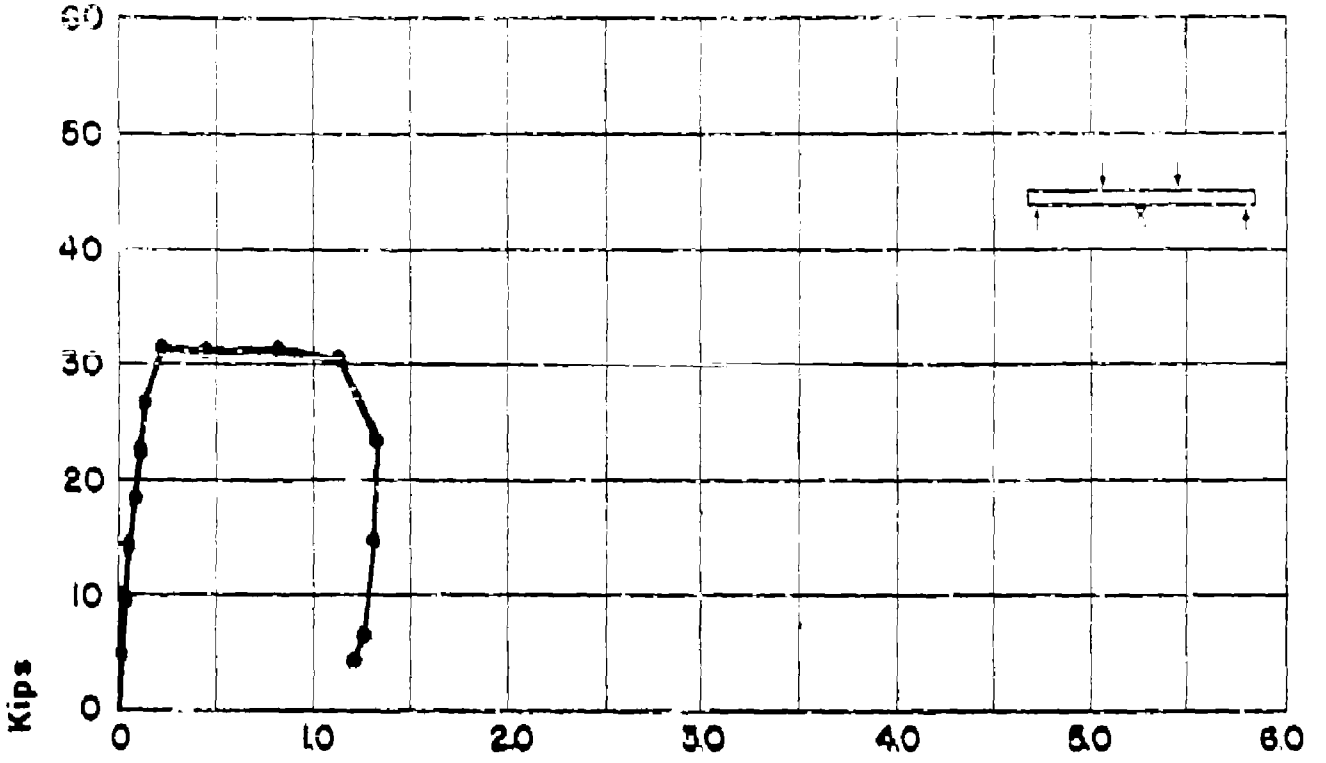

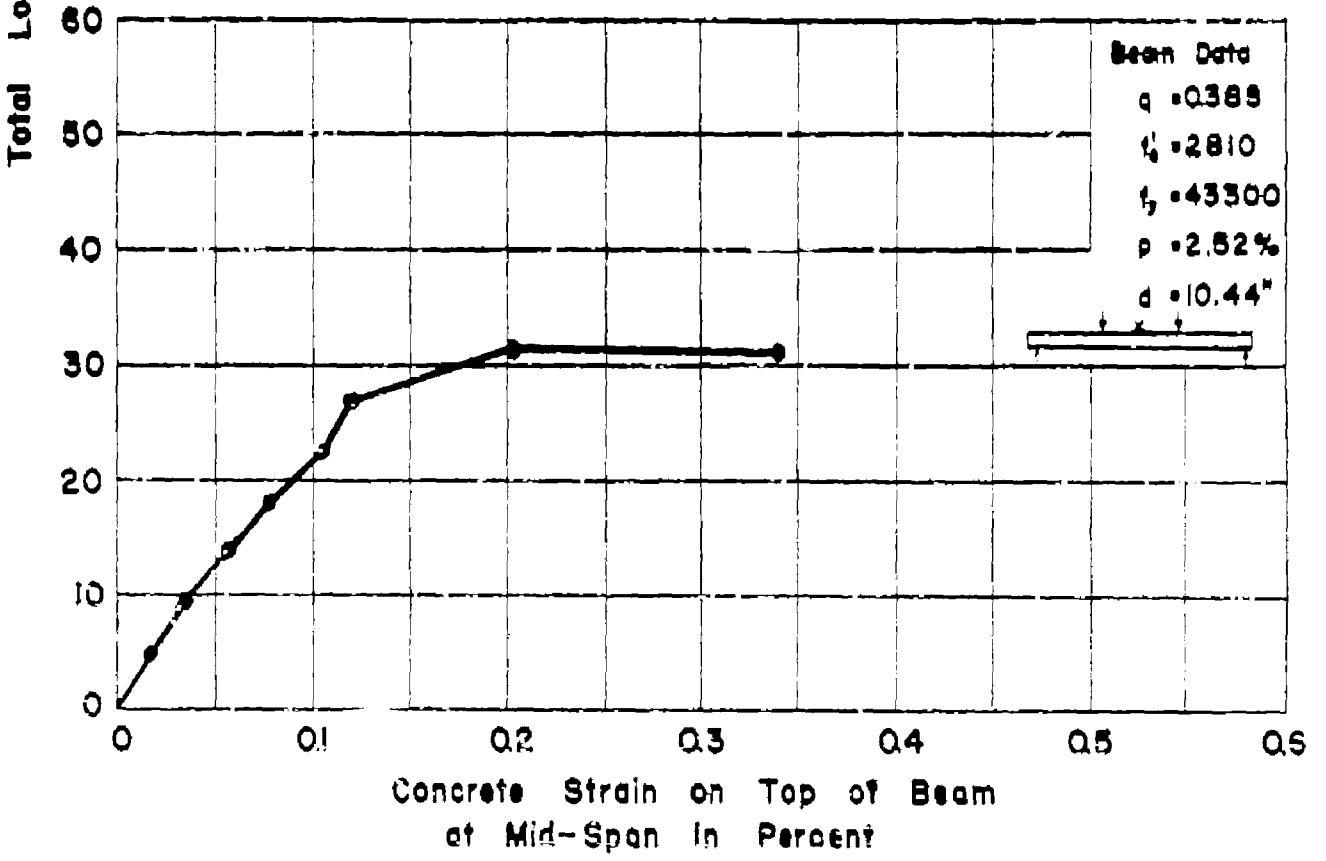

APP FIG. 72 LOAD-STRAIN CURVES FOR BEAM NO.T4Lb

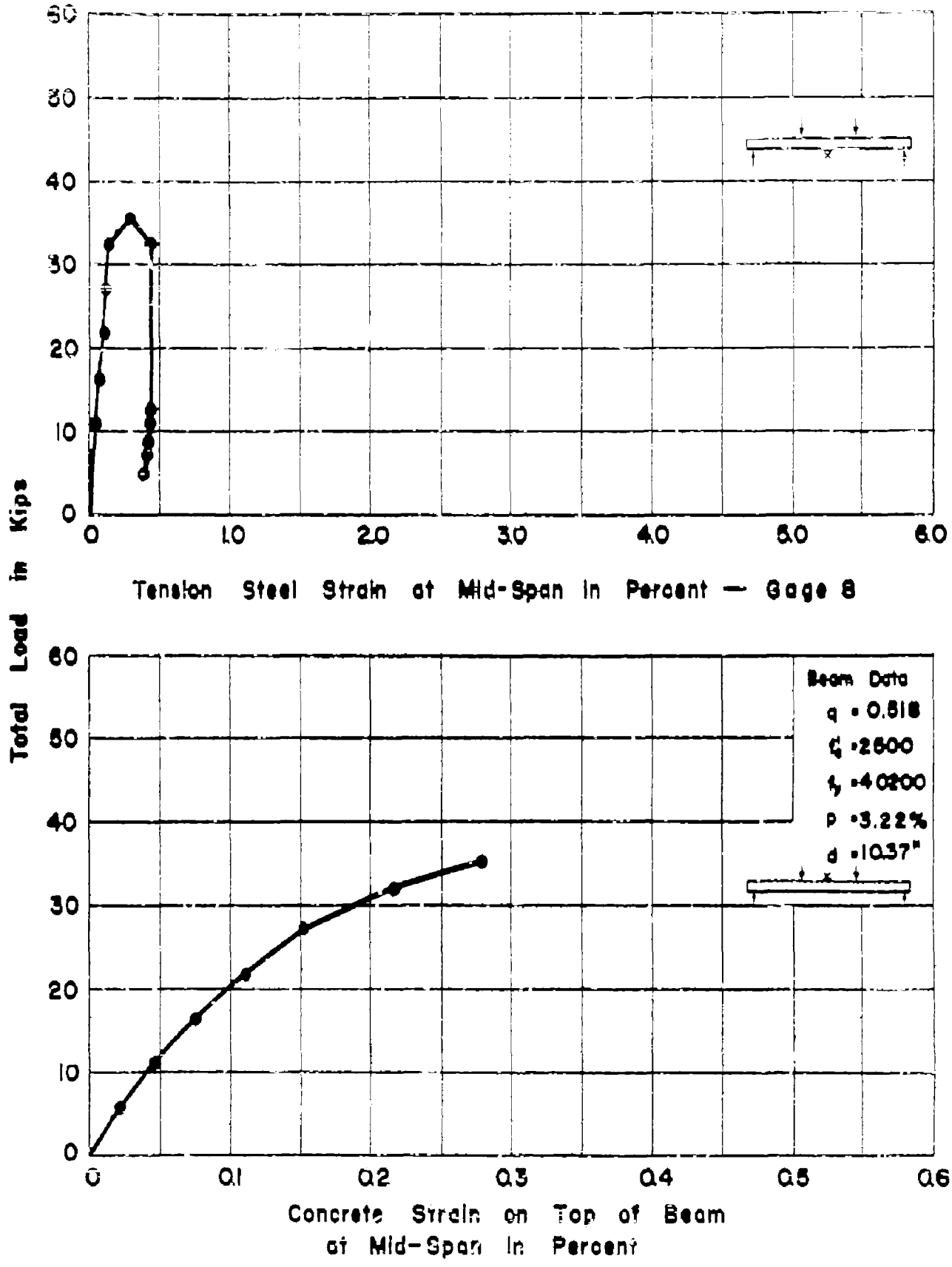

APP. FIG. 73 LOAD-STRAIN CURVES FOR BEAM NO.T5L

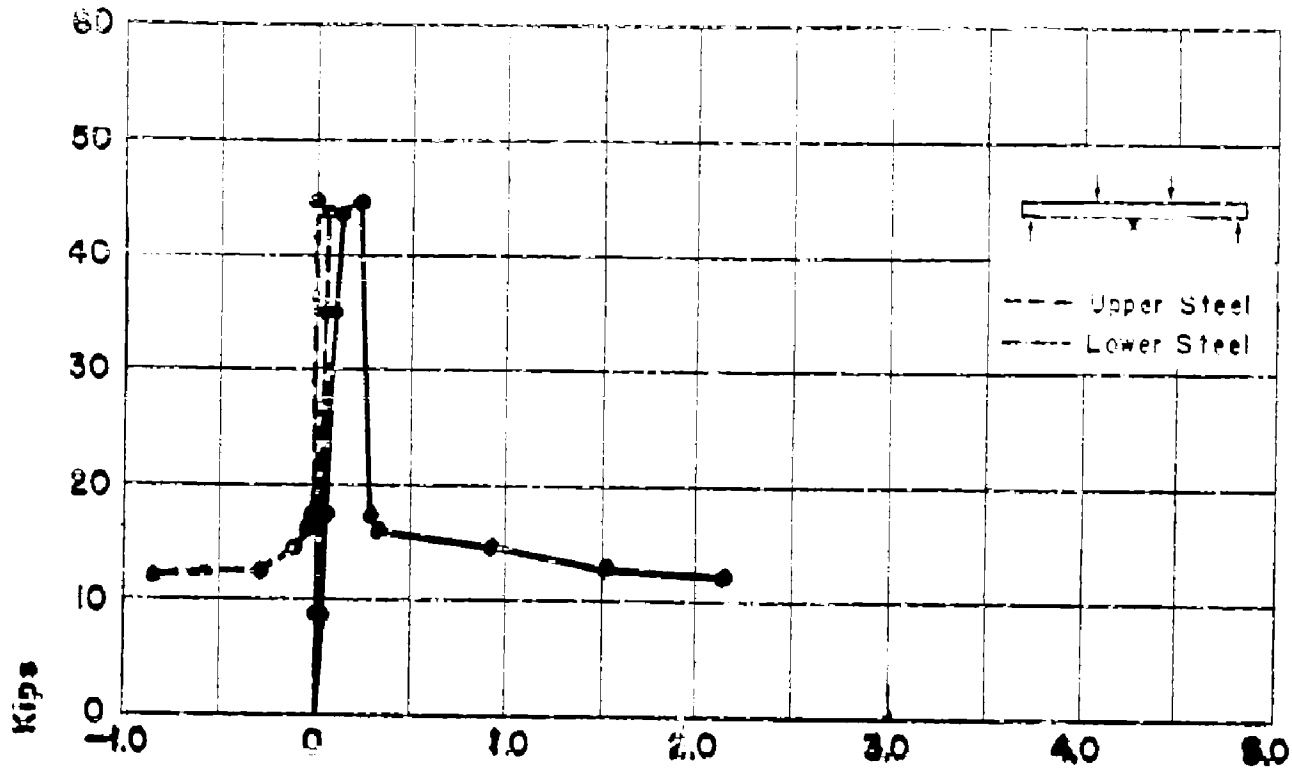

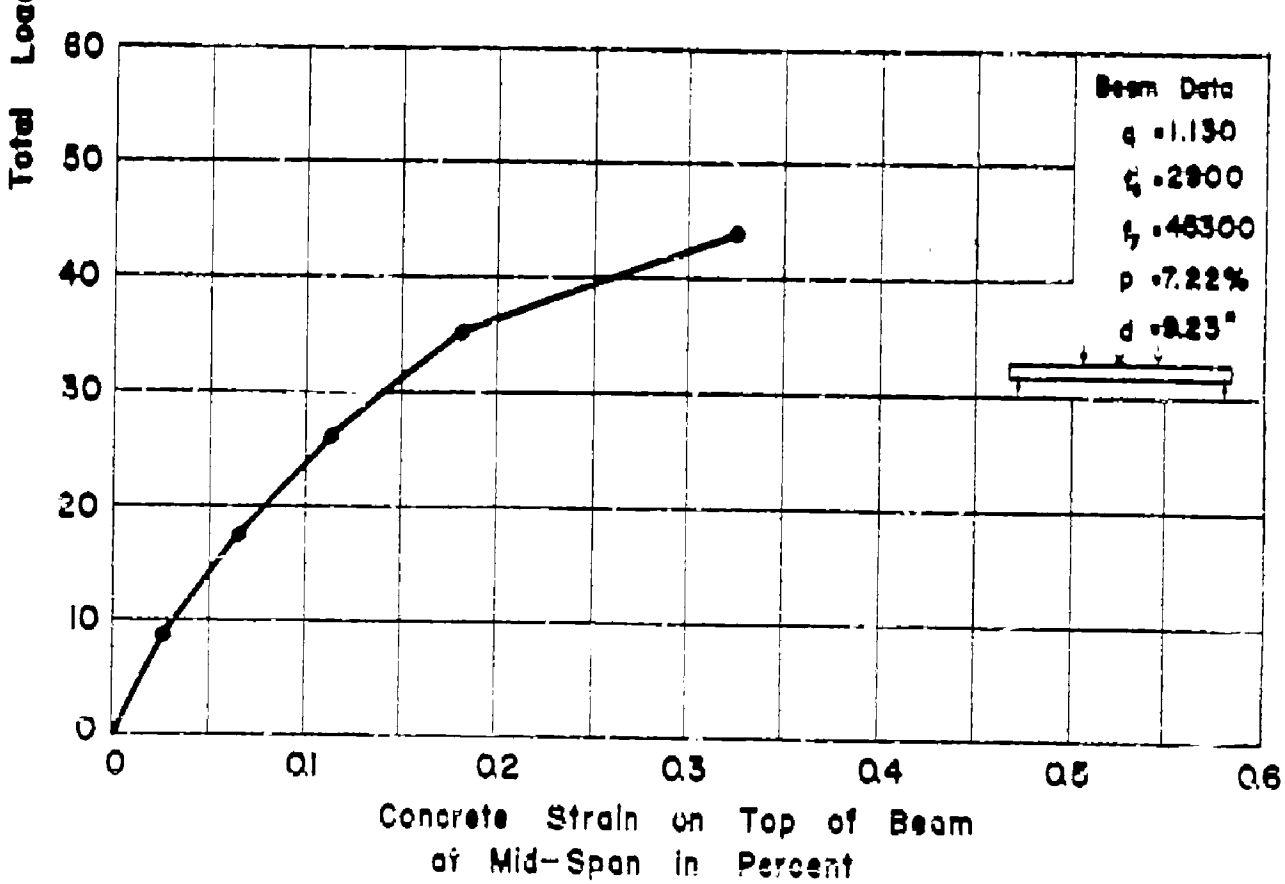

APP. FIG. 74 LOAD-STRAIN CURVES FOR BEAM NO. T11L

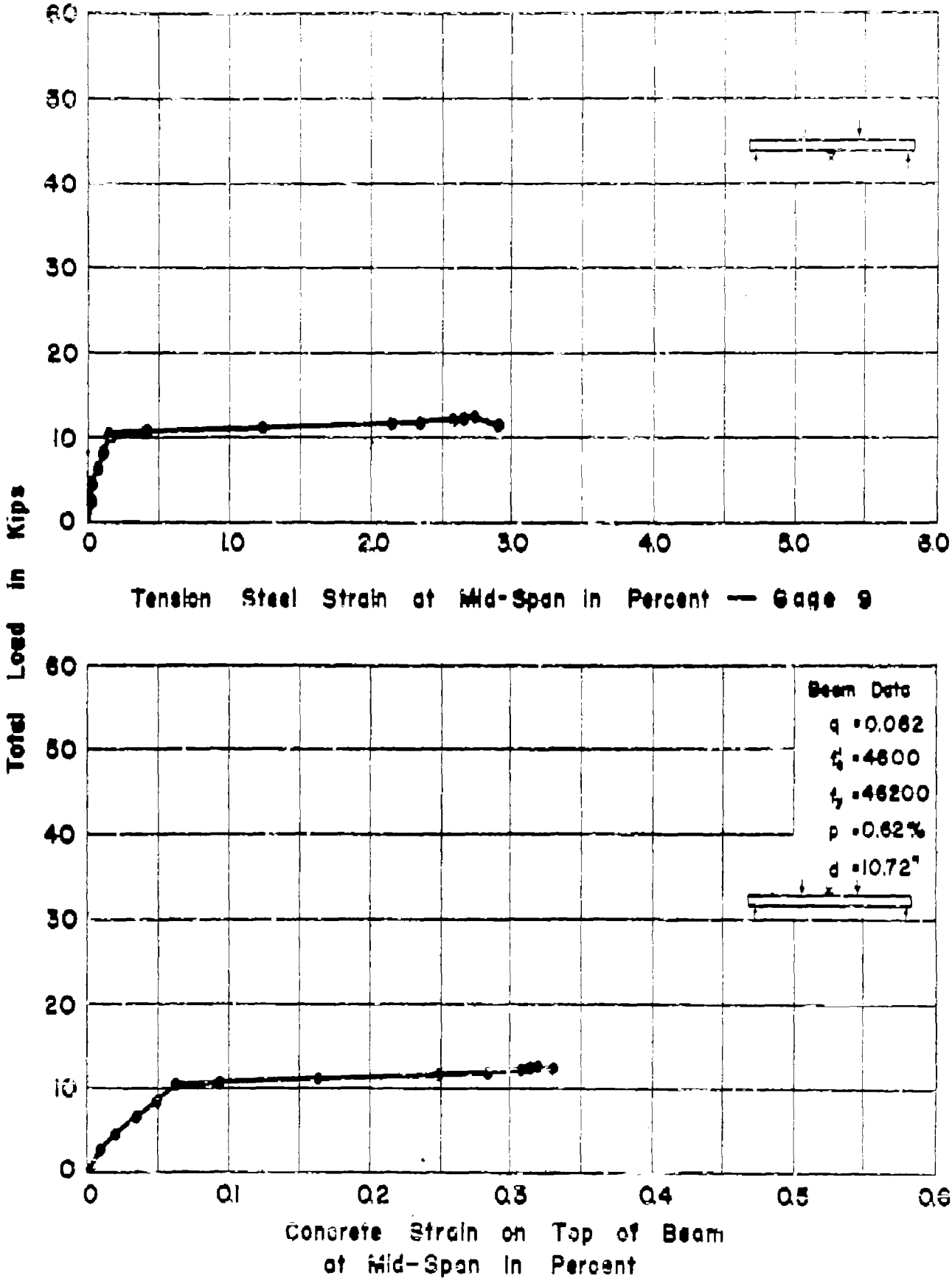

APP. FIG. 75 LOAD-STRAIN CURVES FOR BEAM NO. T1M2

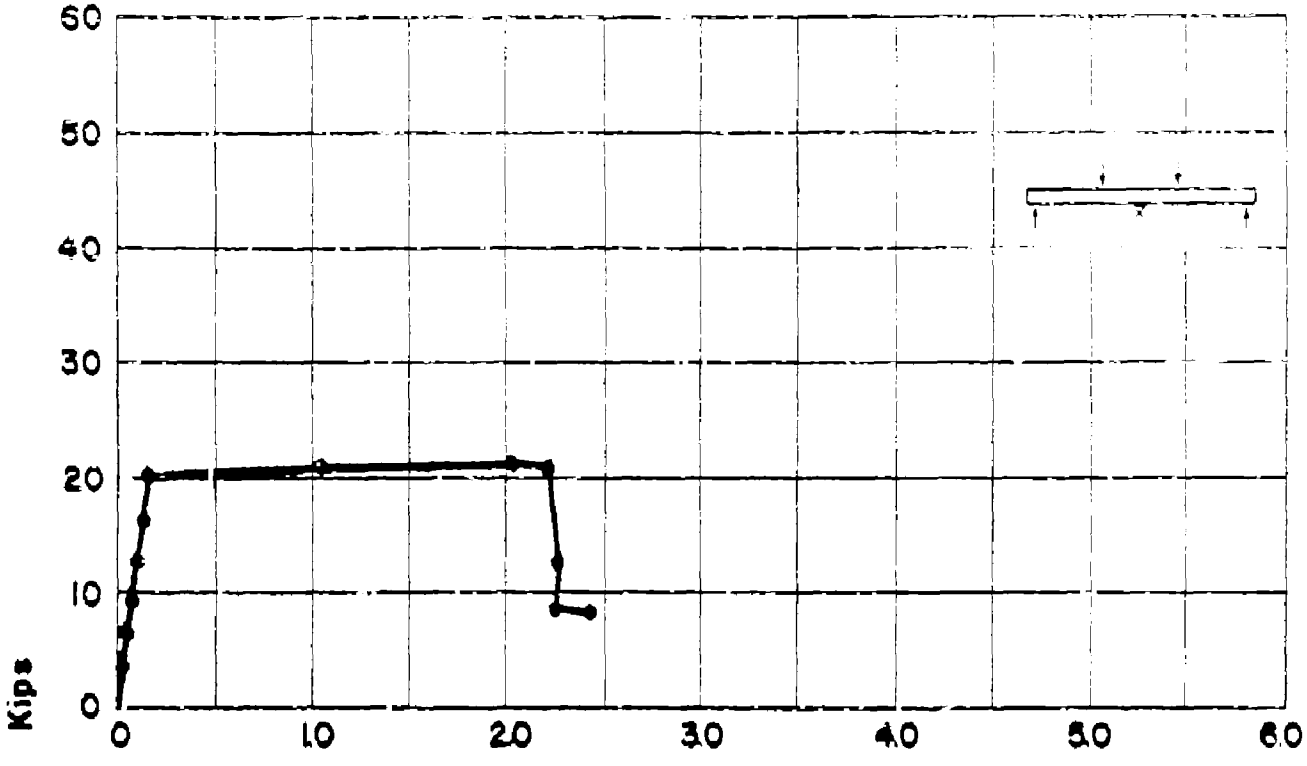

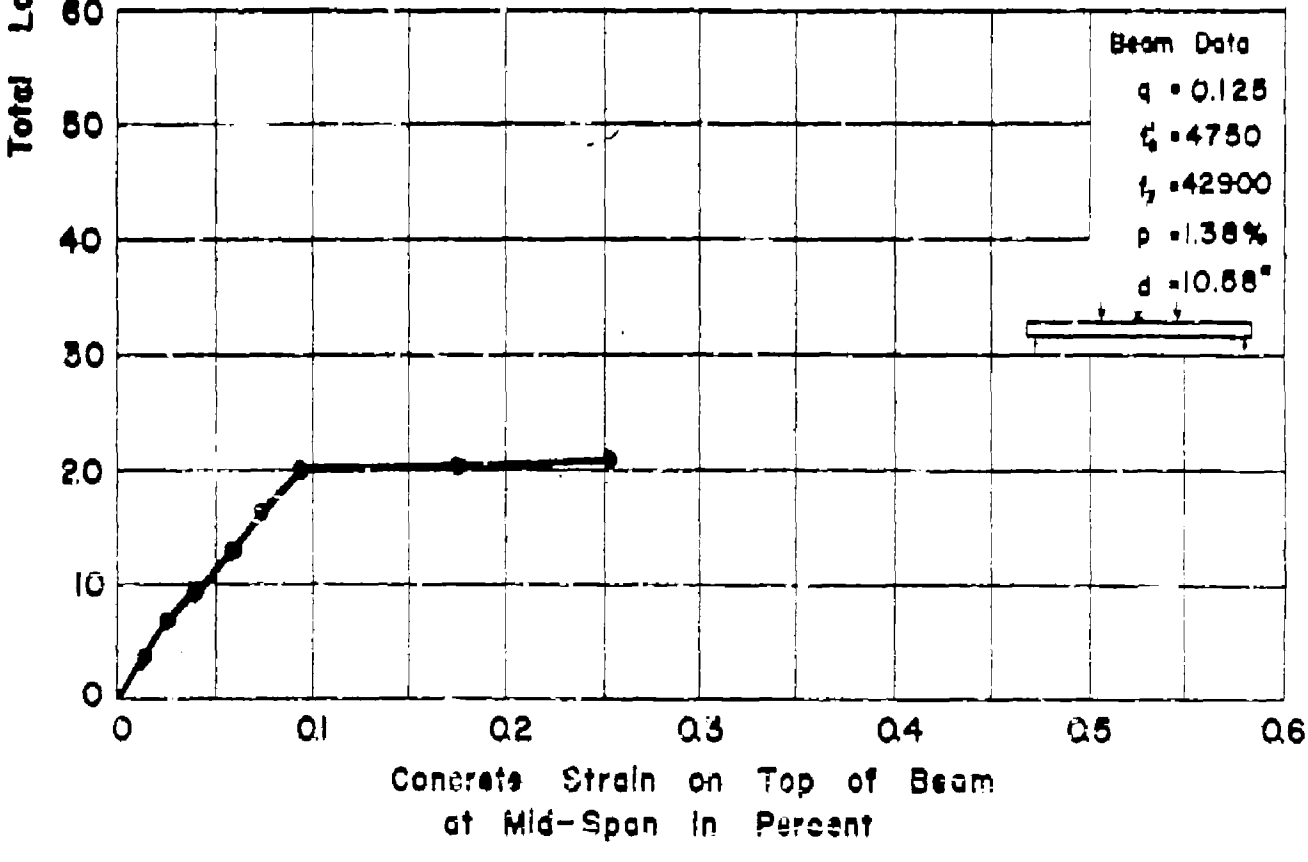

APP. FIG. 76 LOAD-STRAIN CURVES FOR BEAM NO. T1M6

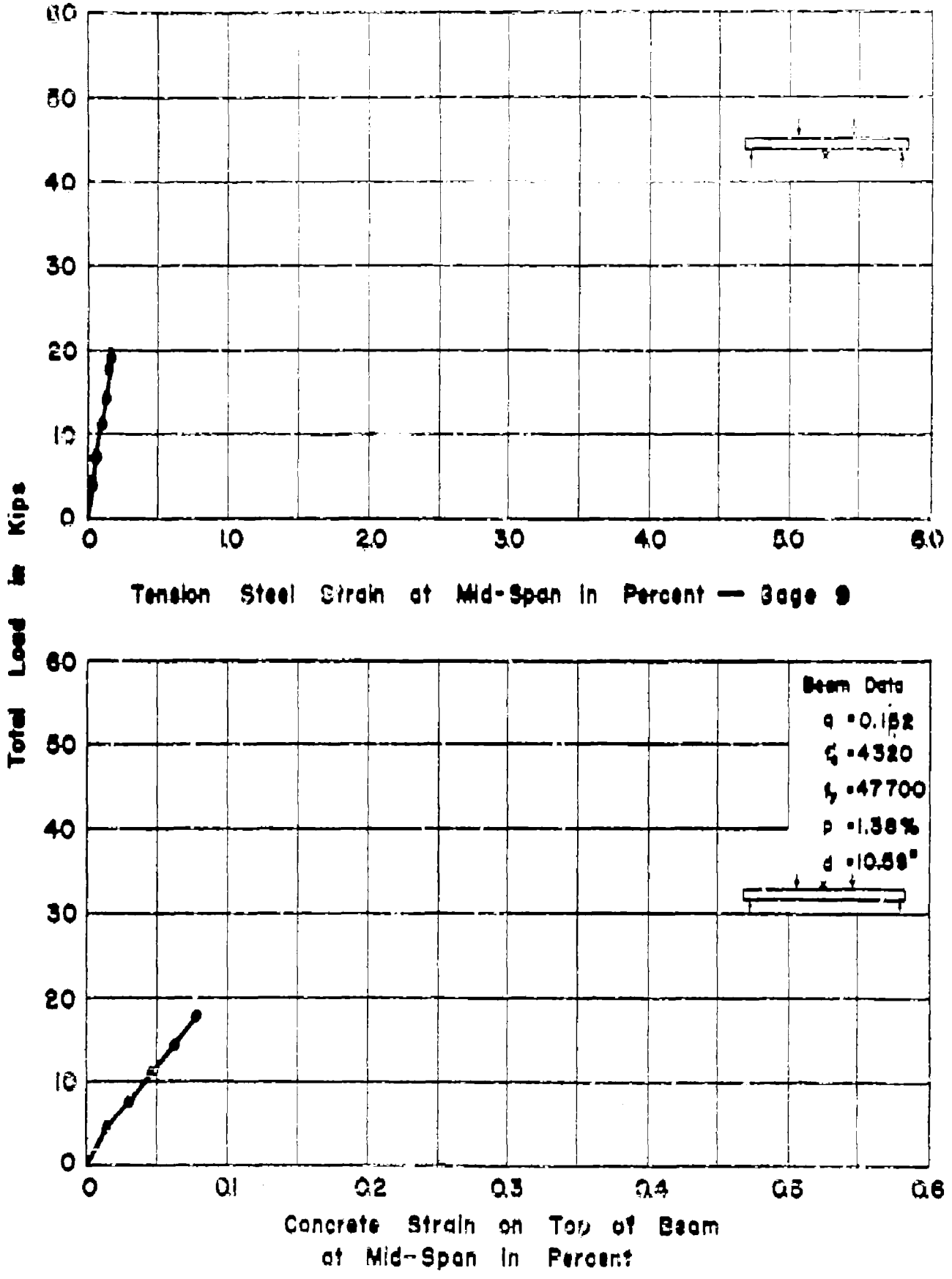

APP. FIG. 77 LOAD-STRAIN CURVES FOR BEAM NOT2Mo

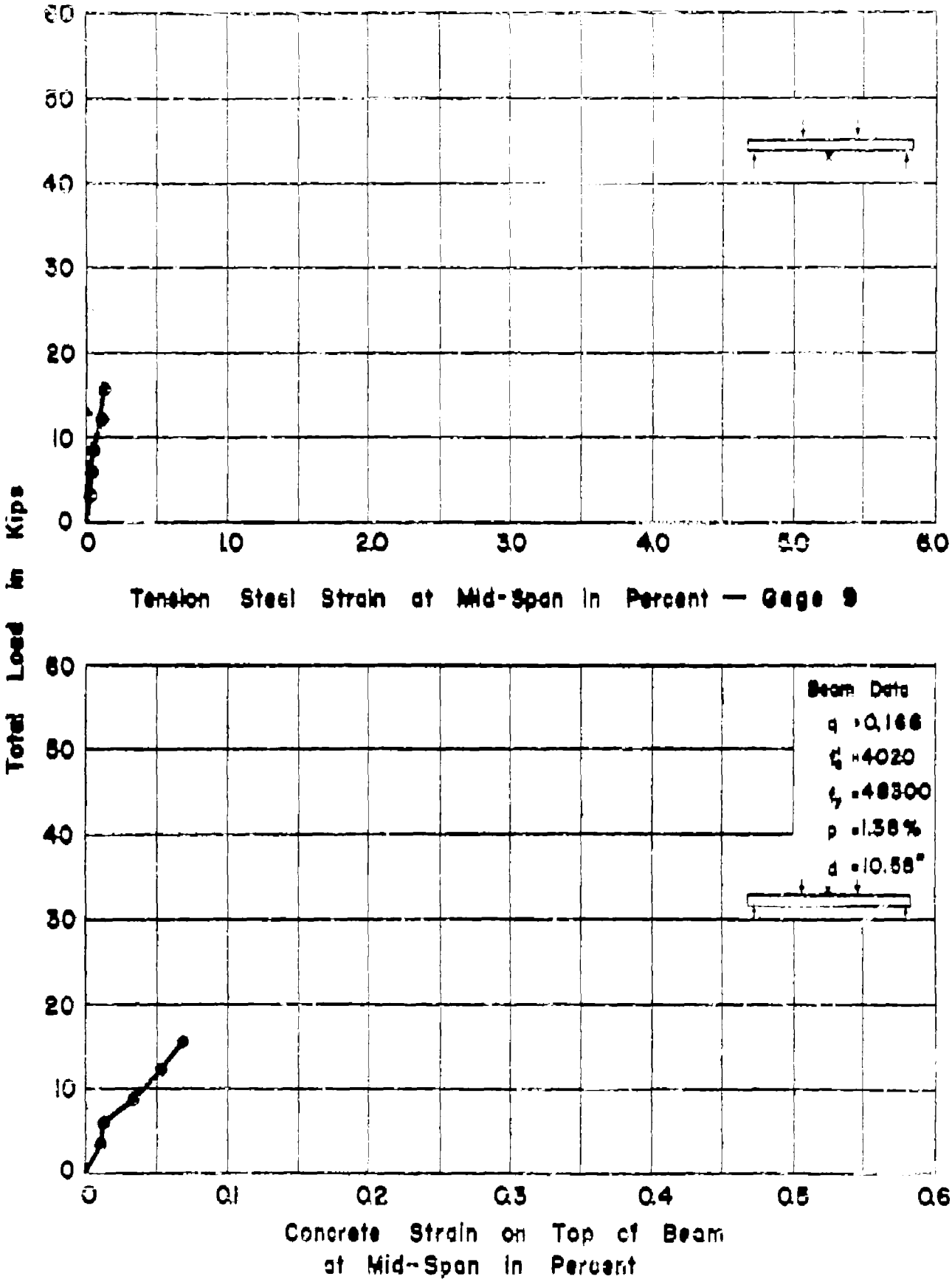

APP. FIG. 78 LOAD-STRAIN CURVES FOR BEAM NO.T2Mb

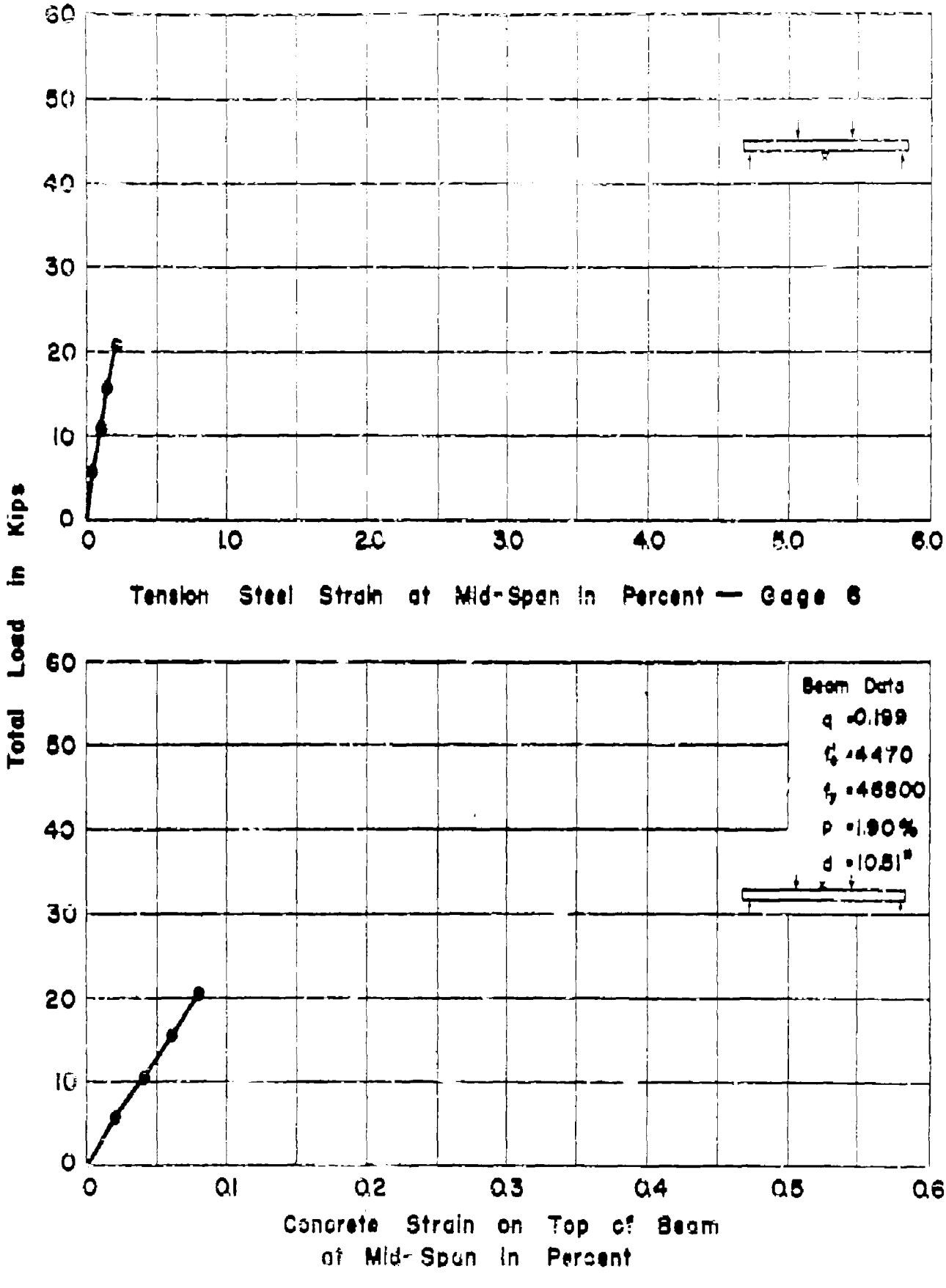

APP. FIG. 79 LOAD-STRAIN CURVES FOR BEAM NO. T2Mc

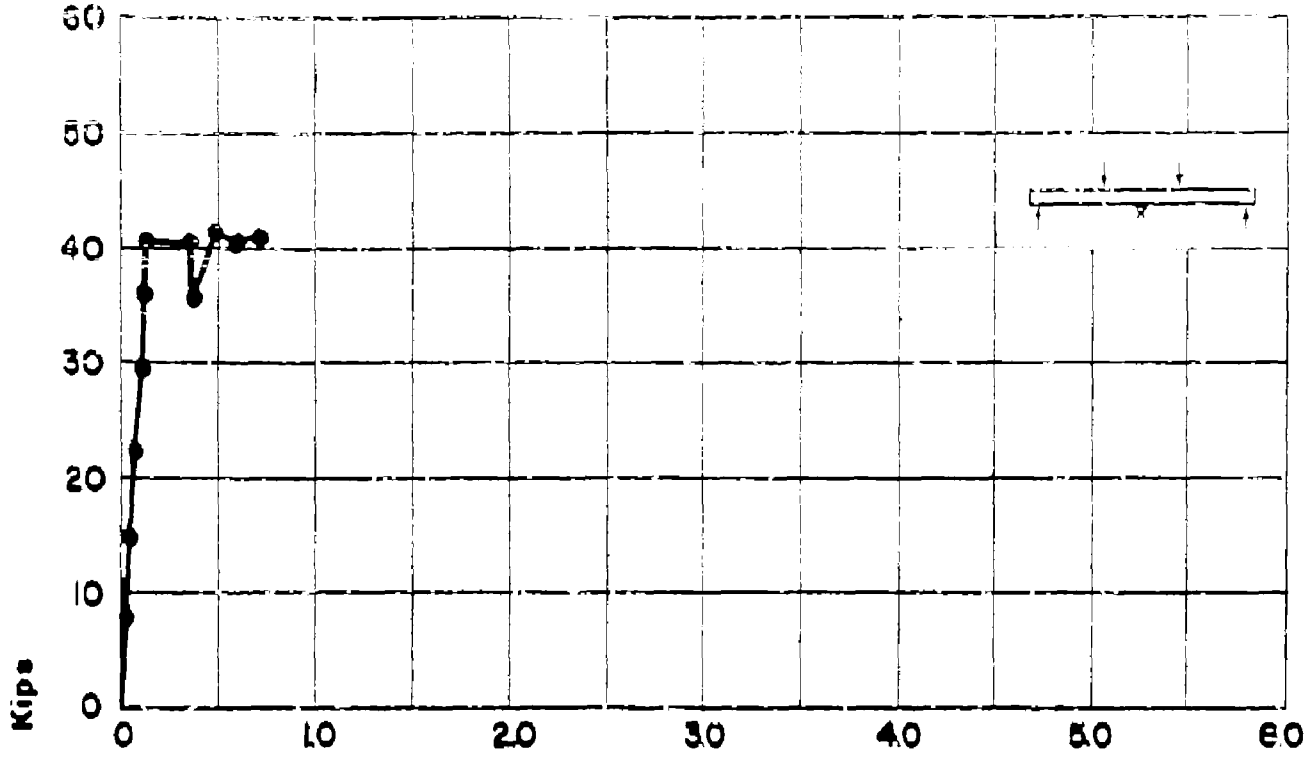

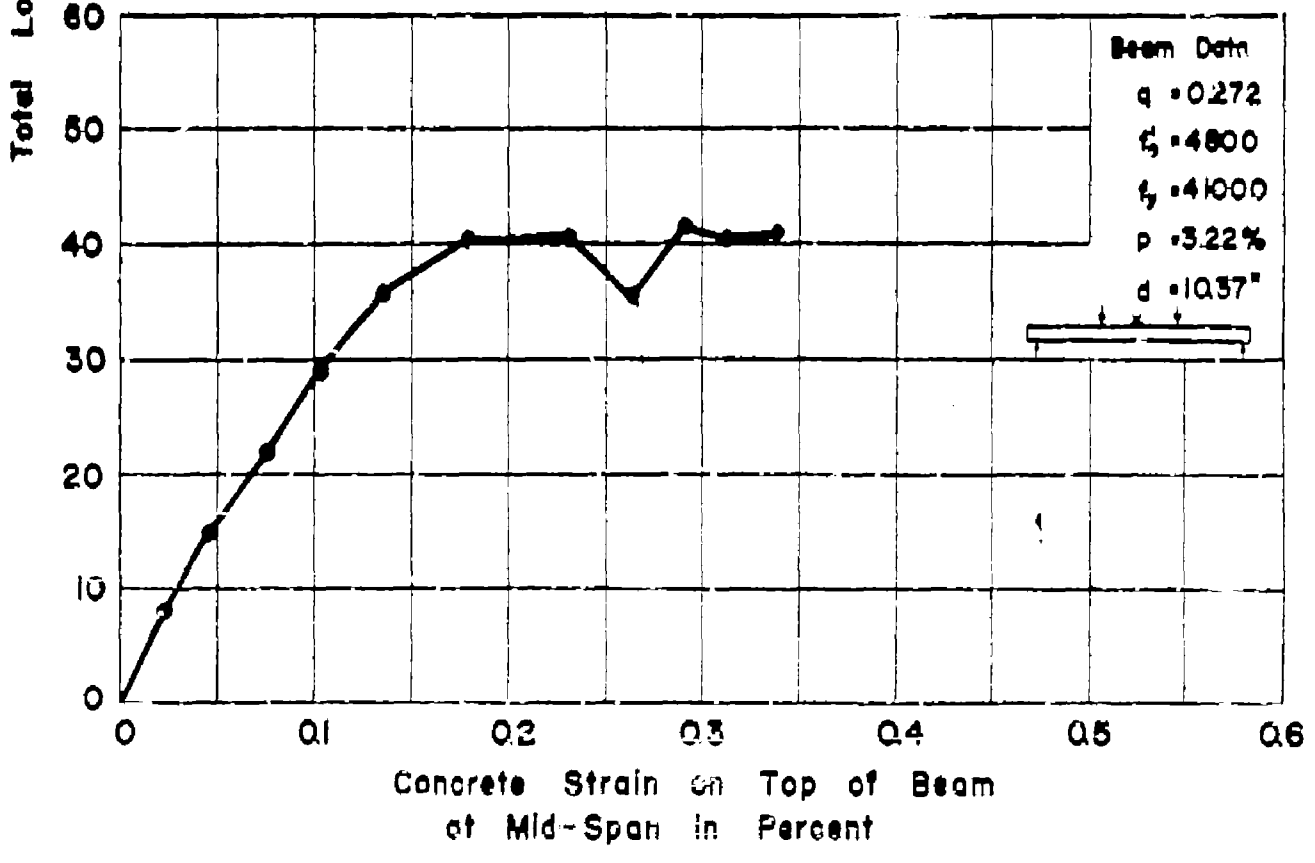

APP. FIG. 80 LOAD-STRAIN CURVES FOR BEAM NO. T3Ma

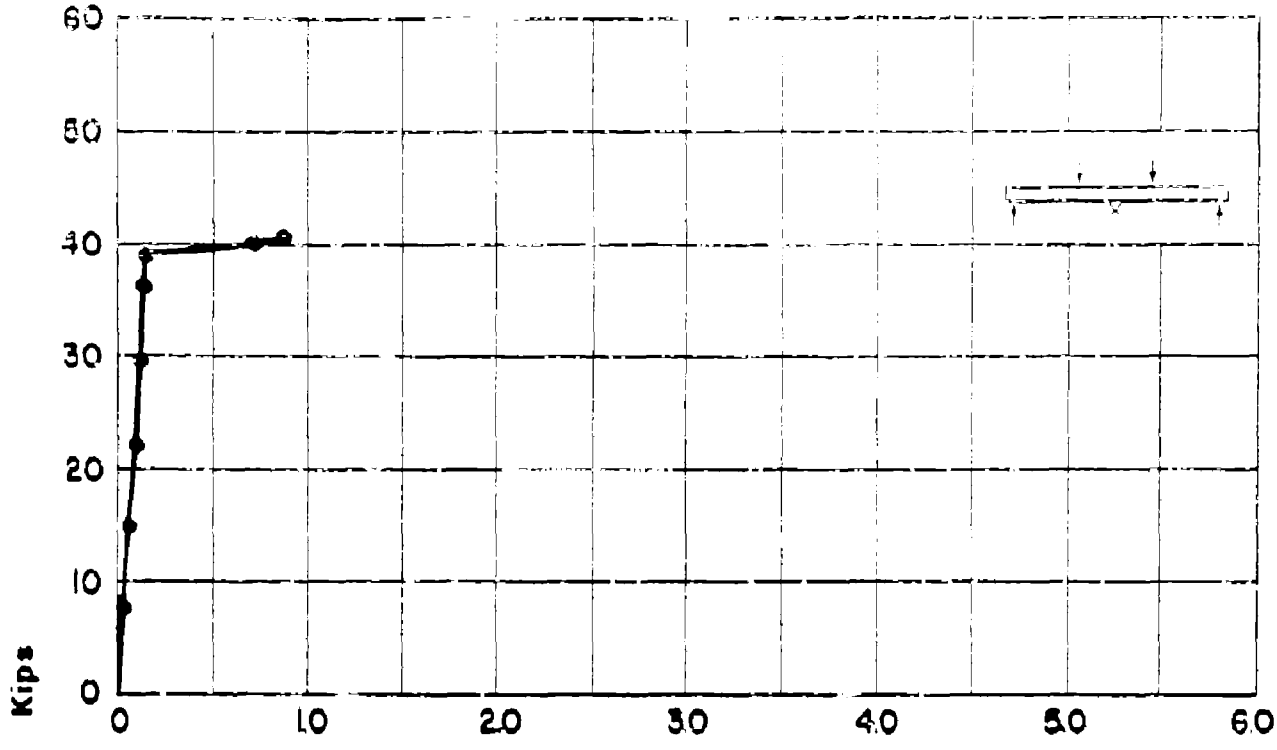

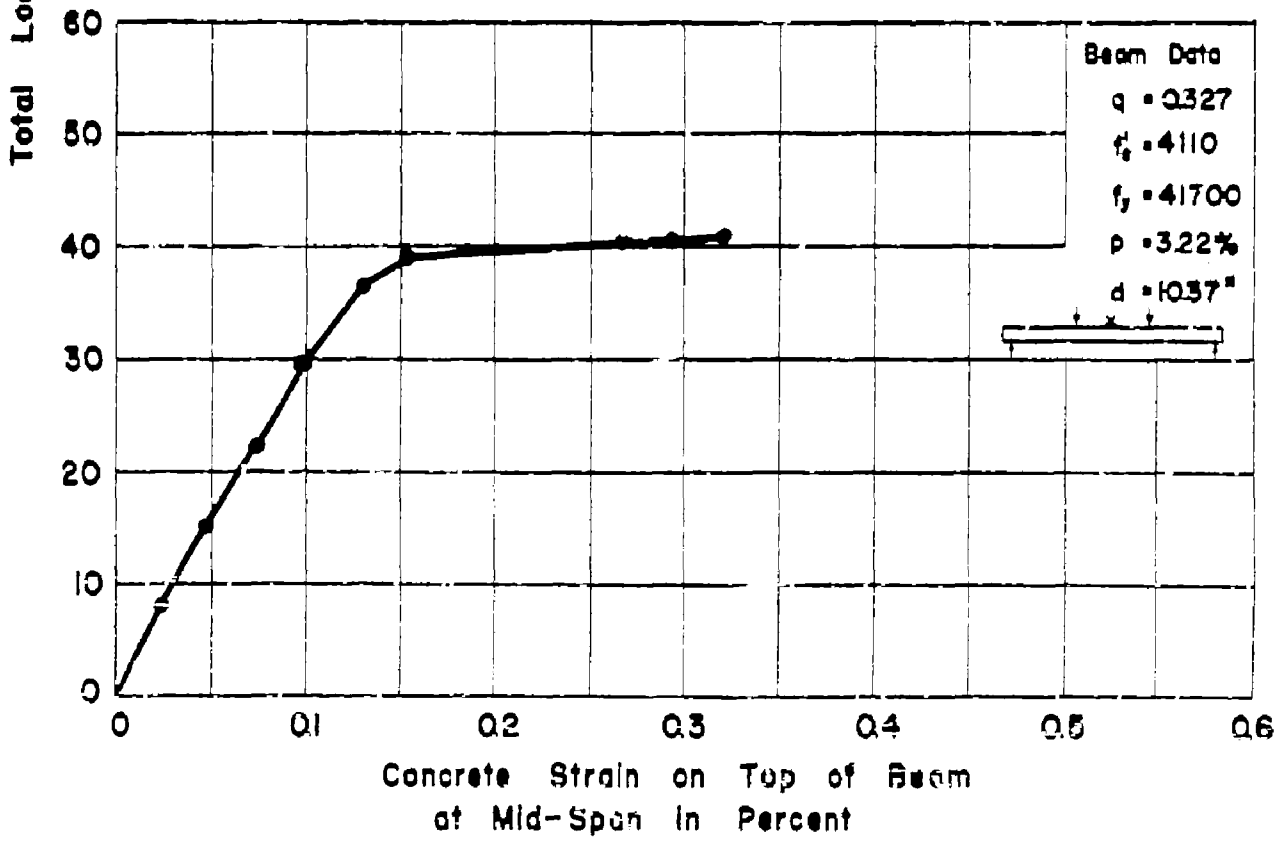

APP FIG. 81 LOAD-STRAIN CURVES FOR BEAM NO. T3Mb

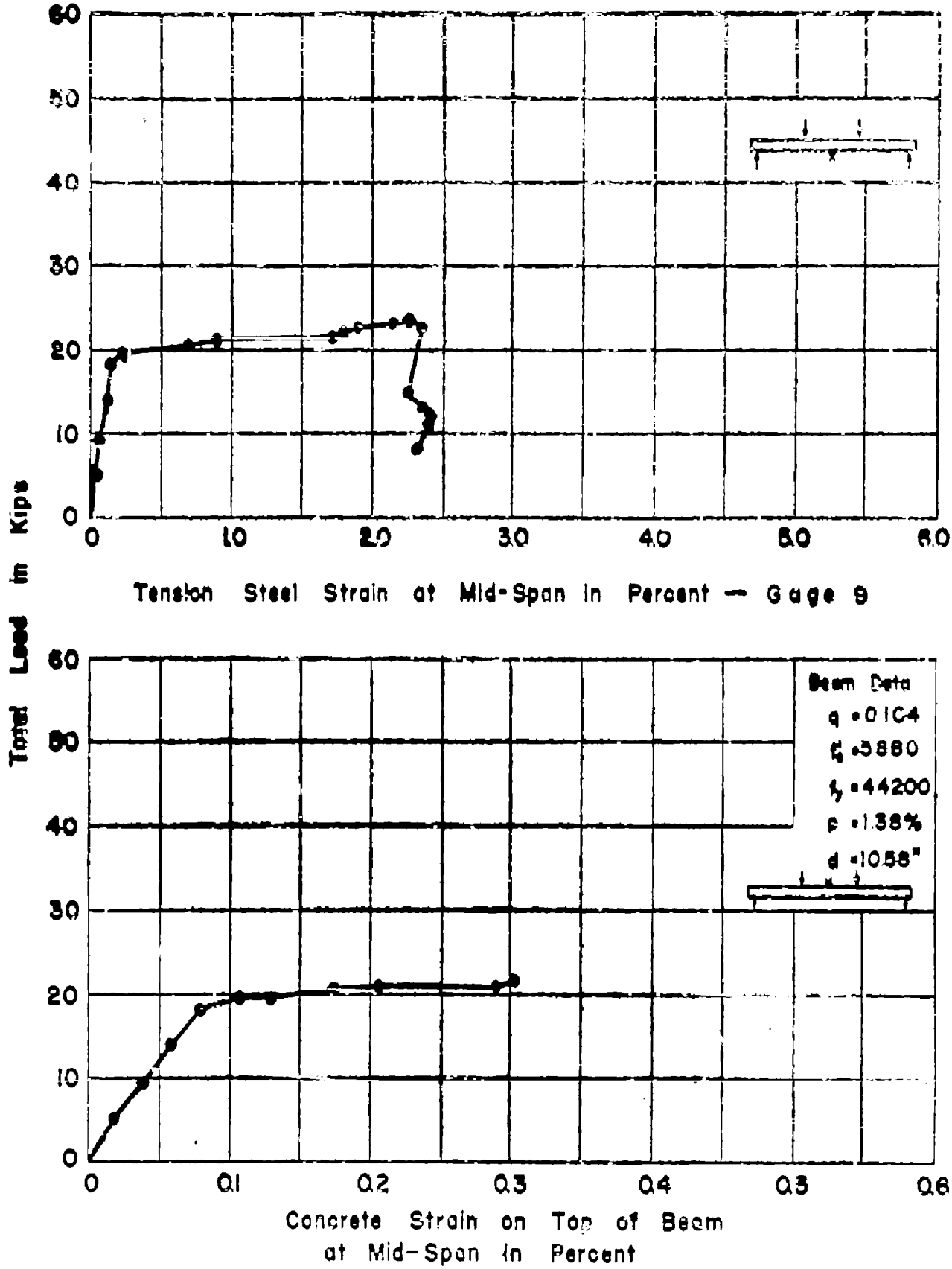

APP. FIG. 82 LOAD-STRAIN CURVES FOR BEAM NO. T1Ha

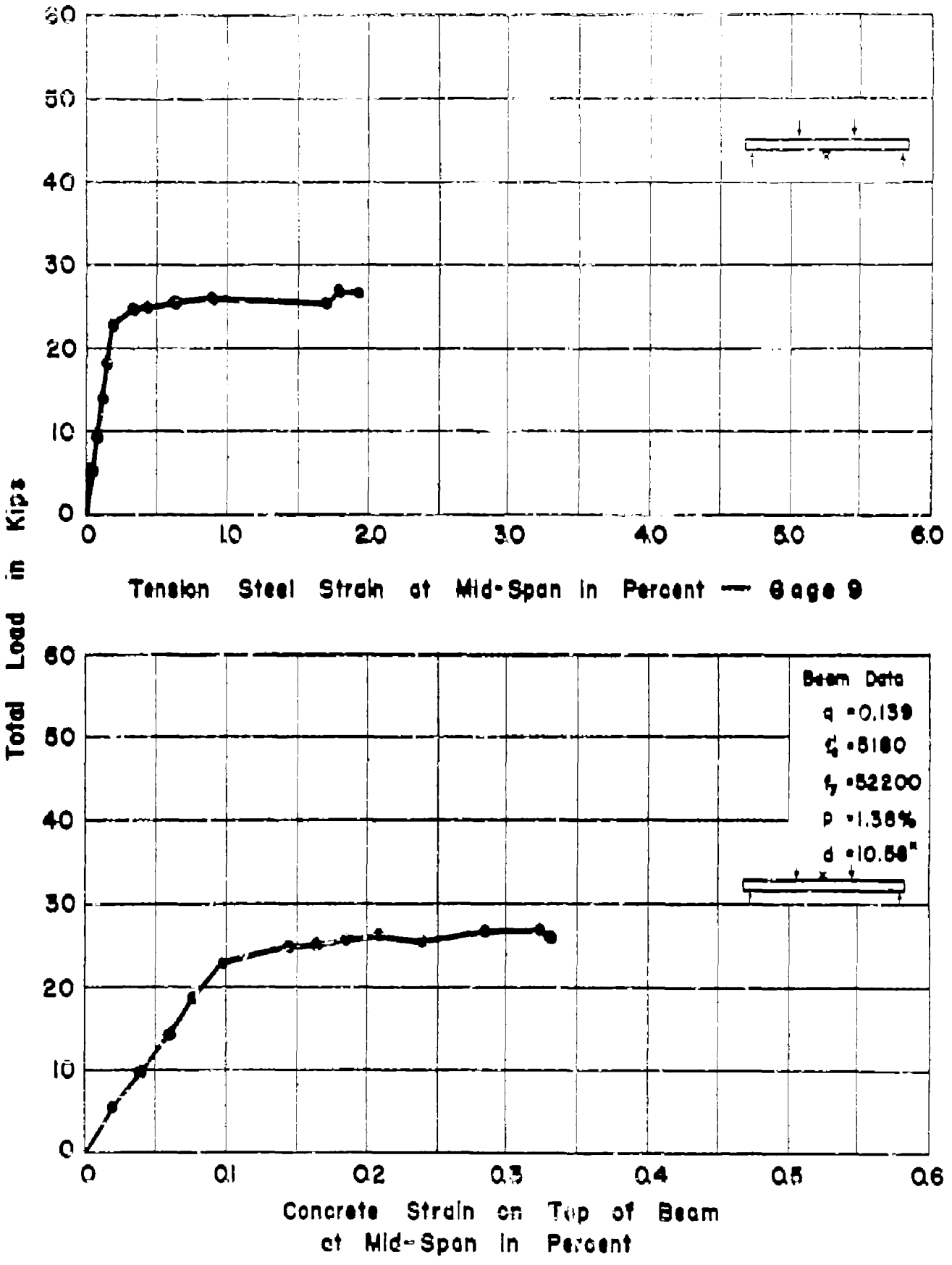

APP. FIG. 83 LOAD-STRAIN CURVES FOR BEAM NO. TIHb

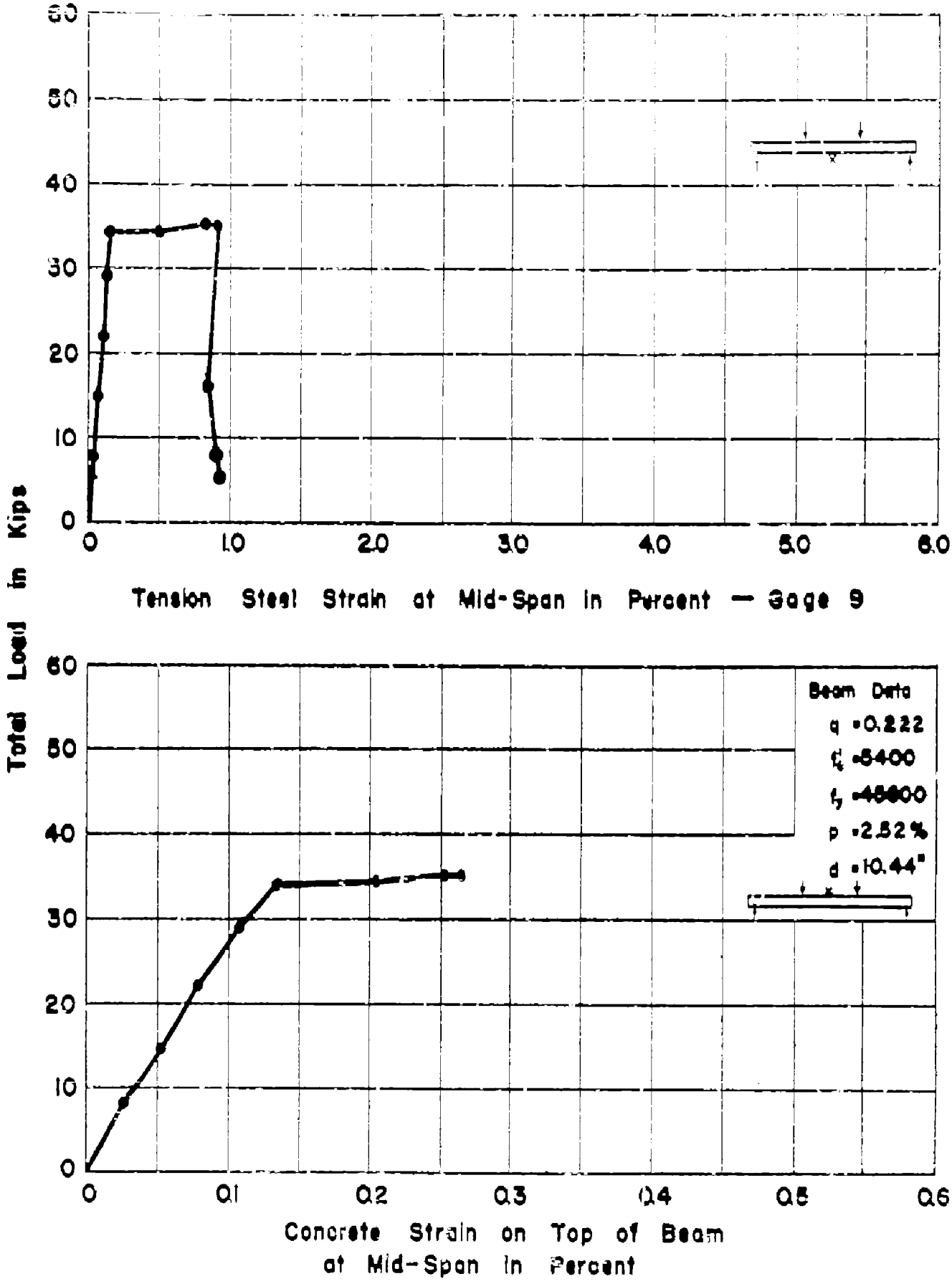

APP. FIG. 84 LOAD-STRAIN CURVES FOR BEAM NO. T2H

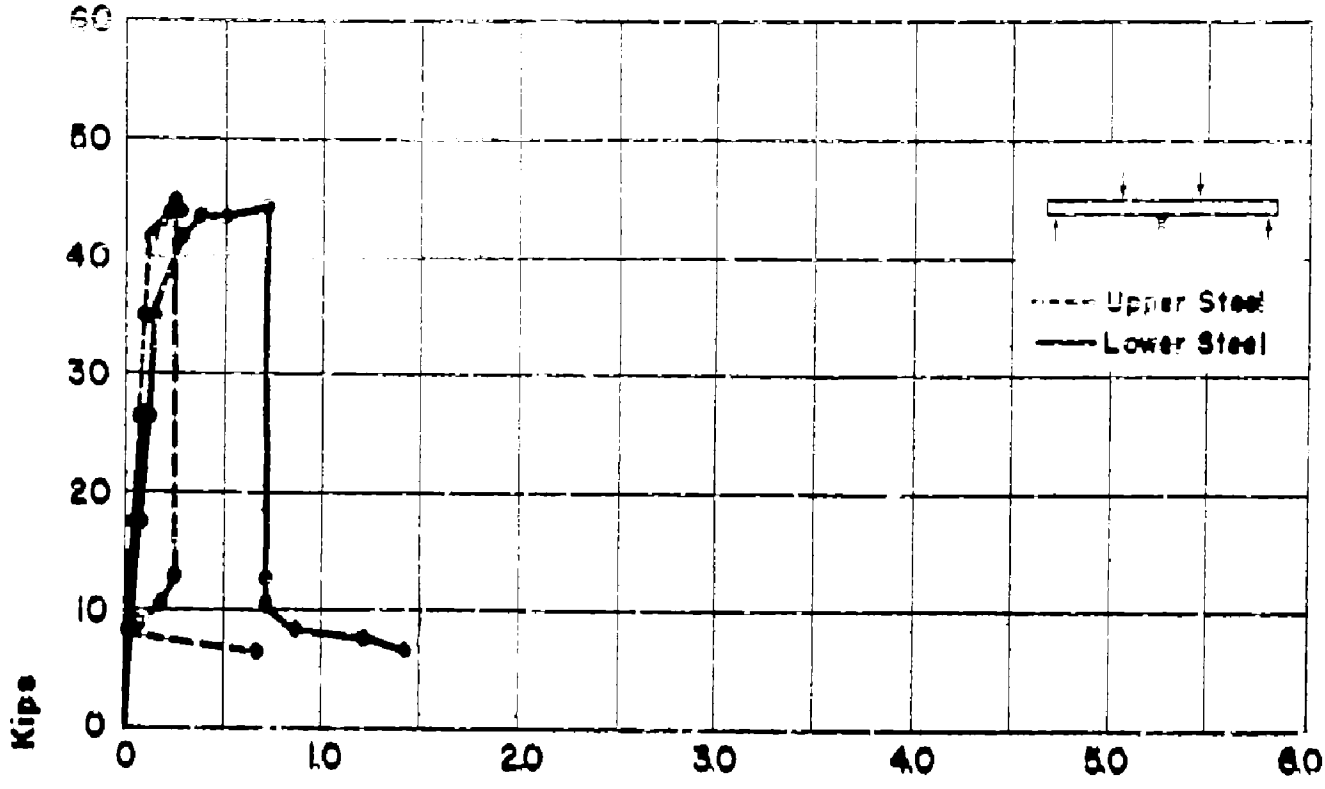

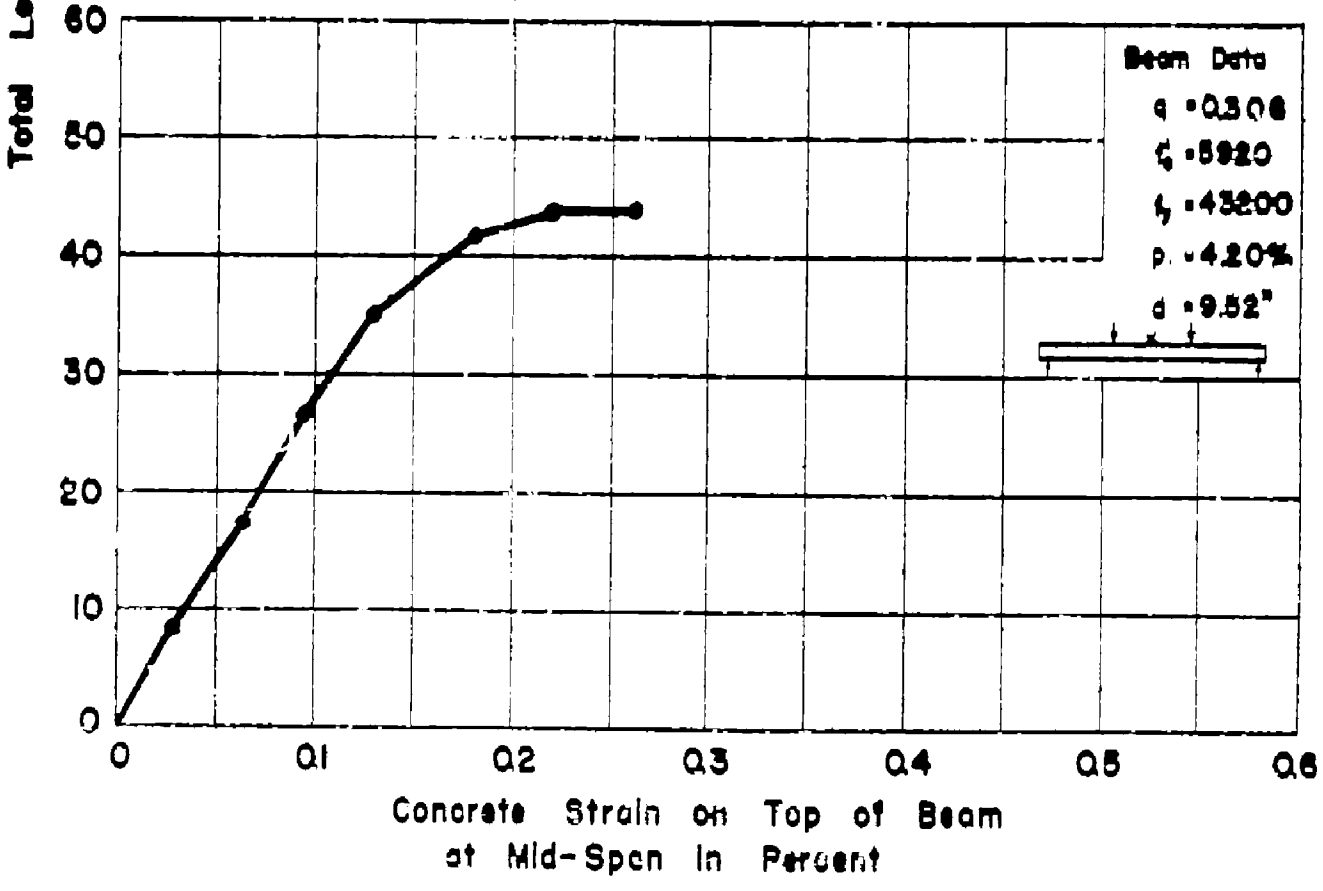

APP. FIG. 85 LOAD-STRAIN CURVES FOR BEAM NO.T3H

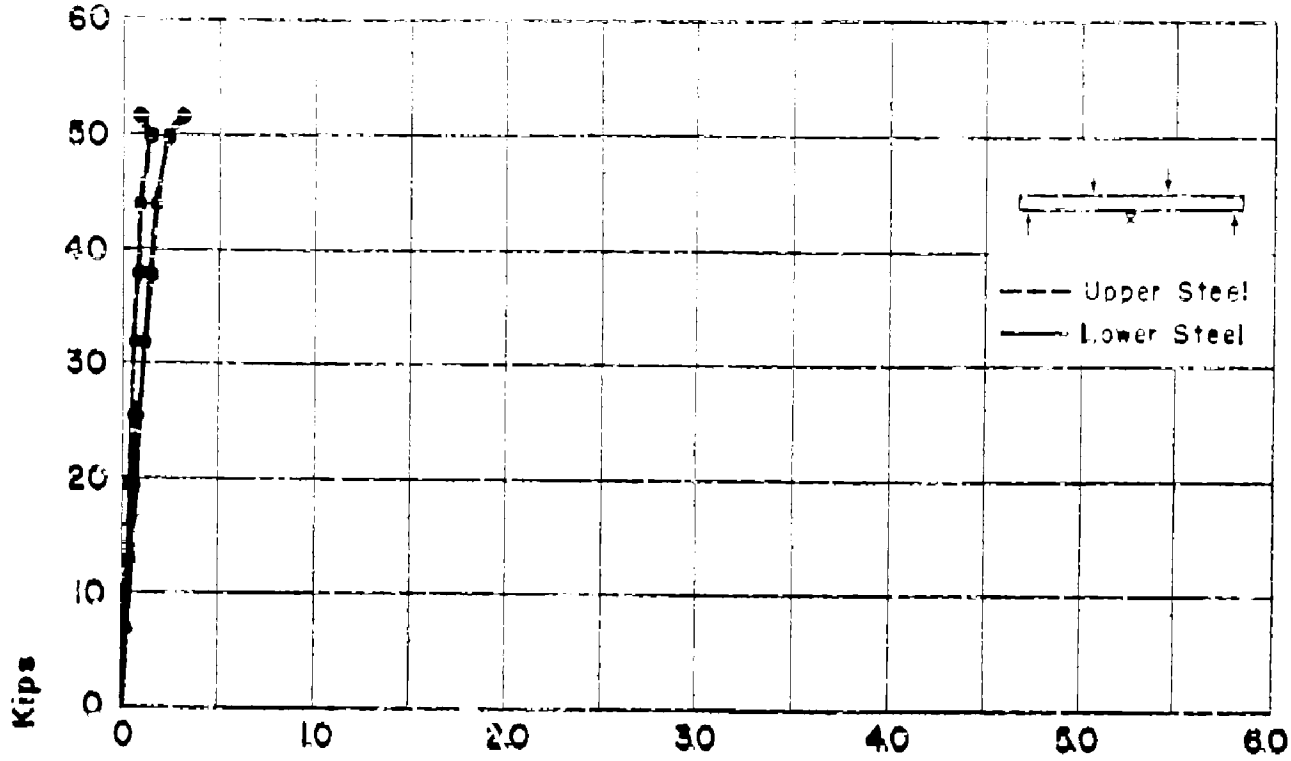

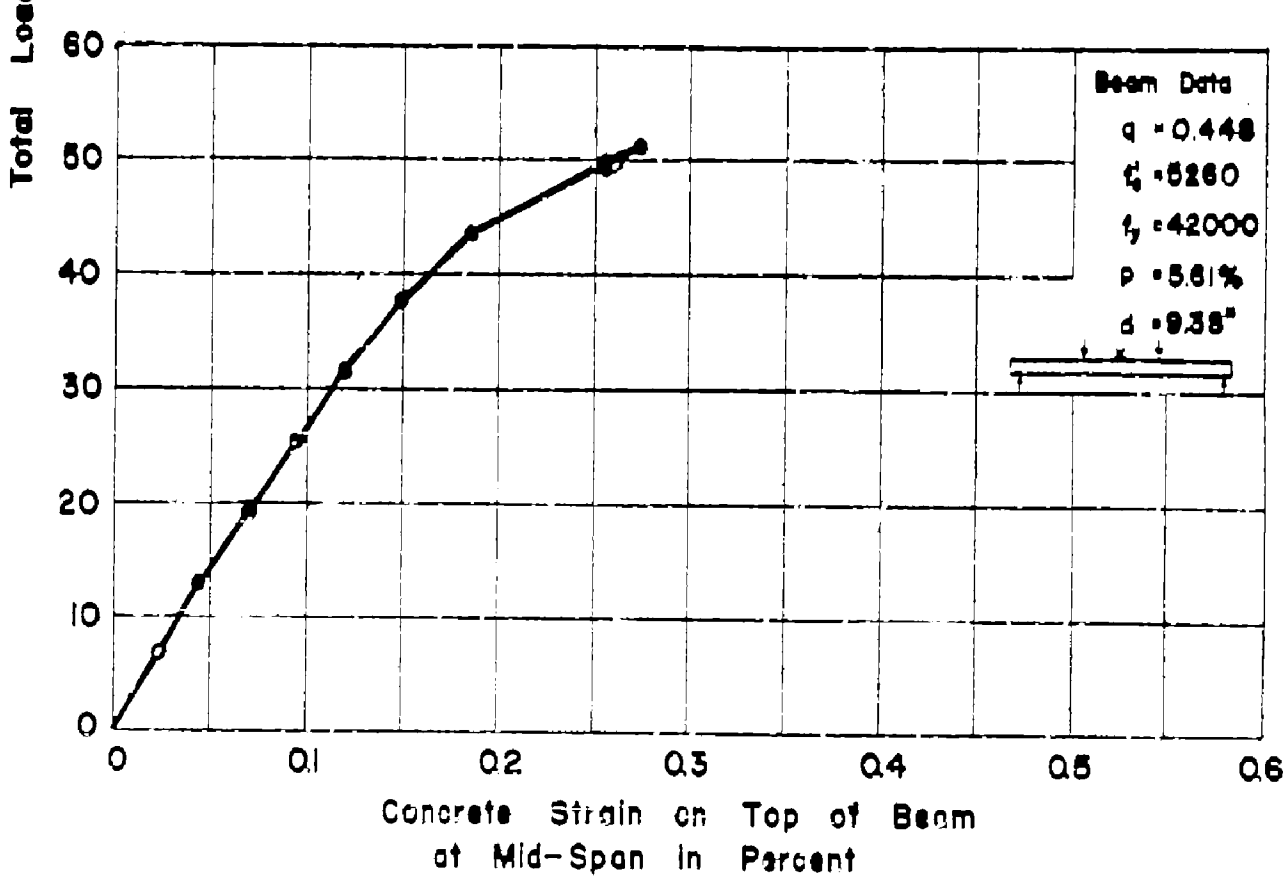

APP. FIG. 86 LOAD-STRAIN CURVES FOR BEAM NO. T4H

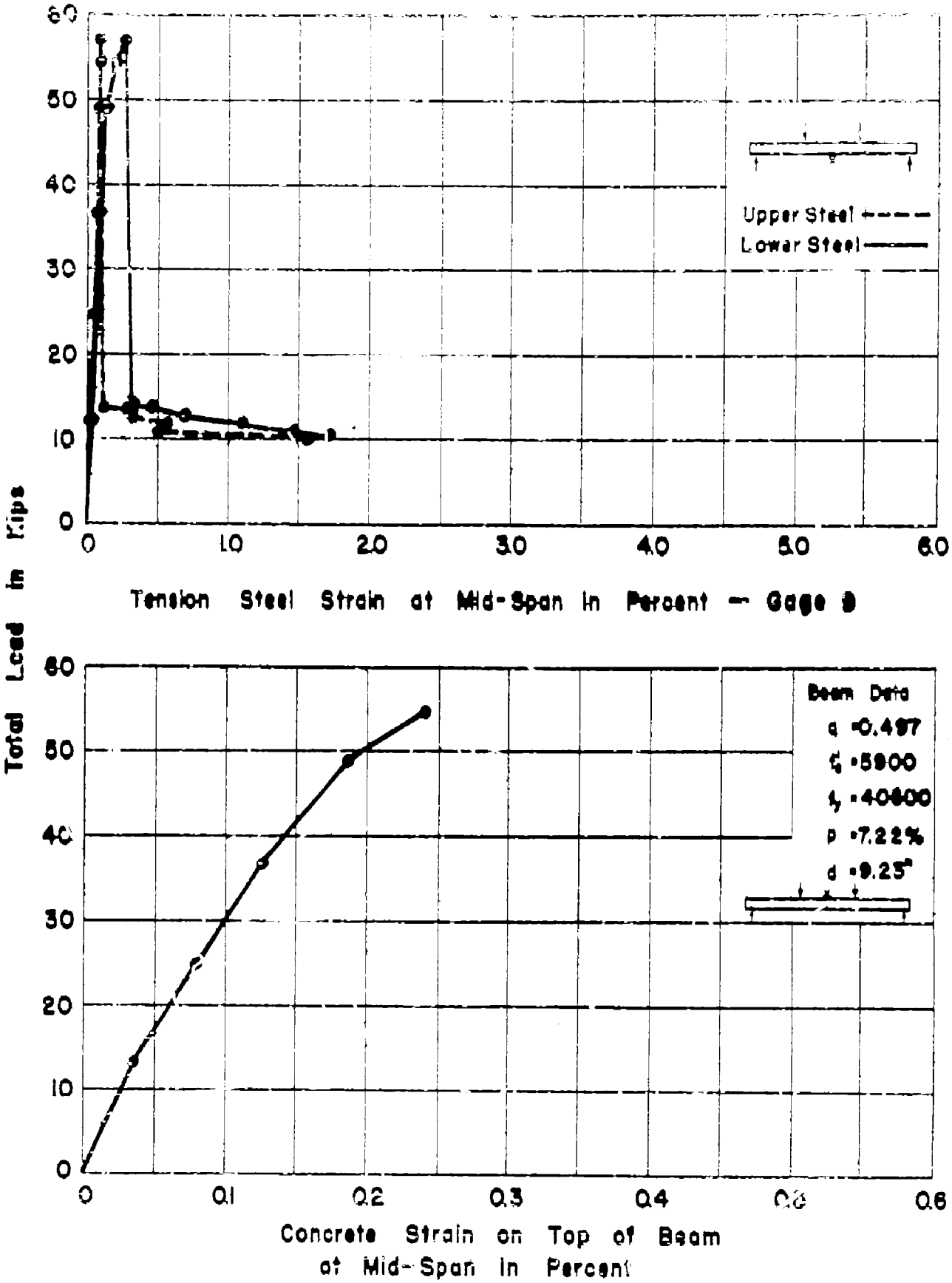

APP. FIG. 87 LOAD-STRAIN CURVES FOR BEAM NO.T5H

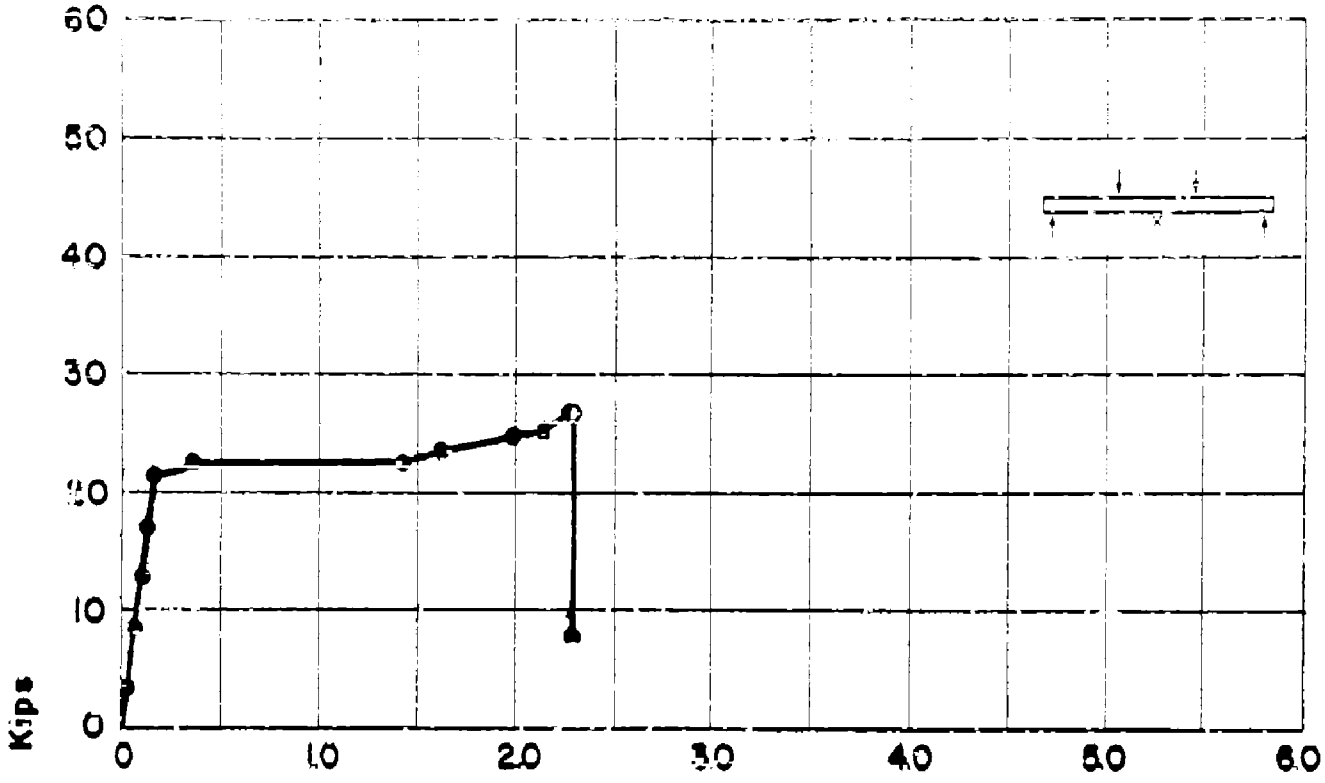

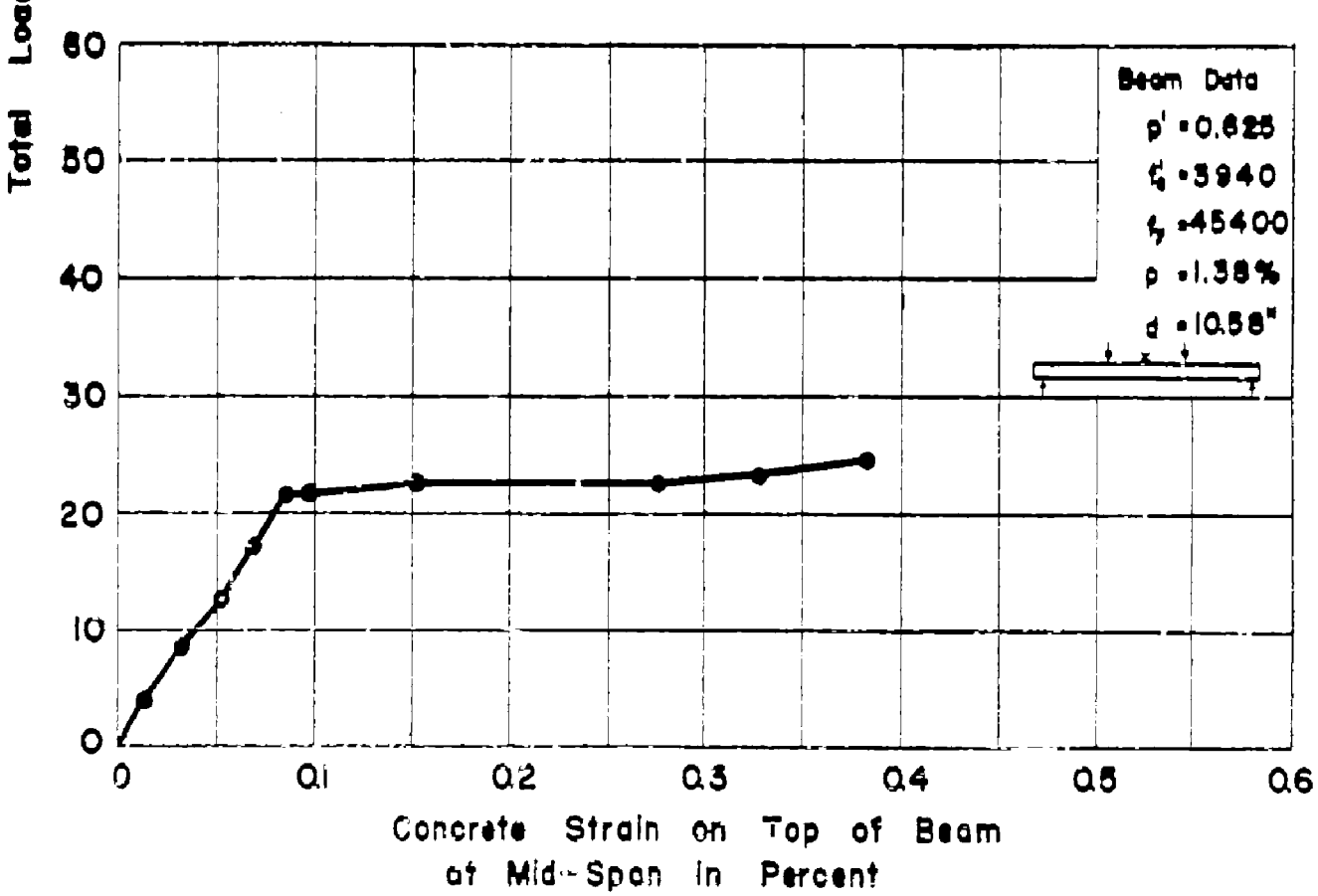

APP. FIG. 88 LOAD-STRAIN CURVES FOR BEAM NO. C2W

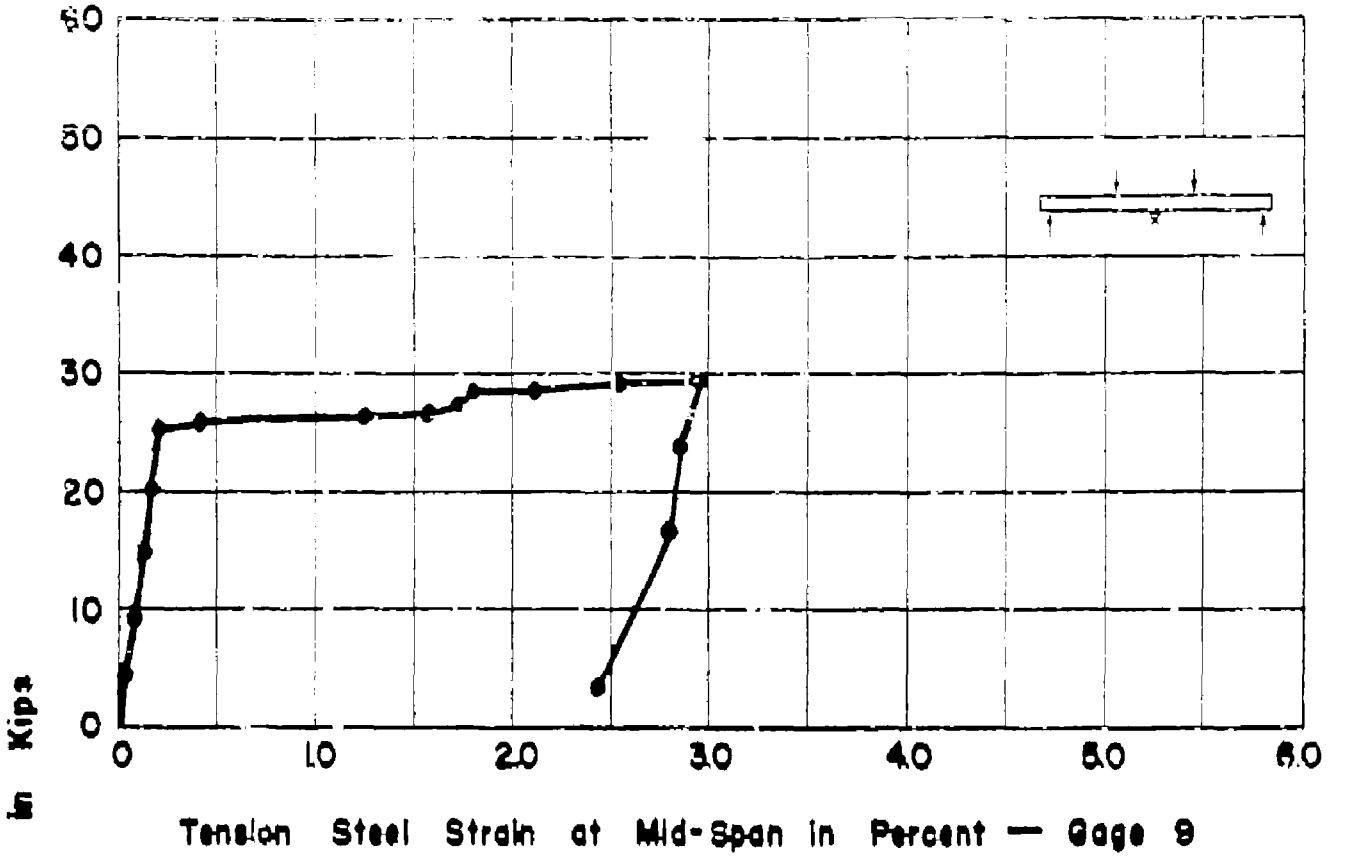

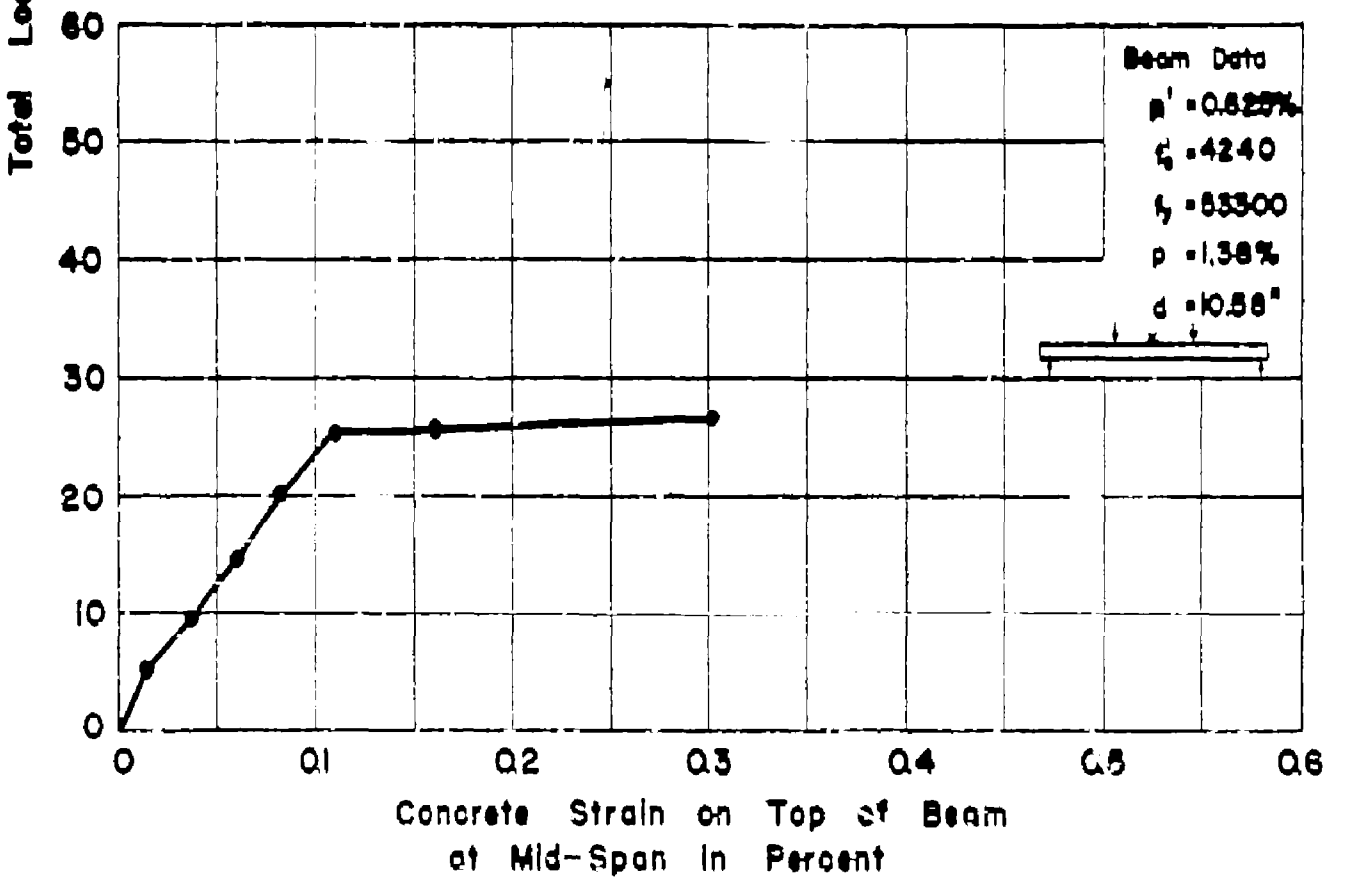

APP. FIG. 89 LOAD-STRAIN CURVES FOR BEAM NO.02xm

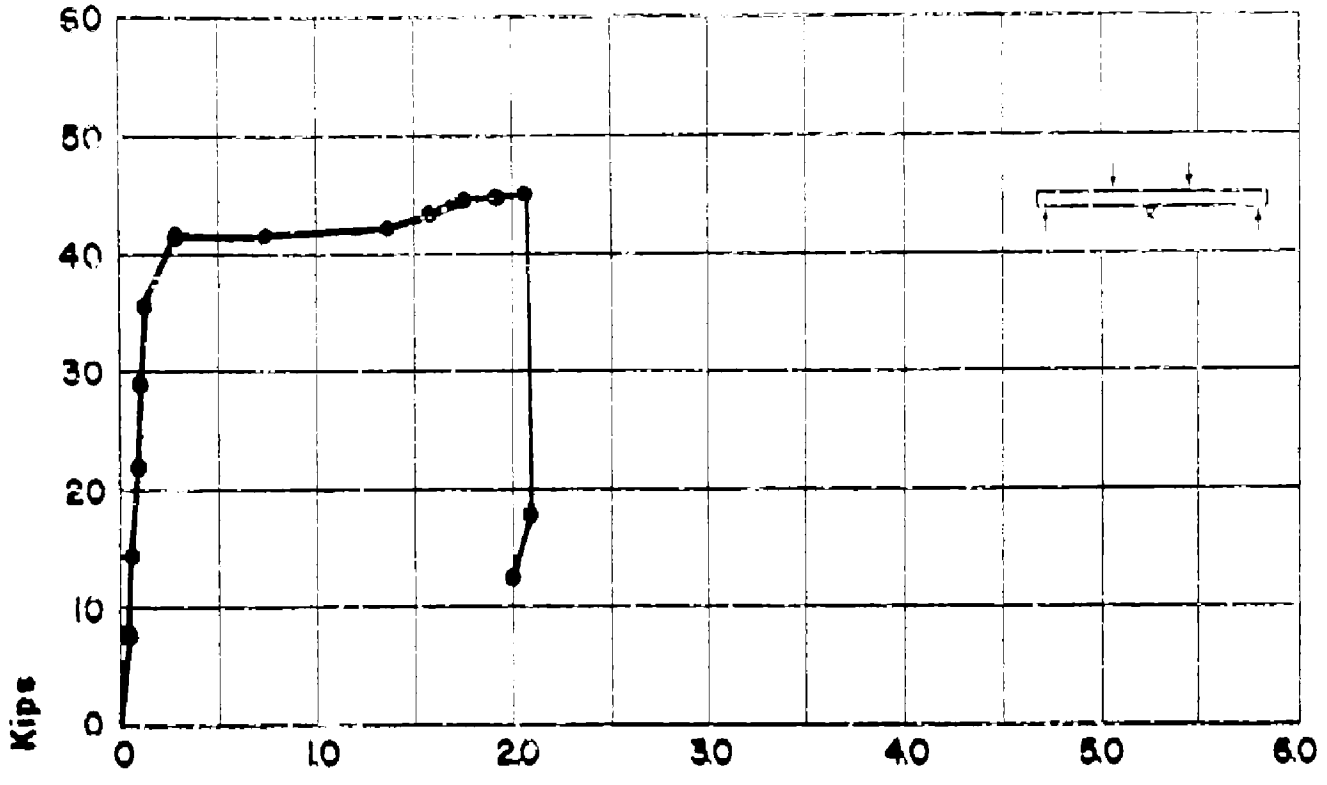

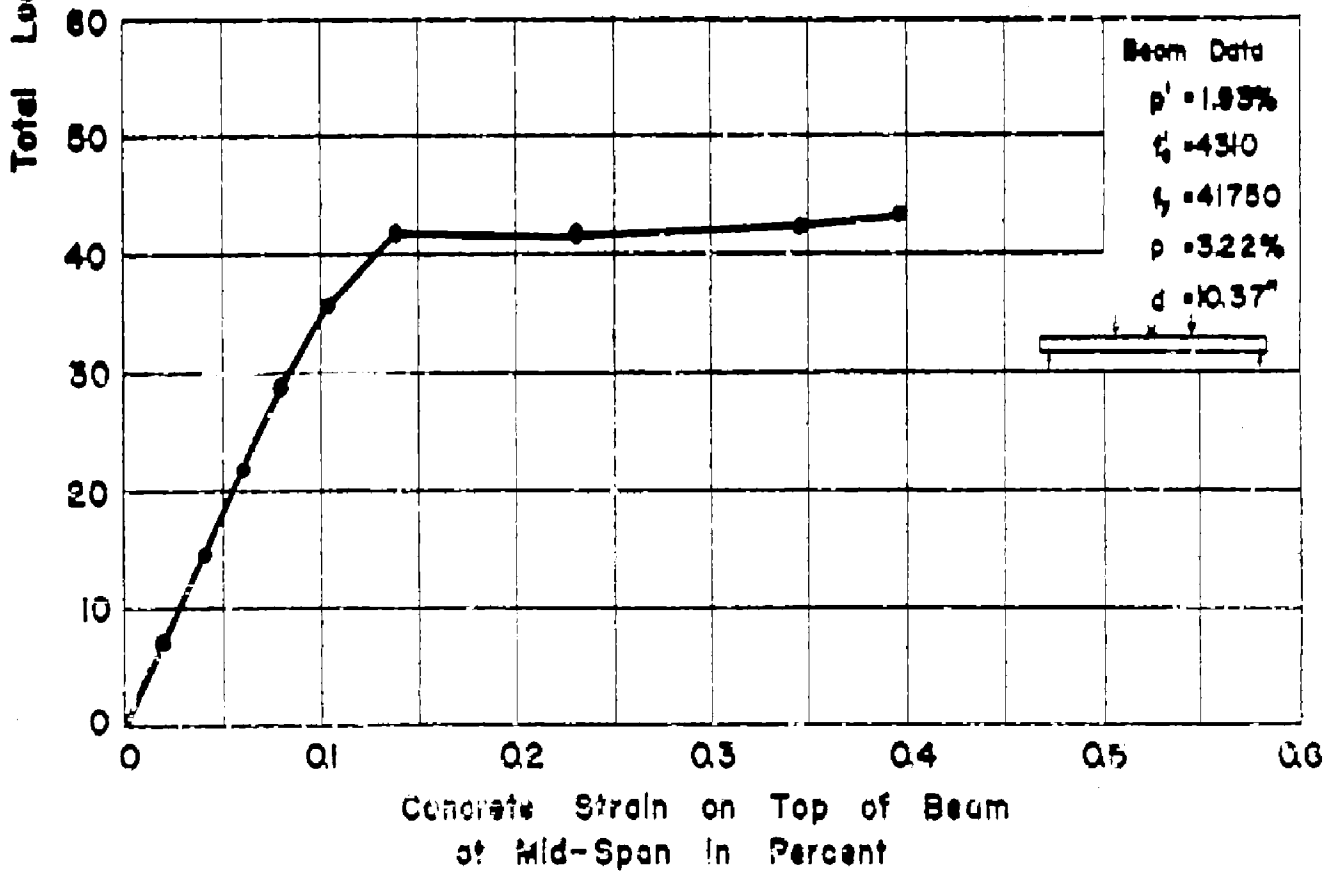

APP. FIG. 90 LOAD-STRAIN CURVES FOR BEAM NO.C3W

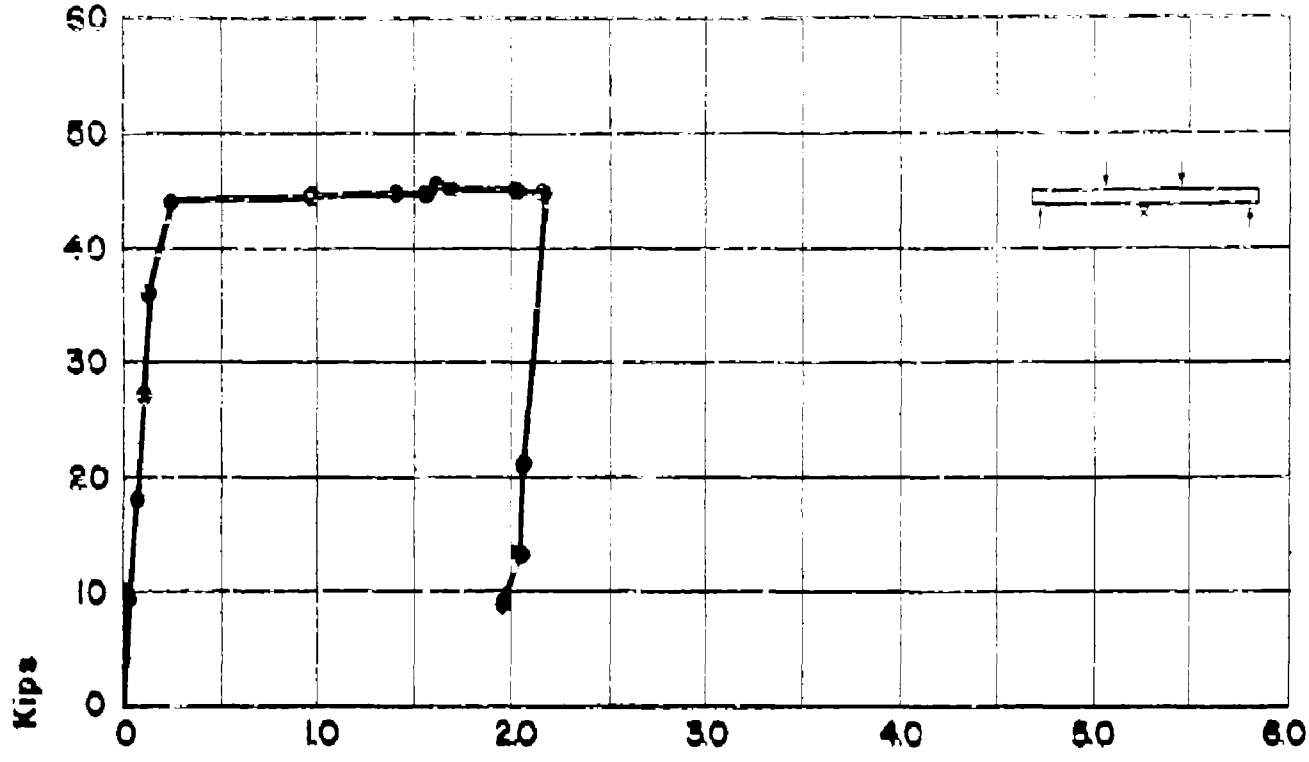

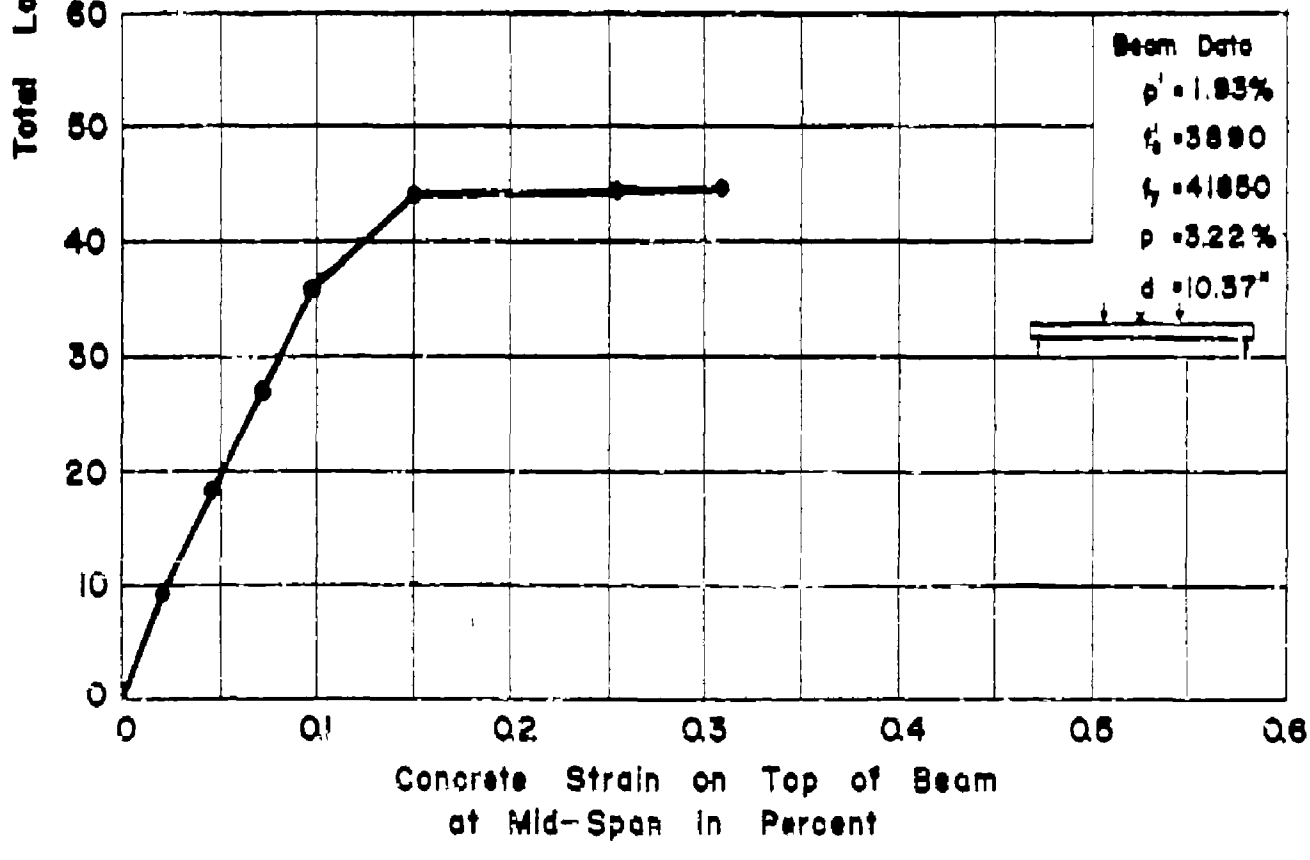

APP. FIG. 91 LOAD-STRAIN CURVES FOR BEAM NO.C3xm

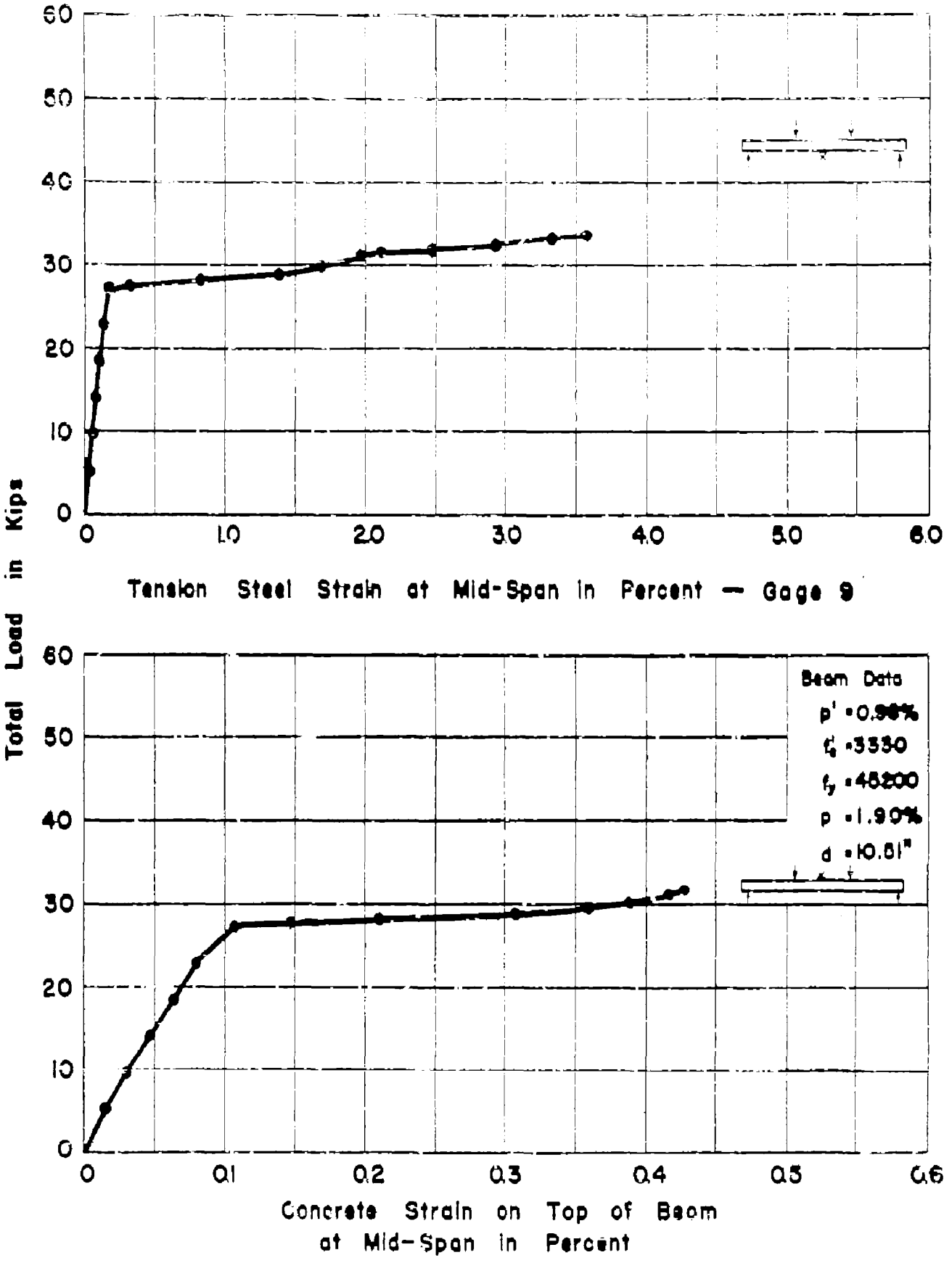

APP. FIG. 92 LOAD-STRAIN CURVES FOR BEAM NOC3yna

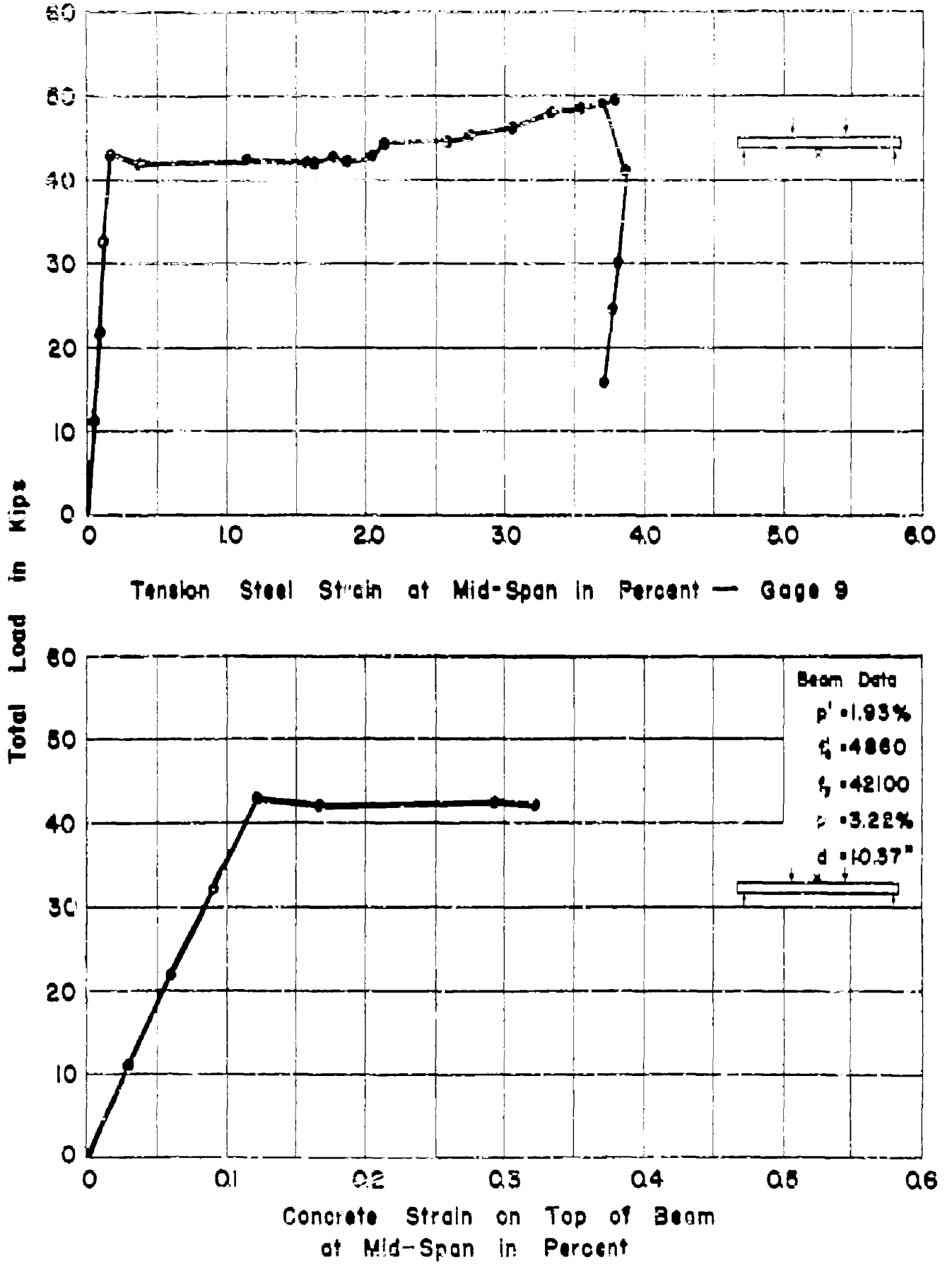

APP. FIG. 93 LOAD-STRAIN CURVES FOR BEAM NO.C3ynb

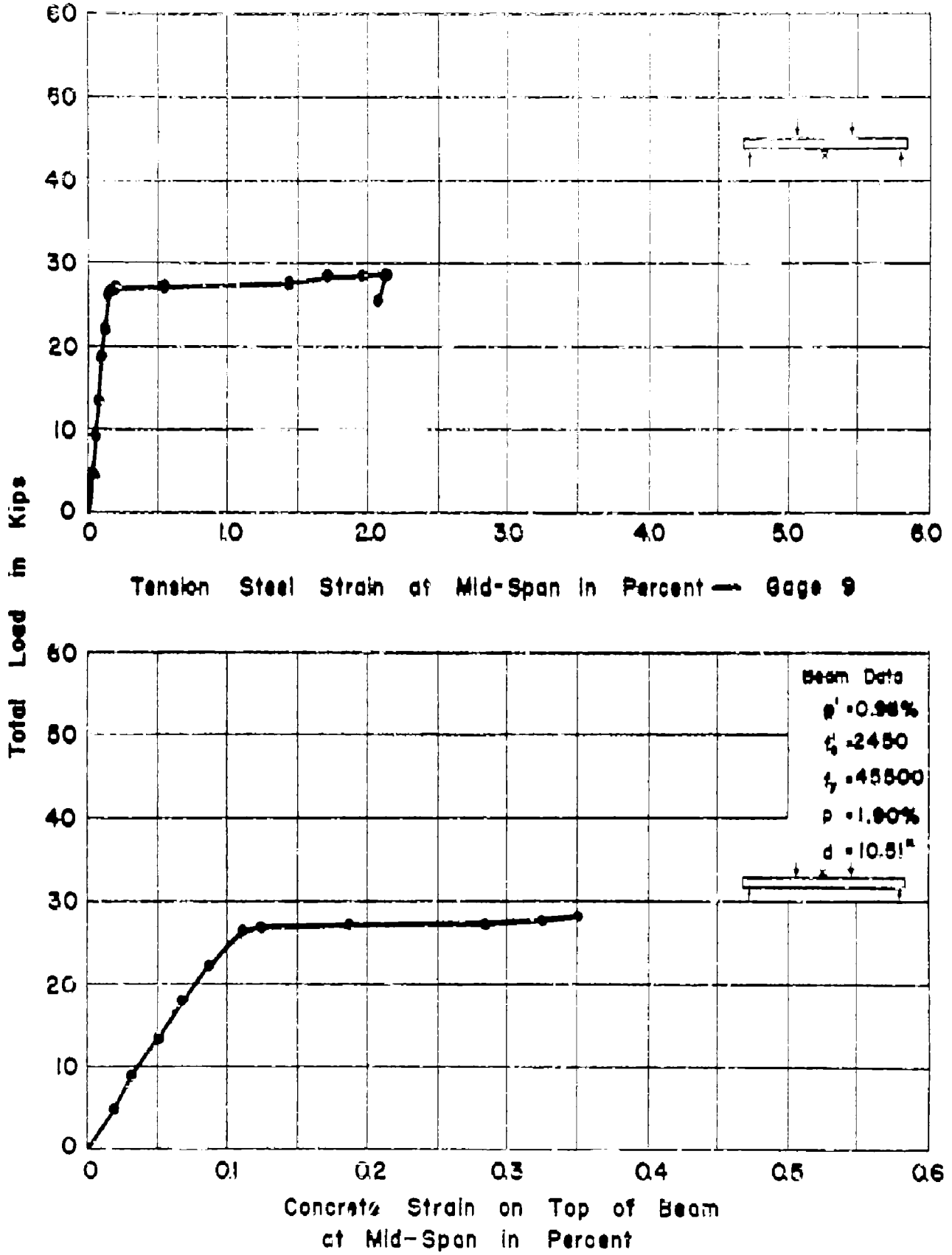

APP. FIG. 94 LOAD-STRAIN CURVES FOR BEAM NOC4xnd

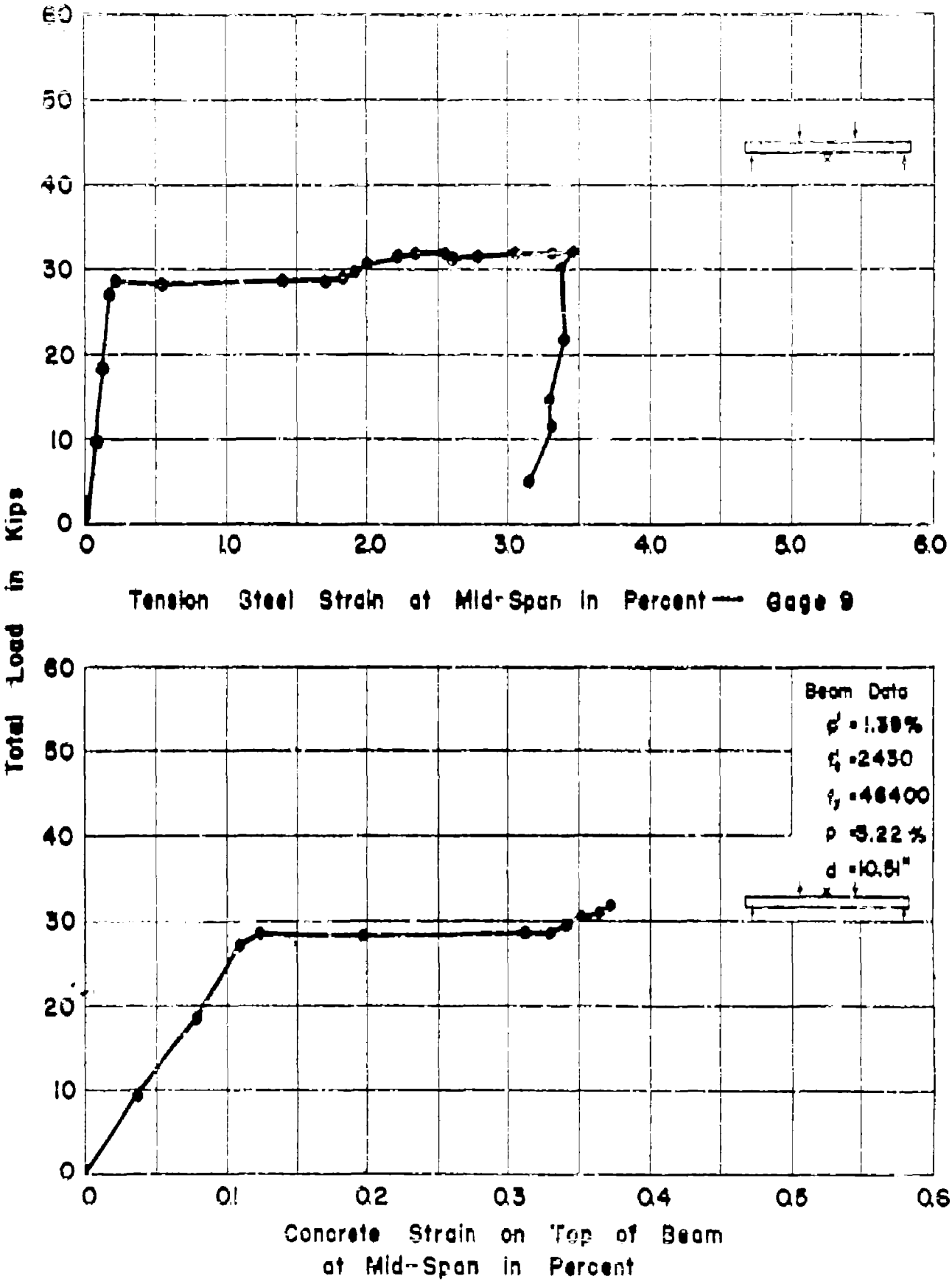

APP. FIG. 95 LOAD-STRAIN CURVES FOR BEAM NOC4xnb

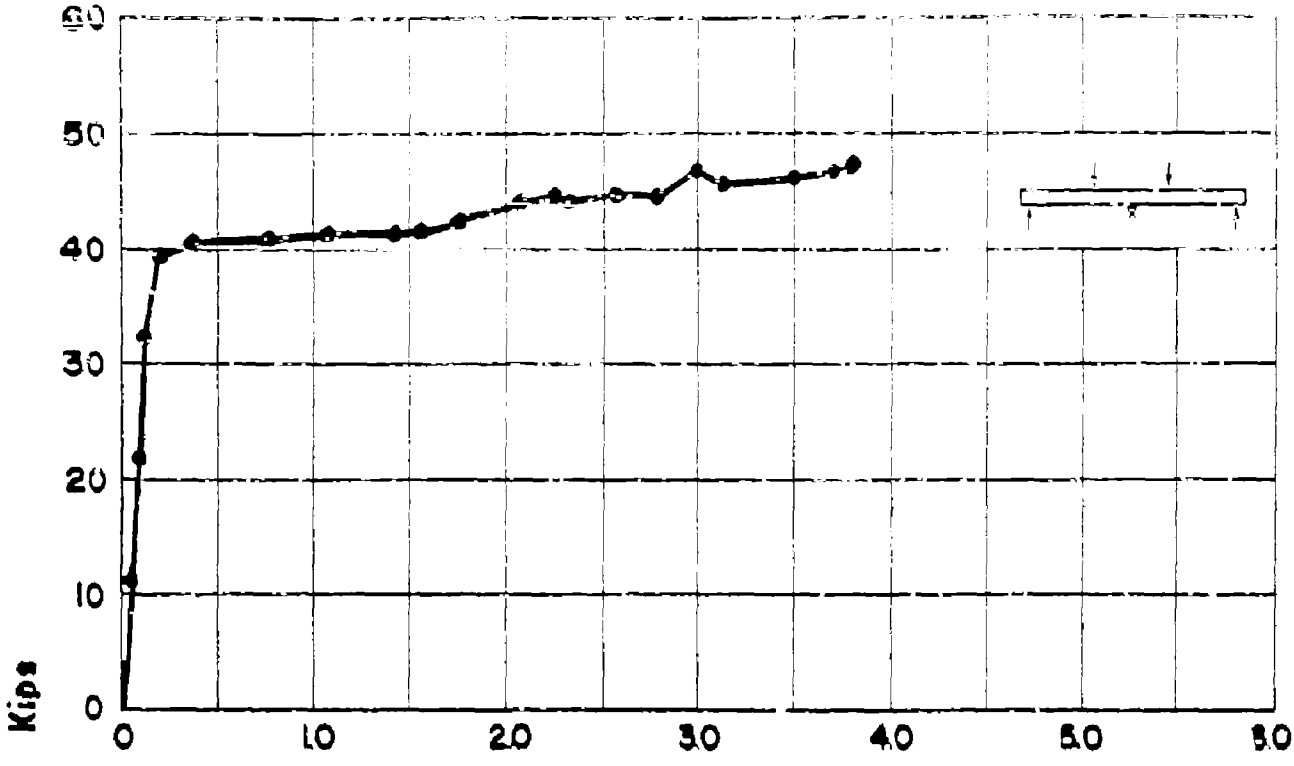

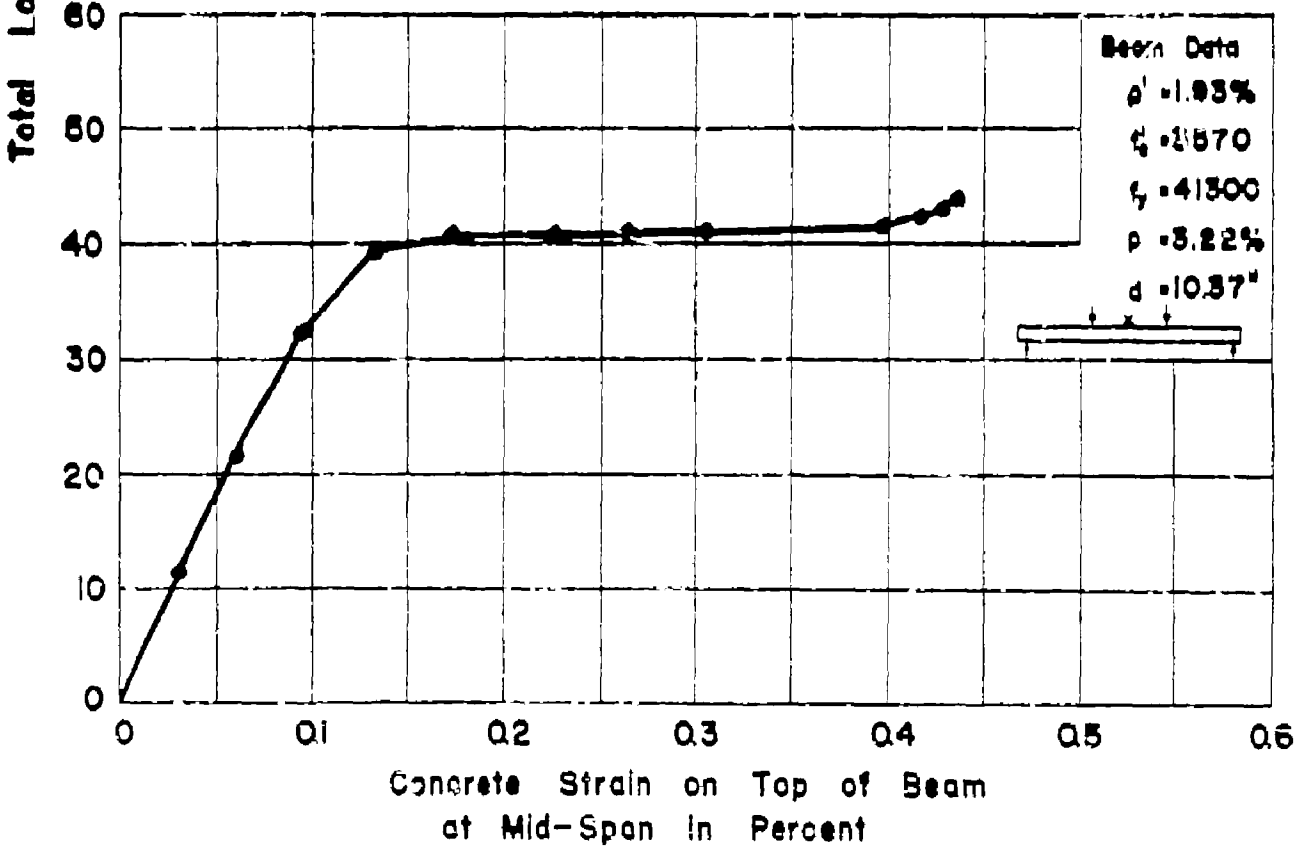

APP. FIG. 96 LOAD-STRAIN CURVES FOR BEAM NCC4zn

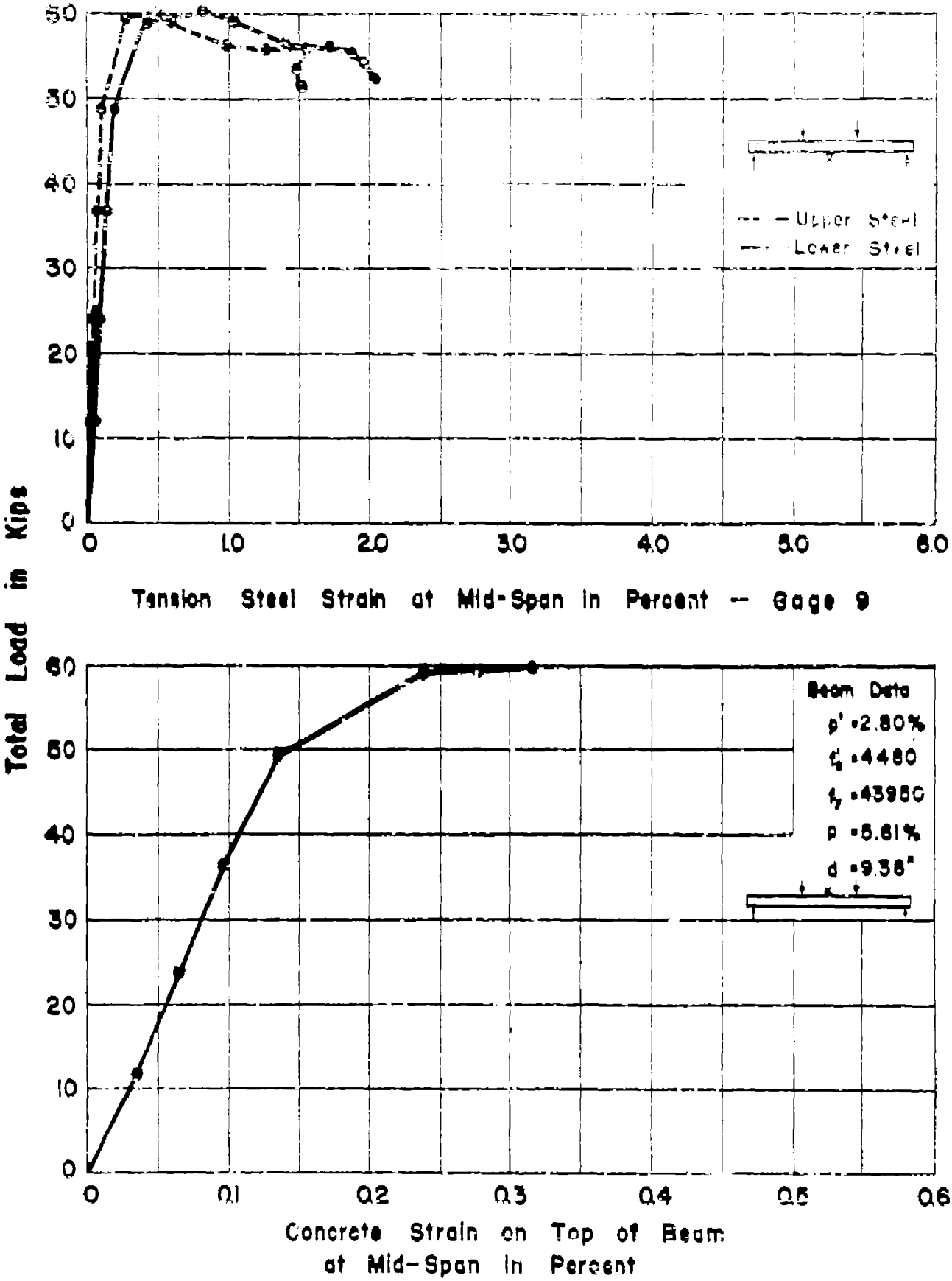

APP. FIG. 97 LOAD-STRAIN CURVES FOR BEAM NO.C5yn

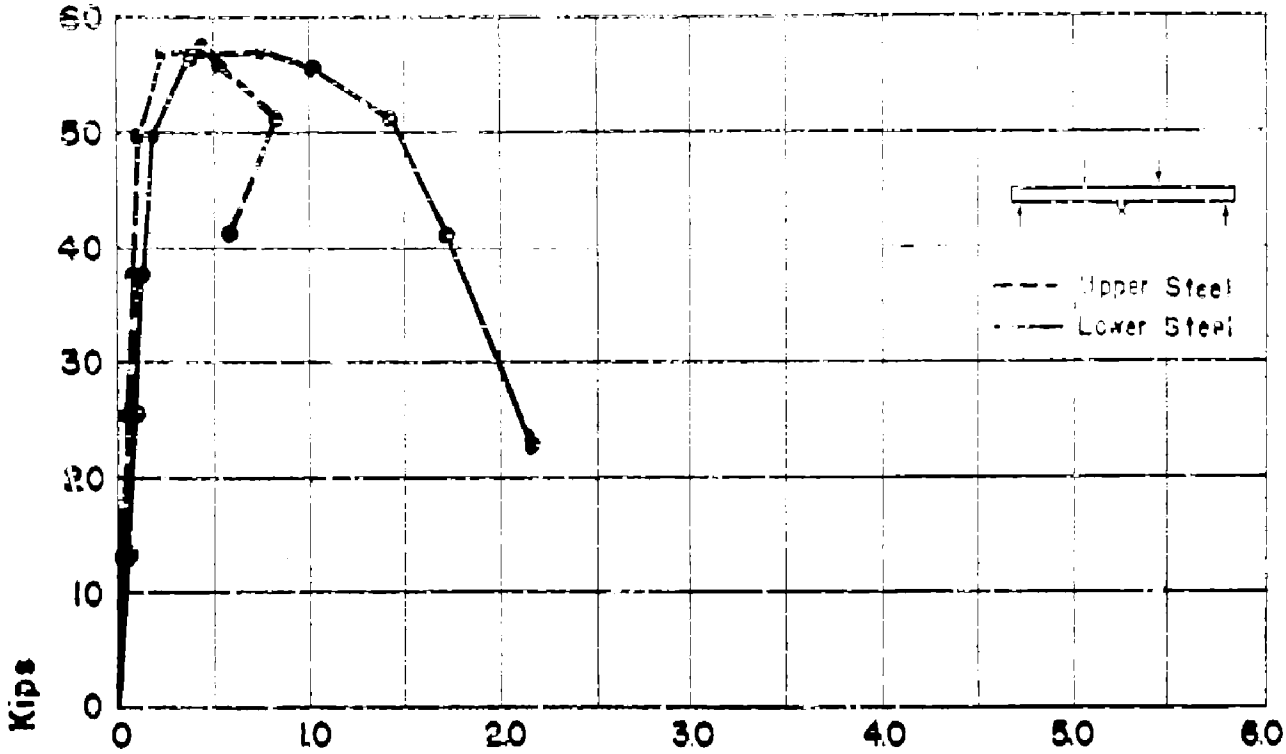

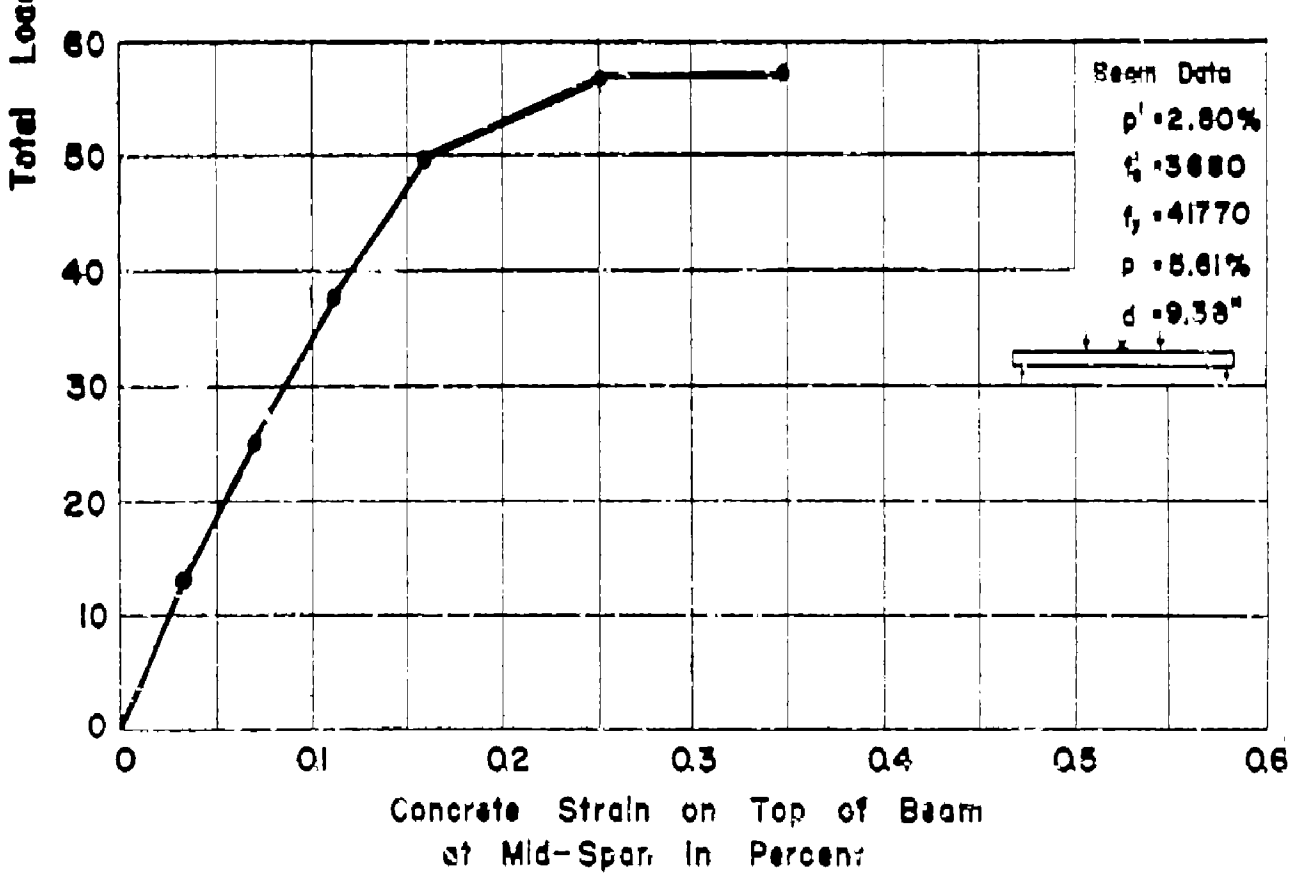

APP. FIG. 98 LOAD-STRAIN CURVES FOR BEAM NO.C6xm

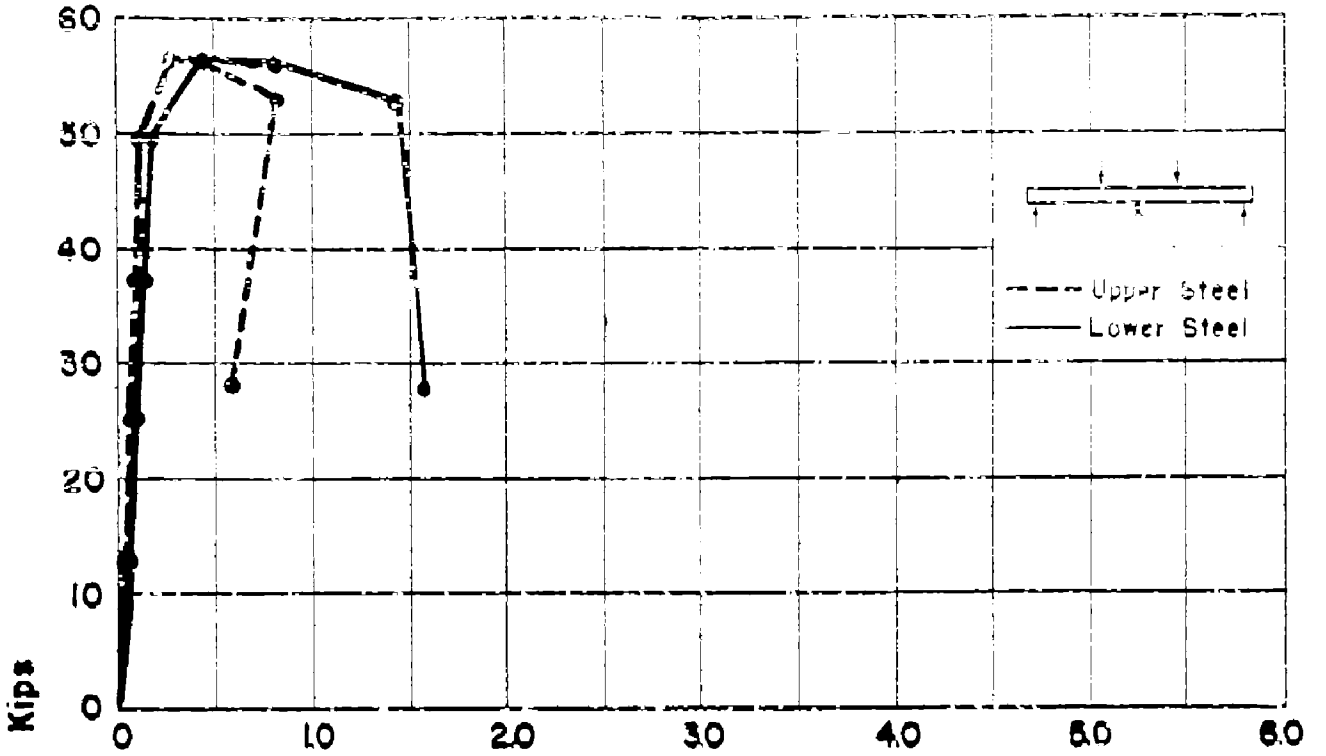

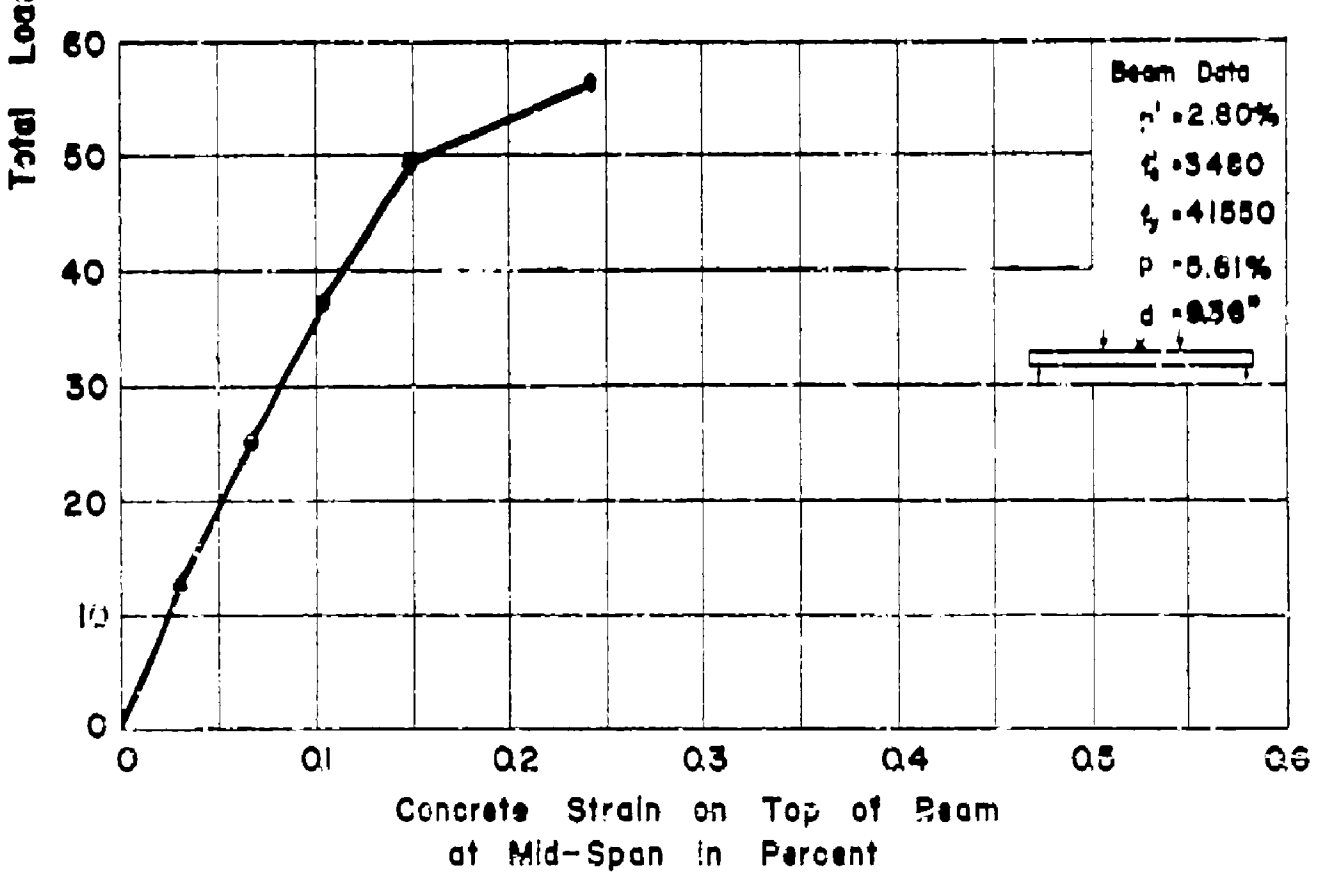

APP. FIG. 99 LOAD-STRAIN CURVES FOR BEAM NO. C7w

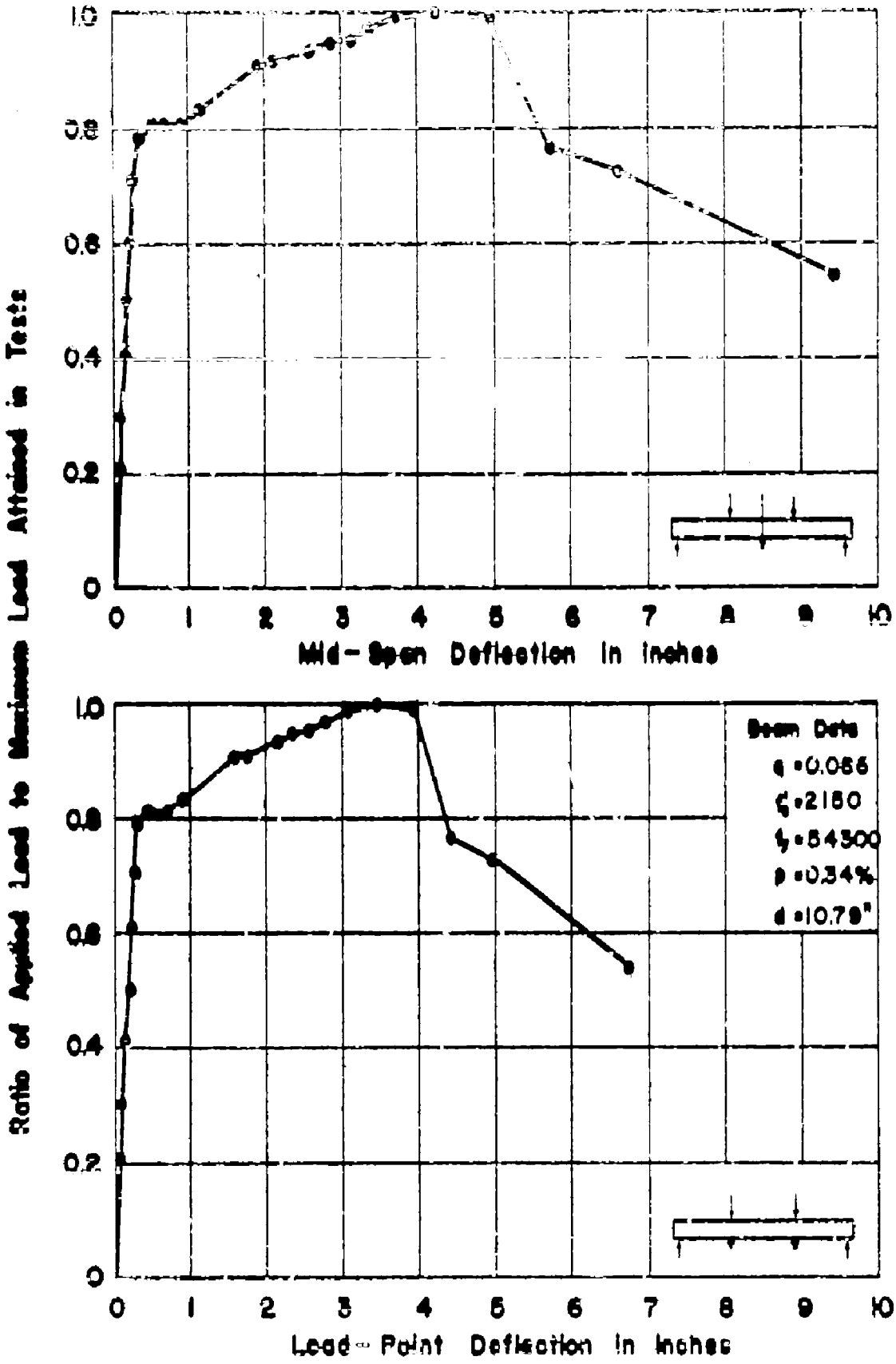

APP. FIG. 100 LOAD-RATIO VS. DEFLECTION FOR BEAM NO. T1L2

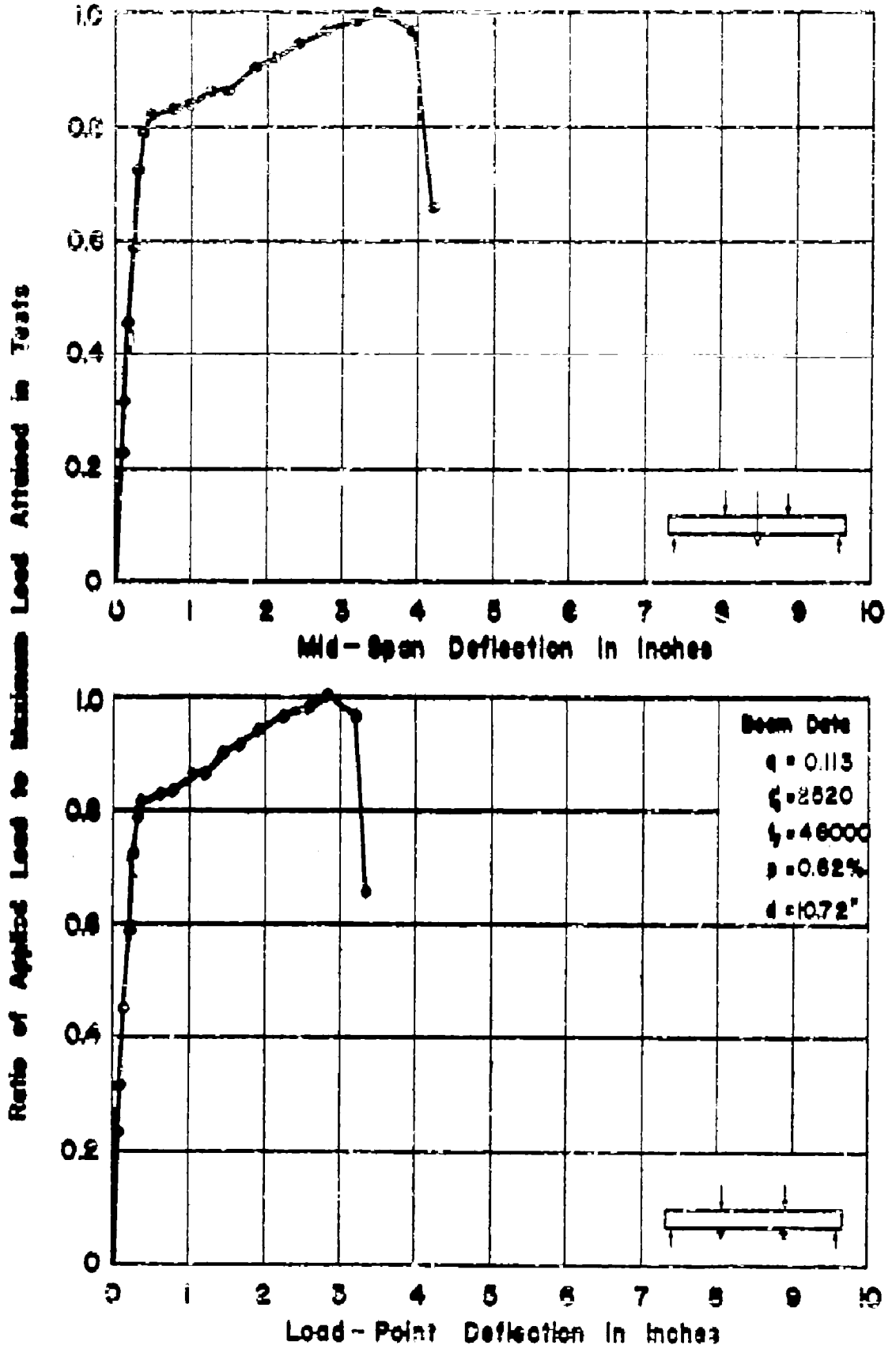

APP FIG. 101 LOAD-RATIO VS. DEFLECTION FOR BEAM NO. T1Lb

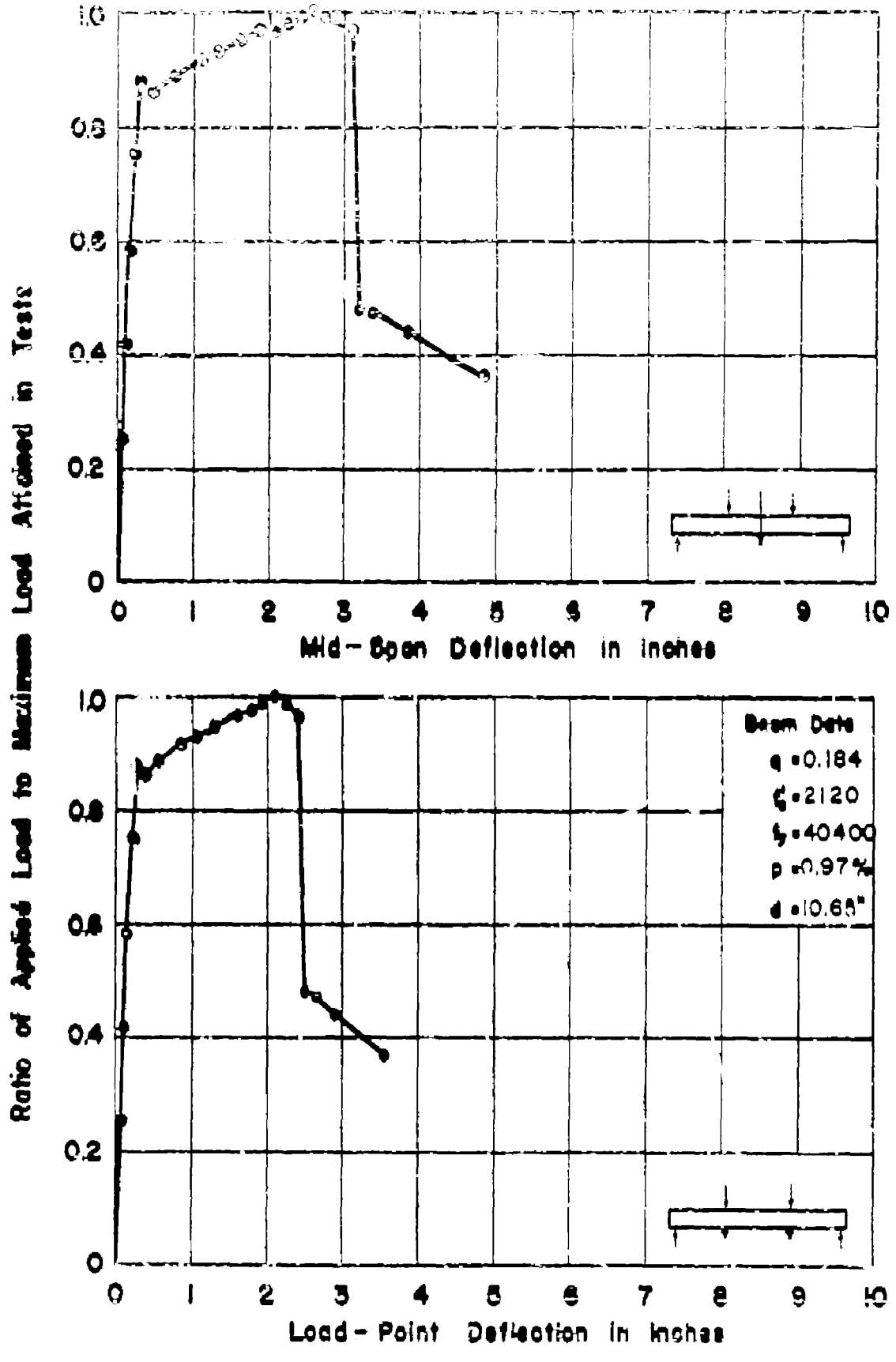

APP. FIG. 102 LOAD-RATIO VS. DEFLECTION FOR BEAM NO. T2La

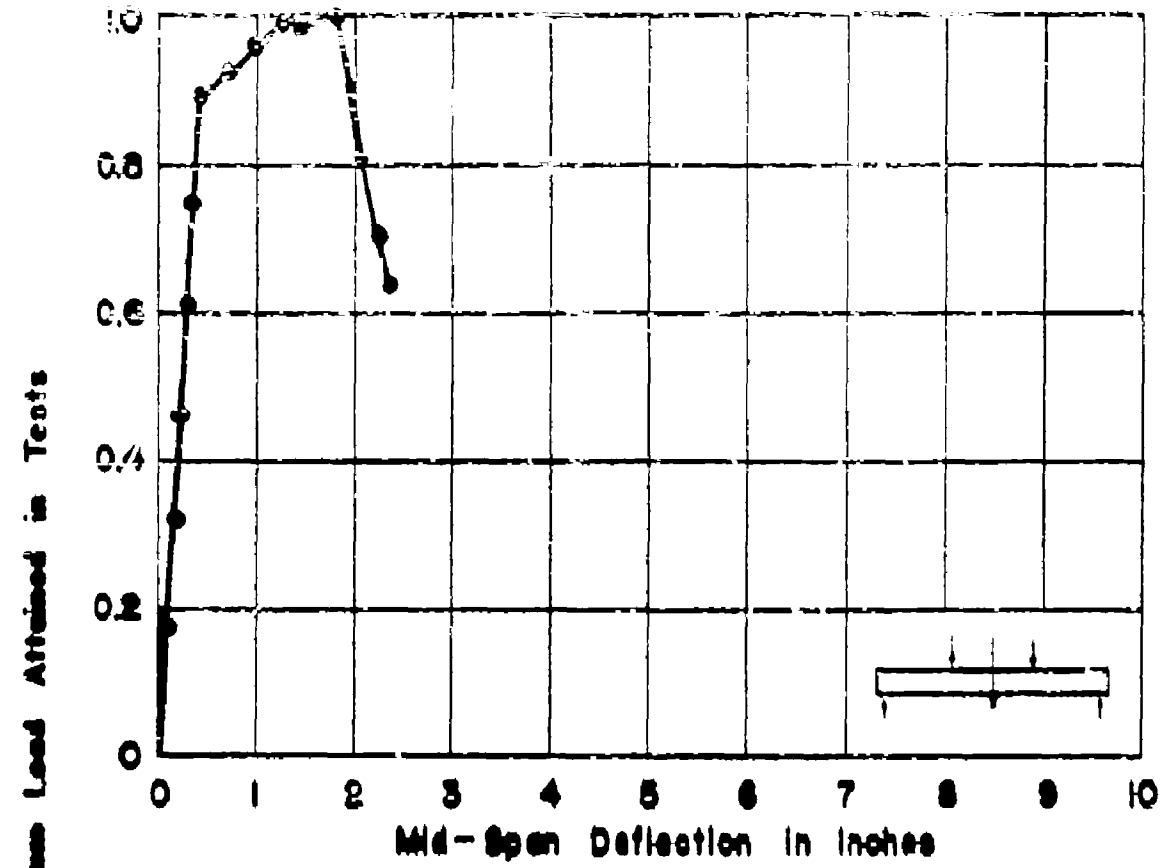

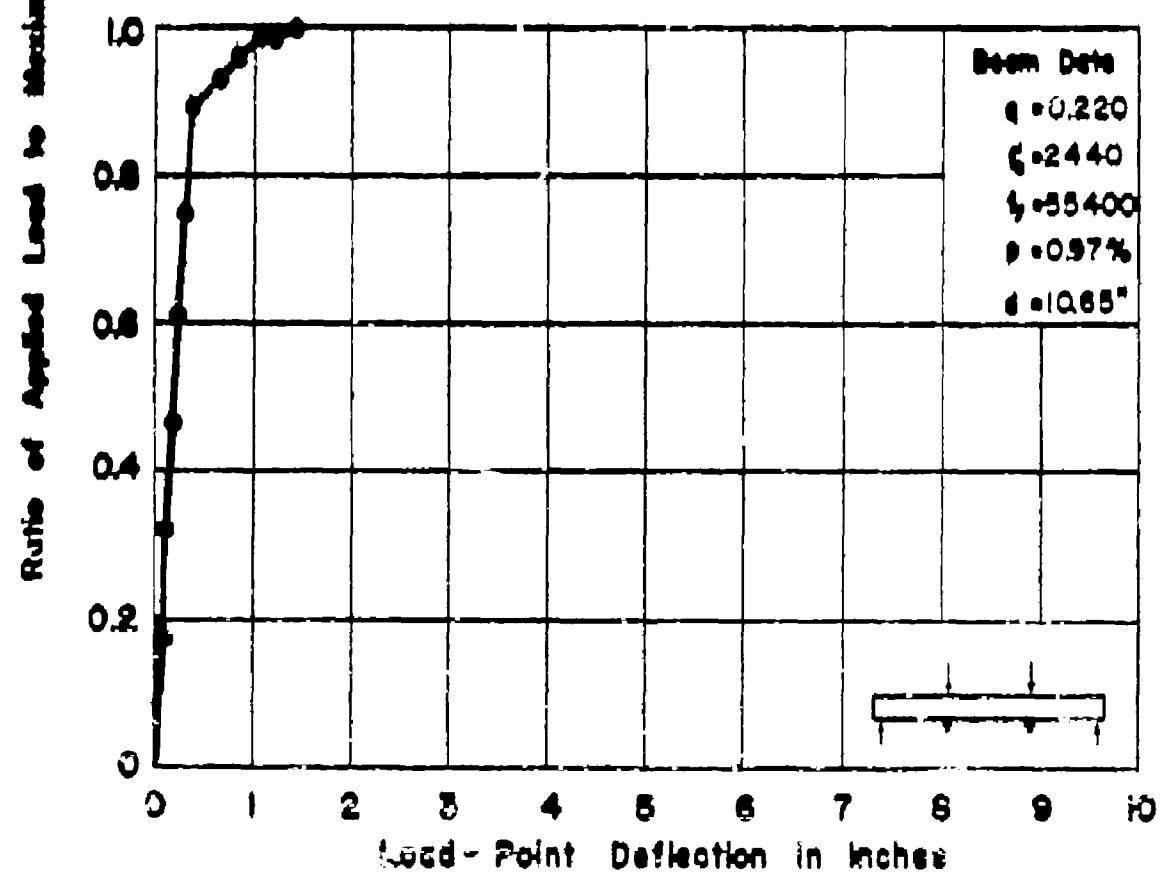

APP. FIG. 103 LOAD-RATIO VS. DEFLECTION FOR BEAM NO. T2Lb

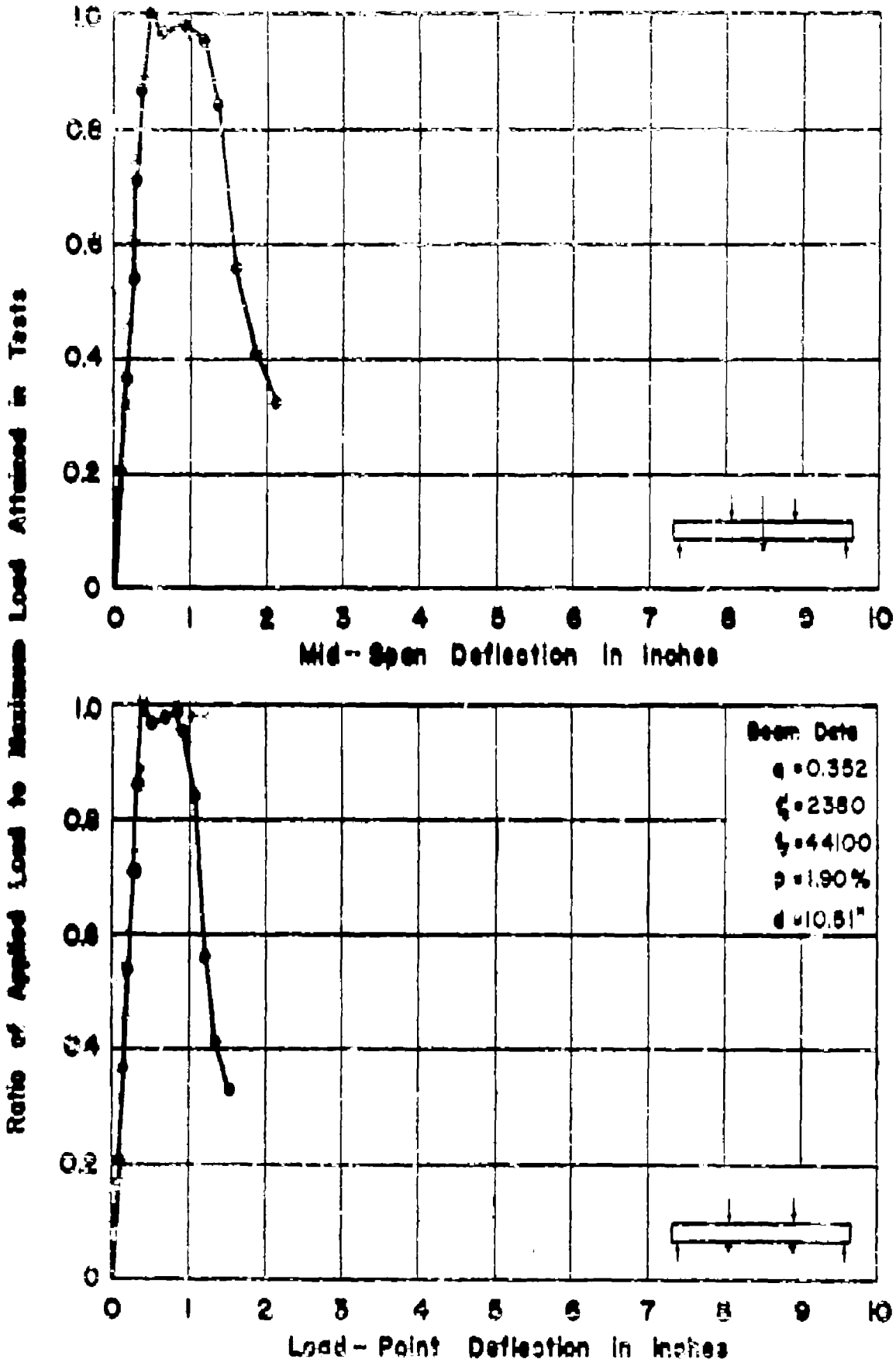

APP. FIG. 104 LOAD-RATIO VS. DEFLECTION FOR BEAM NO. T4L a

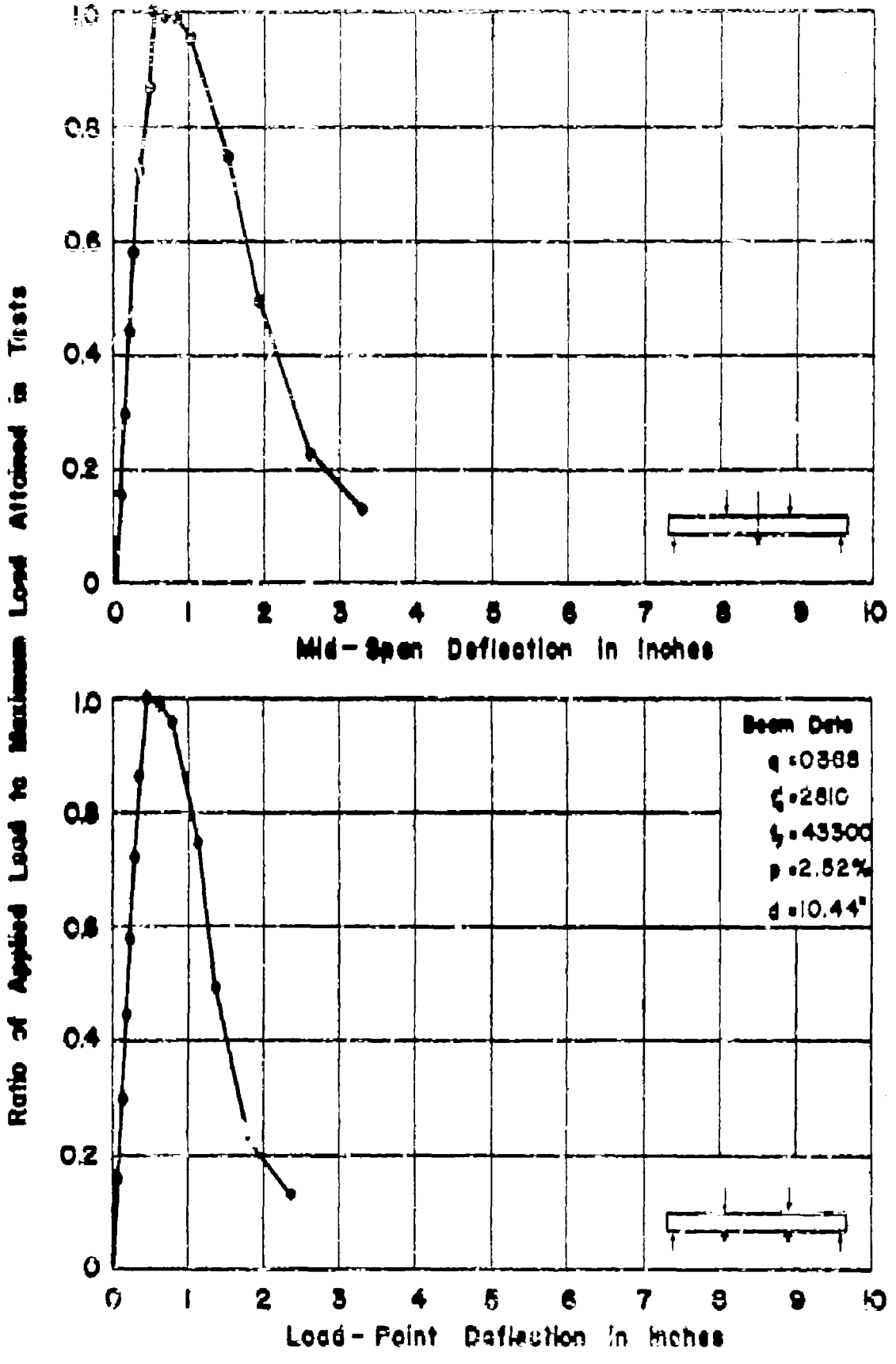

APP. FIG. 105 LOAD-RATIO VS. DEFLECTION FOR BEAM NO. T4Lb

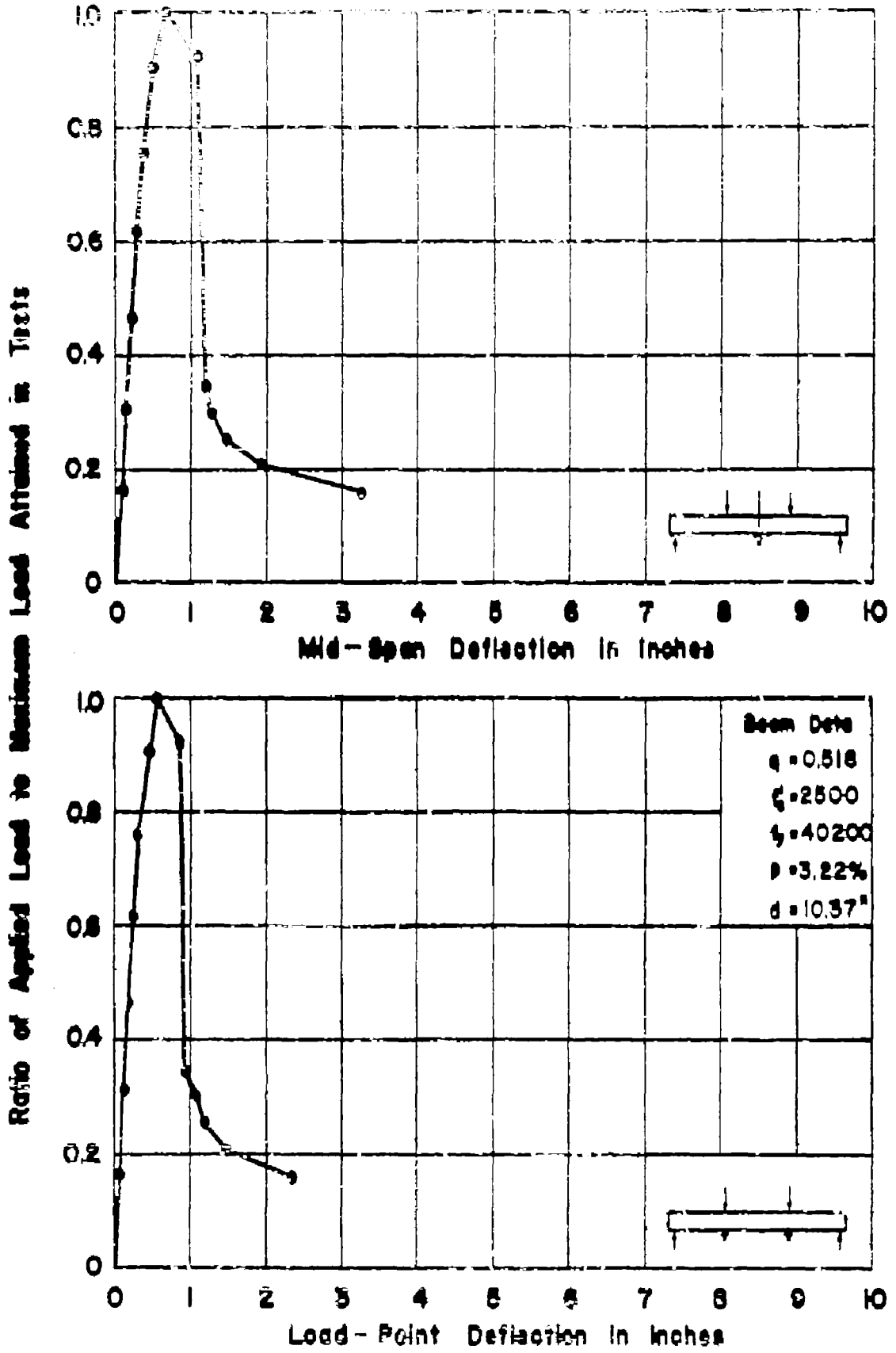

APP. FIG. 106 LOAD-RATIO VS. DEFLECTION FOR BEAM NO. T5L

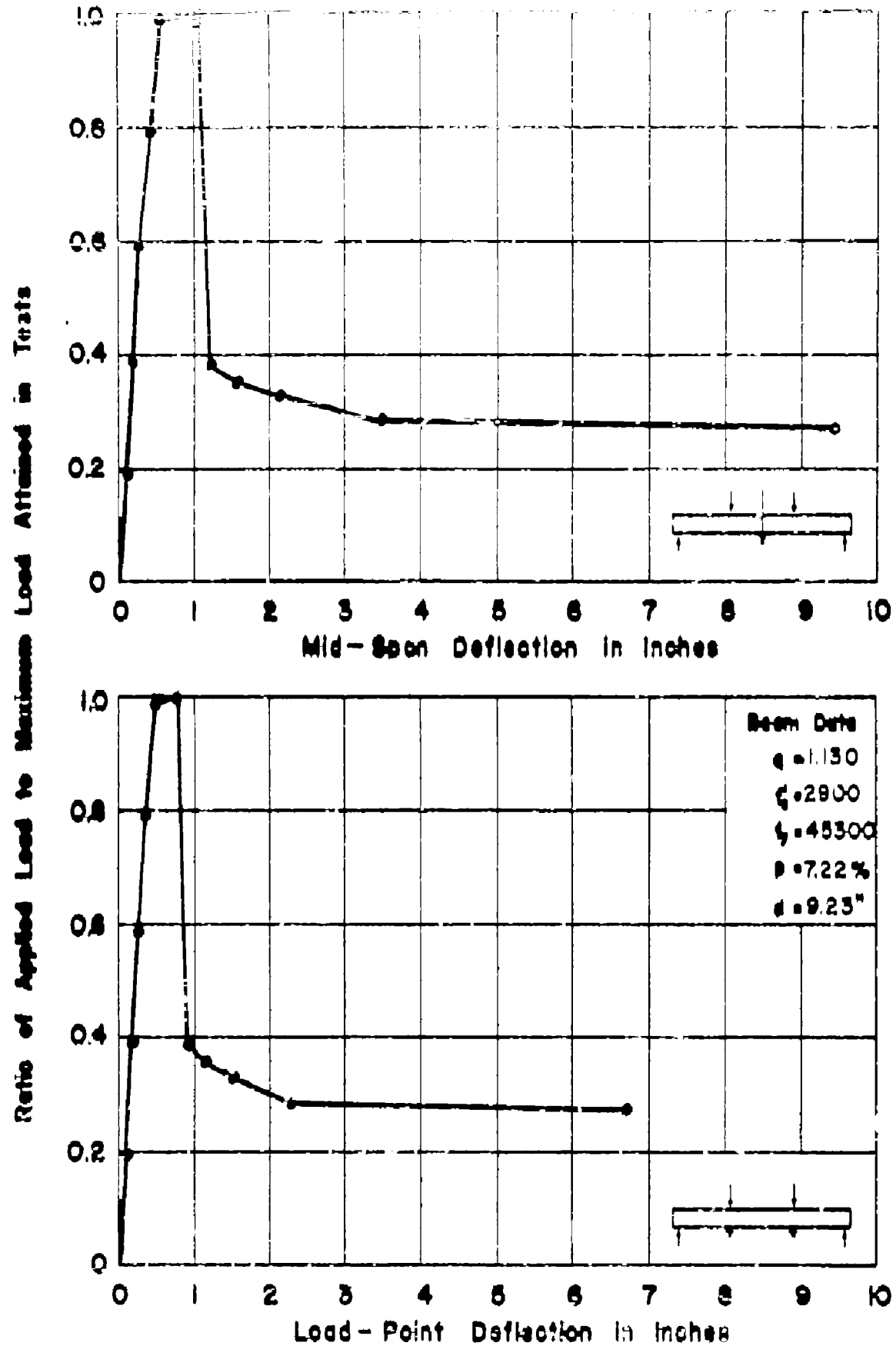

APP. FIG. 107 LOAD-RATIO VS. DEFLECTION FOR BEAM NO. T11L

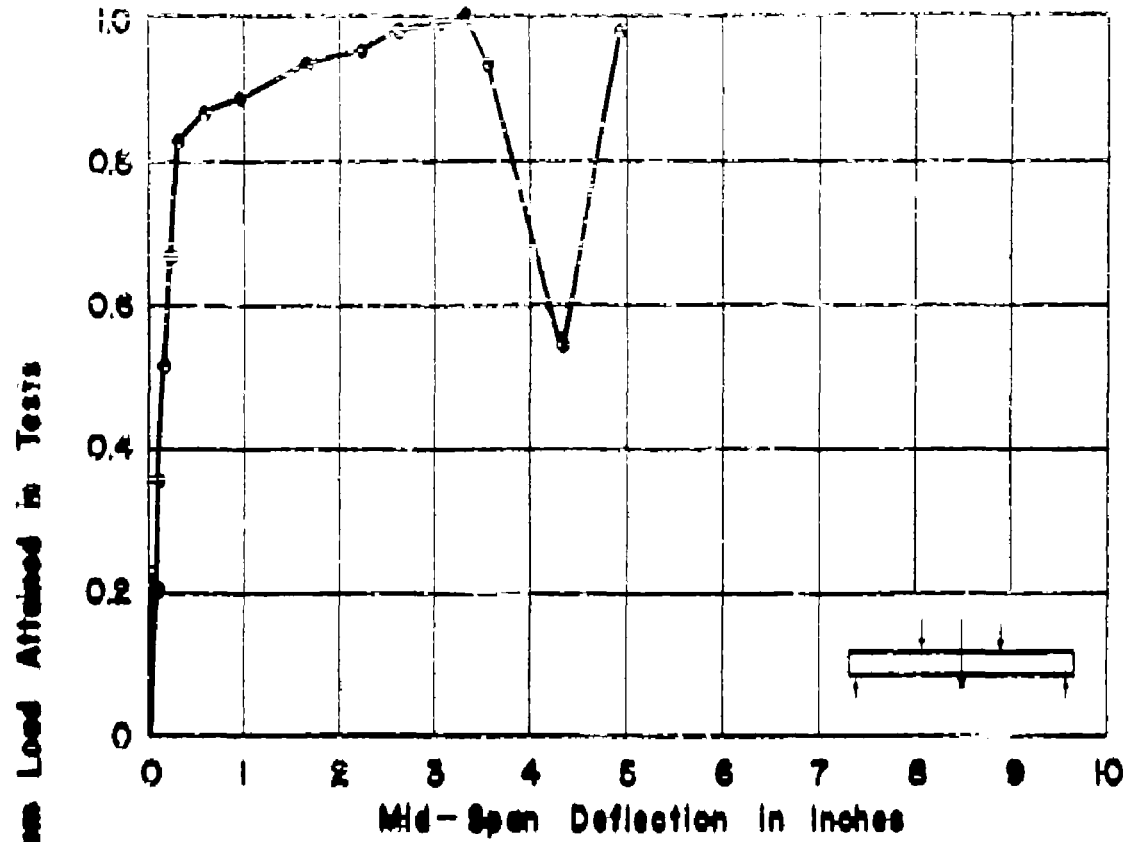

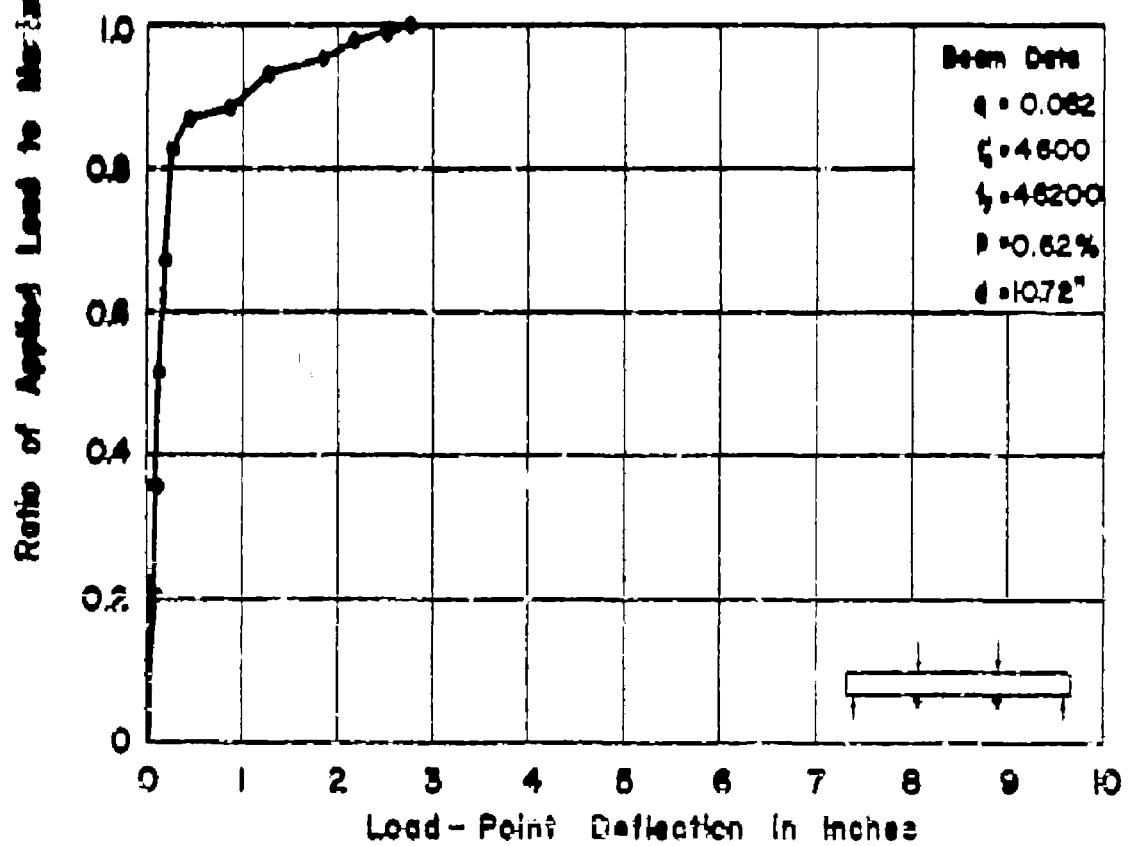

APP FIG. 108 LOAD-RATIO VS. DEFLECTION FOR BEAM NO. T1Ma

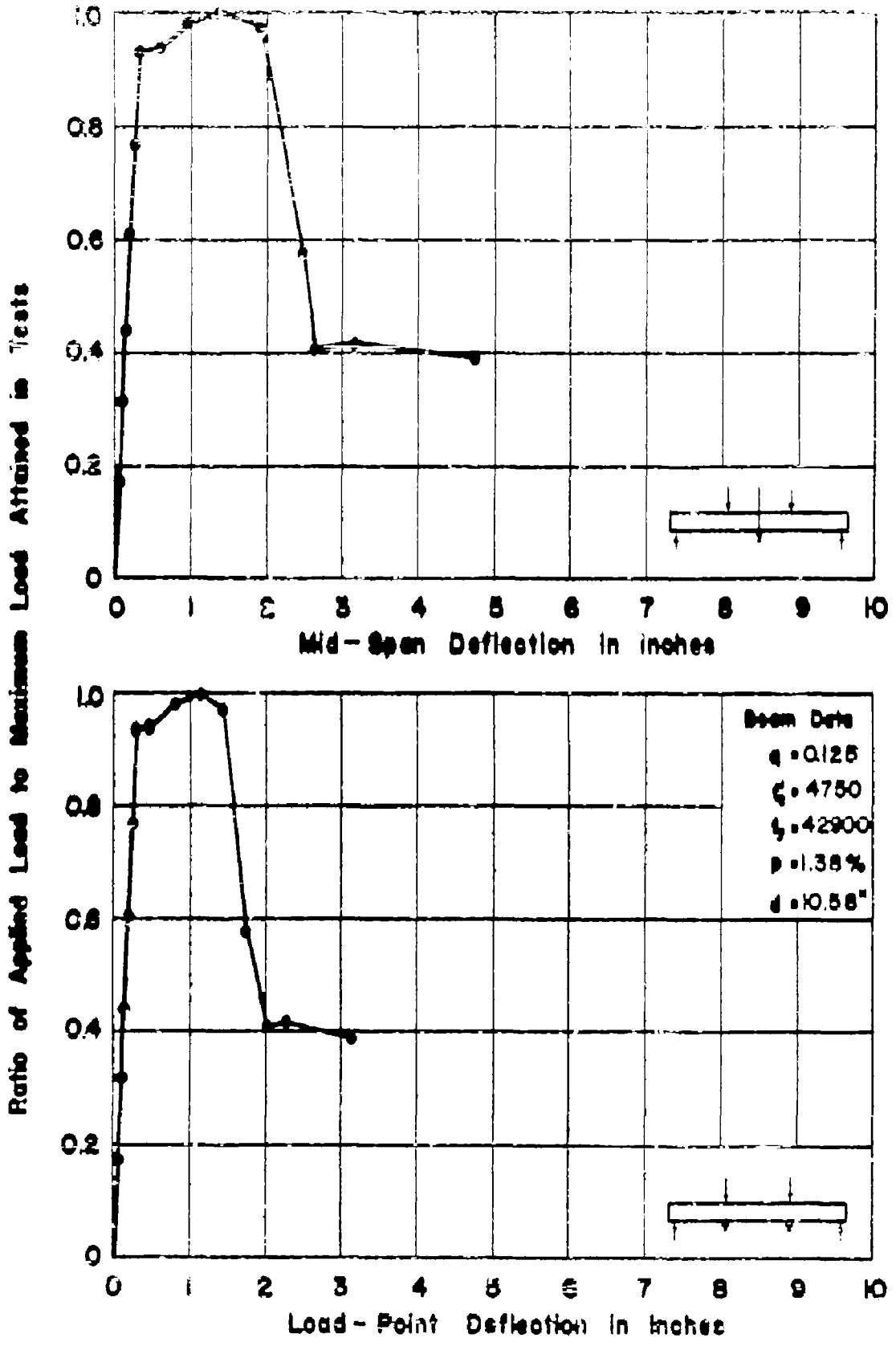

APP. FIG. 109 LOAD-RATIO VS. DEFLECTION FOR BEAM NO. T1Mb

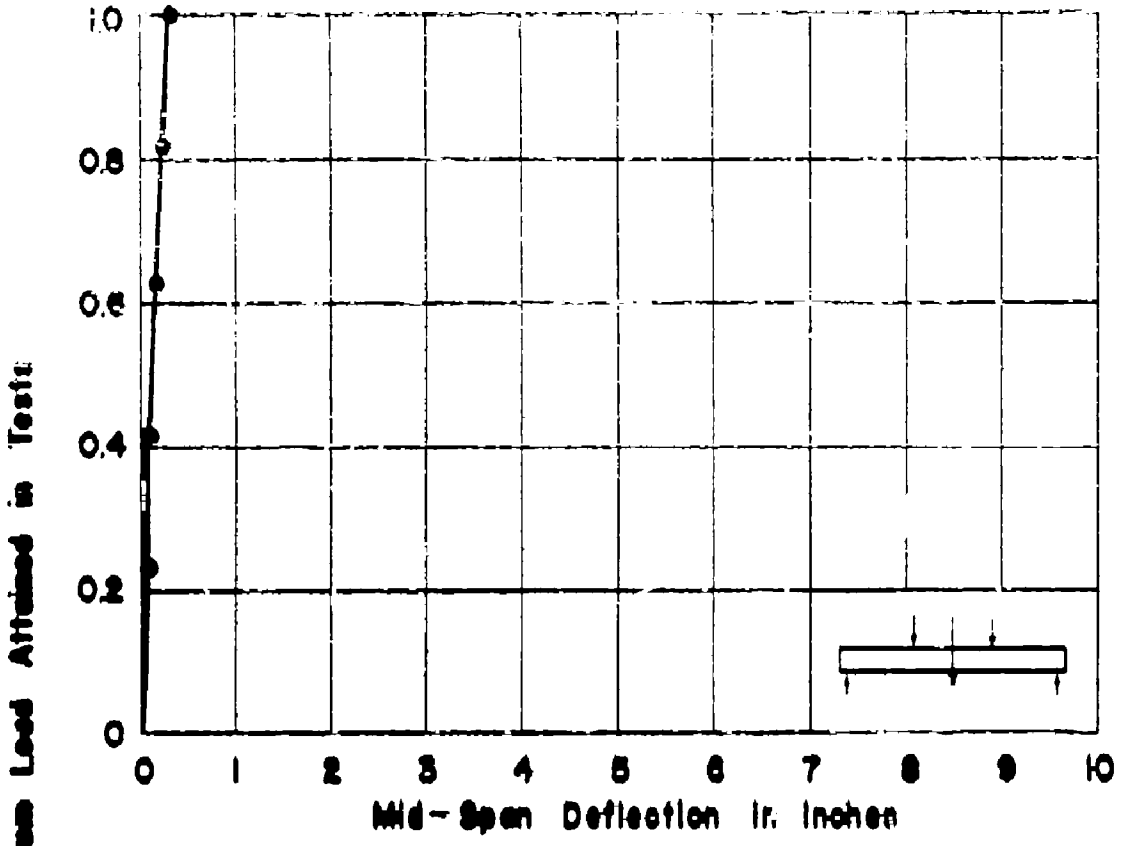

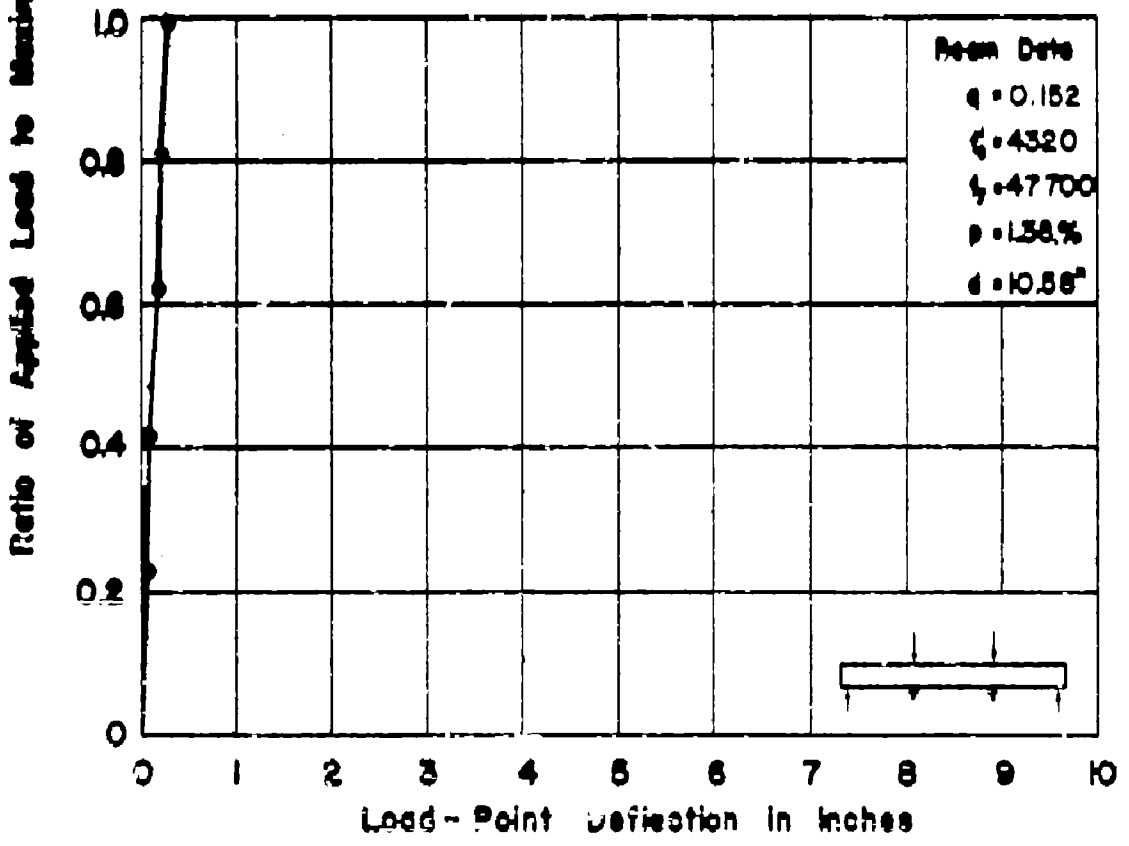

APP. FIG. 110 LOAD-RATIO VS. DEFLECTION FOR BEAM NO. T2Ma

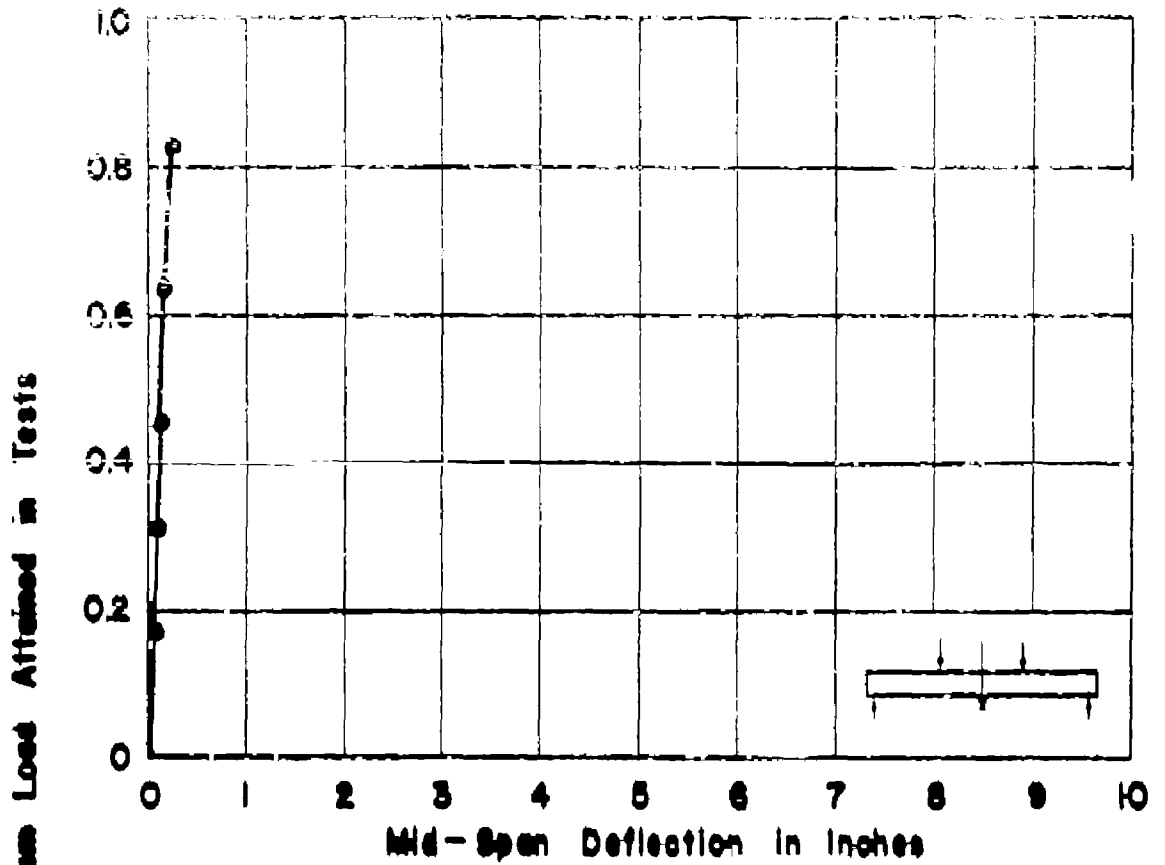

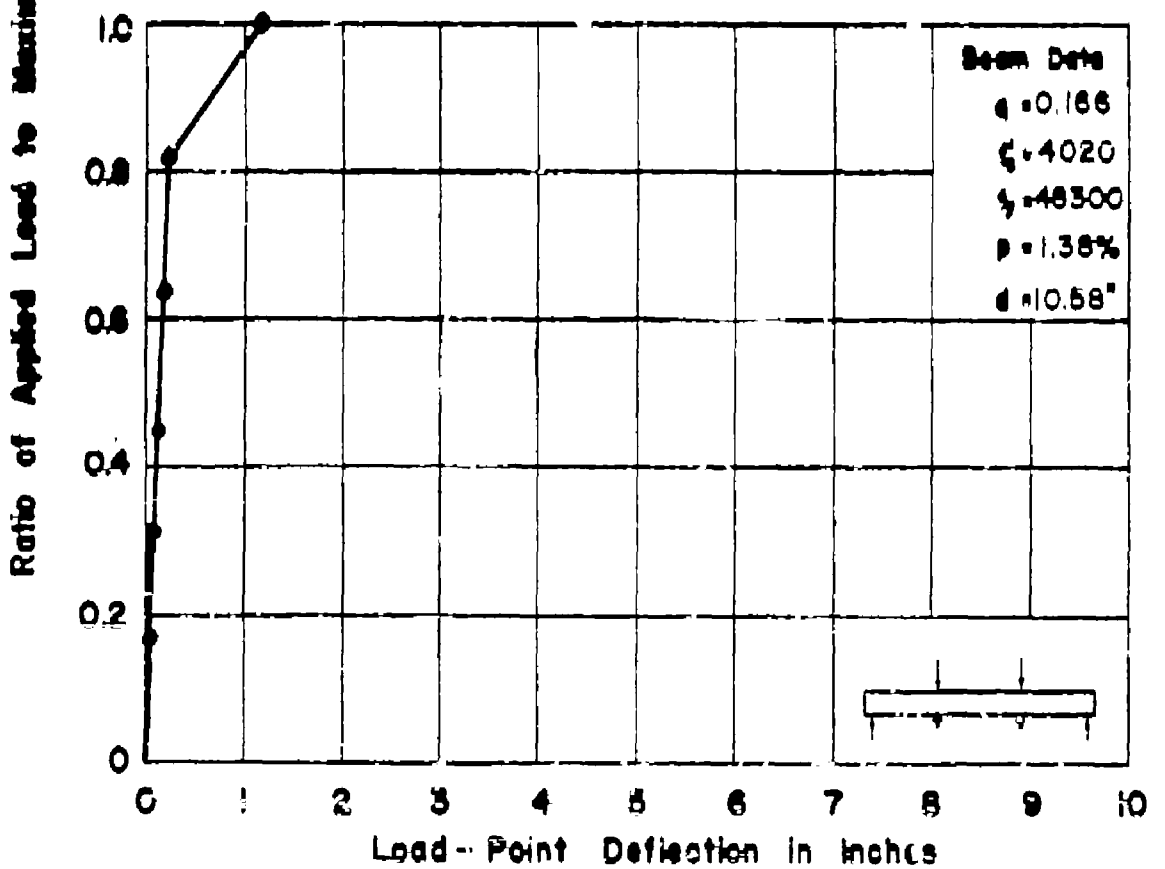

APP. FIG. III LOAD-RATIO VS. DEFLECTION FOR BEAM NO. T2Mb

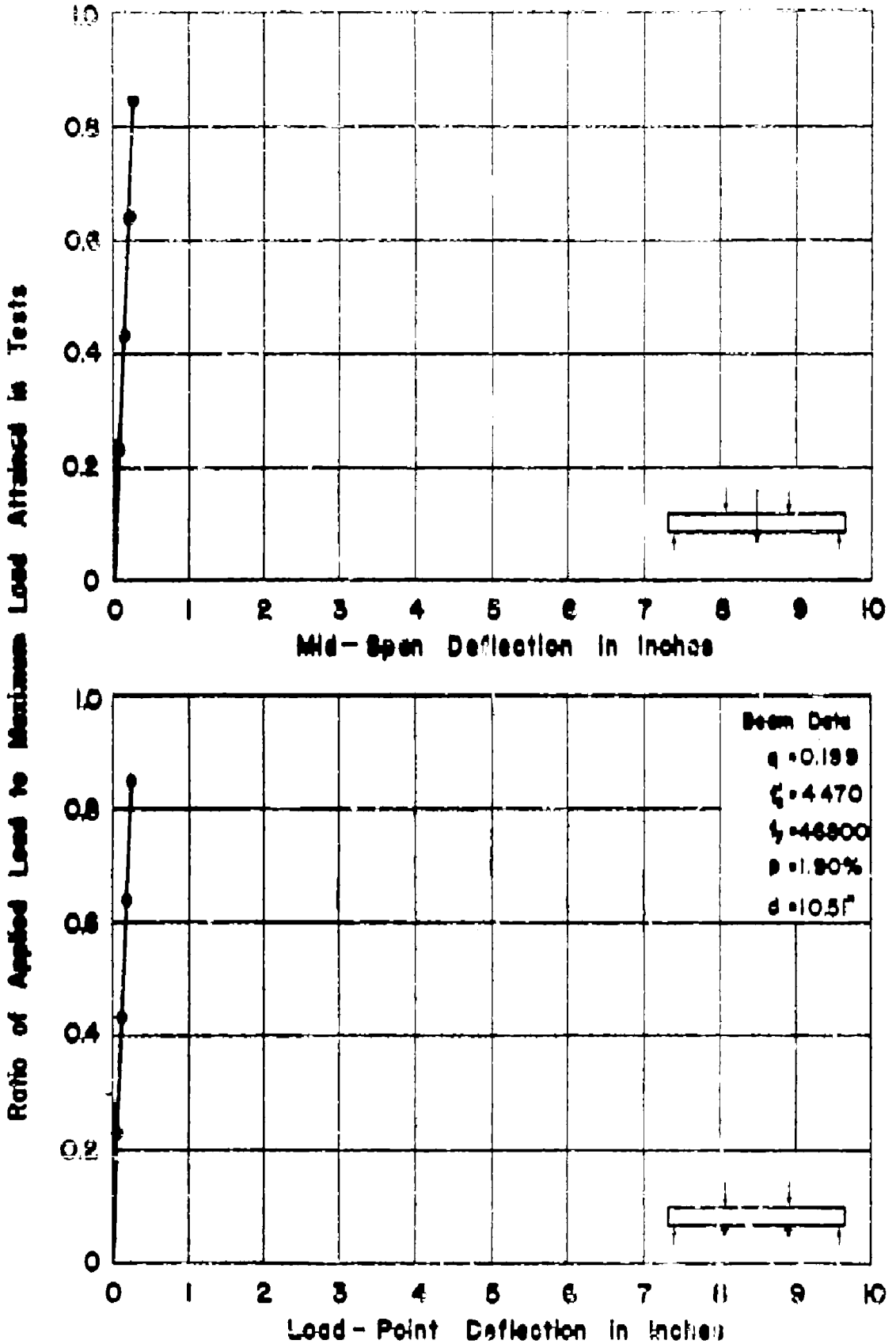

APP. FIG. 112 LOAD-RATIO VS. DEFLECTION FOR BEAM NO. T2Mc

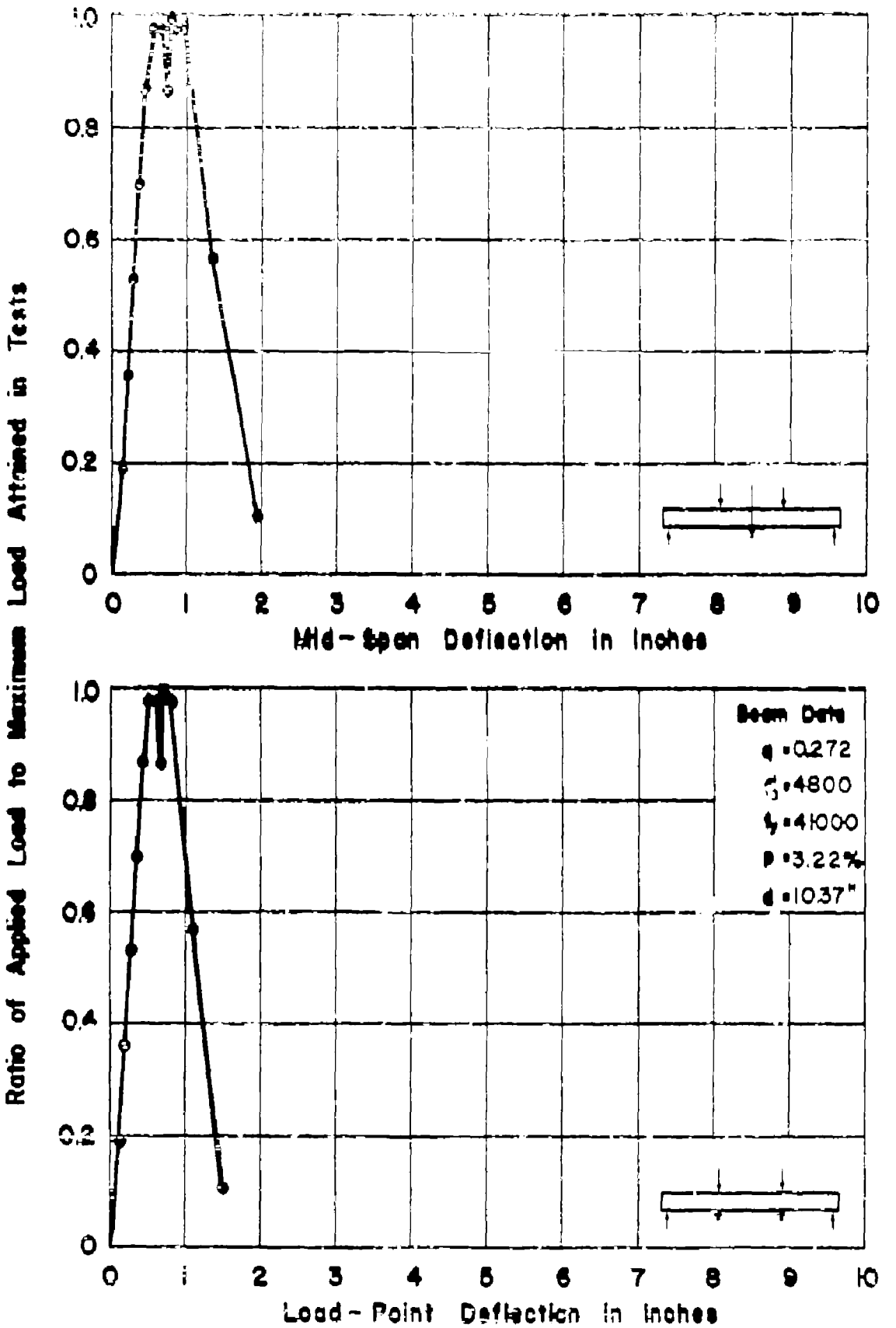

APP. FIG. 113 LOAD-RATIO VS. DEFLECTION FOR BEAM NO. T3Ma

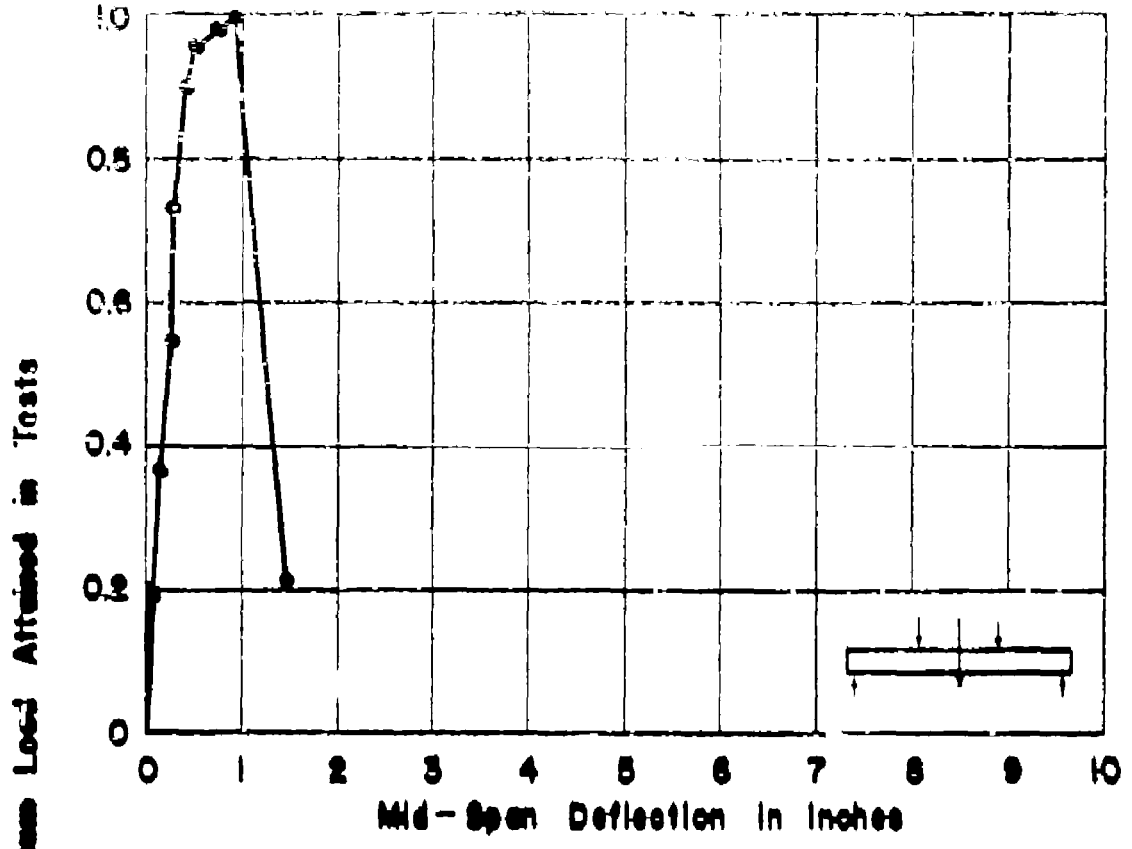

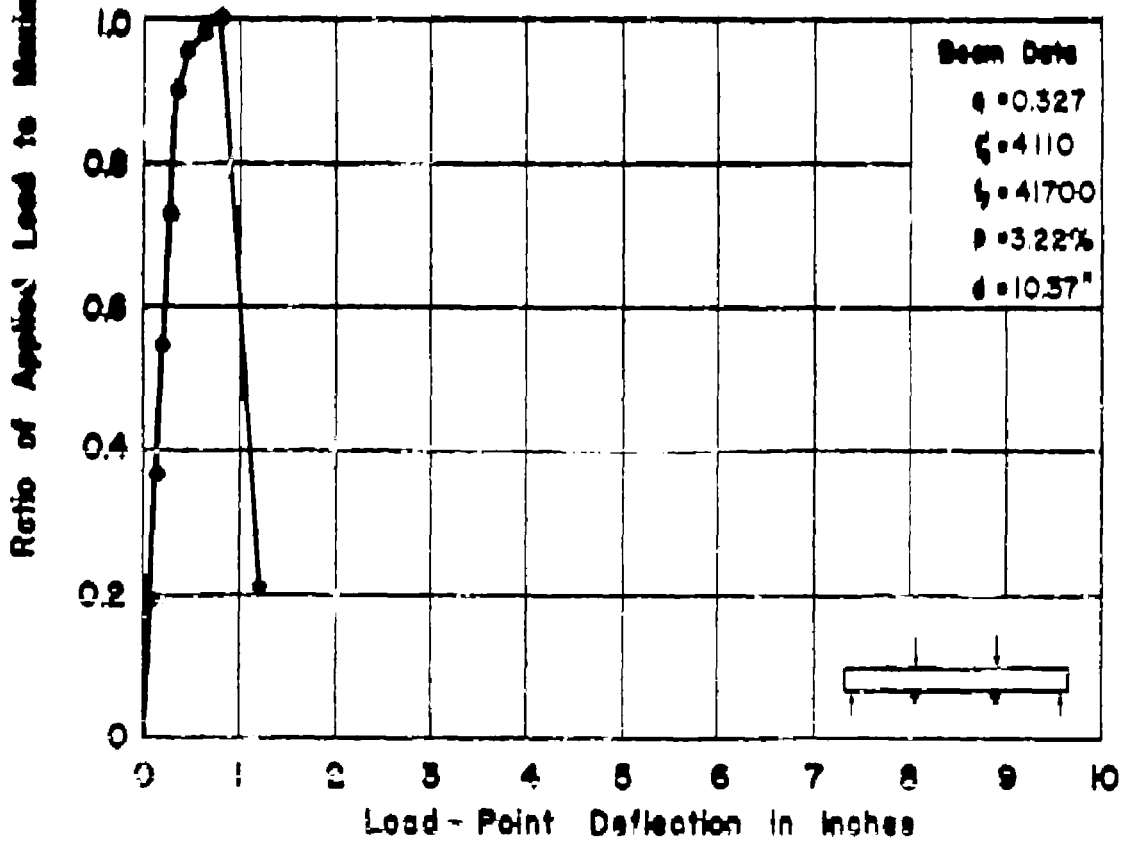

APP FIG. 114 LOAD-RATIO VS. DEFLECTION FOR BEAM NO. T3Mb

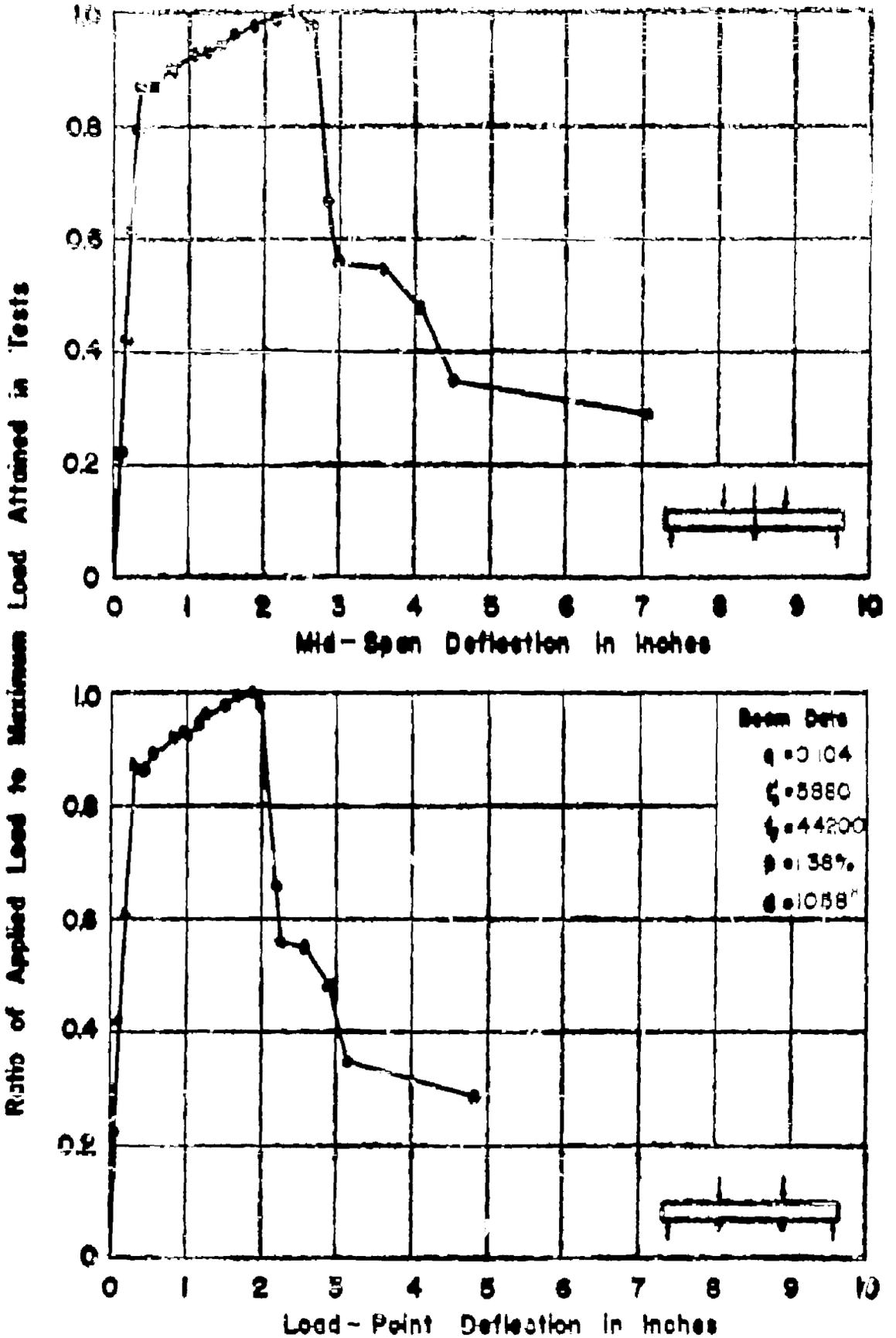

APP. FIG. 115 LOAD-RATIO VS. DEFLECTION FOR BEAM NO. T1Ha

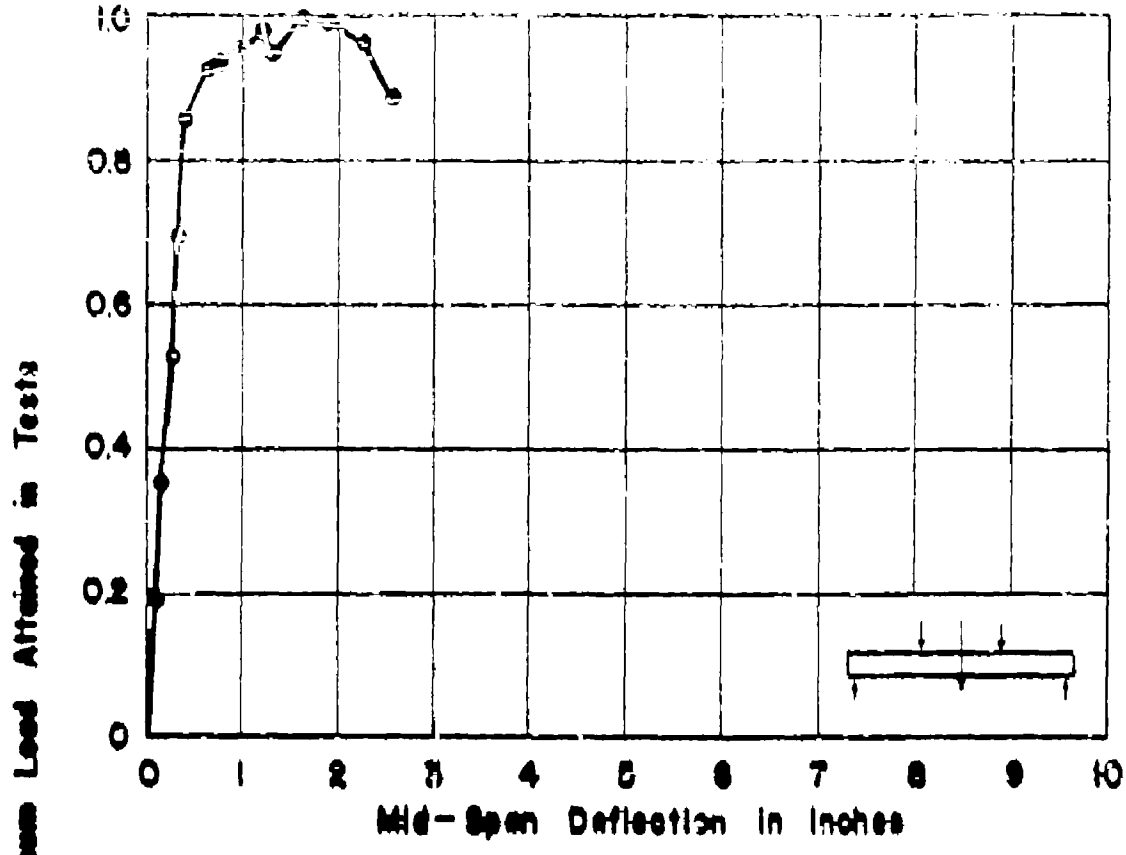

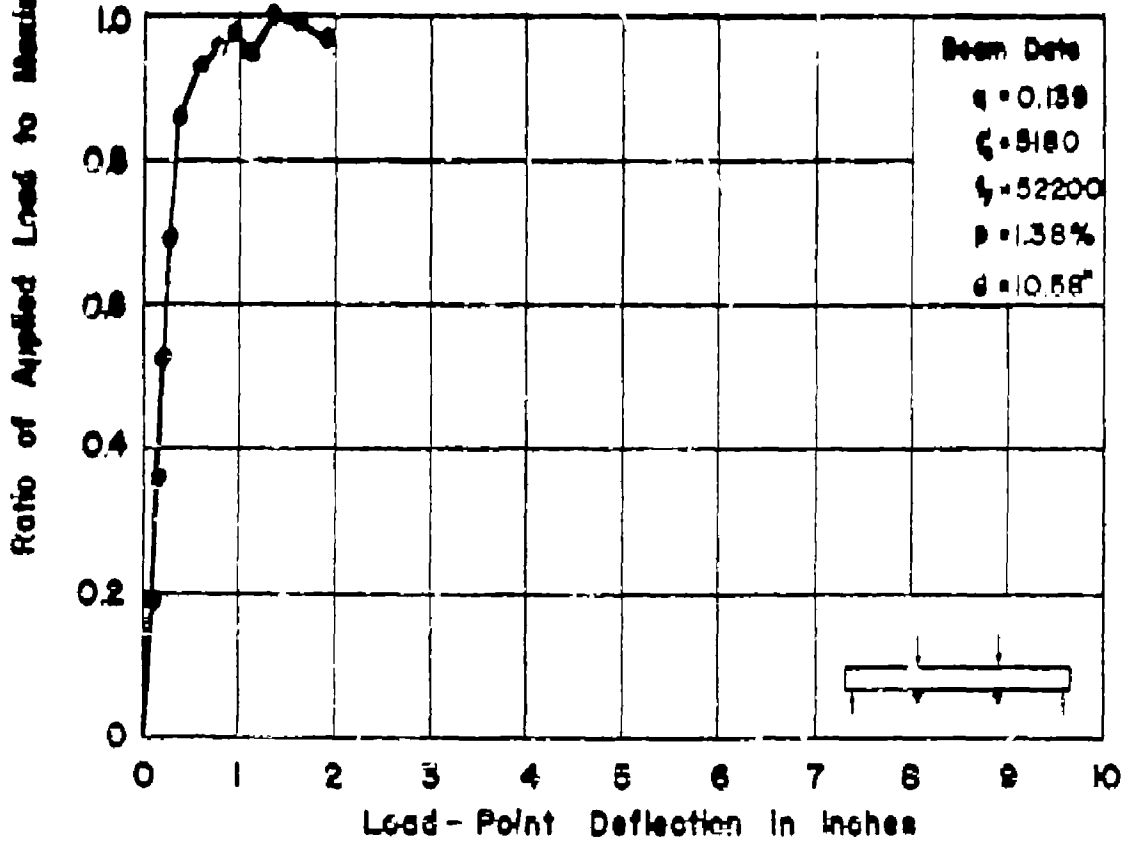

APP. FIG. 116 LOAD-RATIO VS. DEFLECTION FOR BEAM NO. T1Hb

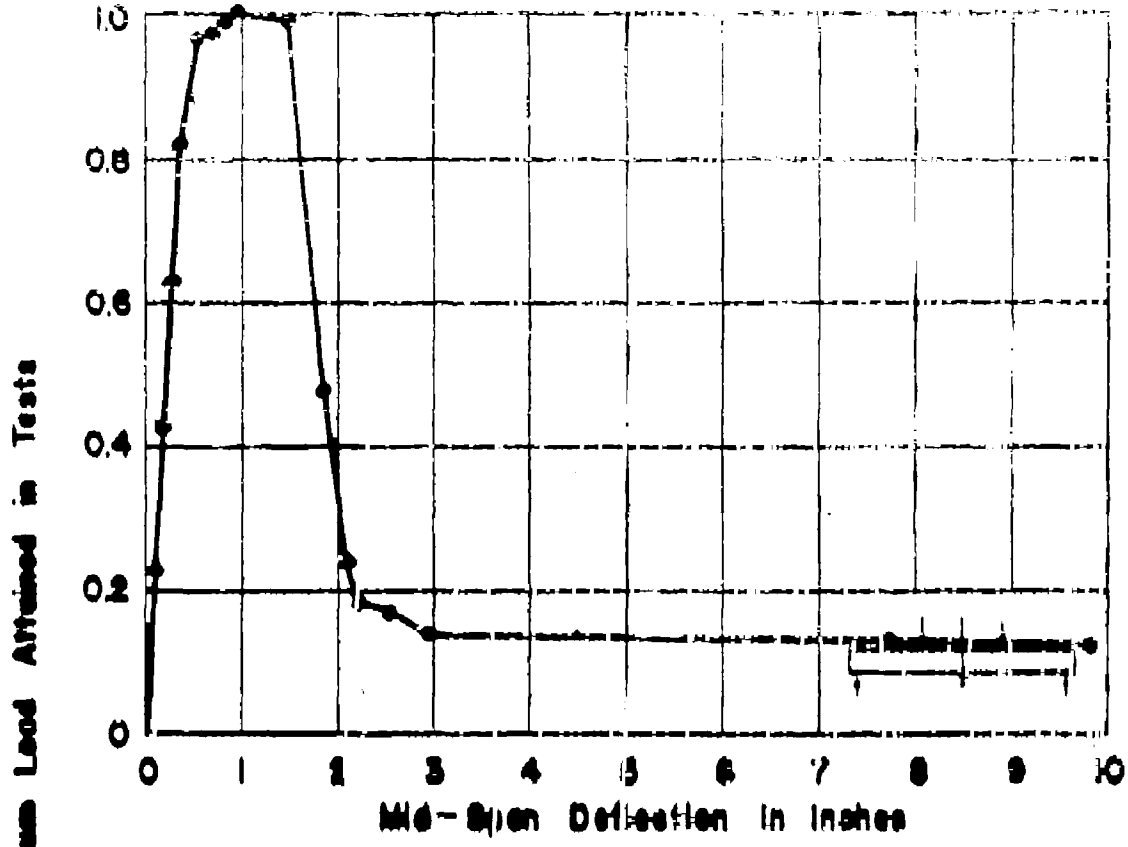

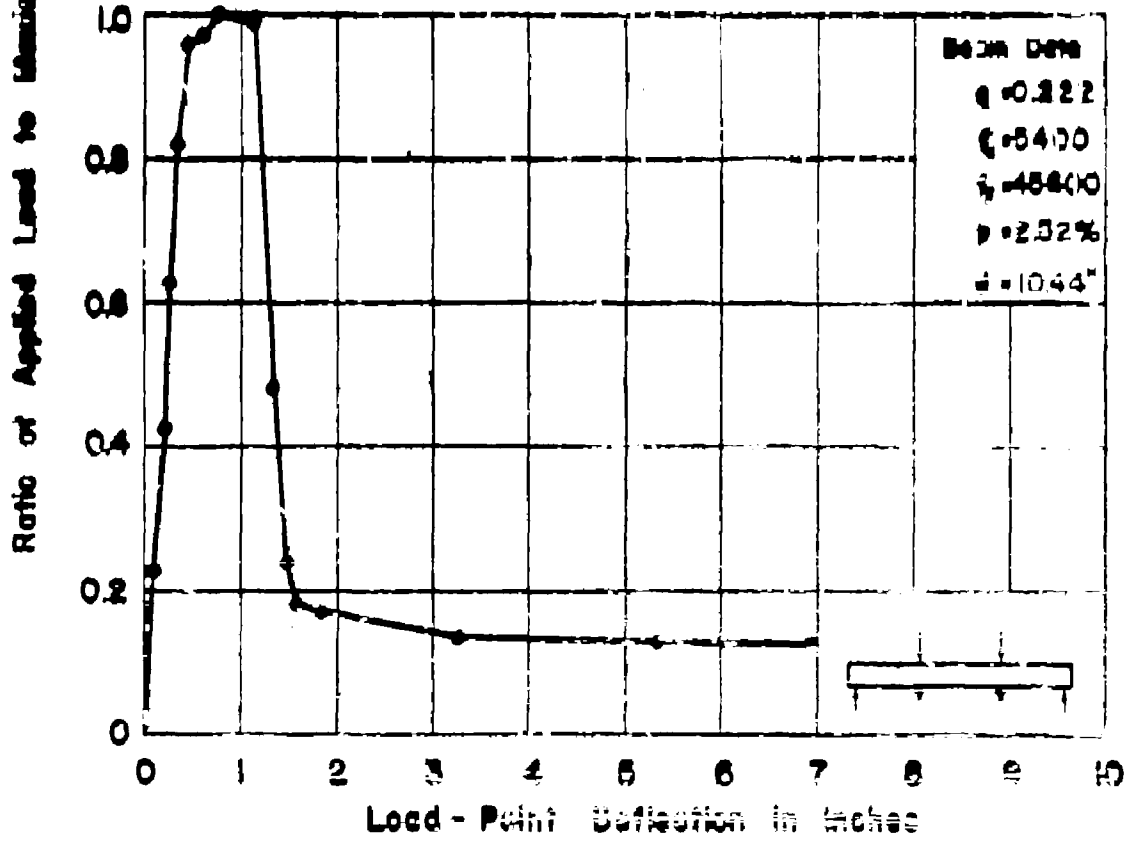

APP. FIG. 117 LOAD-RATIO VS. DEFLECTION FOR BEAM NO. T2H

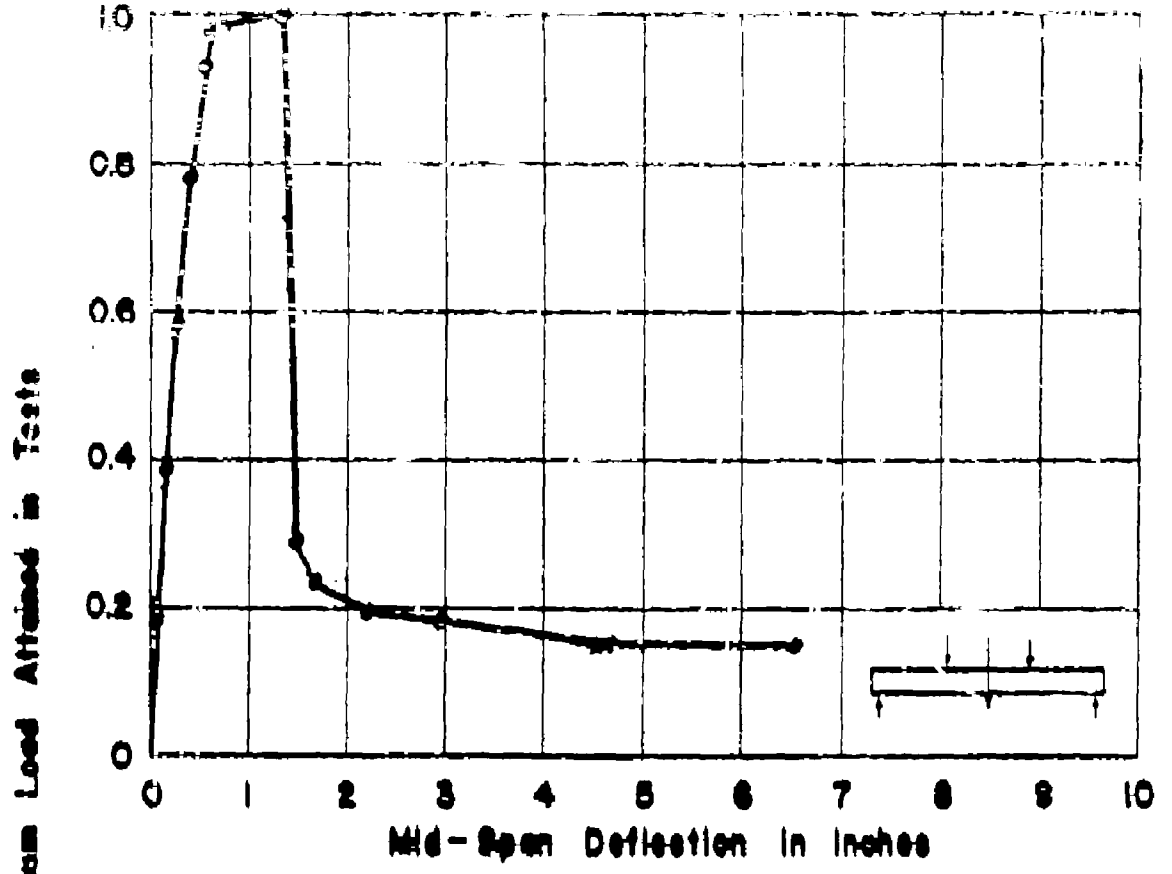

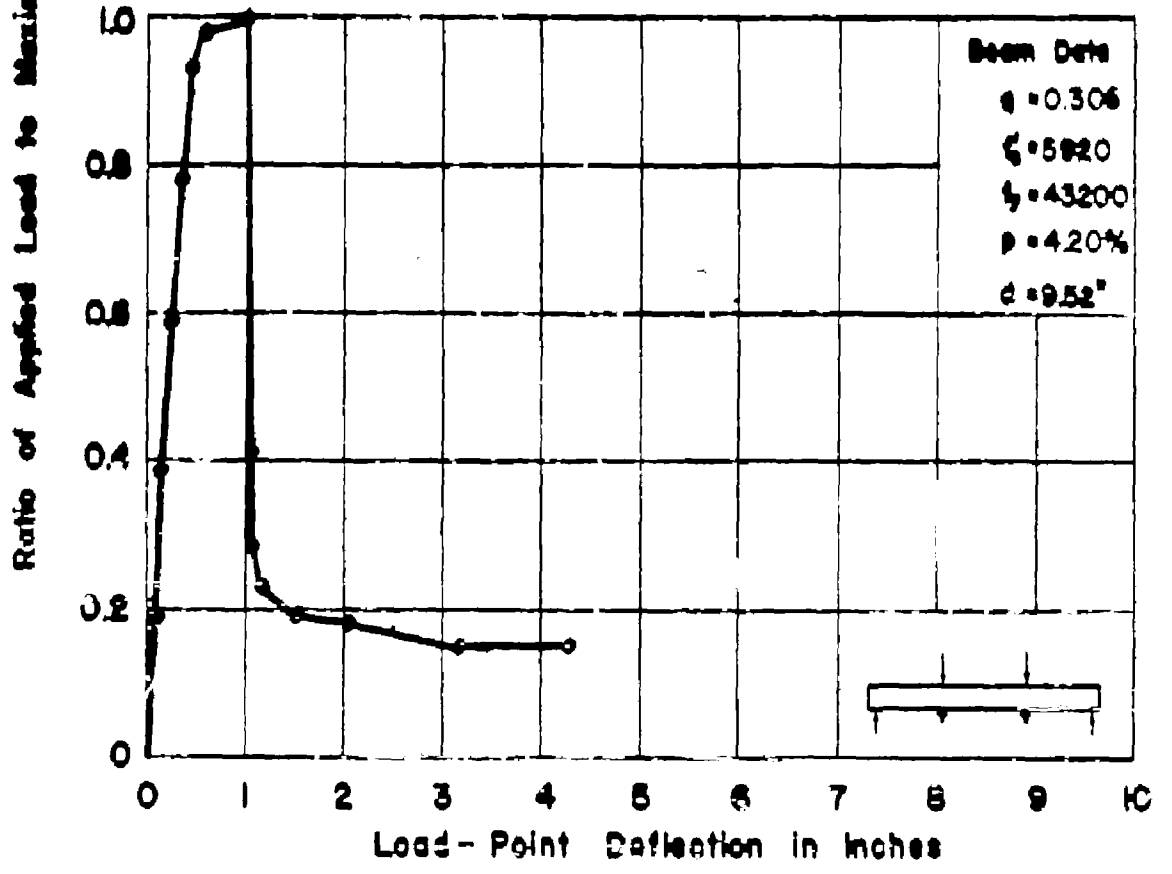

APP. FIG. 11B LOAD-RATIO VS. DEFLECTION FOR BEAM NO. T3H

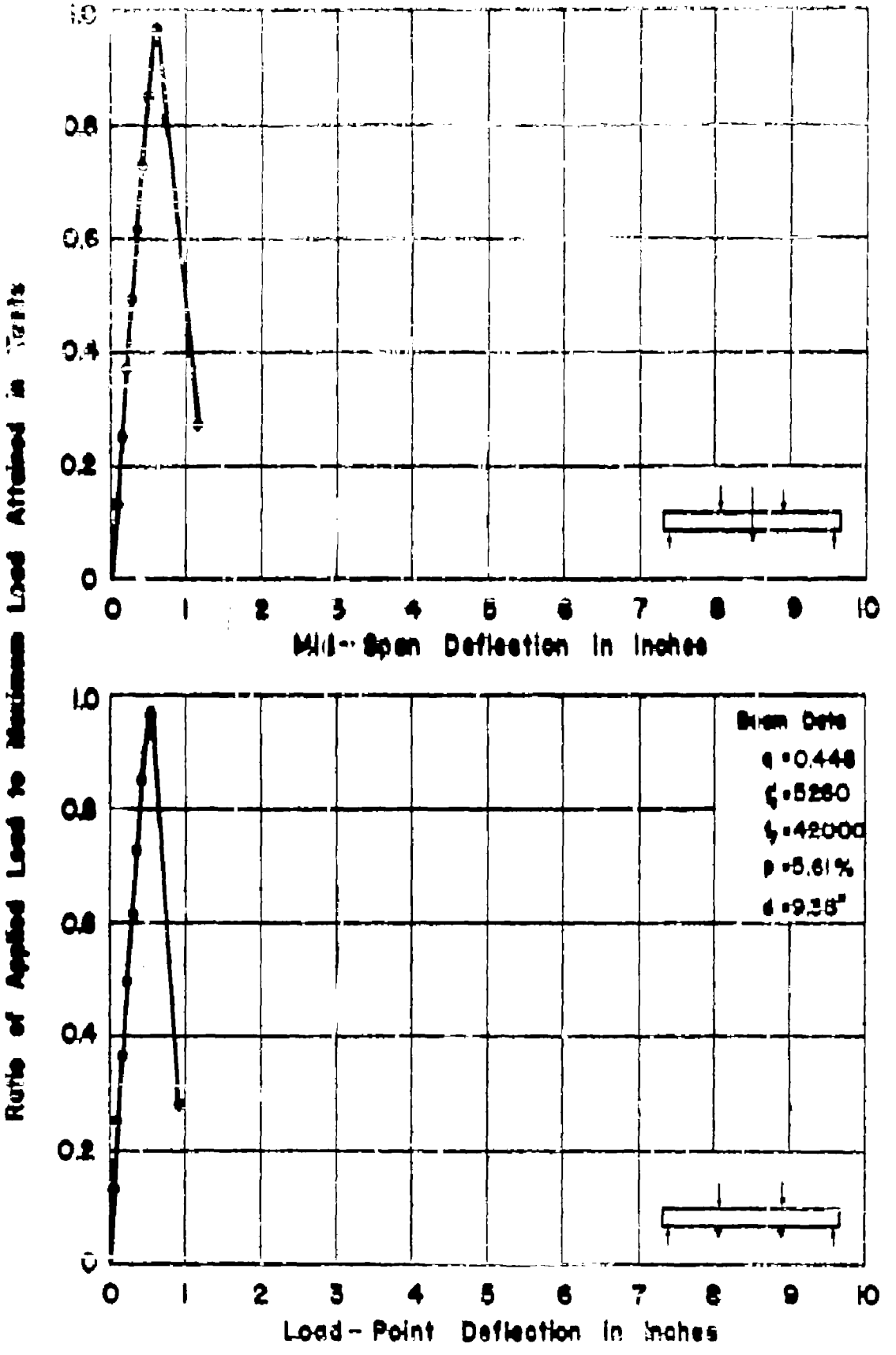

APP. FIG. 119 LOAD-RATIO VS. DEFLECTION FOR BEAM NO. T4H

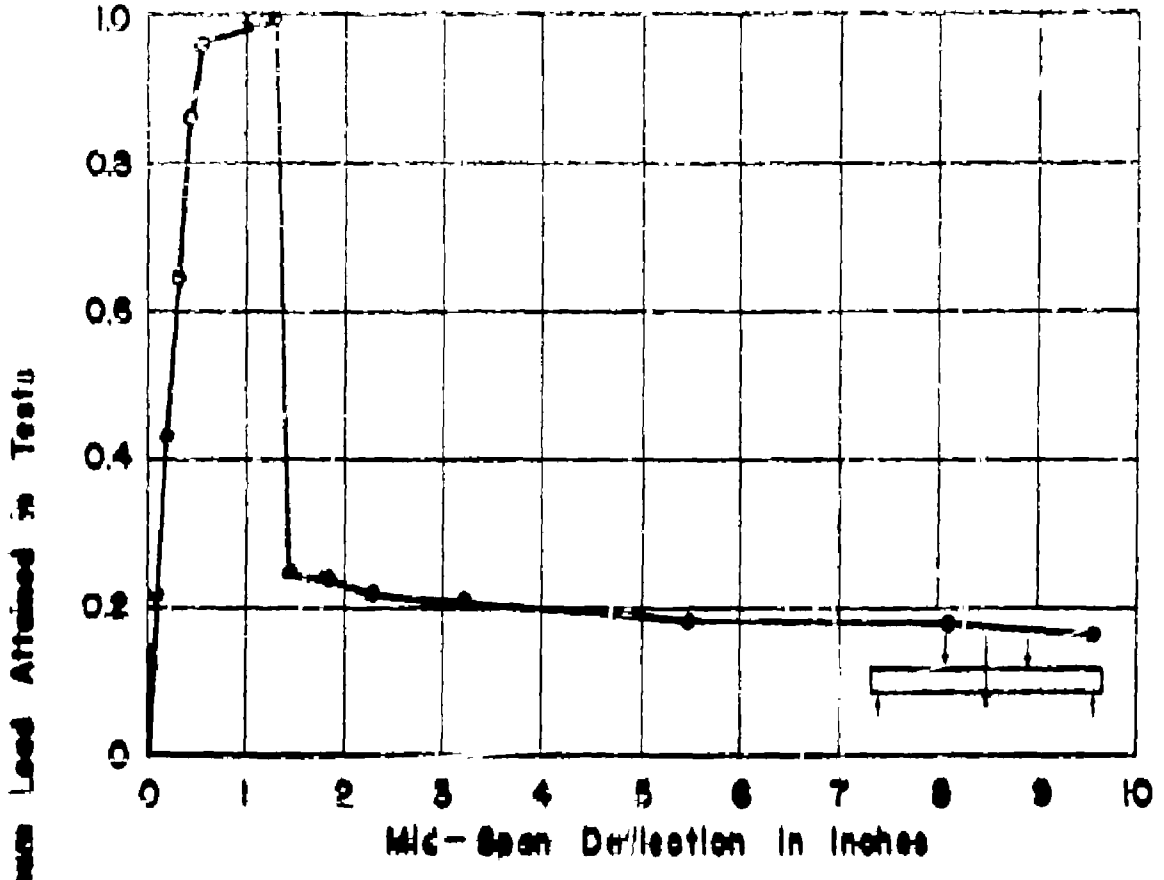

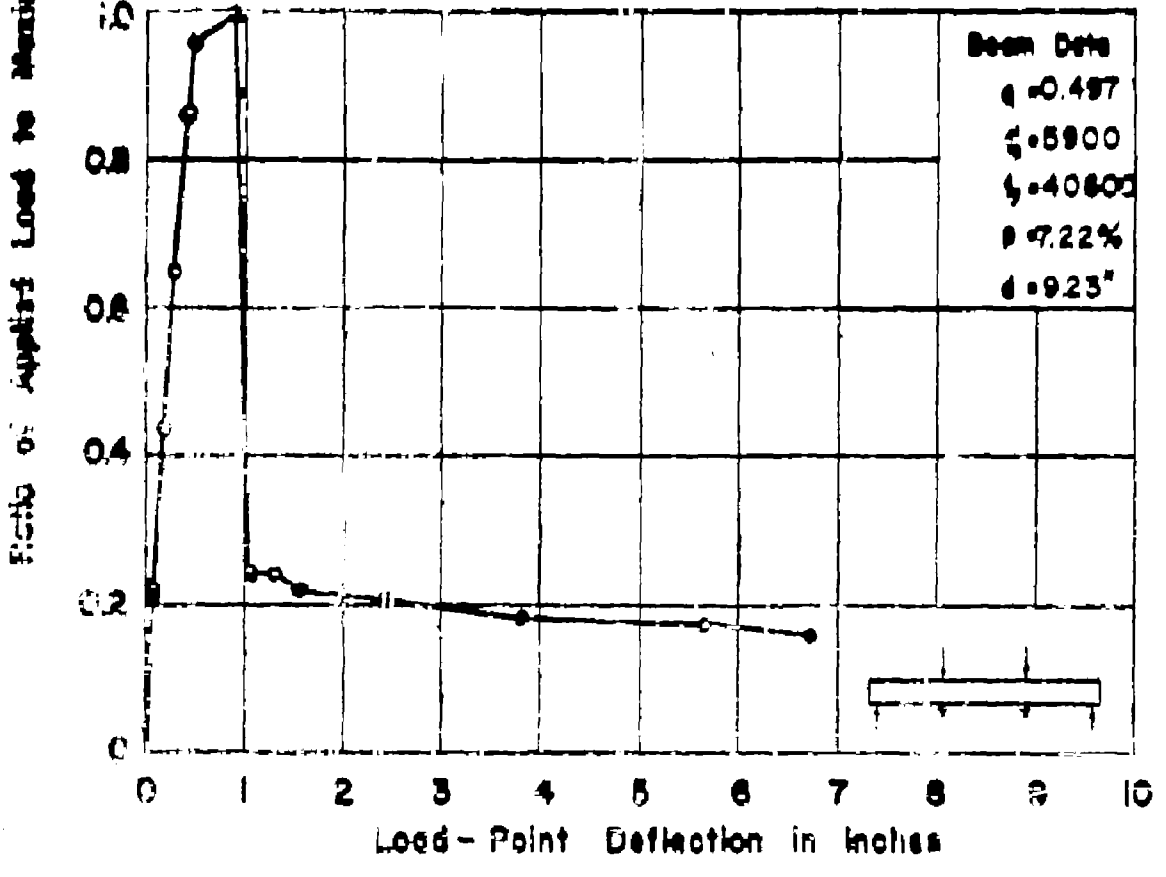

APP. FIG. 120 LOAD-RATIO VS. DEFLECTION FOR BEAM NO.T5H

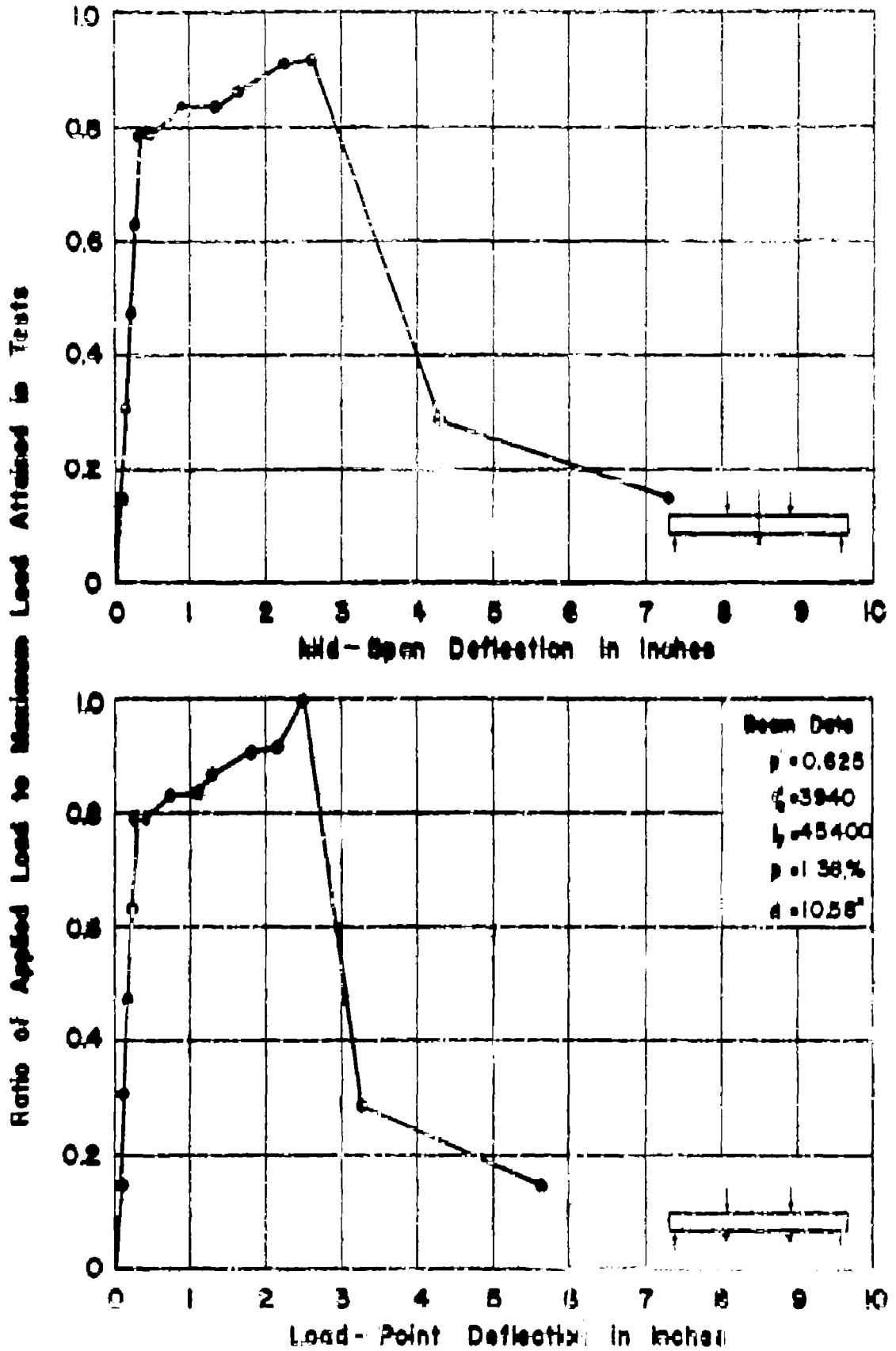

APP. FIG. 121 LOAD-RATIO VS. DEFLECTION FOR BEAM NO. G2w

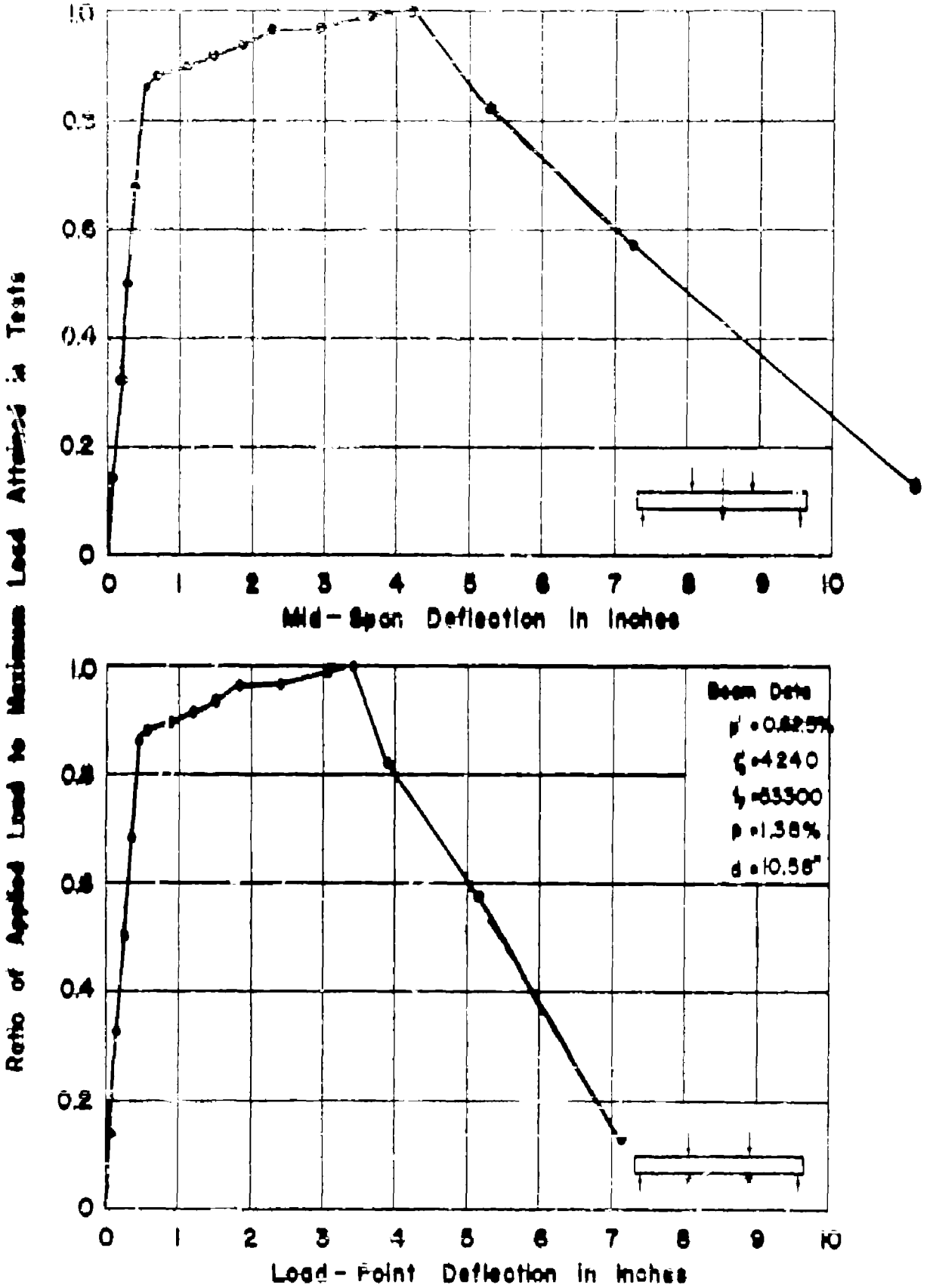

APP. FIG. 122 LOAD-RATIO VS. DEFLECTION FOR BEAM NO C2xm

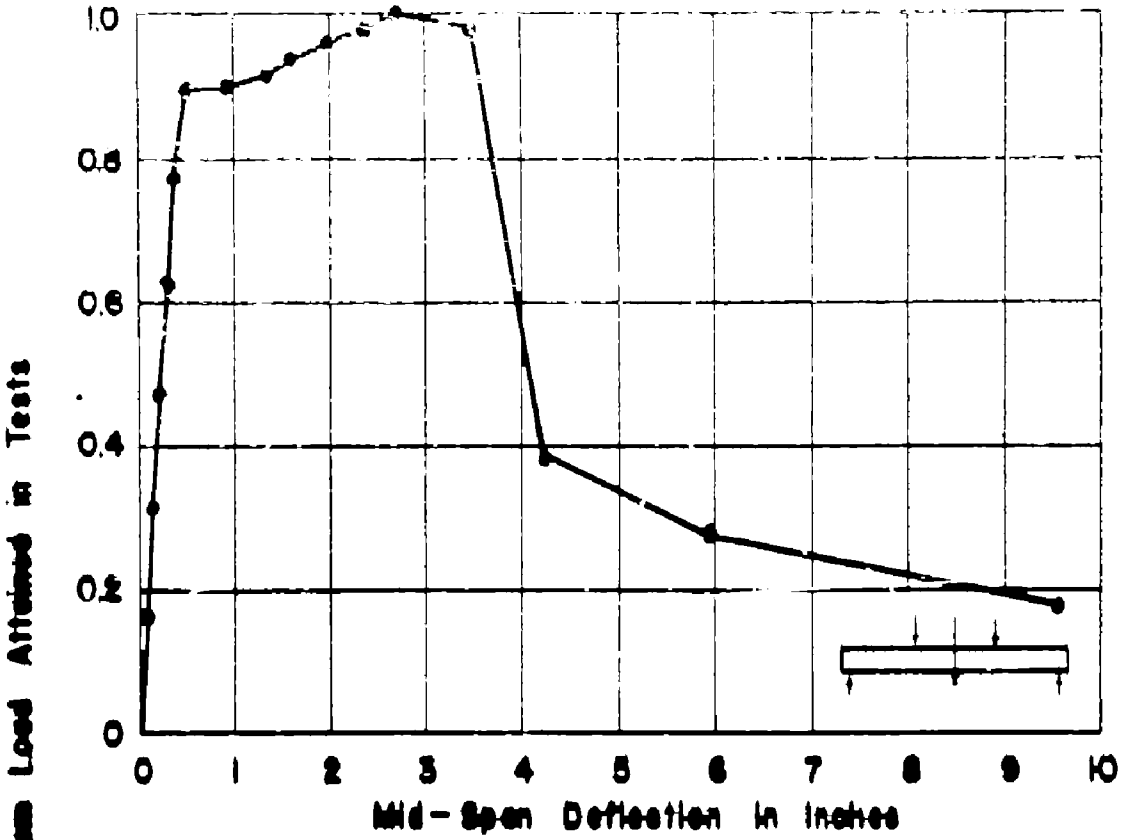

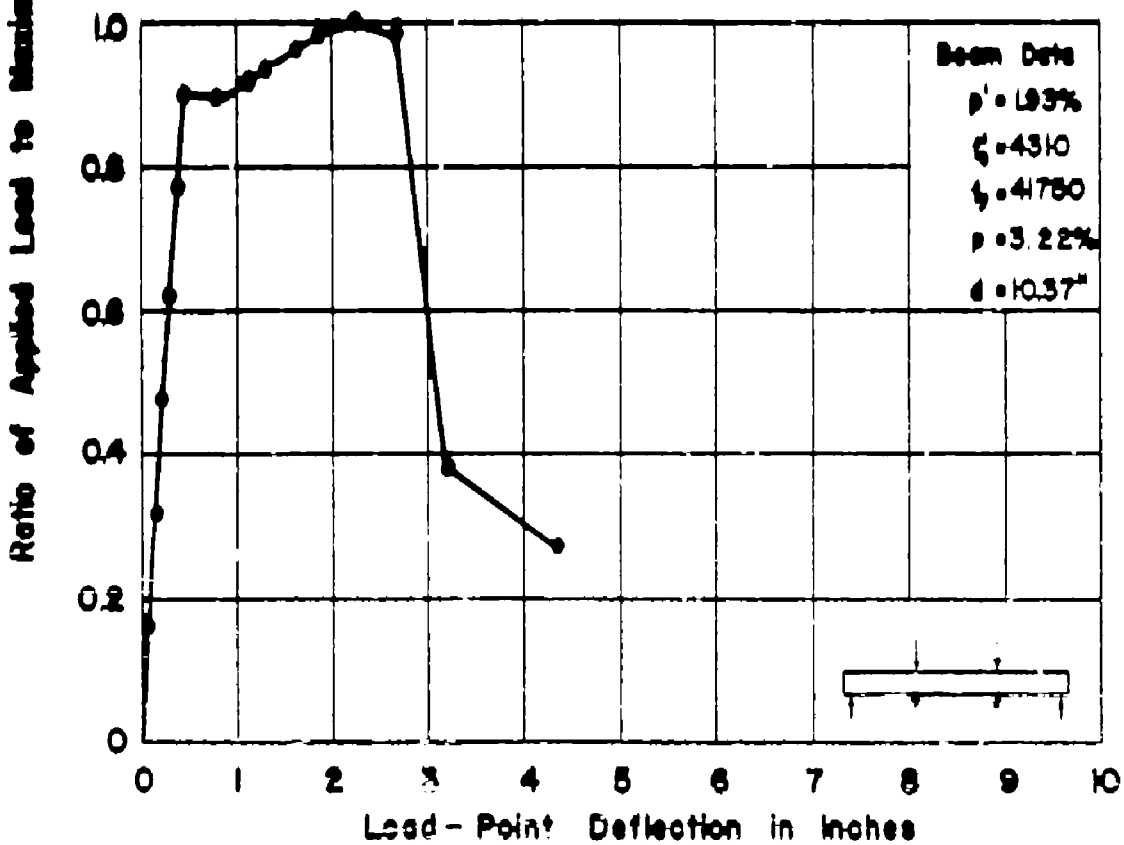

APP. FIG. 123 LOAD-RATIO VS. DEFLECTION FOR BEAM NO. C3w

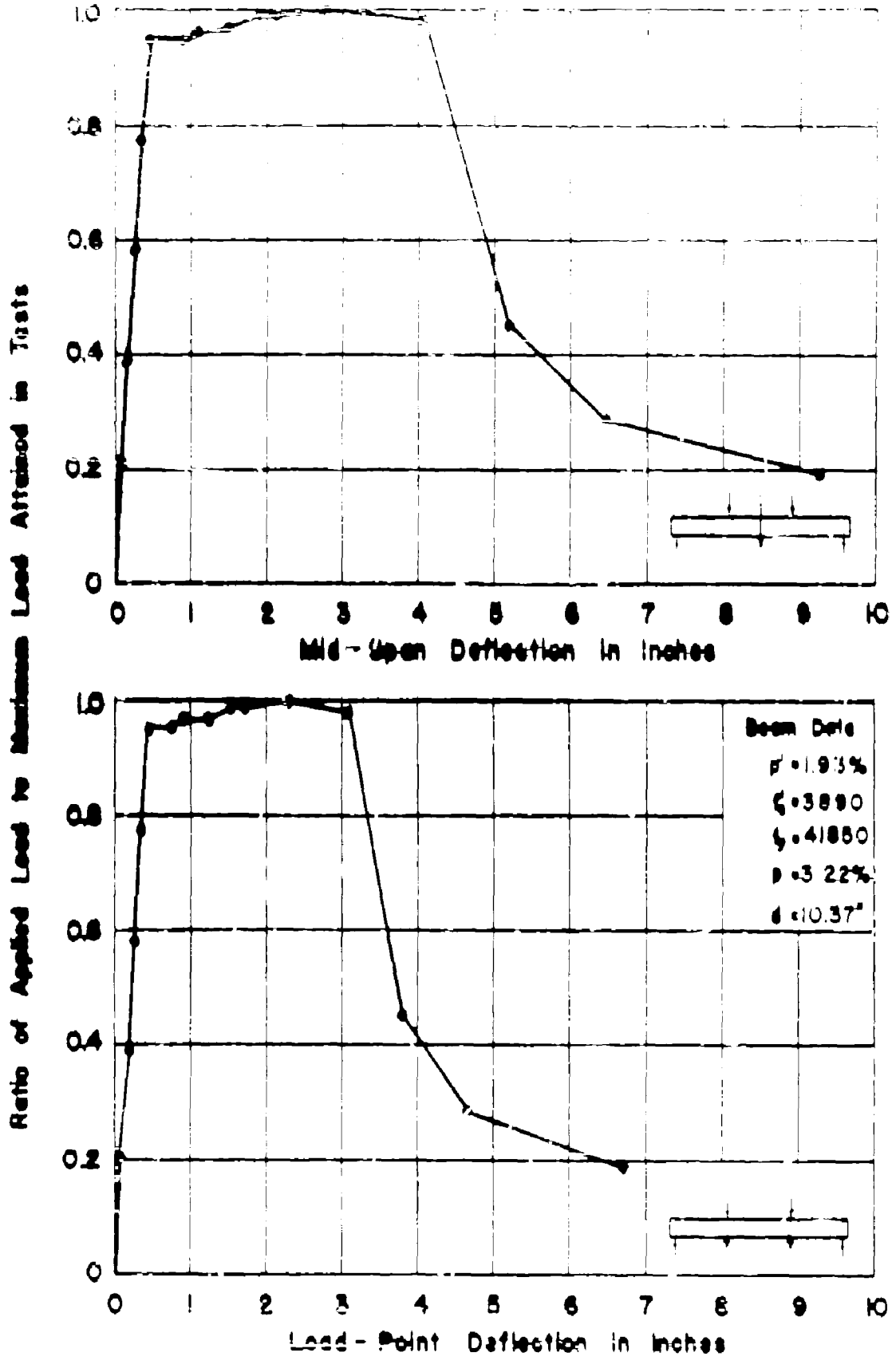

APP. FIG. 124 LOAD-RATIO VS. DEFLECTION FOR BEAM NO.03xm

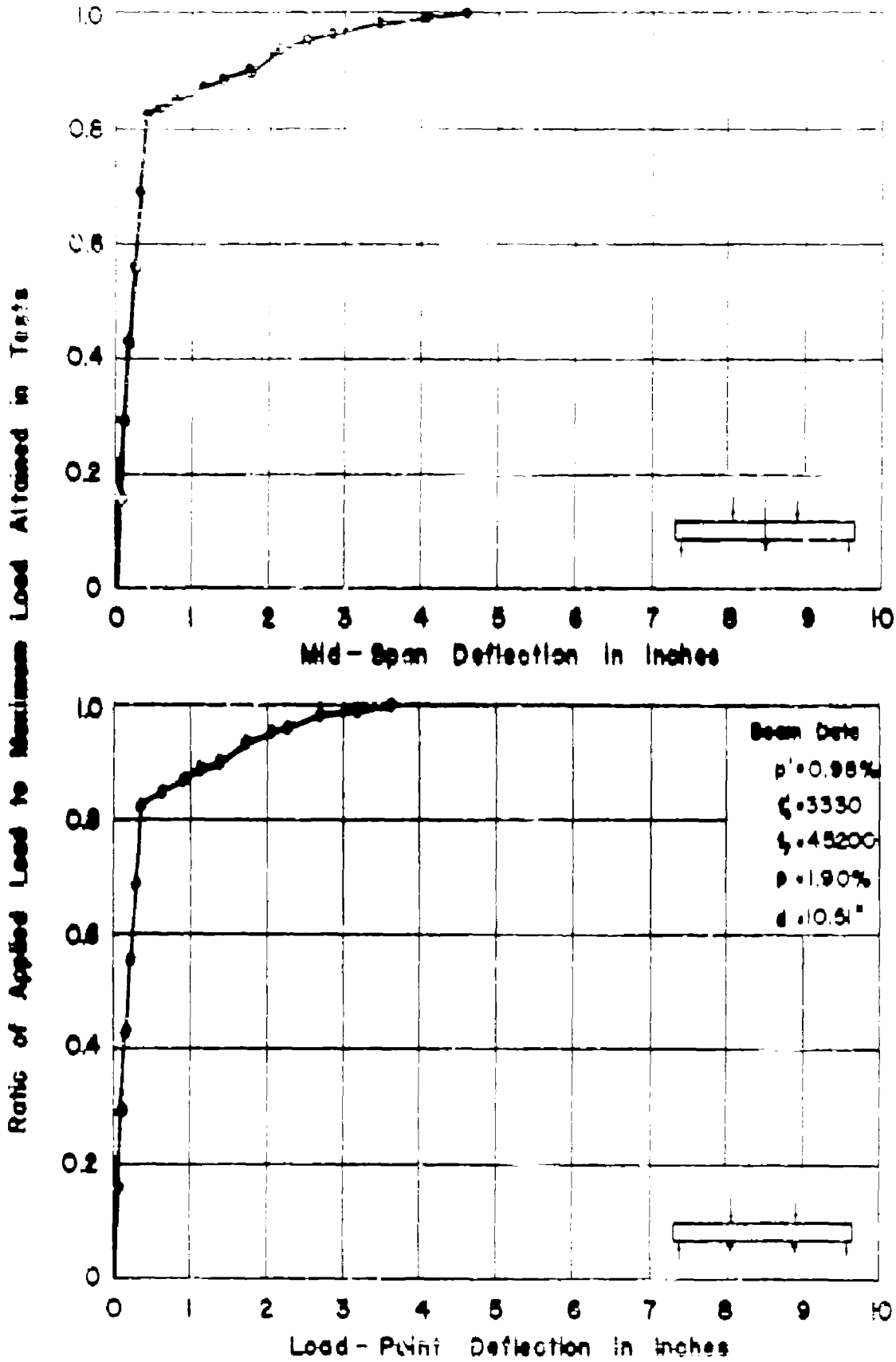

APP. FIG. 125 LOAD-RATIO VS. DEFLECTION FOR BEAM NO. 03yrla

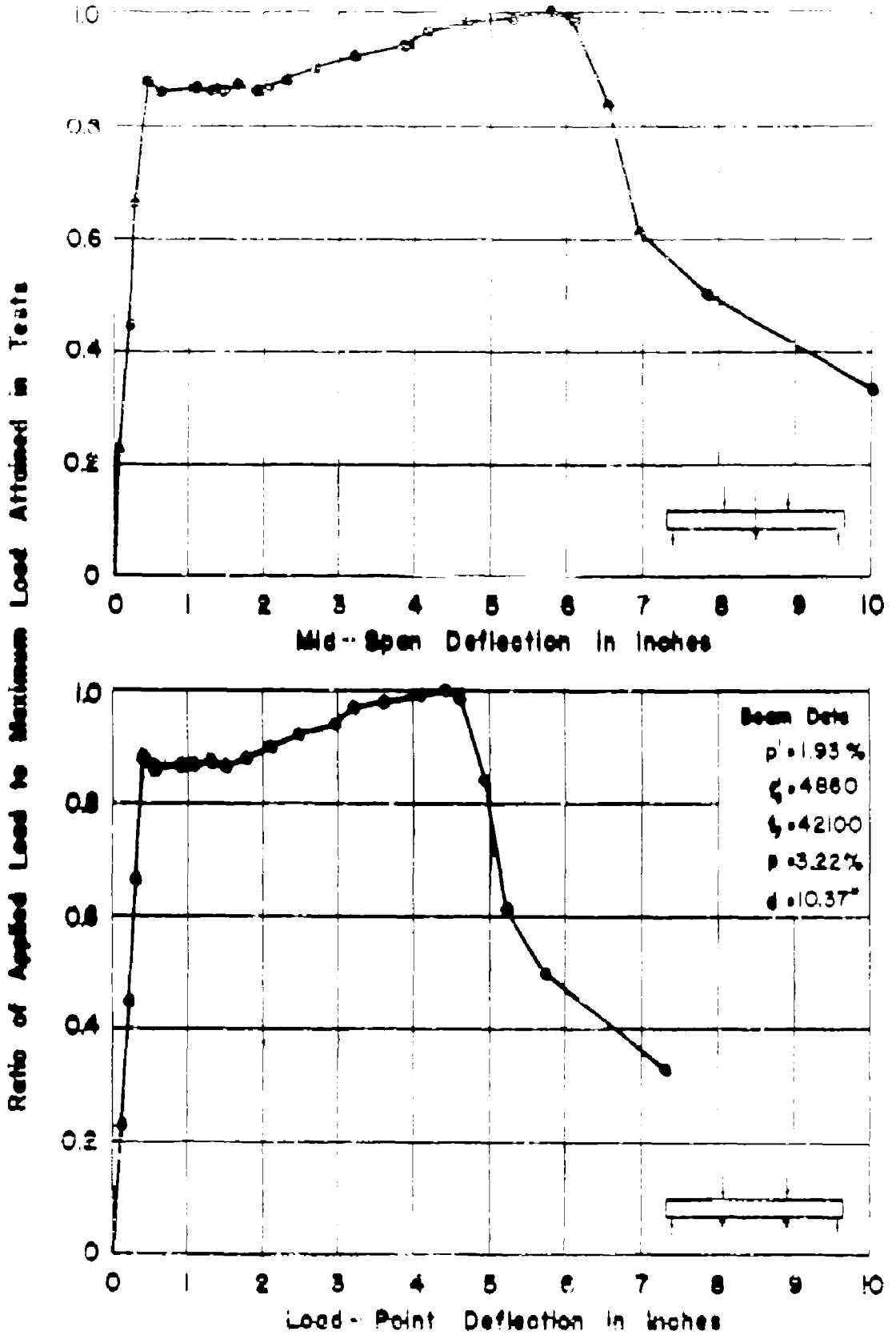

APP. FIG. 126 LOAD-RATIO VS. DEFLECTION FOR BEAM NO. C3ynb

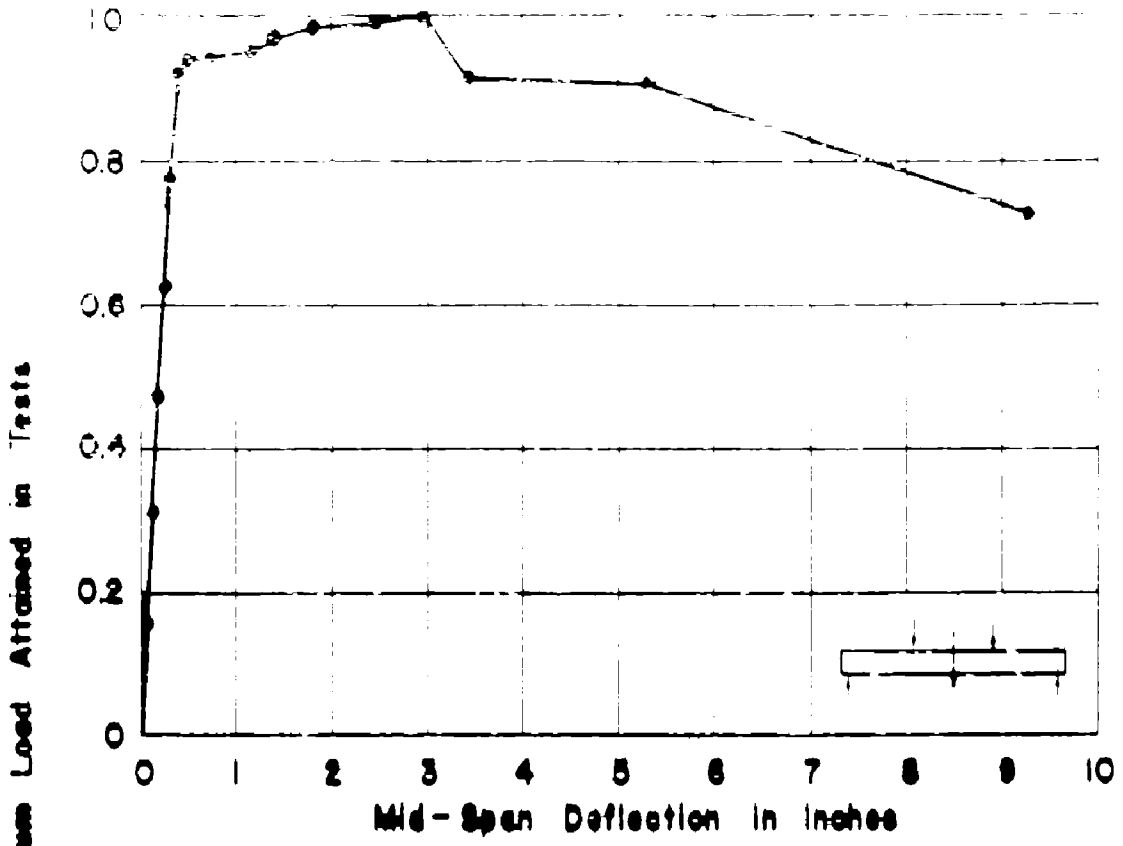

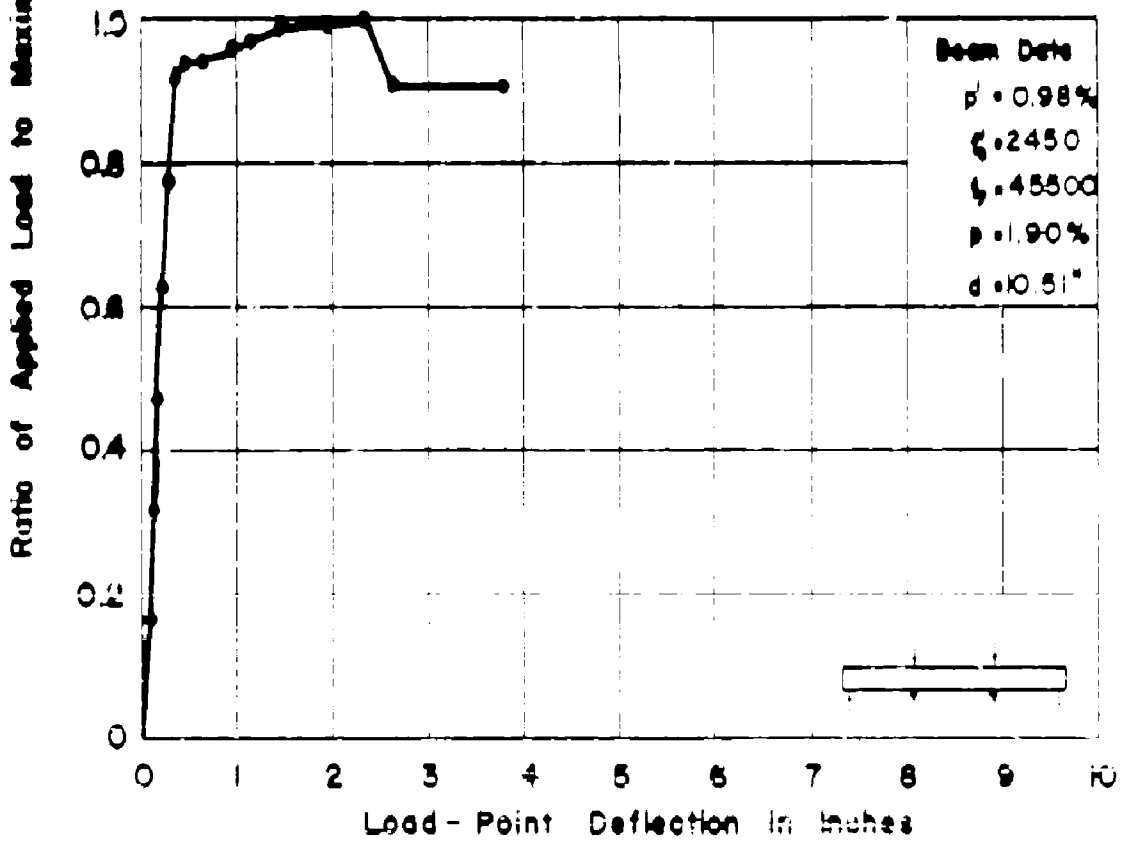

APP. FIG. 127 LOAD-RATIO VS. DEFLECTION FOR BEAM NC.C4xna

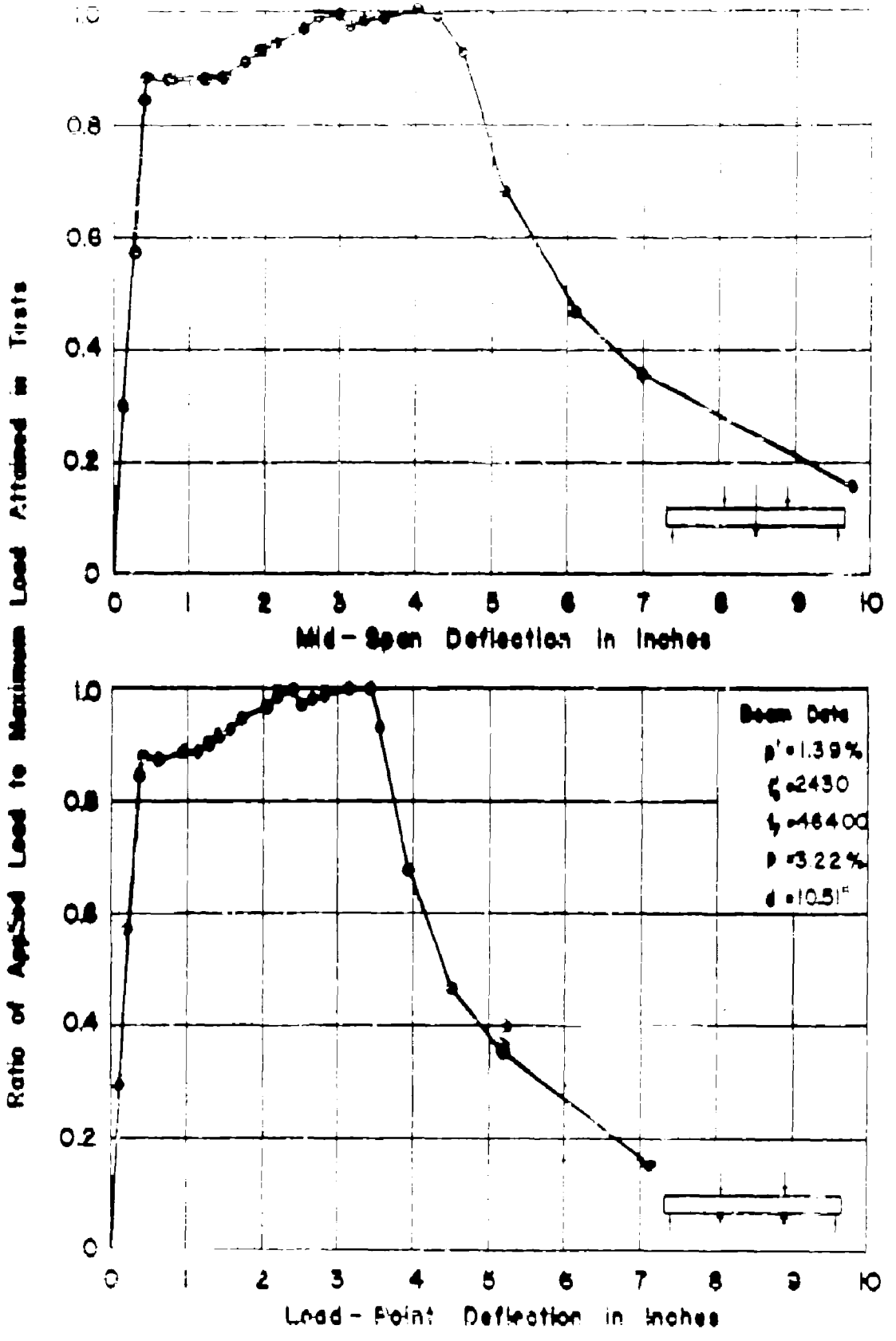

APP. FIG. 128 LOAD-RATIO VS. DEFLECTION FOR BEAM NO. C4xnb

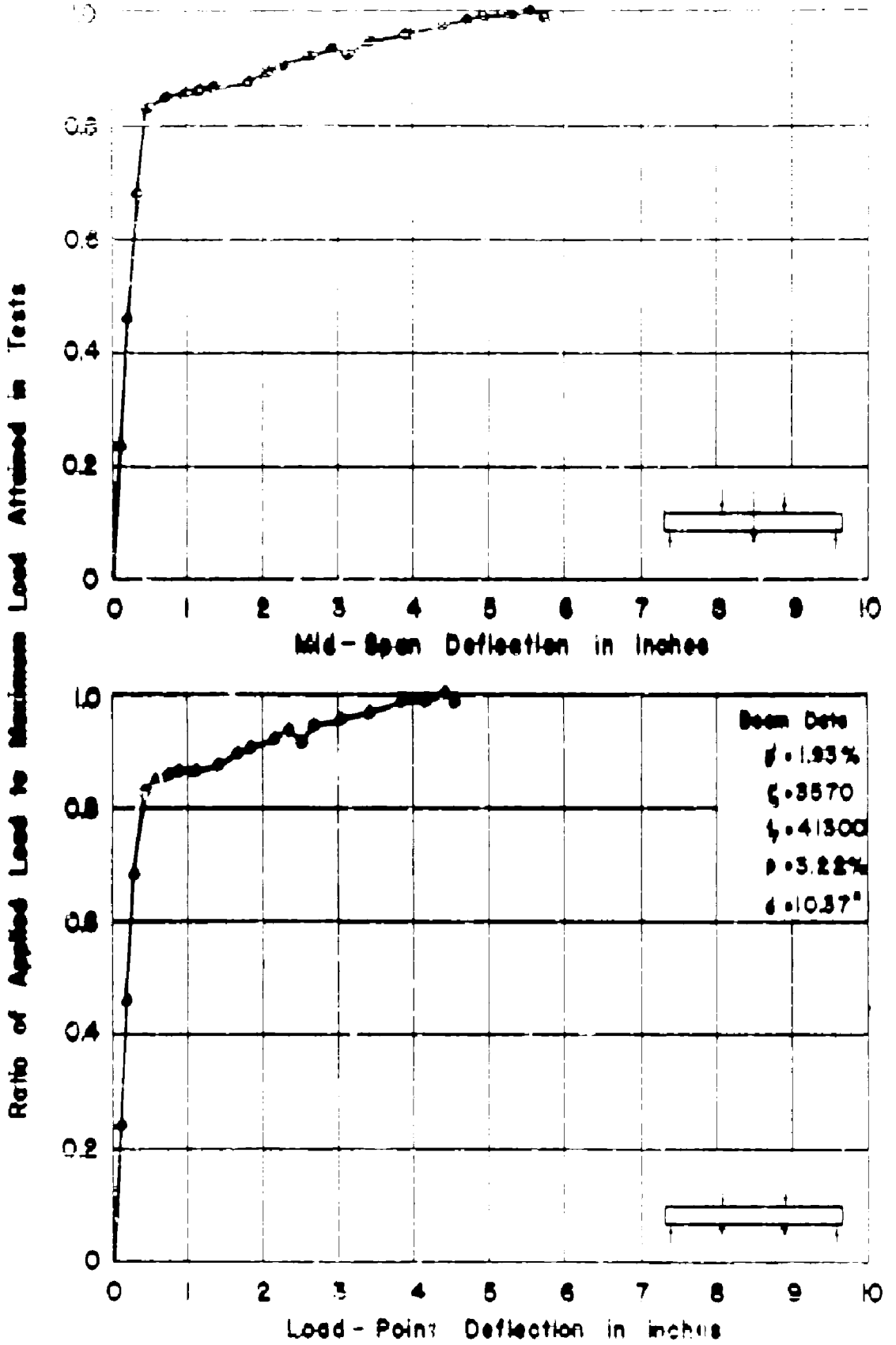

APP. FIG. 129 LOAD-RATIO VS. DEFLECTION FOR BEAM NO.04zn

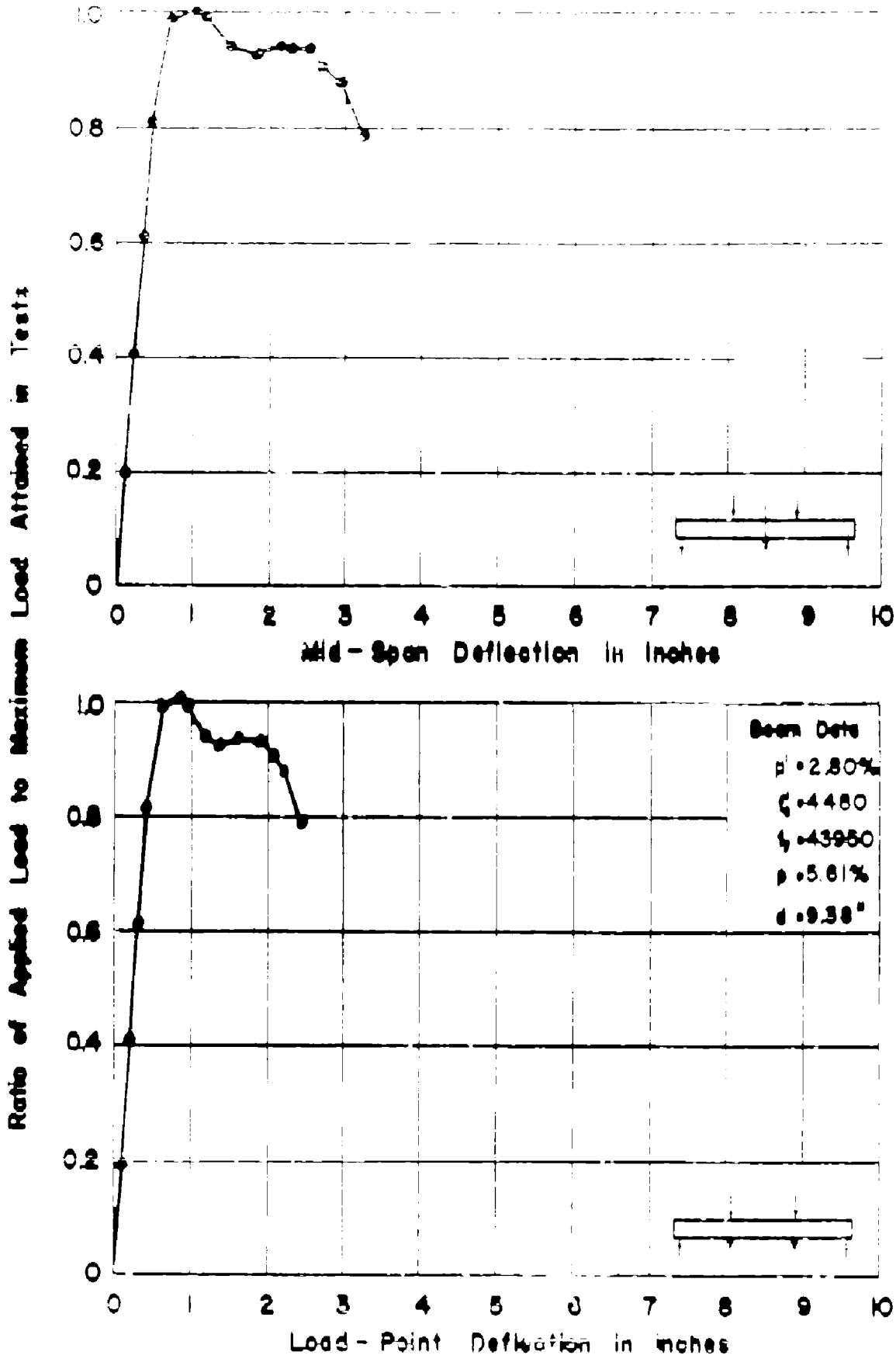

APP. FIG. 130 LOAD-RATIO VS. DEFLECTION FOR BEAM NO. C5vn

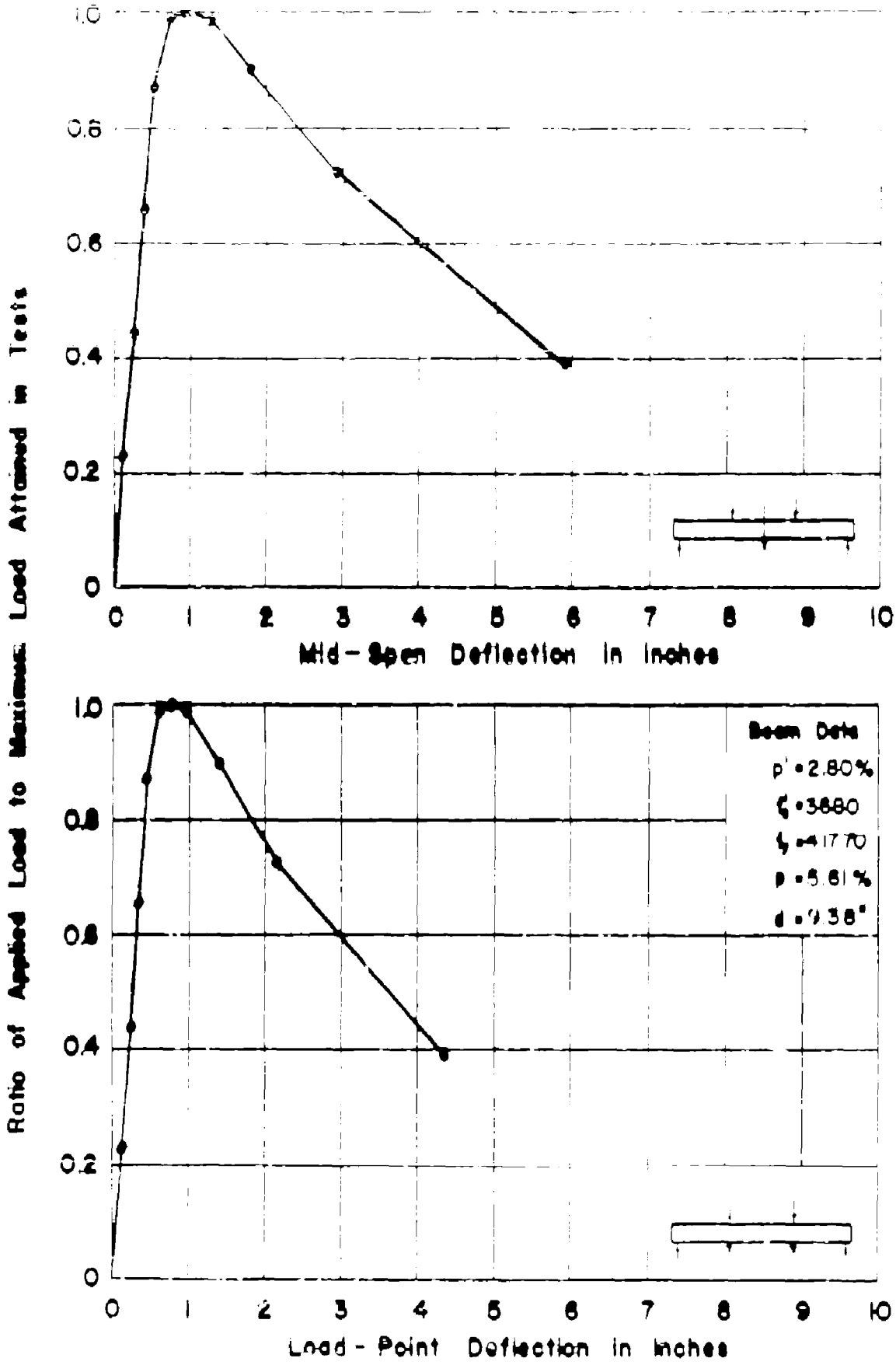

APP. FIG. 131 LOAD-RATIO VS. DEFLECTION FOR BEAM NO. C6xm

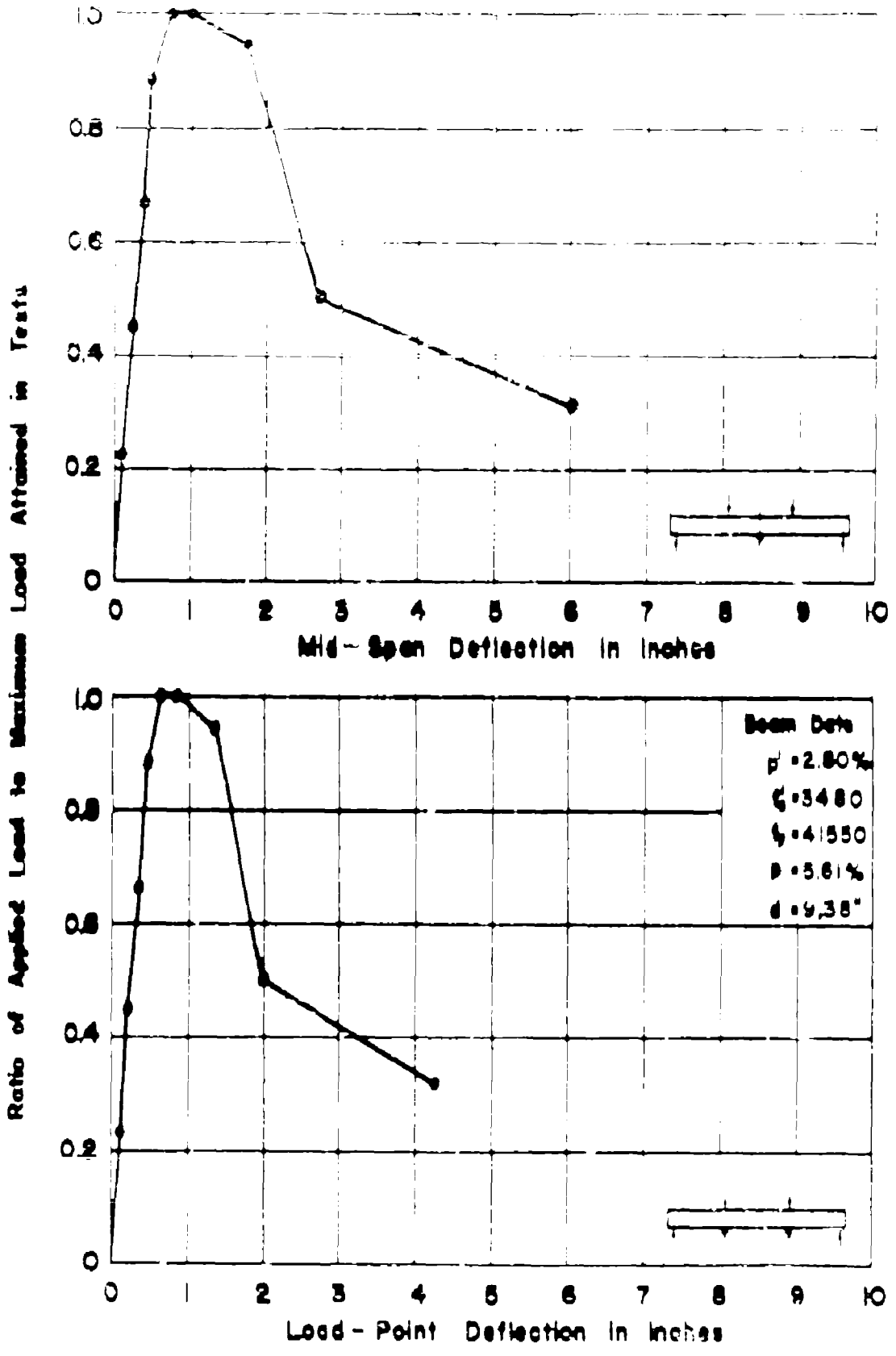

APP. FIG. 132 LOAD-RATIO VS. DEFLECTION FOR BEAM NO. C7w

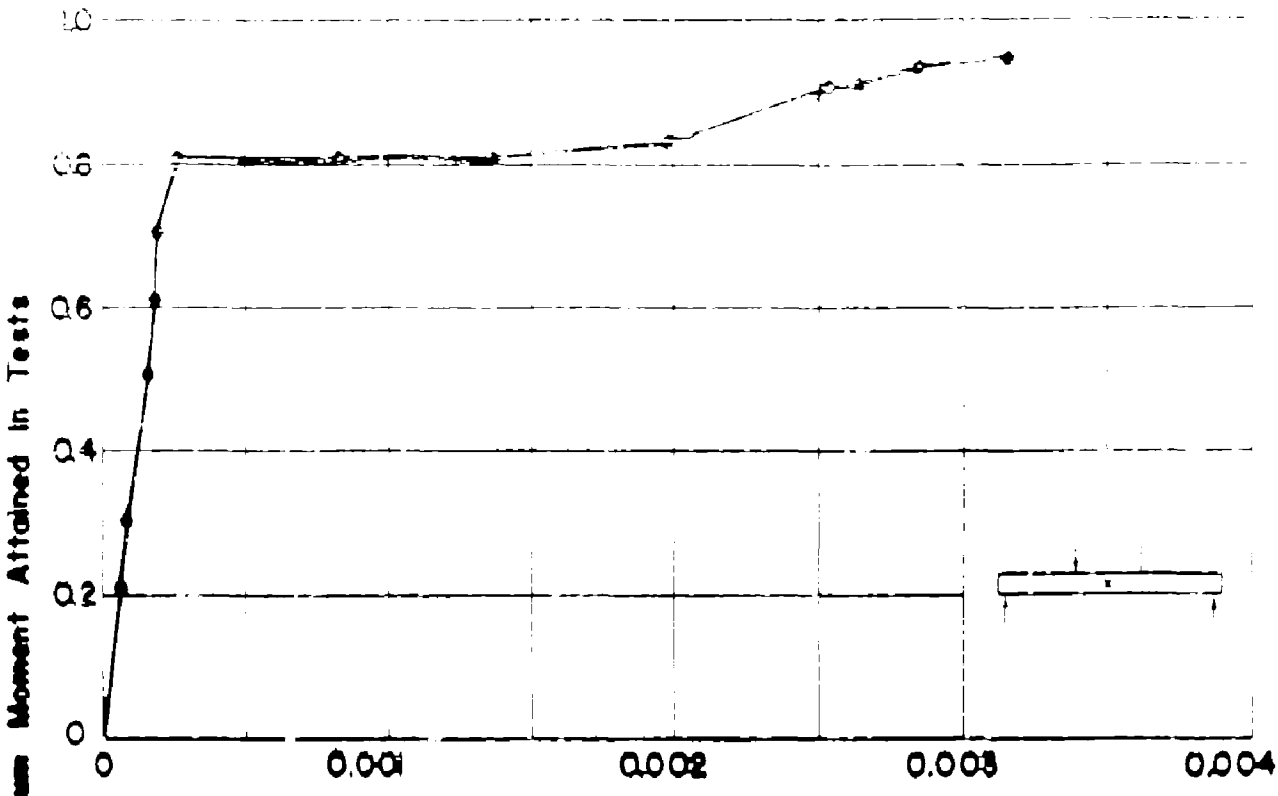

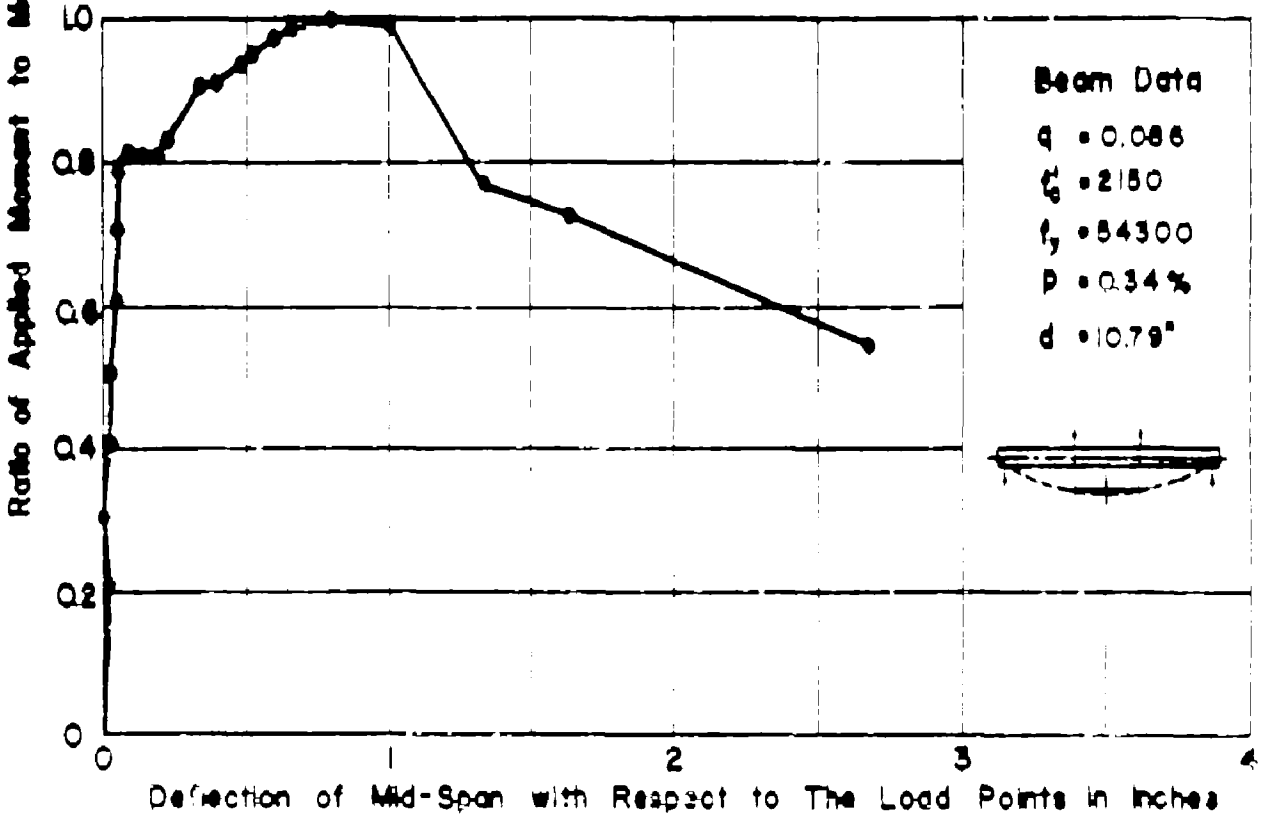

APP FIG. 133 MOMENT RATIO VS. PURE MOMENT DEFORMATIONS FOR BEAM NO. T1L2

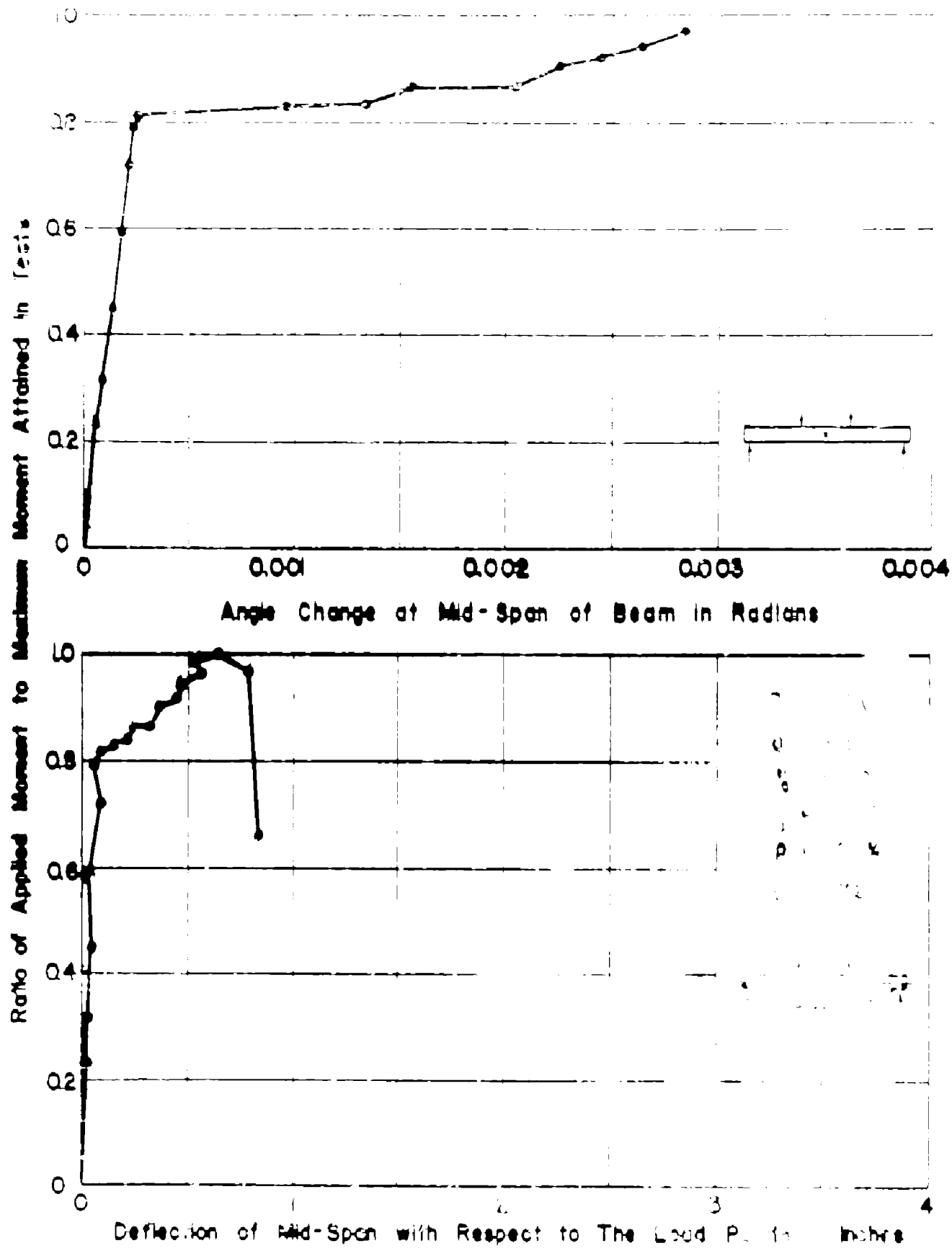

APP. FIG. 134 MOMENT RATIO VS. PURE MOMENT DEFORMATIONS FOR BEAM NO. T1Lb

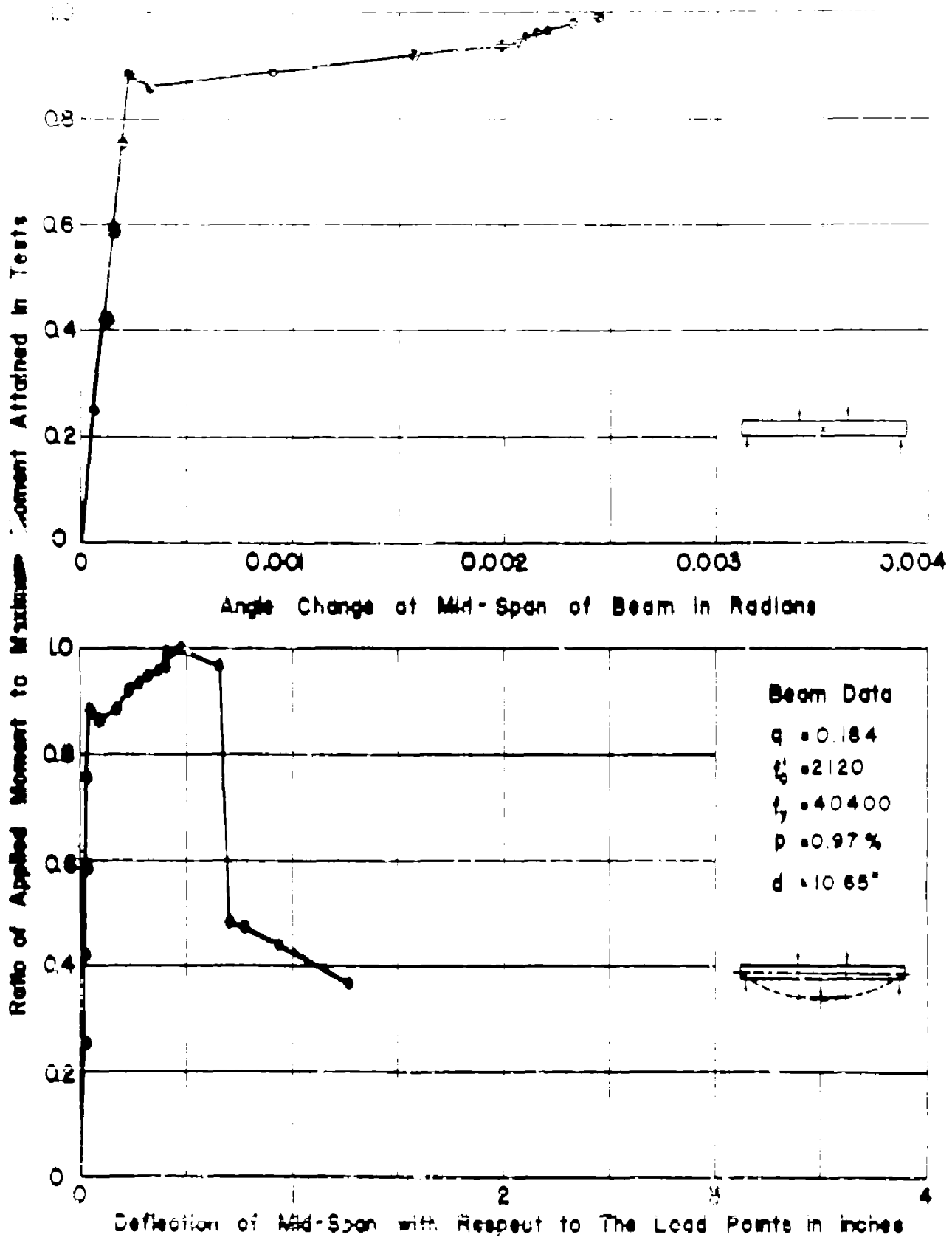

APP FIG 135 MOMENT RATIO VS. PURE MOMENT DEFORMATIONS FOR BEAM NO T2 Lo

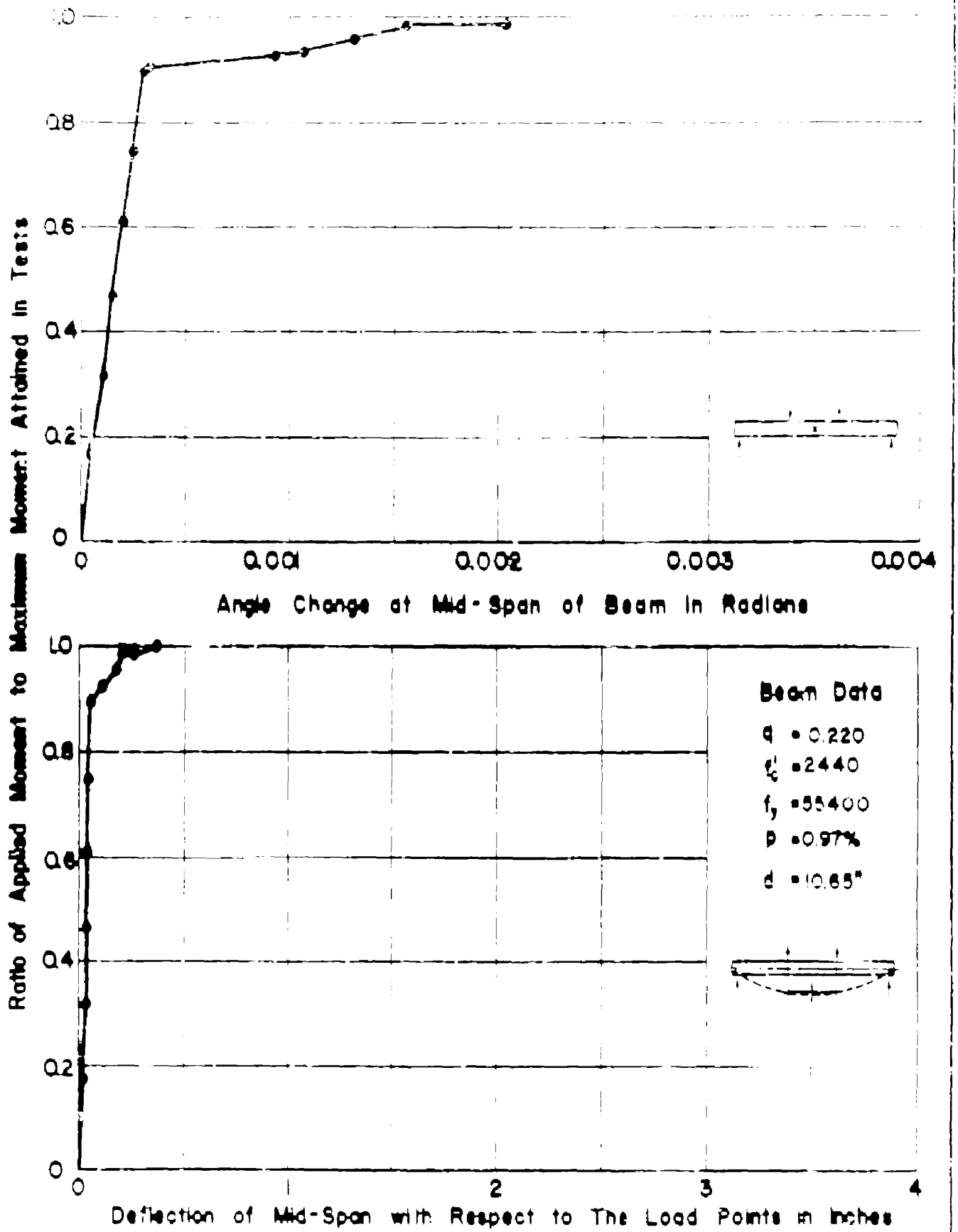

APP. FIG. 136 MOMENT RATIO VS. PURE MOMENT DEFORMATIONS FOR BEAM NO. T2Lb

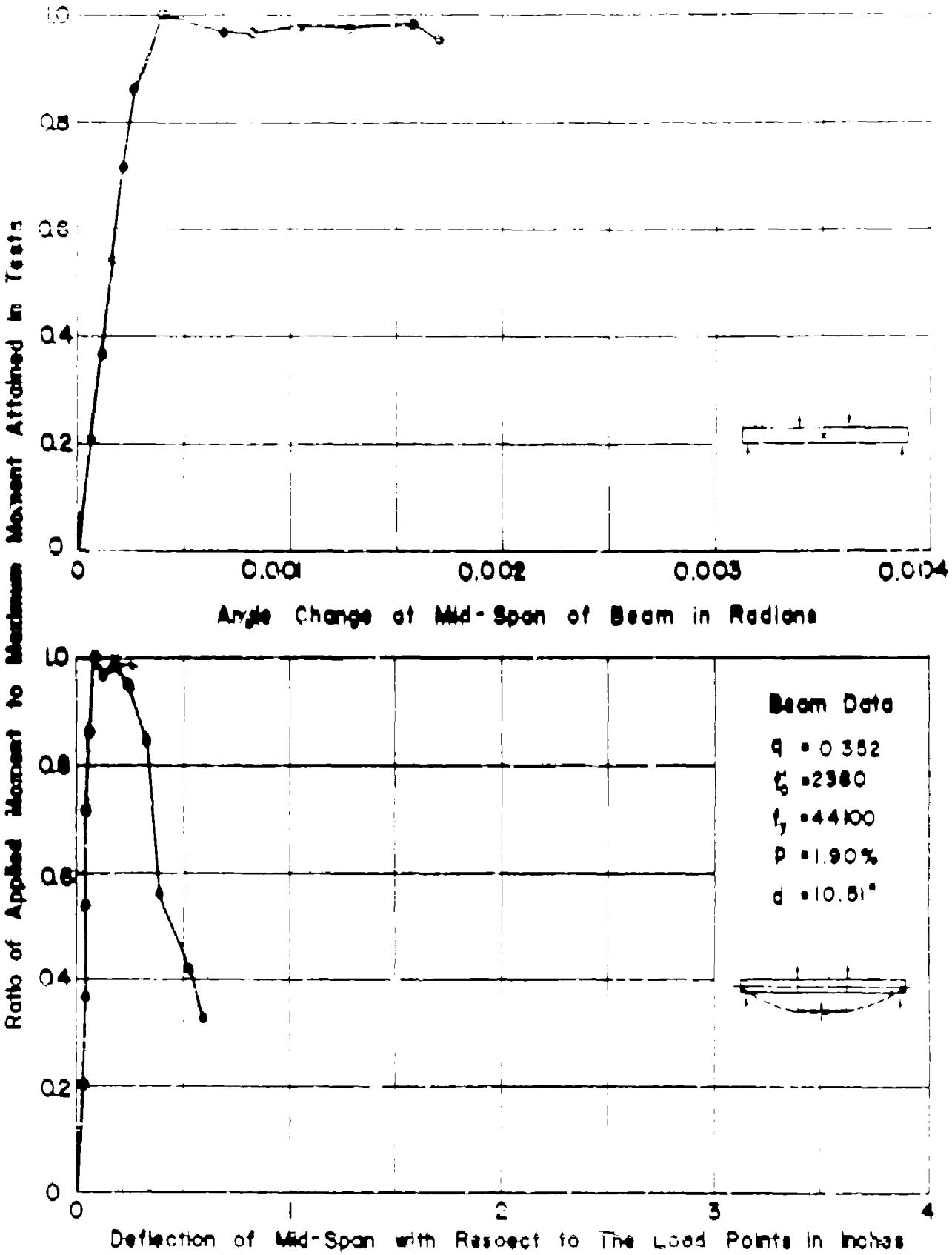

APP. FIG. 137 MOMENT RATIO VS. PURE MOMENT DEFORMATIONS FOR BEAM NQT4L0

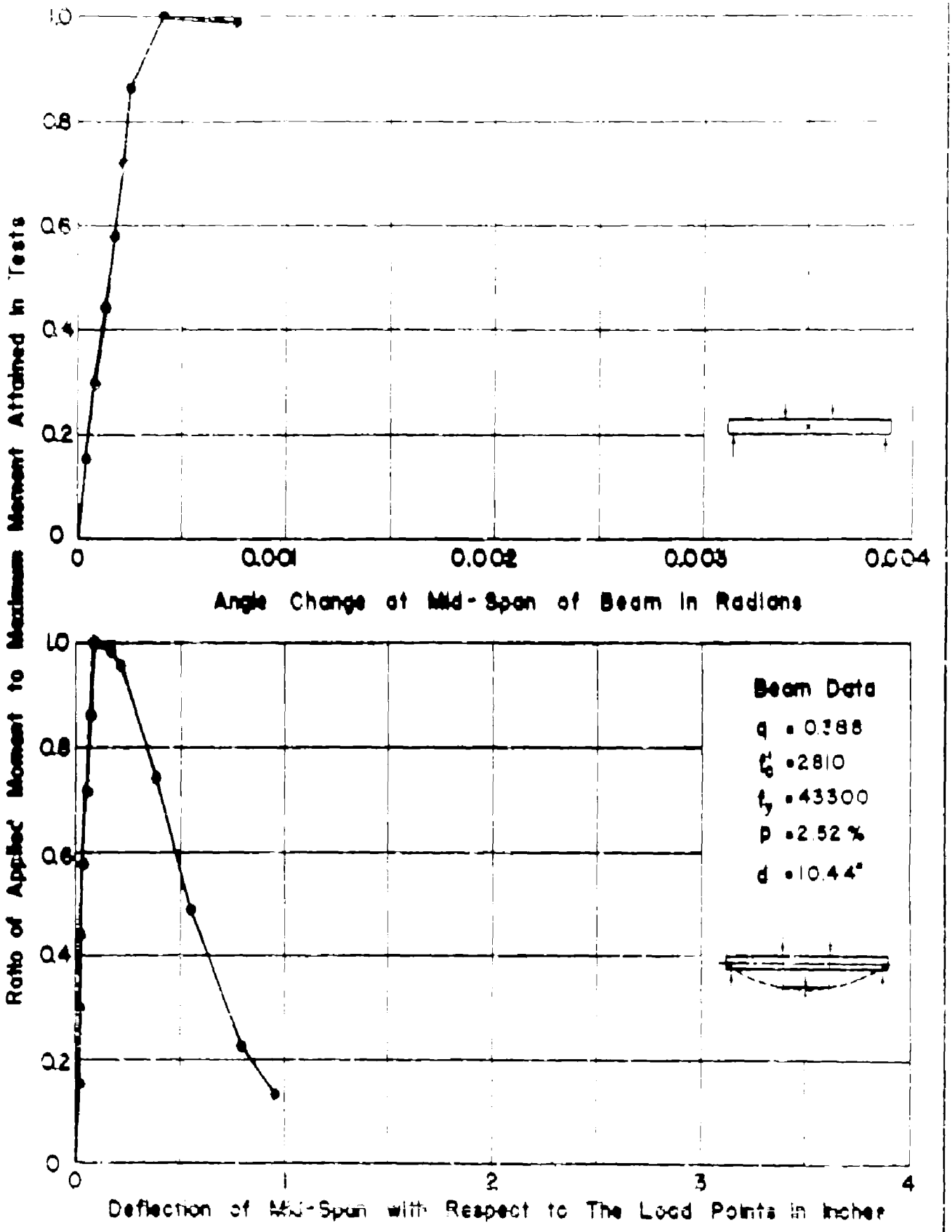

APP. FIG. 138 MOMENT RATIO VS. PURE MOMENT DEFORMATIONS FOR BEAM NO. T4Lb

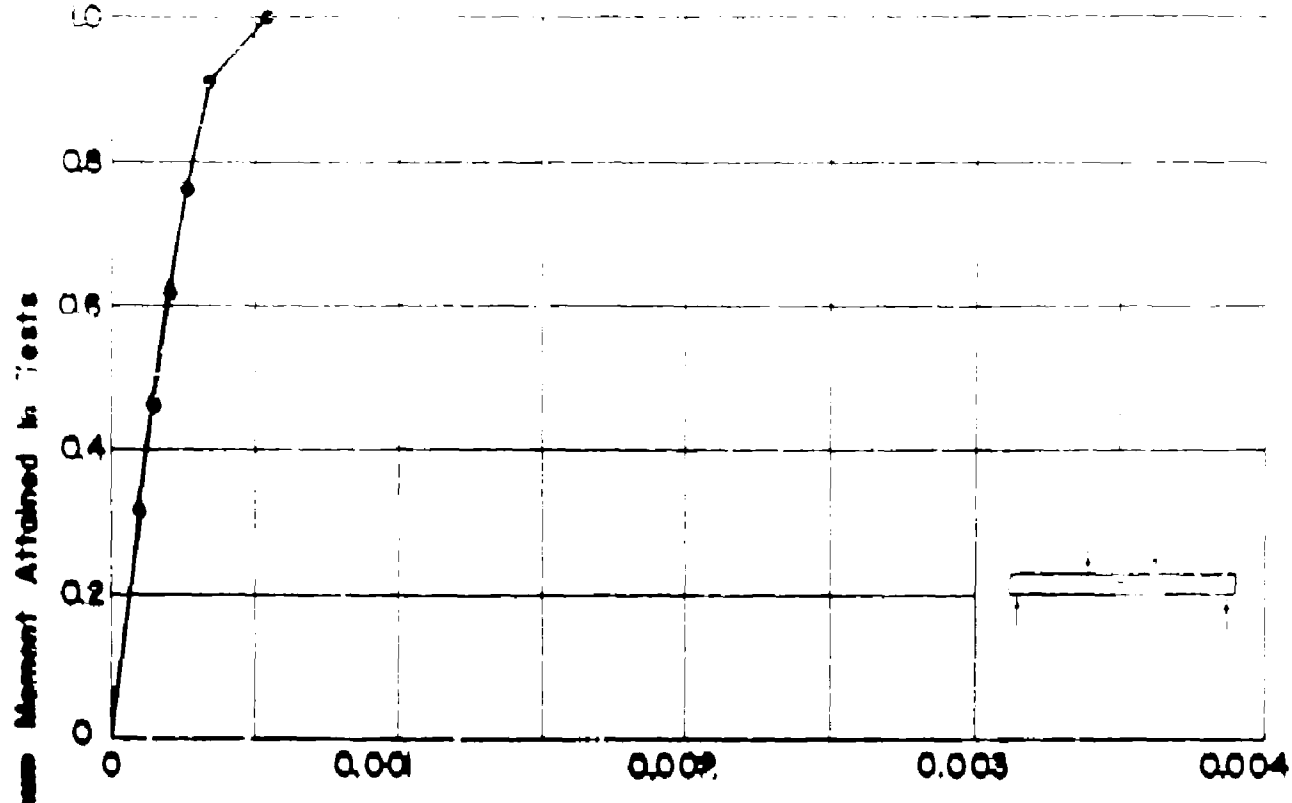

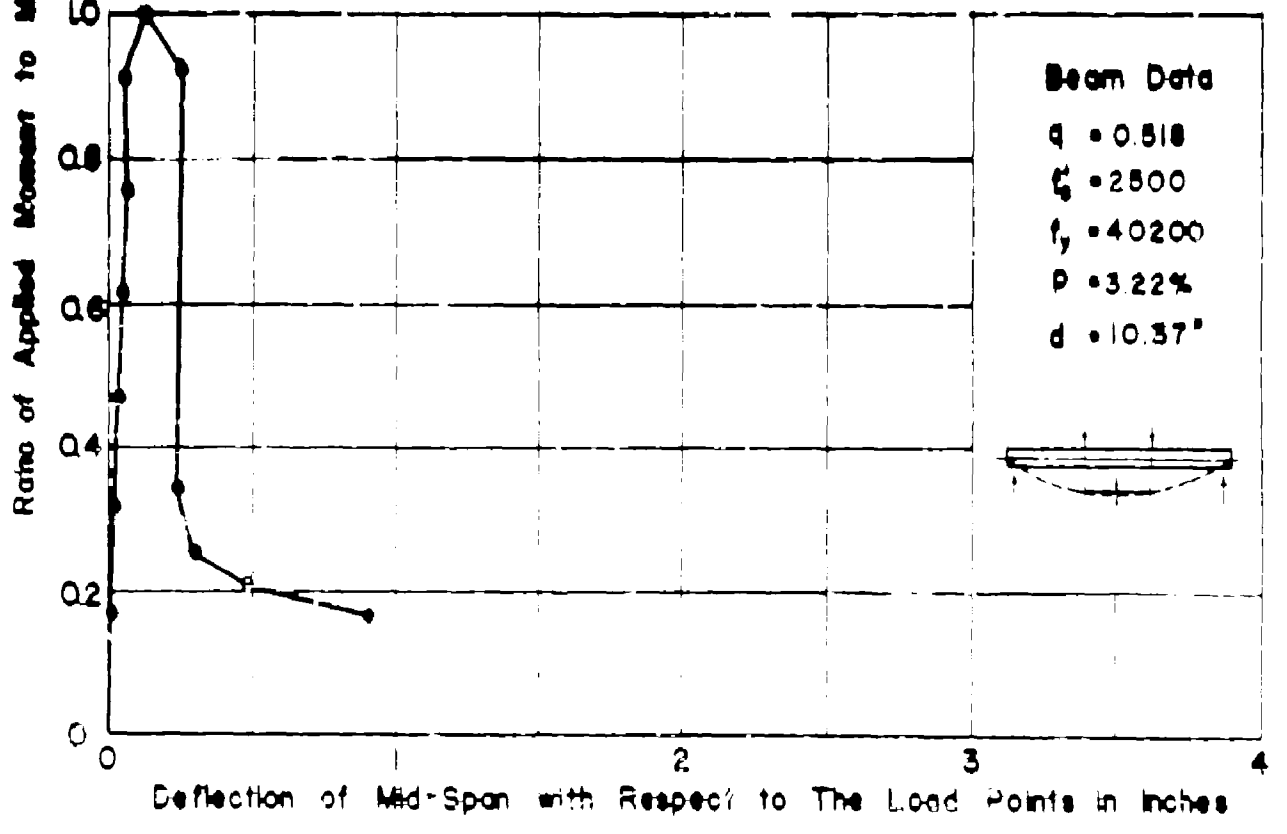

APP FIG 139 MOMENT RATIO VS. PURE MOMENT DEFORMATIONS FOR BEAM NO T5L

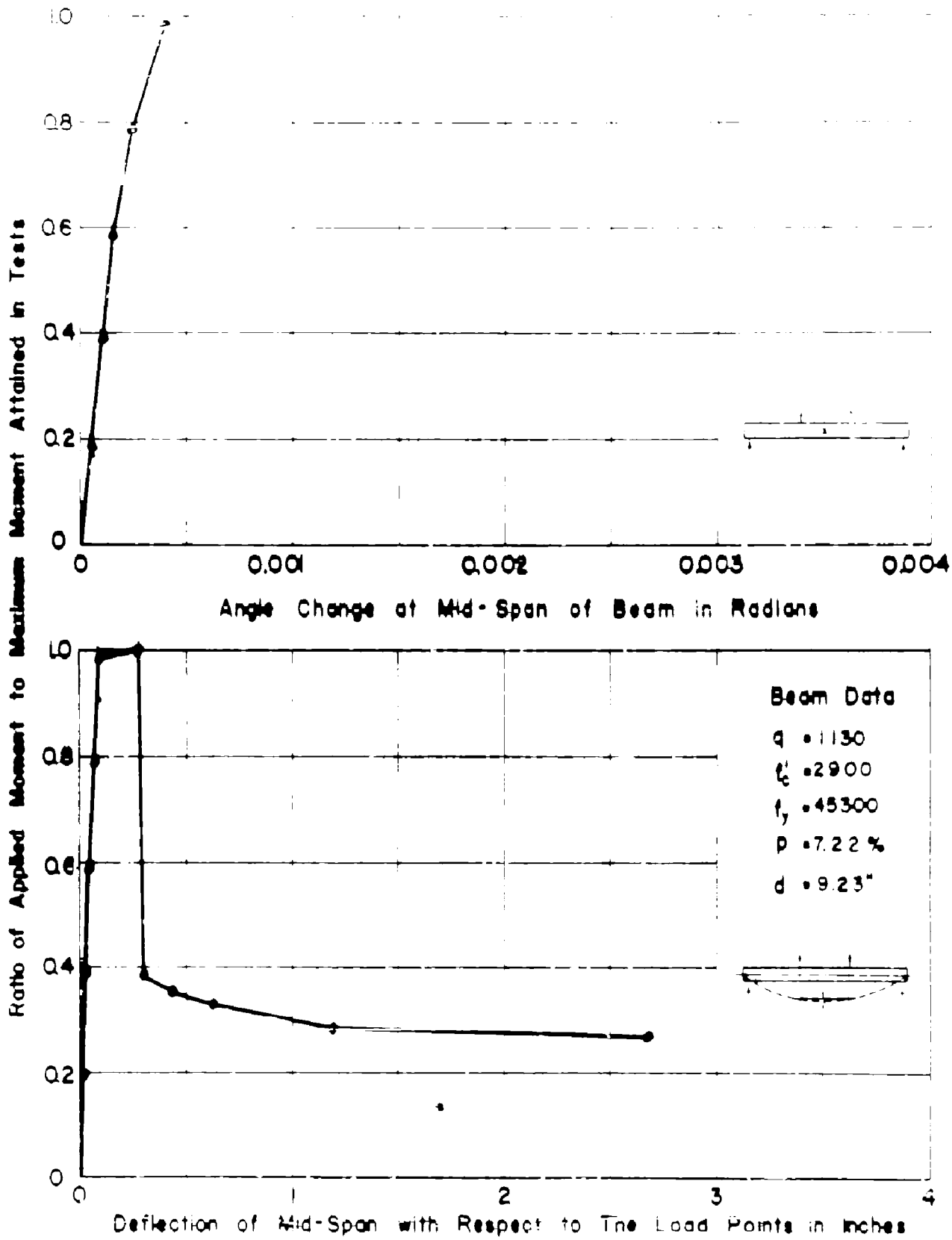

APP. FIG 140 MOMENT RATIO VS. PURE MOMENT DEFORMATIONS FOR BEAM NO. T11L

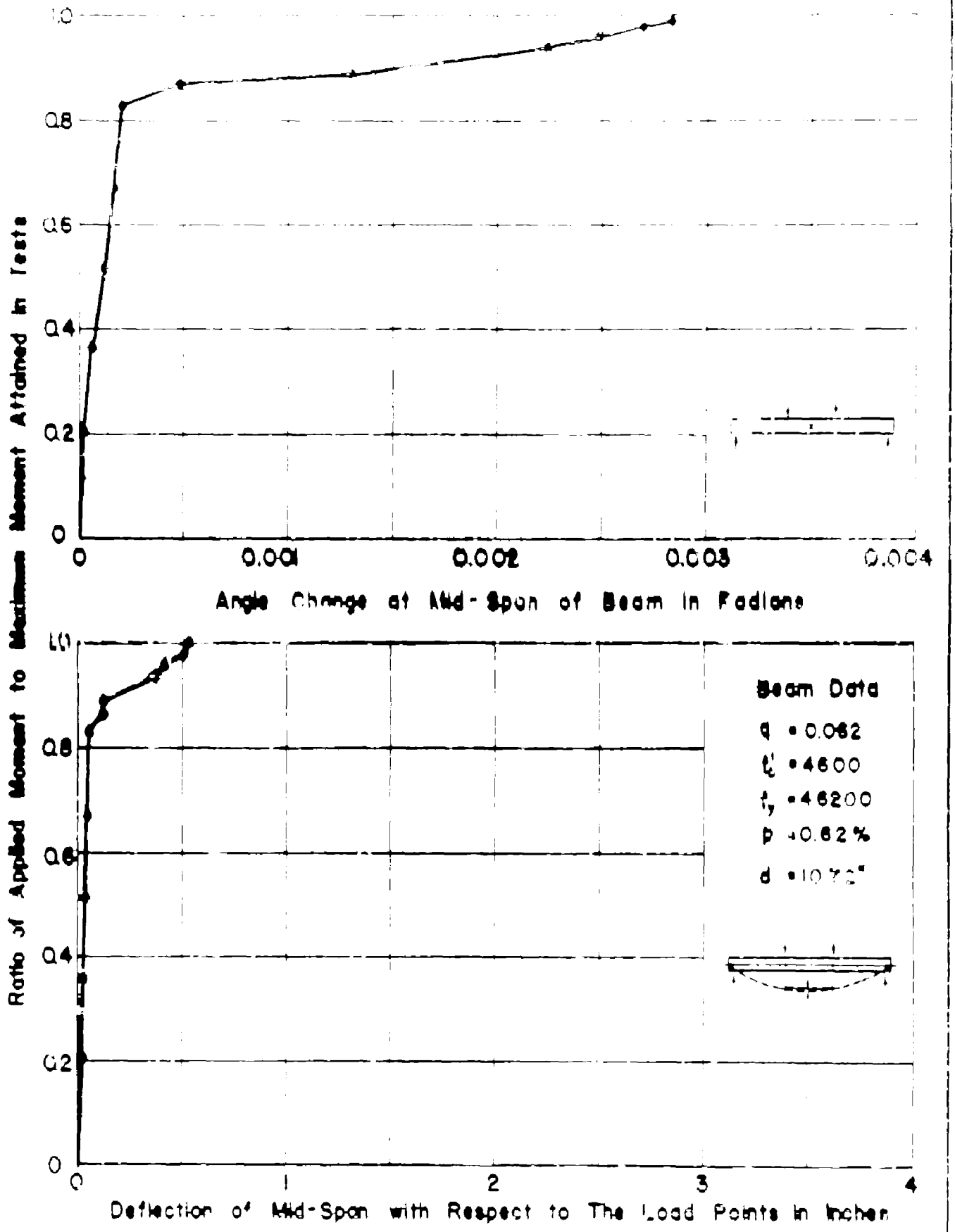

APP. FIG. 141 MOMENT RATIO VS. PURE MOMENT DEFORMATIONS FOR BEAM NO TIMa

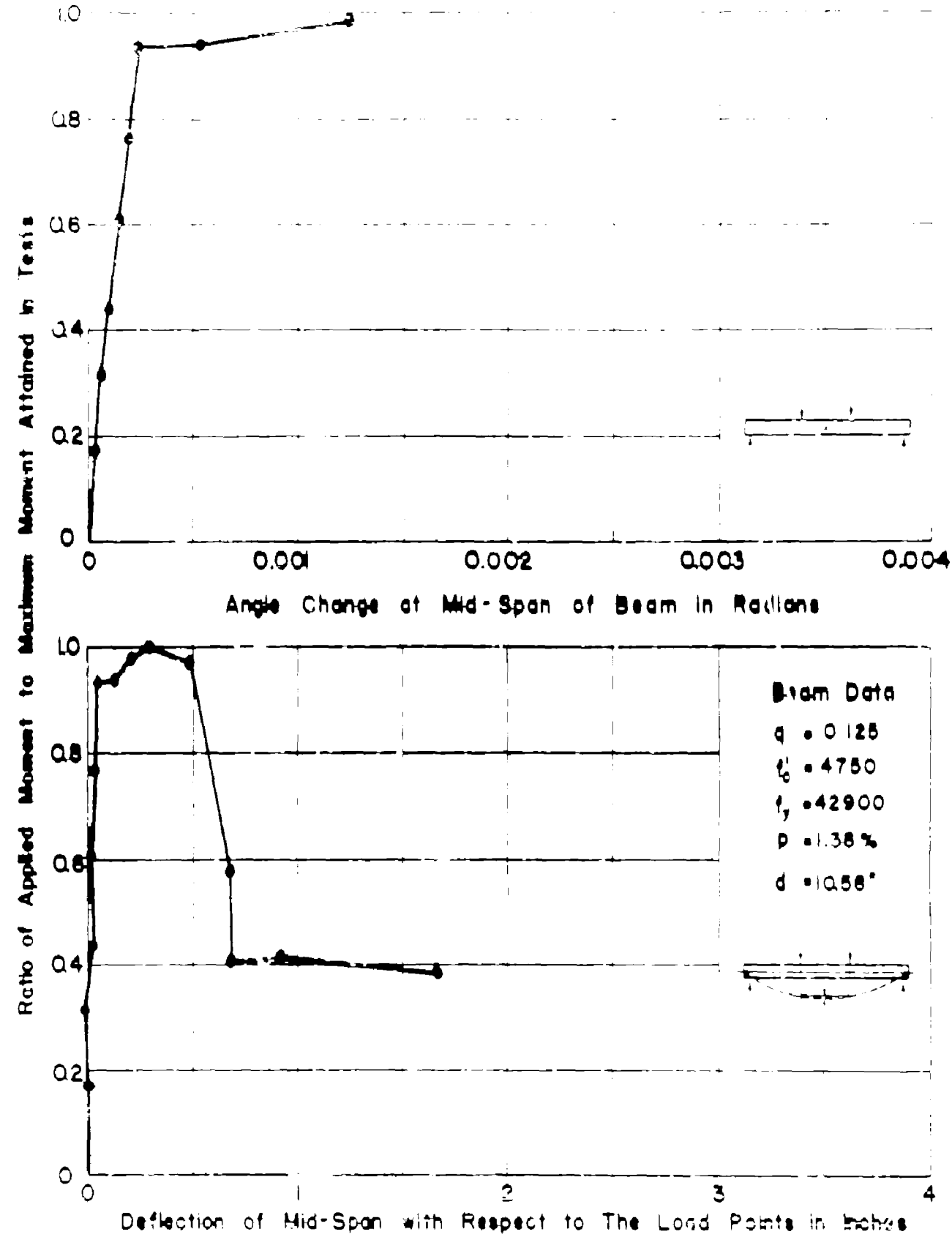

APP FIG. 142 MOMENT RATIO VS. PURE MOMENT DEFORMATIONS FOR BEAM NO. T1Mb

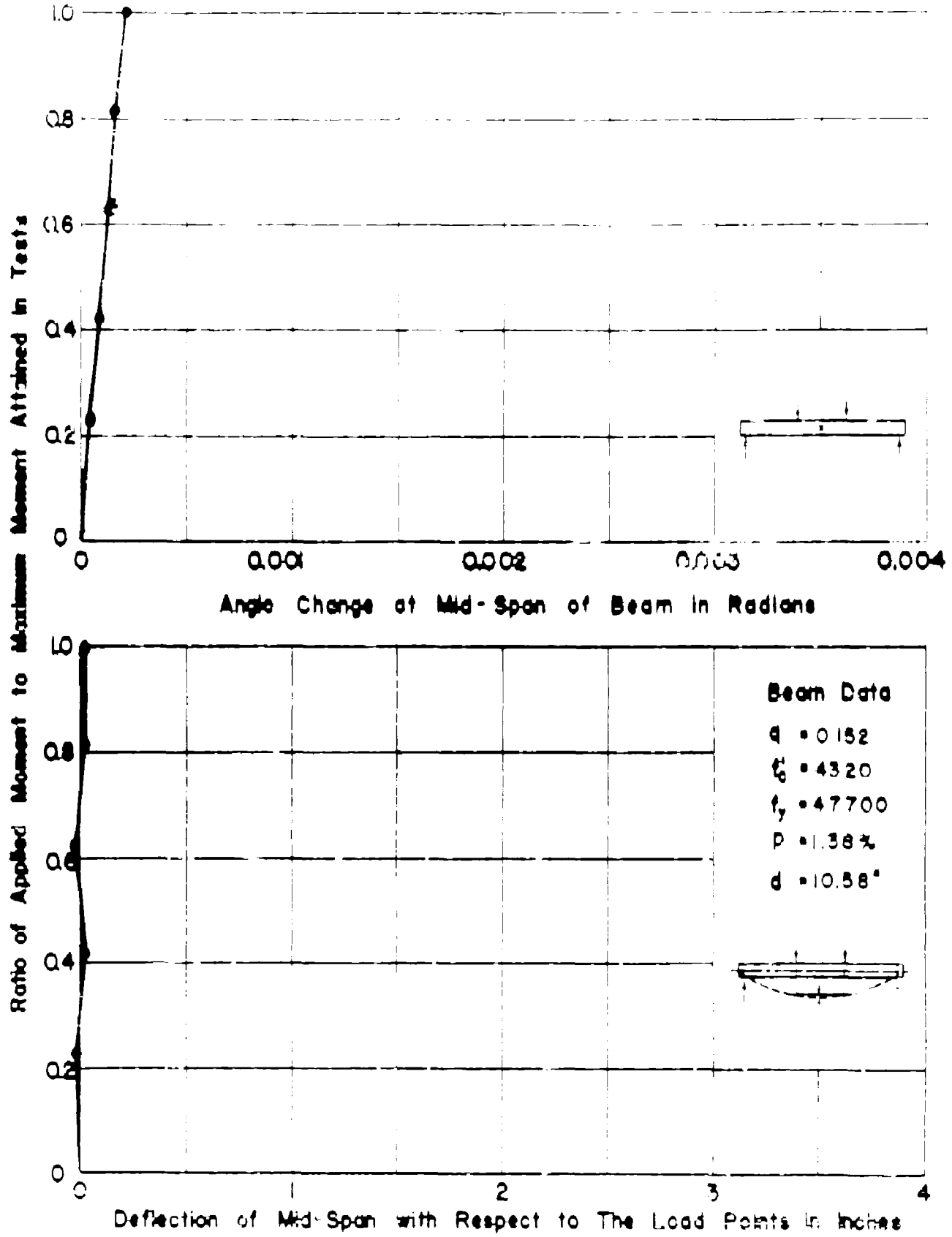

APP. FIG. 143 MOMENT RATIO VS. PURE MOMENT DEFORMATIONS FOR BEAM NOT2Ma

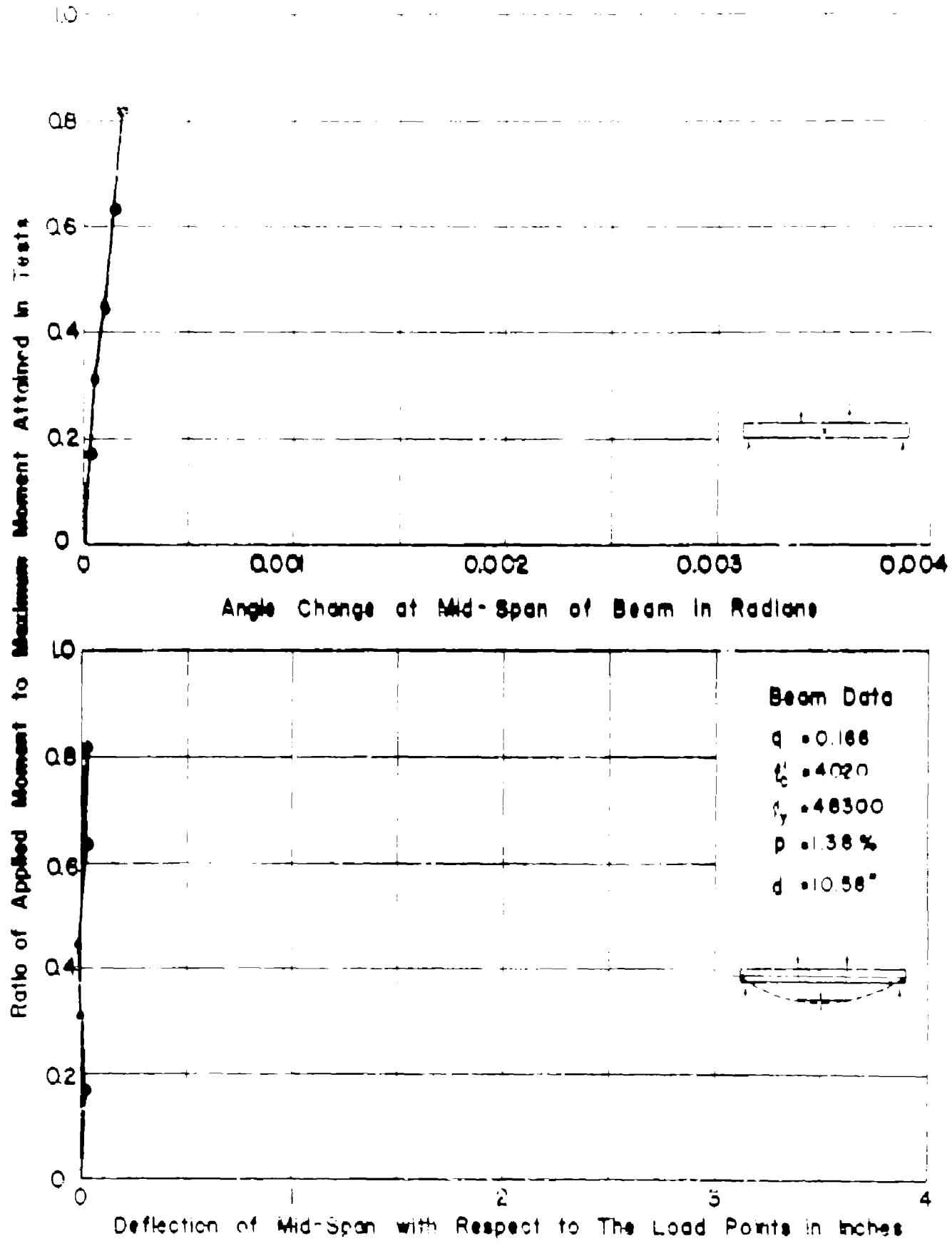

APP. FIG. 144 MOMENT RATIO VS. PURE MOMENT DEFORMATIONS FOR BEAM NO. T2M6

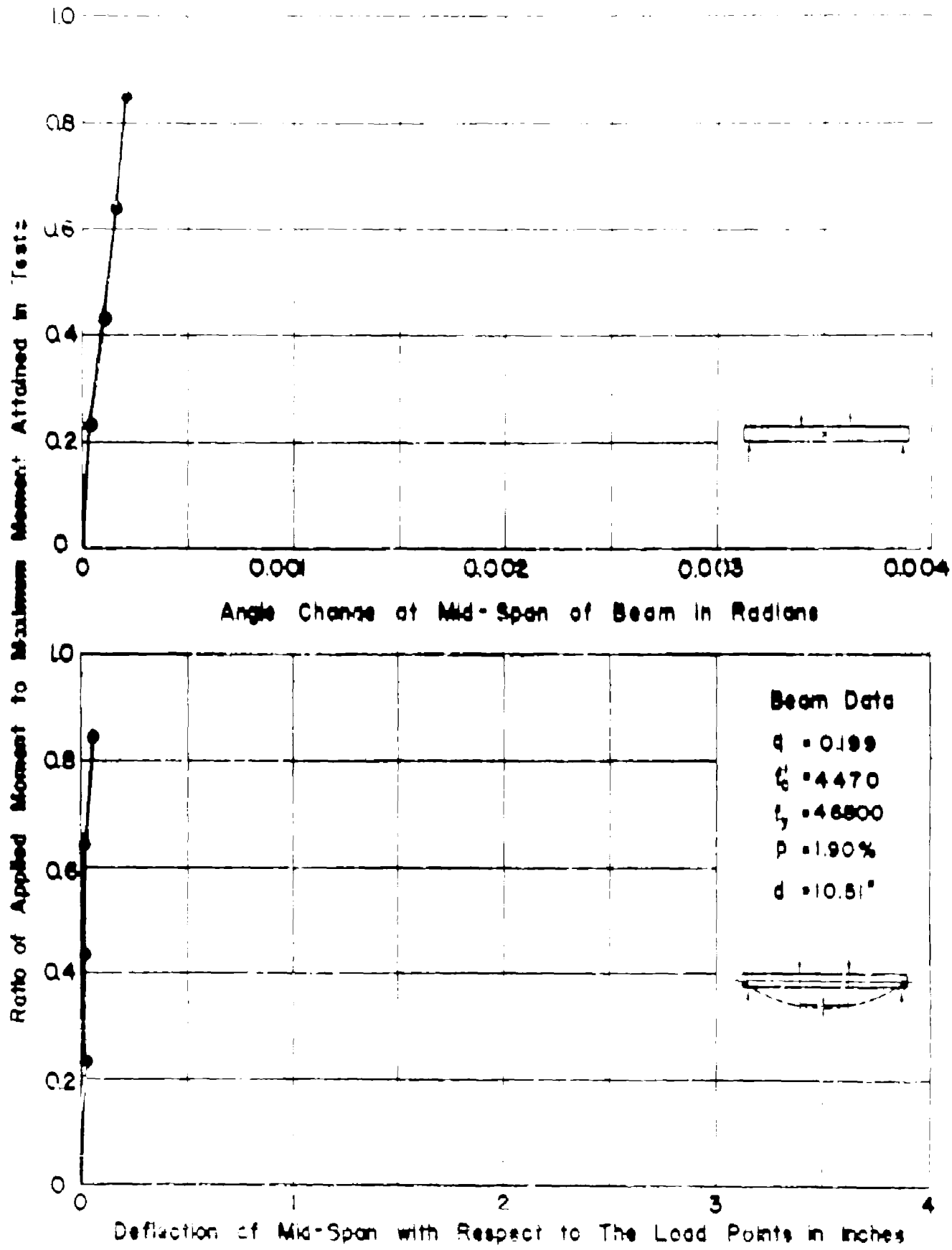

APP. FIG. 145 MOMENT RATIO VS. PURE MOMENT DEFORMATIONS FOR BEAM NO. T2M6

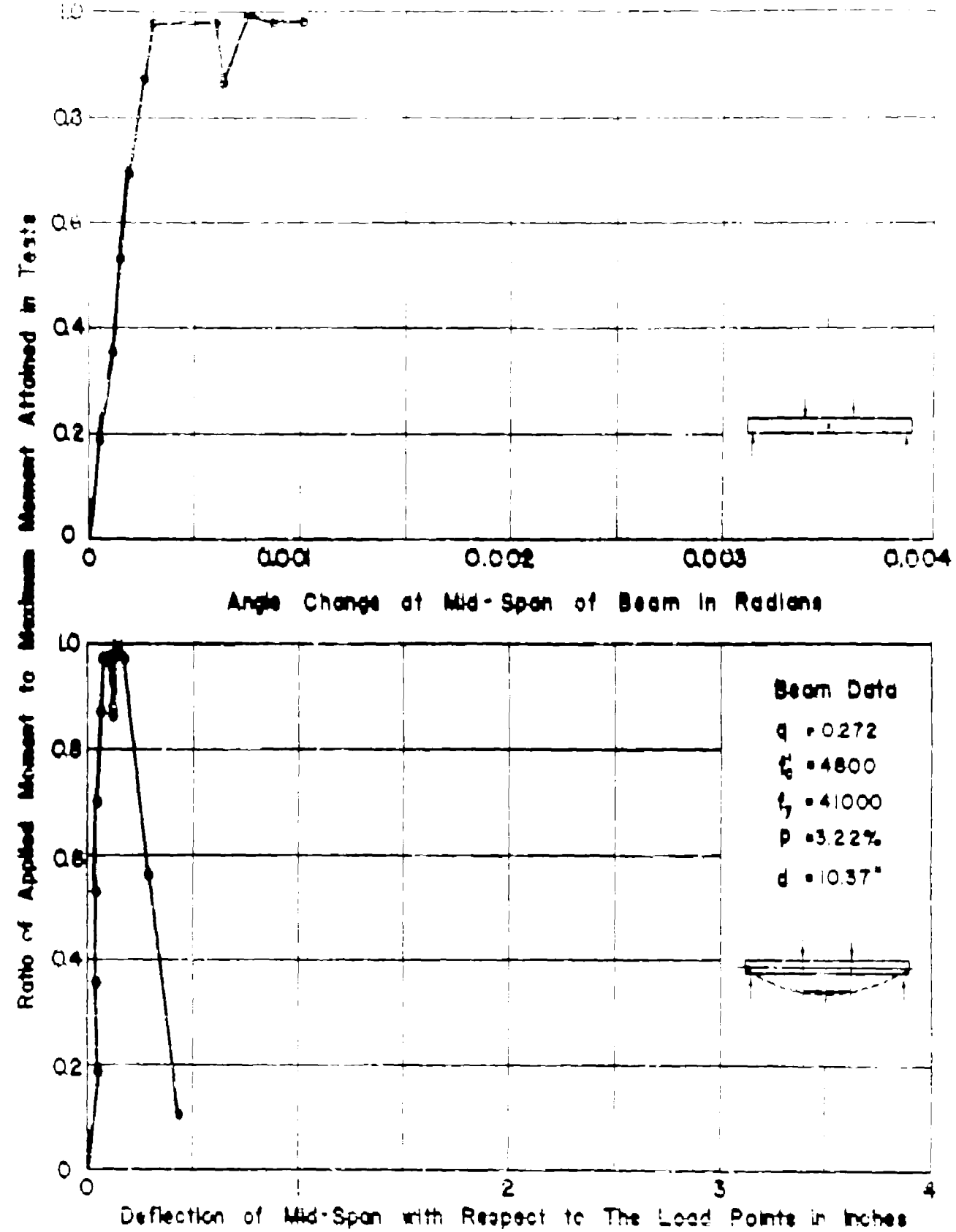

APP FIG. 146 MOMENT RATIO VS. PURE MOMENT DEFORMATIONS FOR BEAM NO. T3Ma

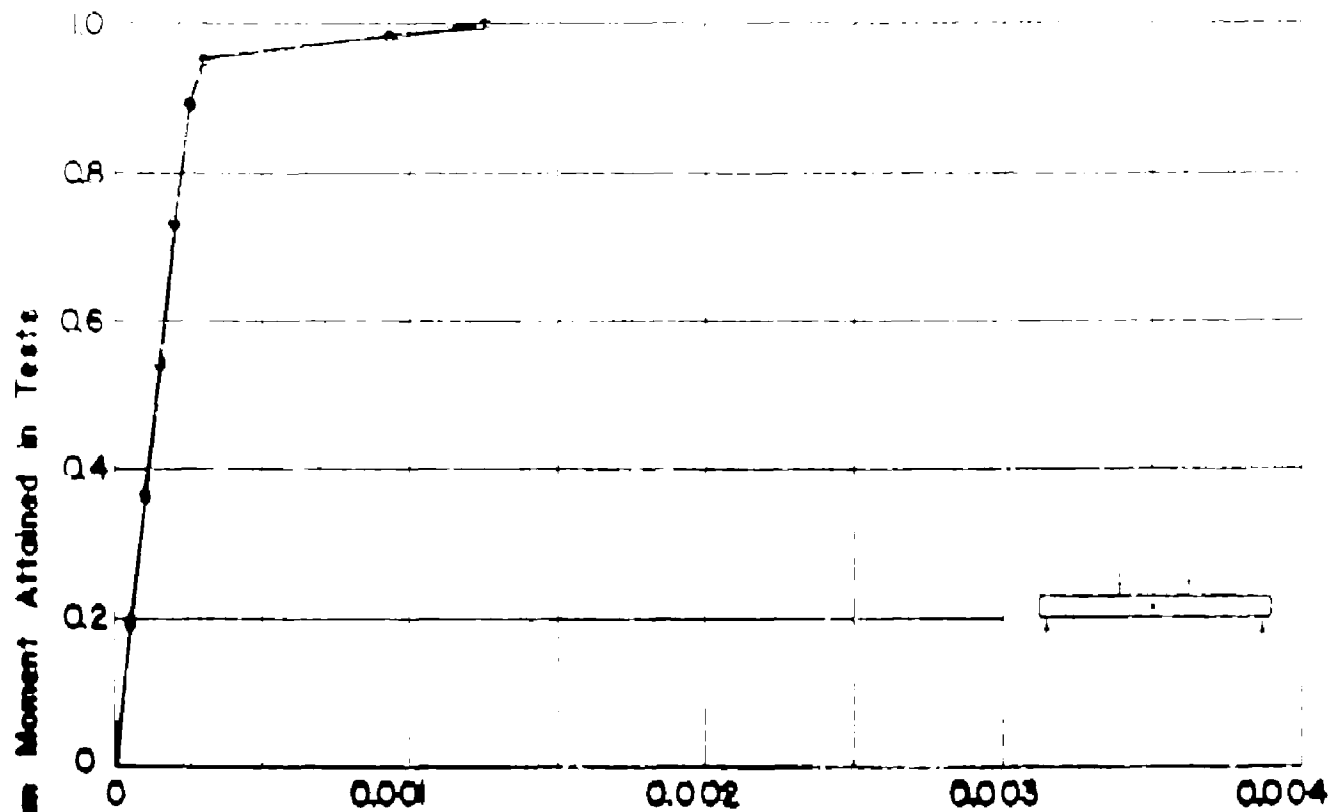

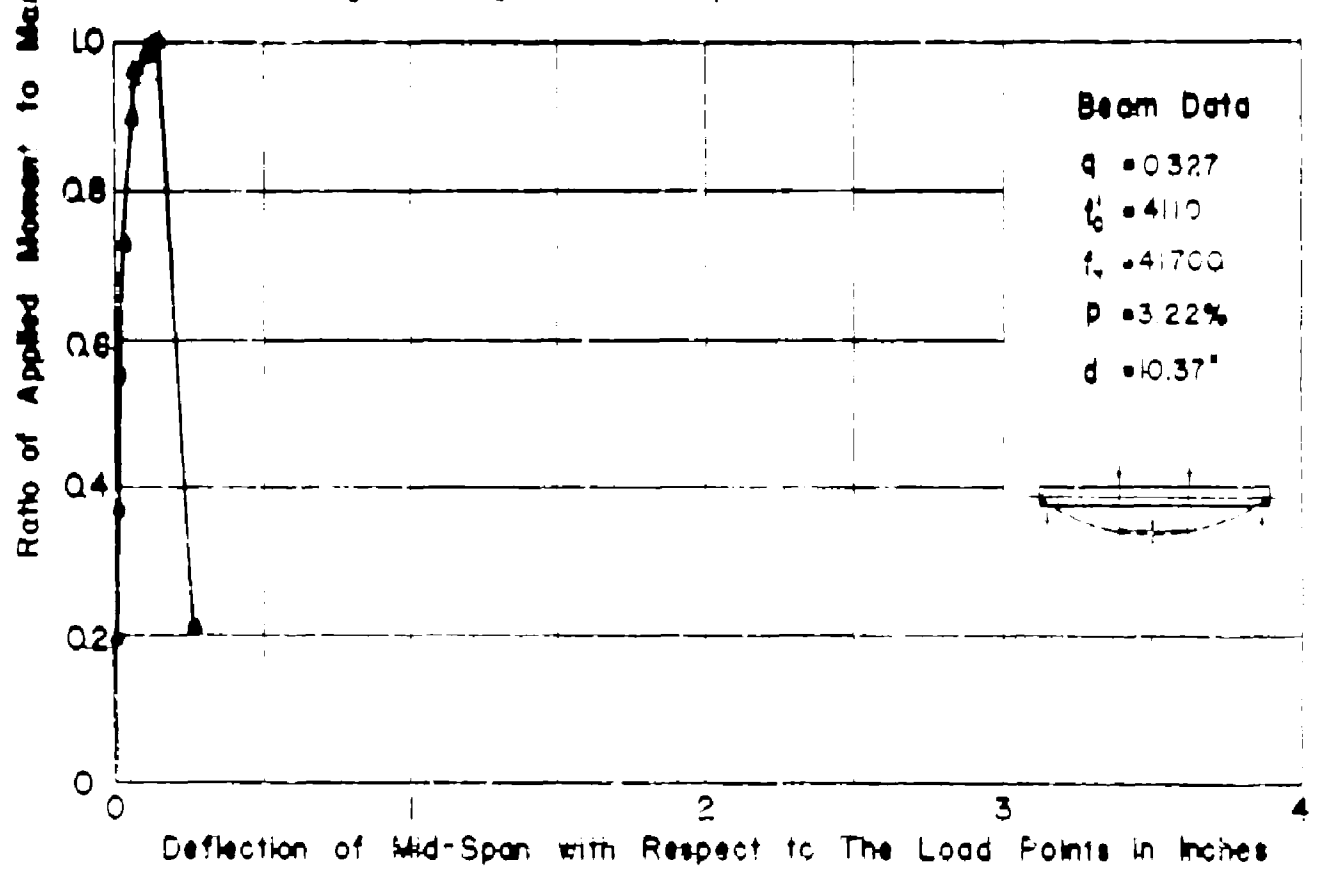

APP FIG147 MOMENT RATIO VS. PURE MOMENT DEFORMATIONS FOR BEAM NO. T3Mb

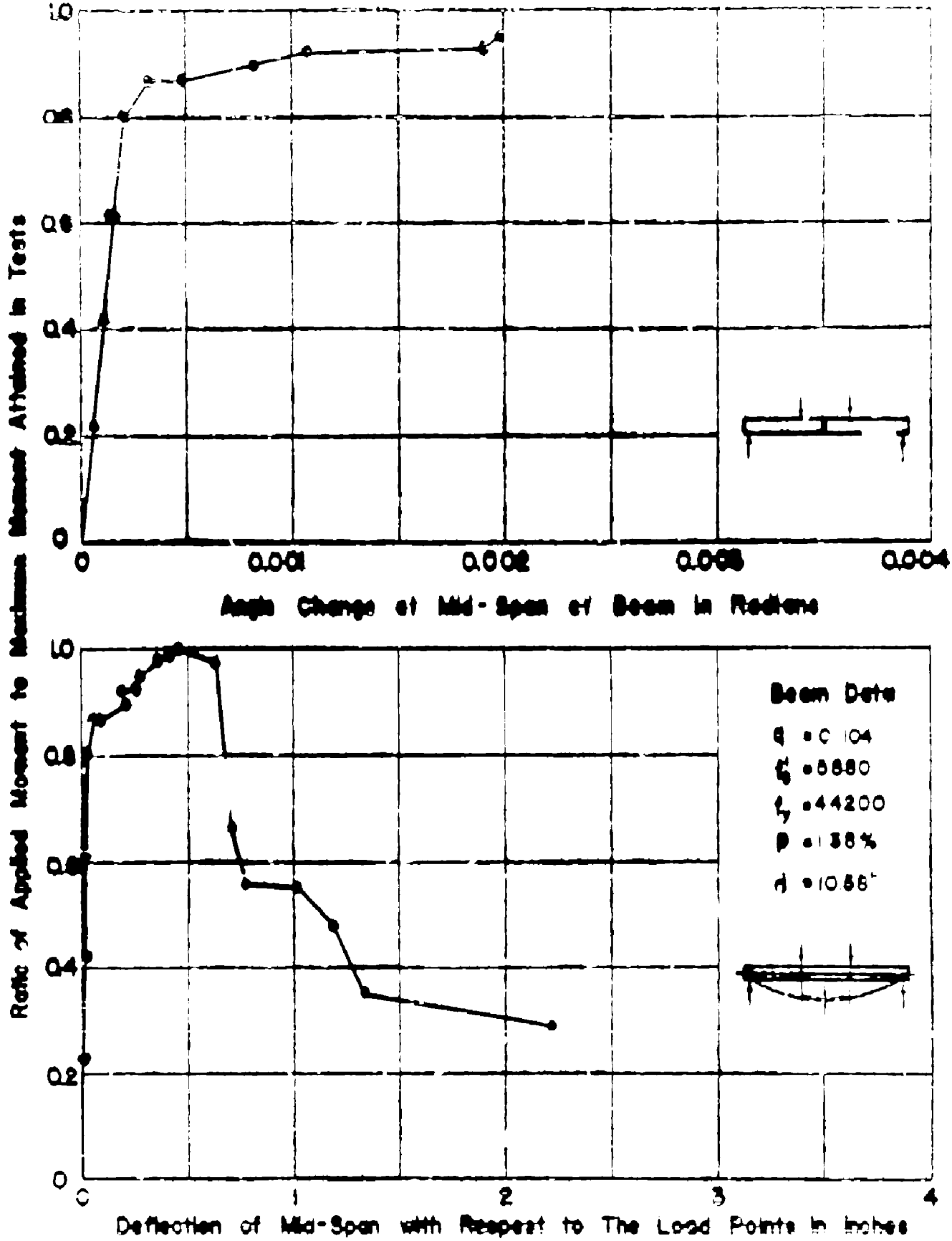

APP FIG.148 MOMENT RATIO VS. PURE MOMENT DEFORMATIONS FOR BEAM NO. T1H2

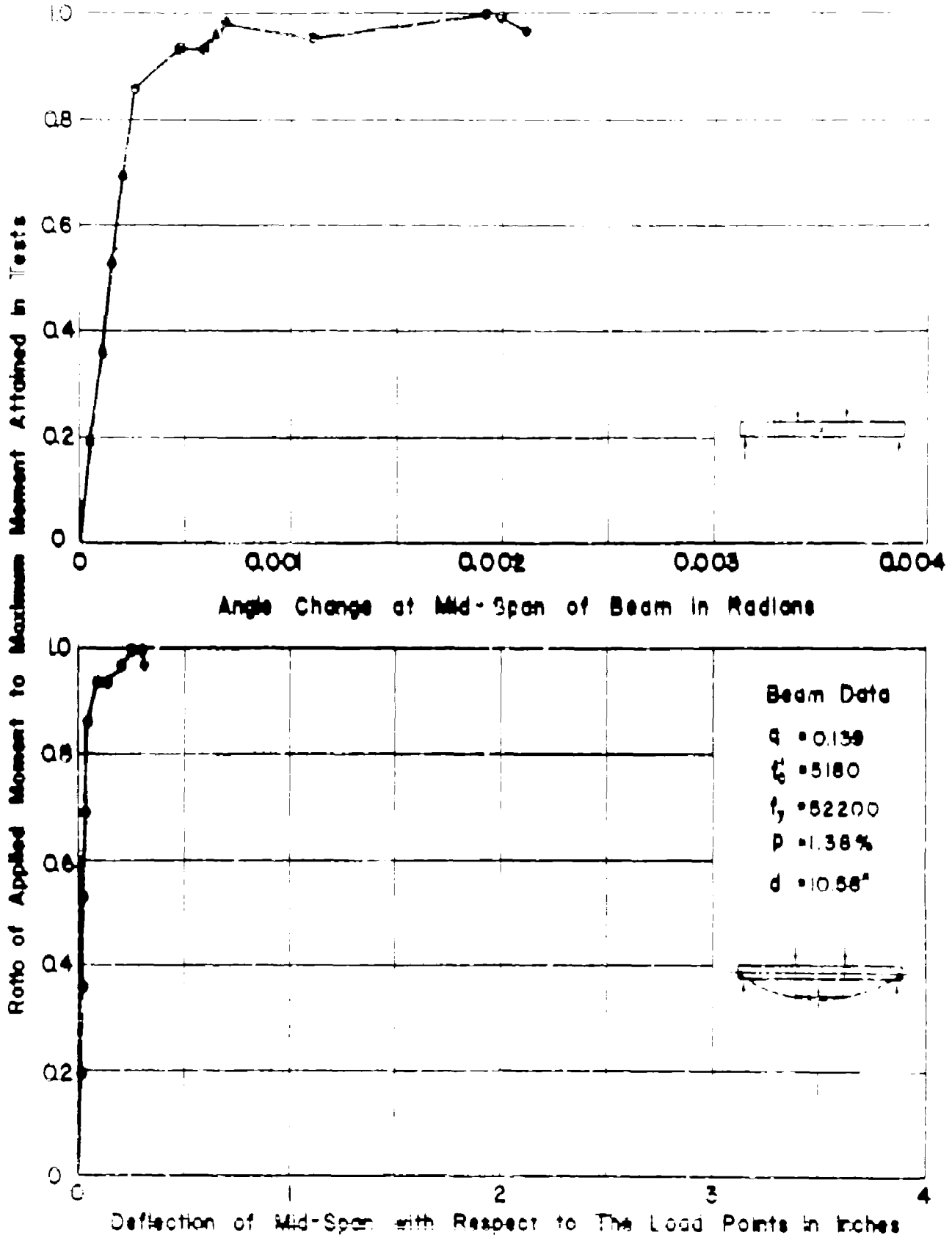

APP. FIG. 14S MOMENT RATIO VS. PURE MOMENT DEFORMATIONS FOR BEAM NO. T1Hb

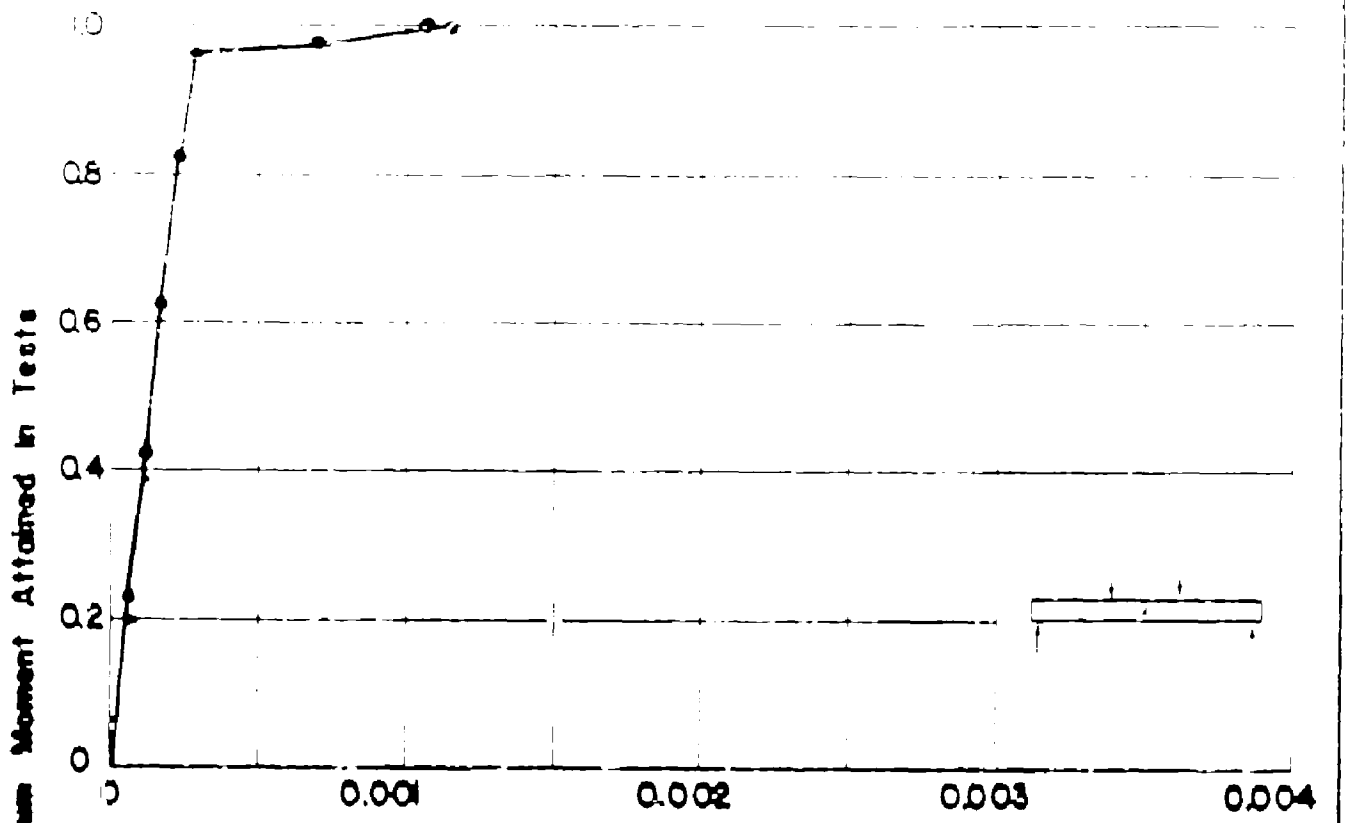

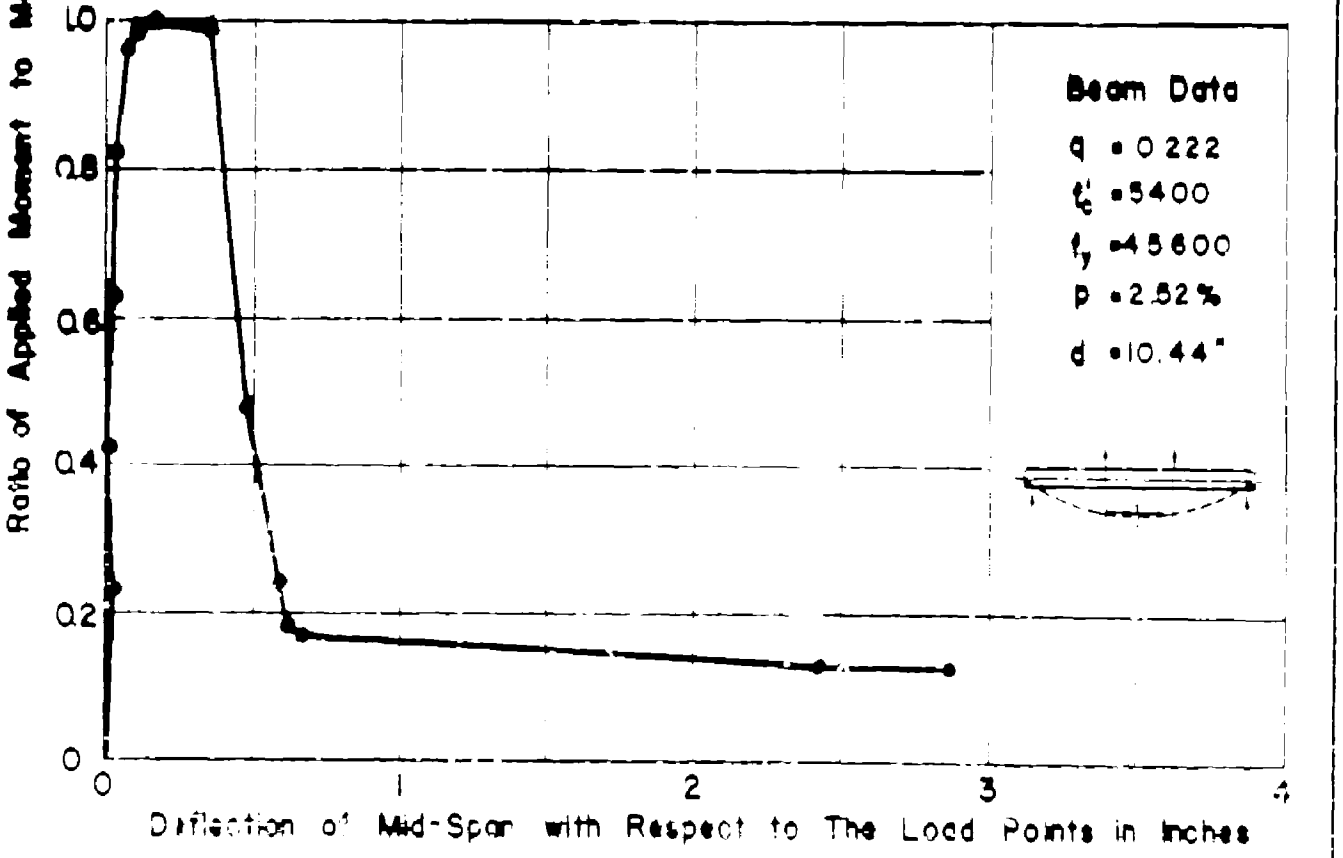

APP. FIG 150 MOMENT RATIO VS. PURE MOMENT DEFORMATIONS FOR BEAM NO. T2H

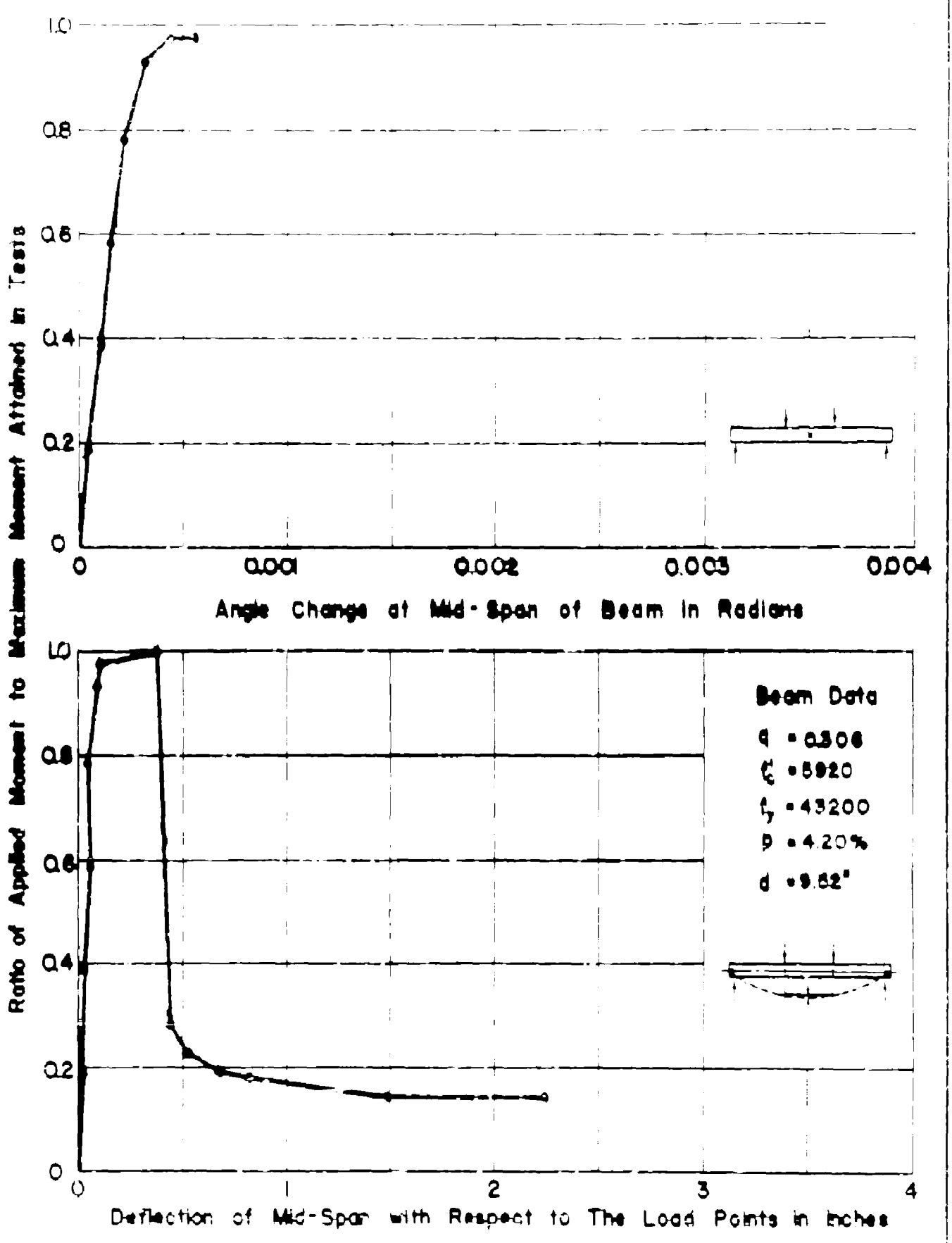

APP FIG 151 MOMENT RATIO VS. PURE MOMENT DEFORMATIONS FOR BEAM NO T3H

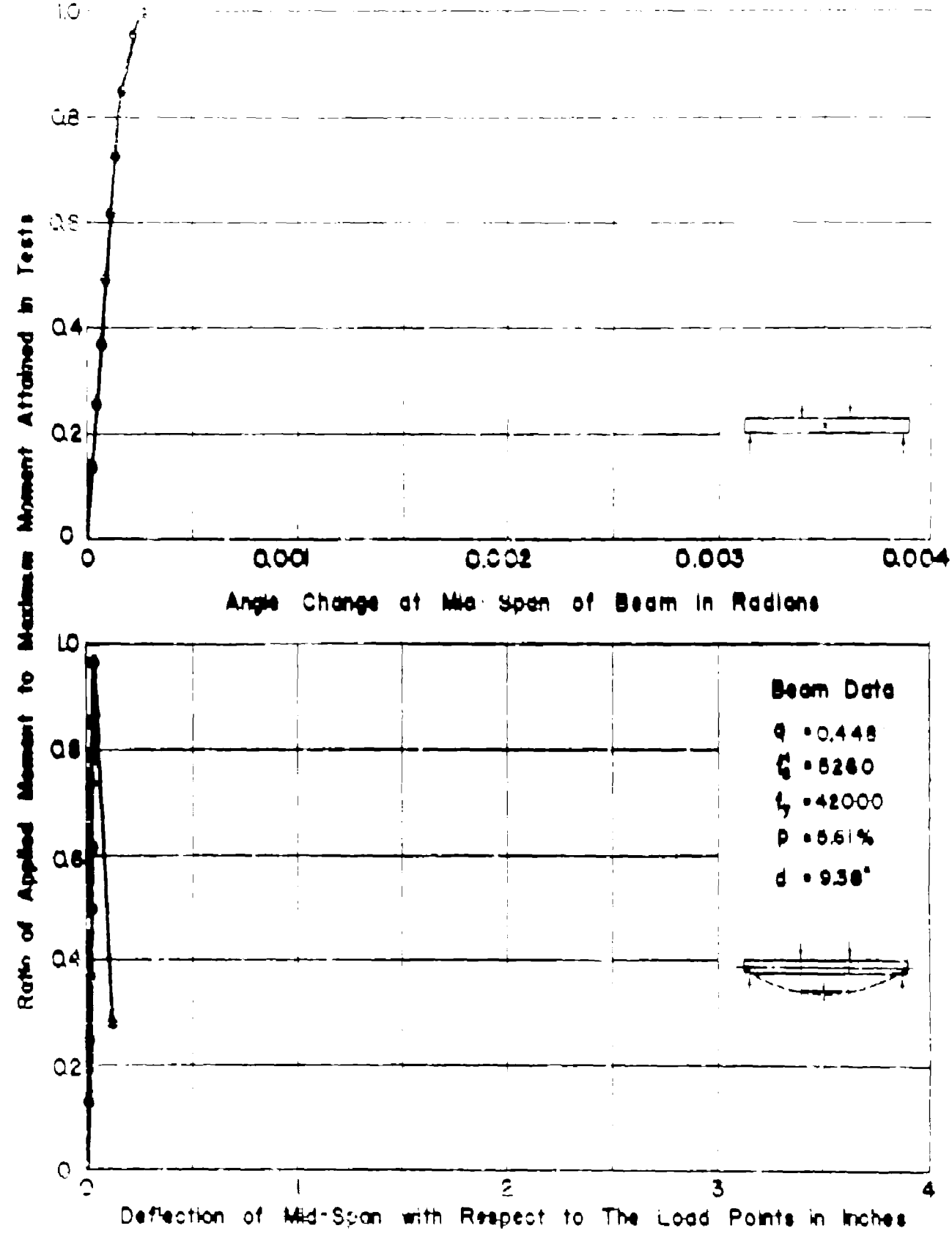

APP. FIG. 152 MOMENT RATIC VS. PURE MOMENT DEFORMATIONS FOR BEAM NO T4H

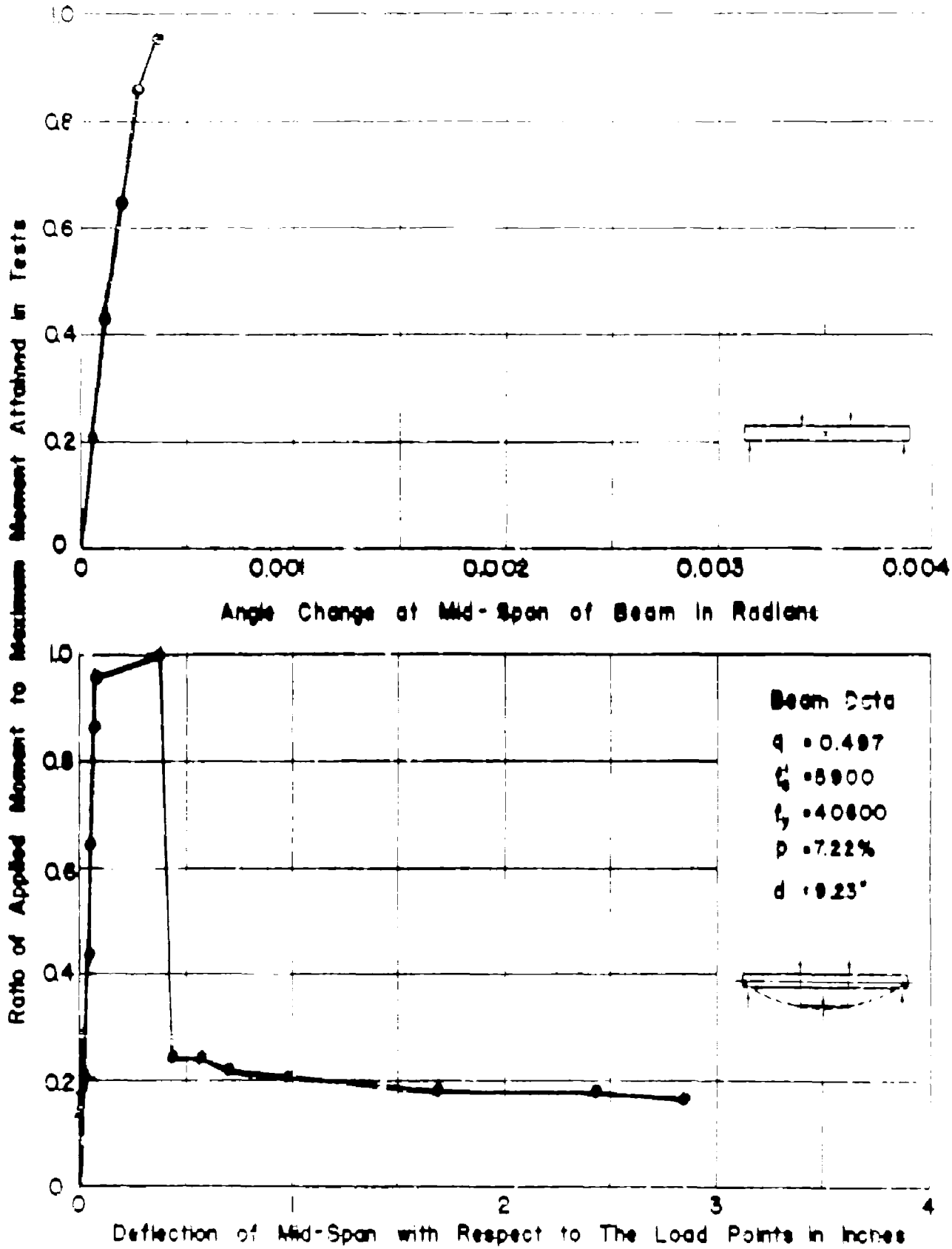

APP. FIG. 153 MOMENT RATIO VS. PURE MOMENT DEFORMATIONS FOR BEAM NO. T5H

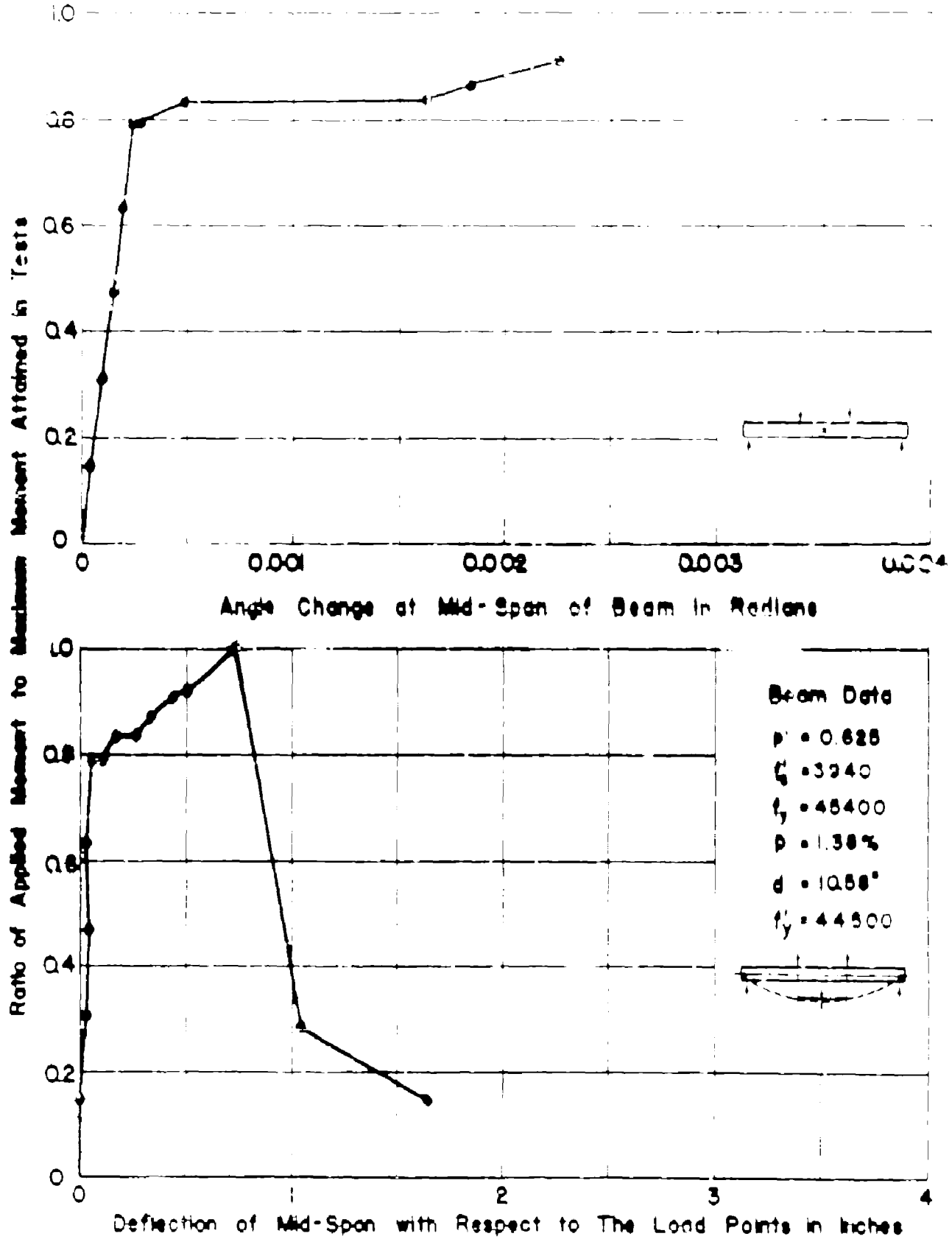

APP. FIG. 154 MOMENT RATIO VS. PURE MOMENT DEFORMATIONS FOR BEAM NO. C2W

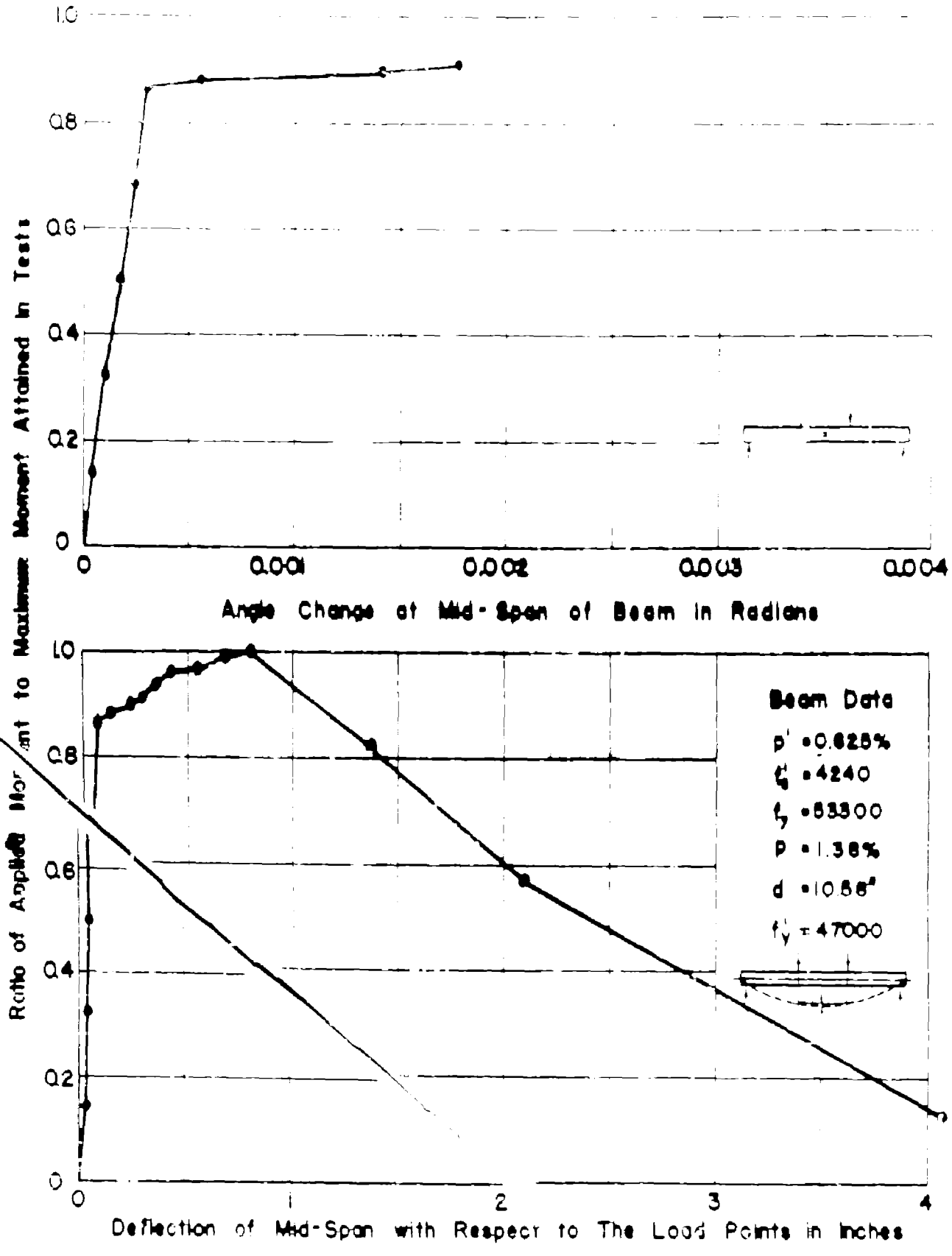

APP. FIG. 155 MOMENT RATIO VS. PURE MOMENT DEFORMATIONS FOR BEAM NO. 2xm

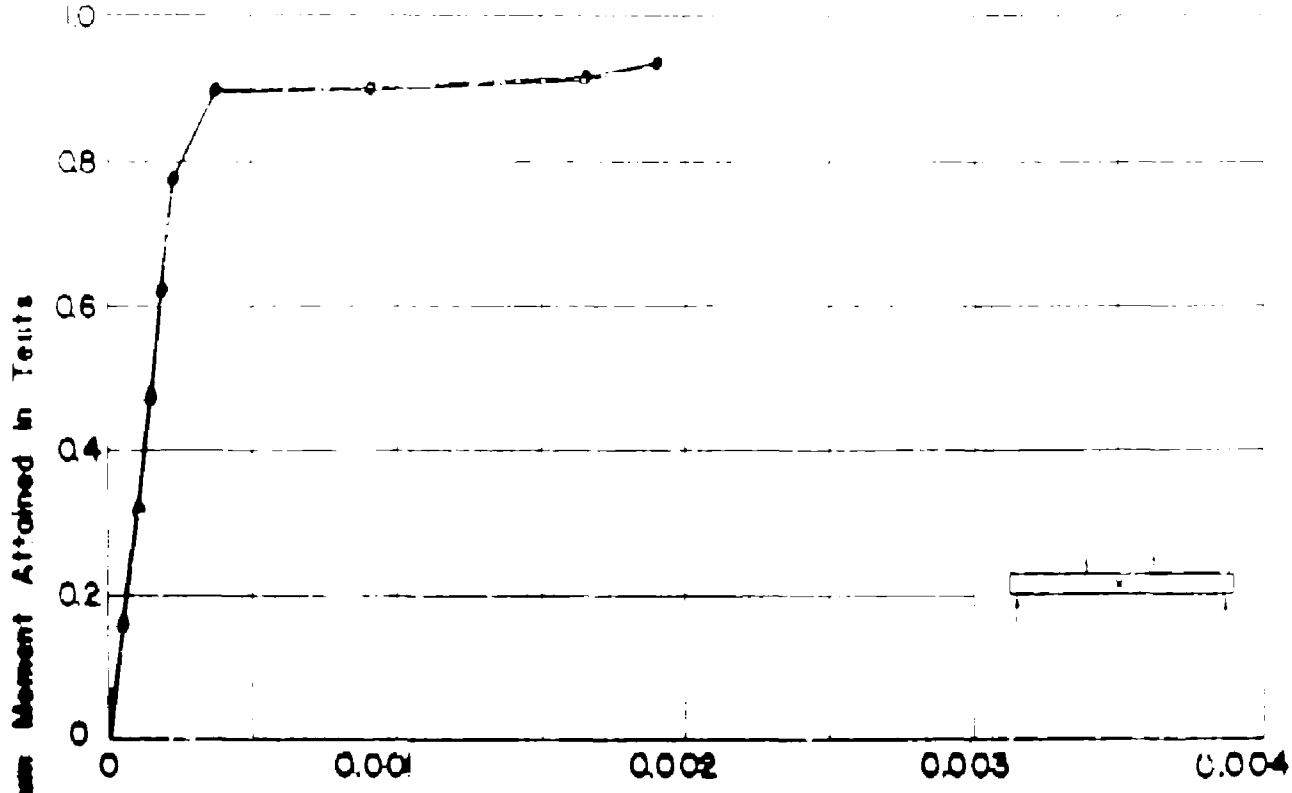

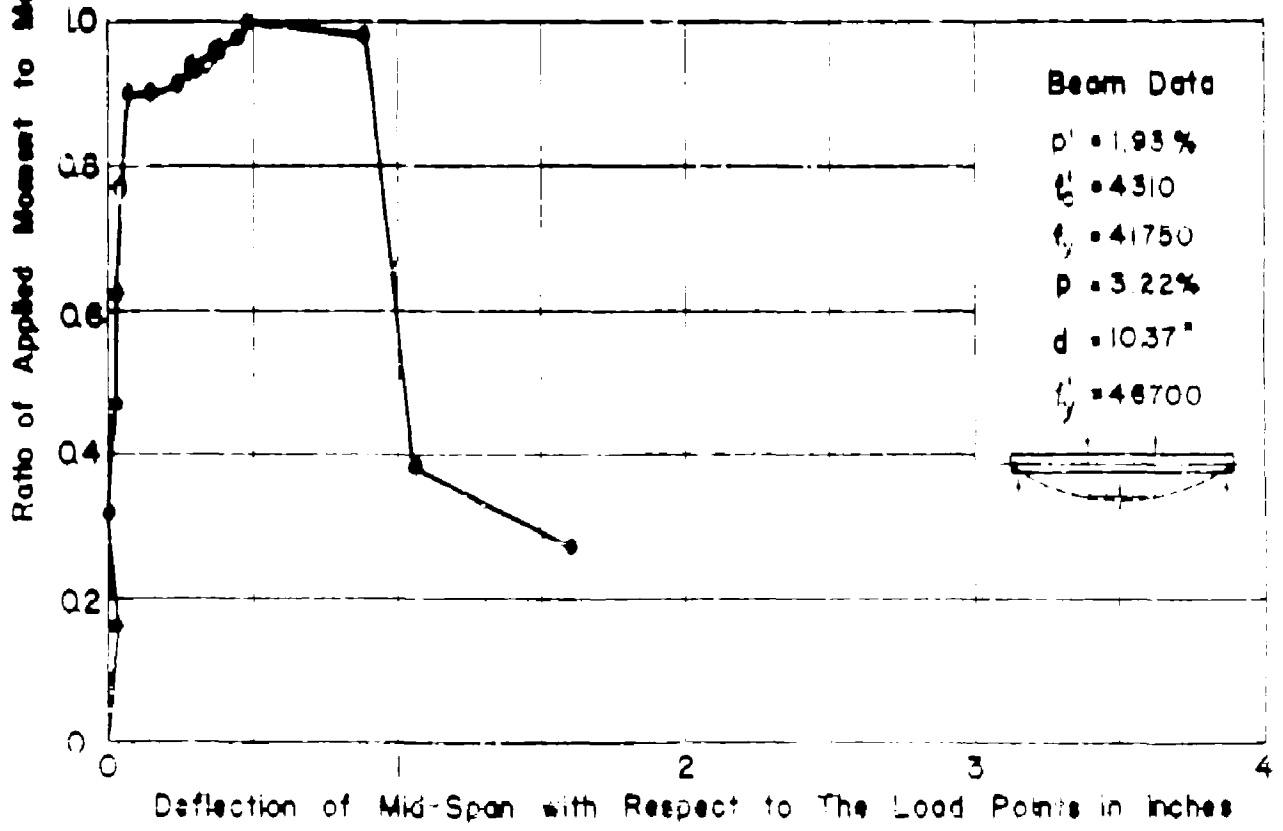

APP. FIG. 156 MOMENT RATIO VS. PURE MOMENT DEFORMATIONS FOR BEAM NO. 3W

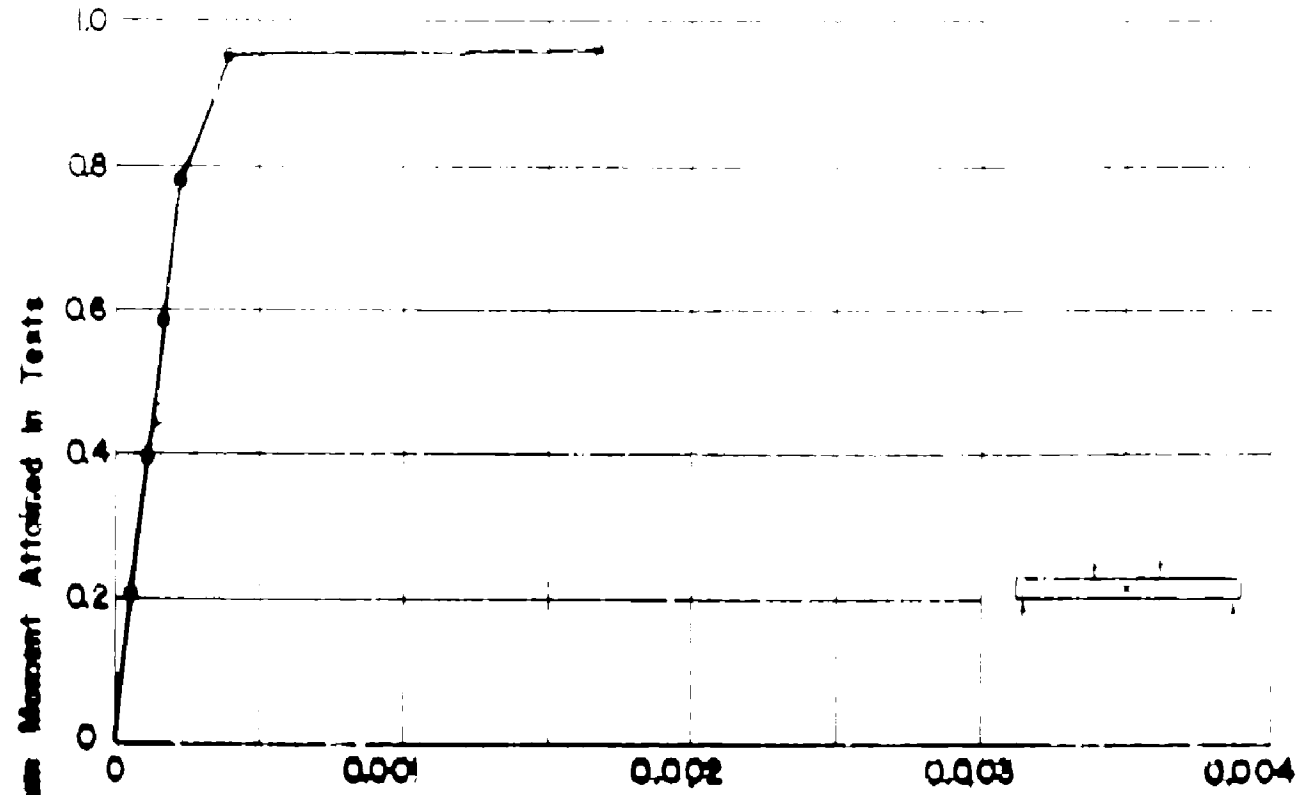

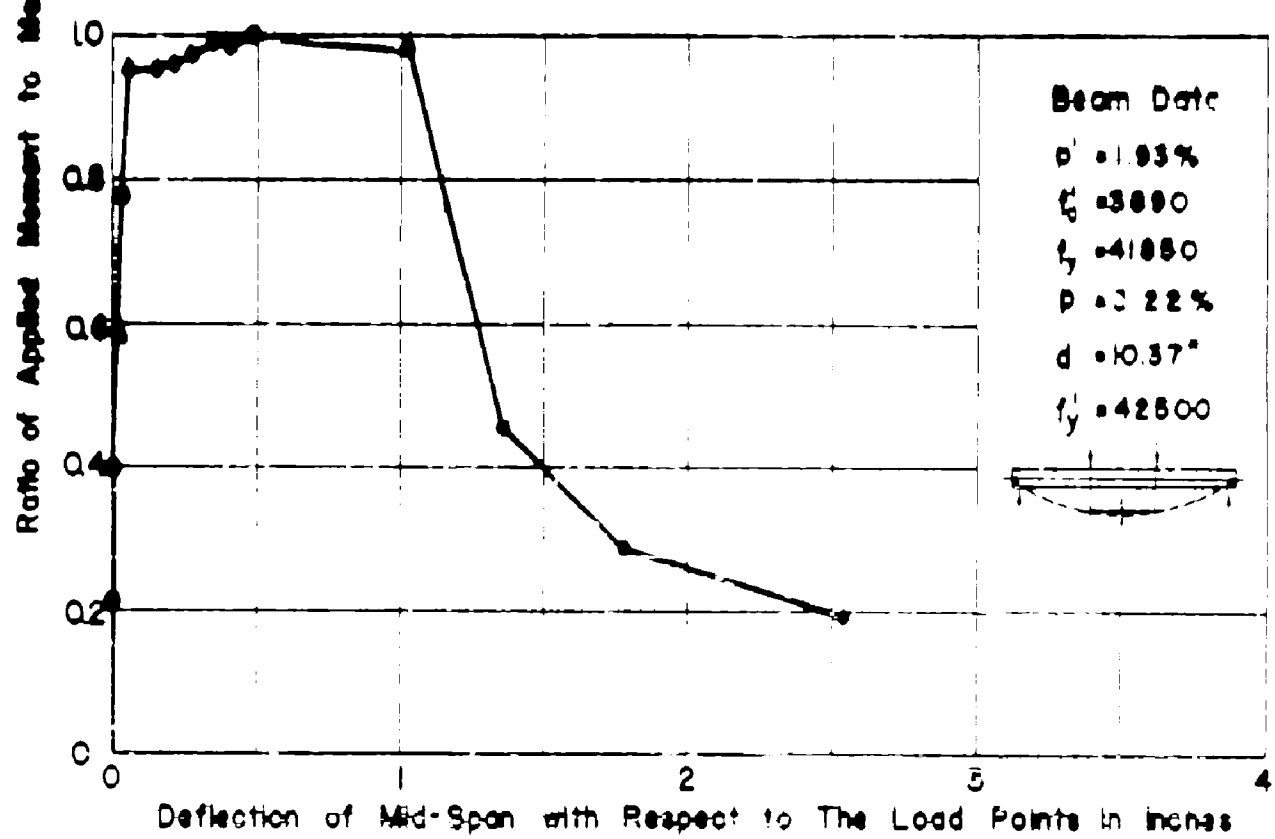

APP. FIG. 157 MOMENT RATIO VS. PURE MOMENT

DEFORMATIONS FOR BEAM NO. 3xm

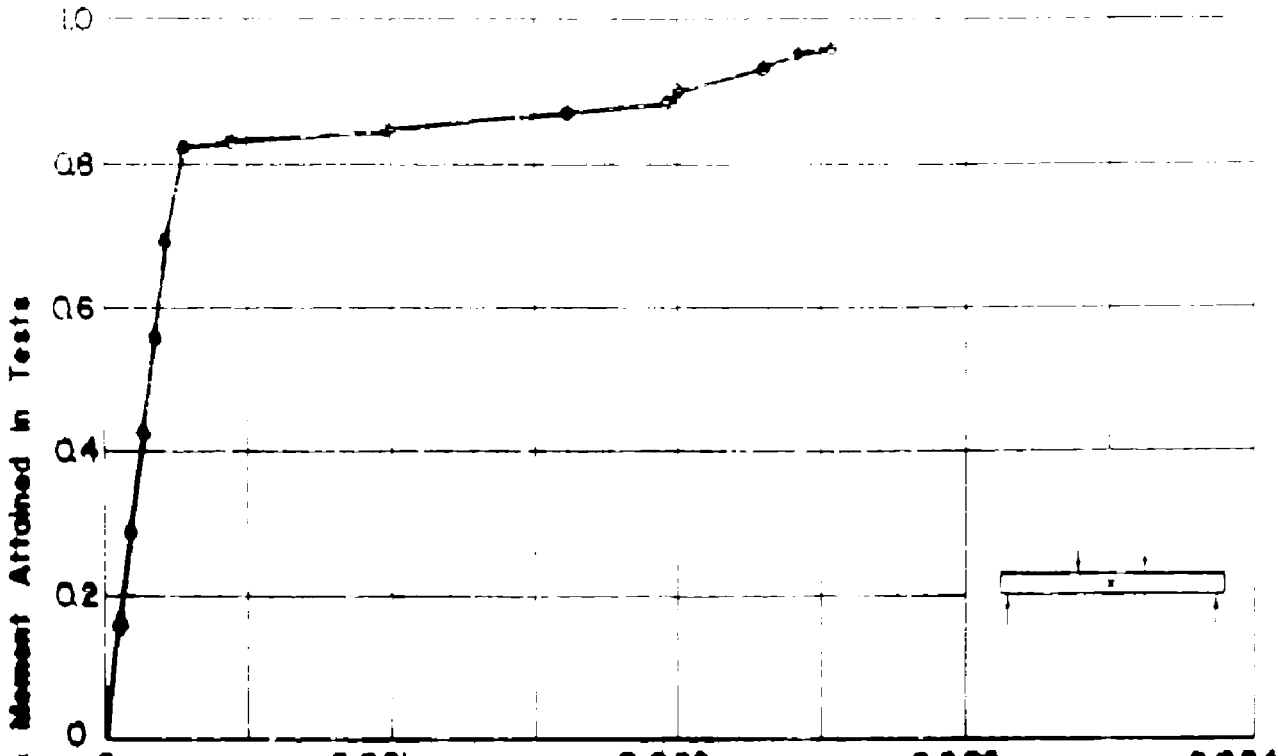

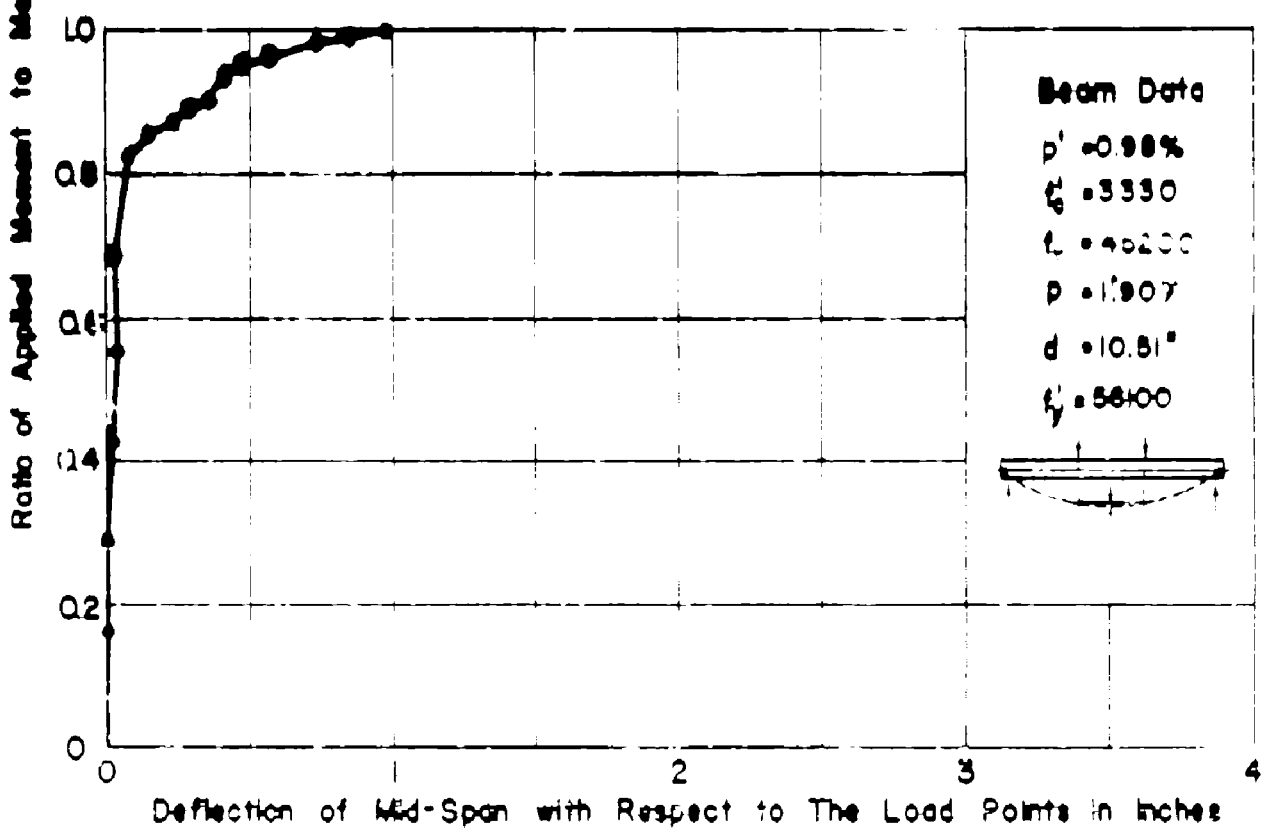

APP. FIG. 158 MOMENT RATIO VS. PURE MOMENT DEFORMATIONS FOR BEAM NQC3yna

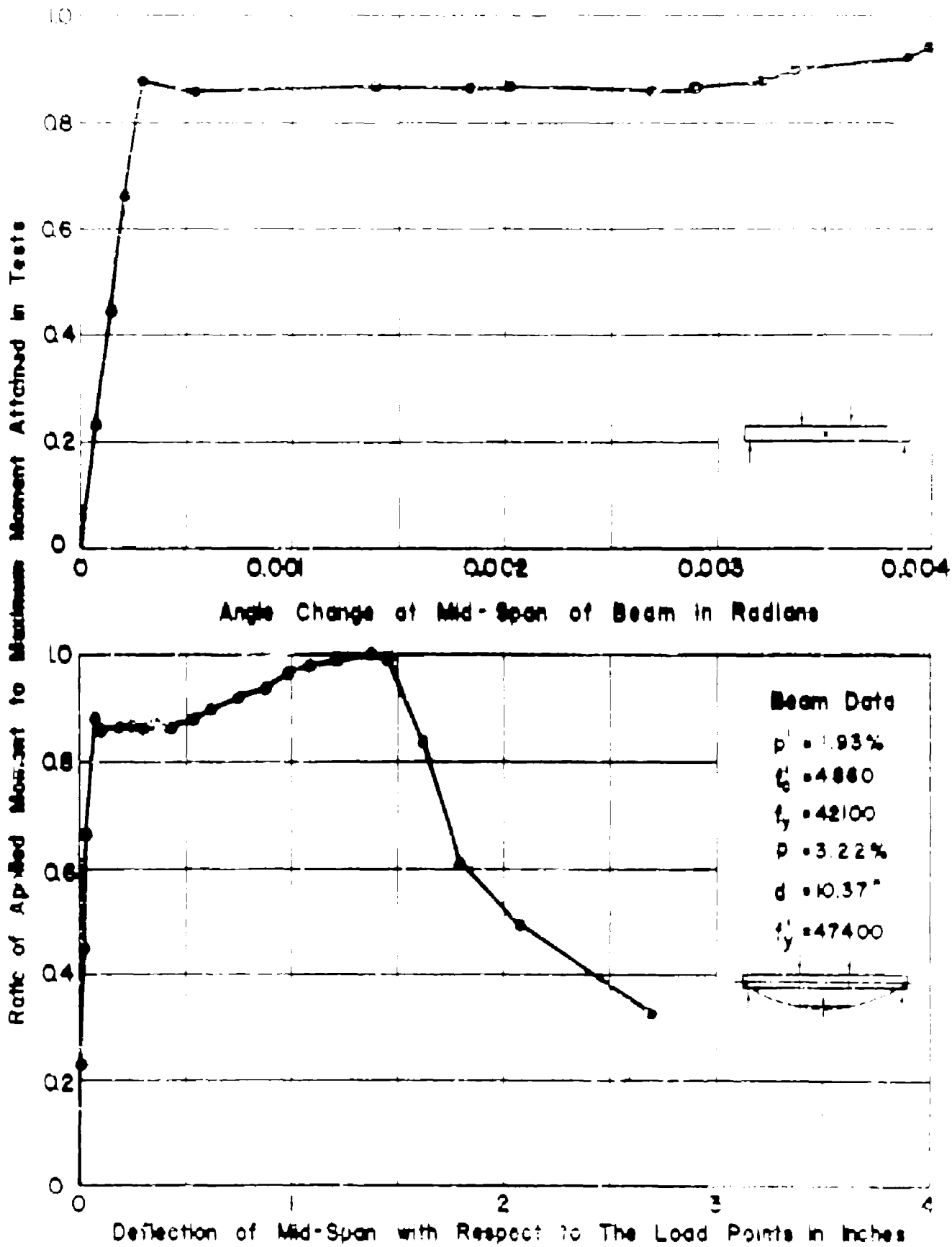

APP. FIG 159 MOMENT RATIO VS. PURE MOMENT DEFORMATIONS FOR BEAM NO.C3ynb

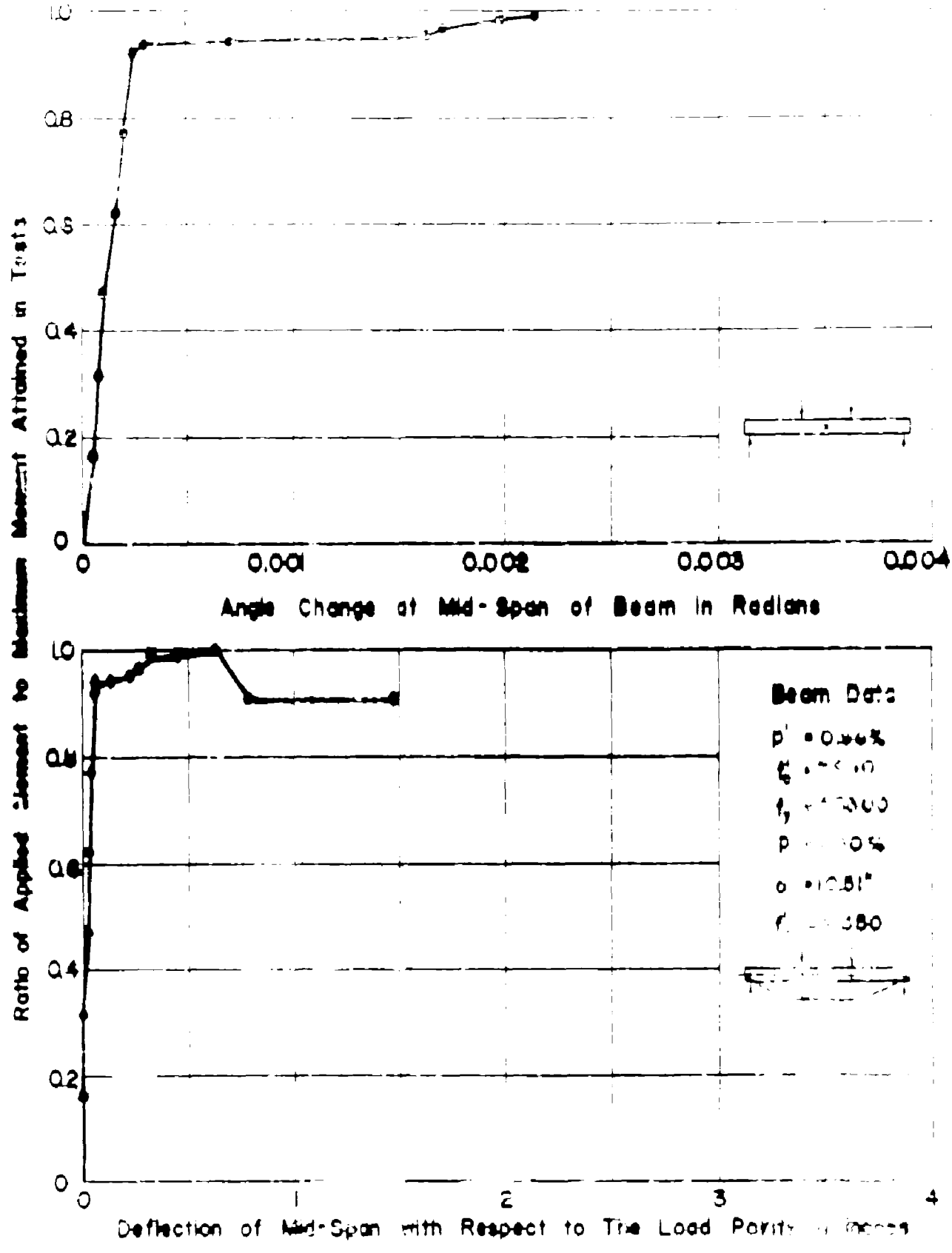

APP. FIG. 160 MOMENT RATIO VS. PURE MOMENT DEFORMATIONS FOR BEAM NO. C-4x[illegible]

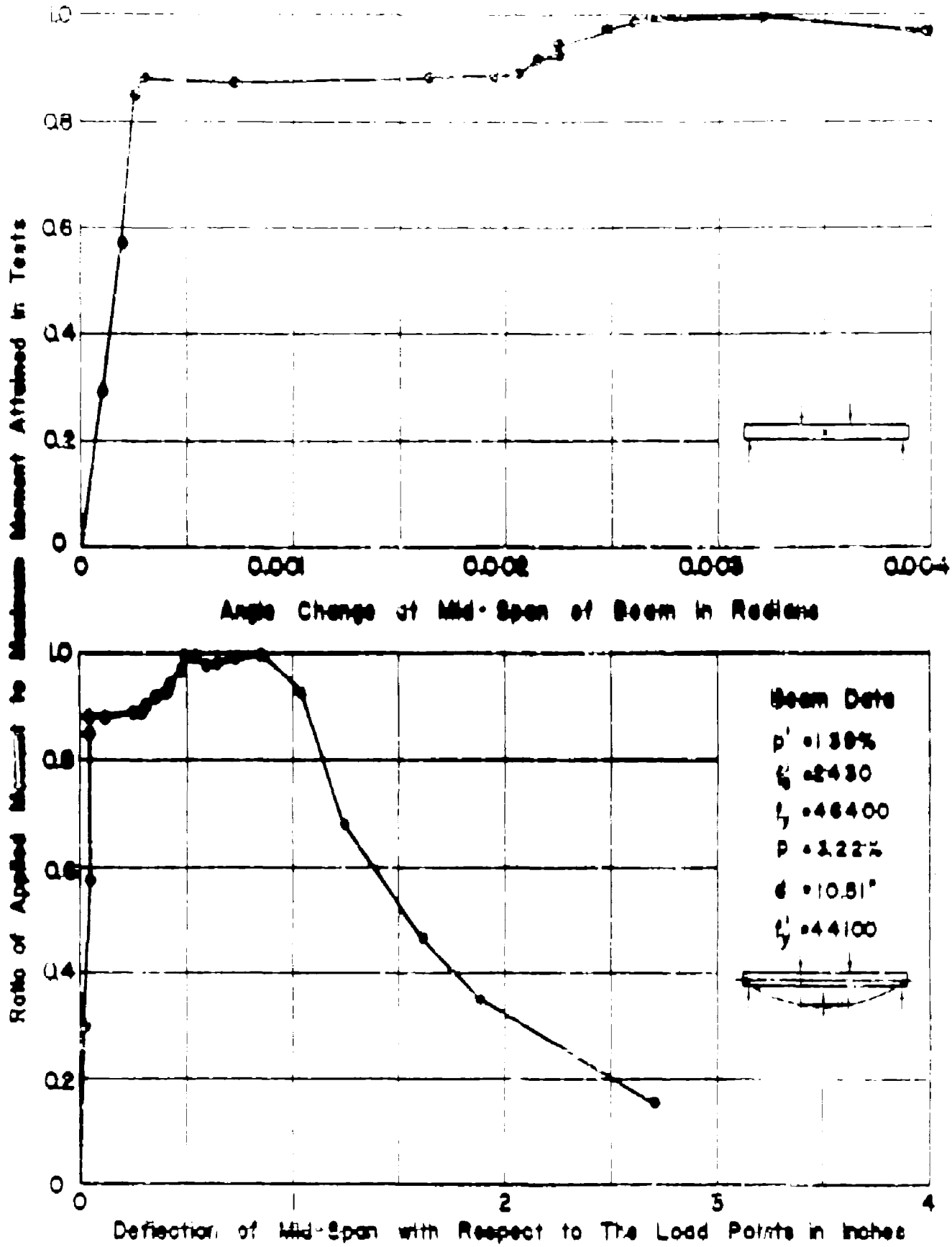

APP. FIG. 161 MOMENT RATIO VS. PURE MOMENT DEFORMATIONS FOR BEAM NO. 4xnb

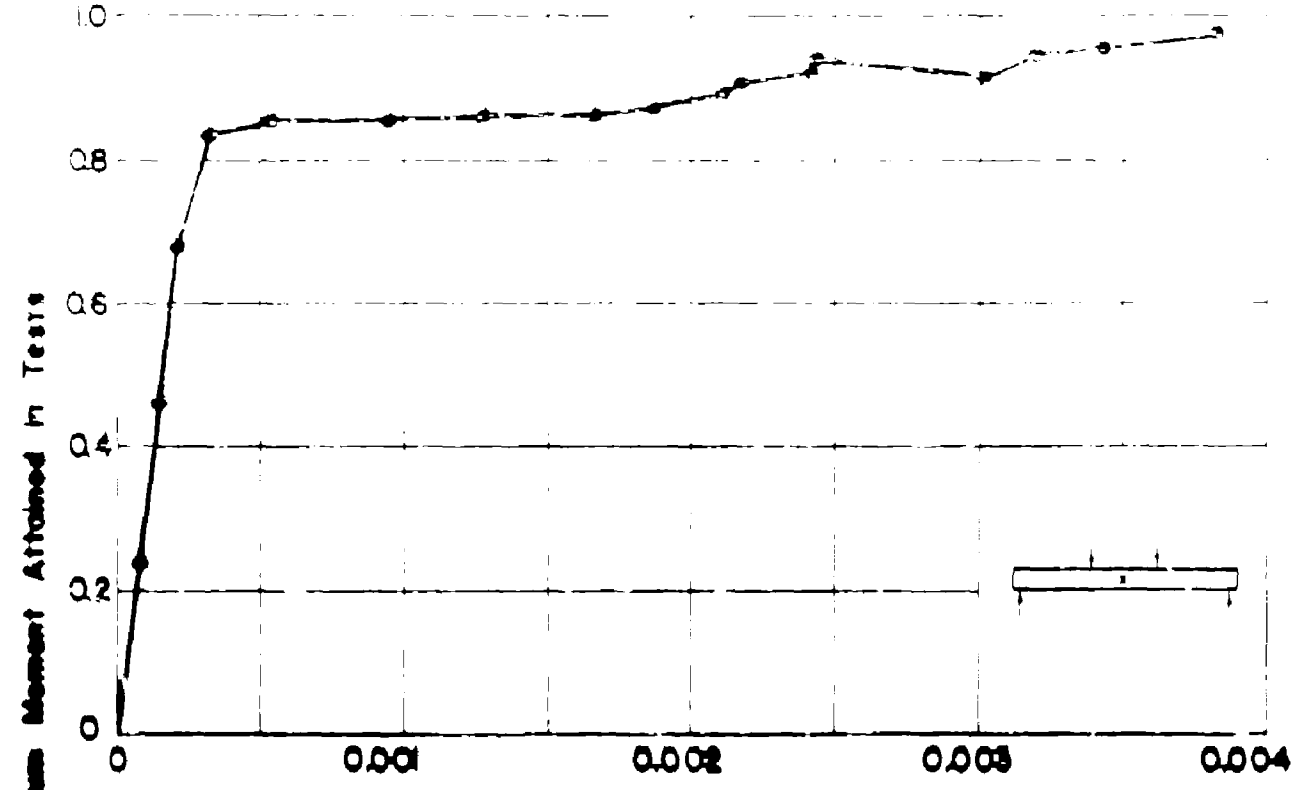

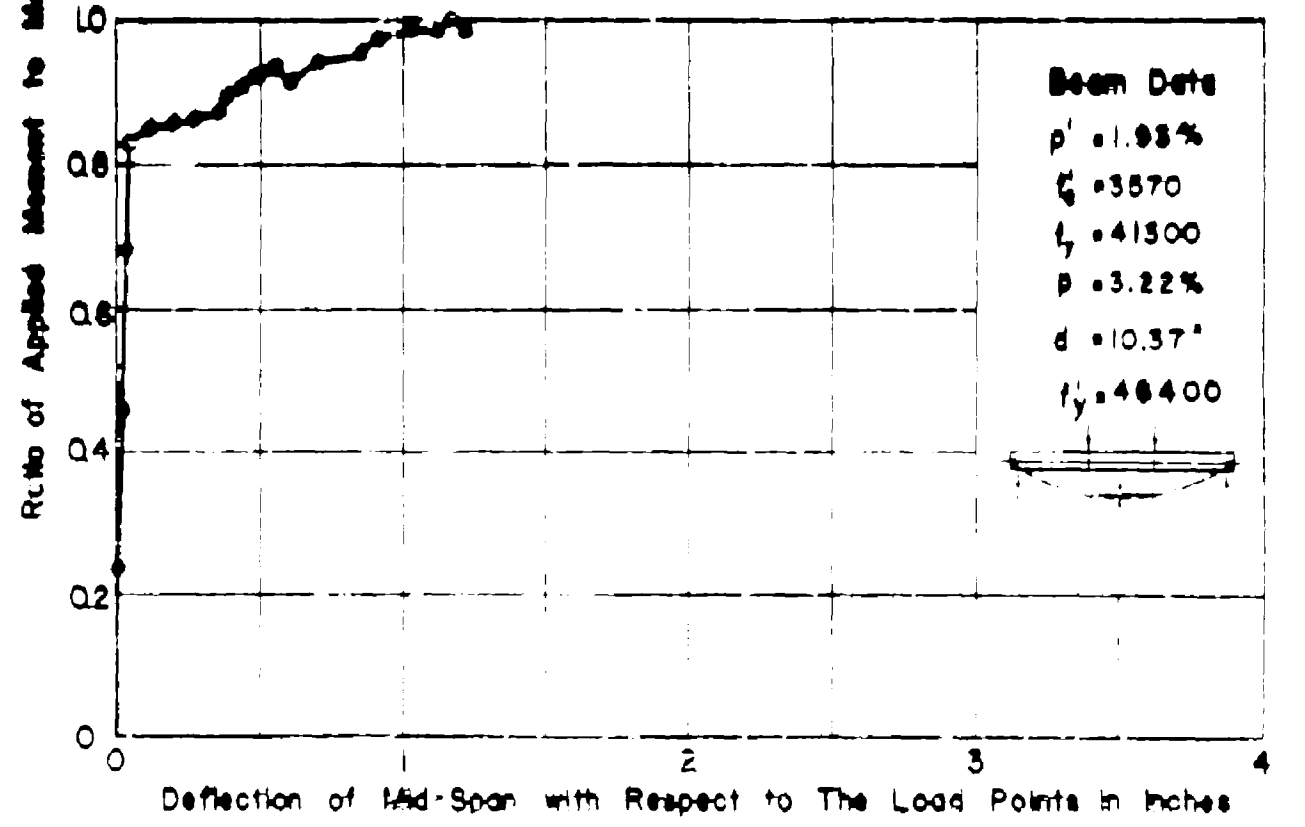

APP. FIG. 162 MOMENT RATIO VS. PURE MOMENT DEFORMATIONS FOR BEAM NO. C4zn

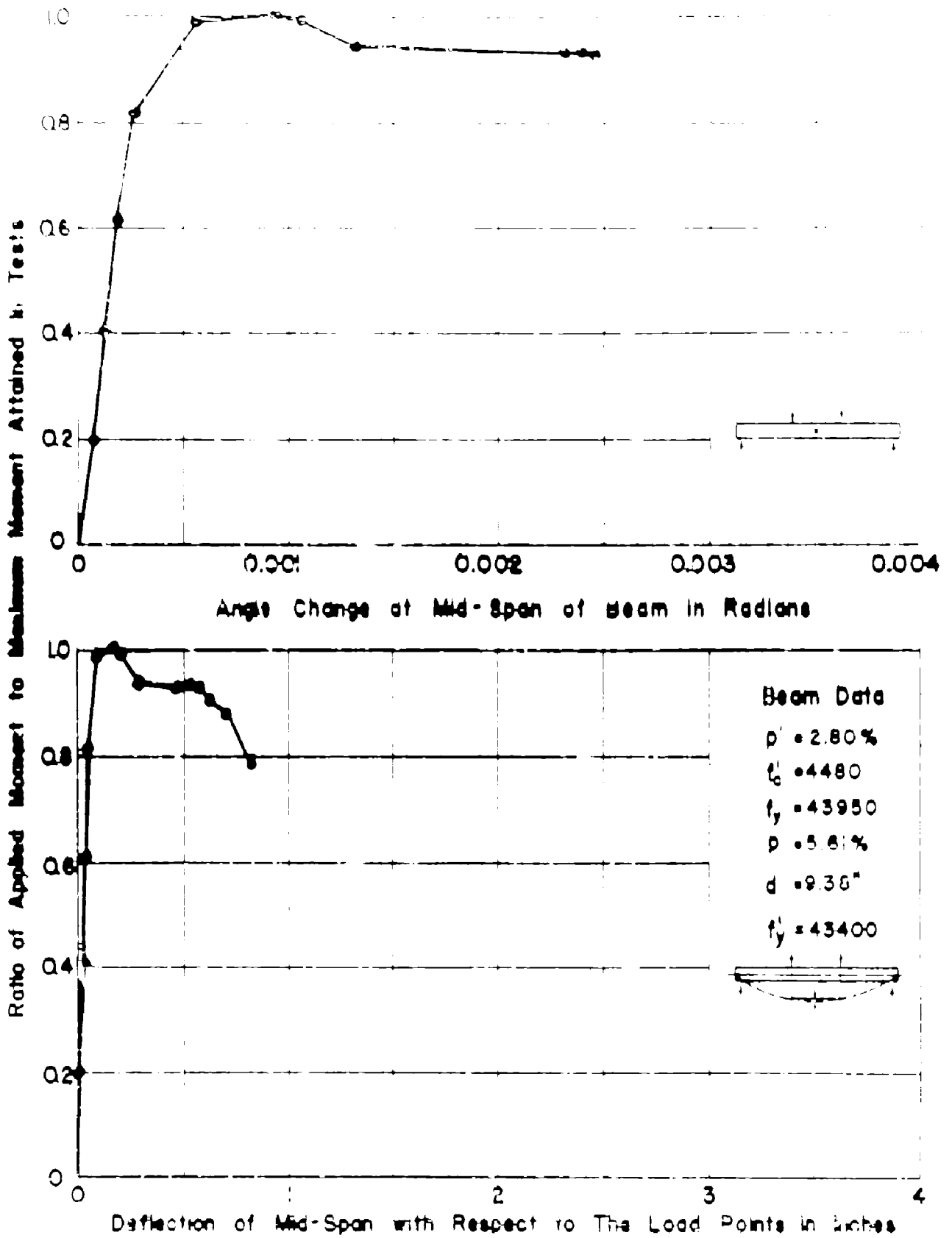

APP. FIG. 163 MOMENT RATIO VS. PURE MOMENT DEFORMATIONS FOR BEAM NO. C5yn

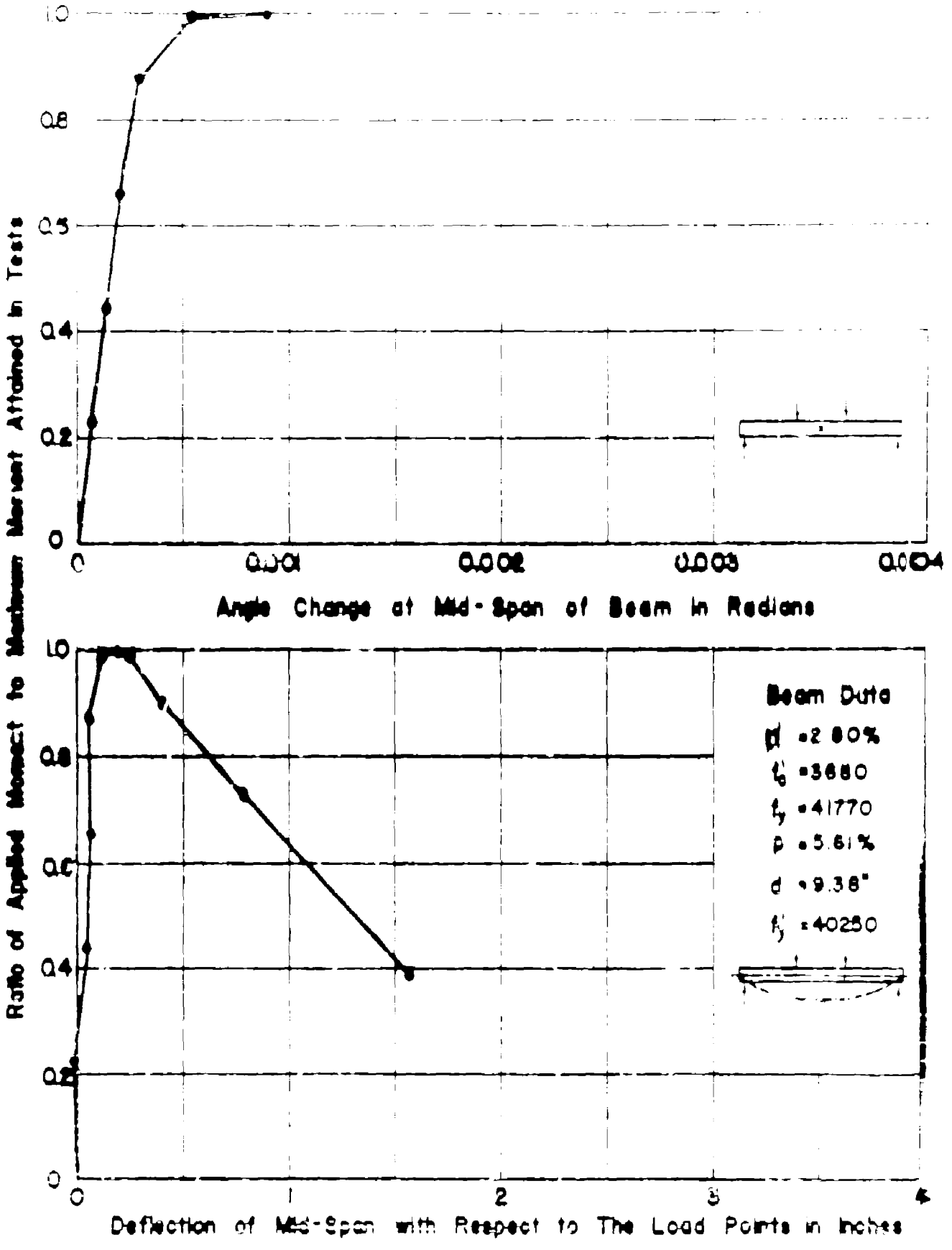

APP. FIG. 164 MOMENT RATIO VS. PURE MOMENT DEFORMATIONS FOR BEAM NQC6xm

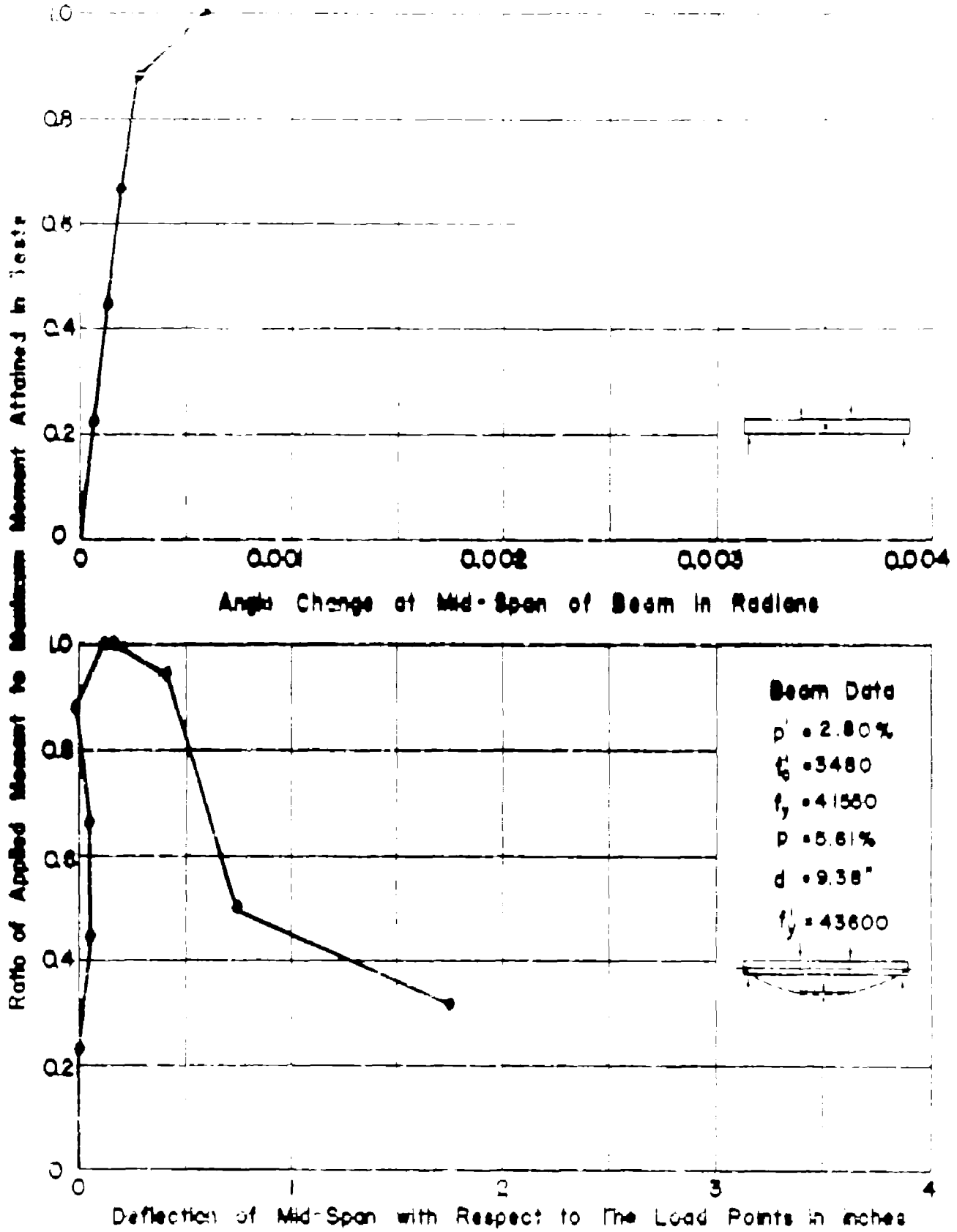

APP FIG. 165 MOMENT RATIO VS. PURE MOMENT DEFORMATIONS FOR BEAM NQC7w

DISTRIBUTION LIST

ARMY:

The Assistant Chief of Staff, G-4
Department of the Army
Washington 25, D. C. (1)

Chief of Engineers
Department of the Army
Washington 25, D. C.
ATTN: Military Construction Div. (1)

Chief of Engineers
Department of the Army
Washington 25, D. C.
ATTN: Structural Br. Civil Works (1)

Chief of Army Field Forces
Fort Monroe, Virginia (1)

Commanding Officer, Frankfort Arsenal
Bridesburg Station
Philadelphia 37, Pennsylvania
ATTN: Laboratory Division (1)

Chief of Ordnance
Department of the Army
Washington 25, D. C.
ATTN: Technical Reference Unit (1)

Director, Operations Research Office
6410 Connecticut Avenue
Chevy Chase, Maryland
ATTN: Technical Library (1)

Chief of Ordnance, Department of Army
R and D Division
Washington 25, D. C.
ATTN: ORDTB-AE (1)

Commanding Officer, Ballistics
Research Laboratory
Aberdeen Proving Ground
Aberdeen, Maryland
ATTN: Dr. C. W. Lampson (1)

Chief of Engineers
Department of the Army
Washington 25, D. C. (1)
ATTN: Engineer Research and Dev. Div.

Commanding General, Army Chemical
Center, Maryland
ATTN: Technical Command (1)

Director, Waterways Experiment St.
Box 631
Vicksburg, Mississippi (1)

Commanding Officer, Watertown Arsenal
Watertown 72, Massachusetts
ATTN: Laboratory Division (1)

NAVY:

Chief of Naval Operations
Department of the Navy
Washington 25, D. C.
ATTN: Op-36 (1)

Commandant, U.S. Coast Guard
1800 E Street, N.W.
Washington D. C.
ATTN: Chief, Testing and Dev. Div. (1)

Commanding Officer
U. S. Naval Radiological Defense Lab
San Francisco 24, California (1)

Chief of Naval Operations
Department of the Navy
Washington 25, D. C.
ATTN: Dr. J. Steinhardt, Operational
Readiness Division (1)

Chief, Bureau of Ships
Department of the Navy
Washington 25, D. C.
CODE: 432 (1)

Commander Operational Dev. Force
U. S. Atlantic Fleet
U. S. Naval Base
Norfolk 11, Virginia (1)

Commandant, Marine Corps Schools
Quantico, Virginia
ATTN: Marine Corps Dev. Center (1)

Director
U. S. Naval Research Laboratory
Washington 25, D. C.
ATTN: Mechanics Division
Code 3805 (1)

NAVY: (Cont'd)

Chief, Bureau of Ordnance
Department of the Navy
Washington, D. C. (1)

Commander, Naval Ordnance Test St.
Inyokern, China Lake, California
ATTN: Code 501 (1)

Commanding Officer and Director
David W. Taylor Model Basin
Washington 7, D. C.
ATTN: Structural Mechanics Div. (1)

Commander, U.S.Naval Ord. Lab
White Oak, Silver Spring 19, Md.
ATTN: Dr. C. J. Aronson (1)

Commanding Officer, U. S. Naval
Civil Engineering Research and
Evaluation Laboratory
U. S. Naval Construction Batt.
Center
Port Hueneme, California (1)

Commanding Officer and Director
U. S. Naval Electronics Lab
San Diego 52, California
ATTN: Dr. A. B. Focke (1)

Commanding Officer and Director
U. S. Naval Eng. Exp. Station
Annapolis, Maryland (1)

U. S. AIR FORCE:

Asst. for Atomic Energy, Headquarters
U. S. Air Force
Washington 25, D. C. (1)

Commanding General, Air Mat'l Command
Wright-Patterson Air Force Base
Dayton, Ohio
ATTN: MCREXA-B1 (1)

Commanding General, Strategic Air
Command, Offutt Air Force Base,
Nebraska
ATTN: Directorate of Plans (1)

Commanding General, Air University
Maxwell Air Force Base, Alabama (1)

Commanding Officer
Air Force Cambridge Research Center
230 Albany Street
Cambridge 39, Massachusetts
ATTN: CRUB-1, Geophysical Res. Lab (1)

Commanding General, Wright Air Dev.
Center
Wright-Patterson Air Force Base
Dayton, Ohio, ATTN: WCSSN (1)

Commanding General, Strategic Air Cmd
Offutt Air Force Base, Nebraska
ATTN: Directorate of Intelligence (1)

Deputy Chief of Staff for Dev.
Headquarters, U.S. Air Force
Washington 25, D. C.
ATTN: AFDRD (1)

Commanding General, Wright Air
Dev. Center, Wright-Patterson
Air Force Base, Dayton, Ohio
ATTN: FRL (1)

Commanding General, Strategic Air
Command, Offutt Air Force Base,
Nebraska, ATTN Directorate of
Operations (1)

Commanding General, Air Material
Command
Wright-Patterson Air Force Base
Dayton, Ohio, ATTN: MCAIRD (1)

Commanding General, Wright Air
Dev. Center,
Wright-Patterson Air Force Base
Dayton, Ohio
ATTN: Eng. Div., Mat'ls Lab (1)

Commanding General, Air Proving Grd.
Eglin Air Force Base, Florida
ATTN: Deputy for Operations (1)

Commanding General, Air Force Special
Weapons Center, A.R.D.C.
Kirtland Air Force Base, New Mexico
ATTN: Research and Development (1)

U. S. AIR FORCE: (Cont'd)

Director of Intelligence
Headquarters, U.S. Air Force
Washington 25, D. C.
ATTN: Air Targets Div., Physical Vulnerability Branch (1)

Director of Research and Development
Headquarters, U.S. Air Force
Washington 25, D. C.
ATTN: Chief, Research Division (1)

Commanding General, Air Res. and Dev. Command
P.O. Box 1395
Baltimore 3, Maryland
ATTN: RDDN (1)

A.S.T.I.A. - Document Service Center
U B Building
Dayton 2, Ohio
ATTN: DSC-SA (1)

OTHERS.

Commanding General, Field Command
Armed Forces Special Weapons Project
P. O. Box 5100
Albuquerque, New Mexico (2)

The Assistant for Civil Defense Liaison
Office of the Sec'y of Defense
Washington 25, D. C. (2)

Executive Secretary, Military Liaison Committee
U. S. Atomic Energy Commission
Washington 25, D. C. (1)

Dr. A. C. Graves, Director
J-1 Division
Los Alamos Scientific Laboratory
P. O. Box 1663
Los Alamos, New Mexico (1)

J Division, Los Alamos Scientific Lab
P. O. Box 1663
Los Alamos, New Mexico
ATTN: Lt. Col. F. B. Forzel (1)

Chairman, Res. and Dev. Board
Department of Defense
Washington 25, D. C.

Executive Secretary
Weapons System Evaluation Group
Office of the Sec'y of Defense
Washington 25, D. C.

National Advisory Committee for Aeronautics
1724 F Street, N. W.
Washington, D. C.
ATTN: Mat'ls Res. Coord Group (1)

Director, Division of Research
U.S. Atomic Energy Commission
Washington 25, D. C. (1)

Executive Director, Committee on Atomic Energy, Research and Dev. Board
Washington 25, D. C.
ATTN: Mr. David Beckler (1)

Director, Div. of Military Appl.
U. S. Atomic Energy Commission
Washington 25, D. C. (1)

Chairman, Armed Services Explosives Safety Board
Department of Defense, Room 2E073
Barton Hall, Washington 25, D.C. (1)

RAND Corporation, 1500 4th St.
Santa Monica, California
ATTN: Dr. E.H. Plesset (1)

Director
National Bureau of Standards
Washington, D. C.
ATTN: Dr. W.H. Rambarg (1)

Professor B. J. Lazan
Syracuse University
Syracuse, New York (1)

Dr. Otto Laporte
Engineering Research Institute
University of Michigan
Ann Arbor, Michigan (1)

Dr. W. H. Hoppmann
Department of Applied Mechanics
The Johns Hopkins University
Baltimore, Maryland (1)

Dr. L. B. Zoll
Stanford Research Institute
Palo Alto, California (1)

Dr. H. J. Neff
Department of Aeronautical Eng.
and Applied Mechanics
Polytechnic Institute of Brooklyn
99 Livingston Street
Brooklyn, New York (1)

Dr. G. Raynor
Armour Research Foundation
Illinois Institute of Technology
Chicago, Illinois (1)

Professor R. L. Bisplinghoff
Mass. Institute of Technology
Cambridge 39, Massachusetts (1)

Dr. Walker Bleakney
Department of Physics
Princeton University
Princeton, New Jersey (1)

Director, Construction Div.
U. S. Atomic Energy Commission
Washington 25, D. C.
ATTN: Mr. C. Beck (1)

SUPPLEMENTAL -- DISTRIBUTION LIST

ARMY:

Chief of Ordnance
Department of the Army
R and D Division
Washington 25, D. C.
ATTN: ORDTB-PS (1)

Engineering Research and Development Lab
Fort Belvoir, Virginia
ATTN: Structures Branch (1)

Chief of Engineers
Department of the Army
Washington 25, D. C.
ATTN: Code ENGWE (1)

NAVY:

Chief of Naval Research
Department of the Navy
Washington 25, D. C.
ATTN: Code 438 (2)

Officer in Charge
Office of Naval Research, Navy No. 100
Fleet Post Office
New York, New York (5)

Chief, Bureau of Ships
Department of the Navy
Washington 25, D. C.
ATTN: Code 324 (1)
: Code 442 (1)

Chief, Bureau of Yards and Docks
Department of the Navy
Washington 25, D. C.
ATTN: P-300 Research Div. (1)
P-312 Defensive Const. (1)
C-313 Spec. Structures Br. (1)

Superintendent
U. S. Naval Post Graduate School
Monterey, California (1)

Director, Office of Naval Research
Branch Office
844 N. Rush St., Chicago 11, Ill. (2)
150 Causeway St., Boston, Mass. (1)
346 Broadway, New York 13, N.Y. (1)
1000 Geary St., San Francisco 9 (1)
1030 E. Green St., Pasadena 1, California (1)

Director
U. S Naval Research Laboratory
Washington, D. C.
ATTN: Tech. Information Officer
Code 2028 (9)

Chief, Bureau of Ordnance
Department of the Navy
Washington 25, D. C.
ATTN: Code Re (1)

Commander
U. S. Naval Proving Grounds
Dahlgren, Virginia (1)

OTHERS:

Director, Nat'l Bureau of Standards
Washington, D. C.
ATTN: Mr. D. E. Parsons (1)

National Science Foundation
2144 California St., N.W.
Washington 25, D. C. (1)

OTHERS: (Cont'd)

Professor Lynn S. Beedle
Fritz Engineering Laboratory
Lehigh University
Bethlehem, Pennsylvania (1)

Professor Bruce G. Johnston
University of Michigan
Ann Arbor, Michigan (1)

Corps of Engineers, U. S. Army
Office of the Division Engineer
Ohio River Division
536 U. S. Post Office and Courthouse
P. O. Box 1159
Cincinnati 1, Ohio
ATTN: Mr. R. G. West (2)

Professor Hans Bleich, Columbia Univ.
Department of Civil Engineering
Broadway at 117th Street
New York 27, New York (1)

Corps of Engineers, U. S. Army
Ohio River Division Laboratories
5851 Mariemont Avenue, Mariemont,
Cincinnati 27, Ohio
ATTN: Mr. F. M. Mellinger (3)

Project File (2)

Project Staff (4)

For future distribution by
University (6)

Commanding Officer
Office of Naval Research
The John Crerar Library Bldg.
Tenth Floor, 86 East Randolph Street
Chicago 1, Illinois

ERRATA FOR

1778

AD

ATI NO. 1778 CLASSIFICATION U

DSC-PP11 Camera Unit

Strip into Original Film

~~Reproduce one copy to forward to DSC-SD11 (Mrs. Grant)~~

Forward Original copy to DSC-PR3 (Mrs. Pitsinger)

2 copies to Wash (LM)(W)

AIR FORCE-WPAFB-L-20 JUN 51 250M

IMMEDIATE ATTENTION

AMC Form 7D (14 Mar 51)

AD 17 9 2

ADDITIONS AND CORRECTIONS

TO THE REPORT

AN INVESTIGATION OF THE LOAD-DEFORMATION CHARACTERISTICS OF REINFORCED CONCRETE BEAMS UP TO THE POINT OF FAILURE

The following additions and corrections are to be made to the report An Investigation of the Load-Deformation Characteristics of Reinforced Concrete Beams Up to the Point of Failure, by J. R. Gaston, C. P. Siess, and N. M. Newmark, which was issued to the Office of Naval Research under Contract N6ori-071(34), Task Order 34, Project NR-064-372 in December 1952:

BEAM DESIGNATION

The significance of the letter and numeral symbols used to designate the various beam specimens was not given in the original report.

The letters and numerals serve to identify the various beams in the following manner:

For beams reinforced in tension only:

The letter T indicates that the beam was reinforced in tension only in the region of pure flexure.

The numeral following the letter T is the value of the reinforcing index $q = \frac{pf_y}{f'_c}$ in tenths, rounded to the nearest tenth.

The letter L, M, or H appearing next designates the concrete strength; that is low, medium, or high, where low is from 2000 psi to 3000 psi, medium is from 3000 psi to 4000 psi and high is from 4000 psi to 6000 psi.

The lower case letter a, b, or c following the concrete strength designation identifies the individual beams when two or more similar specimens were tested.

For beams reinforced in compression as well as tension:

The letter C indicates that the beam was reinforced in compression as well as tension in the region of pure flexure.

The numeral following the letter C is the value of $q = \frac{pf_y}{f'_c}$ in tenths, as before.

The letter w, x, y, or z appearing next indicates the spacing of the ties in the region of pure flexure. The letter w refers to compression reinforcement without ties; x indicates that the tie spacing was that specified by ACI 318-51; y indicates that the tie spacing was one-half that specified by ACI 318-51; and z indicates that the tie spacing was one-fourth that specified by ACI 318-51.

The letters n or m indicate the type of tie used, as shown in Fig. 4 of the report.

The lower case letter a or b, where it appears, indicates that two similar specimens were tested.

Examples:

Beam T1La is reinforced in tension only, has a value of the reinforcing index q equal to 0.1, a concrete strength between 2000 and 3000 psi, and is one of two or more similar beams.

Beam C3yna is reinforced in compression as well as tension, has a value of q equal to 0.3, has a tie spacing in the region of pure flexure one-half that specified by ACI 318-51, has type n ties, and is one of two or more similar beams.

ADDITION TO TABLE NO. 2

SUMMARY OF RESULTS

FOR BEAMS REINFORCED IN TENSION AND COMPRESSION

Beam	k^n +
C2w	0.897
C2xm	0.878
C3w	0.857
C3xm	0.857
C3yna	0.866
C3ynb	0.850
C4xna	0.884
C4xnb	0.856
C4zn	0.857
C5yn	0.833
C6xm	0.833
C7w	0.833

+$k^n d$ = distance between the centroids of the tension and compression reinforcement; where d = distance from the top of the beam to the centroid of the tension reinforcement.

CORRECTION TO TABLE 9a

COMPARISON OF EXPERIMENT AND THEORETICAL VALUES

OF YIELD-POINT MOMENT

Beams with Tension and
Compression Reinforcement

Beam	M_y - kip-ft		
	Exp	Theo	Exp / Theo
C2w	32.4	31.1	1.04
C2xm	38.0	35.4	1.07
C3w	62.4	60.4	1.03
C3xm	66.3	61.5	1.09
C3yna	41.0	40.1	1.02
C3xnb	62.4	62.0	1.01
C4xna	40.1	41.4	0.97
C4xnb	42.8	42.2	1.01
C4zn	59.3	60.7	0.98
C5yn	87.8	89.5	0.98
C6xm	84.9	85.2	1.00
C7w	84.0	84.7	0.99
	Average Ratio		1.02
	Range		0.98-1.09

OTHER CORRECTIONS AND ADDITIONS

A value of the modulus of elasticity of the reinforcing steel, E, of 30 x 10^6 psi was used throughout the report.

Page 32:

Equation (31) should read:

$$f_c = \frac{pf_y}{\frac{1}{2}k' + \frac{np'(k' + k''-1)}{k'}}$$

Equation (32) should read:

$$f'_s = \left[\frac{k'' + k'-1}{k'}\right] nf_c$$

Page 38:

Third line below Eq. (47)

"For $q' > q'_{cr}$, . . ."

Fifth line below Eq. (47)

" . . ., that is, $f_s < f_y$ "

Second line below Eq. (48)

" . . . and $f_s > f_y$ "

TABLE 1, "SUMMARY OF RESULTS FOR BEAMS REINFORCED IN TENSION ONLY"

The entry under the column entitled "Stirrups" should read "None" for beam T1Ma instead of "Clamp-on".

TABLE 2, "SUMMARY OF RESULTS FOR BEAMS REINFORCED IN TENSION AND COMPRESSION

The heading for column 9 should read " p'- %", instead of " p -%".

TABLE 4, PROPERTIES OF REINFORCING STEEL

The heading for column 9 should read "Elongation in 8 in., %" instead of "Elongation in 6 in., %".

Fig. 14 BEAM AND TESTING APPARATUS

The following note should be added, "The 8"-dimension of all bearing plates is parallel to the axis of the beam".